NASA

Technical Memorandum **79619**

Gamma Ray Spectroscopy
In Astrophysics

EDITED BY

T. L. Cline and R. Ramaty

AUGUST 1978

National Aeronautics and
Space Administration

Goddard Space Flight Center
Greenbelt, Maryland 20771

Proceeding of a Symposium held at the Goddard Space Flight Center April 28 and 29, 1978.

GAMMA RAY SPECTROSCOPY

IN ASTROPHYSICS

Edited by

T. L. Cline and R. Ramaty

August 1978

GODDARD SPACE FLIGHT CENTER
Greenbelt, Maryland

PREFACE

This volume contains the papers presented at the Symposium on Gamma Ray Spectroscopy in Astrophysics held at the Goddard Space Flight Center, Greenbelt, Maryland on April 28 and 29, 1978.

This was the first symposium devoted entirely to spectroscopy in gamma ray astronomy. Its purposes were to bring together most of the scientists contributing to all the aspects, experimental and theoretical, of this new field and to discuss and compare ideas, measurements, calcu- . lations and technical experience in what we confidently expect to be a very important new discipline in high energy astrophysics.

This goal was achieved, we feel, in that a very large fraction of all that is known about gamma ray spectroscopy in astrophysics was indeed presented or discussed at the Symposium, yet many of these results are new, presented here for the first time. Further, the discipline is on the brink of moving to the next level of development within the coming year, with a number of satellite experiments and major balloon experiments in gamma ray spectroscopy and in related astrophysical sciences about to be launched. We therefore felt that we should publish the Proceedings as soon as possible, without the delays involved in reformatting the manuscripts and extensive editing. We hope that the information that will thus become available will prove to be useful to all workers in these fields.

We have ordered the papers approximately as presented, with experimental and theoretical papers combined in each session. The introductory session is followed by the sessions on solar, stellar, and planetary gamma ray spectroscopy, and on cosmic gamma ray spectroscopy, with the technical discussions and previews of new experiments in the last two sessions.

The Symposium was organized by the editors of these proceedings, T. L. Cline and R. Ramaty. We wish to thank the Symposium Session Chairmen, D. D. Clayton, and M. M. Shapiro, and the Workshop Session Chairmen, G. J. Fishman and N. S. Wall, for their assistance. We are grateful to R. C. Reedy for supplying us the manuscript on Planetary Gamma Ray Spectroscopy which was not presented at the Symposium. This paper is taken from the Proceedings of the Ninth Lunar and Planetary Science Conference (Pergamon Press 1978, with permission). We are also indebted to R. W. Bussard and R. P. Weaver for their help in running the conference. We thank F. B. McDonald for his continued support of this Symposium, and R. S. Cooper for his interest and his contribution. We thank Barbara Pratt in particular for her excellent secretarial help with both the organization of the Symposium and the preparation of this document.

T. L. Cline
R. Ramaty

TABLE OF CONTENTS

I. OPENING REMARKS AND REVIEWS

OPENING REMARKS

Robert S. Cooper
Director, Goddard Space Flight Center
Greenbelt, Maryland 20771, USA

It is a pleasure for me to be here and welcome you all to the Goddard Space Flight Center. I noticed from the agenda that we have speakers from all the major groups that are interested in high energy astronomy and in particular in gamma ray astronomy virtually in the entire free world. The agenda is particularly interesting to me and I intend to spend as much of my time here over the next day as I can. I would like to make a couple of points. The people here at Goddard know that when they give me an opportunity to come and welcome you, the potential is always there for me to say something. But they have to suffer through that. I have only been at the center a couple of years now, yet it is clear to me that one of the most interesting and vital areas of research in the space program is high energy astrophysics. Also, the high energy astrophysics group here is vital and strong and they have a great deal of enthusiam for what they do. The other point is that high energy astrophysics and particularly gamma ray astronomy is in a very fermenting intellectual period right now.

Because it is in such ferment, I have tried to sort through exactly why and how the high energy activity has grown and what its development has been by reading and by talking to people such as Frank McDonald, Reuven Ramaty and others. The developments have been outstanding and rapid over the last 10 or 15 years and particularly over the last few years as the detector development and the capability to put larger and larger objects in space has grown.

One of the things I did last night, while thinking through these developments, was to compare the development of the activity in this scientific area to the development of the intellect of the human child. There is an interesting analogy that can be made. When a child is born he comes into the world with the ability only to have large scale perceptions or sense impressions of the various physical

phenomena about him. His eyes don't focus well; he feels heat and cold only in a very diffuse manner; he is unable to integrate any of the sense impressions that he has and it must be a chaotic universe to him. In the beginning he complains about that a great deal. I think that is a stage through which this intellectual activity has passed, and if you think carefully about the details many of these correspondences will come to your mind. Now, as this conference attests, we are passing from that early development into a period when the details of the sensory stimuli that come to us will be understood. That is a major advancement in maturation of any scientific discipline when an essentially observational science moves from the general to the particular, from the photometry to the spectroscopy of the science. We are at the threshold of that period in both gamma ray and x-ray astronomy now. It is going to give new intellectual insights into mysteries of the universe.

Continuing the analogy, in human intellectual development there is another period of maturation that occurs during the teens. That is the time when the human mind is able to overcome its emotional impulses and to begin to intellectualize things, and where the sensory apparatus are largely matured, perhaps even at their highest capability and sensitivity. There is every evidence that high energy astrophysics is moving into that developmental period. The development of the instrumentation has reached a level where I believe over the next few years it will have matured essentially to what the current state-of-the-art will allow and perhaps in many cases to what the fundamental physical limits will allow. Also, I believe that the vitality, the intellectual maturity of the maybe few hundred people who are working in this area will have reached a stage where the intellectual development of the physical discipline itself will be accelerating at a maximum pace. Society stands to benefit in many ways from the intellectual developments in this area over the next 5 to 10 years. There exists in the life of every human being

and in the life of activities of this sort a period of mature activity and senescence; but I don't believe that we can even see when that period is likely to occur for the high energy astrophysical discipline.

One more point. Without the ability to do significant experiments in space, there really would be no gamma ray and x-ray astronomy of any note. People have been doing experiments in the upper atmosphere with balloons for a number of years and we still do some of them here at the center, but I think that almost all of the interest now has turned to the HEAO spacecraft, to the prospects for the Gamma Ray Observatory, and to follow-on x-ray experiments of major proportions in space. The reason, of course, is because of our ability to do major large scale space experiments. That is where Goddard can make some contributions. We have in the past by placing the SAS spacecraft into orbit and helping to make them successful. We contributed to the HEAO program substantially and we are looking forward to the major new high energy programs of the future. So, we have a great interst in this. I am glad that you are all here today and I look forward to participating with you in this exciting review.

Mechanisms and Sites for

Astrophysical Gamma Ray Line Production

R. Ramaty
Laboratory for High Energy Astrophysics
NASA/Goddard Space Flight Center
Greenbelt, MD. 20771 USA

1. INTRODUCTION

Gamma-ray lines result from nuclear deexcitations, positron annihilation and neutron capture, processes which are expected to occur at many astrophysical sites. Supernova and nova explosions synthesize long-lived radioactive isotopes and eject them into space where they produce observable gamma-ray lines by decaying into excited levels of daughter nuclei or by emitting positrons. Energetic charged particles in the interstellar medium, in supernova remnants, in solar or stellar flares, and possibly in the vicinity of compact objects, produce gamma-ray lines by inelastic collisions which either excite nuclear levels or produce positrons and neutrons. The energetic particles could result from acceleration in time-varying magnetic fields, as for example in solar flares, or from gravitational accretion onto neutron stars and black holes. Electromagnetic processes in the strong magnetic fields of pulsars could produce positron-electron pairs, and line emission can result from the annihilation of these positrons. Deexcitations of quantized states in strong magnetic fields can also produce lines, and these have energies of tens of keV for magnetic fields typical of neutron star surfaces.

The purpose of the present paper is to review the production mechanisms of gamma-ray lines of astrophysical interest, to briefly discuss the sites at which detectable line emission could be produced, and to present realistic estimates of line fluxes that could be expected from these sites.

The general scope of gamma-ray line astronomy prior to this Symposium has been reviewed by Lingenfelter and Ramaty (1978), and some of the material of the present review is based on that paper. The numerical results for gamma-ray line production in energetic particle reactions that are used in both these reviews are based on the extensive calculations of Ramaty, Kozlovsky and Lingenfelter (1978) which will be published shortly.

The status of astrophysical gamma-ray line observations was reviewed at the Symposium by E. L. Chupp whose paper appears elsewhere in this volume (Chupp 1978). Here we only briefly mention some of the key observations, and give the appropriate references for treatments of their interpretation.

Gamma-ray lines were seen from the solar flares of 1972, August 4 and 7 (Chupp et al. 1973) and possibly from the flare of 1977, November 22 (Chambon et al. 1978). The implications of solar gamma-ray observations were treated in detail by Ramaty, Kozlovsky and Lingenfelter (1975) and Ramaty et al. (1978), and are discussed in this volume by Lin and Ramaty (1978). Gamma-ray lines were possibly detected from the galactic center (Haymes et al. 1975) and from Centaurus A (Hall et al. 1976). Interpretations of the galactic center observations were given by Lingenfelter and Ramaty (1976) and Audouze et al. (1976), and in the present volume by Lingenfelter Higdon and Ramaty (1978). Upper limits on gamma-ray lines from Nova Cygni were given by Leventhal, MacCallum and Watts (1977), and the implications of these observations are discussed by Truran (1978). A 20 minute burst of gamma-ray lines was observed in 1974 (Jacobson 1977, Jacobson et al. 1978), and an interpretation of this very exciting event is given in the present volume by Lingenfelter, Higdon and Ramaty (1978). The cyclotron line from Hercules X-1 was first observed by Trumper et al. (1978), and several papers in this volume provide further observational results and theoretical discussions of cyclotron line emission (Trumper 1978, Durouchoux, Boclet and Rocchia 1978, Dennis et al. 1978, Daugherty 1978, Bussard 1978, Weaver 1978, Meszaros 1978). The observation of positron annihilation radiation from the galactic center was reported at this Symposium by Leventhal, MacCallum and Stang (1978a,b), and some of the implications of this very important observation are given in the present paper.

The principal mechanisms for gamma-ray line production (decay of radioactivity from processes of nucleosynthesis, excitation of nuclei by energetic particle reactions, positron annihilation, neutron capture, and cyclotron line emission) are reviewed in Section 2; the astrophysical sites and the estimates of line fluxes are discussed in Section 3; the implications of the 0.511 MeV gamma-ray line observations from the galactic center are given in Section 4; and a Summary is provided in Section 5.

2. EMISSION MECHANISMS

Radioactivity. Excited nuclear levels can be populated by the decay of long-lived radioactive species which are formed during processes of nucleosynthesis. The decay chains which are likely to produce detectable gamma-ray lines are listed in Table 1, together with the relevant mean lives, yield of radioactive nuclei per supernova, photon energies, and the number of photons per disintegration (Clayton, Colgate and Fishman 1969, Lingenfelter and Ramaty 1978, Arnett 1978). The supernova yields relative to the ^{56}Ni yield are based on solar system abundances (Cameron 1973), and the assumption that all the ^{56}Fe, ^{57}Fe and ^{44}Ca in the galaxy, and 2%, 1% and 0.1% of the galactic ^{22}Ne, ^{60}Ni and ^{26}Mg, respectively, are produced via the decay chains shown in this table. The absolute yield of ^{56}Ni is normalized to the production of the galactic abundance of ^{56}Fe by approximately 1.7×10^{9} supernovae (Clayton 1973). It should be emphasized that these assumptions are strongly model dependent and that their validity could be best tested by the line observations themselves.

The ^{22}Na yield per nova is from Truran (1978). With a nova rate of about 40 events per year and a supernova rate of one every 25 years, the average ^{22}Ne production from novae is smaller than that from supernovae. But because of the higher nova frequency, there is a better chance for observing the 1.275 MeV line from novae than from supernovae.

The half-lives of the radioactive isotopes are of crucial importance for the detectability of the lines. Because the nucleosynthesis takes place in dense regions, the gamma rays cannot escape unless significant expansion occurs before the decay of the nuclei and the emission of the lines. For the lines of ^{56}Co one expects that the medium will just become transparent in 100 days provided that in the explosion one solar mass is ejected with a velocity of at least 10^4 km/sec. If, however, the explosion leads to the ejection of a larger mass, the lines from the ^{56}Ni decay chain may not be observable, but in any case the opacity of the medium should present no problems for the detection of the lines from the other decay chains shown in Table 1.

The widths of gamma-ray lines from nucleosynthesis are determined by Doppler broadening due to the velocity of the expanding medium. For supernova ejecta the appropriate velocity, 10^4 km/sec, results in line widths of about 6%. The isotopes ^{60}Fe and ^{26}Aℓ have long mean lives and essentially come to rest before they decay; their lines have widths of only $\sim$ 0.2%, mostly due to galactic rotation. For the ^{22}Na line (1.275 MeV) from novae, the ejection velocity of $\sim 10^3$ km/sec results in a width of $\sim$ 0.6%.

Among the lines listed in Table 1, the 1.809 MeV line from ^{26}Aℓ decay has a very good prospect for detection. The long lifetime of this radioactive nucleus guarantees an emitting region (most likely the interstellar medium) which is transparent to gamma rays; this lifetime also implies that the width of the line is very narrow. Both these features are important for a high probability of detection. Moreover, the discovery of anomalous ^{26}Mg in the Allende meteorite (Lee, Papanastassiou, and Wasserburg 1977) lends support to the notion that large quantities of freshly nucleosynthesized ^{26}Aℓ are ejected by supernova explosions, and it is the decay of these nuclei which should produce the 1.809 MeV gamma-ray line (Ramaty and Lingenfelter 1977).

Inelastic Collisions. Nuclear reactions between energetic charged
particles and ambient interstellar material lead to gamma-ray line emission
following the excitation of nuclear levels both in the accelerated particle
population and in the ambient medium. Lines of this nature have been observed
from the large solar flare of 1972, August 4 (Chupp et al. 1973), and their
interpretation has been treated in several publications (e.g. Ramaty,
Kozlovsky and Lingenfelter 1975, Ramaty, Kozlovsky and Suri 1977). An
example of the gamma-ray spectrum due to inelastic collisions is shown in
Figure 1. Here three line components can be distinguished. There is a broad
component from deexcitation of excited energetic nuclei which have energies
of a few MeV/nucleon or more, a narrow line component from deexcitation of
excited ambient nuclei which pick up recoil energies of a few tens of keV/
nucleon, and a very narrow line component from deexcitation of those excited
nuclei which can essentially come to rest before deexcitation, because the
lifetime of the level, or its radioactive parent, is long enough and the
ambient density high enough. In solids with densities of the order of a
gm/cm^3, the slowing down time and distance are about 10^{-12}sec and 10^{-4}cm.
The broad lines with widths of up to an MeV merge into the underlying
continuum upon which the narrow and very narrow lines are superimposed. The
widths of the narrow lines are less than about one hundred keV (e.g. the
4.438 MeV line from ^{12}C), while the widths of the very narrow lines (e.g.
the sharp component of the 6.129 MeV line from ^{16}O) are only a few keV. In
the interstellar medium, very narrow lines may be produced in interstellar
grains (Lingenfelter and Ramaty 1977). The strongest lines from energetic
particle interactions are expected at 4.44 MeV from ^{12}C, at 6.129 MeV from
^{16}O and at 0.847 MeV from ^{56}Fe.

The production rates, q, of the 4.44, 6.129 and 0.847 MeV lines and of
the total nuclear radiation, normalized to the energy density, W, in energetic

particles and 1H atom in the ambient medium are shown in Figure 2. These

results are based on solar abundances for both the ambient medium and the

energetic particles. For the 4.44, 6.129 and 0.847 MeV lines, the q's

of this figure are those resulting from proton and alpha interactions, i.e.

the narrow component of the 4.44 MeV line and the sums of the narrow and

very narrow components of the other two lines. For the total, q is the

sum of the production rates of photons of all energies in all three line

components. The production rates can also be normalized to the energy

deposition rate, $\dot{W}$, of the energetic particles in the ambient medium. The

ratios $q/\dot{W}$ are shown in Figure 3. As in Figure 2, the q's are the production

rates of the narrow 4.44 MeV and narrow plus very narrow 6.129 MeV line, and

both the ambient medium and energetic particles have solar abundances. The

energy loss rates in a neutral medium of 90% H and 10% He are from Northcliffe

and Shilling (1970) and Barkas and Berger (1964). The parameters s and E_c

in Figure 2 and 3 define the spectrum of the energetic particles: the number

of particles per unit energy per nucleon is proportional to E^{-s} for $E > E_c$ and

to a constant otherwise.

Positrons. Positron annihilation leads to gamma-ray line emission at

0.511 MeV. The principal mechanism for positron production are the decay of

radioactive nuclei from processes of nucleosynthesis, inelastic collisions

which produce nuclei that decay by positron emission, and possibly pair

production in pulsar magnetospheres. We now consider these in turn.

The yield of positrons that accompanies nucleosynthesis is given for

the various decay chains in Table 1. In assessing the contribution of each

chain to detectable 0.511 MeV radiation, we distinguish between short-lived

and long-lived decay processes. Positrons from short lived chains (e.g.

$^{56}Ni \rightarrow ^{56}Co \rightarrow ^{56}Fe$ and $^{22}Na \rightarrow ^{22}Ne$) annihilate in relatively dense regions of

the expanding supernova-envelope on time scales much shorter than the longest

mean life in the chain. Such positrons produce a 0.511 MeV line whose

time history is similar to that of the characteristic gamma rays that accom-

pany the decays in the chain. The considerations for the detectability

of the 0.511 MeV line from these positrons, therefore, should be the same

as those of the characteristic gamma rays, and these considerations are dis-

cussed separately below. On the other hand, the positrons from decay chains

with relatively long mean lives (e.g. the $^{44}Ti \rightarrow ^{44}Sc \rightarrow ^{44}Ca$ and $^{26}A\ell \rightarrow ^{26}Mg$) are

expected to annihilate on time scales longer than the time interval between

supernova explosions, and hence to produce an essentially steady flux of

0.511 MeV photons. For $^{26}A\ell$ decays, the positrons almost surely annihilate

in the interstellar medium; for the ^{44}Ti chain, the positrons probably

annihilate inside supernova remnants. Positrons resulting from the decay of

^{22}Na produced in nova explosions should also annihilate in the interstellar

medium, on time scales much longer than the interval between nova explosions.

The production of nuclear gamma-ray lines by energetic particle reactions

is accompanied by positron production from the decay of radioactive positron

emitters produced in these reactions. Such positron production has been

treated in considerable detail by Ramaty et al. (1975). The cross sections

used by these authors have been recently updated, and several new positron

emitters such as $^{16}O^*6.052$ and ^{56}Co have been added (Ramaty et al. 1978). In

Figure 4 we show the ratio of positron production, q_+, to the narrow 4.44 MeV

line production, $q_{4.44}$, as a function of s and E_c for solar abundances. We

note that q_+ in this figure does not include positron production from π^+

decay. An upper limit on the intensity of the 0.511 MeV line from π^+ decay

can be obtained from the observed >100 MeV gamma-ray emission from the galactic

center by assuming that all the high energy gamma rays are from π^o decay.

This upper limit is lower by at least an order of magnitude than the 0.511 MeV

line intensity observed by Leventhal et al. (1978a,b) from the galactic center.

The production of positrons by electromagnetic processes in pulsar magnetospheres has been treated by Sturrock (1971). It is suggested that about $3x10^{51}$ positrons are produced in the lifetime of a pulsar, and that the production rate by the Crab pulsar at the present time is about 10^{41} positrons/second.

We turn now to a discussion of the positron annihilation process. The recent results of Bussard, Ramaty and Drachman (1978) are shown in Figure 5, 6 and 7. Figure 5 shows the fraction of positrons that form positronium in flight as a function of the degree of ionization of the ambient medium. As can be seen, in a neutral gas over 90% of the positrons from positronium in flight before they thermalize, but this percentage drops rapidly with increasing ionization fraction. As we shall see below, positronium formation in flight leads to a fairly broad 0.511 MeV line whose width is independent of the temperature of the ambient medium.

The rates of the various processes that affect thermal positrons are shown in Figure 6: R_{ce}/n_H and R_{da}/n_H are the rates for charge exchange with neutral hydrogen and direct annihilation with atomic electrons per unit target density, while R_{rr}/n_e and R_{da}/n_e are the radiative recombination and direct annihilation rates with free electrons, also per unit target density. As can be seen, only for temperatures greater than 10^6K is direct annihilation the dominant process. At lower temperatures, the bulk of the positrons ($\gtrsim 90\%$) form positronium, either by radiative recombination or by charge_ exchange. The relative rates of these two processes depend on the amount of residual neutral hydrogen present. For example, at $T = 10^5$K, the rate of charge exchange is greater than that of radiative recombination if $n_H/n_e > 5x10^{-6}$. Since for temperatures less than 10^5K, we expect larger neutral hydrogen concen-

trations, charge exchange should be the dominant process down to temperatures around 10^4K. At 8000 K, $R_{ce}/n_H = R_{rr}/n_e$, so that for a medium that is half ionized, the rates of charge exchange and radiative recombination are about equal. At lower temperatures, radiative recombination should remain the dominant process as long as there is an appreciable concentration of free electrons. However if n_e/n_H becomes small, a large fraction of the positrons form positronium in flight, as can be seen from Figure 5.

In Figure 7 we show the shapes of the 0.511 MeV line resulting from annihilation in cold neutral hydrogen and from charge exchange after thermalization. As can be seen, the full width at half maximum (FWHM) of the line produced in a cold medium is about 5 keV; however, a narrower line (e.g. FWHM ≃ 1.5 keV for T = 8000K) can result from positronium formation after thermalization.

Neutrons. The radiative capture of neutrons by protons ($n + p \rightarrow d + \gamma$) produces a gamma-ray line at 2.223 MeV. The strongest line from solar flares has been observed at this energy (Chupp et al. 1973), and is believed to be due to neutrons produced in inelastic collisions of energetic particles in the solar atmosphere. The 2.2 MeV line is produced in the photosphere where the density is sufficiently high ($\sim 10^{17} cm^{-3}$) to allow the capture of the neutrons before they decay. Neutrons in the photosphere can also be captured, nonradiatively, by ^{3}He nuclei (Wang and Ramaty 1974). Because of this effect, observations of the 2.2 MeV line from flares set meaningful upper limits on the abundance of ^{3}He in the photosphere. The width of the 2.2 MeV line from solar flares reflects the photospheric temperature and is of order 0.1 keV. A detailed discussion of the physics of solar gamma-ray production is given elsewhere in this volume (Lin and Ramaty 1978).

The detection of the 2.223 MeV line from non-solar sources would have important implications on the question of the origin of deuterium in the

universe. It is believed that deuterium is of cosmological origin produced
in the Big Bang. However, for this interpretation to be correct, the
density in the universe has to be low, which implies that the universe is open.
If other sources of deuterium were known, less deuterium production would be
required in the Big Bang, and hence a higher universal density would be possible.

Radiative neutron capture also leads to other lines. Of considerable
astrophysical interest is the reaction $n+^{56}Fe \rightarrow ^{57}Fe + \gamma$ which produces two
lines at 7.632 and 7.646 MeV. Since the capture cross section of neutron
on ^{56}Fe is larger than that on H by a factor of 8, in a medium with Fe/H
ratio $\geqslant 0.1$, the above two lines will have comparable or larger intensities
than the 2.2 MeV line. A large Fe/H ratio may exist on the surfaces of neutron
stars. Three of the 4 lines observed by Jacobson et al. (1978) in the 20 minute
burst of June 1974 can be associated with neutron capture on H and Fe, according
to the model of Lingenfelter et al. (1978) presented elsewhere in this volume.

Cyclotron Emission. Emission lines in the soft gamma-ray region could
result from cyclotron radiation in the very strong magnetic fields believed
to exist at the surfaces of neutron stars. The square of the perpendicular
momentum of an electron in a magnetic field B is quantized, $p_{\perp}^2 = 2B/B_q (m^2c^2)j$,
where j is an integer and $B_q = 4.414 \times 10^{13}$ gauss (e.g. Daugherty and Ventura
1977). Cyclotron and synchroton radiations are produced by transitions between
these levels. While for low fields, the separation in levels is so small
that the radiation can be approximated by a continuum, for magnetic fields
at neutron star surfaces, the energy level separations are large and transitions
among them can produce discrete line emission. In the nonrelativistic case
($E_\gamma \ll mc^2$), the energies at the line centers for transitions between j and j-n
are given by $mc^2 (B/B_q)n$, i.e. they are independent of j. But in the relativistic
quantum case, significant line splitting is introduced if more than one quantum

level j is excited. This is illustrated in Table 2, where we show the line

center energies for transitions among the first three quantum levels in a

magnetic field of 6.62×10^{12} gauss. As mentioned in the Introduction, the

observations and theory of cyclotron line emission from pulsars is treated

in detail in other papers in this volume.

3. ASTROPHYSICAL SITES

We proceed now to discuss the various astrophysical sites that could

produce detectable gamma-ray line emission.

Supernovae. Radioactivity is the most important mechanism for gamma-ray

line production in supernovae. The various lines listed in Table 1 should

be observable from a galactic supernova for differing periods of time after

the explosion. For the higher energy lines, these times are determined by the

detector sensitivity. For a sensitivity of $\sim 5 \times 10^{-5}$ photons/cm^2sec for a line

of FWHM ~ 60 keV at 1 MeV, the 0.847 and 1.238 MeV lines of the $^{56}Ni \to ^{56}Co \to ^{56}Fe$

chain, the 1.275 MeV line of the $^{22}Na \to ^{22}Ne$ chain, and the 1.156 MeV line of

$^{44}Ti \to ^{44}Sc \to ^{44}Ca$ chain should be observable for about 4, 25 and 120 years. If,

on the average, there is one supernova explosion every 25 years in the galaxy,

then there should exist several galactic supernova remnants with detectable

^{44}Ti radioactivity, and perhaps one remnant with detectable ^{22}Na. But there

is only a 10% chance for detecting ^{56}Co radioactivity from a galactic super-

nova, provided that the supernova envelope is transparent to the lines of ^{56}Co.

The detectability of the 0.122 MeV line from $^{57}Co \to ^{57}Fe$ decay is limited by

the universal background, and it could be observed for about 5 to 8 years after

the explosion for detector opening angles ranging from 20° to 5°. With the

above supernova rate, there is about a 25% chance for finding a supernova

remnant with detectable ^{57}Co in the galaxy.

The ^{44}Ti decay chain could be observed from the supernova remnant

Cassiopeia A (distance = 2.8kpc, age ~ 300 years). The predicted flux is

$\sim 4 \times 10^{-5}$ photons/cm^{2}sec. The 0.847 and 1.238 MeV lines from the decay chain $^{56}\text{Ni} \rightarrow {}^{56}\text{Co} \rightarrow {}^{56}\text{Fe}$ could be observed from a single supernova out to a distance of 3Mpc. The Virgo cluster of galaxies at 10Mpc could present a steady source of 0.847 and 1.238 MeV lines provided that the supernova rate in this cluster exceeds about 10 events per year. Here again, these predictions assume that the individual supernovae are transparent to these gamma-ray lines.

Novae. Accretion from a large, cool companion onto a white dwarf leading to thermonuclear runaway in the CNO cycle has been suggested as the cause of novae (e.g. Starrfield et al. 1972). If so, novae could also be sources of gamma-ray line emission from the decay of synthesized radionuclei (Clayton and Hoyle 1974). The easiest line to detect is at 1.275 MeV from ^{22}Na decay. For the ^{22}Na yield per nova as given in Table 1, the flux of the 1.275 MeV line from a nova at 1 kpc, in photons/cm^{2}sec, is $\sim 8 \times 10^{-5}$ exp(-t/3.8 years) (Truran 1978). The limit of 8×10^{-4} photons/cm^{2}sec set by Leventhal et al. (1977) on Nova Cygni (distance = 1.5 kpc) 9 months after the explosion is larger by more than an order of magnitude than the expected flux from this nova.

Nevertheless, for an estimated nova rate of ~ 40 per year, a few closeby novae should occur during a two year gamma-ray astronomy mission. With a detector sensitivity of $\sim 2 \times 10^{-5}$ photons/cm^{2}sec for a line of FWHM ~ 10 keV at 1 MeV, an individual nova could be detected from a maximal distance of about 2kpc. But because the time between nova explosions is much shorter than the ^{22}Na mean life, a detector with a broad field of view observing the galactic plane in the direction of the galactic center would probably observe diffuse emission at 1.275 MeV. We provide a rough estimate of the expected diffuse 1.275 MeV intensity below.

Interstellar Medium. Line emission intensities from the interstellar medium can be estimated by considering the emissivities per hydrogen atom in the vicinity of the solar system. Such emissivities are shown for several lines in Table 3. For inelastic collisions, the emissivities of the 4.44, 6.129 and 0.847 MeV lines are from Figure 2 for $s = 4$, $E_c = 10$ MeV/nucleon, $W = 1$ eV/cm^3, and a solar composition for the ambient medium. We take half the O in grains and the other half in gas, and all the Fe in grains. For the interstellar lines from nucleosynthesis, we assume that the production rates of ^{26}Aℓ and ^{60}Fe at the present epoch are a factor of 10 less than the average rates required to produce over the age of the galaxy (1.2×10^{10} years) 0.1% and 1% of the ^{26}Mg and ^{60}Ni abundances, respectively, and that 1% of the galactic mass is in the interstelar medium.

For the 1.275 MeV line from unresolved novae, we assume a nova rate larger by a factor of 10^3 than the supernova rate and a yield of 10^{48} ^{22}Na nuclei per nova. This yields a 1.275 MeV line emissivity larger by a factor of 2.5 than the 1.809 MeV emissivity.

For positron annihilation in the interstellar medium, we consider inelastic collisions, ^{26}Aℓ decay from supernovae and ^{22}Na decay from novae. The 0.511 MeV photon production rate per H atom from these processes is about 2×10^{-26}, 5×10^{-26} and 1×10^{-25} photons/(H atom sec), respectively, where we have used $q_+/q_{4.44} = 1$ from Figure 1, the positron yields of Table 1, and the 4.44 MeV, 1.809 MeV and 1.275 MeV line emissivities of Table 3. Since about 93% of the positron annihilate via positronium, the annihilation of 1.6 positrons is required to produce one photon in the 0.511 MeV line.

The emissivity of gamma rays of energies greater than 100 MeV is shown

for normalization purposes. Since gamma rays in this energy range have

been observed from the galactic disk with an intensity of $\sim 10^{-4}$ photons/cm^2

sec rad for longitudes between 330° and 30° (Fichtel et al. 1975), the expected

flux of a given line can be estimated by scaling its emissivity to the >100 MeV

emissivity given in the table. For the 0.511 MeV line from processes of

nucleosynthesis and the lines from ^{26}Aℓ, ^{60}Fe and ^{22}Na decay we thus obtain

the fluxes as given in Table 3. For the lines from inelastic collisions, we

take the average emissivities along a line of sight near the galactic center

to be larger by a factor of 3 than the local emissivities. This is based

on evidence (Peimbert, Torres-Peimbert and Rayo 1978 and references therein)

for a substantial increase in the relative abundance of elements heavier

than helium compared to hydrogen with decreasing distance from the galactic

center. Thus, the estimated fluxes of lines from inelastic collisions given

in Table 3 are 3 times larger than those estimated for a constant heavy element-

to-hydrogen ratio.

Compact Objects. Neutron stars and black holes could produce gamma-ray

lines in several ways.

Accretion of matter on neutron stars produces gamma-ray lines by

inelastic collisions induced by the accreted particles which can reach the

neutron star surface with energies in the range 10 to 100 MeV/nucleon (e.g.

Ramaty, Borner and Cohen 1973). Gamma-ray lines could also be produced from

quasithermonuclear excitation of matter, either in a standing shock above

the surface of a neutron star or in an accretion disk around a neutron star or

a black hole (Higdon and Lingenfelter 1977). The strongest lines from these

processes should be at 4.438 and 6.129 MeV. Inelastic collisions on and around

compact objects also produce neutrons and positrons. It is possible that the

413.2 and 1789.7 keV lines of the June 10, 1974 burst (Jacobson et al. 1978)

could be redshifted lines from positron annihilation and neutron capture on H. The other two lines observed from this burst could also be due to neutron capture (Lingenfelter, Higdon and Ramaty 1978).

Neutron stars could be strong sources of quantized cyclotron emission, as the observations of Hercules X-1 (Trumper et al. 1978) and of the Crab Nebula (Jacobson 1977, Jacobson et al. 1978) have shown. We would expect cyclotron lines from other x-ray or gamma-ray pulsars: Cen X-3, Vela X-1, 3U0115+63 and the Vela pulsar.

The origin of gamma-ray bursts is not known, but it is possible that compact objects could be responsible for their production. Metzger et al. (1974) have observed radiation up to $\sim$ 5 MeV from the gamma-ray burst of April 14, 1972, and at this energy nuclear processes could be responsible for the bulk of the radiation as they are in solar flares (Ramaty, Kozlovsky and Suri 1977). Therefore, we expect considerable line structure from gamma-ray bursts at energies above an MeV. These lines could be very broad; but by measuring the line shapes, unique information could be obtained on the distribution of matter in the gravitational wells of compact objects.

Extragalactic Emission. Both discrete extragalactic sources and the universal background should be examined for possible line emission. As mentioned, in the Introduction, Hall et al. (1976) have reported line emission from the radiogalaxy Centaurus A. Objects in which non-thermal processes are dominant, could be important sources of gamma-ray lines. Schonfelder et al. (1978) reported at this Symposium the observations of MeV gamma rays from NGC4151, and it is conceivable that this emission contains lines as well. As already mentioned, clusters of galaxies, e.g. the Virgo cluster, could produce detectable line emission from radioactivity in supernovae.

Nucleosynthesis in extragalactic supernovae in the past could have contributed significantly to the universal background around 0.5 to 0.8 MeV through

photon emission from the decay chain $^{56}Ni \rightarrow ^{56}Co \rightarrow ^{56}Fe$ (Clayton and Silk 1969).
These authors suggest that, even though the cosmological redshift considerably
broadens the nuclear lines, they nevertheless could be discernable in the
background and thereby provide information on the rate of nucleosynthesis
in the past.

4. IMPLICATIONS OF THE 0.511 MEV LINE OBSERVATIONS FROM THE GALACTIC CENTER.

One of the highlights of the Symposium was the presentation of convincing
evidence for positron annihilation radiation from the galactic center (Leventhal,
MacCallum and Stang 1978a,b). The observed line at 0.511 MeV line has an
intensity of $(1.21 \pm 0.22) \times 10^{-3}$ photons/$(cm^2 sec)$, and a full width at half
maximum of less than 3.2 keV. There is also evidence for the 3-photon continuum
from triplet positronium annihilation.

Bussard, Ramaty and Drachman (1978) have recently analyzed the implication
of the very narrow width of this line, and they conclude that a fraction of the
positrons should annihilate in a medium which is at least partially ionized.
Possible annihilation sites are the warm ($\sim 10^4 K$) component of the interstellar
medium (McKee and Ostriker 1977), filaments or knots in supernova remnants,
and the extended HII region in the nuclear disk at the galactic center.

The possible detection of triplet positronium annihilation radiation
from the galactic center (Leventhal et al. 1978a,b) has the implication that
in the annihilation region the density of matter is less than about $10^{15} cm^{-3}$
and the temperature less than about $10^6 K$. At a higher density triplet posi-
tronium would dissociate before it could annihilate (Crannell et al. 1976),
and at higher temperatures positronium formation would be suppressed (Figure 7).

The origin of the positrons which produce the observed 0.511 MeV line is
not well understood, and all the mechanisms discussed in Section 2 (radioactivity,
inelastic collisions, pulsars) could be possible candidates. As already

mentioned, positrons from π^+ decay cannot produce the observed line, because such an origin would imply more high energy gamma rays from π° decay than observed (e.g. by Fichtel et al. 1975). It is also unlikely that diffuse emission from the interstellar medium could produce a 0.511 MeV flux as strong as observed (see Table 3). Future measurements of other gamma-ray lines from the galactic center, however, should provide a much better indication regarding the origin of the positrons responsible for the observed 0.511 MeV line.

The detection of a strong 1.809 MeV line from $^{26}A\ell$ decay would indicate that the positrons result predominantly from processes of nucleosynthesis. To provide an estimate of the expected intensity, we assume that the observed 0.511 MeV line is steady emission from the annihilation of positrons from ^{44}Ti and $^{26}A\ell$ decay. From Table 1, we then obtain a positron-to-1.809 MeV gamma-ray production ratio of about 16. Since $\sim$ 90% of the positrons are expected to annihilate via positronium, the observed 0.511 MeV line intensity of 1.2×10^{-3} photons/cm^{2}sec (Leventhal et·al. 1978a,b) implies a 1.809 MeV intensity of $\sim 10^{-4}$ photons/cm^{2}sec.

If, on the other hand, the positrons are produced predominantly in inelastic collisions, then the results of Figure 4 imply a positron-to-4.44 MeV photon production ratio of about 1 (Figure 4), and a 4.44 MeV line intensity from the galactic center of about 2×10^{-3} photons/cm^{2}sec. For a detector of 15° opening angle (Leventhal et al. 1978a, b), this intensity is larger by two orders of magnitude than that calculated for diffuse emission in the interstellar medium (Table 3). But the energetic particles could be confined to their sources; in particular, the nuclear reactions could occur in the accretion disk of a massive black hole at the galactic nucleus, as suggested in this volume by Lingenfelter et al. (1978). The observations of Haymes et al. (1975) of a spectral feature around 4.4 MeV from the galactic center would support this possibility; this measurement, however, needs to be confirmed by independent

observations.

Unlike radioactivity and inelastic collisions, positron production by pulsars is not accompanied by strong line emission due to processes other than annihilation. However, if pulsars are the major contributor to the observed 0.511 MeV line from the galactic center, positron annihilation radiation, perhaps redshifted, should be observed from known pulsars.

5. SUMMARY

The positive detection of gamma-ray lines promises to open a new area of observational astronomy with enormous potential for making fundamental contributions to astrophysics. The observation of gamma-ray lines can provide direct evidence for the existence of freshly nucleosynthesized matter and supply observational tests for theories nucleosynthesis. In particular, these observations would prove that some of the elements are synthesized in short time intervals in supernova explosions and not during the long evolution of the presupernova star. Gamma-ray line observations could also detect new supernovae and unknown supernova remnants in the galaxy, and confirm the thermonuclear theory of novae.

The detection of gamma-ray lines could reveal the existence of large fluxes of hitherto undetected low-energy cosmic rays and give unique information on the composition, size and distribution of interstellar dust grains. The combination of high energy-resolution with spatial resolution could give information of the rotation of interstellar dust on a galactic scale.

Nuclear reactions due to gravitationally accelerated ions around neutron stars and black holes could be strong sources of gamma-ray lines through neutron and positron production and the excitation of nuclear levels in abundant heavy nuclei (e.g. C, O and Fe). The observation of gravitational redshifts would yield exciting information on the physics of compact objects

as pointed out by Brecher (1978) at this Symposium. The best example to date of gravitational redshift from compact objects has been provided by the observation of Jacobson et al. (1978) of a 20 minute burst of gamma-ray line emission.

The observation of Leventhal et al. (1978a, b) of positron annihilation radiation from the galactic center implies the existence of very powerful high energy processes in our galaxy. A variety of other gamma-ray lines should accompany the 0.511 MeV line. The intensities of these lines are lower by one to two orders of magnitude than that of the observed line. Their detection, however, would not only unambiguously determine the origin of the positrons, but also provide new and unique information on the high energy processes (e.g. supernova explosion, energetic particle interactions) that take place in the central parts of our galaxy.

REFERENCES

Arnett, W. D. 1978, Gamma Ray Spectroscopy in Astrophysics, Symposium

Proceedings, eds. T. L. Cline and R. Ramaty, this Volume, p. 310.

Audouze, J., Lequeux, J., Reeves, H., Vigroux, L. 1976, Ap. J. (Letters),

208, L51.

Barkas, W. H. and Berger, M. J. 1964, Tables of Energy Losses and Ranges

of Heavy Charged Particles, NASA SP-3013 (Washington, D.C.).

Brecher, K. 1978, Gamma Ray Spectroscopy in Astrophysics, Symposium

Proceedings, eds. T. L. Cline and R. Ramaty, this Volume, p. 275.

Bussard, R. W. 1978, Gamma Ray Spectroscopy in Astrophysics, Symposium

Proceedings, eds. T. L. Cline and R. Ramaty, this Volume, p. 404.

Bussard, R. W., Ramaty, R. and Drachman, R. J. 1978, to be published.

Cameron, A. G. W. 1973, Space Science Review, 15, 121.

Chambon, G., Hurley, K., Niel, M., Talon, R., Vedrenne, G., Likine, O. B.,

Kouznetsov, A. V., and Estouline, I. V. 1978, Gamma Ray Spectroscopy

in Astrophysics, Symposium Proceedings, eds. T. L. Cline and R. Ramaty,

this Volume, p. 70.

Chupp, E. L. 1978, Gamma Ray Spectroscopy in Astrophysics, Symposium Proceedings,

eds. T. L. Cline and R. Ramaty, this Volume, p. 42.

Chupp, E. L., Forrest, D. J., Higbie, P. R., Suri, A. N., Tsai, C., and

Dunphy, P. P. 1973, Nature, 241, 333.

Clayton, D. D. 1973, Gamma Ray Astrophysics, (NASA SP 339), p. 263.

Clayton, D. D., Colgate, S. A. and Fishman, D. J. 1969, Ap. J. 155, 75.

Clayton, D. D. and Hoyle, F. 1974, Ap. J. (Letters) 187, L101.

Clayton, D. D. and Silk, J. 1969, Ap. J. (Letters) 158, L43.

Daugherty, J. K. 1978, Gamma Ray Spectroscopy in Astrophysics, Symposium

Proceedings, eds. T. L. Cline and R. Ramaty, this Volume, p. 394.

Daugherty, J. K. and Ventura, J. 1977, Astron. and Astrophys. 61, 723.

Dennis, B. R., Maurer, G. S., Cutler, E. P., Crannell, C. J., Dolan, J. F. and Frost, K. J. 1978, Gamma Ray Spectroscopy in Astrophysics, Symposium Proceedings, eds. T. L. Cline and R. Ramaty, NASA, this Volume, p. 371.

Durouchoux, Ph., Boclet, D. and Rocchia, R. 1978, Gamma Ray Spectroscopy in Astrophysics, Symposium Proceedings, eds. T. L. Cline and R. Ramaty, NASA, this Volume, p. 346.

Fichtel, C. E., Hartman, R. C., Kniffen, D. A., Thompson, D. J., Bignami, G. F., Ogelman, H., Ozel, M. E., and Tumer, T. 1975, Ap. J. 198, 163.

Graml, F., Penningsfeld, F. P. and Schonfelder, V. 1978, Gamma Ray Spectroscopy in Astrophysics, Symposium Proceedings, eds. T. L. Cline and R. Ramaty, this Volume, p. 207.

Hall, R. C., Meegan, C. A., Walraven, G. D., Djuth, F. T., Shelton, D. H. and Haymes, R. C. 1976, Ap. J. 210, 631.

Haymes, R. C., Walraven, G. D., Meegan, C. A., Hall, R. D., Djuth, F. T. and Shelton, D. H. 1975, Ap. J. 201, 593.

Higdon, J. C. and Lingenfelter, R. E. 1977, Ap. J. (Letters) 215, L53.

Jacobson, A. S. 1977, Invited paper presented at the APS Spring Meeting, April, Washington, D.C..

Jacobson, A. S., Ling, J. C., Mahoney, W. A. and Willett, J. B. 1978, Gamma Ray Spectroscopy in Astrophysics, Symposium Proceedings, eds. T. L. Cline and R. Ramaty, this Volume, p. 228.

Lee, T., Papanastassiou, G. J. and Wasserburg, G. J. 1977, Ap. J. (Letters) 211, L107.

Leventhal, M., MacCallum, C. J. and Stang, P. D. 1978a, Ap. J. (Letters), in press.

Leventhal, M., MacCallum, C. J. and Stang, P. D. 1978b, Gamma Ray Spectroscopy in Astrophysics, Symposium Proceedings, eds. T. L. Cline and R. Ramaty, this Volume, p. 169.

Leventhal, M., MacCallum, J. C. and Watts, A. C. 1977, Ap. J. 216, 491.

Lin, R. P. and Ramaty, R. 1978, Gamma Ray Spectroscopy in Astrophysics,

Symposium Proceedings, eds. T. L. Cline and R. Ramaty, this Volume, p. 76.

Lingenfelter, R. E., Higdon, J. and Ramaty, 1978, Gamma Ray Spectroscopy in

Astrophysics, Symposium Proceedings, eds. T. L. Cline and R. Ramaty, NASA,

this Volume, p. 252.

Lingenfelter, R. E. and Ramaty, R. 1976, The Structure and Content of the

Galaxy and Galactic Gamma Rays, NASA CP002, p. 237.

Lingenfelter, R. E. and Ramaty, R. 1977, Ap. J. (Letters) 211, L19.

Lingenfelter, R. E. and Ramaty, R. 1978, Physics Today 31, 40.

McKee, C. F. and Ostriker, J. P. 1977, AP. J. 218, 148.

Meszaros, P. 1978, Gamma Ray Spectroscopy in Astrophysics, Symposium

Proceedings, eds. T. L. Cline and R. Ramaty, this Volume, p. 425.

Metzger, A. E., Parker, R. H., Gilman, D., Peterson, L. E. and Trombka, J. I.

1974, Ap. J. 194, L19.

Northcliffe, L. C. and Schilling, R. F. 1970, Nuclear Data Tables, A7, 233.

Peimbert, M., Torres-Peimbert, S. and Rayo, J. F. 1978, Ap. J. 220, 516.

Ramaty, R., Borner, G. and Cohen, J. M. 1973, Ap. J. 181, 891.

Ramaty, R., Colgate, S. A., Dulk, G. A., Hoyng, P., Knight, J. W., Lin, R. P.,

Melrose, D. B., Paizis, C., Orrall, F., Shapiro, P. R., Smith, D. F.,

Van Hollebeke, M. 1978, Chapter 4 in the Proceedings of the Second Skylab

Workshop, P. A. Sturrock Editor, University of Colorado Press, in press.

Ramaty, R., Kozlovsky, B. and Lingenfelter, R. E. 1975, Space Sci. Rev. 18, 341.

Ramaty, R., Kozlovsky, B. and Lingenfelter, R. E. 1978, to be published.

Ramaty, R., Kozlovsky, B. and Suri, A. N. 1977, Ap. J. 214, 617.

Ramaty, R. and Lingenfelter, R. E. 1977, Ap. J. (Letters) 213, L5.

Starrfield, S., Truran, J. W., Sparks, W. M. and Kutter, G. S. 1972, Ap.
176, 169.

Sturrock, P. A. 1971, Ap. J. 164, 529.

Trumper, J. 1978, Gamma Ray Spectroscopy in Astrophysics, Symposium
Proceedings, eds. T. L. Cline and R. Ramaty, this Volume, p. 331.

Trumper, J., Pietsch, W., Reppin, C., Voges, W., Staubert, R. and
Kendziorra, E. 1978, Ap. J. (Letters) 219, L105.

Truran, J.W., Starrfield, S. G. and Sparks, W. M. 1978, Gamma Ray Spectroscopy
in Astrophysics, Sumposium Proceedings, eds. T. L. Cline and R. Ramaty,
this Volume, p. 315.

Wang, H. T. and Ramaty, R. 1974, Solar Physics 107, 1065.

Weaver, R. P. 1978, Gamma Ray Spectroscopy in Astrophysics, Symposium
Proceedings, Eds. T. L. Cline and R. Ramaty, NASA, to be published.

FIGURE CAPTIONS

1. Theoretical gamma-ray spectrum from inelastic collisions. The energetic particles are assumed to have a spectrum proportional to E^{-3}, and both the energetic particles and the ambient medium have solar composition. Interstellar grains are assumed to have mean radii of 5×10^{-5} cm, and half the C, N, O, Ne and S, and all the Mg, Si, and Fe is assumed in grains.

2. Gamma ray emissivity per unit energy density in the energetic particles. The emissivities are for the narrow 4.44 MeV line, the narrow plus very narrow 6.129 and 0.847 MeV lines, and the total broad, narrow and very narrow emissions. Both the energetic particles and ambient medium have solar compositions.

3. Emissivities of the narrow 4.44 MeV and narrow plus very narrow 6.129 MeV lines per unit energy deposition rate of the energetic particles in a neutral medium. Both the energetic particles and ambient medium have solar compositions.

4. Ratio of positron production to narrow-line 4.4 MeV photon production. Both the energetic particles and ambient medium are assumed to have solar composition.

5. The fraction of positrons forming positronium atoms before thermalizing, by charge exchange with atomic hydrogen as a function of the ionization fraction of the gas for two sets of parameters.

6. The rates (per unit target density) at which thermal positrons form positronium by charge exchange with neutral H (R_{ce}/n_H) or by radiative recombination with free electrons (R_{rr}/n_e), and annihilate directly with free electrons (R_{da}/n_e) or with bound electrons (R_{da}/n_H), as functions of the gas temperature.

7. The calculated profiles of the 0.511 MeV line in (a) molecular hydrogen

   in which 95% of the positrons from positronium in flight and 5% annihilate

   directly, and (b) following charge exchange of thermal positrons in

   a partially ionized gas.

TABLE I

GAMMA RAY PRODUCING DECAY CHAINS FROM SUPERNOVAE AND NOVAE

Decay Chain	Mean Life (yr)	Nuclei/ Supernova	Photon Energy (MeV)	Photons or positrons/ disintegration
$^{56}Ni \to {}^{56}Co \to {}^{56}Fe$	0.31	3×10^{54}	0.847	1
			1.238	0.70
			2.598	0.17
			1.771	0.16
			1.038	0.13
			e^+	0.2
$^{57}Co \to {}^{57}Fe$	1.1	7×10^{52}	0.122	0.88
			0.014	0.88
			0.136	0.12
$^{22}Na \to {}^{22}Ne$	3.8	3×10^{52} $(10^{48}/nova)$	1.275	1
			e^+	0.9
$^{44}Ti \to {}^{44}Sc \to {}^{44}Ca$	68.	6×10^{51}	1.156	1
			0.078	1
			0.068	1
			e^+	0.94
$^{60}Fe \to {}^{60}Co \to {}^{60}Ni$	4.3×10^{5}	5×10^{50}	1.332	1
			1.173	1
			0.059	1
$^{26}Al \to {}^{26}Mg$	1.1×10^{6}	4×10^{50}	1.809	1
			1.130	0.04
			e^+	0.85

Table 2

Line center energies for $j \rightarrow j-n$,

$B = 0.15\ B_q = 6.62 \times 10^{12}$ G,

QUANTUM NUMBER	HARMONIC NUMBERS		
J	$n = 1$	$n = 2$	$\dot{n} = 3$
1	71.64 keV		
2	63.72 keV	135.36 keV	
3	58.00 keV	121.72 keV	193.36 keV

TABLE 3

Approximate Local Interstellar Emissivities and Diffuse Galactic Fluxes from the Direction of the Galactic Center

Mechanism	Photon Energy (MeV)	FWHM keV	Local Emissivity (photons/H atom sec)	Flux Photons/ cm^2 sec rad
Inelastic	4.44	100	3×10^{-26}	6×10^{-5}
collisions	6.129(grain)	8	5×10^{-27}	1×10^{-5}
($w=1eV/cm^3$)	6.129 (gas)	150	1×10^{-26}	2×10^{-5}
	0.847 (total)	2	6×10^{-27}	1×10^{-5}
e^+ annihilation	0.511	5	2×10^{-25}	1×10^{-4}
$^{26}Al \rightarrow ^{26}Mg$	1.809	3	1×10^{-25}	7×10^{-5}
$^{60}Fe \rightarrow ^{60}Co \rightarrow ^{60}Ni$	1.332	2	1×10^{-25}	7×10^{-5}
	1.173	2	1×10^{-25}	7×10^{-5}
	0.059	0.1	1×10^{-25}	7×10^{-5}
$^{22}Na \rightarrow ^{22}Ne$	1.275	10	2×10^{-25}	1×10^{-4}
π^o decay + bremsstrahlung	>100	--	1.5×10^{-25}	1×10^{-4}

Fig. 1

35

Fig. 2

Fig. 3

37

SOLAR ABUNDANCES

$q_+/q_{4.44}$

E_C (MeV / NUCLEON)

Fig. 4

Fig. 5

Fig. 6

40

RATES/TARGET DENSITY ($CM^3 SEC^{-1}$) vs T (K)

R_{ce} / n_H

$R_{ce} / n_H \times 10^{-2}$

R_{rr} / n_e

R_{da} / n_e

R_{da} / n_H
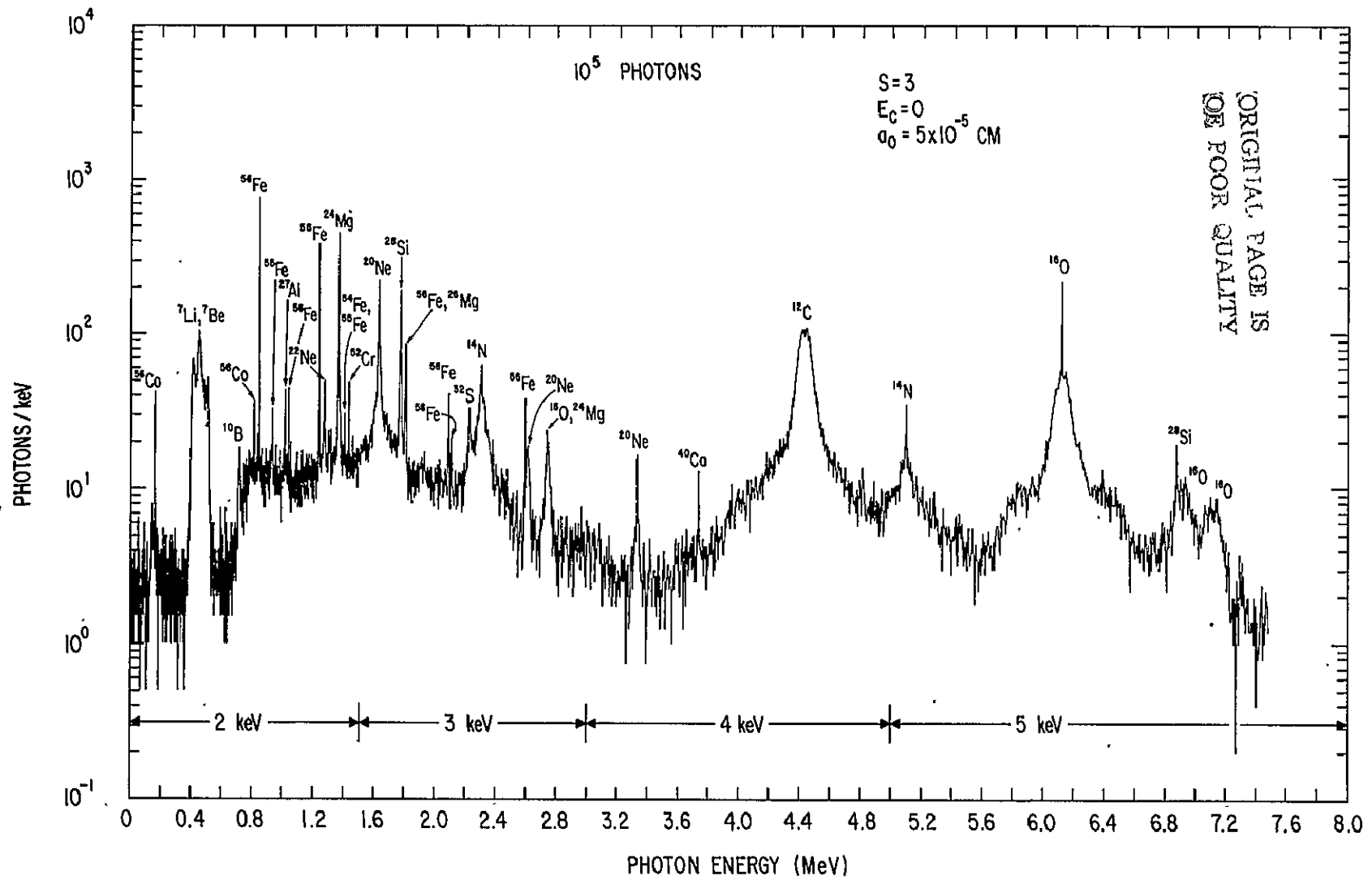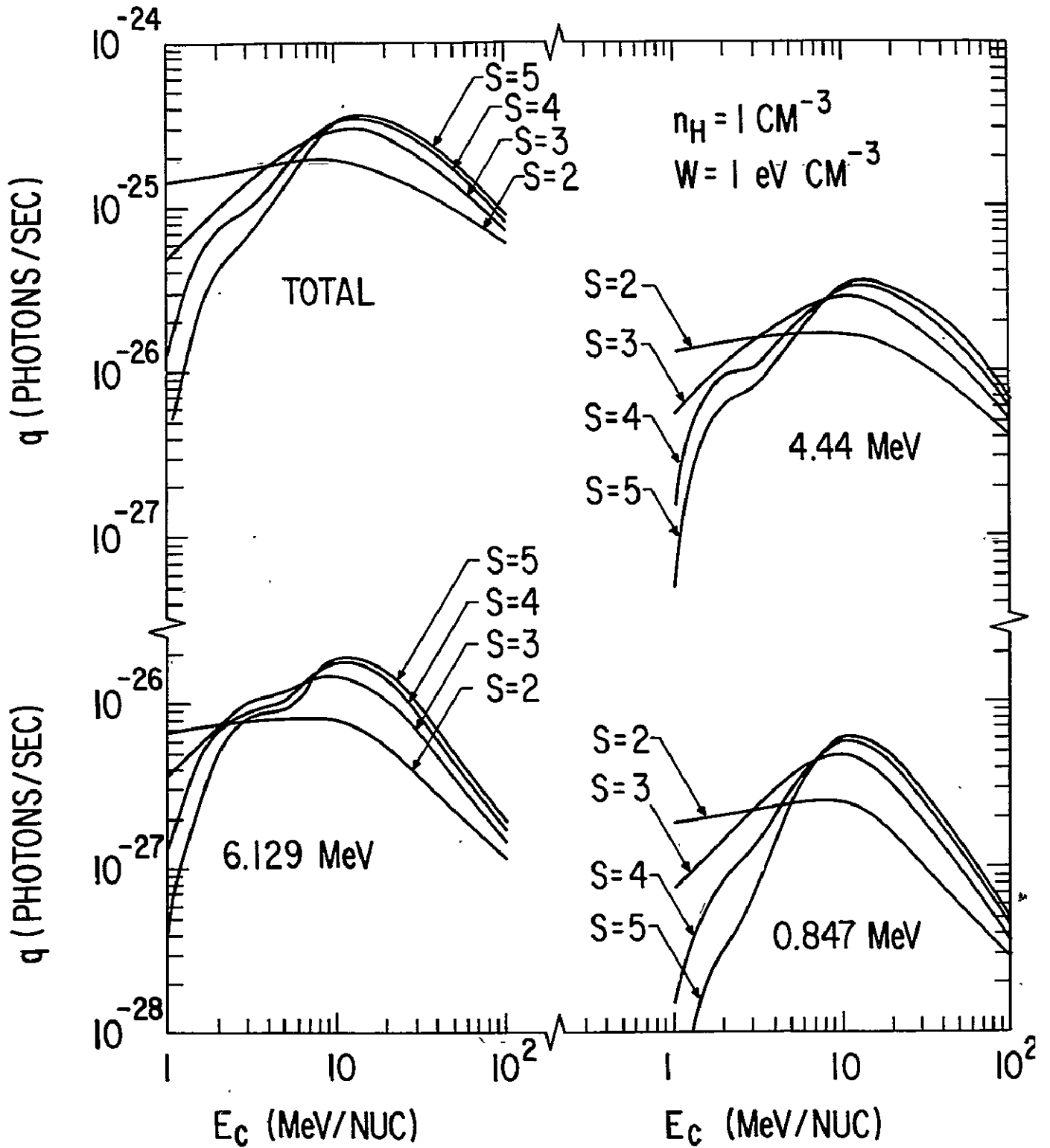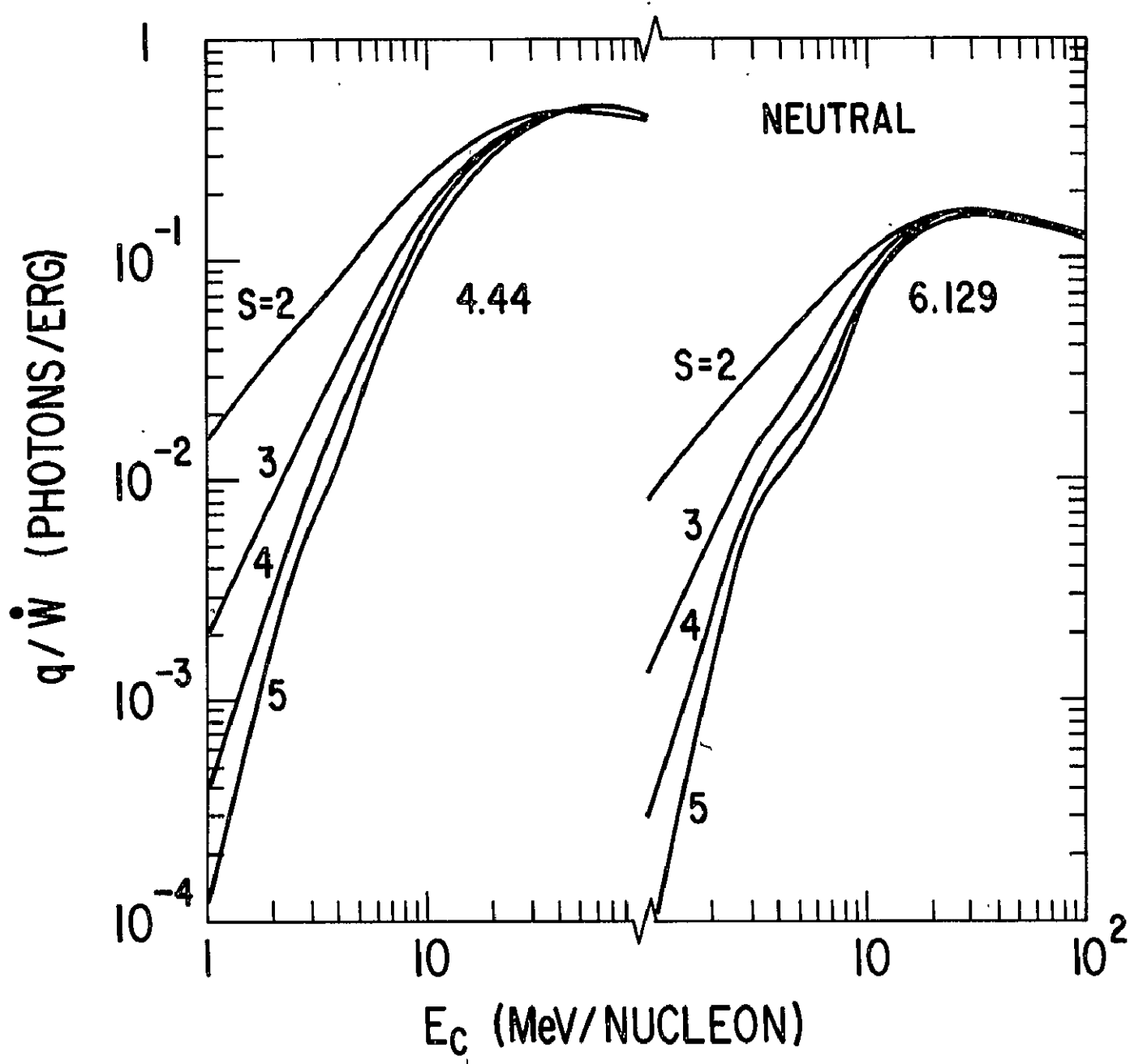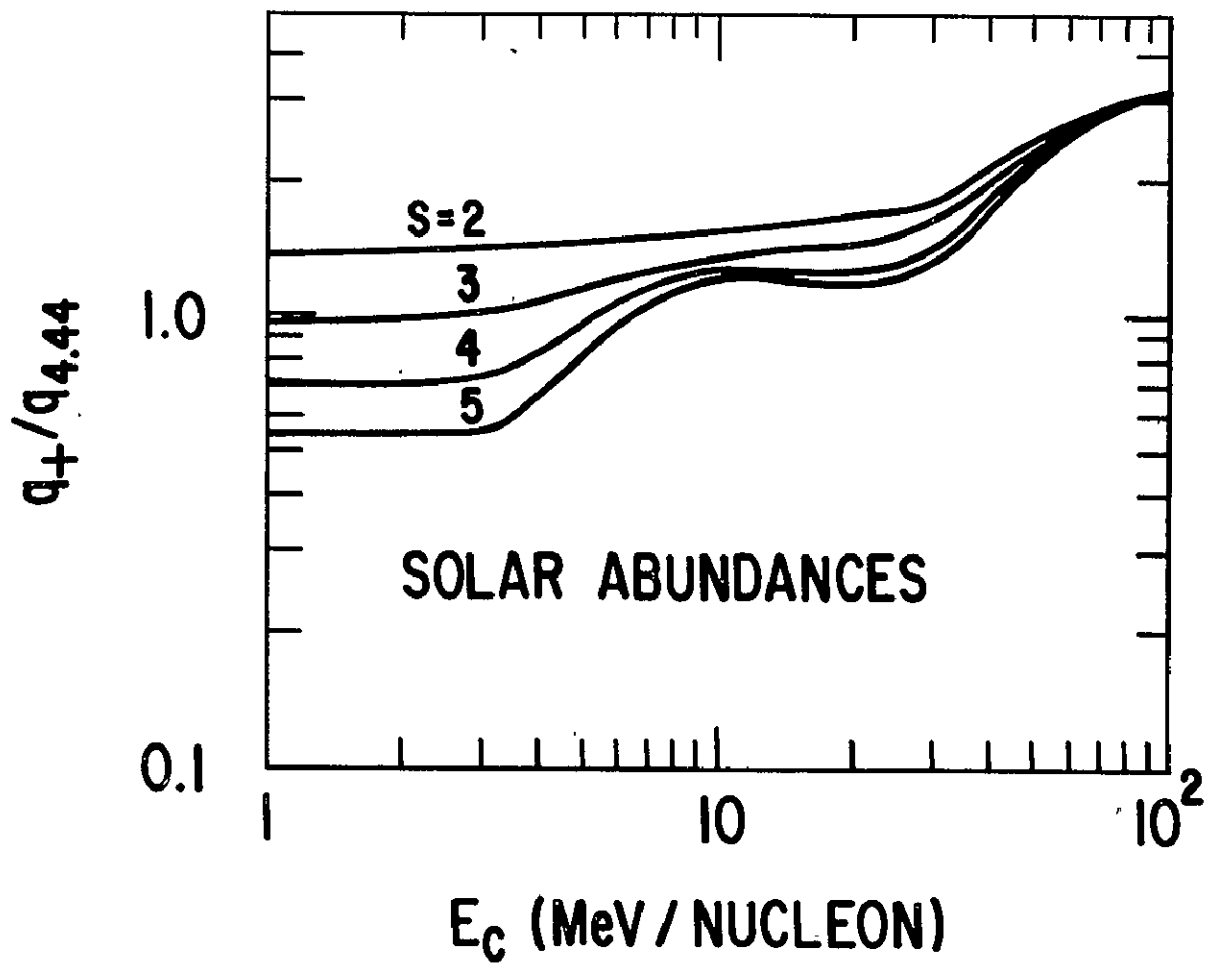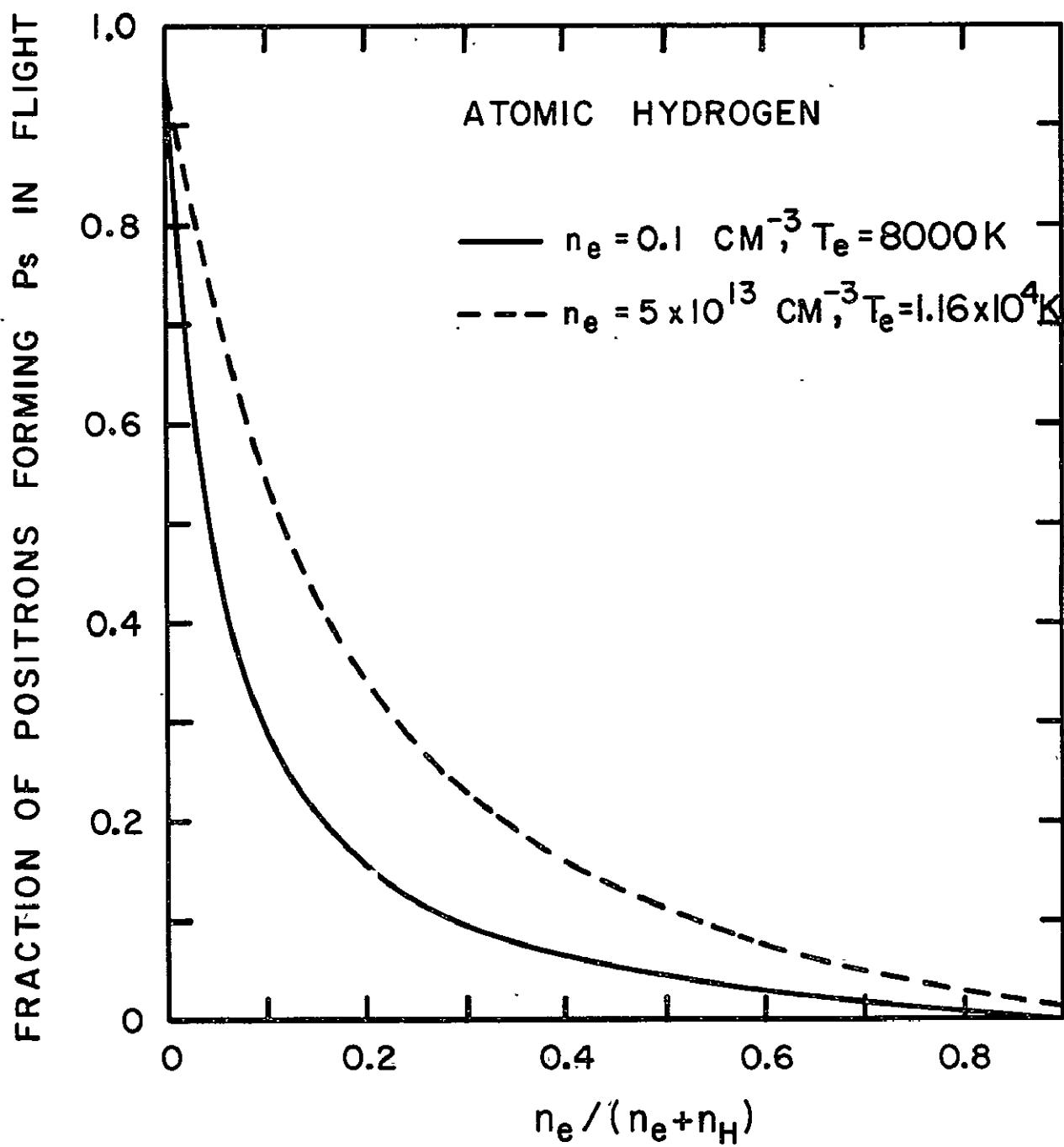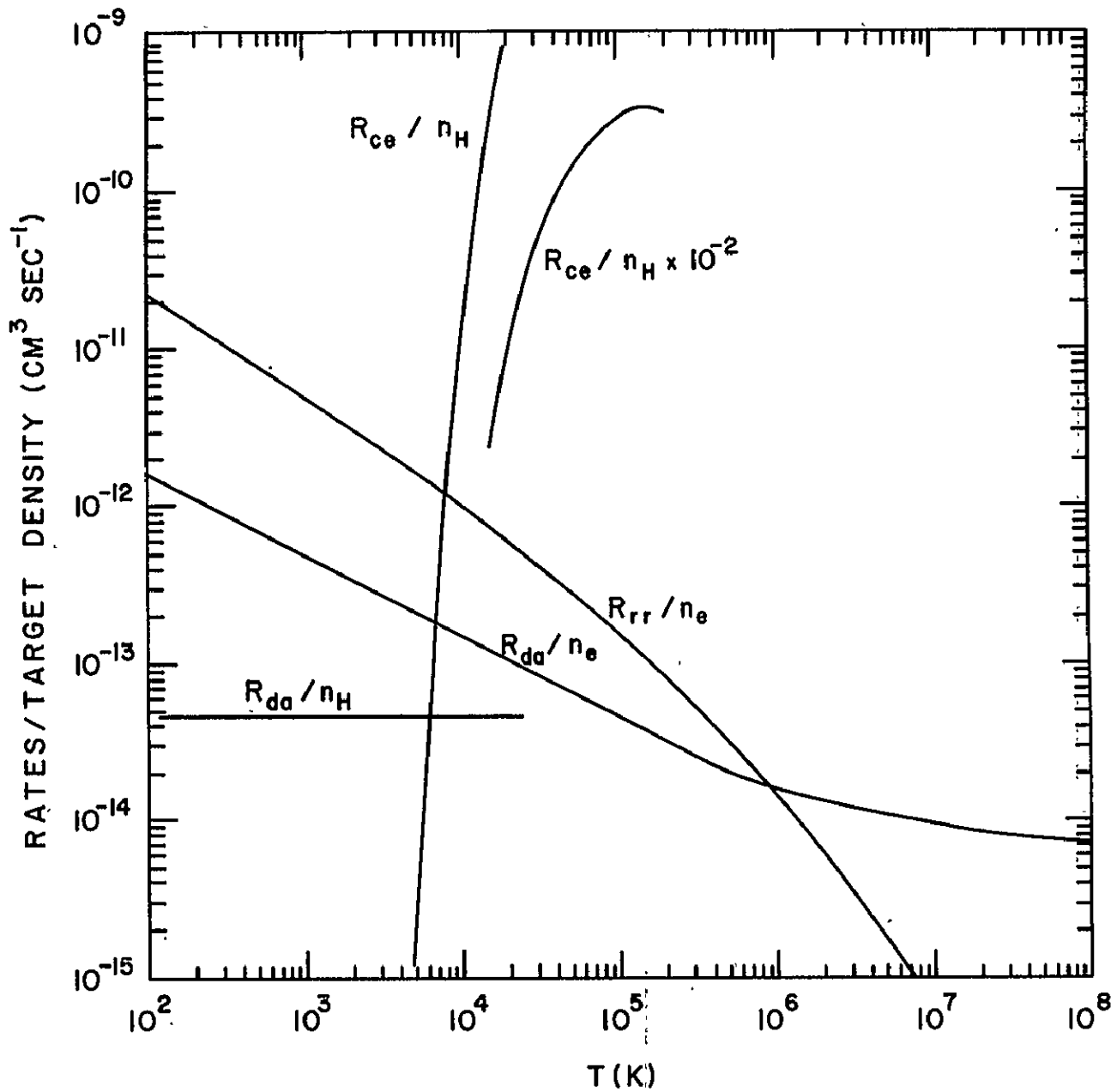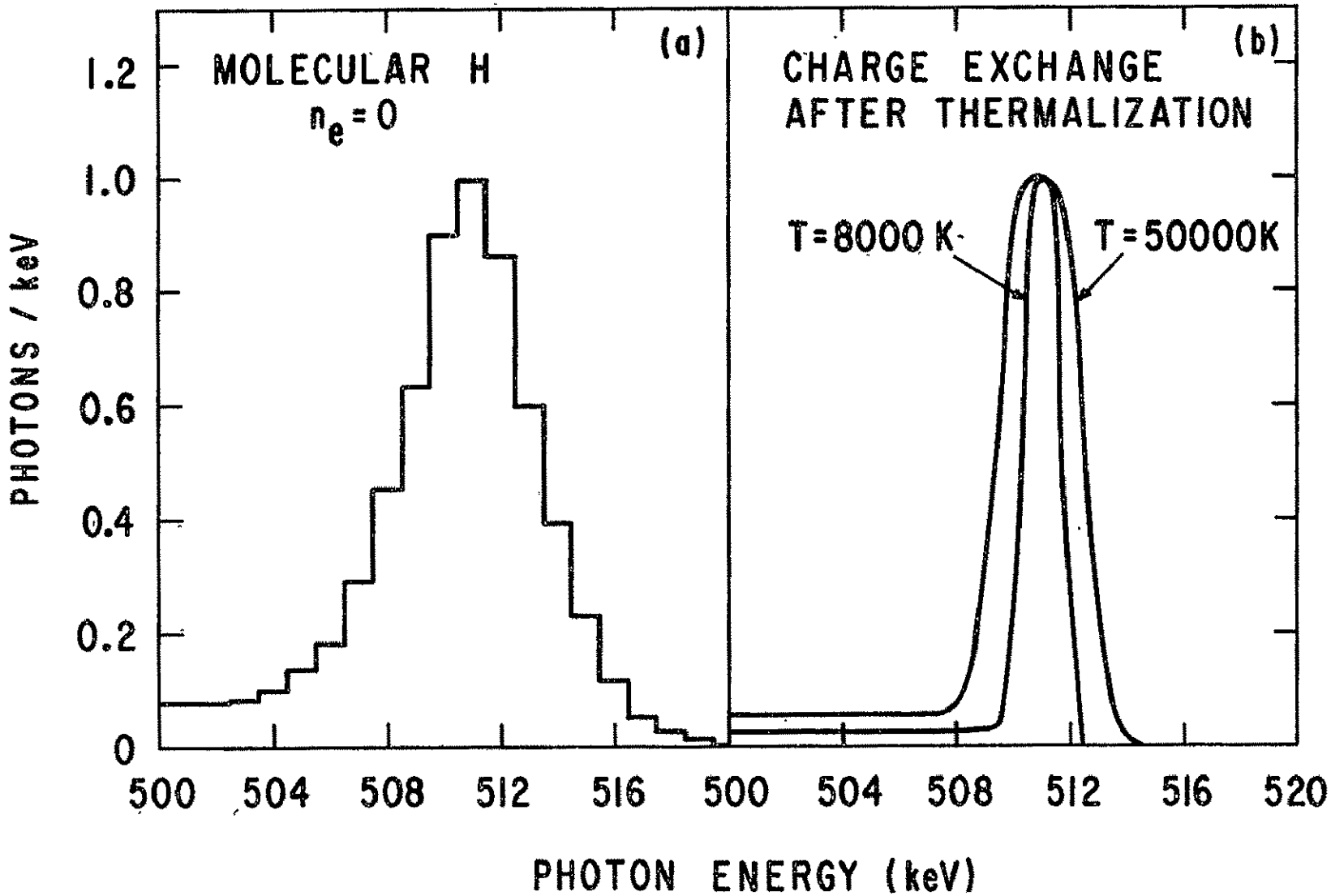
Fig. 7

Gamma Ray Spectroscopy in Astrophysics

An Observational Overview*
(50 keV-20 MeV)

E. L. Chupp
Department of Physics
University of New Hampshire
Durham, New Hamsphire   03824

ABSTRACT

An overview of the observational status of gamma ray astronomy based on results reported prior to April 1978 is presented. Specific line observations are reviewed from the Sun, the galactic plane, the Galactic Center region, the active Galaxy NGC 5128 (Cen A), the Crab Nebula region, and a transient source in the general direction of the anti-Galactic Center region. A statistical method is described which determines the relative probability that a given, reported observation is due to an external source as compared to a random fluctuation in the experimental background counting rate. We conclude that only a few of the many reported observations can be considered likely extraterrestrial observations of an extraterrestrial source made with a confidence level of 99%.

1.0 INTRODUCTION

Gamma ray spectroscopy, as a potential probe for the study of astrophysical phenomena, was first discussed by Morrison in 1958; however, only now, some 20 years later, have experimental results in this field begun to bear out early expectations. The reason, which is well known, is that experimental efforts have been plagued with high background and low fluxes and that instruments with suitable telescopic properties in the energy range of interest have not been available. Yet gamma ray spectroscopy today is a strong, viable field of research because of recently acquired observational evidence and because of the convictions of researchers in the field that gamma ray line astronomy will become a very effective tool in probing the Universe due to the unique signature of gamma ray spectral lines, the penetrability of gamma rays, and their origin in high energy astrophysical processes.

In this report we will first present an overview of observational evidence
for gamma rays of discrete energy in the range from ∿ 50 keV to 20 MeV reported
prior to 28 April 1978. Therefore, we will not include yesterday's report
by McCallum at the Washington, D.C. Meeting of the American Physical Society
where evidence was presented for the existence of a sharp Galactic Center
region gamma ray line at 0.511 MeV, and further evidence for a Galactic Center
line at 4.4 MeV from HEAO-1 observations was reported by Matteson. Papers
on both of these experiments will be given at this conference and are found
in these proceedings (cf. Leventhal et al., 1978; Matteson, 1978).

Following our review of the observations, the likelihood method we have adopted
for evaluating experimental results will be described. We will conclude with
a discussion of the results of applying this method to the reported observations
of gamma ray lines.

2.0 REPORTED OBSERVATIONS OF GAMMA RAY LINES

In general, gamma ray spectroscopy experiments can be carried out by using
various techniques, depending on the energy range of interest. Table 1
summarizes the instrumentation techniques by energy range that are used in
gamma ray spectroscopy observations. Also shown are the platforms that
have been used, or that will be used, in the near future (cf. Lingenfelter and
Ramaty, 1978). The gamma ray spectroscopy measurements we will discuss today
have all been carried out using actively shielded scintillation or solid state
spectrometers.

One of the most likely expected sources of gamma ray lines is the Sun,
especially during periods of high solar activity when energetic particles
(solar cosmic rays) are known to be produced. For early predictions of solar
gamma ray line fluxes, see Lingenfelter and Ramaty (1967). However, not
until 1972 was it possible (due to a combination of a suitable instrument
in satellite orbit, and a period of dramatic solar activity) to obtain the
first spectrum of solar gamma rays. In Figure 1 we show the results obtained
with a small (3" x 3") actively shielded NaI(Tℓ) scintillation spectrometer
onboard the OSO-7 satellite during the rising phase of the large solar flare
which erupted at ∿0621 UT on 4 August 1972 (Chupp et al., 1973, 1975). The

Table 1. Gamma ray experiments - conducted,
in progress, or development.

DETECTORS	ENERGY RANGE	PLATFORM
ACTIVELY SHIELDED INORGANIC SCINTILLATION SPECTROMETERS	0.1 → 10 MEV	BALLOONS AND SATELLITES (OSO-7, OSO-8, HEAO-A, SIGNE, SMM, ARIEL V, ERS, APOLLO)
ACTIVELY SHIELDED COOLED SOLID STATE SPECTROMETERS	0.1 → 10 MEV	BALLOONS AND SATELLITES (OTZB, HEAO-C, ISEE-C, S78-1)
COMPTON TELESCOPES	0.5 → 20 MEV	BALLOONS
SPARK CHAMBERS (LOW MASS) AND PROPORTIONAL CHAMBERS	5 → 50 MEV	BALLOONS
SPARK CHAMBERS	>50 MEV	BALLOONS AND SATELLITES (EX 11, OSO-3, SAS-II, CCS 3)
CERENKOV LIGHT TELESCOPE AIR SHOWER ARRAY	>50 MEV	TERRA FIRMA

satellite was spin stabilized (30 rpm) so that the spectrometer could alternately
view a quadrant in the direction of the Sun and in a direction away from the
satellite-Sun direction. Therefore, spectra could be obtained in these two
directions, stored in separate buffers, and read out every three minutes. The
dotted curve in Figure 1 shows the background spectra (anti-solar direction)
obtained during three full spectrum accumulations ($\sim$ 9 minutes) covering the
impulsive rise of the flare as observed in X-ray, optical, and radio frequency
emissions. The solid curve, the solar quadrant, shows strong spectral features
at 0.51 and 2.22 MeV and weaker features at 4.4 and 6.1 MeV with the following
average respective flux values: $(6.3 \pm 2.0) \times 10^{-2}$, $(2.8 \pm 0.22) \times 10^{-1}$,
$(3.0 \pm 1.0) \times 10^{-2}$, $(3.0 \pm 1.0) \times 10^{-2}$ photons $cm^{-2}sec^{-1}$. Leakage calibration
lines from ^{60}Co at 1.17 MeV and 1.33 MeV appear in both the solar and background
quadrant spectra. (See Forrest et al., 1972 and Higbie et al., 1972 for

Figure 1. The gamma ray spectrum observed during the
impulsive phase of the large solar flare on
4 August 1972. (From Chupp et al., 1975.)
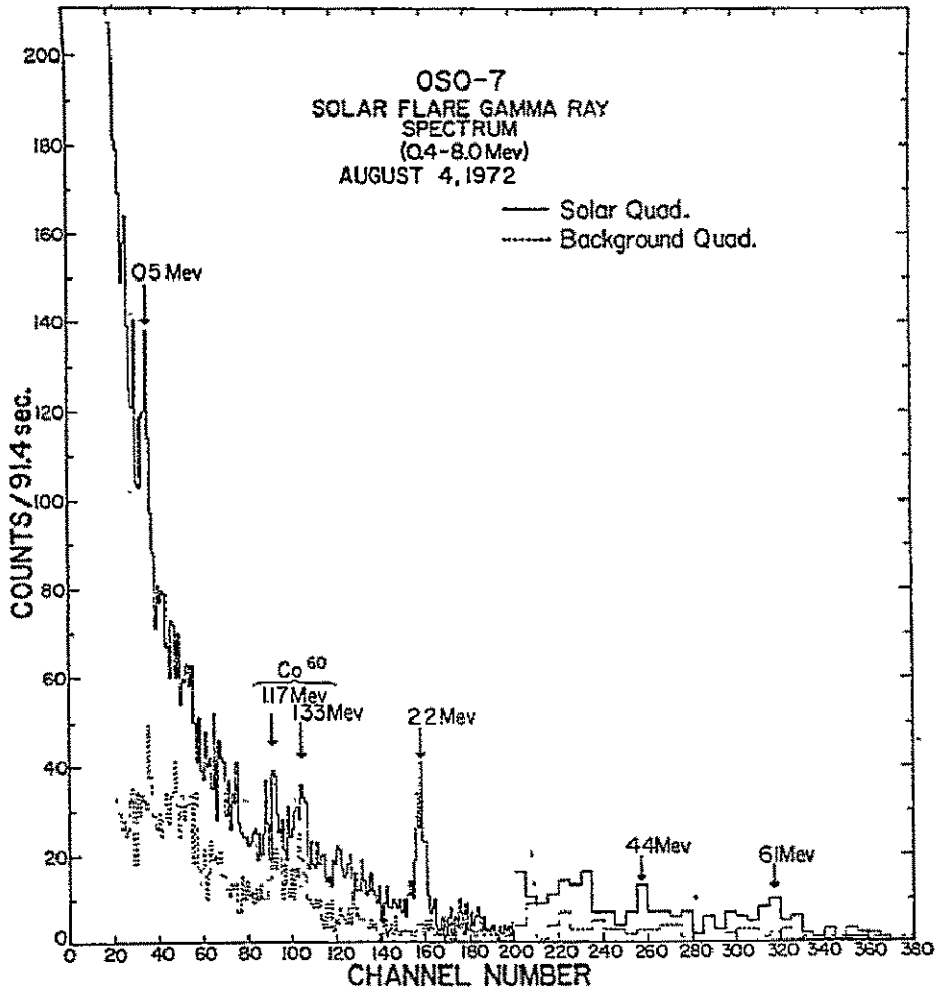
details of the instrument.) The 0.51 MeV line has as its origin the annihila-
tion of solar cosmic ray produced positrons with ambient electrons in the
solar atmosphere; the line at 2.22 MeV is a result of capture of flare produced
neutrons with photospheric hydrogen. Finally, the weaker features at 4.4 and
6.1 MeV are expected to be the result of inelastic scattering of energetic
protons and alpha particles on ambient carbon (^{12}C) and oxygen (^{16}O) nuclei.
The relative intensities of the observed lines are in agreement
with that expected from the Sun during sufficiently intense solar flares.
Gamma ray lines at 0.51 and 2.2 MeV were also seen by the same OSO-7 instru-
ment during the decaying phase of another large solar flare which erupted on

7 August 1972; however, in this case the satellite was on the dark side of Earth during the initial phase of the flare. A general discussion of the interpretation of these solar flare gamma ray observations may be found in Ramaty and Lingenfelter (1975), Ramaty et al. (1975), and Ramaty et al. (1977).

Probably the first report of an observation of a cosmic gamma ray line was by Johnson et al. (1972) of Rice University, who reported on a spectral feature observed from the direction of the Galactic Center. In November 1970 an actively collimated scintillation spectrometer was used to scan the Galactic Center region including the bright X-ray source GX5-1 for gamma rays in the energy range 23 to 930 keV. The balloon experiment, carried out from Paraná, Argentina (P_c = 11.5 GV), utilized a large NaI(Tℓ) crystal (4" diameter x 2" thickness) in a thick NaI(Tℓ) anticoincidence shield collimator, which formed a crude telescope with a 12° half angle. By use of an orientable gondola, alternate source (GX5-1) and background spectra were taken for a time period of ∿ 7 hours on 25 November 1970. Source and background observations were taken in alternate 10 minute segments by shifting the azimuth of the telescope by 180° so, in effect, the source would rise in the east and set in the west while the background moved in the opposite sense. The net Galactic Center source spectrum was found for a single source observation interval by sub-tracting the average counting rate/channel during the two adjacent 10 minute background measurements, giving the counting rate spectrum from the source, assuming the background is independent of azimuth. With this procedure applied to all source and background segments, evidence was obtained for a Gaussian shaped line centered at 473 $\pm$ 30 keV with a flux (1.8 $\pm$ 0.5) x 10^{-3} photons $cm^{-2}sec^{-1}$. The existence of this spectral feature was reportedly confirmed by an additional balloon flight experiment on 20 November 1971 using the same apparatus. In this case a similar method of data analysis gave a Galactic Center spectral feature at 485 $\pm$ 35 keV. The weighted average energy and flux for this Galactic Center feature reported by Johnson and Haymes (1973) is 476 $\pm$ 24 keV and (1.8 $\pm$ 0.5) x 10^{-3} photons $cm^{-2}sec^{-1}$ respectively.

This evidence for a Galactic Center gamma ray line under 500 keV was drastically altered by new observations reported by the same group from a balloon launched at Rio Cuarto, Argentina on 2 April 1974 (Haymes et al., 1975). The gamma ray

instrument used for the new observations was very similar to that used previously and had only marginally better efficiency and energy resolution, but a significantly smaller angular resolution, 15° (FWHM) as compared to 24° (FWHM). The method of taking Galactic Center and background spectra was effectively the same as used in the previous flights. The difference spectrum obtained from a 219 minute observation of the Galactic Center now gave evidence for a gamma ray line centered at 530 ± 11 keV with a flux of $(8.0 \pm 3.2) \times 10^{-4}$ photons $cm^{-2}sec^{-1}$. Figure 2 is this latest result on the galactic gamma ray spectrum below 1.0 MeV.

Figure 2. Measured differential energy spectrum of the Galactic Center region for energies below 1.0 MeV. The solid curve is the best-fit power law. The spectral line at 0.5 MeV is at the 3.5σ confidence level. (From Haymes et al., 1975.)
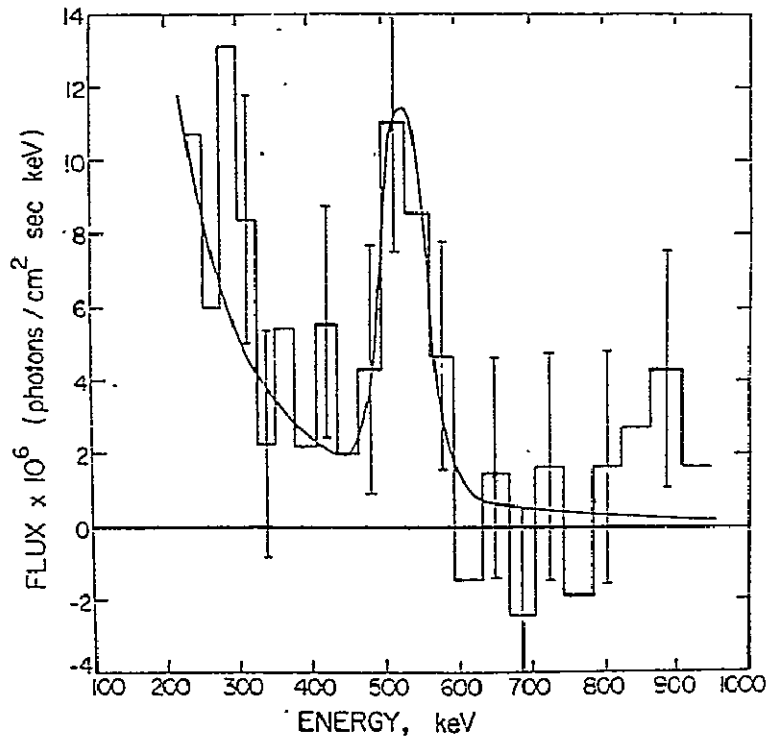
These two sets of results are at variance with one another and Haymes et al.
(1975) offer three possible hypotheses to explain them:

- Since the solid angle in the latest experiment was 0.4 of that used previously, the lower flux may be evidence that the Galactic Center source is larger than the 15° beam width,

- The apparent time variation of the flux values and the line energy may be a result of nova activity in the Galactic Center region as discussed by Clayton and Hoyle (1974), or

- The average energy of the 0.5 MeV line may depend on the galactic coordinates being observed and since there was a slight difference in the viewing directions for the two observations there may be evidence for such a correlation.

Also, the 1974 Rice experiment gave evidence for an additional significant Galactic Center line feature located at 4.6 + 0.1 MeV with a flux of $(9.5 \pm 2.7) \times 10^{-4}$ photons $cm^{-2}sec^{-1}$. This result is shown in Figure 3 as

Figure 3. Measured differential energy spectrum of the Galactic Center region for energies greater than 1.0 MeV. The line between 4 and 5 MeV is at the 3.5σ confidence level, the sum of the overlapping spectral lines between 1.2 and 2.0 MeV is at the 4.1σ level. (From Haymes et al., 1975.)
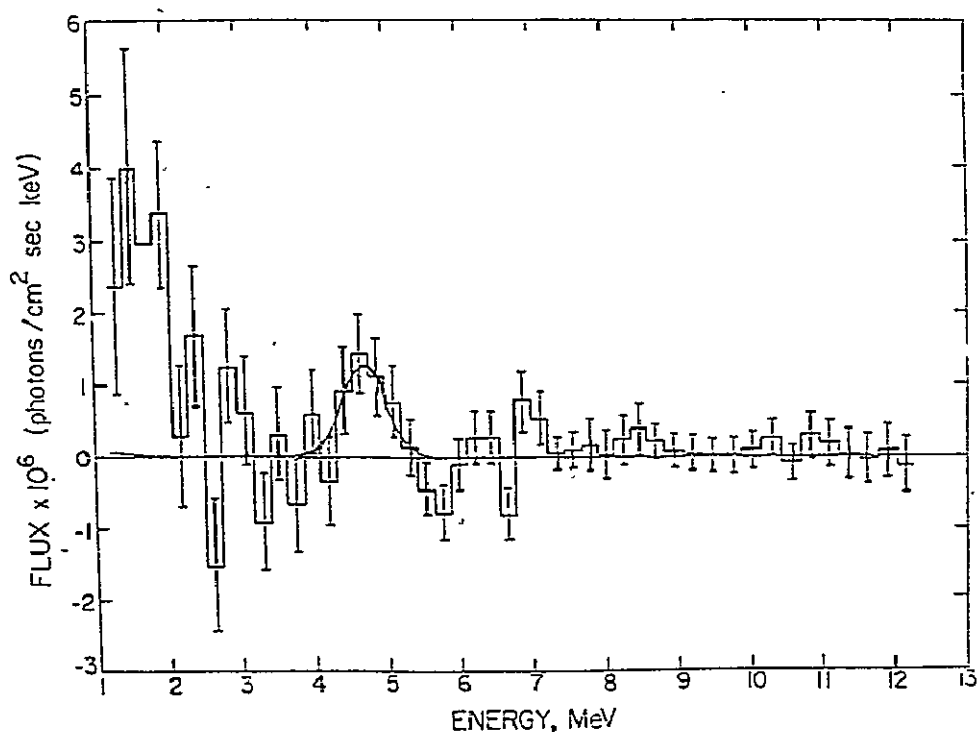
a difference spectrum for energies above 1 MeV. The line in question, which
appears to be broadened, is attributed to emission from the first excited
state of ^{12}C at 4.43 MeV. There is also an indication of gamma ray emission
(not necessarily a single line) over the energy region from 1.2 to 2.0 MeV.
[See the paper in . these proceedings by Leventhal et al. (1978)
    for recent results on Galactic Center gamma ray emission.]

A further report of a gamma ray line, possibly from explosive supernova nucleo-
synthesis, was given recently by the Rice University group (Walraven and Haymes,
1976). By studying data from the background scans of the celestial sphere taken
by Haymes et al. (1975), these authors found that one particular background
segment had anomalously high counts in a certain spectral region. The "back-
ground, segment" in question was near the galactic plane but centered $\sim$ 15°
away from the Galactic Center. By using another background scan measured
$\sim$ 30 minutes earlier at a higher galactic latitude and subtracting it from the
anomalous scan a hypothetical source energy spectrum was obtained as shown in
Figure 4. Two features of this spectrum have been pointed out; first the
continuum spectrum, fit by a power law shown by the solid line, which has a

Figure 4. A spectrum of gamma rays obtained from a
possible source in the galactic plane. A
possible spectral line exists $\sim$ 1.16 MeV.
(From Walraven and Haymes, 1976.)
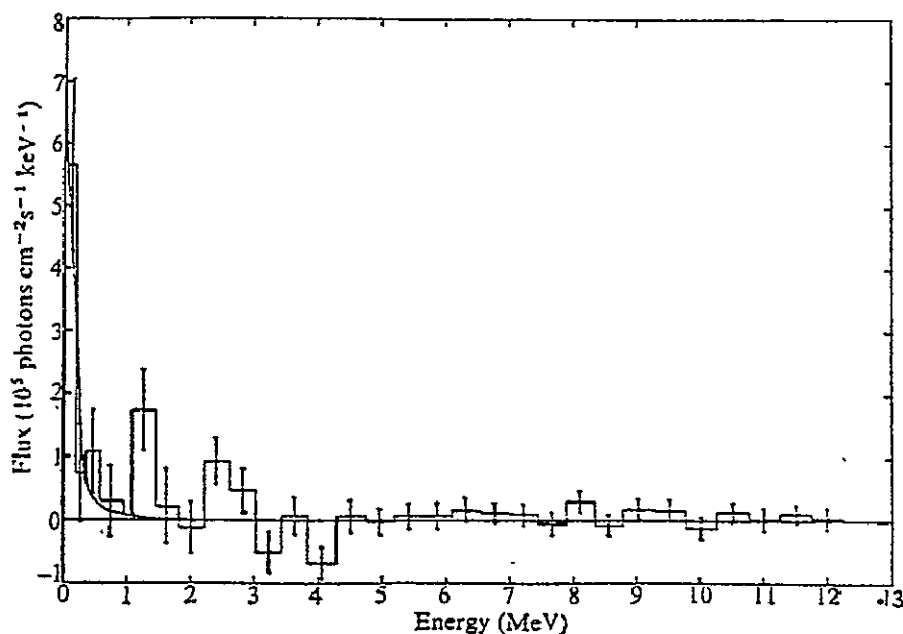
harder spectral shape than measured at lower energies for the Galactic Center
and second, the spectral feature centered at $\sim$ 1.16 MeV. Hypothesizing the
presence of a Gaussian line superposed on the power law spectrum in Figure 4
gave a line flux of $(3.4 \pm 1.5) \times 10^{-3}$ photons $cm^{-2}sec^{-1}$ at an energy of
(1.15 ± 0.07) MeV; that is, the spectral feature is $\sim$ 2σ above the continuum.
Even though this spectral feature is marginally significant, it was considered
to be tantalizing since some calculations of explosive nucleosynthesis predict a
line at 1.156 MeV. In particular, Clayton et al. (1969) predict that
$^{44}Ti(T_{1/2} \sim 48$ yrs) is produced in sufficient quantity in a supernovae event
that its decay to $^{44}Sc(T_{1/2} \sim 3.9$ hrs) and subsequently to ^{44}Ca will give a
strong line at 1.156 MeV from an excited state of ^{44}Ca. This would
be the case for events occurring within the past 100 years or so within
our galaxy; thus for this reason and the fact that the background segment in
question was located near the galactic disk, the presence of the reported
line feature is believed by the Walraven and Haymes (1976) to be more than
coincidence even though the statistical significance is low.

Mention should also be made of gamma ray observations of the galactic
plane using a high resolution spectrometer on board a spinning polar
orbiting satellite in 1972. Imhof and Nakano (1977) used a 50 cm^3 Ge(Li)
detector having a FWHM energy resolution of $\sim$ 3.5 keV in a passively collimated
shield forming a crude telescope with broad angular acceptance of $\sim$ 90°
degrees. For a time period from 3-12 October 1972 the satellite scanned across
the galactic plane, but some distance away from the Galactic Center. By choosing
other portions of the sky for background determination, difference energy
spectra were obtained, which could be studied for evidence of line emission
over an energy range 38 keV-2700 keV. This method gave net galactic plane
spectra for cases where the satellite was near the Earth's magnetic equator
at local noon or at local midnight. The two portions of the galactic plane
that were scanned were separated by $\sim$ 170° and covered a galactic longtitude
range of $\sim$ 100°-170° and 260°-330°. The difference spectra obtained from local
noon passes is shown in Figure 5. In short, there was no strong evidence for
any gamma ray line emission from either galactic plane scan. A special study
was made of the spectral region around 0.5 MeV to see if evidence existed for
the lines reported by Rice University discussed above.   Unfortunately, the

Figure 5. Energy spectra measured during local noontime passes near the geomagnetic equator in the period 3-12 October 1972. The original 4096 channels in the spectrometer data have been combined by fours and are presented for 827 keV-2700 keV. The spectrum in the bottom section is a sum over all zenith angles within a spin. In the middle and top sections are presented the difference spectra over the central zenith angle sweep intervals indicated. (From Imhof and Nakano, 1977.)
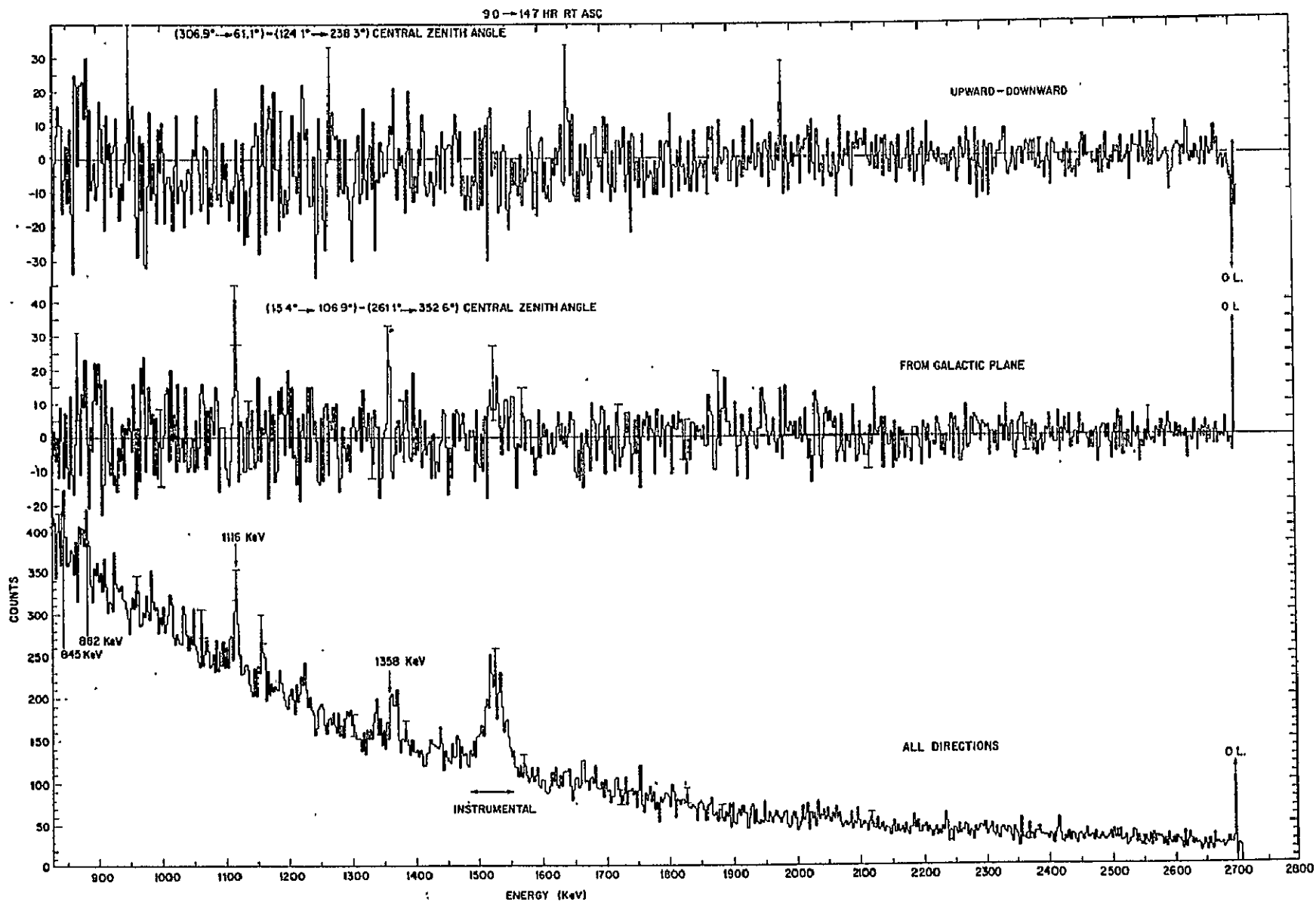
flux sensitivity achievable by Imhof and Nakano (1977) was just about at the level of the strongest fluxes reported by Johnson and Haymes (1973) and Haymes et al. (1975), that is $\sim 2 \times 10^{-3}$ photons $cm^{-2}sec^{-1}$. It should be remembered nevertheless that the Galactic Center region was not covered in these observations. The difference spectra shown in Figure 5 do show weak peaks at 1116 and 1358 keV, which are suggested as possibly from levels of ^{46}Ti and ^{24}Mg (cf. Lingenfelter and Ramaty, 1976); however, the lines are statistically marginal $\sim 3.1\sigma$ and 2.9σ, respectively.

Besides the strong possibility that our own galaxy may emit observable gamma ray lines, there is a reasonable chance that the powerful radio galaxies may be intrinsically stronger sources of gamma ray lines than presumably ordinary galaxies. This possibility has also been investigated by the Rice University group, who searched for gamma ray emission from the radio source Cen A associated with the optical galaxy NGC 5128. Hall et al. (1976) observed this source during the same balloon flight that made the Galactic Center observation (Haymes et al., 1975). The same instrument, a NaI(Tℓ) spectrometer, was used for both observations. For further details on the instrument, see Walraven et al. (1975). Source plus background and background spectra were taken in a manner identical to that used for the Galactic Center observations. By this method Hall et al. (1976) recorded from Cen A a flux of hard X-rays and gamma ray lines that was not present during a 1968 observation of the same source. In addition to a continuum flux observed in the X-ray region, the existence of two gamma ray lines was reported as illustrated in Figure 6. The first line is a broad feature centered at about 1.6 MeV and extending from 1.27 MeV to 1.95 MeV, a range much larger than the instrument FWHM resolution of 0.12 MeV at this energy. The line flux for this broad feature is $(3.4 \pm 1.0) \times 10^{-3}$ photons $cm^{-2}sec^{-1}$. The second line feature extends from 4.42 to 4.65 MeV with a line flux of $(9.9 \pm 3.0) \times 10^{-4}$ photons $cm^{-2}sec^{-1}$. This latter line is suggested to be a result of excitation of ambient ^{12}C to its first excited state by low energy cosmic rays and the broad feature at 1.16 MeV is suggested to be a blend of nuclear lines from excited states in $^{24}Mg^*$(1.37 MeV), $^{20}Ne^*$(1.63 MeV), and $^{28}Si^*$(1.78 MeV). If these spectral features are indeed from Cen A, then the luminosity of this radio galaxy in gamma ray lines is $\sim 4.8 \times 10^{43}$ ergs sec^{-1}. The continuum spectrum observed has about the same luminosity, so the total gamma ray luminosity is

Figure 6. The Centaurus A spectrum at energies above
0.686 MeV. The curve is the sum of the
best-fit power law and two spectral lines
as indicated by Gaussian shape. (From
Hall et al., 1976.)
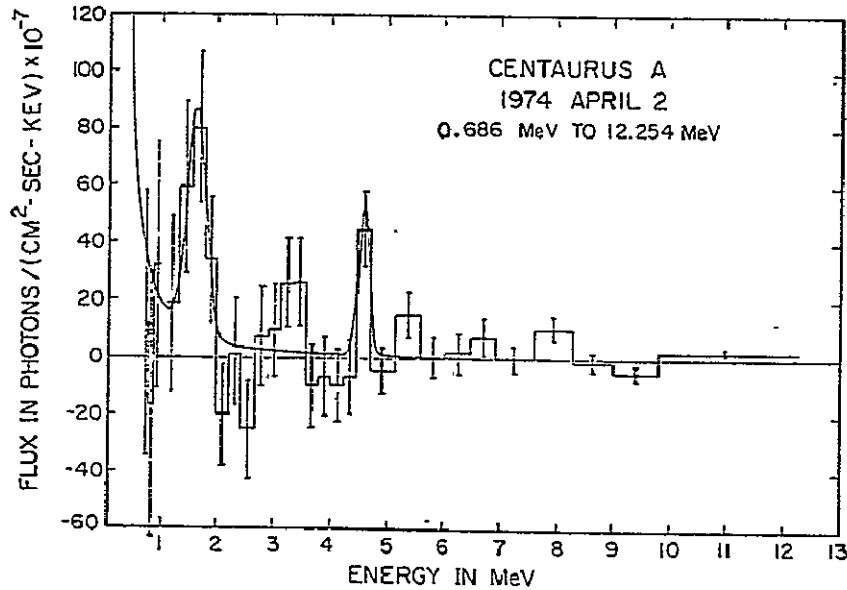
~ 10^{44} ergs sec^{-1} which is ~ 10 times greater than the radio luminosity of
Cen A! If confirmed, this observation is of considerable importance for
understanding the behavior of dramatic objects such as Cen A.

Recently there have been reports of positive fluxes of gamma ray lines from
the Crab Nebula region by two different groups using high resolution spectro-
meters. The first was a reported line at (400 ± 1) keV by Leventhal et al.
(1977) observed during a balloon flight on 10-11 May 1976. Their measurement
was made with a 93 cm^3 cooled Ge(Li) spectrometer. Crab target and background
spectra were taken in a manner very similar to that adopted by the Rice
University group as discussed above. By taking difference spectra,
Leventhal et al. (1977), found a possible line feature at ~ 400 keV with a
reported intensity of (2.24 ± 0.65) x 10^{-3} photons $cm^{-2}sec^{-1}$ and a width
$\lesssim$ 3 keV (see Figure 7). This line feature corresponds to a 4σ deviation above
a continuum background. These authors have suggested that this line may be a
result of gravitationally red-shifted 0.511 MeV annihilation radiation
emanating from the surface of the neutron star. Verification of the existence

Figure 7. The Crab target energy spectrum in the vicinity of 400 keV and the Crab background energy spectrum from the JPL observation. The lower data is adopted from Leventhal et al., (1977). (From Ling et al., 1977.)

ENERGY LOSS SPECTRA

10 JUNE 1974 BALLOON FLIGHT

PALESTINE, TEXAS

$+$ CRAB + BACKGROUND — 104 min

$\lozenge$ BACKGROUND — 128 min

COUNTS/sec keV

10^{-2}

5×10^{1}

CRAB TARGET

10^{1}

5×10^{1}

LEVENTHAL et al.(1976)

CRAB BACKGROUND

COUNTS/keV

10^{1}

388   392   396   400   404   408   412   414

ENERGY (keV)
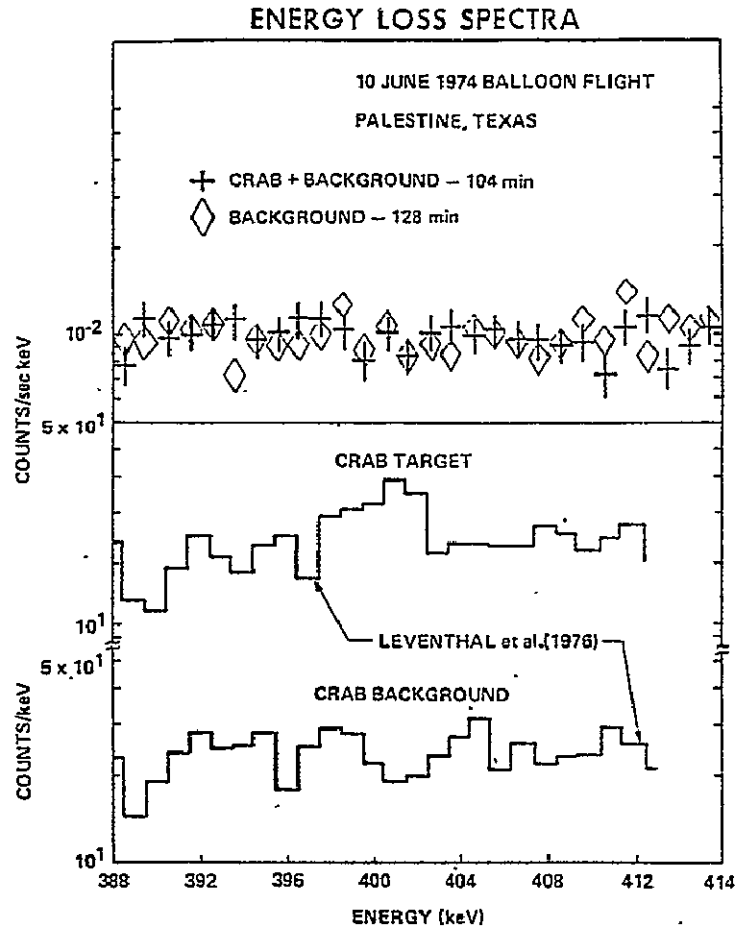
of this line is of considerable astrophysical importance; but Ling et al. (1977), after searching the JPL group's high resolution spectra from the Crab Nebula taken on 10 June 1974, failed to find any evidence for it. The JPL instrument used four 40 cm^3 Ge(Li) crystals in a CsI(Na) anticoincidence shield giving collimation to 25° FWHM. However, only three crystals functioned in flight. In viewing sources with this instrument, the telescope viewing axis is kept at a fixed altitude and azimuth thus, in this case, the Crab Nebula made a transit of the field of view. In this way, source and background observations are made

under identical (or nearly identical) conditions as contrasted to the method
used by the Rice University and Bell/Sandia groups. Ling et al. (1977) should
have seen a 3.9σ signal in their Crab spectra if the flux was (2.24 ± 0.65) x 10^{-3}
photons $cm^{-2}sec^{-1}$ as reported by Leventhal et al. (1977). Instead Ling et al.
(1977) gave a 3σ upper limit for a 400 keV Crab line of 1.75 x 10^{-3} $cm^{-2}sec^{-1}$.
Figure 7 from Ling et al. (1977) shows a comparison of the spectra from both
experiments in the vicinity of 400 keV.

At energies below 100 keV, there have been reports of spectral lines from two
objects, the Crab Nebula and the X-ray source Hercules X-1. First, the high .
resolution experiment described above (Jacobson, 1977; Ling et al., 1977)
which viewed the Crab Nebula gave evidence for a spectral line at 73.3 keV
with a line flux above the Crab continuum of (4.0 ± 1.1) x 10^{-3} photons $cm^{-2}sec^{-1}$
and a width < 4.9 keV FWHM. In Figure 8 the total Crab Nebula spectrum from

Figure 8. The net photon spectrum from the Crab Nebula in the energy
range of about 50 keV to 300 keV, measured on 10 June 1974.
The solid and dashed curves indicate, respectively, power
law fits to the data with and without a Gaussian shaped
line at 73.3 keV. The inset shows details of the fit in
the vicinity of the possible line on a channel-by-channel
basis. (From Jacobson, 1977.)

CRAB NEBULA SPECTRUM - TOTAL EMISSION
10 JUNE 1974 BALLOON FLIGHT
PALESTINE, TEXAS
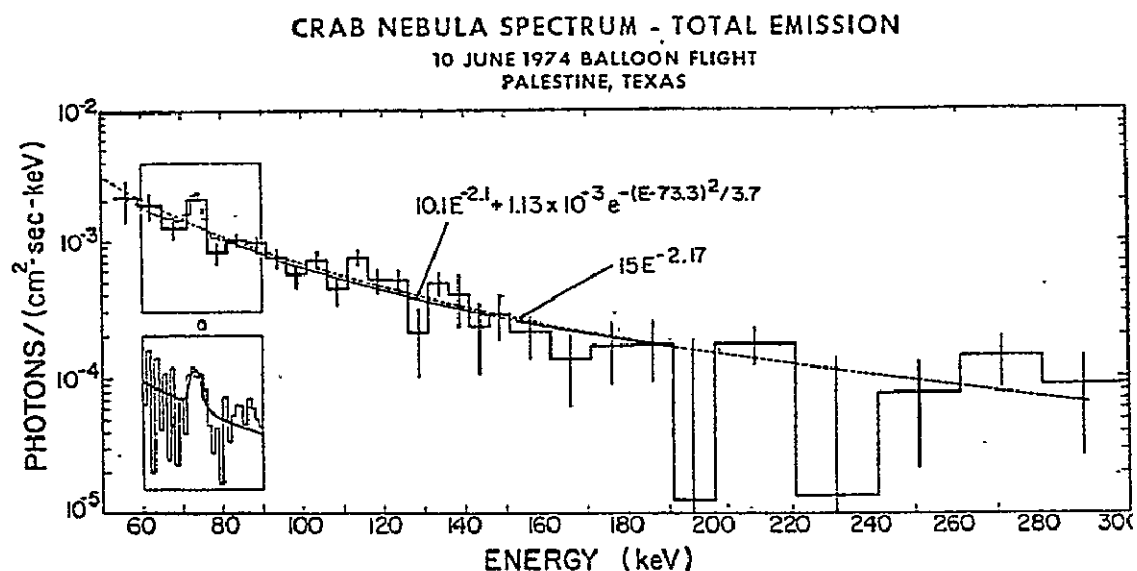
∿ 50-300 keV observed by Ling et al. (1977) is shown. The flux value given
above is based on a best fit to the overall spectrum by the function
$10.1 \ E^{-2.1} + (1.15 \ x \ 10^{-3})e^{-(E - 73.3)^2/3.64}$. The excess counts in the line
correspond to a 3.8σ effect over the Crab continuum. Jacobson (1977)
suggested that this line observed from the direction of the Crab Nebula may
be produced by cyclotron emission in the strong magnetic field of the Crab
pulsar as proposed by Trümper et al. (1978a,b) in the case of line emission from
Her X-1. If the 73 keV line is the first harmonic and is red-shifted by
∿ 20%, then the magnetic field strength would be ∿ $8 \ x \ 10^{12}$ Gauss. Later in
this conference Dr. J. Trümper will give a detailed discussion of the pulsed
line observation from Her X-1 and its possible interpretation as cyclotron
radiation. We, therefore, will not review this important result here (cf.
(Trümper et al., 1978b).

The last important observation of gamma ray lines are those recorded in the
transient event seen in the JPL balloon flight of 10 June 1974. The experiment
was intended to study line emissions from the Crab Nebula as was discussed
above (Jacobson, 1977, Ling et al., 1977). Near the end of this balloon
flight a transient burst was recorded by the experiment, which lasted for
about 20 minutes resulting in the appearance of four gamma ray lines in the
measured spectrum (cf. Jacobson, 1977).

Figure 9 shows the spectra obtained in three energy intervals containing the
four lines during the time interval during which the transient source was
present ∿ 2020-2041 UT. The average background spectra based on earlier and later
time intervals are also shown for comparison. Comparison of these two
spectra provide the evidence for the four lines at ∿ 413 keV, 1.8 MeV, 2.2 MeV,
and 5.9 MeV. The pertinent information concerning these lines is shown in
Table 2, which gives the centroid location of each feature and the error in
this position, the approximate width of each line, and the line flux intensity
(cf. Jacobson, 1977). One unique aspect of these features is that they are
all much broader than the instrument's energy resolution. The belief that this
is a true extraterrestrial transient event is greatly strengthened by the fact
that the anticoincidence shield elements of the detector also registered simul-
taneous counting rate increases corresponding to 3-5σ deviations from the average.
Information on the direction of this source is not too good but the telescope

field of view included several interesting objects including the gamma ray source γ 195+5 and the supernova IC 443. In a later paper in this symposium, Dr. Lingenfelter will present a possible model to interpret this interesting event (cf. Lingenfelter, 1978).

Figure 9. Those portions of the spectrum containing the lines measured during the transient event of 10 June 1974 observed by the JPL group. All the lines widths are greater than the resolution width of the instrument. (From Jacobson, 1977.)
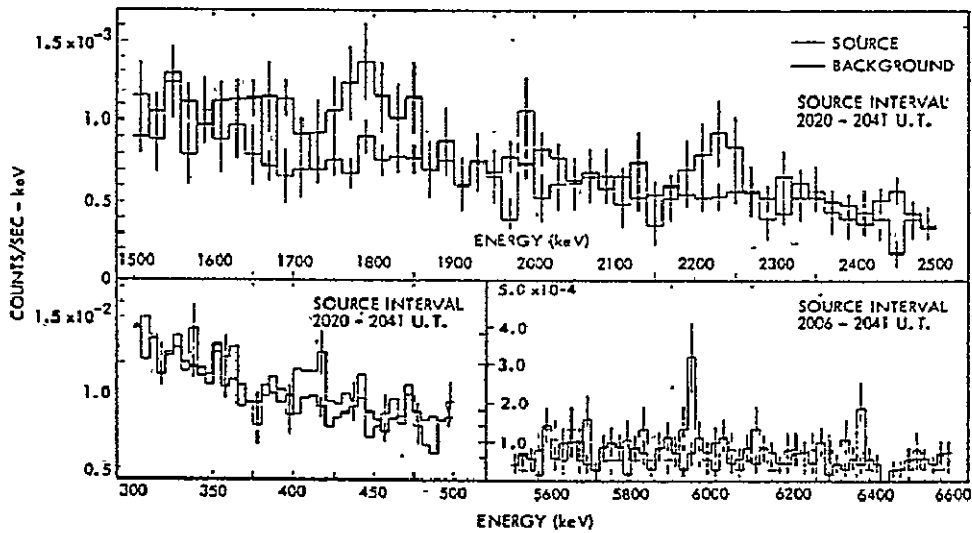
Table 2. The detailed properties of the lines observed in the transient burst spectrum shown in Figure 9. (From Jacobson, 1977.)

LIVE ENERGY (keV)	COUNT RATE (SEC)$^{-1}$	FLUX* (CM^2 - SEC)$^{-1}$	FWHM (keV)	TIME INTERVAL SPANNED (U.T.)
413.2 ± 1.8	$(5.5 \pm 1.6) \times 10^{-2}$	$(7.0 \pm 2.0) \times 10^{-3}$	15	2020 - 2041
1789.7 ± 6.0	$(6.78 \pm 1.55) \times 10^{-2}$	$(3.15 \pm 0.74) \times 10^{-2}$	95	2026 - 2041
2218.6 ± 6.3	$(2.67 \pm 0.87) \times 10^{-2}$	$(1.51 \pm 0.49) \times 10^{-2}$	70	2020 - 2041
5946.5 ± 3.7	$(7.06 \pm 2.18) \times 10^{-3}$	$(1.47 \pm 0.46) \times 10^{-2}$	25	2006 - 2041

*ASSUMES SOURCE ON THE DETECTOR AXIS

3.0 SIGNIFICANCE OF THE REPORTED OBSERVATIONAL RESULTS.

The observational results in gamma ray line astronomy discussed above are generally not of high statistical significance. It seems clear in this circumstance that some standardized statistical method should be used to determine quantitatively the confidence that can be attached to a given report in terms of its astrophysical presence. Of course, it must be taken for granted that the experimenter has taken every precaution to insure that some systematic instrumental or observational effect cannot produce an "apparent" extraterrestrial flux of a gamma ray line. With the understanding that this is the case, then various statistical methods can be used to determine the significance of an observation. The approach we have adopted in our laboratory has already been used by Hearn (1969) and O'Mongain (1973) in evaluating the earlier reports of various sources of high energy gamma rays (> 50 MeV). The method consists of determining the probability that a given number of suspected source events is due to the presence of a real source relative to the probability that it is due to a statistical fluctuation in the number of background counts. This basic approach, apparently first proposed by Greisen (see Hearn, 1969), has been modified by Cherry et al. (1978) to take into account uncertainties in experimental conditions under which gamma ray astronomy experiments are usually conducted. We will briefly review the basic principles involved and apply the technique to several of the results previously discussed.

In particular, consider an experiment in which B background counts are accumulated in a given time interval. Now take the number of counts obtained when looking at the source for an equal time interval as N, where N > B. Now since B is only a best estimate of the true mean background B', one can write down the Poisson probability that the measured background is obtained from a distribution with average background counts B':

$$P(B,B') = \frac{(B')^B e^{-B'}}{B!} \qquad\qquad 1.$$

By summing over all possible values of the true mean background B', since B' is in principle unknown, one can then compute the probability that the total number of events N is due only to background by computing the following quantity:

$$\sum_{B' = 0}^{\infty} P(N,B') \; P(B,B') \qquad\qquad 2.$$

Similarly, the probability that N counts are produced by a background plus a source S is the corresponding summation:

$$\sum_{B' = 0}^{\infty} P(N,S+B') \; P(B,B') \qquad\qquad 3.$$

The ratio of these probabilities, that is, the probability that the N counts are due to a source plus background divided by the probability that the N counts are due to background alone, is defined as the relative likelihood L(N,S,B) of S so that:

$$L(N,S,B) \; = \; \frac{\displaystyle\sum_{B' = 0}^{\infty} P(N,S+B') \; P(B,B')}{\displaystyle\sum_{B' = 0}^{\infty} P(N,B') \; P(B,B')} \qquad\qquad 4.$$

By using the explicit form (Equation 1) for the probability distribution P(x,y), the likelihood ratio L(N,S,B) can be rewritten as:

$$L(N,S,B) \; = \; \frac{\displaystyle\sum_{B' = 0}^{\infty} \exp[N \ln(S+B') + B \ln B'-2B'-S]}{\displaystyle\sum_{B' = 0}^{\infty} \exp[(N+B) \ln B'-2B']} \qquad\qquad 5.$$

For background intensities B sufficiently large, L is maximized for values of the source intensity S $\approx$ N-B. We may, therefore, evaluate Equation 5 at S = N-B (where N and B are measured quantities) and introduce the signal-to-background ratio β = S/B. Then B = N/(1+β) and S = βN/(1+β), and the likelihood ratio may be expressed in terms of the two variables β and N:

$$L(\beta,N) = \frac{\displaystyle\sum_{B'=0}^{\infty} \exp N[\ln\left(\frac{\beta N}{1+\beta} + B'\right) + \frac{\ln B'}{1+\beta} - \frac{2B'}{N} - \frac{\beta}{1+\beta}]}{\displaystyle\sum_{B'=0}^{\infty} \exp N[\frac{2+\beta}{1+\beta}\ln B' - \frac{2B'}{N}]} \qquad 6.$$

This expression gives the relative likelihood that a particular single observation is due to a source rather than to a background fluctuation. In a typical experiment, however, many attempts to observe a source are made. One generally searches for a source by scanning an area of the sky or a range of energies, or (in the case of a transient or variable source) by repeating the measurement many times. Then, if M attempts are made to observe the source, the probability of seeing a statistical fluctuation increases roughly by a factor of M. This increased probability of observing a spurious background fluctuation may be taken into account by considering not just the likelihood ratio L but rather the normalized value L/M.

One can also write down the confidence level to which one can claim the presence of a source S:

$$C = 1 - M/L = \frac{L - M}{L} \qquad 7.$$

In order to claim the presence of a source with C = 99%, a normalized likelihood ratio L/M = 100 is required.

Hearn (1969) and O'Mongain (1973) have considered just the B' = B term of Equation 5 or 6. In this case:

$$L(S) = L_{B'=B}(\beta,N) = [(S/B) + 1]^N e^{-S} = (1 + \beta)^N e^{-\beta N/(1+\beta)} \qquad 8.$$

This expression is correct if one knows the background exactly. However, in a gamma ray astronomy experiment, one knows only that the true background B' is probably within the range $B - \sqrt{B} < B' < B + \sqrt{B}$. On the basis of Equation 8, O'Mongain (1973) has evaluated several of the early reported observations of high energy gamma ray ($\gtrsim$ 50 MeV) sources in the directions of the Galactic

Center and anticenter, Cygnus, Cassiopeia, the Crab Nebula, and various pulsars. For each observation, he took the worst-case estimate $B + \sqrt{B}$ for the background, and evaluated the normalized likelihood ration L/M. He considered 60 observations and found 12 with normalized likelihood ratios L/M $\geq$ 20, corresponding to a 95% confidence level. Only 5 observations had L/M $\geq$ 100, the requirement for 99% confidence. The inescapable conclusion was that a large number of reported gamma ray source observations were likely due to statistical background fluctuations. By using the pessimistic background estimate $B + \sqrt{B}$, O'Mongain has introduced a certain arbitrariness into his calculations and has perhaps placed overly strict requirements on the observations. However, even using the value B for the background, one finds only 13 measurements with normalized likelihood ratios in excess of 20, and 9 with L/M above 100.

The more general form for the likelihood ratio (Equation 6) has been evaluated for a range of values of N and β and the result is plotted in Figure 10 as a

Figure 10. The likelihood ratio L(N,β) plotted versus signal-to-background ratio β for different values of the total number of counts N. The dashed line at L = 100 corresponds to a confidence level of 99%. (From Cherry et al., 1978.)
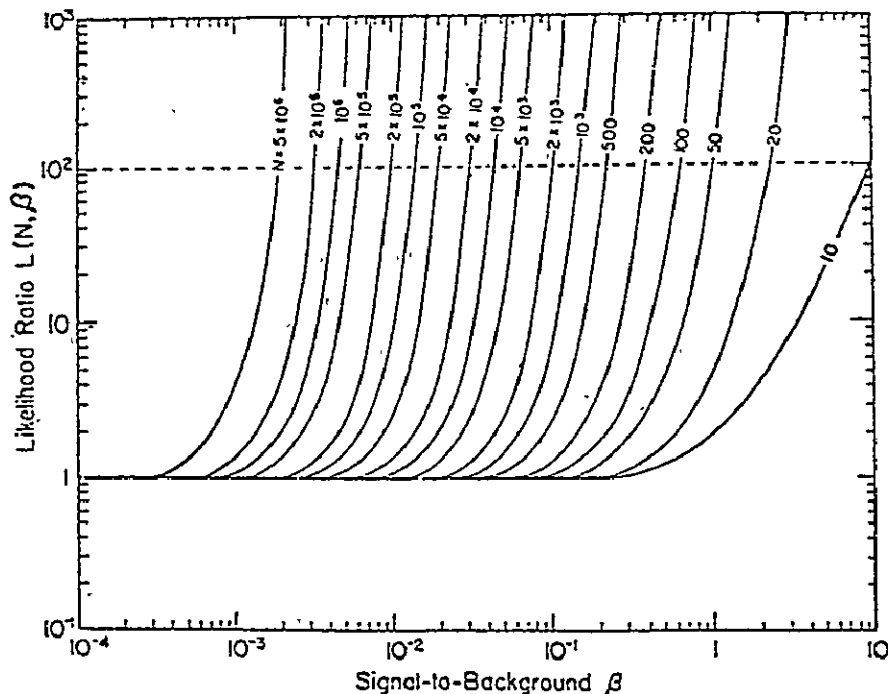
function of the signal-to-background ratio β = S/B with the total number of counts N as a parameter. Curves are shown for L(β,N) for values of the total number of counts N = S+B ranging from N = 10 to 5 x 10^6. For sufficiently small values of signal-to-background, β, the likelihood approaches unity which means that it is no more probable that a number of counts S = N-B is caused by a weak source then by a fluctuation in the background. For larger values of N and β such that $\beta^2 N \lesssim 1$, however, the likelihood increases dramatically with increasing N and β. It should also be noted that if one is dealing with a small number of total counts (N $\sim$ 10), then L(N,β) increases relatively more slowly with β than if a large number of total counts are involved.

In order to evaluate the reported observations of gamma ray lines we discussed earlier, the likelihood ratio will be evaluated for those experiments where there is sufficient published data to determine the basic quantities. These observations are listed in Table 3 with a summary of the basic experiment parameters and the quantities S, B, β, and L. Also listed is the number of standard deviations above background claimed by the experimenters for each specific report. The results are presented in order of general significance. A more extensive discussion of this analysis will be published elsewhere (Cherry et al., 1978).

The first entry in the table and the most significant of these observations is that of 2.2 MeV line seen during the solar flare of 4 August 1972 by the UNH sodium iodide spectrometer aboard OSO-7. (Chupp et al., 1973, 1975). This gives a likelihood ratio of L = 5.6 x 10^{16}. During the same flare, a less significant line was observed at 0.5 MeV, with L = 21, and possible line features were seen at 4.4 and 6.1 MeV, which were reported as circumstantial evidence. In addition, the 2.2 MeV and 0.5 MeV lines were observed during the decaying phase of the large flare which erupted on 7 August 1972. Again the likelihood ratio is extremely high for the neutron-proton capture line giving a confidence level of its presence of $\sim$ 100% while the confidence level for the 0.5 line is $\sim$ 94%–95%. A value of M = 1 corresponding to only one trial was used for evaluating these observations since lines were expected theoretically at the energies observed.

Table 3. The likelihood value obtained for various reported observations of gamma ray line emission. (From Cherry et al., 1978.)

EXPERIMENT	OBJECT	ENERGY (MeV)	S	B	β	σ	L* (M = 1)
CHUPP ET AL. (1973,1975) OSO-7 SATELLITE 1971-1972 3" X 3" NaI(Tℓ) CsI(Na) SHIELD 8% FWHM AT 662 KeV ~90 SEC ON SOURCE ~90 SEC OFF SOURCE	AUG. 4, 1972 SOLAR FLARE AUG. 7, 1972 SOLAR FLARE	2.2 0.5 4.4 6.1 2.2 0.5	147 87 40 48	96 470 20 167	1.5 0.18 2.0 0.29	15 4 3 3 6 3	5.6×10^{16} 21 3.8×10^{4} 16
JACOBSON (1977) BALLOON FLIGHT 6/10/74 135 Cm³ Ge(Li) CsI(Na) SHIELD 2.9 KeV FWHM AT 1.3 MeV 0.2 SR SOLID ANGLE 104 MIN ON SOURCE 128 MIN OFF SOURCE	CRAB NEBULA TRANSIENT EVENT (15-35 MIN DURATION)	0.073 0.413 1.790 2.219 5.947	950 54 52 34 10	2.25×10^{4} 159 101 59 2	4.2×10^{-2} .34 .51 .58 5.0	>3 >3 >3 >3	1.3×10^{4} 40.2 151.5 36.4 41.6
LEVENTHAL ET AL. (1977) BALLOON FLIGHT 5/11/76 92 Cm³ Ge(Li) NaI SHIELD 3.4 KeV FWHM ~12° FWHM 15 HR OBSERVATION	CRAB NEBULA	0.400	47	120	0.39	4	37
HAYMES ET AL. (1975) BALLOON FLIGHT 4/2/74 182 Cm² NaI(Tℓ) NaI COLLIMATOR 13° FWHM 12% FWHM AT 0.5 MeV 219 MIN ON SOURCE 219 MIN OFF SOURCE	GALACTIC CENTER	0.530 0.900 1.2-2 4.6	380	1.15×10^{4}	3.3×10^{-2}	3.5 1.2 4.1 3.5	14
HALL ET AL. (1976) BALLOON FLIGHT 4/2/74 cf. HAYMES et al. (1975) 85 MIN ON SOURCE 109 MIN OFF SOURCE	CENTAURUS A	4.5 1.6	66	356	0.18	3.3 3.3	10
IMHOF AND NAKANO (1977) SATELLITE OBSERVATION 50 Cm³ Ge(Li) 10/72 TUNGSTEN COLLIMATOR 3.5 KeV FWHM ± 45° COLLIMATION.	GALACTIC PLANE LONG=225°-328°	1.121 1.369	136 109	1920 1400	0.07 0.08	3 3	7.8 5.7

*See text for a discussion of the consequence of using the normalized likelihood ratio L/M when there is justification for using M>1.

Jacobson (1977) has discussed a 73.3 keV line seen in the spectrum of the Crab Nebula. He reported a flux of $(3.8 \pm .86) \times 10^{-3} \text{ cm}^{-2}\text{sec}^{-1}$ measured over a time of $\sim 6 \times 10^3$ sec. Assuming the error estimate to be a 1σ statistical error, one can compute the values of S and B given in Table 3. Since the spectra were accumulated in 8192-channel analyzers, we must use M = 8192, since there is no special reason for expecting a line at 73 keV. The normalized likelihood ratio is then L/M = 1.58 but if M = 1 is used the result, of course, becomes highly significant at $L \simeq 10^4$. Jacobson (1977) also reports four lines seen between 0.4 and 6 MeV in a transient event in the same experiment but later in the flight (see our previous discussion of this event). In Table 3 we give the values of S and B obtained from Jacobson (1978) for each of the reported lines. The resulting values obtained for L assuming M = 1 range from ~ 40 to ~ 150, so the results are fairly significant with a confidence level of $\sim 96-97\%$ of being due to a true source. On the other hand, if one considers the large number of possible trials in 8192-1 keV channels, then the normalized likelihood ratio, L/M, could be considerably reduced. This, of course, might eliminate the significance of this observation but as mentioned earlier, support for the reality of the transient event comes from the simultaneous increase in the shield counting rates. On the other hand, as far as the presence of spectral lines is concerned, it would be gratifying to know if they are observable in each of the independent Ge(Li) crystals.

In the case of the report of Leventhal et al. (1977) of a 400 keV line from the Crab Nebula, we take the values of S and B from the tabulation of Leventhal's data by Ling et al. (1977). The resulting value of L is 37; however, in general one should consider that there is no reason to expect a sharp line at 400 keV, therefore, one should use the normalized likelihood ratio. If the line is interpreted as due to red-shifted 511 keV gamma rays from positron annihilations near the surface of a 1.4 $M_\odot$ neutron star then a reasonable value for M, the number of trials, is M = 96 corresponding to the number of data channels between 400 and 511 keV. The resulting value of L/M is so low that there is a significant probability that the feature observed by Leventhal et al. (1977) may have been caused by a background fluctuation.

If a second observation were to yield a feature at the same energy, then one could reasonably use M $\approx$ 1 and much more confidently attribute a weak feature to a real gamma ray line source. Ling et al. (1977) had earlier (1974) flown another solid state detector which viewed the Crab Nebula. They carried out a search of their data for a 400 keV line from the Crab, but reported negative results. The reported line flux of 2.24×10^{-3} photons $cm^{-2}sec^{-1}$ by Leventhal et al. (1977) would have increased the counting rate in the earlier experiment by a factor of $\sim$ 6.

The Rice group has reported lines from the Galactic Center (Johnson and Haymes, 1973; Haymes et al., 1975) and Centaurus A (Hall et al., 1976), obtained with a balloon-borne NaI(Tℓ) detector. The line observations were first reported at 476 keV and later at 530 keV. It is not clear whether this difference in energy, which is significantly larger than the quoted uncertainty in the energy measurement, is due to instrumental effects or to variation in real source. Hence, the lowest value one can use for M is the number of channels (15) between the expected 511 keV and the reported energy. Taking the values for S and B from the graphs in the published papers, one finds L/M $\approx$ 1 for the more recent 530 keV measurement of Haymes et al. (1975). Galactic Center lines were also reported by Rice University in the range near 1.2–2 MeV, at 900 keV, and at 4.6 MeV, but the published data is insufficient to permit a detailed analysis. For the Centaurus A line feature at 4.5 MeV observed by the same group one can again take S and B from the published graphs. In this case, we take M as 1 since the ^{12}C line at 4.4 MeV is very nearly at the reported energy. The resulting value for L is 10 corresponding to a 90% confidence level.

Imhof and Nakano (1977) using data from a Ge(Li) spectrometer on a satellite, have reported possible distinct line features at 1121 and 1369 keV from the galactic plane. Using values for the counting rates supplied by one of the authors (Imhof, 1978), we compute values of L = 7.8 and 5.7 respectively for these two lines assuming the lines are expected. However, since it was necessary to scan through a large number of channels, there were, therefore, 4096 chances for a large statistical fluctuation to occur. Although the observed features were sharp and distinct, the probability is quite high that they were due to background fluctuations.

Of the 20 reported line observations in Table 3, we have applied a likelihood
analysis to the most significant. Although each line was reported at the 3σ
level or higher, the present discussion shows that only the OSO-7 solar flare
lines at 2.2 MeV were clearly due to an extraterrestrial gamma ray source.
In all other cases, either the reported line features are weak or their
statistical significance is drastically reduced when one considers the
number of trials made in searching for a line. We, therefore, must draw a
conclusion similar to that of O'Mongain (1973), that a 3σ criterion is neither
a significant nor a reliable criterion to use in the detection of weak gamma
ray sources. One must be especially wary of designing experiments to detect
sources at the 3σ level, or of using this criterion to predict very low
minimum detectable fluxes. A much more reliable criterion is the requirement
that a measurement be made at a confidence level of 99%, or a normalized,
likelihood value of 100.

4.0 CONCLUDING REMARKS

This review and evaluation of the reported results in gamma ray line astronomy
should be tempered with the following statement. We have presented a method
for evaluating the significance of a suspected extraterrestrial gamma ray line
observation that we believe is more reliable than the usual 2σ-3σ statement and
less subject to bias. This method, determination of the likelihood ratio for
the result, should not be applied until after all systematic effects have either
been eliminated or carefully evaluated, quantitatively if possible. In our
application of the likelihood method to the reported observations of gamma ray
lines, we *are not* saying that experimental situations giving low L values should
be discarded, but rather that the case for a cosmic gamma ray line should be
held open until one or more additional experiments confirm the same line or
fails to find it. One can safely claim success when a normalized likelihood
value of approximately 100 is achieved.

Finally, the significance of an observation as indicated by the likelihood ratio
L(N,β) (see Figure 10) depends critically on an accurate determination of the
appropriate background for the source observation since L varies so strongly
with β = S/B, the ratio of suspected sources counts to the background counts.

This is even more true when $\beta << 1$. The background counts we have used for the likelihood analysis of reported line observations presented here have been, for most cases, our own estimates of backgrounds based on the published data; however, in some instances we have used background data provided by the experimenters themselves.

This same likelihood method can be used to predict in advance the sensitivity expected for a given new experimental design. Again, a design goal to achieve an L value of ~ 100 should be the guiding criterion.

In conclusion, it is the author's conviction that with the larger and more sensitive gamma ray telescopes that will be available in the future many more significant results in gamma ray line astronomy should be obtained and the value of this new astronomical tool as an effective probe of the Universe will be realized.

ACKNOWLEDGEMENTS

REFERENCES

Cherry, M. L. and collaborators: 1978, (in preparation).

Chupp, E. L., Forrest, D. J., Higbie, P. R., Suri, A. N., Tsai, C., and Dunphy, P. P.: 1973, Nature 241, 333.

Chupp, E. L. Forrest, D. J., Suri, A. N.: 1975, in S. Kane (ed.), Proceedings of the IAU-COSPAR Symposium, D. Reidel Publishing Company, 68.

Clayton, D. D., Colgate, S. A., and Fishman, G. J.: 1969, Astrophys. J. 155, 75.

Clayton, D. D., and Hoyle, F.: 1974, Astrophys. J. (Letters) 181, L101.

Forrest, D. J., Higbie, P. R., Orwig, L. E., and Chupp, E. L.: 1972, Nucl. Instrum. Methods 101, 567.

Hall, R. D.; Meegan, C. A., Walraven, G. D., Djuth, F. T., and Haymes, R. C.: 1976, Astrophys. J. 210, 631.

Haymes, R. C., Walraven, G. D., Meegan, C. A., Hall, R. D., Djuth, F. T., and Shelton, D. H.: 1975, Astrophys. J. 201, 593.

Hearn, D.: 1969, Nucl. Instrum. Methods 70, 200.

Higbie, P. R., Chupp, E. L., Forrest, D. J., and Gleske, I. U.: 1972, IEEE Trans. Nucl. Sci. NS-19, 606.

Imhof, W. L., and Nakano, G. H.: 1977, Astrophys. J. 214, 38.

Imhof, W. L.: 1978, (private communication).

Jacobson, A. S.: 1977, Invited Paper, American Physical Society Meeting, Washington, D.C., 25-28 April.

Jacobson, A. S.: 1978, (private communication).

Johnson, W. N. III, Harnden, F. R., Jr., and Haymes, R. C.: 1972, Astrophys. J. (Letters) 172, L1.

Johnson, W. N. III, and Haymes, R. C.: 1973, Astrophys. J. 184, 103.

Leventhal, M., MacCallum, C., and Watts, A.: 1977, Astrophys. J. 216, 491.

Leventhal, M et al.: 1978, In these proceedings, see page 169.

Ling, J. E.: 1974, Doctoral Thesis, University of California San Diego, La Jolla, California.

Ling, J. E., Mahoney, W. A., Willett, J. B., and Jacobson, A. S.: 19774, Nature 270, 36.

Lingenfelter, R. E.: 1978, In these proceedings, see page 252.

Lingenfelter, R. E. and Ramaty, R. 1967 High Energy Nuclear Reactions in Astrophysics, B. S. P. Shen, Editor (Beryamin, N. T.) p. 99.

Lingenfelter, R. E. and Ramaty, R. 1976, The Structure and Content of the Galaxy and Galactic Gamma Rays NASA CP 002, p. 237.

Morrison, P.: 1958, Nuovo Cimento 7, 858.

O'Mongain, E.: 1973, Nature 241, 376.

Ramaty, R., and Lingenfelter, R. E.: 1975, in S. Kane (eds.), Solar Gamma X-, and EUV Radiation, 363.

Ramaty, R., Kozlovsky, B., and Lingenfelter, R. E.: 1975, Space Sci. Rev. 18, 341.

Ramaty, R., Kozlovsky, B., and Suri, A. N.: 1977, Astrophys. J. 214, 617.

Ramaty, R., and Lingenfelter, R. E.: 1977, Astrophys. J. (Letters) 213, L5.

Trümper, J. et al.: 1978a, In these proceedings, see page .

Trümper, J., Pietsch, W., Reppin, C., and Voges, W.: 1978b, Astrophys. J. (Letters) 219, L105.

Walraven, G. D., Hall, R. D., Meegan, C. A., Coleman, P. L., Shelton, D. H., and Haymes, R. C.: 1975, Astrophys. J. 202, 502.

Walraven, G. D., and Haymes, R. C.: 1976, Nature 264, 42.

II. .SOLAR, STELLAR AND PLANETARY LINE EMISSION

A HARD X RAY AND GAMMA RAY OBSERVATION OF
THE 22 NOVEMBER 1977 SOLAR FLARE

by

G. Chambon, K. Hurley, M. Niel, R. Talon, and G. Vedrenne
C.E.S.R. Toulouse, France

and

O.B. Likine, A.V. Kouznetsov, and I.V. Estouline,
IKI, Moscow, U.S.S.R.

The Franco-Soviet experiment package Signe 2 MP for solar and cosmic X and gamma ray observations was launched aboard a Soviet Prognoz satellite on 22 September 1977 into a highly eccentric earth orbit. The experiment operated successsfully until around February 1978, when the satellite ceased to function. It consists of several different detectors, which were built at the C.E.S.R. An uncollimated NaI detector (Fig. 1) 37 mm. thick by 90 mm. diameter is placed on the upper surface of the satellite, and faces the sun; a collimated lateral NaI detector 14 mm. thick by 38 mm. diameter also faces the sun, and a similar lateral detector faces the anti-solar direction. These instruments have as their primary objectives the detection of cosmic gamma ray bursts and solar X and gamma rays. A more detailed description is currently being prepared ; briefly, however, these detectors measure X rays in the energy range 20 keV-5 MeV, approximately, with a time resolution which is variable, but reaches 2 ms. for strong events.

The upper detector has a photopeak efficiency of about 8 % at 2 MeV. Its energy resolution at this energy is about 8 % FWHM. Typically, spectra over the energy range 160 KeV - 5 MeV are transmitted in 9 channels. Therefore, this instrument cannot be considered a true gamma ray spectrometer. However, in the data tapes which were received at the end of February, it was found that an exceptionally intense solar flare was observed around 10:00 UT on 22 November 1977, up to energies of 5 MeV, with evidence for line emission at 2.23 MeV and possibly 4.4 MeV. We report here the results of a very preliminary treatment of these data . Due to the presence of line emission, which has been observed for only two other solar flares (August 4 and 7, 1972), the results of the complete analysis should be especially interesting; they will be presented at a later date.

According to the Prompt Boulder Reports (Nos 400 and 401), the event which we observed was associated with the Mc Math Plage Region 15031, and an H-alpha flare of importance 2B; it is not yet clear what radio emission is associated with our X-ray observations.

Figure 2 shows the counting rates in different energy bands for the uncollimated upper detector, which always faces the sun. The time scale is approximately 163 seconds/measurement. The onset and decay are visible most clearly in the low energy bands. The unique feature of the event, however, is revealed by the two higher energy bands at the bottom of the figure. In the curve (1.59-2.95 MeV) we note that the counting rate does not increase at the onset of the event, but rather, 163 seconds after. However, in the curve (2.95-4.9 MeV) an onset is evident which is coincident with the onset at low energy. We take this as evidence that the increase in one band is due to the 2.23 MeV line produced by neutron capture on protons, which should be slightly delayed due to the capture time, while the other increase can be attributed to the excited state of ^{12}C, which should de-excite promptly. Although we are not prepared at the moment to quote the statistical significance of these results, our conclusions are strengthened by a consideration of Figure 3, which shows two spectra observed by the same detector. Around 4.4 MeV, both spectra are inconsistent with a simple power law; around 2.2 MeV, the earlier spectrum lies below the later one. A rough estimate of the 2.2 MeV flux is 0.15 photons/cm^2.sec, which is comparable with Chupp's observation of the 2.2 MeV line during the August 4, 1972 event (Chupp et al., 1973). If the 4.4 MeV excess is indeed due to a line, its intensity is about a factor of 3 less. This would in turn mean that the 511 KeV line should be about a factor of 2 less intense than the 2.2 MeV line (Ramaty and Lingenfelter, 1973) and that it should not be detected in these data. These intensities are subject to some uncertainty, since a complete spectral fitting program has not yet been applied to these data ; they have been estimated by subtracting the simple power laws shown in Fig. 3 from the observed spectra. An additional uncertainty comes from the possible presence of many unresolved lines at MeV energies, which would make this simple power law fit inappropriate.

The experiment contains high time resolution memories, storage into which is triggered by a rapid increase in the counting rate. These memories were triggered by this event, and during the most intense part, the counting rates were sampled every 2 ms for a total of 2 secs. During the less intense part, there was a 16 ms sample time for a total of 16 secs, and 250 ms sample times for 32 secs. The analysis of these results has only begun as of this writing.

Chupp, E.L., Forrest, D.J., Higbie, P.R., Suri, A.N., Tsai, C. and Dunphy, P.P.
    1973, Nature, 241, 333.

Ramaty, R., and Lingenfelter, R.E., 1973, in High Energy Phenomena on the Sun ,
    R. Ramaty and R.G. Stone Eds., NASA SP-342.

FIELD OF VIEW

PLASTIC

PM   NaI (Tl)   PM

UPPER DETECTOR

PROGNOZ VI SATELLITE

SPIN AXIS

LATERAL DETECTORS

SUN

20°

3   3'

1L
2L

4   4'

20°

ANTISOLAR
DIRECTION
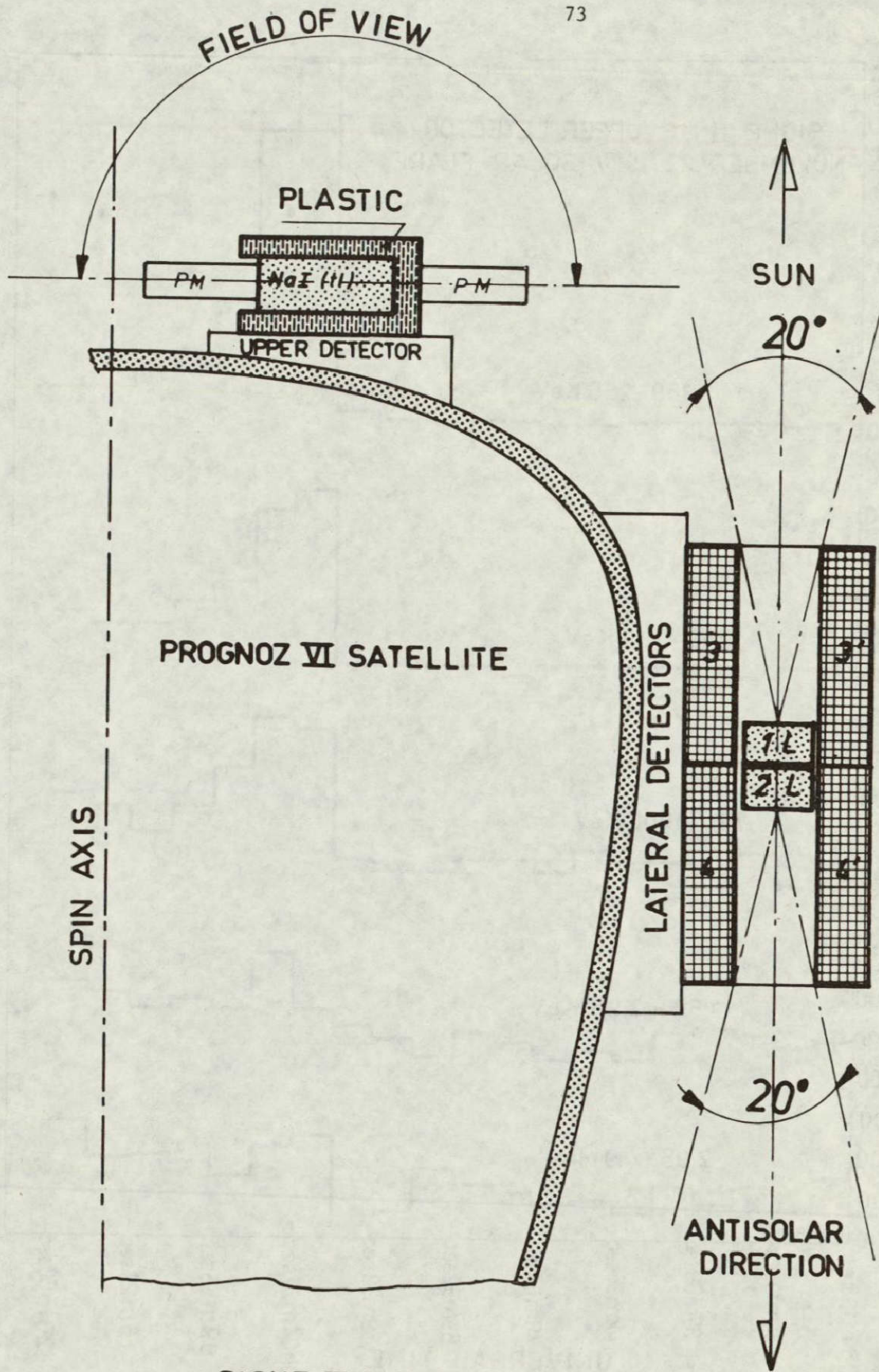
SIGNE II MP EXPERIMENT

Fig. 1

SIGNE II MP UPPER DETECTOR
NOVEMBER 22 1977 SOLAR FLARE

169 - 255 KeV

368 - 780 KeV

780 - 1200 KeV

1.59 - 2.95 MeV

2.95 - 4.9 MeV

COUNTS / 163.8 SEC

UNIVERSAL TIME
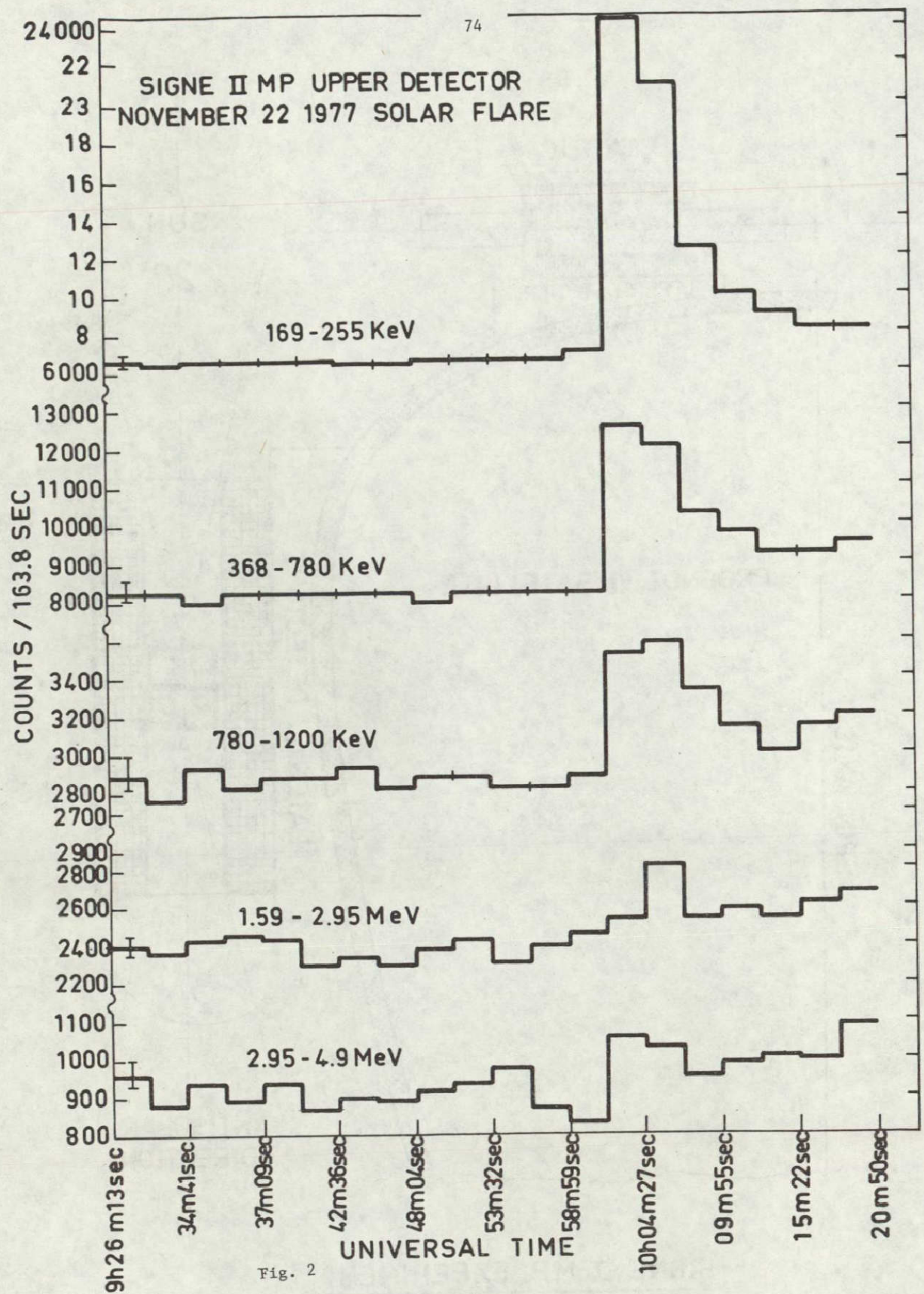
Fig. 2

Gamma Ray Emission and Solar Flares

R. P. Lin
Space Sciences Laboratory
University of California
Berkeley, CA 94720

R. Ramat,
Goddard Space Flight Center
Greenbelt, MD 20771

Abstract

Solar gamma-ray line and continuum emission can provide unique information about particle acceleration and its temporal behavior; the energy spectrum, composition and directivity of the accelerated particles; and the composition, density and temperatures of the ambient medium. This information, coupled with the comprehensive photon and particle observations available for the sun, give a detailed picture of the particle acceleration and flare energy release processes. In addition information on elemental and isotopic abundances, surface nuclear reactions and coronal heating mechanisms can be obtained. We discuss the implications of the present observations and the potential return from future observations.

I. Introduction

Gamma-ray emission from the Sun results from the interactions of energetic protons, nuclei and electrons with the solar atmosphere. These interactions produce gamma-ray lines from the captures, annihilations and deexcitations of neutrons, positrons and excited nuclear levels, respectively, and continuum emission from bremsstrahlung of relativistic electrons and Doppler-broadened nuclear lines. The observation of these gamma rays provides unique information on high energy processes at the Sun, including properties of energetic particles such as the timing of their acceleration, the ratio of electrons to protons, and the number, energy spectrum, chemical composition and possible beaming of the particles. Comparisons of the gamma-ray observations with the comprehensive photon observations available for the sun and with the spacecraft observations of solar energetic particles which escape the sun will provide crucial information on particle acceleration processes. In addition since energetic particles accelerated in solar flares contain a significant and possibly dominant fraction of the total flare energy, information on the flare energy release mechanism and the generation of other flare phenomena by energetic particles may also be obtained.

The same gamma-ray lines should occur prominently in non-solar objects whose gamma-radiation results from energetic particles. The solar gamma-ray observations can thus provide a basis for the interpretation of the spectra of cosmic gamma-ray emitters. Additionally, solar observations can provide information on elemental and isotopic (particularly He^3) abundances, surface nuclear reactions, and coronal heating mechanisms.

II.   The Present Observations and their Implications

Solar gamma rays were first observed from the 1972, August 4 and 7 flares

by a detector employing a NaI (Tℓ) crystal flown on OSO-7 (Chupp et al., 1973,

1975). The August 4 observations detected two strong lines, at 2.223 and

0.511 MeV, provided reasonable evidence for lines at 4.44 and 6.13 MeV, and

mapped the continuum from about 0.35 to 8 MeV. The measured relative inten-

sities of these four lines were consistent with earlier calculations (Lingen-

felter and Ramaty, 1967) which showed that the strongest lines from flares, in

decreasing order, should be at 2.223 MeV from neutron caputre, at 0.511 MeV

from positron annihlation, and at 4.438 and 6.129 MeV from ^{12}C and ^{16}O de-

excitations. The latter two lines are prompt so that their production varies

as the instantaneous number of energetic particles, while the 2.223 and 0.511

MeV lines are delayed because of the finite neutron-capture and positron-

annihlation times. Indeed, on August 7, when OSO-7 emerged into sunlight from

behind the Earth after the peak of the flare, only the 2.223 and 0.511 MeV

lines were detected (Wang and Ramaty, 1975).

In Figure 1 we show a theoretical solar gamma-ray spectrum calculated for

spectral parameters of the accelerated particles and nuclear abundances which

best fit the 1972, August 4 observations. These calculations are obtained from

a computer program which employs a Monte Carlo simulation and data for close

to 100 nuclear lines derived from either laboratory measurements or theoretical

interpolations and evaluations (Ramaty, Kozlovsky and Lingenfelter, 1978). The

shapes of the lines are calculated by taking into account nuclear kinematics

and data on the differential cross sections of the reactions. The 2.223 and

0.511 MeV lines are based on separate calculations of neutron and positron pro-

duction (Ramaty et al., 1975), and the bremsstrahlung, which contributes to the

underlying continuum, is taken from the calculations of Bai (1977). The results

of the simulation are binned into energy intervals ranging from 2 to 5 keV, as

indicated in the figure. With energy resolution of 3 keV at 2.2 MeV, the intensity of the neutron capture line is larger than that of the neighboring solar continuum by more than two orders of magnitude.
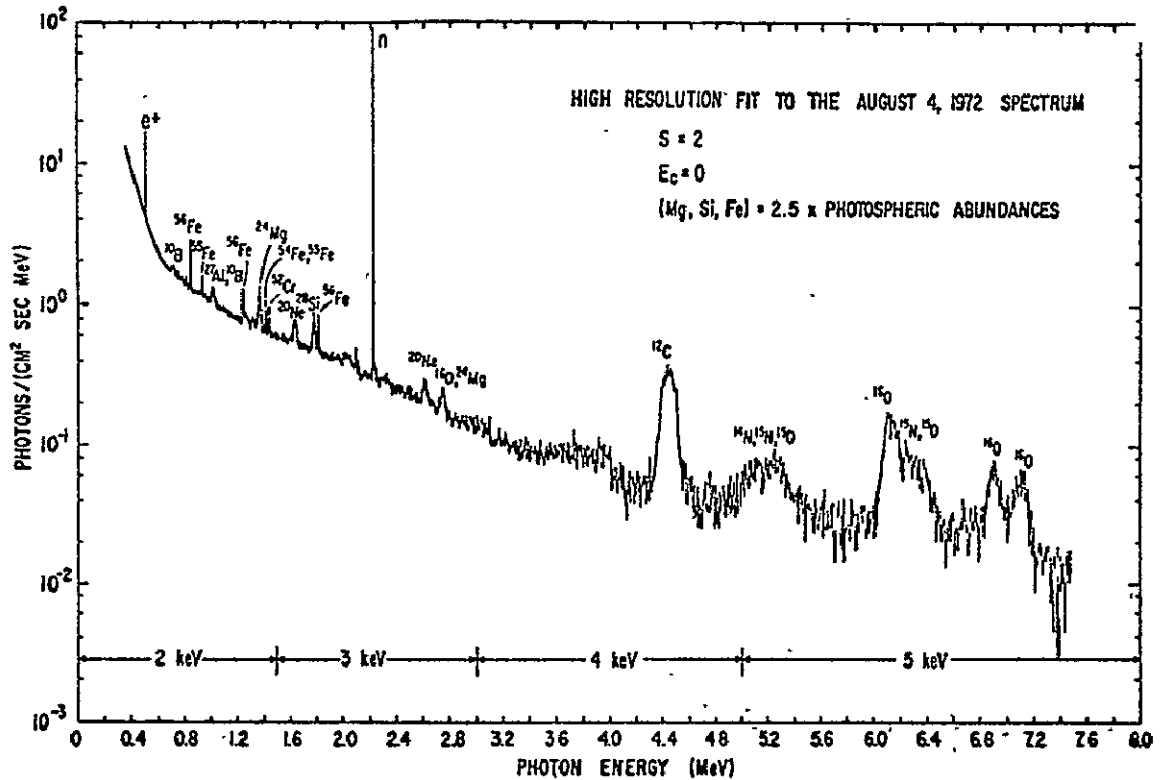
Fig. 1 — Calculated high resolution spectrum of the 1972 August 4 flare. The calculation represents the incident photon spectrum and thus does not take into account any detector background or efficiency correction; the figure does show an assumed energy resolution (FWHM) of the detector system. The spectral and abundance parameters are indicated on the figure.

The widths of other strong lines mentioned above are about 5 keV at 0.847 MeV, 18 keV at 1.369 MeV, 13 keV at 1.434 MeV, 100 keV at 4.44 MeV, and 150 keV at 6.129 MeV. The width of the 0.511 MeV line depends on the temperature and density, and in Figure 1 a width of 5 keV was used. The spallation features at ~5.2 and ~6.3 MeV are a few hundred keV wide. There are many other weaker lines, which together with Doppler broadened nuclear

emission produced by heavy accelerated particles, merge into a strong continuum which dominates the solar gamma-ray spectrum in the 4 to 8 MeV band (Ramaty et al., 1977). At higher energies, an important line occurs at 15.11 MeV (Crannell, Ramaty and Cannell, 1977). Even though its intensity is less than 2% of the 4.44 MeV line intensity, its high energy could make this line detectable above background for large flares.

III. The Particle Acceleration Process

Detailed information on particle acceleration processes can be obtained from gamma-ray observations as discussed below:

Timing.

The timing of the acceleration of protons and nuclei in relation to the acceleration of electrons can be obtained from comparison of gamma-ray line emission with x-ray and gamma-ray continuum. Figure 2 shows the timing for the 4 August 1972 flare event. Here only the 2.2 MeV neutron capture line was sufficiently above background for comparison. The observed 29-41 keV x-ray and $\gtrsim$.35 MeV gamma-ray continuum (produced primarily by electron brem-sstrahlung) time profiles were used as inputs to compute the expected time dependence of the 2.2 MeV line, using a Monte-Carlo model for the neutron capture in the photosphere. The protons and nuclei appear to be accelerated at the same time as the relativistic electrons which produce the $\gtrsim 0.35$ MeV gamma-ray continuum, and several minutes after the acceleration of the lower energy electrons. This two-stage acceleration is consistent with observations of two stages in the low energy x-ray emission, with a harder x-ray spectrum in the second stage (Frost and Dennis, 1971). Also observations of flare accelerated electrons and ions escaping into the interplanetary medium indicate a few minutes delay in the time of release from the sun for the energetic ions and relativistic electrons after the $^-10-10^2$ keV electrons (see Lin; 1974 for

review). However, the best direct timing evidence for two stages of acceleration would be obtained by comparing the time dependences of prompt gamma-ray lines such as those at 4.44, 6.129 and 0.847 MeV with the time dependences of hard x-rays, gamma-ray continuum and high frequence microwaves.
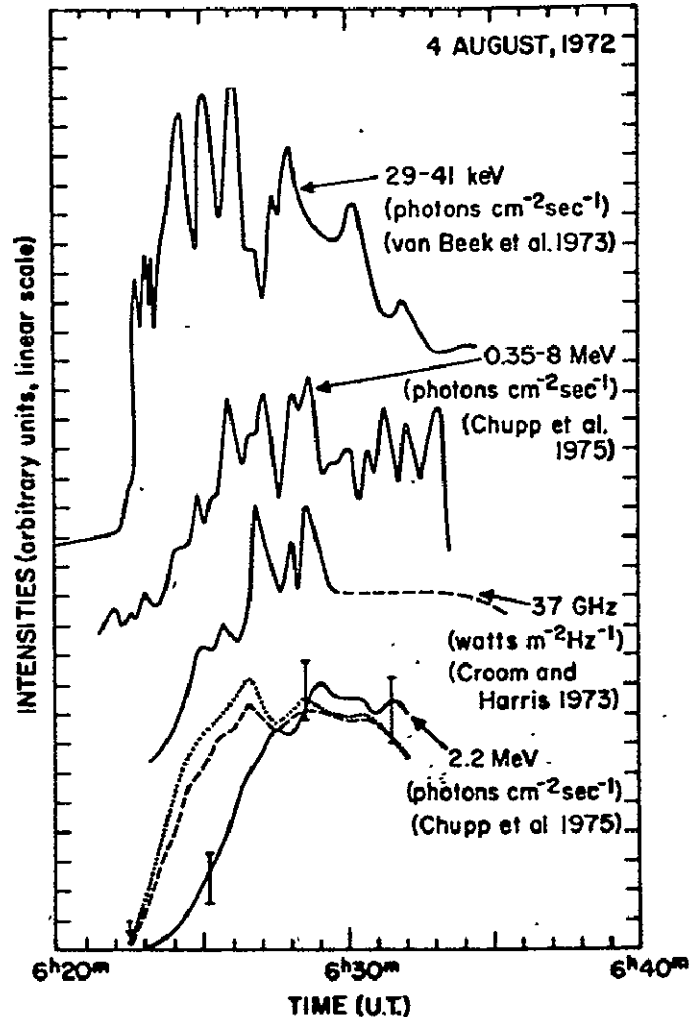
Figure 2. Time dependences of radiations of the 1972 August 4 flare from Bai and Ramaty (1976). The three upper lines are the measured time profiles of x-rays (29 to 41 keV), gamma rays (0.35 to 8 MeV), and microwaves (37 GHz). The error bars in the lower part of the figure represent the measured intensities of the 2.2 MeV line. The solid, dashed, and dotted lines are calculated time profiles of the 2.2 MeV line. The solid line is obtained by assuming that the instantaneous number of energetic nuclei in the flare region has the same time dependence as that of the observed 0.35 to 8 MeV gamma-rays. The dashed and dotted lines are obtained by assuming that the time dependence of the nuclei is the same as that of the 29 to 41 keV x-rays. For the solid and dotted lines we use a photospheric ^{3}He abundance ^{3}He/H = 5 X 10^{-5}, for the dashed line ^{3}He/H = 0.

The delayed onset of the second stage acceleration coincides with the onset of the type II radio burst. Type II bursts are produced by a shock wave travelling through the corona. Eventually these shock waves are observed by spacecraft near 1 A.U., where they are often observed to be locally accelerating ions up to the 1-10 MeV energy range.

Energy Spectrum

The spectrum of energetic particles in the 1972, August 4 flare has been estimated by comparing the calculated and observed ratios of the intensities of the 4.44 and 2.223 MeV lines (Ramaty and Lingenfelter, 1973; Ramaty et al., 1975), or of the total 4 to 8 MeV radiation and the 2.223 MeV line (Ramaty et al., 1977). Under the assumptions of a power law proton spectrum and a thick target, i.e., the protons are stopped by collisions in the medium, the accelerated proton spectrum is found to be

$$\frac{dN}{dE} = 1.3 \times 10^{36} \, E^{-2.7 \pm 0.2} \quad \text{protons/MeV}$$

For a thin target, i.e., where collision losses are assumed negligible, the spectral exponent would be -1.8 ± 0.2.

The gamma-ray ratios used above depend strongly on spectral parameters, but because they also depend on chemical abundances, the deduced spectrum is subject to uncertainties caused by possible deviations of the compositions of both the energetic particles and the ambient medium from standard photospheric abundances. A better determination of the spectrum of energetic particles could be obtained from the comparison of the intensities of lines that are produced from the same target nucleus, but whose production cross sections have markedly different energy dependences. Two such lines are at 0.847 MeV from ^{56}Fe and 1.434 MeV from ^{52}Cr, and, as can be seen from Figure 1, a high resolution spectrometer is needed for their detection above the continuum and to avoid blending. The ratio of the intensities of the 1.434 and 0.847 MeV

lines is shown in Figure 3 as a function of the spectral parameters of s and

E_c. These are defined such that the proton spectrum is proportional to E^{-s}

for $E > E_c$ and to a constant otherwise. Since the target nucleus for both

these lines is ^{56}Fe, they provide an excellent diagnostic of the proton spec-

trum, independent of elemental abundances. The ratio of the intensities of

the 15.11 and 4.44 MeV lines from ^{12}C gives a similar diagnostic of the ener-

getic proton spectrum in flares (Crannell et al. 1977).
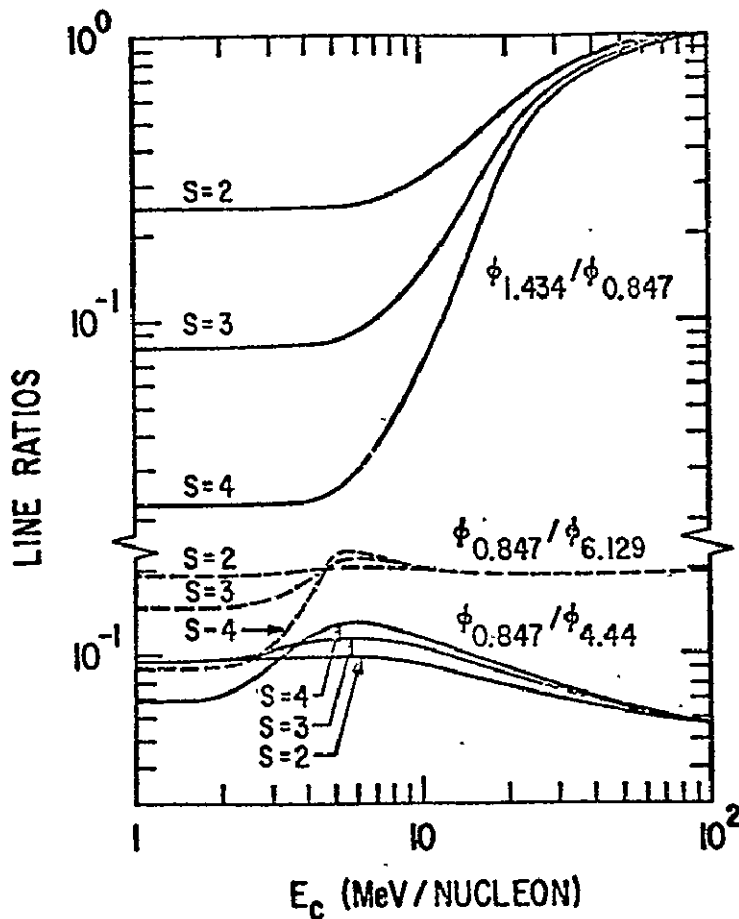
Figure 3. Line intensity ratios. The 0.847 MeV line is from deexcitation of the first excited state of ^{56}Fe, the 1.434 MeV line is from the deexcitation of ^{52}Cr, a spallation product of ^{56}Fe, and the 4.44 and 6.129 MeV lines are from ^{12}C and ^{16}O. The weak dependence of the 0.846 to 6.129 MeV line ratio upon the spectral index s and the cutoff energy E_c implies correspondingly good precision in abundance determination for Fe.

The number and spectrum of protons escaping from the sun can be obtained from direct spacecraft observations (Lin and Hudson, 1976). The angular and radial extent of the cone of field lines in the interplanetary medium filled with particles was estimated for the 4 August 1972 flare from observations on the Pioneer 9 and 10 plus near-earth observations from IMP-6 (Roelof et al., 1974) to be about 10^2 degrees and about 1.5 AU, respectively, giving a total volume of $V \sim 10^{40}$ cm^3. Then the total number is just

$$\frac{dN}{dE} \text{ (escape)} \doteq V \frac{dJ}{dE} \frac{4\pi}{v}$$

We find the integral number of escaping >10 MeV protons is $\sim 5 \times 10^{35}$ compared with a maximum of $\sim 10^{34}$ for the thick target interpretation, implying that most of the energetic protons either escaped to the interplanetary medium or were accelerated there. Furthermore, the spectrum of the energetic protons at 1 AU was approximately $\propto E^{-2}$ in the energy range $\sim 10-10^2$ MeV, closer to the think-target interpretation of the 4.43/2.23 MeV gamma-ray line ratio than the thick target. The observations therefore indicate that the gamma-rays originated in thin-target emission as the energetic protons escaped from the sun.

This would be consistent with shock wave acceleration of the protons in the upper corona, where escape would be relatively easy. The ionization state has been measured for low energy ≤ 1 MeV/nucleon O, N and Fe, ions from solar flares (Gloeckler et al., 1976). There measurements give ionization states typical of the 1-2 X 10^6 $^{\circ}$K corona rather than the $\sim 10^7$ $^{\circ}$K flare plasma, again consistent with acceleration in the corona.

Proton to Electron Ratio

The 4 to 8 MeV region, seen in Figure 1, was studied by Ramaty, Kozlovsky and Suri (1977), who showed that all the observed counts in this energy band from the August 4, 1972 flare are consistent with a pure nuclear

origin. This result has the important implication that the energetic proton to electron ratio at a given particle energy above a few MeV is quite high ($\gtrsim 100$), of the same order as in the galactic cosmic rays. The 1972 August 4 flare is the first astronomical object in which the proton-to-electron ratio has been determined inside the source region. This determination is of general importance for other astronomical sources such as supernovae, radio-galaxies, and quasars. The deduced p/e ratio for flares is an important parameter for acceleration theories (it is consistent with Fermi acceleration), and should be further explored with new gamma-ray data.

Chemical Composition

The ratio of protons to heavy nuclei for the accelerated particles can be studied by comparing the intensities of narrow lines from heavy nuclei in the ambient medium excited by protons to the broad continuum, which is due, in part, to excited heavy nuclei in the energetic particle population. For example, one of the persistent puzzles of the OSO-7 data has been the presence of a bump in the gamma-ray spectrum between 1 to 2 MeV (Suri et al, 1975). It is possible that this bump is due to an overabundance of the heavy nuclei (Mg, Si, Fe) in the solar energetic particles, and possibly also in the corona relative to the photosphere. But only high resolution observations can distinguish narrow lines from excited nuclei in the ambient medium from the broad continuum due to the deexcitation of accelerated heavy particles.

Directivity

An exciting objective of high resolution solar gamma-ray spectroscopy is the possibility for detecting the beaming of the energetic particles in the flare region. If the energetic particles have isotropic momentum distributions, the lines peak at the rest-frame transition energies, but if the particles stream appreciably, the lines shift in energy (e.g. the 6.13 MeV line, Ramaty

and Crannell, 1976); they may also become anomalously narrow (the 0.438 and

0.478 MeV lines, Kozlovsky and Ramaty, 1977), or they may exhibit a deep dip

at the line center (e.g. the 4.44 MeV line, Dyer, Chiang and Bodansky, 1977,

Ramaty et al., 1978). The continuum in the 4 to 8 MeV region is also strongly

affected by the directionality of the accelerated particles (Ramaty et al.,

1977). These effects, if present in the solar flare spectrum, should provide

valuable information on the flare mechanism. For example, significant beaming

of energetic protons is expected in the flare model of Colgate (1978), or if

energetic protons excite the white-light flare continuum (Najita and Orrall,

1970; Svestka, 1970).

^{3}He Rich Solar Cosmic Ray Events

A question of great interest for high energy solar physics is the

origin of the ^{3}He enrichments in energetic particle events (Garrard, Stone and

Vogt, 1973). The possibility that these enrichments originate in nuclear pro-

cesses (Ramaty and Kozlovsky, 1974; Colgate, Audouze and Fowler, 1977) could

be best tested by correlating ^{3}He-rich events with gamma-ray producing flares,

the 2.223 MeV line being the best candidate for monitoring the gamma rays. The

absense of gamma rays from ^{3}He-rich flares would support Fisk's (1978) model

for preferential ^{3}He heating by ion cyclotron waves.

Characteristics of the Positron Annililation Region

The temperature and density of the ambient medium in the positron

annihilation region can be determined by measuring the width of the 0.511 MeV

line, and the ratio of 2-photon to 3-photon positron annihilations. Since

the positrons are expected to be produced close to the flare site in the

chromosphere or lower corona, and since they probably annihilate close to

their production site, they may provide a measurement of the temperature and

density in the flare region.

The most important sources of positrons are radiative nuclei
(e.g. ^{11}C, ^{13}N, ^{14}O, and ^{15}O), the first excited state in oxygen,
$^{16}O^{*6.052}$, and π^+ mesons. The positrons are produced with initial energies
ranging from several hundreds. of keV to tens of MeV (depending on the pro-
duction mode), but if trapped by magnetic fields close to the sun, the
positrons can be slowed down to energies of tens of eV on time scales
less than $\sim10^2$ sec (if the ambient density is $\gtrsim10^{12}$ cm^{-3}). The positrons
then annihilate, either directly or from a bound positronium atom. The
latter annihilation mode dominates if the temperature is less than $\sim10^6K$
and the densitiy is $<10^{15}$ cm^{-3} (Crannell et al., 1976). In this case the
0.511 MeV line is accompanied by a characteristic 3-photon continuum at
energies just below 0.511 MeV.

The width of the 0.511 MeV line can depend on the state of ionization,
density and temperature of the ambient medium.(Crannell et al. 1975). In
a medium which is mostly neutral, the bulk of the positrons from positronium
in flight, in which case the width depends only on the density: it is about
5 keV if the density is less than about 10^{15} cm^{-3}, and decreases to about
3 keV if the density is higher. If, however, the ionization fraction of the
medium is higher than about 10%, the bulk of the positrons thermalize
before annihilation.__In this case, the width of the line is determined
by the temperature of the medium. At 10^5K the full width at half maximum
is about 3 keV, and it varies roughly as the square root of the temperature.
For partially ionized media of temperatures less than about 10^6K, positronium
formation has a higher probability than free annihilation and the 3-photon
continuum is formed as long as the density is less than about 10^{15} cm^{-3}

IV. The Flare Process

Gamma ray observations can provide fundamental information on the flare process. High sensitivity, high resolution measurments of the 2.2 MeV line prior to a flare should provide a straightforward test of the Elliott (1959) hypothesis that the basic energy source for flares is provided by protons slowly accelerated and accumulated in coronal storage regions. Observations during flares provide a measure of the total energy deposited in the solar atmosphere by accelerated protons. It is known from x-ray measurements that $\sim 10-10^2$ keV electrons may carry a substantial and possibly dominant fraction of the total energy released in a flare (Lin and Hudson, 1971, 1976). For the 4 August 1972 flare >10 MeV protons appear to carry only a small fraction of the energy in the $\sim 10-10^2$ keV electrons. However, there is some indication that for the 7 August flare approximately an order of magnitude more >10 MeV protons are accelerated (Wang and Ramaty, 1975). Thus the basic energy release mechanism in these flares may be the acceleration of particles.

Energetic particles may play a critical role in the transport of energy in a flare and in the production of other flare phenomena via their interactions with the ambient medium. White light continuum emission observed in very large flares has been attributed to heating of the photosphere by energetic protons (Najita and Orrall, 1970). Figure 4 shows the energy deposition into the solar atmosphere from energetic electrons and protons for the 4 August 1972 flare, computed under the assumption that the particles are accelerated high in the solar atmosphere and then precipitate downward. It is possible under this naive model to produce most of the observed flare phenomena, including the electromagnetic radiation, flare hot plasma production, and mass ejection and shock wave formation. For this flare the energetic protons appear to be less of a factor than the electrons; however they may play a major role in the 7 August 1972 flare.
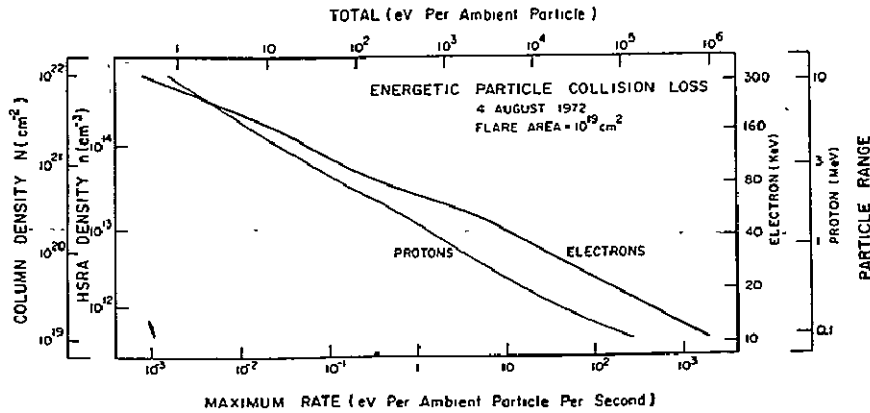
Figure 4. The energy deposited in the solar atmosphere by energetic electrons and protons in the 4 August 1972 large proton flare is plotted here as a function of column density for a flare area of 10^{19} cm^2 and for the thick target model (from Lin and Hudson, 1976). The rate of energy deposition per ambient particle is given by the lower scale and the total energy deposited (flare duration ~500 sec) by the upper scale. The particle ranges are shown on the right. Note that the energy deposition for protons is substantially less than for electrons to a column density of $<10^{21}$ cm^{-2}.

V. ₁ Abundances, Coronal Heating and Surface Nuclear Reactions

Heavy Elements

It is possible to determine the abundances of some heavy nuclei in the ambient medium of the gamma-ray emitting region (probably the corona). We show in Figure 3 the ratios of the intensities of the 0.847 MeV to the 4.44 and 6.129 MeV line intensities as functions of s and E_c. and normal photospheric abundances of C, O, and Fe. As can be seen, these ratios are almost independent of spectral parameters. Furthermore, since the 0.847 and 6.129 MeV lines are almost entirely due to ^{56}Fe and ^{16}O, respectively (spallation of ^{16}O contributes significantly to the 4.44 MeV line), the measurement of ϕ (0.847)/ ϕ (6.129) leads to a unique determination of the Fe to O ratio. Even if no restrictions are placed on the spectral parameters, the uncertainty in this deduction does not exceed a factor of 2. But the measurement of $\phi(1.434)/\phi$ (0.847),

for example, can considerably restrict s and E_c, and hence reduce the uncertainty in the deduced Fe/O ratio, to probably less than 50%. Implicit in this statement is the requirement for precise nuclear cross sections. Some of these are already available (e.g. Ramaty, Kozlovsky and Lingenfelter, 1978), while others will have to be measured in the laboratory.

Using similar techniques, high resolution gamma-ray spectroscopy can determine the abundances of Si, Mg and Ne. The determination of the Si and Mg abundances is quite straightforward because the characteristic lines of these nuclei are not much contaminated by spallation reactions of heavier nuclei. (The main other contributor to the 1.369 MeV line of ^{24}Mg is ^{28}Si, and ^{32}S contributes to the 1.779 MeV line of ^{28}Si.) But the determination of the Ne abundance is complicated by the 1.632 MeV line of ^{14}N, which cannot be resolved from the 1.634 MeV line of ^{20}Ne.

^{3}He Abundance

Non-radiative capture of neutrons by ^{3}He in the photosphere, a process whose cross sections exceeds that of radiative capture on H by four orders of magnitude, is an important neutron sink. But rather than hindering the observability of the neutron capture line, this process can place meaningful limits on the photospheric ^{3}He abundance. If the number and spectrum of the accelerated ions is determined from other lines, then the expected 2.2 MeV line strength can be calculated as a function of the photospheric ^{3}He abundance. The observed 2.2 MeV intensity then gives the ^{3}He abundance.

Quiet Time Observations

Finally, solar gamma ray observations should be carried out during quiet times. We estimate that if ~3 X 10^{-4} of the energy required to accelerate the solar wind is deposited in the corona by protons of energies greater than 10 MeV, then the sun would be a steady 2.2 MeV source with a flux of ~10^{-4} photons/ (cm^{2}sec) in a very narrow line at this energy. The detection of this radiation

would greatly clarify the mechanisms which heat the corona. Quiet time measurements would also determine the rate of nuclear reactions on the solar surface. By analyzing lunar soils, Fireman, Défelice and D'Amico (1976) have concluded that very large amounts of ^{14}C are produced at the sun and carried into the interplanetary medium by the solar wind. If this ^{14}C is due to nuclear reactions, then the implied steady state flux of 2.223 MeV gamma rays from the sun would exceed the peak flux in this line observed from the 1972 August 4 flare by an order of magnitude, or the above quiet time flux by 4 orders of magnitude. These are clear inconsistencies even with the present meager solar gamma-ray data, and hence their most likely implication is that not all the lunar ^{14}C is from the solar wind. But these results also point to the greatest potential of solar gamma-ray astronomy: future measurements will determine the nuclear reaction rate at the solar surface without the uncertainties that were inherent in this problem in the past when only charged particle observations near the earth were available.

VI. Flare Observations and Sensitivity

The solar flares which produce the largest energetic particle events, i.e. the events likely to produce intense gamma-ray emission, occur not at solar maximum but several years later on the descending phase of the solar cycle. Figure 6 shows the distribution over the past 3 solar cycles of flare events that caused ground-level increases (GLE) in the cosmic-ray counting rates of ionization chambers or neutron monitors. Ground level events are the highest energy and most intense solar cosmic ray acceleration events observed from the sun. Based on Figure 5 we expect to see ~2 truly major (GLE) flare events in one year of observation in the 1983-85 period. This estimate is based on ~60% duty cycle, and an equivalent duty cycle for observing energetic particles at 1 A.U. from a flare (due to particle propagation in the spiral interplanetary

magnetic field, energetic flare particles are generally only observed from Western hemisphere flares.) We note that there are no solar missions planned after the Solar Maximum Mission (expected lifetime 1980-1981) which can provide the long-term observing necessary for solar gamma-ray flare observations.
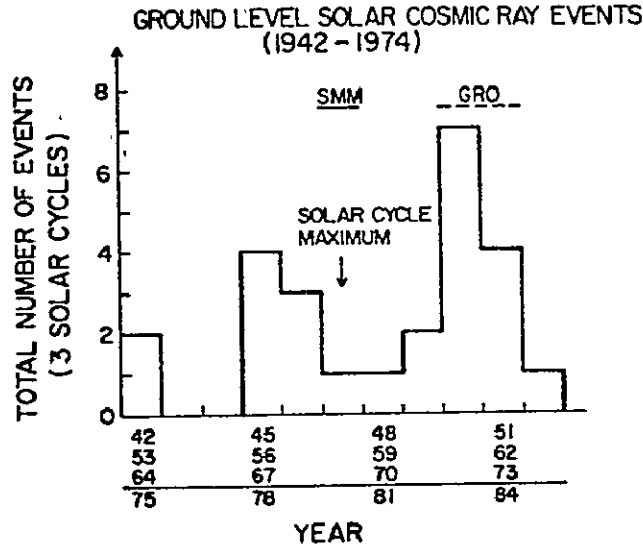
Figure 5. The occurrence of ground level solar cosmic ray events observed over the last three solar cycles, plotted versus year in the solar cycle (adapted from Pomerantz and Duggal, 1974).

With the next generation of gamma-ray instruments, it should be possible to achieve a 2.2 MeV line sensitivity for transient flare events of $\sim 10^{-3}$ the level of the 4 August 1972 event. By scaling the gamma-ray fluxes from the single previously observed gamma-ray event (August 4, 1972) by the observed energetic >10 MeV proton flux at 1 A.U., and using the energetic-particle event observations over the 1972-1974 period, we estimate that ~ 6 flare events/year could be detected in 1983-1985. Clearly, this estimate is highly speculative since it is based on only one gamma-ray observation. Analysis of the delayed gamma-ray line emission in the 7 August 1972 flare suggests that the prompt emission (not observed) was an order of magnitude higher than in the 7 August 1972 event (Wang and Ramaty, 1975), even though the energetic particle flux was

lower. Also, many flare events show high. He^3 abundance, suggesting that relatively more spallation had occurred than did in the 4 August 1972 event.

Acknowledgements

References

Bai, T. 1977, "Studies of solar hard x-rays and gamma rays: Compton backscatter, anistropy, polarization and evidence for two phases of acceleration", Ph.D. thesis, University of Maryland.

Bai, T. and Ramaty, R. 1976, Solar Physics, 49, 343.

Chupp, E. L., Forrest, D. J., Higbie, P. R., Suri, A. N., Tsai, C., and Dunphy, P. P. 1973, Nature, 241, 333.

Chupp, E. L., Forrest, D. J. and Suri, A. N. 1975 in S. Kane (ed.), "Solar γ, X and EUV radiations" IAU Symp. 68, 341.

Colgate, S. A., Audouze, J. and Fowler, W. A. 1977, Ap. J. 213, 849.

Crannell, C. J., Joyce, G., Ramaty, R. and Werntz, C. 1976, Ap. J. 210, 582.

Crannell, C. J., Ramaty, R., and Crannell, H. 1977, "Recent advances in gamma ray astronomy," European Space Agency, ESA SP 124, p. 213.

Dyer, P., Chiang, D. and Bodansky, D. 1977, Bull. Amer. Phys. Soc. 22, 583.

Elliott, H., 1959, in Solar Flares and Space Research (eds. C. deJager and Z. Svestja), North-Holland, p. 356.

Fisk, L. A. 1978, Ap. J. (to be published).

Fireman, E. L., Defelice, J. and D'Amico, J. 1976, Earth and Planetary Science Letters, 32, 185.

Frost, K. J. and Dennis, B, R. 1971, Astrophys. J. 165, 655.

Garrard, T. L., Stone, E. C., and Vogt, R. 1973, in R. Ramaty and R. G. Stone (eds.) "High energy phenomena on the sun", NASA SP-342, p. 341.

Gloeckler, G., Sciambi, R. K., Fan, C. Y., Hovestadt, D. 1976, Astrophys. J. 209, L93, 95.

Kozlovsky, B. and Ramaty, R. 1977, Astrophys. Letters, 19, 19

Lin, R. P. 1974, Space Sci. Revs. 16, 189.

Lin, R. P. and Hudson, H. S. 1976, Solar Physics, 50, 153.

Lin, R. P. and Hudson, H. S. 1971, Solar Phys. 17, 412.

Lingenfelter, R. E. and Ramaty, R., 1967, "High energy nuclear reactions in astrophysics," W. A. Benjamin, New York, p. 99.

Najita, K. and Orall, F. Q., 1970, Solar Phys. 15, 176.

Pomerantz, M. A., and Duggal, S. P. 1974, Rev. Geophys. and Space Phys., 12, 343.

Ramaty, R. and Crannell, C. J. 1976, Ap. J. 203, 766.

Ramaty, R. and Kozlovsky, B. 1974, Ap. J. 193, 729.

Ramaty, R., Kozlovsky, B. and Lingenfelter, R. E. 1975, Space Sci. Rev. 18, 341.

Ramaty, R. Kozlovsky, B. and Lingenfelter, R. E. 1978 (to be published).

Ramaty, R., Kozlovsky, B. and Suri, A. N. 1977, Ap. J. 214, 617.

Ramaty, R. and Lingenfelter, R. E. 1973, in R. Ramaty and R. G. Stone (eds.) "High energy phenomena on the sun" NASA SP-342, p. 301.

Roelof, E. C., Lezniak, J. A., Webber, W. R., McDonald, F. B., Teegarden, B. J., and Trainor, J. H. 1974, in D. E. Page (ed.) Correlated Interplanetary and Magnetospheric Observations, D. Reidel Publ., p.563.

Suri, A. N., Chupp, E. L., Forrest, D. J., and Reppin, C. 1975, Solar Physics 43, 415.

Svestka, Z. 1970, Solar Phys. 13, 471.

Wang, H. T. and Ramaty, R. 1974, Solar Physics 107, 1065.

Wang, H. T. and Ramaty, R. 1975, Ap. J. 202, 532.

DISCRETE GAMMA-RAY LINES FROM THE MOON

J. I. Trombka and C. J. Crannell
Laboratory for Astronomy and Solar Physics
NASA-Goddard Space Flight Center

L. E. Evans and M. J. Bielefeld
Computer Sciences Corporation
Silver Spring, MD 20910

A. E. Metzger
Jet Propulsion Laboratory

The γ rays emitted from the moon or any condensed object carry information on the composition of the surface layer and on the characteristics of the exciting flux. At energies below a few MeV, the major sources of γ-ray line emission from planetary bodies are the radioactive elements potassium, thorium, and uranium. The next most important source of line radiation results from bombardment of the surface by cosmic-ray particles. Both the primary and the secondary particles induce significant γ-ray emission by interactions with the abundant nuclear species: oxygen, magnesium, aluminum, calcium, silicon, titanium, and iron. In our lunar observations, more γ rays are produced by secondary neutrons than by primary cosmic rays. The processes include both inelastic scattering of fast neutrons and prompt capture of thermal neutrons. Discrete γ-ray line emission observed during the Apollo 15 and Apollo 16 missions was used to determine the abundances of the radioactive elements and the abundant nuclear species in the lunar surface. Iterative methods were employed for separating discrete γ-ray lines from continuous spectra. The lunar source spectrum was obtained from the observed spectrum by least-squares matrix inversion techniques with constraints. From the relative intensities of discrete lines resulting from different reactions in a particular nuclear species, variations in the neutron spectrum were mapped around the lunar surface. Spectral diagnostics were used to locate areas of significant depression in the thermal neutron flux associated with high rare-earth concentrations. The power of these analytic techniques has been verified by independent confirmation of our results based on the chemical analysis of returned moon rocks. The lunar investigations may now be regarded as the proving ground for methods of studying the characteristics of the energetic particle flux and the elemental composition of cosmic sources through γ-ray observations.

PLANETARY GAMMA-RAY SPECTROSCOPY

by

Robert C. Reedy

Los Alamos Scientific Laboratory

Los Alamos, NM   87545

ABSTRACT

The distribution of certain elements over a planet's surface specifies important constraints on models of its origin and evolution. The measured intensities of certain gamma rays of specific energies escaping from a planetary surface can be used to determine the abundances of a number of elements. The major sources of these gamma-ray lines are the decay of natural radionuclides, reactions induced by energetic galactic-cosmic-ray particles, the capture of low-energy neutrons, and solar-proton-induced radioactivities. The fluxes of the more intense gamma-ray lines emitted from 32 elements have been calculated using current nuclear data and existing models for the source processes. The source strengths for neutron-capture reactions have been modified from those previously used. The fluxes emitted from a surface of average lunar composition are reported for 292 gamma-ray lines. These theoretical fluxes have been used elsewhere to convert the data from the Apollo gamma-ray spectrometers to elemental abundances and can be used with measurements from future missions to map the concentrations of a number of elements over a planet's surface. Detection sensitivities for these elements are examined and applications of gamma-ray spectroscopy for future orbiters to Mars and other solar-system objects are discussed.

INTRODUCTION

Determining the chemical composition of a planet's surface is an essen-, tial part of the investigation of the planet. The abundances of certain elements with different condensation temperatures and with various types of geochemical behavior can provide valuable clues to a planet's origin and evolution (Anders, 1977). A planet's gross chemistry is established during its accretion from the solar nebula and certain elements are indicative of the nature of the early condensate, e.g., uranium (a refractory element in the early condensates), iron (condensed as metallic iron-nickel), and magnesium (the first silicate formed). Planetary processes, such as core and crust formation during differentiation and later magma formation and emplacement, greatly modify the distribution of the elements in the planet and produce the present crusted rocks. Geochemical clues to the evolution of a planet (Anders, 1977) include the supply of sulfur and metallic iron (formation of FeS), the ratio FeO/MnO (the oxidation of iron), the ratio K/U (remelting of the primordial condensates), and the ratio Tl/U (relative abundance of volatiles). Since many elements can be grouped according to their condensation and geochemical behavior, chemical abundance data for only a few key elements are needed to determine the origin and evolution of a planet.

The surface layers of most planets usually involve a regolith consisting of rock fragments and reworked materials, such as glasses. The extent to which regolith material has been transported away from its origin influences the chemistry of the surface layers of a planet. Transport mechanisms possible on various planets include volcanism, meteoroid impact (ballistic or flow processes), water and wind movement, and electrostatically charged particles in electric fields. The lateral movement of material into geologically different provinces can be detected by photogeology or chemical analyses.

Another source of foreign material is vertical mixing in regions with relatively thin layers of different composition. The composition of ejecta near a large crater often is different from that of the surface layer.

The chemical nature of a planetary surface can be determined from returned samples, by experimental instruments placed on the surface, or by remote-sensing experiments. Returned samples allow extensive analyses to be performed and surface instruments (on penetrators, rovers, or landers) can provide valuable data, but these results only apply to a localized region. Orbital experiments allow global surveys to be made of a planet's surface, and complement surface measurements (Haines et al., 1976).

Some orbital remote-sensing experiments, such as mass spectrometers and alpha-particle spectrometers, provide only a limited amount of information on surface chemistry. Measurements of the spectrum of albedo neutrons above a planet's surface can indicate the presence of hydrogen and the macroscopic properties for the transport of neutrons in the surface layers (Lingenfelter et al., 1961). The relative abundances of the major elements with atomic numbers up to about 20 can be.measured by X-ray fluorscence, using solar X-rays as the exciting source (Haines et al., 1976). Successful X-ray fluorescence experiments were flown on Apollos 15 and 16 (Adler et al., 1973). Orbital X-ray fluorescence is applicable only to planets with no atmosphere because X-rays have very. short mean free paths in matter. The relative reflectance in the wavelength region from 0.3 to 3.0 µm and absorption bands at certain wavelengths can be used to map several elements, such as titanium and iron, in a number of minerals. Earth-based multispectral measurements have been used to classify lunar regions on the basis of spectral type (McCord et al., 1976). The physical properties of the regolith, such as soil maturity, also affect the reflectance spectrum. The above two techniques can map the distribution of a few elements in the uppermost surface layers of a planet with good spatial resolution.

Gamma-ray lines emitted by various isotopes allow the abundances of many elements to be determined by gamma-ray spectroscopy. These gamma rays are produced in the top few tens of centimeters of the planet's surface and can be detected above planets with no or little atmosphere. The spatial resolution for an isotropic detector is fairly poor but can be improved by collimation of the detector (Haines et al., 1976) and by deconvolution techniques (Haines et al., 1978). The flux of gamma-ray lines from a planetary surface is low, so long counting times over a given region are required, especially if collimation is used. These four geochemical mapping techniques generally complement each other, and their inclusion on future planetary polar orbiters will provide valuable chemical data with which to study the planet's origin and evolution.

Gamma-Ray Spectroscopy

This paper discusses the applications of gamma-ray spectroscopy in mapping the distribution of certain elements in planetary surfaces. The fluxes of gamma-ray lines expected from the moon are given and used to examine the ability of orbital gamma-ray spectrometers to determine the concentrations of a number of elements in the surface of the moon, Mars, Mercury, asteroids, and comets. ——

Gamma-ray spectrometers were carried to the moon on Luna 10 and Apollos 15 and 16 and to Mars on the Soviet Mars-5. The Apollo spectrometers allowed the relative variations of the natural radioelements (K, U, and Th) and certain other elements (such as Fe) to be mapped on a relatively fine scale over 20% of the lunar surface (Arnold et al., 1977). The abundances of Th, K, Fe, Mg, and Ti were determined for a number of lunar regions overflown by the Apollo spectrometers by analyses of their gamma-ray spectra (Bielefeld et al., 1976).

The spectrometers flown on these missions used scintillator detectors made of NaI(Tl). Future planetary missions will probably use solid-state detectors of high-purity germanium, which allow greatly improved resolution of the detected gamma-ray lines (Metzger et al., 1975). Because of the poor resolution of NaI(Tl) detectors, only a few gamma-ray lines were actually observable in the Apollo lunar spectra. Since germanium detectors can distinguish between gamma-ray lines only a few keV in energy apart, they will detect many lines in the energy region of geochemical interest (0.2 to 10 MeV). To plan for such missions flying with high-resolution spectrometers, the fluxes expected for less intense gamma-ray lines (minor lines from major elements and major lines from minor elements) as well as those for strong lines must be calculated.

The fluxes of gamma-ray lines from the moon have been calculated by Gorenstein and Gursky (1970), Armstrong (1972), and Reedy et al. (1973). All three of these papers gave fluxes for only the strongest gamma-ray lines. This work is an extension of the calculations in Reedy et al. (1973), hereafter called RAT. It uses the same models as in RAT to determine source strengths for gamma-ray lines, although the absolute magnitude of the neutron-capture rate in the moon has been modified using recent experimental results. The spatial resolution of an isotropic spectrometer is given in RAT and the effects of collimation on detection sensitivities are discussed in Metzger et al. (1975). The procedure presented in RAT for unfolding the NaI(Tl) spectra has evolved to that described in Bielefeld et al. (1976). Other procedures for reducing the Apollo gamma-ray data have also been developed (Metzger et al., 1977; Arnold et al., 1977).

The first spectral unfolding of the Apollo gamma-ray data (Metzger et al., 1974) used the lunar gamma-ray line fluxes of RAT. It was found that the RAT library of fluxes was too small for good spectral unfolding (several

lines unaccounted for and other lines poorly fitted), so a greatly expanded library of gamma-ray line fluxes was calculated. This improved library was used by Bielefeld et al. (1976) in unfolding the Apollo spectra and resulted in better fits to the lunar data. It was also used by Metzger et al. (1977) in mapping lunar thorium via integral count rates in the 0.55-2.75 MeV energy band. Arnold et al. (1978) used this library to remove contributions of iron gamma rays from an energy band used to map titanium. The gamma-ray line fluxes used by Bielefeld et al. (1976), Metzger et al. (1977), and Arnold et al. (1978) are included here with only a few minor changes.

The major improvement in the gamma-ray line fluxes presented here is that more recent and better nuclear data were used in calculating the source strengths. In RAT, the energies of gamma-ray lines often were given only to the nearest 0.01 MeV and some lines several keV apart in energy were combined. Since germanium detectors have energy resolutions of several keV, the energies given here are as accurate as possible (usually to better than a keV) and only a very few lines with almost identical energies are combined. Many more gamma-ray lines were calculated for the major sources of lunar gamma rays (O, Mg, Al, Si, K, Ca, Ti, Fe, Th, and U) than were given in RAT. Also, gamma-ray line fluxes were calculated for 22 other elements, and any element likely to produce gamma-ray lines in planets, comets, or spacecraft was considered. The quality of the models used to calculate the fluxes and of the nuclear data (and hence of the calculated fluxes) is discussed. The fluxes are given for the average lunar chemical composition given in Table I; RAT used the Apollo 11 soil chemistry. These calculated gamma-ray line fluxes are used to discuss the ability of orbital gamma-ray spectroscopy to determine elemental abundances on future planetary missions.

CALCULATED FLUXES

The general procedure used to calculate the flux of gamma-ray lines from a planetary surface is that described in RAT, and depends on the gamma-ray source strength as a function of depth and on the mass attenuation coefficient for each gamma-ray energy. The calculated fluxes are for the photons which escape from a semi-infinite plane without undergoing any interactions. Four sources of gamma-ray lines are considered: decay of naturally occurring radionuclides, decay of solar-proton-induced radionuclides, reactions by energetic galactic-cosmic-ray (GCR) particles (nonelastic neutron scattering, proton spallation, and radionuclide production), and neutron-capture reactions. With a few exceptions, only gamma-ray lines with energies greater than about 0.2 MeV are considered here. For the gamma-ray fluxes tabulated below, the limit below which fluxes are not given was chosen so that the minimum fluxes for all major elements at their average lunar abundances were about the same.

Natural Radionuclides

The naturally occurring primordial radioactive nuclei (^{40}K, ^{138}La, ^{176}Lu, and the U and Th decay chains) were assumed to be uniformly distributed in the top few meters of the lunar surface. For each radionuclide, the half-life and the elemental atom abundance were 1.250 x 10^9 y and 0.0001167 (^{40}K), 1.35 x 10^{11} y and 0.00089 (^{138}La), 3.6 x 10^{10} y and 0.026 (^{176}Lu), 1.40 x 10^{10} y and 1 (^{232}Th), 7.04 x 10^8 y and 0.0072 (^{235}U), and 4.47 x 10^9 y and 0.9928 (^{238}U).

The parameters for ^{40}K, including the 0.1048 yield per ^{40}K disintegration for the 1.4608-MeV gamma-ray line from excited ^{40}Ar, are from Steiger and Jager (1977). The decay parameters for ^{138}La are from Pancholi and Martin (1976), and those for ^{176}Lu are from Horen and Harmatz (1976). Data for the 185.72 keV line of ^{235}U are from Schmorak (1977).

For gamma-ray lines produced by the daughters of ^{232}Th, recent measurements made by high-resolution gamma-ray spectrometers were evaluated to get energies and yields per disintegration of ^{232}Th. Beck (1972) reported absolute gamma-ray yields for the entire decay chain. Evaluated yields for the decay of ^{228}Ac were given by Horen (1976) and are adopted here. For the gamma rays emitted by the daughters of ^{228}Th, Heath (1974) and Avignone and Schmidt (1978) reported relative yields (which were normalized assuming a yield of 0.307 for the 583.1 keV line produced by the decay of ^{208}Tl). The relative yields for the decay of ^{208}Tl presented by Pakkanen et al. (1969) and by Larsen and Jorgensen (1969) were normalized using a 0.360 yield for the 2.6146-MeV gamma ray. I evaluated these data to get the yields used for the daughters of ^{228}Th.

For the ^{238}U decay chain, the energies and yields in recent evaluations were adopted. All the gamma-ray lines with energies above 200 keV are emitted in the decay of ^{214}Pb and ^{214}Bi (Toth, 1977b). The 1.0010-MeV line emitted by the decay of ^{234m}Pa has only a 0.6% yield and was not included. The only other ^{238}U daughter emitting a relatively strong gamma ray is ^{226}Ra, which produces a gamma ray at 186.0 keV in its alpha-particle decay to ^{222}Rn (Toth, 1977a).

Table II gives the energy, yield, decaying nuclide, and flux escaping the moon for each of the gamma-ray lines emitted by natural radionuclides. For the ^{238}U and ^{232}Th decay chains, only lines with yields above about 1% are given. (Results are given to lower yields for high-energy gamma rays since they can travel farther in matter.) Most of the yields used here probably have uncertainties of ± 5% or less. Under the assumption of a source uniform with depth, the only other parameters involved in calculating the flux escaping the moon are the source strength (determined from the half-life of the radionuclide) and the mass attenuation coefficient, both of which

are known quite well. The overall uncertainties in the fluxes of most gamma rays from natural radionuclides are about ± 10%. The yield of the 2.614-MeV gamma ray per decay of ^{232}Th is well known, and the uncertainty in its flux is about ± 5%.

Solar-Proton-Induced Radioactivity

About 90% of the nuclear particles emitted from the sun during strong solar flares are protons and these protons travel only a few centimeters in the lunar surface before they are stopped by ionization energy losses (Reedy and Arnold, 1972). Some of these solar protons induce reactions before they are stopped, producing several radionuclides which emit gamma-rays. Because of the relatively low energy of these solar protons, these product radionuclei are close in mass and charge to the target nucleus. Prompt gamma rays produced by solar protons will be extremely difficult to detect since the high proton flux incident on an actual detection system will saturate the spectrometer and charged-particle anti-coincidence circuits.

The lunar gamma-ray fluxes reported in RAT for solar-proton-induced radioactivities were for three different incident solar-proton spectral shapes (exponential-rigidity parameter, R_0, values of 50, 100, and 150 MV) and an omnidirectional proton flux above 10 MeV of 100 protons/cm^{2}s. As discussed in Reedy and Arnold (1972), the activity of any solar-proton-induced radionuclide at a given time depends on the solar-proton fluxes during the last few mean-lives of that nuclide. The gamma-ray fluxes reported here are those for solar-proton-induced radioactivities at the times of the Apollo 15 and Apollo 16 missions. The radionuclides considered are 7 x 10^5-year ^{26}Al, 2.6-year ^{22}Na, 303-day ^{54}Mn, and 78-day ^{56}Co; their activities were calculated using the model and cross sections of Reedy and Arnold (1972).

The activities of the short-lived radionuclides depend on the fluxes of solar protons since 1956. The evaluated solar-proton data of Reedy (1977)

were used to calculate the activity-versus-depth profiles for ^{22}Na, ^{54}Mn, and ^{56}Co. For the Apollo 11, 12, and 14 missions, the agreements between calculated and observed profiles were quite good (Reedy, 1977). There are no detailed depth-versus-activity profiles measured in samples from the Apollo 15 and 16 missions, so the profiles used to calculate gamma-ray fluxes were determined from the solar-proton fluxes of Reedy (1977). The solar-proton fluxes just previous to these missions were relatively low, so the induced ^{54}Mn and ^{56}Co activities were low and the uncertainties in their gamma-ray fluxes are large because the satellite solar-proton fluxes have not been confirmed by lunar sample measurements. Most of the ^{22}Na atoms present in the Apollo 15 and 16 samples were made before Apollo 14, so the measured lunar rock data insures that the activity-versus-depth profiles used here are probably good to within about ± 20%.

The half-life of ^{26}Al is so long that contemporary solar-flare activity has a negligible effect on the lunar radioactivity-versus-depth profile. The ^{26}Al data in Apollo 12 and 14 rocks were used to derive the average solar-proton flux over its mean life of 80 protons/cm^{2}s above 10 MeV with a spectral shape of R_0 = 100 MV (Whalen et al., 1972). The uncertainties in this average flux and in the excitation functions used to calculate the expected activities for monoelemental targets result in an overall uncertainty for ^{26}Al gamma-ray fluxes of about ± 20%.

Table III gives the gamma-ray fluxes for these solar-proton-produced radioactivities at the times of the Apollo 15 and 16 missions. Because of its long half-life, the ^{26}Al values will be applicable to future lunar missions. The August 1972 solar flares produced much ^{22}Na, and more recent flares will produce additional atoms of ^{22}Na, ^{54}Mn, and ^{56}Co, so the fluxes of these and other short-lived radionuclides will need to be calculated from solar-proton measurements before future orbiter missions. If a strong solar

flare occurs shortly before or during such a mission, activities of short-lived solar-proton-produced radionuclides, such as ^{56}Co and especially 16-day ^{48}V (made from titanium), will be very large, and their gamma-ray fluxes will be much larger than those reported here.

Solar-proton fluxes at other planets will vary depending on their distance from the sun (higher fluxes at Mercury, lower ones at Mars) and the positions of the planets in their orbit relative to the sun (since solar protons are not emitted isotropically from the sun, but travel out from the sun along specific magnetic field lines). Since solar protons are the least important of the four gamma-ray sources reported here, the inability to predict solar-proton-induced radioactivity fluxes for other planets won't be a serious limitation. Relative ratios of gamma-ray fluxes measured for radionuclides which are produced mainly from one target element, such as ^{48}V from titanium and ^{56}Co from iron, could be used to study the relative spatial distributions of such elements. The measured fluxes of other gamma-ray lines from the same target element could be used to convert these relative results to absolute abundances.

Energetic GCR Particle Reactions

The bombardment of the moon by the primary galactic cosmic rays (about 90% protons) produces many reactions and numerous secondary particles. Most secondary charged particles have low enough energies that they are stopped before they can induce a nuclear reaction, leaving neutrons as the major nuclear particle (Reedy and Arnold, 1972). Most of these secondary neutrons are produced with energies between 0.5 and 20 MeV, and can produce gamma-rays via nonelastic-scattering, $(n,x\gamma)$, reactions. These secondary neutrons also can be slowed by scattering in the moon and captured via (n,γ) reactions. The production of gamma rays by neutron-capture reactions is discussed in the next section. High-energy GCR particles also can produce gamma-rays, denoted

here as (p,xγ) reactions, and some gamma-ray-emitting radionuclides.

The model used for the fluxes of energetic GCR particles as a function of depth in the moon was that of Reedy and Arnold (1972). For radionuclides at various depths in lunar samples, the ratios of the measured activities to the calculated production rates usually are within 30% of unity. No systematic trends in these ratios were observed either as a function of depth in the moon (including near the surface where gamma-ray production is most important) or of the effective energy of the nuclear reaction involved (low-energy reactions usually produce the strongest fluxes of gamma rays). As described in RAT, the source strengths for gamma rays produced by energetic GCR particles were calculated using excitation functions for the relevant reactions and the Reedy-Arnold GCR fluxes. The sources and quality of the cross-section data are discussed below and the changes in the gamma-ray fluxes relative to those in RAT also are mentioned. A complete listing of references containing information on neutron reactions are given in CINDA (the Computer Index of Nuclear Data), issued periodically by the International Atomic Energy Agency, Vienna. Neutron cross section data are compiled for many reactions in Garber and Kinsey (1976) and Bormann et al. (1974). For gamma-ray-production cross-sections, the data measured at angles of about 55° or 125° with respect to the incident neutrons usually were used since these data are more typical of the values averaged over angle than those measured at other angles (such as 90°). Table IV gives the fluxes of gamma rays produced from the major elements (O, Mg, Al, Si, Ca, Ti, and Fe) by neutron nonelastic-scattering reactions and by the decay of GCR-produced radionuclides. The uncertainties given below should not be considered absolute, but are intended to indicate the relative quality of these fluxes. Low uncertainties were given to fluxes calculated with well-determined excitation functions for gamma-ray production, i.e., for cross sections measured with high resolution Ge(Li) (as opposed to NaI(Tl)) spectrometers, for cross

sections available at many different energies, and for good agreement among the excitation functions measured by different experiments.

The evaluated oxygen photon-production cross sections of Foster and Young (1972) and P. G. Young (private communication, 1975) were used for $(n,n\gamma)$, $(n,\alpha\gamma)$, and $(n,n\alpha\gamma)$ reactions. The cross sections used for the $^{16}O(n,p)^{16}N$ reaction were those in RAT. Relative to RAT, the gamma-ray fluxes from $(n,n\gamma)$ reactions are slightly lower, those from $(n,\alpha\gamma)$ reactions are up a factor of about 1.25, and that from the $(n,n\alpha\gamma)$ reaction up by 2.64. These new fluxes for oxygen gamma rays gave better fits to the Apollo data than those in RAT, especially for the $^{16}O(n,n\alpha\gamma)^{12}C$ line at 4.438 MeV (Bielefeld et al., 1976). The quality of the evaluated cross section data for oxygen is quite good, comparable to some of those used for radionuclides, and I would estimate the uncertainties in these fluxes as of the order of ± 20%.

The quality of the magnesium cross-section data is poor, especially for gamma rays other than the one at 1.3686 MeV, since there have been few high-resolution measurements made of $Mg(n,x\gamma)$ reactions. The evaluated cross sections of Drake and Fricke (1975) and P. G. Young (private communication, 1975) were used for the 1.3686-MeV gamma ray. The flux calculated for this line is 1.07 of that in RAT. The gamma-ray lines produced by the decay of ^{24}Na were calculated using the same cross sections as in RAT, and that from ^{22}Na decay was calculated using the cross sections of Reedy and Arnold (1972). The uncertainties in the above magnesium gamma-ray fluxes are estimated to be about ± 25%. The $(n,n\gamma)$ cross sections for other gamma rays from ^{24}Mg, ^{25}Mg, and ^{26}Mg were derived from various measurements below about 4.5 MeV and at 14-15 MeV. Their uncertainties are estimated to be of the order of ± 50%. Two gamma rays identified in NaI(Tl) spectra at about 6.2 and 7.2 MeV were not included here because of the uncertainties in their energies and because their fluxes are lower than those of the others reported here.

For aluminum (n,xγ) reactions, the evaluated cross sections of P. G. Young (private communication, 1975), based mainly on the measurements of Orphan and Hoot (1971), were used. The cross sections for ^{26}Al and ^{22}Na production were those of Reedy and Arnold (1972). The measurements of Bayhurst et al. (1975) were used for the ^{27}Al(n,α)^{24}Na reaction and the evaluated data of Young and Foster (1972) were adopted for the ^{27}Al(n,p)^{27}Mg reaction. The calculated gamma-ray fluxes are similar to those in RAT and their estimated uncertainties are about ± 25%.

The strongest silicon gamma-ray line is that at 1.7788 MeV via the ^{28}Si(n,nγ) reaction, and the measured cross sections of Dickens and Morgan (1974) and the evaluated ones of P. G. Young (private communication, 1975) were used. The cross sections used for other Si (n,xγ) reactions were based on the measurements of Dickens (1970) from 5.3 to 9.0 MeV, various other measurements, and evaluations of P. G. Young (private communication, 1975). The fluxes of the two strongest (n,nγ) gamma rays are 1.22 times greater than those in RAT. The same cross sections as were used for RAT were used for the production of ^{22}Na, ^{24}Na, and ^{26}Al. The evaluated cross sections of Bhat et al. (1973) were used for the ^{28}Si(n,p)^{28}Al reaction. The gamma-ray fluxes from the decay of these radionuclides are identical or very similar to those of RAT. The uncertainties in the fluxes for silicon gamma rays are estimated to be of the order of ± 30%, although that for the 1.7788-MeV gamma ray probably is less.

The calcium cross-section measurements of Dickens (1972) and Dickens et al. (1974) were used for the gamma rays at 3.7366 and 3.9044 MeV from ^{40}Ca (n,nγ) reactions and that at 0.7705 MeV from the ^{40}Ca(n,pγ) reaction. Cross sections for other Ca(n,xγ) reactions were based on the measurements of Dickens (1972) and miscellaneous other workers. In some NaI(Tl) spectra of calcium nonelastic-scattering gamma rays, there was a fairly strong peak at about 3.15 MeV, but only a number of weak peaks were observed near this energy

in Ge(Li) spectra. The ^{40}Ca(n,nγ) fluxes are about factors of 1.3 greater than those in RAT. The estimated uncertainties in these gamma-ray fluxes are about ± 40%.

The measured titanium gamma-ray-production cross sections of Dickens (1974) for 4.9-, 5.4-, and 5.9-MeV neutrons were used and extended to and beyond various measurements at about 14.5 MeV. For the production of ^{46}Sc, various measured cross sections for the ^{46}Ti(n,p) and ^{47}Ti(n,np) reactions (cf., Garber and Kinsey, 1976) and estimated cross sections for the ^{48}Ti(n,x) ^{46}Sc reaction were used. The flux of the 0.9834-MeV gamma ray reported in RAT was based only on estimated cross sections and was a factor of 1.85 lower than that calculated here. Because of the scarcity of measured cross sections for the Ti(n,xγ) and ^{48}Ti(n,x)^{46}Sc reactions, the gamma-ray fluxes reported here probably have uncertainties of the order of ± 50%.

The Fe(n,nγ) cross sections used were those of Orphan et al. (1975) and the cross sections for the production of ^{54}Mn were those of Reedy and Arnold (1972). The gamma-ray fluxes calculated here for these sources were very similar to those in RAT and their estimated uncertainties probably are about ± 25%. Cross sections for the production of gamma rays by ^{56}Fe(n,2nγ) reactions were measured by Korkal'chuk et al. (1975) and extended to higher energies using the ^{56}Fe(n,2n)^{55}Fe excitation function of Reedy and Arnold (1972). Fluxes for two gamma rays produced by ^{56}Fe(n,2nγ) reactions are included here and their uncertainties are estimated to be of the order of ± 40%.

Table V gives the fluxes of gamma rays produced from 16 other elements by neutron nonelastic-scattering reactions or by the decay of GCR-produced radionuclides. Generally, because of low elemental abundances, these gamma rays will not be detectable for small regions of a planet's surface, although some could be (such as nickel and sulfur on asteroids of chondritic composition or carbon in comets). Some of these gamma rays will be detectable with

long counting times for large regions of a planet (e.g., sodium, chromium, and manganese). The quality of the cross-section data is quite variable, ranging for different elements from very good to virtually non-existent.

The cross-section data for the $^{12}C(n,n\gamma)$ reaction producing the 4.4383-MeV gamma ray (Rogers et al., 1975) are very good, agreeing well with other measurements, and the flux uncertainty is about ± 20%. The cross-section data for $^{14}N(n,x\gamma)$ reactions of Rogers et al. (1975) are also of good quality and result in flux uncertainties of about ± 30%. The quality of the data of Morgan and Dickens (1976) for the 0.1971-MeV inelastic-scattering gamma ray of ^{19}F are about as good as those for nitrogen, while the quality for other prompt fluorine gamma rays are very poor, resulting in large uncertainties (of the order of a factor of two) in their gamma-ray fluxes. The cross sections used for $^{23}Na(n,n\gamma)$ reactions are based mainly on the measurements of Donati et al. (1977) and Dickens (1973), plus various ones near 14.5 MeV. The data for the $^{23}Na(n,2n)^{22}Na$ and $^{23}Na(n,\alpha)^{20}F$ are from Reedy and Arnold (1972) and from various sources (cf., Garber and Kinsey, 1976), respectively. The estimated uncertainties in the sodium gamma-ray fluxes are about ± 30%.

Kellie et al. (1973) was used for the $^{31}P(n,n\gamma)$ reactions and, since their data for iron agreed well with those adopted here, the data are probably of reasonably good quality (about ± 40% uncertainty). The data for the $^{32}S(n,n\gamma)$ reaction producing the 2.2301-MeV gamma ray are of poor quality (uncertainty of over ± 50%) and probably include cross sections for gamma rays produced by the decay of the 4.47-MeV level to the 2.23-MeV level of ^{32}S. The nonelastic-scattering gamma-ray fluxes for ^{35}Cl, ^{40}Ar, and ^{39}K are based on only a few measured cross sections and are of poor quality.

The scatter in the measured $^{52}Cr(n,n\gamma)$ and $^{55}Mn(n,n\gamma)$ cross sections is fairly large, and the resulting prompt gamma-ray fluxes are of poor quality. The evaluated data of Magurno and Takahashi (1975) for the $^{55}Mn(n,2n)^{54}Mn$

reaction is of fairly good quality. The data for the inelastic-scattering reactions with ^{58}Ni and ^{60}Ni from many sources are of good quality, and those for the ^{58}Ni(n,p)^{58}Co reactions are also very good.

For the ^{88}Sr(n,nγ) reaction, I know of only one cross section (at 14.4 MeV), so the uncertainty in its flux is large. There is a fair amount of spread in the data which exist for the ^{89}Y(n,nγ) reactions, and there are no measurements between 5 and 14 MeV. The ^{89}Y(n,2n)^{88}Y and ^{90}Zr(n,2n)^{89}Zr cross sections of Bayhurst et al. (1975) are of very good quality, but the decay of these products produces gamma rays from levels in ^{88}Sr and ^{89}Y, respectively, so these particular gamma rays, originating from reactions with two different elements, are less suitable for geochemical mapping. The data for the ^{90}Zr(n,nγ) gamma ray is of good quality, but the inelastic-scattering cross sections for the ^{92}Zr and ^{94}Zr nuclei are poorly known, being assumed equal to half of the measured values for 0.92-MeV gamma rays from natural zirconium. There exist no cross section data above 1.73 MeV for the ^{138}Ba(n,nγ) reaction, and the quality of the calculated gamma-ray flux is very poor. This 1.4359-MeV gamma ray is also made by the decay of the natural radionuclide ^{138}La.

Table VI gives fluxes of gamma rays produced by several high-energy reactions induced by GCR particles. The energies required to induce these spallation reactions are considerably above those for the (n,xγ) reactions considered above because several nucleons or alpha particles are removed from the target nucleus by these reactions. These reactions are denoted here as (p,xγ) since protons are more numerous than neutrons at these incident particle energies. These spallation reactions were not considered in RAT as a source of lunar gamma rays. A gamma-ray line in the Apollo spectra at 1.63 MeV can be explained and its flux reasonably well calculated by (p,xγ) reactions with Mg, Al, and Si producing the 1.6337-MeV excited level in ^{20}Ne

(cf., Bielefeld et al., 1976, and Metzger et al., 1977). The measurements of
Foley et al. (1962), Chang et al. (1974), and Artun et al. (1975) for the
bombardment of various targets with energetic protons show many $(p,x\gamma)$ gamma
rays. Their observations indicate that these reactions produce relatively
strong fluxes of gamma rays from the de-excitation of the first level of 4n
nuclei with even numbers of protons and neutrons and that most of these
strong gamma rays are from product nuclei which are equivalent to the target
nucleus minus one to three alpha particles.

In addition to the production of the ^{20}Ne line at 1.6337 MeV, other
strong spallation lines observed include 2.6133 MeV (^{20}Ne), 1.3686 MeV (^{24}Mg
from Al and Si), 2.2104 and 1.0144 MeV (^{27}Al from Si), 1.9704 (^{36}Ar from Ca),
and 1.4342 MeV (^{52}Cr from Fe). The ^{20}Ne line at 2.6133 MeV will interfere
with the detection of the thorium line at 2.6146 MeV. The only cross sec-
tions measured for this line were those of Foley et al. (1962), and result in
fairly high calculated lunar gamma-ray fluxes (equivalent to about 0.4 ppm of
thorium in the moon). The lunar gamma-ray data indicate that the flux of the
2.613-MeV line of ^{20}Ne is considerably lower than calculated and is equivalent
to about 0.1 ppm of Th or less (Metzger et al., 1977). The Foley et al.
(1962) cross section for the production of this line from magnesium is greater
than that for the 1.634-MeV line of ^{20}Ne, which is inconsistent since, in
^{20}Ne, a 1.634-MeV gamma ray is always emitted after a 2.613-MeV gamma ray.
For these reasons, the Foley et al. (1962) data for the 2.613-MeV line of
^{20}Ne were not used.

The scarcity of measured $(p,x\gamma)$ cross sections and the possible uncer-
tainties in the few measured data result in poor quality gamma-ray fluxes.
These spallation gamma rays generally are not suitable for elemental deter-
minations, but are given here as examples of interferences which can occur in
planetary gamma-ray spectra. The production of the 1.3686-MeV gamma-ray of

^{24}Mg by reactions with aluminum and silicon must be considered in determining magnesium abundances from this line, otherwise there will be an offset in these determined abundances. The low "ground truth" factors for magnesium of Bielefeld et al. (1976) could result from the presence of such spallation lines, although hopefully most of these (p,xγ) lines were removed in the data analysis.

Neutron Capture

Many of the neutrons in the lunar surface have energies below the thresholds for nonelastic-scattering reactions (i.e., below about 0.5 MeV), and, as these low-energy neutrons travel through the lunar surface, they scatter from nuclei until they either escape from the surface or are captured by a nucleus. Many gamma rays, including some with high energies, are produced by such neutron-capture reactions. The energy spectra of these low-energy neutrons in the moon and their capture rates were calculated as a function of chemical composition by Lingenfelter et al. (1972), hereafter called LCH. The various effects of chemical composition on neutron-capture gamma-ray fluxes are discussed in RAT.

The total neutron-capture rates used in RAT were based on computer printouts provided by R. E. Lingenfelter and E. H. Canfield (private communication, 1971) with the rates for the capture of neutrons with energies below 3 eV. The factor used in RAT to convert these rates to total neutron-capture rates was 1.77. This factor included nonelastic-scattering reactions in addition to (n,γ) reactions, and so resulted in an overestimation of the rates of lunar (n,γ) reactions. Detailed neutron fluxes in the moon as a function of depth and energy were provided by E. H. Canfield (private communication, 1973). Using neutron-capture cross sections which were inversely proportional to the neutron velocity ("1/v" cross sections) and these calculated neutron fluxes at a lunar depth of 4 g/cm^2, the ratio of the total

"1/v" capture rate to that for neutrons with energies below 3 eV was determined to be 1.31, which is 0.74 of the factor used in RAT.

The best measurement of the neutron density in the moon was made by the Apollo 17 Lunar Neutron Probe Experiment -LNPE- (Woolum and Burnett, 1974, and Woolum et al., 1975). From tracks produced by the $^{10}B(n,\alpha)$ and $^{235}U(n,f)$ reactions, the lunar fluxes of low-energy neutrons were determined and compared with the theoretical fluxes of LCH. Woolum et al. (1975) concluded that the actual lunar neutron density was 0.8 of that used by LCH.

To convert the Apollo 17 LNPE results to a solar-cycle average, Woolum and Burnett (1974) derived a solar-cycle correction factor based on neutron fluxes measured in the Earth's atmosphere and on neutron-monitor counting rates. Since the neutron-monitor counting rate was greater at the time of the Apollo 17 mission than that averaged over a solar cycle, the Apollo 17 flux of neutrons was estimated to be a factor of 1.21 greater than the average flux of neutrons (Woolum and Burnett, 1974). Using this neutron-monitor approach, I determined the solar-cycle correction factors for the Apollo 15 and 16 missions to be about 1.15 and 1.19, respectively. A factor of 1.17 was adopted for the increase in the lunar neutron fluxes observed by the Apollo Gamma Ray Spectrometer Experiment relative to the solar-cycle-averaged flux.

The lunar neutron-capture gamma-ray fluxes calculated here are those applicable at the times of the Apollo experiments. These fluxes will need to be modified for future missions using solar-cycle correction factors determined during those missions. To convert RAT neutron-capture gamma-ray fluxes to those relevant for the Apollo experiments, the above three factors (0.74, 0.8, 1.17) must be multiplied to get the final conversion factor, 0.69.

Because the neutron fluxes at the times of the Apollo 15, 16, and 17 missions were very similar, the Apollo 17 LNPE neutron-capture rates can be used directly to determine a correction factor for those used in RAT. At a

lunar depth of 150 g/cm^2, the measured ^{10}B capture rate in the LNPE (Woolum et al., 1975) was 467 ± 74 captures/s g(^{10}B) and that calculated by the capture rates used in RAT was 719. Thus the LNPE neutron-capture rates were 0.65 ± 0.10 of those used in RAT. A value of 0.67, the average of this factor and the 0.69 factor calculated above, was adopted to convert the neutron-capture rates used in RAT to those applicable to the Apollo gamma-ray data. Some of the neutron-capture rates used in these calculations (in units of captures/g s) for various lunar depths (in units of g/cm^2) were (0.00131,0), (0.00255,5), (0.00367,10), (0.00579,20), (0.00962,40), and (0.01437,70). The fraction of the neutrons captured by each element is given in Table I.

The neutron-capture gamma-ray fluxes reported in RAT were those calculated for the chemical composition of the Apollo 11 soil. This composition is not typical of the average lunar composition given in Table I, especially in its neutron-capture properties. The effective 1/v cross section for a given composition is $\Sigma_{eff} = N_0 \Sigma(f_i\sigma_i/A_i)$, where N_0 is Avogadro's Number, f_i is the weight fraction of element i, A_i is its atomic weight, σ_i is its effective 1/v capture cross section (cf., LCH; for major elements, σ_i is just its thermal cross section), and the sum is over all elements. For the average lunar and the Apollo 11 chemical compositions, the Σ_{eff} values are about 0.0066 and 0.0098 cm^2/g, respectively. The neutron-capture gamma-ray fluxes for a given element vary with Σ_{eff}, the ratio of the fluxes for a given chemical composition to those for the average lunar composition being denoted the "chemical correction factor" (CCF). For 1/v - capturing nuclides, CCF is about 0.01237 $(\Sigma_{eff})^{-0.876}$. Chemical correction factors calculated with this formula give values very similar to those given in RAT for several chemistries. A CCF factor of 1.40 should be used to convert the neutron-capture fluxes for an Apollo 11 chemistry to those for an average lunar chemistry.

The flux of a neutron-capture gamma ray for a given element depends on the gamma-ray's energy (which determines its mass attenuation coefficient), its yield per capture in that element, and the elemental neutron-capture rate. For all the elements reported here, the yields per capture were assumed to be those determined for the capture of thermal neutrons. The cross sections for the capture of thermal neutrons by these elements were taken from the evaluations of Mughabghab and Garber (1973). The capture cross section used for silicon in RAT was 10% higher than that used here. The yields per thermal capture were evaluated from literature data and the references used for my evaluations are cited below. Table VII gives the calculated fluxes of neutron-capture gamma rays produced by reactions with the major elements in the moon. The lowest fluxes given for each element were selected so that their values for an average lunar chemistry were about the same.

The magnesium neutron-capture yields of Spilling et al. (1967) are in very good agreement with other measurements. The aluminum measured yields of Nichol et al. (1969) and Ishaq et al. (1972) were emphasized in determining the evaluated yields. The three sources mentioned in Bhat et al. (1973) for silicon were used in getting the yields. The calcium yields of Arnell et al. (1969) are the bases of the yields adopted here. For titanium, emphasis was placed on the yields of Tripathi et al. (1969). The iron yields used in RAT were modified slightly using various other measurements. The agreement among the few measurements of iron's neutron-capture yields is good.

The quality of these neutron-capture yields for the major elements is quite good. Neutron-capture gamma rays were used to determine iron and titanium abundances from the Apollo data and the ground truth factors for these elements in Bielefeld et al. (1976) varied about unity by only ± 20% or less. These ground truth factors indicate that the neutron-capture gamma-ray fluxes probably are accurate.

Table VIII gives neutron-capture gamma-ray fluxes for 15 other elements. The quality of the data for neutron-capture yields varied from very good to very poor, but only when the data is not good is there a comment. Neutron capture by hydrogen always results in a 2.2233-MeV gamma ray, the only gamma ray produced by hydrogen. Carbon, oxygen, and fluorine have very low (n,γ) cross sections and are not included here. The energies and neutron-capture yields given in Ajzenberg-Selove (1976) were used for ^{14}N. For sodium, the yields of Nichol et al. (1969) were emphasized in my evaluation. Phosphorus has a relatively low capture cross section and no gamma rays with high yields. The sulfur gamma-ray yields essentially were those of Egri et al. (1969). For chlorine, which has a high capture cross section, about six sources, cited in Spits and Kopecky (1976), were used to derive the yields adopted here. The yields for potassium were similar to those measured by Op den Kamp et al. (1972). There is only fair agreement among the yield data for chromium and nickel and various sources were used to get the yields used here. The yield data of Mellema and Postma (1970) were used for the prompt neutron-capture gamma rays of manganese. There are large spreads among the yields measured for strontium and yttrium. There is fairly good agreement among the reported yields for the capture gamma rays of neodymium and the decay gamma rays of ^{152g}Eu. The spreads among the yields given for samarium and gadolinium capture gamma rays were considerable.

DISCUSSION

These fluxes for gamma rays from the moon should include all the gamma rays likely to be seen on any future gamma-ray-spectroscopy mission to various planets, asteroids, or comets. Since the fluxes of nuclear particles in a spacecraft are similar to those used here, these gamma-ray fluxes also can be used to estimate backgrounds from materials in a spacecraft. The most intense

gamma ray emitted from the moon for each element is given in Table I. Fig. 1 shows the fluxes of the lunar gamma rays as a function of energy.

An earlier version of this library of lunar gamma-ray fluxes, similar to the one given here, was used by Bielefeld et al. (1976) in unfolding the Apollo gamma-ray data. The only gamma-ray line in the Apollo spectra which was not fitted reasonably well by this library was one at about 2.2 MeV and it probably was produced via the capture of lunar-albedo neutrons by hydrogen in matter around the detector. Another preliminary version of this library was used by Metzger et al. (1975) in determining detection thresholds as a function of counting time for high-resolution detectors in orbit about the moon and Mars. Haines et al. (1976) discuss a large number of geochemical questions, such as the presence of volatiles at the lunar poles, which can be addressed by future gamma-ray-spectroscopy missions.

Several relatively strong gamma rays from different elements have energies similar enough that even a high-resolution detector could not resolve them. There are neutron-capture lines from Ca and Ti at energies of 6.420 and 6.419 MeV, respectively. The interference between the ^{208}Tl line at 2.6146 MeV and the (p,xγ) line of ^{20}Ne at 2.6133 MeV was mentioned above, but it should be a problem only for very low abundances of thorium (Metzger et al., 1977). Another example is the lines from Fe (0.8467), Al (0.8438), and Th (0.8402). Various gamma rays from the decay of uranium and thorium have energies close to those from other elements: e.g., 1.3777 MeV (U) and the ^{48}Ti(n,γ) line at 1.3815 MeV; 0.7684 (U), 0.7721 (Th), and the ^{40}Ca(n,pγ) line at 0.7705 MeV; 1.2381 (U) and the ^{56}Fe(n,nγ) line at 1.2383 MeV; 1.5092 (U) and the ^{89}Y(n,nγ) line at 1.5074 MeV; 1.4080 (U) and the ^{152g}Eu decay line at 1.409 MeV; and 0.7859 (U) and the ^{138}La decay line at 0.7887 MeV.

In a number of cases, the same gamma-ray line can be produced by reactions with several different elements. Many of the (p,xγ) reactions dis-

cussed above can produce gamma rays which also can be made by inelastic-scattering reactions. Such $(p, x\gamma)$ gamma rays will be a serious problem in analyzing for minor elements whose major isotope is one to three "alpha particles" away from a major nuclide, e.g., the ^{32}S line at 2.2301 MeV made from ^{40}Ca and the ^{52}Cr line at 1.4342 being made from ^{56}Fe. Since the fluxes for the spallation gamma rays are not well determined, it will be hard to correct for the spallation contributions to these inelastic-scattering gamma rays for minor elements. The relative variations in the abundance of a minor element could be mapped by comparing changes in the nonelastic-scattering gamma-ray fluxes for the minor element's gamma rays relative to those for the major element's gamma rays. Most neutron-capture gamma rays are not produced by nuclear reactions with other elements, so such gamma rays should be free of interferences. A few radionuclides made from various elements will produce gamma rays which are also made by inelastic-scattering reactions in a different element. The decay of ^{24}Na (made readily from Al or Si) produces the 1.3686- and 2.7539-MeV gamma rays of ^{24}Mg.

The $^{16}O(n, n\alpha\gamma)$ reaction produces a strong flux of the 4.4383-MeV gamma ray from ^{12}C. An oxygen abundance of 5.83% produces the same flux of this gamma ray as a 1.00% abundance of carbon. Since oxygen is usually in most planetary surfaces with abundances of about 40 - 45%, the detection of carbon via this line will be difficult. Most of the excited levels in ^{12}C decay by the emission of three alpha particles. The level at 15.110 MeV is one of the few levels in ^{12}C which decays by gamma-ray emission, mainly decaying to the ground state. Cross sections for the production of this 15.110-MeV gamma ray have not been measured, so its flux can't be calculated. Another possible way to map carbon in a planet is to compare the flux of the 4.4383-MeV gamma ray with the fluxes for other oxygen gamma rays.

For an element, its most intense gamma ray emitted from a planetary surface generally is the best one for determining its abundance. However, 11 of the 32 most intense elemental gamma rays listed in Table I have interferences strong enough either to hamper or to make impossible the use of that gamma ray for elemental determinations. Several interferences were discussed above. Sodium, sulfur, and chromium have spallation interferences from $(p,x\gamma)$ reactions with major elements; neutron-capture gamma rays from ^{23}Na (6.395 MeV), ^{32}S (5.424 MeV), and ^{53}Cr (8.884 MeV) are strong lines from these elements which are suitable for determining their abundances. For manganese, its neutron-capture gamma ray at 7.244 MeV is free of interferences. Yttrium and europium can be studied using the ^{89}Y$(n,n\gamma)$ gamma ray at 1.7445 MeV and the ^{152g}Eu decay gamma ray at 1.113 MeV, respectively. The ^{138}Ba$(n,n\gamma)$ reaction produces the same gamma ray as made in the decay of ^{138}La and the other ^{138}La gamma ray is close in energy to one from uranium, so studies of these two elements will be difficult using gamma rays.

Mars is different enough from the moon that the emission of gamma rays from its surface should be discussed. Metzger and Arnold (1970) discussed the general aspects of martian gamma-ray spectroscopy, including atmospheric attenuation of gamma rays and spatial resolution. The presence of about 1% ^{40}Ar in the martian atmosphere will produce a flux of 1.4608-MeV gamma rays which is comparable to the flux from the decay of ^{40}K in approximately 100 ppm of K in the martian surface. Thus martian atmospheric argon will not seriously interfere with the detection of ^{40}K.

The presence of about 0.7% hydrogen in the martian surface would increase the thermal-neutron flux near the surface and decrease the neutron leakage from the surface (Lingenfelter et al., 1961) and would result in a neutron-capture chemical correction factor of approximately two (cf., discussion in RAT about the effects of hydrogen on neutron-capture gamma-ray fluxes); hence

neutron-capture gamma-ray fluxes will be enhanced. If chlorine is present in the martian surface at the about 0.7% abundance reported by the Viking landers (Toulmin et al., 1977), its neutron-capture gamma rays will have fairly high fluxes. Similarly, the hydrogen line at 2.2233 MeV will be observable if the surface contains clay minerals like those used by Toulmin et al. (1977) to match the Viking lander chemical analyses or if it contains appreciable amounts of water.

Gamma-ray spectroscopy, especially from orbiters, is an excellent technique to map the distributions of a number of elements in a planetary surface. It is able to detect most major elements and several minor elements, including the natural radionuclides K, U, and Th, which are important sources of heat in a planetary interior. The spatial resolution possible with gamma-ray spectrometers is relatively poor, though more than adequate for the detailed study of a planet. Gamma rays can be used for the determination of elemental abundances in the moon, Mars, Mercury, asteroids, and comets. Hopefully, high-resolution gamma-ray spectrometers soon will be flown on missions to these interesting planets and solar-system objects.

ACKNOWLEDGMENTS

REFERENCES

Adler I., Trombka J. I., Lowman P., Schmadebeck R., Blodget H., Eller E., Yin L., Lamothe R., Osswald G., Gerard J., Gorenstein P., Bjorkholm P., Gursky H., Harris B., Arnold J., Metzger A., and Reedy R. (1973) Apollo 15 and 16 results of the integrated geochemical experiment. The Moon 7, 487-504.

Ajzenberg-Selove F. (1976) Energy levels of light nuclei A = 13-15. Nucl. Phys. A268, 1-204.

Anders E. (1977) Chemical compositions of the moon, Earth, and eucrite parent body. Phil. Trans. R. Soc. Lond. A285, 23-40.

Armstrong T. W. (1972) Calculation of the lunar photon albedo from galactic and solar proton bombardment. J. Geophys. Res. 77, 524-536.

Arnell S. E., Hardell R., Skeppstedt O., and Wallander E. (1969) Gamma rays from thermal neutron capture in ^{40}Ca, ^{42}Ca, ^{43}Ca, ^{44}Ca and ^{48}Ca. In Neutron Capture Gamma-ray Spectroscopy, p. 231-255. International Atomic Energy Agency, Vienna.

Arnold, J. R., Davis, P. A., and Reedy R. C. (1978) Gamma ray maps of lunar titanium and iron (abstract). In Lunar and Planetary Science IX, p. 25-26. The Lunar and Planetary Institute, Houston.

Arnold J. R., Metzger A. E., and Reedy R. C. (1977) Computer-generated maps of lunar composition from gamma-ray data. Proc. Lunar Sci. Conf. 8th, p. 945-948.

Artun O., Cassagnon Y., Legrain R., Lisbona N., Roussel L., Alard J. P., Baldit A., Costilhes J. P., Fargeix J., Roche G., and Tamain J. C. (1975) Multinucleon removal induced by high-energy protons. Phys. Rev. Lett. 35, 773-775.

Avignone F. T. and Schmidt A. G. (1978) γ-ray and internal-conversion intensity studies of transitions in the decay of ^{228}Th. Phys. Rev. C 17, 380-384.

Bayhurst B. P., Gilmore J. S., Prestwood R. J., Wilhelmy J. B., Jarmie N., Erkkila B. H., and Hardekopf R. A. (1975) Cross sections for (n,xn) reactions between 7.5 and 28 MeV. Phys. Rev. C 12, 451-467.

Beck Harold L. (1972) Absolute intensities of gamma rays from the decay of ^{238}U and ^{232}Th. AEC report number HASL-262. 14 pp.

Bhat M. R., Goldberg M. D., Kinsey R. R., Prince A., and Takahashi H. (1973) Neutron and gamma ray production cross sections for silicon. AEC report BNL-50379. 52 pp.

Bielefeld M. J., Reedy R. C., Metzger A. E., Trombka J. I., and Arnold J. R. (1976) Surface chemistry of selected lunar regions. Proc. Lunar Sci. Conf. 7th p. 2661-2676.

Bormann M., Neuert H., and Scobel W. (1974) Tables and graphs of cross-sections for (n,p), (n,α), and (n,2n) reactions in the neutron energy region 1-37 MeV. In Handbook on Nuclear Activation Cross-Sections, p. 87-272. International Atomic Energy Agency, Vienna.

Chang. C. C., Wall N. S., and Fraenkel Z. (1974) Gamma rays observed from 100-MeV protons interacting with ^{56}Fe and ^{58}Ni. Phys. Rev. Lett. 33. 1493-1496.

Dickens J. K. (1970) $^{28-30}$Si(n,xγ) reactions for $5.3 \leqslant E_n \leqslant 9.0$ MeV. Phys. Rev. C 2, 990-1005.

Dickens J. K. (1972) Neutron induced gamma-ray reactions in calcium in the energy range $4.85 \leqslant E_n \leqslant 8.05$ MeV. Nucl. Sci. Eng. 48, 78-86.

Dickens J. K. (1973) The neutron-induced gamma-ray reactions in sodium-23 in the energy range $4.85 \leqslant E_n \leqslant 7.5$ MeV. Nucl. Sci. Eng. 50, 98-107.

Dickens J. K. (1974) Neutron-induced gamma-ray production in titanium for incident-neutron energies of 4.9, 5.4, and 5.9 MeV. Nucl. Sci. Eng. 54, 191-196.

Dickens J. K., Love T. A., and Morgan G. L. (1974) Neutron-induced gamma-ray production in calcium in the energy range $0.7 \leqslant E_n \leqslant 20$ MeV. Nucl. Sci. Eng. 53, 277-284.

Dickens J. K. and Morgan G. L. (1974) $^{28}Si(n,n'\gamma)$ photon production cross sections for $E_\gamma = 1.78$ MeV, $5.0 \leqslant E_n \leqslant 9.5$ MeV. Phys. Rev. C 10, 958-960.

Donati D. R., Mathur S. C., Sheldon E., Barnes F. K., Beghian L. E., Harihar P., Kegel G. H. R., and Schier W. A. (1977) Cross sections, angular distributions, and magnetic substate populations in the $^{23}Na(n,n'\gamma)$ reaction. Phys. Rev. C 16, 939-957.

Drake M. K. and Fricke M. P. (1975) Evaluation of neutron and photon-production cross sections for natural magnesium. DNA 3479F. 86 pp.

Egri Sh., Kardon B., Poch L., Sheresh Z., and Zamori Z. (1969) Spectrum of γ rays produced during thermal neutron capture by sulfur nuclei. Izv. Akad. Nauk SSSR, Ser. Fiz. 33, 1259-1262 (In Russian).

Foley K. J., Clegg A. B., and Salmon G. L. (1962) Gamma-radiation from the medium energy proton bombardment of sodium, magnesium, aluminium, silicon, phosphorus and sulfur. Nucl. Phys. 37, 23-44.

Foster D. G. and Young P. G. (1972) A preliminary evaluation of the neutron and photon-production cross sections of oxygen. AEC report LA-4780. 30 pp.

Garber D. I. and Kinsey R. R. (1976) Neutron cross sections volume II, curves. ERDA report number BNL 325, Third Edition, Volume II. 489 pp.

Gorenstein P. and Gursky H. (1970) Characteristic γ- and X-radiation in the planetary system. Space Sci. Rev. 10, 770-829.

Haines E. L., Arnold J. R., and Metzger A. E. (1976) Chemical mapping of planetary surfaces. IEEE Trans. Geosci. Electronics GE-14, 141-153.

Haines, E. L., Etchegaray-Ramirez M. I., and Metzger A. E. (1978) Thorium concentrations in the lunar surface II: Deconvolution modeling and its application to the regions of Aristarchus and Mare Smythii. Proc. Lunar Planet. Sci. Conf. 9th. This volume.

Heath R. L. (1974) Gamma-ray spectrum catalogue: Ge(Li) and Si(Li) spectrometry. AEC report number ANCR-1000-2. Volume 2. (numbered in sections).

Horen D. J. (1976) Nuclear data sheets for A = 228. Nucl. Data Sheets 17, 367-390.

Horen D. J. and Harmatz B. (1976) Nuclear data sheets for A = 176. Nucl. Data Sheets 19, 383-444.

Ishaq A. F. M., Colenbrander A. H., and Kennett T. J. (1972) Study of thermal neutron capture in aluminum. Can. J. Phys. 50, 2845-2855.

Kellie J. D., Islam M. N., and Crawford G. I. (1973) Inelastic neutron scattering by ^{56}Fe and ^{31}P in the energy range 0.8 to 9.0 MeV. Nucl. Phys. A208, 525-544.

Korkal'chuk V., Prokopets G. A., and Holmqvist B. (1975) Interaction of 16-22-MeV neutrons with iron nuclei. Sov. J. Nucl. Phys. 20, 574-578.

Larsen J. S. and Jorgensen B. C. (1969) The decay of ^{208}Tl. Gamma-ray measurement. Z. Physik 227, 65-70.

Lingenfelter R. E., Canfield E. H., and Hess W. N. (1961) The lunar neutron flux. J. Geophys. Res. 66, 2665-2671.

Lingenfelter R. E., Canfield E. H., and Hampel V. E. (1972) The lunar neutron flux revisited. Earth Planet. Sci. Lett. 16, 355-369.

Magurno B. A. and Takahashi H. (1975) Evaluation of the ^{55}Mn(n,2n)^{54}Mn cross section for ENDF/B-IV. In ENDF/B-IV Dosimetry File (B. A. Magurno, Ed.), p. 70-79. Brookhaven National Laboratory, Upton.

McCord T. B., Pieters C., and Feierberg M. A. (1976) Multispectral mapping of the lunar surface using ground-based telescopes. Icarus 29, 1-34.

Mellema J. and Postma H. (1970) Investigation of nuclear level spins of ^{56}Mn by means of nuclear orientation. Nucl. Phys. A154, 385-406.

Metzger A. E. and Arnold J. R. (1970) Gamma ray spectroscopic measurements of Mars. Applied Optics 9, 1289-1303.

Metzger, A. E., Haines E. L., Parker R. E., and Radocinski R. G. (1977) Thorium concentrations in the lunar surface. I: Regional values and crustal content. Proc. Lunar Sci. Conf. 8th, p. 949-999.

Metzger A. E., Parker R. H., Arnold J. R., Reedy R. C., and Trombka J. I. (1975) Preliminary design and performance of an advanced gamma-ray spectrometer for future orbiter missions. Proc. Lunar Sci. Conf. 6th, p. 2769-2784.

Metzger, A. E., Trombka J. I., Reedy R. C., and Arnold J. R. (1974) Element concentrations from lunar orbital gamma-ray measurements. Proc. Lunar Sci. Conf. 5th, p. 1067-1078

Morgan G. L. and Dickens J. K. (1976) Production of low-energy gamma rays by neutron interactions with fluorine for incident neutron energies between 0.1 and 20 MeV. Nucl. Sci. Eng. 60, 36-43.

Mughabghab S. F. and Garber D. I. (1973) Neutron cross sections volume I, resonance parameters. AEC report number BNL 325, Third Edition, Volume I. (paged in sections.)

Nichol L. W., Colenbrander A. H., and Kennett T. J. (1969) A study of the $^{23}Na(n,\gamma)^{24}Na$ and $^{27}Al(n,\gamma)^{28}Al$ reactions. Can. J. Phys. 47, 953-961.

Op den Kamp A. M. F. and Spits A. M. J. (1972) Gamma rays from thermal-neutron capture in natural and ^{39}K enriched potassium. Nucl. Phys. A180, 569-586.

Orphan V. J. and Hoot C. G. (1971) Gamma-ray production cross sections for iron and aluminum. DNA 2736F (Gulf-RT-A10743) 199 pp.

Orphan V. J., Hoot C. G., and Rogers V. C. (1975) Gamma-ray production cross sections for iron from 0.86 to 16.7 MeV. Nucl. Sci. Eng. 57, 309-327.

Pakkanen A., Kantele J., and Suominen P. (1969) Levels in ^{208}Pb populated in the decay of $^{208}Tl(ThC")$. Z. Physik 218, 273-281.

Pancholi S. C. and Martin M. J. (1976) Nuclear data sheets for A = 138. Nucl. Data Sheets 18, 167-222.

Reedy R. C. (1977) Solar proton fluxes since 1956. Proc. Lunar Sci. Conf. 8th, p. 825-839.

Reedy R. C. and Arnold J. R. (1972) Interaction of solar and galactic cosmic-ray particles with the moon. J. Geophys. Res. 77, 537-555.

Reedy R. C., Arnold J. R., and Trombka J. I. (1973) Expected γ ray emission spectra from the lunar surface as a function of chemical composition. J. Geophys. Res. 78, 5847-5866.

Rogers V. C., Orphan V. J., Hoot C. G., and Verbinski V. V. (1975) Gamma-ray production cross sections for carbon and nitrogen from threshold to 20.7 MeV. Nucl. Sci. Eng. 58, 298-313.

Schmorak M. R. (1977) Nuclear data sheets for A = 231, 235, 239. Nucl. Data Sheets 21, 91-200.

Spilling P., Gruppelaar H., and Op den Kamp A. M. F. (1967) Thermal-neutron capture gamma rays from natural magnesium and enriched ^{25}Mg. Nucl. Phys. A102, 209-225.

Spits A. M. J. and Kopecky J. (1976) The reaction ^{35}Cl$(n,\gamma)^{36}$Cl studied with non-polarized and polarized thermal neutrons. Nucl. Phys. A264, 63-92.

Steiger R. H. and Jager E. (1977) Subcommission on geochronology: convention on the use of decay constants in geo- and cosmochronology. Earth Planet. Sci. Lett. 36, 359-362.

Toth K. S. (1977a) Nuclear data sheets for A = 222. Nucl. Data Sheets 21, 479-492.

Toth K. S. (1977b) Nuclear data sheets for A = 214. Nucl. Data Sheets 21, 437-466.

Toulmin P., Baird A. K., Clark B. C., Keil K., Rose H. J., Christian R. P., Evans P. H., and Kelliher W. C. (1977) Geochemical and mineralogical interpretation of the Viking inorganic chemical results. J. Geophys. Res. 82, 4625-4634.

Tripathi K. C., Blichert-Toft P. H., and Boreving S. (1969) Thermal neutron capture gamma-ray studies of natural titanium. In Neutron Capture Gamma-Ray Spectroscopy, p. 183-198. International Atomic Energy Agency, Vienna.

Wahlen M., Honda M., Imamura M., Fruchter J. S., Finkel R. C., Kohl C. P., Arnold J. R., and Reedy R. C. (1972) Cosmogenic nuclides in football-sized rocks. Proc. Lunar Sci. Conf. 3rd, p. 1719-1732.

Woolum D. S. and Burnett D. S. (1974) In-situ measurement of the rate of ^{235}U fission induced by lunar neutrons. Earth Planet. Sci. Lett. 21, 153-164.

Woolum D. S., Burnett D. S., Furst M., and Weiss J. R. (1975) Measurement of the lunar neutron density profile. The Moon 12, 231-250.

Young P. G. and Foster D. G. (1972) A preliminary evaluation of the neutron and photon-production cross sections for aluminum. AEC report number LA-4726. 40 pp.

Table I

For each element considered here, its average abundance in the moon (as adopted for these calculations), the fraction of low-energy neutrons it captures, and its most intense gamma ray escaping from the moon.

Element	mg/g[a]	Fraction captured	Strongest lunar gamma ray		
			Source[b]	Energy (MeV)	photons/cm^2 min
H	0.04	0.0012	$^1_1H(n,\gamma)$	2.2233	0.00349
C	0.1[c]	---	$^{12}C(n,n\gamma)$	4.4383[d]	0.00163
N	0.1[c]	---	$^{14}N(n,n\gamma)$	2.3127	0.000323
O	435.	0.0007	$^{16}O(n,n\gamma)$	6.1294	2.592
F	0.1	---	$^{19}F(n,n\gamma)$	0.1971	0.00144
Na	3.5	0.0075	$^{23}Na(n,n\gamma)$	0.4399[d]	0.0558
Mg	40.	0.0096	$^{24}Mg(n,n\gamma)$	1.3686[d]	0.727
Al	110.	0.0868	$^{27}Al(n,n\gamma)$	2.2104	0.675
Si	200.	0.105	$^{28}Si(n,n\gamma)$	1.7788	3.223
P	0.6	0.0003	$^{31}P(n,n\gamma)$	1.2661	0.0038
S	0.7	0.0010	$^{32}S(n,n\gamma)$	2.2301[d]	0.0067
Cl	0.02	0.0017	$^{35}Cl(n,\gamma)$	6.111	0.00215
Ar	0.1[c]	---	$^{40}Ar(n,n\gamma)$	1.4608[d]	0.0013
K	1.2	0.0059	^{40}K	1.4608	2.352
Ca	100.	0.099	$^{40}Ca(n,n\gamma)$	3.7366	0.346
Ti	14.	0.165	$^{48}Ti(n,\gamma)$	6.7615	0.412
Cr	1.0	0.0055	$^{52}Cr(n,n\gamma)$	1.4342[d]	0.0160
Mn	0.8	0.0179	^{56}Mn	0.8467[d]	0.0243
Fe	90.	0.380	$^{56}Fe(n,n\gamma)$	0.8467	1.149
Ni	0.4	0.0028	$^{58}Ni(n,\gamma)$	8.999	0.00732

Table I, (cont.)

Element	mg/g[a]	Fraction captured	Strongest lunar gamma ray		
			Source[b]	Energy (MeV)	photons/cm^2 min
Sr	0.18	0.0002	$^{88}Sr(n,n\gamma)$	1.8360	0.0019
Y	0.06	0.0001	$^{89}Y(n,n\gamma)$	1.5074[d]	0.00024
Zr	0.25	---	$^{90}Zr(n,n\gamma)$	2.1865	0.00089
Ba	0.20	0.0002	$^{138}Ba(n,n\gamma)$	1.4359[d]	0.00147
La	0.010	---	^{138}La	1.4359[d]	0.00247
Nd	0.017	0.0005	$^{143}Nd(n,\gamma)$	0.697	0.00043
Sm	0.007	0.027	$^{149}Sm(n,\gamma)$	0.3340	0.014
Eu	0.0005	0.0008	^{152g}Eu	1.409[d]	0.00024
Gd	0.008	0.072	$Gd(n,\gamma)$	1.187	0.014
Lu	0.0005	---	^{176}Lu	0.3069	0.00756
Th	0.0019	---	^{208}Tl	2.6146	2.193
U	0.0005	---	^{214}Bi	0.6093	1.118

[a]The abundance as mg of element per g of lunar surface material.

[b]The reaction or radionuclide producing the most intense gamma ray.

[c]Nominal abundance used in these calculations, not a lunar abundance.

[d]Study of this element using this gamma ray is hampered or impossible because of interferences by other gamma rays of the same or nearly the same energy. See the text for discussions of the interferences and of other gamma rays suitable for determining abundances of some of these elements.

Table II

The fluxes of gamma rays produced by the decay of the natural radionuclides at the lunar elemental abundances of Table I. The yield is per disintegration of the parent radionuclide.

Element	Nuclide	Energy (MeV)	Yield	Flux (photons/cm^2 min)
K	^{40}K	1.4608	0.1048	2.352
La	^{138}La	1.4359	0.671	0.00247
	^{138}La	0.7887	0.329	0.00090
Lu	^{176}Lu	0.3069	0.94	0.00756
	^{176}Lu	0.2018	0.85	0.00573
Th	^{208}Tl	2.6146	0.360	2.193
	^{228}Ac	1.6304	0.019	0.0919
	^{212}Bi	1.6205	0.016	0.0771
	^{228}Ac	1.5879	0.037	0.177
	^{228}Ac	1.4958	0.010	0.0464
	^{228}Ac	1.4592	0.010	0.0458
	^{228}Ac	0.9689	0.175	0.656
	^{228}Ac	0.9646	0.054	0.202
	^{228}Ac	0.9111	0.290	1.054
	^{208}Tl	0.8605	0.045	0.159
	^{228}Ac	0.8402	0.010	0.0349
	^{228}Ac	0.8356	0.018	0.0627
	^{228}Ac	0.7948	0.048	0.163
	^{212}Bi	0.7854	0.010	0.0338
	^{228}Ac	0.7721	0.016	0.0537
	^{228}Ac	0.7552	0.011	0.0366
	^{212}Bi	0.7271	0.070	0.229
	^{208}Tl	0.5831	0.307	0.916
	^{228}Ac	0.5623	0.010	0.0294
	^{208}Tl	0.5107	0.083	0.234
	^{228}Ac	0.4630	0.046	0.125

Element	Nuclide	Energy (MeV)	Yield	Flux (photons/cm^2 min)
Th	^{228}Ac	0.4094	0.022	0.0566
	^{228}Ac	0.3384	0.120	0.285
	^{228}Ac	0.3280	0.034	0.0797
	^{212}Pb	0.3000	0.031	0.0700
	^{208}Tl	0.2774	0.024	0.0524
	^{228}Ac	0.2703	0.038	0.0821
	^{224}Ra	0.2410	0.038	0.0783
	^{212}Pb	0.2386	0.47	0.964
	^{228}Ac	0.2094	0.045	0.0874
	^{214}Bi	2.4477	0.016	0.0753
	^{214}Bi	2.2041	0.050	0.224
	^{214}Bi	2.1185	0.012	0.0526
	^{214}Bi	1.8474	0.021	0.0861
	^{214}Bi	1.7645	0.159	0.637
	^{214}Bi	1.7296	0.031	0.123
	^{214}Bi	1.6613	0.012	0.0467
	^{214}Bi	1.5092	0.022	0.0817
	^{214}Bi	1.4080	0.025	0.0897
	^{214}Bi	1.4015	0.014	0.0501
	^{214}Bi	1.3777	0.040	0.142
	^{214}Bi	1.2810	0.015	0.0514
	^{214}Bi	1.2381	0.059	0.199
	^{214}Bi	1.1552	0.017	0.0554
	^{214}Bi	1.1203	0.150	0.481
	^{214}Bi	0.9341	0.032	0.0939
	^{214}Bi	0.8062	0.012	0.0328
	^{214}Pb	0.7859	0.011	0.0297
	^{214}Bi	0.7684	0.049	0.131

Element	Nuclide	Energy (MeV)	Yield	Flux (photons/cm^2 min)
U	^{214}Bi	0.6655	0.016	0.0403
	^{214}Bi	0.6093	0.461	1.118
	^{214}Pb	0.3519	0.371	0.714
	^{214}Pb	0.2952	0.192	0.343
	^{214}Pb	0.2419	0.075	0.123
	^{226}Ra	0.1860	0.055	0.0810
	^{235}U	0.1857	0.54	0.0366

Table III

Fluxes of lunar gamma rays produced by the decay of solar-proton-produced radionuclides at the times of the Apollo 15 and 16 missions. The yield is the fraction of the disintegrations which emit that gamma ray. The elemental abundances of Table I were used.

Element	Nuclide	Energy (MeV)	Yield	Flux (photons/cm^2 min) Apollo 15	Apollo 16
Mg	^{22}Na	1.2745	1.00	0.0573	0.0496
Al	^{26}Al	1.808?	0.997	0.444	0.444
	^{22}Na	1.274?	1.00	0.0820	0.0710
Si	^{26}Al	1.808?	0.997	0.300	0.300
	^{22}Na	1.274?	1.00	0.0609	).0530
Fe	^{56}Co	1.238?	0.70	0.0556	).0187
	^{56}Co	0.8467	1.00?	0.0755	).0254
	^{54}Mn	0.8348	1.00	0.0271	).0229

Table IV 138

The fluxes of gamma rays produced in the moon via neutron nonelastic-scattering reactions or the decay of GCR-produced radionuclides. The elemental abundances used for these major elements were those of Table I. The source is the reaction or radionuclide producing the gamma ray. The yield is the fraction of gamma rays with that energy produced per de-excitation of the excited level or per decay of the radionuclide.

Element	Source	Energy (MeV)	Yield	Flux (photons/cm^2 min)
O	$^{16}O(n,n\gamma)$	8.8691	0.072	0.059
	$^{16}O(n,n\gamma)$	7.1170	1.00	0.808
	$^{16}O(n,n\gamma)$	6.9172	1.00	0.736
	$^{16}O(n,n\gamma)$	6.1294	1.00	2.592
	^{16}N	6.1294	0.69	0.277
	$^{16}O(n,n\gamma)$	4.949	0.40	0.093
	$^{16}O(n,n\alpha\gamma)$	4.4383	1.00	1.214
	$^{16}O(n,n\gamma)$	4.161	0.44	0.094
	$^{16}O(n,\alpha\gamma)$	3.854	0.691	0.372
	$^{16}O(n,n\gamma)$	3.833	1.00	0.058
	$^{16}O(n,\alpha\gamma)$	3.6842	1.00	0.692
	$^{16}O(n,\alpha\gamma)$	3.086	1.00	0.283
	$^{16}O(n,n\gamma)$	2.7408	0.76	0.359
	$^{16}O(n,n\gamma)$	1.753	0.126	0.046
Mg	$^{24}Mg(n,n\gamma)$	4.238	0.76	0.107
	$^{24}Mg(n,n\gamma)$	3.8671	0.983	0.060
	^{24}Na	2.7539	0.9995	0.106
	$^{24}Mg(n,n\gamma)$	2.7539	1.00	0.091
	$^{26}Mg(n,n\gamma)$	1.8087	1.00	0.152
	$^{25}Mg(n,n\gamma)$	1.6117	1.00	0.060
	$^{24}Mg(n,n\gamma)$	1.3686	1.00	0.727
	^{24}Na	1.3686	1.00	0.069
	^{22}Na	1.2745	0.9994	0.074
	$^{26}Mg(n,n\gamma)$	1.1297	0.90	0.038
Al	$^{27}Al(n,n\gamma)$	4.580	0.75	0.061
	$^{27}Al(n,n\gamma)$	4.409	0.70	0.059
	$^{27}Al(n,n\gamma)$	3.9556	0.88	0.055
	$^{27}Al(n,n\gamma)$	3.2103	0.87	0.061
	$^{27}Al(n,n\gamma)$	3.004	0.91	0.385
	$^{27}Al(n,n\gamma)$	2.981	1.00	0.120
	^{24}Na	2.7539	0.9995	0.209
	$^{27}Al(n,n\gamma)$	2.734	0.24	0.070

Table IV (cont.)

Element	Source	Energy (MeV)	Yield	Flux (photons/cm^2 min)
Al	^{27}Al(n,nγ)	2.2997	0.76	0.057
	^{27}Al(n,nγ)	2.2104	1.00	0.675
	^{26}Al	1.8087	0.997	0.290
	^{27}Al(n,dγ)	1.8087	1.00	0.238
	^{27}Al(n,nγ)	1.7195	0.76	0.167
	^{24}Na	1.3686	1.00	0.139
	^{22}Na	1.2745	0.9994	0.093
	^{27}Al(n,nγ)	1.0144	0.97	0.634
	^{27}Al(n,nγ)	0.8438	1.00	0.305
	^{27}Mg	0.8438	0.71	0.066
Si	^{28}Si(n,nγ)	7.4162	0.90	0.111
	^{28}Si(n,nγ)	6.8777	0.65	0.199
	^{28}Si(n,nγ)	5.6012	0.61	0.050
	^{28}Si(n,nγ)	5.1094	1.00	0.114
	^{28}Si(n,nγ)	5.0992	0.35	0.094
	^{28}Si(n,nγ)	4.4972	0.91	0.105
	^{28}Si(n,nγ)	3.2000	1.00	0.088
	^{28}Si(n,nγ)	2.8387	1.00	0.329
	^{24}Na	2.7539	0.9995	0.309
	^{30}Si(n,nγ)	2.2354	1.00	0.117
	^{26}Al	1.8087	0.997	0.306
	^{28}Si(n,nγ)	1.7788	1.00	3.223
	^{28}Al	1.7788	1.00	0.700
	^{24}Na	1.3686	1.00	0.212
	^{22}Na	1.2745	0.9994	0.152
	^{29}Si(n,nγ)	1.2733	1.00	0.067
Ca	^{40}Ca(n,nγ)	5.2486	0.79	0.042
	^{40}Ca(n,nγ)	3.9044	1.00	0.232
	^{40}Ca(n,nγ)	3.7366	1.00	0.346
	^{40}Ca(n,αγ)	1.6112	1.00	0.106
	^{40}Ca(n,pγ)	1.1589	0.86	0.032
	^{44}Ca(n,nγ)	1.1569	1.00	0.034
	^{40}Ca(n,pγ)	0.8916	1.00	0.031
	^{40}Ca(n,pγ)	0.7705	1.00	0.101
Ti	^{48}Ti(n,nγ)	1.3117	1.00	0.037
	^{48}Ti(n,nγ)	0.9834	1.00	0.163
	^{46}Ti(n,nγ)	0.8892	1.00	0.016
	^{46}Sc	0.8892	1.00	0.013

Table IV (cont.)   140

Element	Source	Energy (MeV)	Yield	Flux (photons/cm^2 min)
Fe	^{56}Fe(n,nγ)	3.6019	0.69	0.040
	^{56}Fe(n,nγ)	2.601	1.00	0.061
	^{56}Fe(n,nγ)	2.5231	0.87	0.053
	^{56}Fe(n,nγ)	2.1129	1.00	0.078
	^{56}Fe(n,nγ)	1.8109	1.00	0.123
	^{54}Fe(n,nγ)	1.4077	1.00	0.061
	^{56}Fe(n,2nγ)	1.3164	1.00	0.091
	^{56}Fe(n,nγ)	1.2383	1.00	0.256
	^{56}Fe(n,nγ)	1.0380	1.00	0.041
	^{56}Fe(n,2nγ)	0.9312	1.00	0.086
	^{56}Fe(n,nγ)	0.8467	1.00	1.149
	^{54}Mn	0.8348	1.00	0.090

Table V

The fluxes of gamma rays produced in the moon via neutron nonelastic-scattering reactions or the decay of GCR-produced radionuclides. The elemental abundances used for these minor elements were those of Table I. The source is the reaction or radionuclide producing the gamma ray. The yield is the fraction of gamma rays with that energy produced per de-excitation of the excited level or per decay of the radionuclide.

Element	Source	Energy (MeV)	Yield	Flux (photons/cm^2 min)
C	$^{12}C(n,n\gamma)$	4.4383	1.00	0.00163
N	$^{14}N(n,n\gamma)$	5.1049	0.80	0.000203
	$^{14}N(n,\alpha\gamma)$	4.4441	1.00	0.000238
	$^{14}N(n,n\gamma)$	2.3127	1.00	0.000323
	$^{14}N(n,\alpha\gamma)$	2.1245	1.00	0.000165
	$^{14}N(n,n\gamma)$	1.6348	1.00	0.000176
F	$^{19}F(n,n\gamma)$	1.3569	1.00	0.00094
	$^{19}F(n,n\gamma)$	1.2358	1.00	0.00046
	$^{19}F(n,n\gamma)$	0.1971	1.00	0.00144
Na	$^{23}Na(n,n\gamma)$	2.6396	1.00	0.0064
	$^{23}Na(n,n\gamma)$	1.6364	1.00	0.0215
	^{20}F	1.6337	1.00	0.0087
	^{22}Na	1.2745	1.00	0.0121
	$^{23}Na(n,n\gamma)$	0.4399	1.00	0.0558
P	$^{31}P(n,n\gamma)$	2.2337	1.00	0.0022
	$^{31}P(n,n\gamma)$	1.2661	1.00	0.0038
S	$^{32}S(n,n\gamma)$	2.2301	1.00	0.0067
Cl	$^{35}Cl(n,n\gamma)$	1.7632	1.00	0.000100
	$^{35}Cl(n,n\gamma)$	1.2194	1.00	0.000075
Ar	$^{40}Ar(n,n\gamma)$	1.4608	1.00	0.0013
K	$^{39}K(n,n\gamma)$	2.8137	1.00	0.00354
	$^{39}K(n,n\gamma)$	2.5225	1.00	0.00275
Cr	$^{52}Cr(n,n\gamma)$	1.5308	1.00	0.00125
	$^{52}Cr(n,n\gamma)$	1.4342	1.00	0.0160
	$^{52}Cr(n,n\gamma)$	1.3338	1.00	0.00192
	$^{52}Cr(n,n\gamma)$	0.9356	1.00	0.00123
Mn	$^{55}Mn(n,n\gamma)$	1.5289	1.00	0.00151
	$^{55}Mn(n,n\gamma)$	1.1660	1.00	0.00186
	$^{55}Mn(n,n\gamma)$	0.8585	1.00	0.00361
	^{54}Mn	0.8348	1.00	0.00301

Table V (cont.)

Element	Source	Energy (MeV)	Yield	Flux (photons/cm^2 min)
Mn	^{55}Mn(n,nγ)	0.1260	1.00	0.00330
Ni	^{58}Ni(n,nγ)	1.4544	1.00	0.00260
	^{60}Ni(n,nγ)	1.3325	1.00	0.00169
	^{58}Co	0.8106	1.00	0.00105
Sr	^{88}Sr(n,nγ)	1.8360	1.00	0.00192
Y	^{88}Y	1.8360	0.994	0.00020
	^{89}Y(n,nγ)	1.7445	1.00	0.00023
	^{89}Y(n,nγ)	1.5074	1.00	0.00024
	^{89}Y(n,nγ)	0.9092	1.00	0.00019
Zr	^{90}Zr(n,nγ)	2.1865	1.00	0.00089
	^{92}Zr(n,nγ)	0.9345	1.00	0.00050
	^{94}Zr(n,nγ)	0.9182	1.00	0.00049
	^{89}Zr	0.9092	1.00	0.00043
Ba	^{138}Ba(n,nγ)	1.4359	1.00	0.00147

Table VI

The fluxes of gamma rays produced in the moon by spallation, (p,xγ), reactions. Table I elemental abundances are used. The source is the excited nuclide made by reactions of GCR particles with the element.

Element	Source	Energy(MeV)	Flux (photons/cm^2 min)
Mg	$^{20}Ne^*$	1.6337	0.07
Al	$^{23}Na^*$	1.6364	0.08
	$^{20}Ne^*$	1.6337	0.11
	$^{24}Mg^*$	1.3686	0.15
Si	$^{27}Al^*$	2.2104	0.10
	$^{20}Ne^*$	1.6337	0.20
	$^{24}Mg^*$	1.3686	0.52
	$^{27}Al^*$	1.0144	0.10
Ca	$^{39}K^*$	2.8137	0.06
	$^{39}Ca^*$	2.793	0.11
	$^{32}S^*$	2.2301	0.05
	$^{36}Ar^*$	1.9704	0.15
Fe	$^{52}Cr^*$	1.4342	0.05

Table VII

The fluxes of gamma rays produced in the moon by neutron-capture reactions with the major elements. (See Table I for the elemental abundances used.) The yield is the fraction of captures by the element which produces the gamma ray. The source indicates the isotope in which the neutron was captured or the radionuclide, produced by neutron capture, which decayed to produce the gamma ray.

Element	Source	Energy (MeV)	Yield	Flux (photons/cm^2 min)
Mg	^{24}Mg(n,γ)	3.918	0.48	0.0205
	^{24}Mg(n,γ)	2.8285	0.36	0.0119
Al	^{27}Al(n,γ)	7.724	0.30	0.173
	^{27}Al(n,γ)	7.694	0.045	0.026
	^{27}Al(n,γ)	4.735	0.057	0.025
	^{27}Al(n,γ)	4.260	0.06	0.025
	^{27}Al(n,γ)	4.134	0.065	0.026
	^{27}Al(n,γ)	3.0345	0.08	0.025
	^{27}Al(n,γ)	2.960	0.09	0.028
	^{28}Al	1.7788	1.00	0.209
Si	^{28}Si(n,γ)	7.200	0.08	0.054
	^{28}Si(n,γ)	6.381	0.13	0.083
	^{28}Si(n,γ)	4.934	0.61	0.336
	^{28}Si(n,γ)	3.5395	0.66	0.286
	^{28}Si(n,γ)	2.0931	0.20	0.058
	^{28}Si(n,γ)	1.2733	0.19	0.037
Ca	^{40}Ca(n,γ)	6.420	0.40	0.241
	^{40}Ca(n,γ)	5.9005	0.07	0.040
	^{40}Ca(n,γ)	4.419	0.18	0.088
	^{40}Ca(n,γ)	2.0015	0.18	0.047
	^{40}Ca(n,γ)	1.9427	0.80	0.205

Element	Source	Energy (MeV)	Yield	Flux (photons/cm^2 min)
Ti	^{48}Ti(n,γ)	6.7615	0.40	0.412
	^{48}Ti(n,γ)	6.557	0.04	0.040
	^{48}Ti(n,γ)	6.419	0.28	0.280
	^{48}Ti(n,γ)	4.967	0.03	0.026
	^{48}Ti(n,γ)	4.882	0.05	0.043
	^{48}Ti(n,γ)	1.7620	0.045	0.018
	^{48}Ti(n,γ)	1.5853	0.09	0.033
	^{48}Ti(n,γ)	1.4983	0.04	0.014
	^{48}Ti(n,γ)	1.3815	0.82	0.269
	^{48}Ti(n,γ)	0.3419	0.38	0.049
Fe	^{54}Fe(n,γ)	9.299	0.034	0.093
	^{56}Fe(n,γ)	7.6457	0.22	0.552
	^{56}Fe(n,γ)	7.6313	0.24	0.602
	^{56}Fe(n,γ)	7.279	0.05	0.123
	^{56}Fe(n,γ)	6.019	0.08	0.178
	^{56}Fe(n,γ)	5.921	0.08	0.176
	^{56}Fe(n,γ)	4.810	0.018	0.035
	^{56}Fe(n,γ)	4.2185	0.04	0.072
	^{56}Fe(n,γ)	1.725	0.09	0.081
	^{56}Fe(n,γ)	1.6126	0.07	0.059
	^{56}Fe(n,γ)	0.6921	0.08	0.036

Table VIII

The fluxes of gamma rays produced in the moon by neutron-capture reactions with minor or trace elements. (See Table I for the elemental abundances used.) The yield is the fraction of captures by the element which produces the gamma ray. The source indicates the isotope in which the neutron was captured or the radionuclide, produced by neutron capture, which decayed to produce the gamma ray.

Element	Source	Energy (MeV)	Yield	Flux $(photons/cm^2 min)$
H	$^1H(n,\gamma)$	2.2233	1.00	0.00349
N	$^{14}N(n,\gamma)$	10.8295	0.135	0.000051
	$^{14}N(n,\gamma)$	6.3225	0.184	0.000055
	$^{14}N(n,\gamma)$	5.5334	0.185	0.000051
	$^{14}N(n,\gamma)$	5.298	0.217	0.000059
	$^{14}N(n,\gamma)$	5.2693	0.311	0.000084
Na	$^{23}Na(n,\gamma)$	6.395	0.20	0.0090
	^{24}Na	2.7539	0.9995	0.0252
	^{24}Na	1.3686	1.00	0.0147
	$^{23}Na(n,\gamma)$	0.4723	1.00	0.0071
S	$^{32}S(n,\gamma)$	5.424	0.55	0.0032
	$^{32}S(n,\gamma)$	2.379	0.40	0.0013
Cl	$^{35}Cl(n,\gamma)$	7.791	0.09	0.00104
	$^{35}Cl(n,\gamma)$	7.415	0.11	0.00124
	$^{35}Cl(n,\gamma)$	6.621	0.09	0.00096
	$^{35}Cl(n,\gamma)$	6.111	0.21	0.00215
	$^{35}Cl(n,\gamma)$	1.951	0.20	0.00090
K	$^{39}K(n,\gamma)$	7.770	0.07	0.00278
	$^{39}K(n,\gamma)$	5.7525	0.07	0.00238
	$^{39}K(n,\gamma)$	5.697	0.07	0.00237
	$^{39}K(n,\gamma)$	5.381	0.09	0.00295
	$^{39}K(n,\gamma)$	0.7705	0.58	0.00444
Cr	$^{53}Cr(n,\gamma)$	9.719	0.10	0.00404
	$^{53}Cr(n,\gamma)$	8.884	0.24	0.00932
	$^{52}Cr(n,\gamma)$	7.939	0.11	0.00407
Mn	$^{55}Mn(n,\gamma)$	7.244	0.10	0.0116
	$^{55}Mn(n,\gamma)$	7.058	0.09	0.0103
	^{56}Mn	1.8109	0.29	0.0127
	^{56}Mn	0.8467	0.988	0.0243

Table VIII (cont.)

Element	Source	Energy (MeV)	Yield	Flux (photons/cm^2 min)
Ni	^{58}Ni(n,γ)	8.999	0.37	0.00732
	^{58}Ni(n,γ)	8.534	0.18	0.00348
Sr	^{87}Sr(n,γ)	1.8360	0.45	0.00026
Y	^{89}Y(n,γ)	6.080	0.4	0.00019
Nd	^{143}Nd(n,γ)	0.697	0.65	0.00043
Sm	^{149}Sm(n,γ)	0.4395	0.4	0.0097
	^{149}Sm(n,γ)	0.3340	0.7	0.014
Eu	^{152g}Eu	1.409	0.15	0.00024
	^{152g}Eu	1.113	0.09	0.00012
Gd	^{157}Gd(n,γ)	6.747	0.02	0.0090
	Gd(n,γ)	1.187	0.11	0.014
	^{157}Gd(n,γ)	0.945	0.07	0.0075
	^{157}Gd(n,γ)	0.182	0.22	0.0084
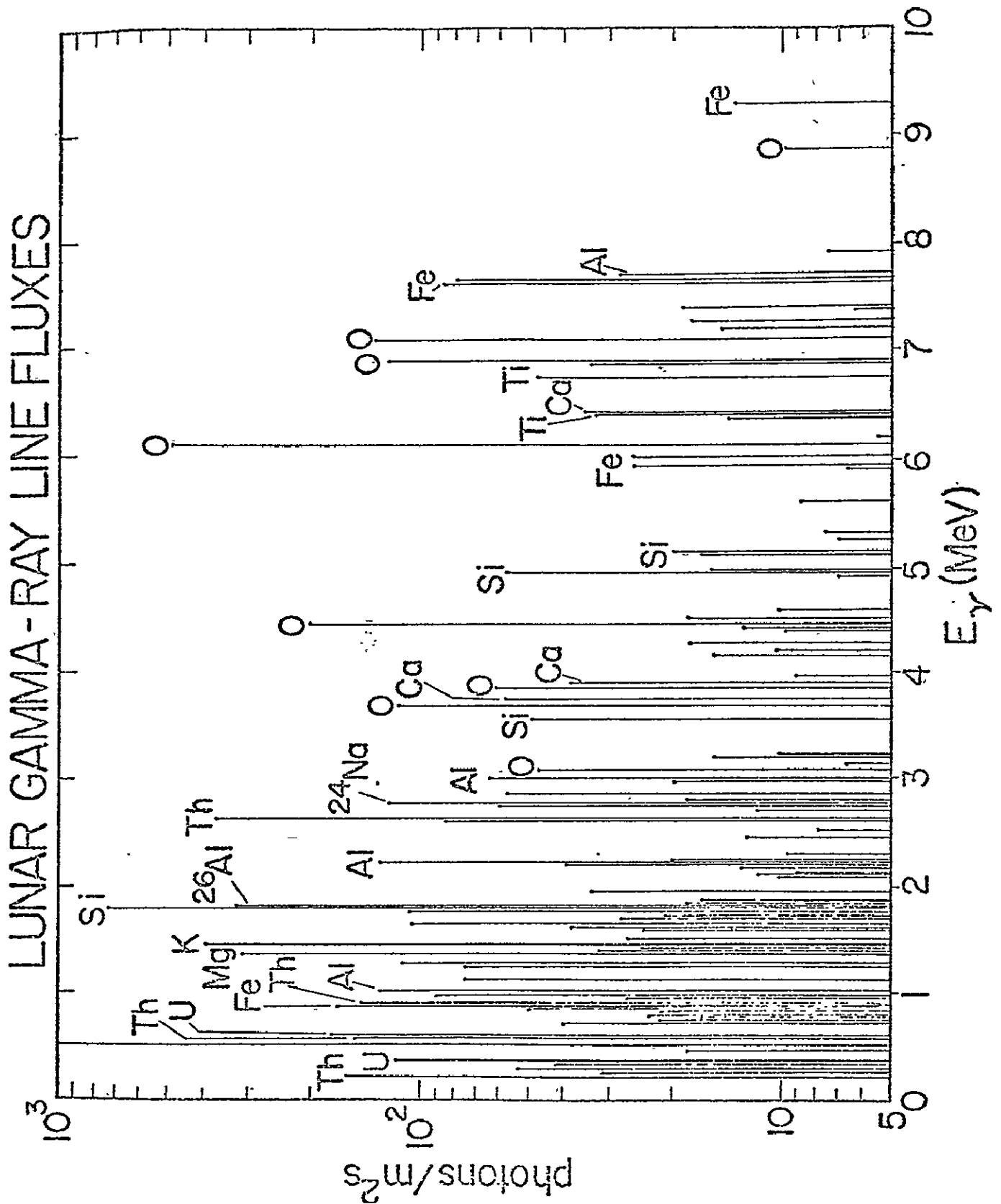
Fig. 1. The gamma-ray fluxes calculated as escaping from the moon for
the average lunar chemical composition of Table I are shown as a function
of their energies. The more intense gamma rays are labeled by the element
or the radionuclide producing them.

ι N78-31977 $\mathcal{D}_{l}$-93

NUCLEAR GAMMA RAYS FROM STELLAR FLARES

by

Stirling A. Colgate
Los Alamos Scientific Laboratory and New Mexico Tech
address: MS 210, LASL, Los Alamos, NM 87545

ABSTRACT

Solar flare observations are consistent with the phenomenological description that a loop of magnetic flux is convected to the surface of the star and twisted. Both deformations are necessary for the presumed dynamo action. The resulting inductive current-parallel to the field is dissipated at an enhanced rate throughout the field volume by current limiting instabilities. The steady state balance between joule heating and thermal conduction along the field lines of force to the denser, cooler surface establishes a temperature distribution. The expansion of heated and ionized surface layers leads to a pressure balance and hence predictable density and x-ray emission measure. The current limitation instabilities result observationally in the parallel current being transferred to run-away ions that reach a kinetic energy of some finite fraction of the inductive potential drop. One can then calculate the nuclear excitation gamma rays produced by such a run-away ion current. A large White Dwarf flare of $B_{max} = 10^7$ gauss, $\ell = 4 \times 10^8$ cm, $r = 2 \times 10^7$ cm, determined by fluid convection arguments then contains $W_T = 2 \times 10^{36}$ ergs. The current dissipation time of several seconds leads to a temperature of several hundred keV, pressure balance in a few tenths of a second, and $n_{e,i} \cong 10^{17}$ cm^{-3}. These conditions describe a typical "γ-burst" (2×10^{36} ergs) where the photons arise from e-e and e-i bremsstrahlung. The parallel current of run-away ions should be $I = 5r B_{max} \cong 10^{15}$ amperes. The total potential drop is $V = d/dt$ (inductance x current) $= W_T/I = 4 \times 10^{14}$ volts. This is so high that we can assume all ions have an energy well above nuclear excitation threshold. Then the production of nuclear γ's (presumably by neutron capture from spallation) becomes ϕ_i n_{He} Vol $\sigma_\gamma \cong 10^{35}$ γ's where ϕ_i = flux of run-away ions, 10^{19} cm^{-2}, $n_{He} \cong 10^{17}$, Vol $= 5 \times 10^{23}$ cm^3, $\sigma_\gamma \cong 10^{-25}$ cm^2. At the

characteristic distance at which the bremsstrahlung would explain a typical γ-burst, 30 pc, this flux of nuclear excitation γ's would correspond to $\cong 10^{-6}$ $cm^2 sec^{-1}$. It is possible that the ion temperature could run away ($kT_i \cong 10$ MeV) because of the small classical electron dynamic friction at $kT_e \cong 150$ keV, but the plasma physics of instability induced coherent dynamic friction is not well enough known. In this case complete spallation would occur giving rise to $\cong 10^{41}$ gamma rays.

INTRODUCTION

The prediction of gamma rays from stellar flares is highly model dependent but on the other hand the fundamental energy flow phenomenology in solar flares can be modeled with surprisingly few free parameters. These are:

1. total energy

2. volume

3. time

We could take all three numbers ad hoc and derive stellar flare phenomena much as Mullan (1974, 1975, 1976) and Worden (1974) have done. Instead we feel that it is far more satisfactory to start with the basic physics of stellar structure and show how this leads to the limiting stress in dynamo theory and how this in turn predicts the maximum field, volume and hence energy. The time of dissipation is then determined by scaling from plasma physics instabilities, and we have the full input parameters necessary to calculate the nuclear spallation. We will use the self consistent description of a solar flare (Colgate 1978) heated throughout its volume, cooled by thermal conduction and where most importantly for this problem the total current necessary to bound the magnetic fields is carried by run-away ions (nucleii). It is these high energy ions comprising the primary current of the flare that we will invoke as the source of the nuclear excitation necessary to give rise to nuclear gamma rays. This is the general description that fits so many measurements of the large solar flare of August 4, 1974.

These nuclear gamma rays are a small fraction of the total radiation. In a solar flare this radiation occurs in the energy range XUV to a few keV, although of course a small fraction emerges as multi kilovolt x rays. In a stellar flare where the total and specific energy may be very much greater,

the radiation will be emitted as bremsstrahlung of 50 to 100 keV x rays. Normally we could interpret this radiation as a "gamma burst" (Stecker and Frost 1973; Mullan 1974, 1975, 1976; Colgate 1977). However we are not as concerned here with the continuum radiation, but instead with the possible line excitation of various nucleii.

The modeling of solar flares frequently starts with the assumption of the release of energy in association with magnetic fields. When one observes that the origin of magnetic field must be associated with more fundamental phenomena of the sun, then this in turn restricts the topology of the fields and determines many of the starting conditions of a solar flare model. Without these restrictions there are very many possible explanations and we do not claim to eliminate these. It is just more comfortable to start with solar dynamics.

A self-gravitating sphere of mass necessarily leads to heat flow and when the mass is in the range of solar magnitudes, regions of the heat flow predictably will be convective as opposed to radiative. The magnitude of convection is prescribed by the requirement of transporting the heat diffusing from the interior. Some effects of convection are clearly manifest on the solar surface, but the depth of convection can primarily be determined only by solar modeling. Pulsations have offered some confirming evidence. Convection and rotation of the star lead to a dynamo (Parker 1971). The generation of magnetic field depends in a fundamental way upon the convection to the solar surface of an ordered, amplified, laminar, deep toroidal field. Convection transports a small fraction of this flux and the Coriolis force causes convective elements to rotate (cyclonic convections) that rotates the flux loops from the toroidal to the poloidal (dipole) plane. The critical closure of the dynamo now

depends upon the dissipation of part of the flux convected away from and rotated othogonal to, the amplified toroidal field. The convected flux is topologically loops; there are no monopoles. A loop that partially dissipates in the dipole plane adds flux to the average dipole field. Laminar differential rotation in the sun amplifies (wraps up many times) the dipole field back into toroidal field and the dynamo is completed.

The partial dissipation of the flux convected to the surface of the sun is the crucial step that still confronts detailed explanation. Without doubt this process is manifested by the observed magnetic activity of the sun. It is conjecture but an extremely plausible conjecture that solar flares are an extremum of this continuing flux dissipation. Sun spot magnetic fields have the correct magnitude, time scale and length scale to correspond to a convected loop of primary toroidal flux (Colgate 1978). Magnitude, time and length are established by the restrictive properties of convecton at the base of the convection zone. We see flares as the explosive dissipation of these sun spot fields. What properties of these fields must be applied to a solar flare model? These are:

1.   The average magnetic field is kilogauss strength or less.

2.   The first order topology of the field is that of a loop.

3.   The second order topology is that the field is force-free because the inferred plasma pressure is very small compared to the field pressure.

4.   The evolution to the state of flare explosion is quasistatic

5.   On the average the field has torsion because vorticity (and cyclonic motion) is a fundamental degree of freedom of turbulence (convection).

From these conditions we argue that a solar flare is most probably, the sudden instability-induced dissipation of a force-free flux loop. The detailed mechanism of this instability and dissipation is the most poorly established part of the theory but there is general agreement that either a combination of hydromagnetic (exceeding the Kuskal-Shafranov limit) or resistive tearing mode (Spicer 1977, Colgate 1977,78) is most likely. The nonlinear limit of these instabilities is conjectural. It should be pointed out that these magnetic instabilities do not exclude the singular case of oppositely directed magnetic fields as is required by the classical neutral point explanation of Petschek (1964). However, the probability of occurrence of exactly oppositely directed fields derived from the random vorticity field of convective turbulence seems small - or at least on the average a significant torsional component of the field must be dissipated first before the oppositely directed neutral point cusp can occur.

There is a significant difference in the two cases for creating accelerated high-energy particles. A "force-free" field is one where the plasma pressure is small compared to the magnetic one, and so of necessity the local current density $\vec{J}$ is primarily parallel, $J_{||}$, to the local field. The neutral point, on the other hand requires a region of zero field and a separating plasma whose pressure equals the field pressure. The gradient of the plasma pressure is balanced by the force $\vec{J} \times \vec{B}$ where $\vec{J}$ is perpendicular, $J_\perp$, to $\vec{B}$. $J_\perp$ is comprised of an ensemble average of individual particles, each orbiting locally perpendicular to the field, and the distance any given particle travels corresponds to a slow drift across the field. $J_{||}$ on the other hand is comprised of particles that may travel a large distance along the field. Since the dissipation or energization is due to $\vec{J} \cdot \vec{E}$, it is evident that run-away acceleration is inherently

more likely for force-free torsion dervied fields because of $E_{||}$ as

opposed to a neutral point configuration where one has only $E_\perp$ and $J_\perp$.

It is therefore more likely that the high energy phenomena observed

in flares is due to the rapid dissipation of the torsion of the field

leading to $E_{||}$ run-away acceleration. It is also currently easier to

explain an enhanced resistivity for $J_{||}$ due to current carrier limited

hybrid or electro-static wave generation than for the $J_\perp$ case. However,

this does not ensure the correctness of the explanation.

If we indeed initiate a flare assuming a twisted force-free loop of

field, and assume a rapid enhanced resistive dissipation of the torsional

component of the field, then do we have even a reasonable description of

the gross phenomena of the flare?

Flare Heating and Cooling

To answer this question we start with our assumption of a twisted

flux loop and ask what happens when we rapidly dissipate part of the field

energy. When this energy is released along the flux tube we expect to heat

the ambient plasma and in turn we expect the plasma to radiate and therm-

-ally conduct heat to the respective ends of the flux tube parallel to the

lines of force. One can observe empirically the rate of energy release

and calculate the thermal conduction. Since the conduction heat flux in a

hot ionized plasma is such a rapid function of the maximum temperature,

being proportional to $\kappa \nabla T \propto T_{max}^{7/2}$, we expect the temperature maximum to

be very broad and relatively insensitive to the length, $\propto L^{2/7}$, heating

rate $\propto (\dot{W})^{2/7}$ and radius, $r^{-4/7}$. Indeed the observed temperatures from

soft x-ray line ratios and x-ray spectra confirm the expected maximum

temperature within rather narrow limits of 1 to 2 keV for a very wide

range of flares. Secondly after a period of time, $\cong$ 10 seconds, plasma

will be expected to rapidly expand from the heated solar surface and because it is ionized it will be constrained to the flux tube, expanding upwards thereby increasing the plasma density along the flux tube. The quasi equilibrium value of the plasma pressure can be calculated assuming that the dense cooler ends radiate almost all the energy flux through the efficient mechanism of line radiation in the XUV. The pressure, 10^3 to 10^4 dynes cm^{-2}, and density, 10^{11} to 10^{12} gm cm^{-3}, so calculated results in an x ray and XUV emission measure in reasonable agreement with observations. This does not say anything about the plasma conditions in the first 10 seconds which will undoubtedly be less dense and hotter, depending upon the dissipation mechanism. Nevertheless, it is comforting to recognize that the quasi equilibrium conditions can be calculated so easily and give good agreement with the general features of observation, especially soft x rays and magnetic fields. As a note on these general flare conditions the quasi steady state phenomena of flares lasting longer than 10 seconds implies that the energization must continue to take place locally for times that are very long compared to thermal and pressure equalization times. This fact alone strongly argues against local shock heating from a single explosion as being the primary source of energization of flares. This must not be construed as arguing against shocks being created by the flare but instead that something must go on initially for times longer than a single shock.

Induction Currents and Run-Away Acceleration

Since we have chosen typical flux loop dimensions of magnetic fields and dissipation times, the induction potential associated with the change in field due to dissipation can be calculated from Maxwell's equations and typically becomes $\cong 10^9$ volts for the full length of the flux tube,

V = d/dt(inductance x current) where the inductance and current are determined by the field configuration and value, but limited by observed dimensions and total energy. Hence the large potential is more than adequate to account for high energies provided particles can run away. The value of $E_{||} \cong \frac{1}{2}$ volt/cm is orders of magnitude more than necessary for classical Coulomb-limited run-away (Dreiser field) $\cong 10^{-4}$ volts/cm at $n_e = 10^{12}$ and kT = 2 keV. This would appear, at first consideration, to be an unlimited source of accelerated particles, but instead the run-away flux can be no greater than the total current, $I = \oint J \, d(\text{area})$, at which value the induction electric field becomes saturated and no further run away can occur. The problem is that this value of the run-away current is some 6 orders of magnitude smaller than the high energy nonthermal electron flux required to account for the hard x-ray spectrum. On the other hand, one notes, that the proton flux, if extrapolated downwards in energy by a power law spectra to 4 MeV from the fiducial value of 30 MeV necessary to account for gamma rays from He, carbon, and oxygen, is almost exactly the total current necessary to bound the magnetic fields. This bizarre circumstance is contrary to normal classical coulomb collision-dominated plasmas where we expect the current carriers to be electrons with a slow drift velocity. On the other hand the equality of the induction current and the ion current is too close to be dismissed as happenstance. Instead, there is, a neat and logical way out of part of the dilemma. We require an enhanced resistivity or magnetic field dissipation mechanism in the first place. Such a phenomena is described as an enhanced dynamic friction of the current carriers. The dynamic friction can be derived and is expected from instabilities associated with a limited number density of current carriers interacting with the magnetic and electric induction fields as well as self-induced electric fields. Such instabilities (Buneman, ion wave, and hybride

waves) are extensively discussed in the literature. They indeed can occur if the current carrier population is sufficiently restricted. If this circumstance were to occur, then indeed we would have a reasonable description of additional flare phenomena. The current carrier limited instabilities would increase the wave dynamic friction to the point where the electron population was essentially immobilized and only ions - with their greater mass and smaller wave particle interaction could run away and carry the induction current of the flare.

The remaining problem is then explaining first, the restriction in the number of current carriers necessary to create the instabilities and secondly the source of the hard x rays. Only current filamentation has been proposed to explain the current carrier limitation. The non-linear limit of the tearing mode naturally leads to some concentration of current channels, called magnetic islands in Tokamac fusion research. However the extreme filamentation $(r_{minimum}/r_{maximum} \lesssim 10^{-4})$ required for flare current carrier limitation confounds modern theory.

THE TRANSITION TO CONVECTION

The sun is a convective star which means that within a distance ΔR from the surface at R all the heat must be carried by thermal convecton. We will summarize the physical arguments for ΔR rather than relying solely upon model calculations.

The boundary between convective and nonconvective core is determined by the condition that the temperature-density distribution must be not less than adiabatic, otherwise an interchange between two fluid elements, vertically, can lead to more work done on the rising element than on the subsiding one

and hence instability and hence turbulence. In the event of no turbulence and just radiative transport and pressure balance in the outer layers of a star where R and M are effectively constant lead uniquely to what is called the "radiative zero" solution (Schwarzschild 1958) where $T \propto \rho^{1/3.25}$ The exponent is quite insensitive to various model parameters and so the convective-nonconvective zone boundary occurs where the effective gas ratio of specific heats, γ, falls below $(1 + 1/3.25)$. Since a free particle gas has $\gamma = 5/3$ we only expect a lower γ where ionization occurs. Radiation pressure also lowers γ, but only asymptotically to $(1 + 1/3)$. Hence, in the sun where radiation pressure is not dominant, the convection zone boundary will occur near the onset of the highest helium ionization potential $\cong$ 50 eV depending upon density. Constituents of higher atomic number are fractionally too small to make a difference in γ.

The surface temperature of the sun, $T_{sur} \cong \frac{1}{2}$ eV and the scale height $h_{sur} = T/gM_p \cong 2 \times 10^7$ cm. $g = M_\odot G/R_\odot^2$, and M_p = mean molecular weight $\cong$ mass of the proton, (nonionized at the surface temperature). Therefore, the scale height at the convective zone boundary, $h_{con} = h_{sur}T_{con}/T_{sur} \cong 2 \times 10^9$ cm. The depth of the convective zone $\Delta R_{con} \cong h_{con}/(\gamma-1) \cong 6 \times 10^9$ cm in reasonable agreement with model calculations where $\Delta R_{con} \cong 10^{10}$ cm, (Schwartzschild 1958). The density of the convective zone boundary scales as

$$\rho_{con} = \rho_{sur}\left(\frac{T_{con}}{T_{sur}}\right)^{\frac{1}{\gamma-1}} \cong \rho_{sur}\left(\frac{T_{con}}{T_{sur}}\right)^3 \cong 2 \times 10^6 \, \rho_{sur}. \tag{1}$$

We note that this result is very sensitive to γ and hence a crude estimate.

Since $\rho_{sur} \cong 1/K_{sur}h_{sur}) \cong 5 \times 10^{-8}$ g/cm^{-3}, where K_{sur} is the surface opacity, then

$$\rho_{con} = 0.1 \ K_{sur}^{-1} \ L^{-1} \ M \ T_{con}^{3} \ g/cm^{-3} \qquad (2)$$

where we have included the scaling in terms of surface opacity, and luminosity, L, radius and mass in solar units, i.e., $\sigma T_{sur}^{4} \ 4\pi R^{2} = L$ etc. In other stars the convection zone boundary may occur at very much larger values of T_{con} than is determined in the sun by helium ionization.

TURBULENT CONVECTION

In a fully convective region, i.e., where heat transport other than by convective motions is negligible, the buoyancy force per unit volume in pressure equilibrium is $F_b = (\Delta T/T \ \rho g)$. If this force is converted into kinetic energy of the buoyancy element rising one scale height, $h = T/g$, and the energy is divided equally between kinetic and potential energy, then $F_b h = \rho v^2 = \Delta T \rho$ or $v^2 = \Delta T$. The convective heat flux ϕ should be a fraction ($\cong \frac{1}{2}$) of the mean convective velocity times ($\rho \ \Delta T$) so that the convective heat flux, which must also be the luminosity, becomes

$$\phi = \frac{1}{2} \ (v\rho \ \Delta T) = \frac{1}{2} \ \rho v^3 = L/4\pi R^2. \qquad (3)$$

The maximum convected fluid stress is $\cong \rho v^2/2$ which must be larger than the stress of the magnetic field that presumably is to be convected to the stellar surface. Therefore $B_{max}^2/8\pi = \rho v^2/2$. Since the convected heat flux in Eq. 3 must be constant, the turbulent stress $\rho v^2 \propto v^{-1} \rho^{1/3}$. In other words as we go radially outwards from the convective zone boundary the turbulent stress decreases so that once a maximum flux loop is "torn" loose, we would not expect further magnetic flux convection to take place and so once torn loose we would expect a loop of magnetic flux to emerge from the surface essentially intact as we see in sun spots. We must also check that our scaling does not violate our convection assumption of local pressure equilibrium; namely, the convection velocities should not exceed sound speed as we approach the suface. If we use equations 2 and 3

$$v_{con} = 1.1 \times 10^4 \; K^{1/3} \; L^{2/3} \; T_{con}^{-1} \; M^{-1/3} \; R^{-2/3} \; cm \; sec^{-1} \qquad (4)$$

where again solar units are used for K, L, R, and M. At the surface the

convective velocity will be larger by $(\rho_{con}/\rho_{sur})^{1/3} = T_{con}/T_{sur} = 100$, or

$v_{sur} \cong 10^6$ cm sec^{-1}. This just slightly exceeds sound speed at $T_{sur} = \frac{1}{2}$ eV

in partially ionized hydrogen so that it agrees with the solar surface con-

vective motions observed where line widths $(\Delta\gamma/\gamma)$ c $\cong 5 \times 10^5$ cm sec^{-1}.

If we use this velocity distribution, then the maximum magnetic field that

can be convected is

$$B_{max} = 1.2 \times 10^4 \left(\frac{ML}{K}\right)^{1/6} R^{2/3} \; T_{con}^{\frac{1}{2}} \; gauss. \qquad (5)$$

The magnetic fields interpreted for some white dwarfs (Angel et al., 1974)

are as large as 5×10^7 to 10^8 gauss. These fields are not obviously within

the scaling of Eq. 5 unless we recognize that in white dwarfs the convection

zone is likely to start at the boundary between a carbon-oxygen core and a

helium atmophere. Hence T_{con} (White dwarf) becomes that of an oxygen boundary

$\sim 16 \; T_{con}$ (solar). Then if L white dwarf $\cong 10^{-2} \; L_\Theta$, and K = compton opacity

at $T_{surface}$ white dward $\sim 15,000$ degrees, then $B_{max} \sim 2 \times 10^7$ gauss. A helium

burning shell will force convection to initiate deeper yet and so may explain

the somewhat larger observed fields.

THE TOPOLOGY OF CONVECTED FIELDS

The absolute maximum average field that could be convected to the surface

of the sun by these arguments if 10^4 gauss. The average fields are very much

less than this, 100 gauss, but typical sun spot fields extend up to 5000

gauss. We do not believe there is yet a strong physical argument leading to

a presiction of the ratio of maximum/average but we note that for the August 4

large flare B $\cong 10^3$ gauss which is comfortably less than the maximum value.

Furthermore, the magnetic pressure of this field, $B^2/8\pi$ is approximately the

same as the gas pressure of the photosphere so that below the photosphere the magnetic pressure will be everywhere small compared to the gas pressure so that the field will only be a small perturbation on th turbulent motions. We expect that a large stellar flare will be that turbulent extremum that convects a loop of flux of the size of the largest eddy and hence scale height, h_{con}, of the convective zone. Such eddies reach the stellar surface only rarely without breaking up roughly each scale height in agreement with the rarety of flares. Finally since vorticity is a stochastic variable in turbulence, we expect such loops to have an arbitrary twist one end relative to the other. The scale size, $h_{con} = 2 \times 10^9 \; T_{con} \; \mu R^2/M$ cm, where μ = molecular weight, and the twist are both in agreement with the topology of solar flares.

WHITE DWARF γ-BURSTS

We now consider the question whether using this model of the origin of flare fields and the associated model of the x rays from stellar flares (Colgate 1978) whether γ-bursts are a reasonable extrapolation as suggested by Mullan (1976). Mullan argues for flare densities based upon chromospheric densities. On the other hand we have pointed out that the photosphere, heated by the thermal conduction flux, expands along the flux tube rapidly and reaches pressure equilibrium in a time short compared to the flare duration. The equilibrium pressure is determined by the condition that the flare radiates at the ends mostly in the XUV, at the rate that energy is released. At constant pressure the bremsstrahlung radiation from the major length of the flare is a small fraction of the total heat.

The maximum magnetic field strength derived on the basis of the convective stress is $B_{max} \cong 10^8$ gauss, and indeed such fields are observed, but we believe a more conservative value analogous to the sun is 1/10 of this or 10^7 gauss.

This gives a pressure large (x 100) compared to the photosphere, but small (10^{-16}) compared to the base of. the convective zone pressure. The size is determined by $\ell = h_{con} \cong 4 \times 10^8$ cm where $R = R_{\Theta}/70 \cong 10^9$ cm, $\mu = 2$ and $T_{con} = 2.5 \times 10^8$ degrees. This flare size agrees with the spot size derived from light variation (Mullan, 1976). Then if we choose the same topology of a twisted flux loop of diameter = 1/10 length, then the total flare energy $W_T = 2 \times 10^{36}$ ergs. This energy places the median size γ-burst at roughly $D \cong 30$ pc as discussed in Mullan (1976). Both his discussion and Strong et al. (1974) and Fishman (1978) conclude that γ-bursts are more likely at $D \cong 300$ to 3000 pc which requires 10^2 to 10^4 times our suggested energy. Mullan models these values by choosing $B_0 = 10^8$ gauss and $\ell = R_0 = 10^9$ cm. The time scale of the flux dissipation is an uncertain modeling parameter but if we use the resistive'instability as the basis of the filamentation and enhanced resistance, then $t = t_{\Theta} \, \ell/\ell_{\Theta} \, (V_A/V_{A\Theta})^{2/3}$ where $\ell =$ length. of the flare, $= h_{con} = 4 \times 10^8$ cm and $V_A =$ the Alven speed. $t_{\Theta} \cong 100$ seconds for typical solar flares, $\ell/\ell_{\Theta} = 1/5$ and $(V_A/V_{A\Theta})^{2/3} \cong 1/10$ so that $t \sim 1$ to 2 sec in agreement with typical γ-bursts (Cline et al, 1973). Then the temperature

··determined by thermal conductivity alone becomes

$$T = 2 \times 10 \left(\frac{W_T \, \ell}{\pi R_0^2 \, t K_0} \right)^{2/7} \tag{6}$$

where the quantities are scaledto the August 4, 1972, solar flare $W_T = 10^{31}$ ergs, $\ell = 2.5 \times 10^9$ cm, $R_0 = 10^8$ cm, $t = 10^3$ seconds, so that for the white dwarf flare $T_{conduction} = 8 \times 10^9$ deg $\cong 800$ keV. This is higher than estimated for γ-bursts $\cong 150$ keV (Cline and Desai, 1975) but the thermal conduction loss solution is unrealistic for these high temperatures. In particular the density distribution based upon thermal conduction, pressure balance and radiation primarily in XUV from the ends assumes that the bremsstrahlung

contribution to the radiation loss is

small. This assumption is valid in the case of solar flares where $T_{max} \cong 1$ to

2×10^7 degrees and the XUV radiation loss $\propto T^{-\frac{1}{2}}$ dominates over bremsstrahlung

$T^{+\frac{1}{2}}$ up to 10^7 deg. In this latter case the above three restrictions result in a

total radiation loss per logarithmic temperature interval $\propto T^{\frac{1}{2}}$. In the case

of nonrelativistic bremsstrahlung this becomes $\propto T$ and for relativistic

bremsstrahlung ($kT_e \geq \frac{1}{4} mc^2$) the radiation loss per logarithmic temperature

interval becomes proportional to $T^{3/2}$. Thus the major energy loss will occur

in the region of T_{max} for the white dwarf flares as opposed to lower tempera-

ture XUV in solar flares. This is simply because high temperature bremsstrah-

lung is a more efficient radiation mechanism than XUV, given the thermal con-

duction solution. Then the surface layers of the star will continue to expand

up the flux tube until the radiation rate equals the heating rate. We note that

the sound speed C_s at 150 keV is $C_s \cong 10^9$ cm sec^{-1} and the time to reach pressure equilib

rium is $\ell/C_s \cong 2/10$ seconds. Thermal stability considerations limit the tempera-

ture to the value separating the relativistic and nonrelativistic bremsstrahlung,

i.e., $kT_e \cong \frac{1}{4} mc^2 \cong 100$ to 150 keV because only below this temperature is the

region of T_{max} stable. Then the bremsstrahlung radiation loss rate in this

region equals the heating rate and using the results of Maxon (1972) for

electron-electron and relativistic bremsstrahlung we obtain

$$n_e \cong 7 \times 10^{10} \left(\frac{W_T}{Vol\ t} \right)^{\frac{1}{2}} = 10^{17}\ cm^{-3}. \tag{7}$$

This is somewhat higher than estimated by Charikov and Starbunov (1975) but

they simply took the limiting dimensions given by $\Delta x = c\Delta t$ and derived a

density of $n_e \geq 10^{16}\ cm^{-3}$ assuming bremsstrahlung. Thus we have a description

of a γ-burst as the largest stellar flare - following the original suggestion

of Mullan, but substituting a solar flare model limited by stellar convection,

and based upon conduction, pressure balance, and XUV radiation.

ACCELERATION AND NUCLEAR SPALLATION

We now consider the likely particle acceleration and spallation in such

a flare. We have already shown in solar flares how it is consistent to assume

that all the current of the flare is carried by run-away ions, and the electrons

are immobilized by instabilities. The current and potential drop in the

present case of a largest white dwarf flare are: $I = 5 R B_\Theta = 10^{15}$ amps and

$V = d/dt$ (inductance x current) $= W_T/I = 4 \times 10^{14}$ volts.

NUCLEAR GAMMA RAYS

The acceleration potential along the field is so large that we can

assume that essentially all the run-away ion current is above nuclear excita-

tion threshold, ie., ≥ 10 MeV/nuclean. Under these circumstances the direct

production of nuclear gamma rays in the "transparent" ($\rho r \cong 2$ gm cm^{-2}) high

temperature plasma becomes

$$\phi_\gamma = \phi_i \, n_{target} \, Vol \, \sigma_\gamma, \tag{8}$$

where ϕ_i is the flux of runaways, 10^{19} cm^{-2} sec^{-1}, n_{target} is $X \, n_e = 10^{17}$

X cm^{-3}. Vol $= 5 \times 10^{23}$ cm^3 and the cross section for production of

nuclear gamma rays, σ_γ, is variously 10 to 100 millibarns. If we consider

the absolute maximum gamma production from the run-away ion current, then

the neutron capture gammas are probably the largest production source. Then

for a helium atmosphere $X \, n_e \cong n_{He} \cong 10^{13}$, $\sigma_\gamma = \sigma_{spallation} \cong 10^{-25}$ cm^2 and

$\phi_\gamma = 10^{35}$ γ's sec^{-1}. Since the flare duration is roughly 1 sec, this is also

roughly the total nuclear gammas expected.

ION TEMPERATURE RUNAWAY

It is possible that the ion temperature could run away ($T_i \cong 10$ MeV) from the electron temperature ($T_e \cong 150$ keV) because the electron temperature is so high and classical dynamic friction so small (Colgate 1975). In this case we might expect that all nucleii in the flare volume would be spalled and then the maximum gamma rays would correspond to the neutron capture of $2 \times N_{He} \cong 10^{41}$ gamma rays. The prediction of an ion temperature runaway corresponds to the case where a major fraction (~25%) of the energy of the flare ends up as ion temperature and spallation. The coherent dynamic friction in flare instabilities is not known well enough to predict this result.

References

Angel, J.R.P., Carswell, R. F., Strittmatter, P. A., Beaver, E. A. and Harms, R. 1974, Ap. J. (Letters) 194, L47.

Charikov, Yu. E. and Starbunov, Yu. N., 1975, 14th International Cosmic Ray Conference, Munich, Vol. 1 paper Og5-4.

Cline, T. L. and Desai, U. D., 1975, Ap. J. (Letters), 196, L43.

Colgate, S. A., 1978, Ap. J. 221, 1068.

Colgate, S. A., 1977, 15th International Cosmic Ray Conf. Plovdiv, Bulgaria.

Colgate, S. A., 1975, Ap. J. 195, 493.

Fishman, J. 1978, NASA Goddard preprint.

Maxon, S., 1972, Phys. Rev. A 5, 1630.

Mullan, D. J. 1974, Ap. J. 192, 149. 1975, Ap. J. 200, 641. 1976, Ap. J. 208, 199.

Parker, E. N., 1971, Ap. J. 164, 491.

Petschek, A., 1964, Physics of Solar Flares, ed. W. N. Hess, (NASA, Sp-50), p. 425.

Schwartzschild, M., 1958, "Structure and Evolution of the Stars," Princeton Univ. Press.

Spicer, D. S., 1977, Solar Phys. 51, 431.

Stecker, F. W. and Frost, K. J., Nat. 245, 70.

Strong, B., Klebesadel, R. W., Olsen, R. A., 1974, Ap. J. (Letters) 188, L1.

III. COSMIC SPECTROSCOPY

N78-31978 D7-93

DETECTION OF 511 keV POSITRON ANNIHILATION
RADIATION FROM THE GALACTIC CENTER DIRECTION*

by

M. Leventhal
Bell Laboratories
Murray Hill, New Jersey 07974

and

C. J. MacCallum** and P. D. Stang**
Sandia Laboratories
Albuquerque, New Mexico 87115

ABSTRACT

A balloon-borne germanium γ-ray telescope was flown over Alice Springs, Australia, in an attempt to detect sharp spectral features from the Galactic Center direction. A 511 keV positron annihilation line was detected at a flux level of $(1.21 \pm 0.22) \times 10^{-3}$ photons/sec/cm^2. Suggestive evidence for the detection of the three-photon positronium continuum is presented. A discussion of the possible origin of the positrons is given.

Historically, the first astrophysical gamma-ray line observation was reported at an energy near 0.5 MeV from the Galactic Center direction. Johnson, Harnden and Haymes (1972) and Johnson and Haymes (1973), employing a NaI scintillation telescope from a balloon platform, originally reported a spectral feature at 476 ± 24 keV with a flux of $(1.8 \pm 0.5) \times 10^{-3}$ photons $cm^{-2} sec^{-1}$ at earth. Based on these pioneering observations, several explanations of the feature were put forth; (i) Fishman and Clayton (1972) and Kozlovsky and Ramaty (1974) suggested cosmic ray excitation of 478 keV interstellar ^7Li nuclear radiation via the reactions $^7Li(p,p')^7Li^*$, and $^4He(\alpha,p)^7Li^*$, respectively; (ii) Ramaty, Borner, and Cohen (1973) and Guthrie and Tademaru (1973) suggested 511 keV positron annihilation radiation gravitationally redshifted from the surface of small neutron stars, and (iii) Leventhal (1973) suggested interstellar positronium (e^+e^- bound state) annihilation radiation. In the latter case an apparent redshift arises when the three-photon annihilation spectrum of $^3S_1$ ortho-positronium is combined with the 511 keV annihilation line of $^1S_0$ para-positronium and the sum is convoluted with the inherently poor energy resolution of a NaI system. Since this earlier work, the Rice University group has repeated the experiment with an improved NaI system and now report the feature to be at 530 ± 11 keV with a flux of $(8.0 \pm 2.3) \times 10^{-4}$ photons $cm^{-2} sec^{-1}$ (Haymes et al., 1975). These workers suggest that the quantitative differences in flux and average energy between their earlier and later flights may be due to several factors, including

a narrower ·beamwidth in the latter experiment (13° FWHM versus 24° FWHM),time dependence, or different aiming directions. They also indicate their belief that the line is really the 511 keV free positron annihilation line shifted to higher energies by a statistical fluctuation in their data. Clearly, an independent study of this feature with finer energy resolution is needed to clarify.what has become a confusing situation. The purpose of this letter is to report the initial results of such a study.

A balloon-borne high-resolution (3.2 keV FWHM at 511 keV) γ-ray telescope was flown on 11-12 November, 1977 from Alice Springs, Australia. While the instrument was essentially the same as that previously described in the literature (Leventhal, MacCallum and Watts, 1977), an important modification made for this flight was the replacement of the central Ge(Li) detector with a larger volume, $\sim$130 cm^3 high-purity germanium detector. This necessitated an increase of the effective entrance aperture in the 400 lbs NaI anticoincidence shield to 15° FWHM at 511 keV. Observations of the Galactic Center direction ($\alpha = 17^h44^m$, $\delta = -28°0'$) were made on two successive days at a mean atmospheric depth of 3.6 grams cm^{-2} Data were accumulated in alternate 20-minute target-background segments with the telescope maintained at the same zenith angle but reflected about the north-south direction in azimuth for the background measurements. Since the Galactic Center rose very nearly in the east and set in the west, the background

may be said to have risen in the west and set in the east. However, the background observations swept over the celestial sphere with fixed declination, $\delta = -28°0'$ and right ascension α varying between 8^h49^m and 3^h09^m paying no special attention to any particular point. This method of data acquisition allows equal background measurements to the east and the west and eliminates the effect of any hypothetical asymmetry. A total of 17.3 hours of data were accumulated in this manner.

In Fig. 1, we show energy spectra in the vicinity of 511 keV for the sum of all GC target runs and the sum of all GC background runs. These are basically raw data having been corrected only for drifts in the energy calibration with time. Three clearly significant, cosmic-ray induced telescope lines are evident in these data and have been seen by us in previous balloon flights. These are at 439 keV from $^{23}Na(n,n')^{23}Na^*$, at 472 keV from $^{23}Na(n,\gamma)^{24}Na$ and/or $^{76}Ge(n,\gamma)^{77}Ge$, and at 511 keV from positron annihilation. The instrumental 511 keV line seen by us and by all other workers in the field arises from cosmic-ray generated positrons in the telescope and the atmosphere. A feeble unidentified line is also evident at 497 keV and has been seen in previous flights. A striking characteristic of this data, however, is the near-doubling of the 511 keV line count rate above continuum when the Galactic Center is in view. None of the other instrumental lines show a statistically significant difference between target and background count rates. The raw target data of Fig. 1 contain an excess of

counts in the energy bins 509 through 512 keV which is

significant at the 4.5 σ level. However we have here

treated each of the 20 minute segments equally and ignored the

real effects of increasing instrumental background and atmospheric

attenuation as the telescope points down toward the horizon.

When target-background pair difference rates are formed,

corrected for atmospheric attenuation, weighted inversely as

to their variances, and averaged, the excess becomes significant

at the 5.6 σ level. When detector area, efficiency, and dead-

time factors are included, the excess represents a 511 keV line

flux of $(1.22 \pm 0.22) \times 10^{-3}$ photons $cm^{-2} sec^{-1}$ at the top of the

atmosphere with a FWHM $\lesssim 3.2$ keV.

The increase in statistical significance which occurs

when the data are weighted in a manner appropriate to an extra-

terrestrial source is strong evidence for such an origin as

opposed to an instrumental or atmospheric origin. The data

were also divided into six subgroups corresponding to Galactic

Center ascending, near zenith, and descending, on each of two

days. The background 511 keV line rate was essentially the same

for each subgroup and a positive target-background excess was

obtained for each subgroup.

The azimuthal dependence of the instrumental 511 keV

line intensity was studied in flight at enhanced count rate with

the anticoincidence shield off. These data are consistent with

there being no azimuthal dependence at all.

Stecker (1969) and Leventhal (1973) have pointed

out that energetic positrons stopping in the cold dilute inter-

stellar gas should annihilate predominantly from one of the

two ground state configurations of positronium. Should this

be the case, 25% of the annihilations will be from the para

state yielding two antiparallel 511 keV photons, whereas 75%

of the annihilation will be from the ortho state yielding

3 γ-rays in a plane. The energy spectrum of the 3 γ-ray photons,

P(E)dE, was calculated originally by Ore and Powell (1949) and

consists of a continuum extending from 511 keV down to 0 keV.

The maximum value of P(E)dE is at 511 keV and it decreases

roughly monatonically to a value of 0 at 0 keV. It is impor-

tant to determine whether or not evidence for a three-photon

contunuum is to be found in our data. Because of the good energy

resolution of the system, no apparent redshift of the 511 keV

peak is expected. Rather, the three-photon continuum would give

rise to a small excess of counts in the channels extending down

from 511 keV to lower energy. Indeed, a slight but ubiquitous

excess is indicated in Fig. 1. However, this might be attributed

to the general x-ray - γ-ray inverse power law continuum

emanating from the Galactic Center direction which is seen very

clearly in the data at lower energy The presence of this

additional continuum radiation greatly complicates the task of

extricating any potential three-photon spectrum.

In. Fig. 2a, the Galactic Center difference spectrum extrapolated to the top of the atmosphere is plotted between 70 keV and 700 keV. This spectrum was obtained by first forming target background pair difference rates on a channel-by-channel basis, correcting each pair for atmospheric attenuation, weighting the pairs as their variances and forming an average. The resulting differential count rate spectrum is then converted to a photon flux on a channel-by-channel basis by dividing by the detector area, photopeak efficiency, and live time factor. This spectrum is shown in Fig. 2a where the data have been lumped into bins of increasing width to reduce the apparent statistical scatter.

In some cases, slight drifts in energy calibration cause large fluctuations in the difference spectrum in the wings of strong instrumental lines. To minimize confusion in curve-fitting a total of five energy segments have been deleted that are potentially contaminated by known telescope lines which appear clearly in both the target and background spectra at 139 keV, 185 keV, 198 keV, 238 keV and 472 keV.

An inverse power law gamma-ray continuum emanating from the Galactic Center is clearly evident in these data as it was in the earlier NaI spectra (Haymes et al., 1975). Most likely, this represents a composite spectrum from the many continuum sources in the field of view, e.g., GCX, GX 3+1, GX 5-1, GX 1+4, etc. An apparent departure from the continuum is evident to the low-energy side of 511 keV. Evidence for any

continuum radiation has disappeared from the data to the high-energy side of 511 keV. The data have been least-squares fit to the sum of three functions, (1) a Gaussian line near 511 keV, (2) a three-photon continuum as determined by Ore and Powell (1949), and (3) an inverse power law continuum. The parameters were the width, intensity, and location of the line, the intensity of the three-photon continuum, and the intensity and exponent of the power law. In Fig. 3, χ^2 is shown as a function of the fraction f (held fixed) of positrons allowed to annihilate via the positronium state. For f = 1.0, corresponding to 100% positronium annihilation, 75% of the intensity is in the three-photon continuum and 25% in the line at 511 keV. For f = 0.0, there is no three-photon continuum at all. This function has a minimum in the vicinity of 100% positronium annihilation which is very suggestive since this is what one expects on theoretical grounds for most astrophysical plasmas (Crannell, Joyce, Ramaty, and Werntz, 1976). However, on the basis of the χ^2 test alone, even the fit for the case f = 0 is acceptable. Application of the F test for an additional term (Bevington, 1969) indicates, at better than the 99% confidence level, however, that a statistically significant improvement in the fit has been made by inclusion of the three-photon continuum. Without belaboring the point, we believe that strong but not conclusive evidence for the three-photon continuum has been presented.

The data presented above, taken in conjunction with the most recent Rice University results, unambiguously establish the existence of a 511 keV positron annihilation line from the direction of the Galactic Center, and suggest the existence of a positronium continuum. While it .seems likely that the radiation is coming from an extended region of space, were it all to originate at the distance of the Galactic Center (d = 10 kpc), 8.1×10^{42} annihilations per second are required, corresponding to a luminosity of 1.4×10^{37} ergs sec^{-1} in the 511 keV line. An additional 2.5×10^{43} annihilations per second are required if one accepts the existence of the positronium continuum. It is interesting to consider possible origins for this radiation and in the space below, we mention four possibilities which have been discussed in the literature.

During the past decade, elaborate explosive nucleo-synthesis calculations have been performed which purport to follow the complex nuclear reaction matrix that takes place when stars explode and hydrodynamically expand. A remarkable result of these calculations has been their ability to repro-duce large portions of the observed cosmic abundance table. The calculations indicate that many of the stable species should be produced first as beta-unstable radioactive elements that often decay with the emission of a positron. Colgate (1970) and Clayton (1973b) have indicated that supernova-produced ^{56}Co or ^{44}Sc could yield enough positrons to account

for the observed feature. Recently, Clayton and Hoyle (1974)
and Truran (1975) have pointed out that nova-produced ^{22}Na
is an abundant source of positrons. In principle, this could
also account for the feature. Support for either of these
hypotheses would come with the detection of other nuclear
gamma-ray lines predicted to accompany the decay of explosively
produced radioactive matter (Clayton, 1973a). No believable
evidence for these lines has yet been produced or exists in
our data.

Radio pulsars like the Crab are spinning neutron
stars whose radiations are powered by a gradual loss of rota-
tional kinetic energy. Although pulsar models which attempt
to explain the energy transfer processes involved must still
be considered uncertain, it is interesting to note that the
more widely accepted models generate large positron fluxes in
the co-rotating magnetosphere above the star via various pair
production processes (Cheng and Ruderman, 1977). For the
Crab in particular, positron fluxes as large as 10^{41} per second
have been envisioned (Sturrock, 1971). The large number of
radio pulsars within the field of view of our γ-ray telescope
could presumably be injecting an adequate number of positrons
into the interstellar medium to account for the observed
feature.

A secondary positron component of the interstellar
medium is expected from cosmic-ray interactions with the cold

interstellar matter leading to positive pion decay and the production of beta-unstable nuclei in spallation reactions. Ramaty, Stecker, and Misra (1970) have indicated that the lower-energy positrons from spallated CNO beta emitters should make the dominant contribution to any 511 keV annihilation line. These workers attempted to estimate a line flux from the Galactic Center direction based upon various models for the cosmic-ray energy spectrum. The largest of their flux estimates is about one order of magnitude smaller than the current observations. However, the calculations are very sensitive to the assumed intensity of low-energy cosmic-rays $(E \lesssim 100$ MeV$)$, about which very little is known because of solar modulation effects. Support for this hypothesis would come with the detection of Doppler-broadened nuclear gamma-ray lines that must be excited in collision processes occurring in parallel with the production of CNO beta emitters. Rygg and Fishman (1973) have calculated the expected relative intensity of the 511 keV line to various nuclear lines. They find six lines which should have an intensity in excess of the 511 keV intensity, e.g., ^{7}Li(478 keV), ^{24}Mg(1.37 MeV), ^{12}C(4.43 MeV), etc. Evidence for the existence of some of these broad lines is to be found in the Galactic Center data of Haymes et al., (1975) and in recent HEAO A observations. Hence a cosmic-ray interaction origin for the annihilation line must be taken seriously. Our own experiment did not have adequate sensitivity

to detect these features which are hundreds of keV in width.
It should be pointed out, however, that the low-energy cosmic-
ray densities considered by Ramaty, Stecker, and Misra (1970)
already lead to problems regarding the stability of the galaxy
if they are distributed over the entire disc. If it is necessary
to increase this density an order of magnitude to bring the
calculations into agreement with observation, the hypothesis may
become untenable.

Perhaps the most exotic possible origin of the 511 keV
line is black hole evaporation. Hawking (1974) originally pointe
out that quantum effects will cause black holes to radiate like
a black body whose temperature is inversely proportional to
mass, leading possibly to a final explosion. However, this
effect appears important only for small black holes presumably
made in the early universe. In the present epoch, primordial
black holes of initial mass near 10^{15} grams will be approaching
their most luminous phase. Calculations indicate that for
these primordial black holes, the energy will be radiated 1
percent as gravitons, 45 percent as neutrinos, 45 percent as
electrons and positrons, and 9 percent as photons. The possi-
bility of detecting these radiations has been discussed by
Page and Hawking (1976), Carr (1976), and Rees (1977). By
attributing the entire observed 511 keV line flux to positrons
from the evaporation or explosion of primordial black holes,
it is in principle possible to set an upper limit on the

number of such objects within the galaxy. However, this calculation is fraught with such uncertainty that it is perhaps best left for a later time. Some idea of the kind of limit which ultimately can be achieved follows from the assumption that the 10^{15} gram primordial black holes are distributed uniformly throughout the galaxy which fills our field of view to a distance of 20 kpc, that the positrons are emitted over a period of 10 billion years with a characteristic energy of 150 MeV, and that most of them annihilate within the galaxy at low energy. This obviously oversimplified picture yields a limit of $\lesssim 10^{22}$ primordial black holes which is somewhat smaller than the present upper limit determined from the diffuse gamma-ray background.

Undoubtedly, the positrons giving rise to the 511 keV feature reported in this letter come from a variety of processes. For the present, only the cosmic-ray interaction processes can be identified as a contributor with some certainty. Future experiments with germanium systems of greater sensitivity and/or spatial resolution such as those planned for HEAO C and the Gamma Ray Observatory should clarify the situation further.

This experiment was performed under difficult circumstances in a remote location. Without the help of many people it would not have been possible. Specifically, the authors would like to thank P. E. Havey, G. C. Hauser, A. F. Huters,

C-3

FIGURE CAPTIONS

Figure 1   Energy spectra in the vicinity of 511 keV for the sum of all GC target (circles) and GC background (squares) measurements. Raw data corrected only for drifts in the energy calibration. Each point represents a 1 keV energy bin. Note that of the instrumental lines shown only the 511 keV line shows an enhanced count rate in the target spectrum.

Figure 2a   Differential photon spectrum for the target direction GC at the top of the atmosphere. The solid line is a least-squares fit to the data as discussed in the text. The line center was found at 510.7 $\pm$ 0.5 keV with a width limited by system resolution at $\stackrel{<}{\sim}3.2$ keV. The parameter f was found to be 0.92

Figure 2l   An expanded version of Fig. 2a in the vicinity of 511 keV.

Figure 3 χ^2 versus f, the fraction of positrons annihilating via the positronium state. For 57 degrees of freedom and 5 parameters.

REFERENCES

Bevington, P.R., 1969,"Data Reduction and Error Analysis for the Physical Sciences", McGraw-Hill, New York.

Carr. B. J., 1976, Ap. J. 206, 8.

Cheng, A. F. and Ruderman, M. A., 1977, Ap. J. 214, 598.

Clayton, D.D., 1973a, "Explosive Nucleosynthesis", edited by Schramm, D. N. and Arnett, W. D., University of Texas Press, page 264.

Clayton, D. D., 1973b, Nature Phys. Sci., 244, 137

Clayton, D. D. and Hoyle, F, 1974, Ap. J. 187, L101.

Colgate, S. A., 1970, Ap. and Sp. Sci., 8, 457.

Crannell, C.J., Joyce, G., Ramaty, R., and Werntz, C, 1976, Ap.J. 210, 582.

Fishman, G. J. and Clayton, D. D., 1972, Ap. J. 178, 337

Guthrie, P. and Tademaru, E., 1973, Nature Phys. Sci. 241, 77.

Hawking, S. W. 1974, Nature, 248, 30.

Haymes, R. C., Walraven, G. D., Meegan, C. A., Hall, R. D., Djuth, F. T., and Shelton, D. H., 1975, Ap. J., 201, 593.

Johnson, W. N., Harnden, F. R., and Haymes, R. C., 1972, Ap. J. 172, L1.

Johnson, W. N. and Haymes, R. C., 1973, Ap. J. 184, 103.

Kozlovsky, B. and Ramaty, R. 1974, Ap. J. 191, L43.

Leventhal, M., 1973, Ap. J. 183, L147.

Leventhal, M., MacCallum, C. J., and Watts, A. C., 1977, Ap. J. 216, 491.

Ore, A. and Powell, J. L., 1949, Phys. Rev. 75, 1696.

Page, D. N. and Hawking, S. W., 1976, Ap. J. 206, 1.

Ramaty, R., Börner, G., and Cohen, J. M., 1973, Ap. J. 181, 891.

Ramaty, R., Stecker, F. W., and Misra, D., 1970, J. Geophys. Res. 75, 1141.

Rees, M. J. 1977, Nature, 266, 333.

Rygg, T. A. and Fishman, G. J., 1973, (Denver) Proc. 13th Intl. Cos. Ray Con. 1, 472.

Stecker, F. W., 1969, Ap. and Sp. Sci., $\underline{3}$, 579.

Sturrock, P. A., 1971, Ap. J. $\underline{164}$, 529.

Truran, J. W., 1975, private communication.
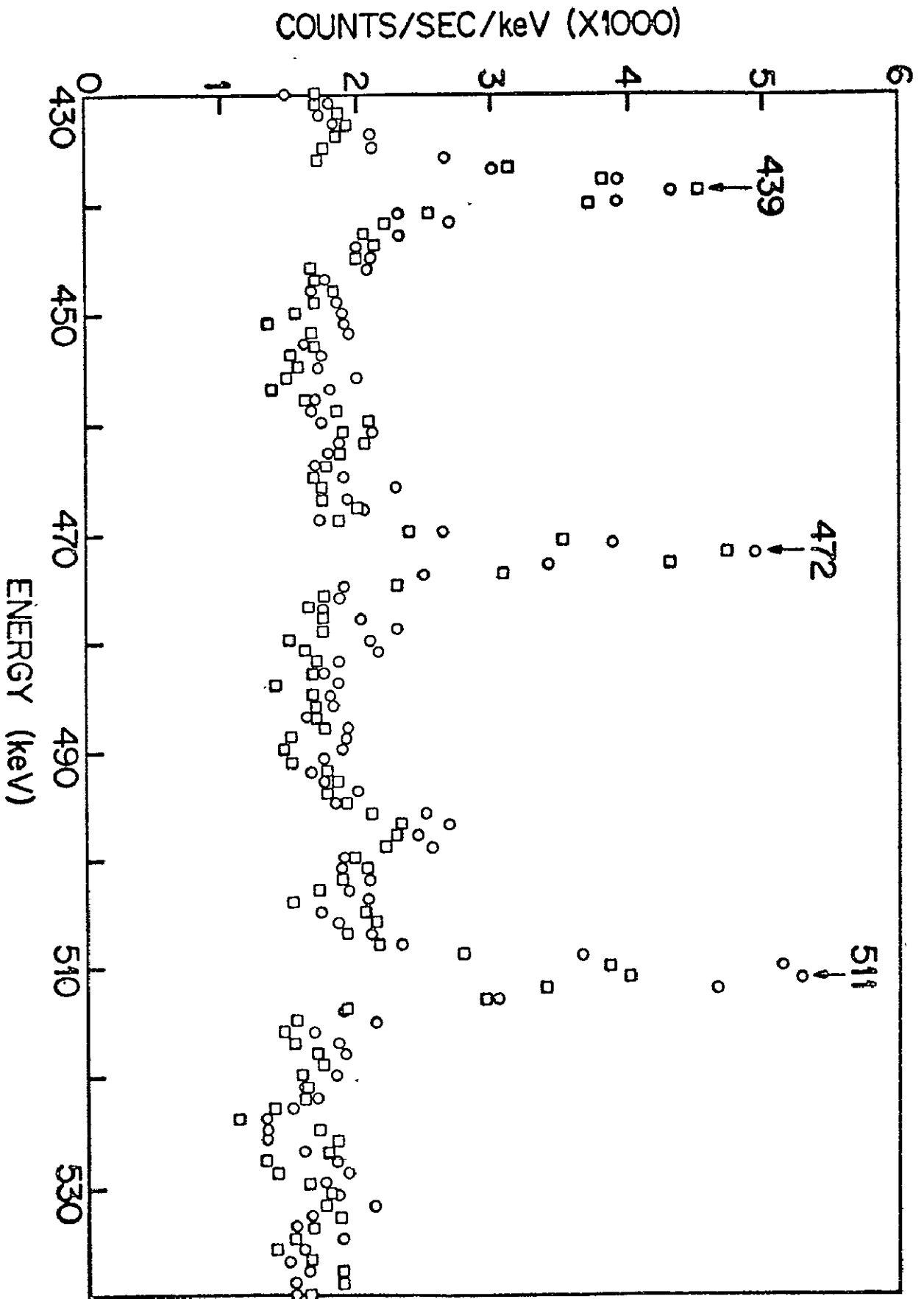
FIGURE 1
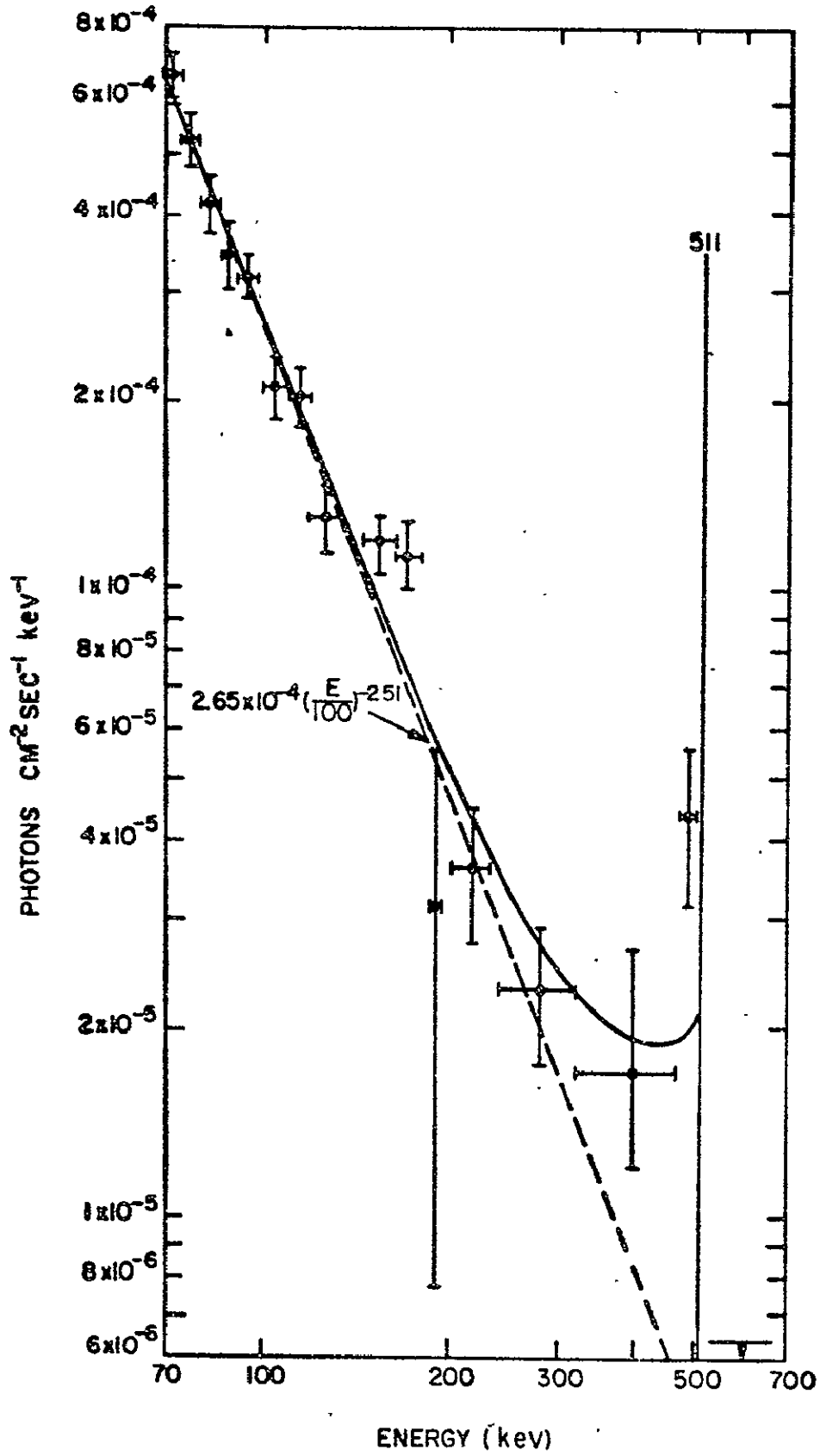
FIGURE 2a
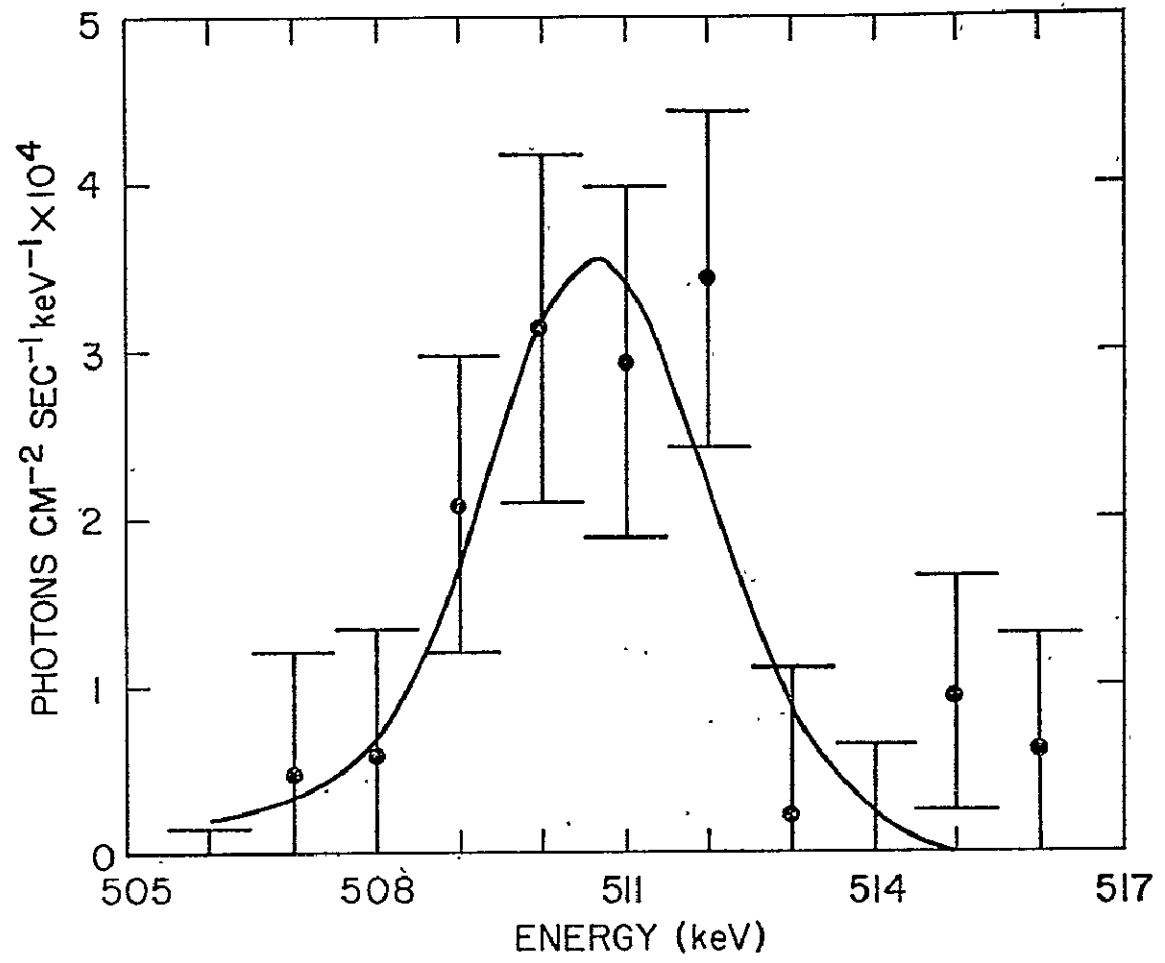
FIGURE 2b
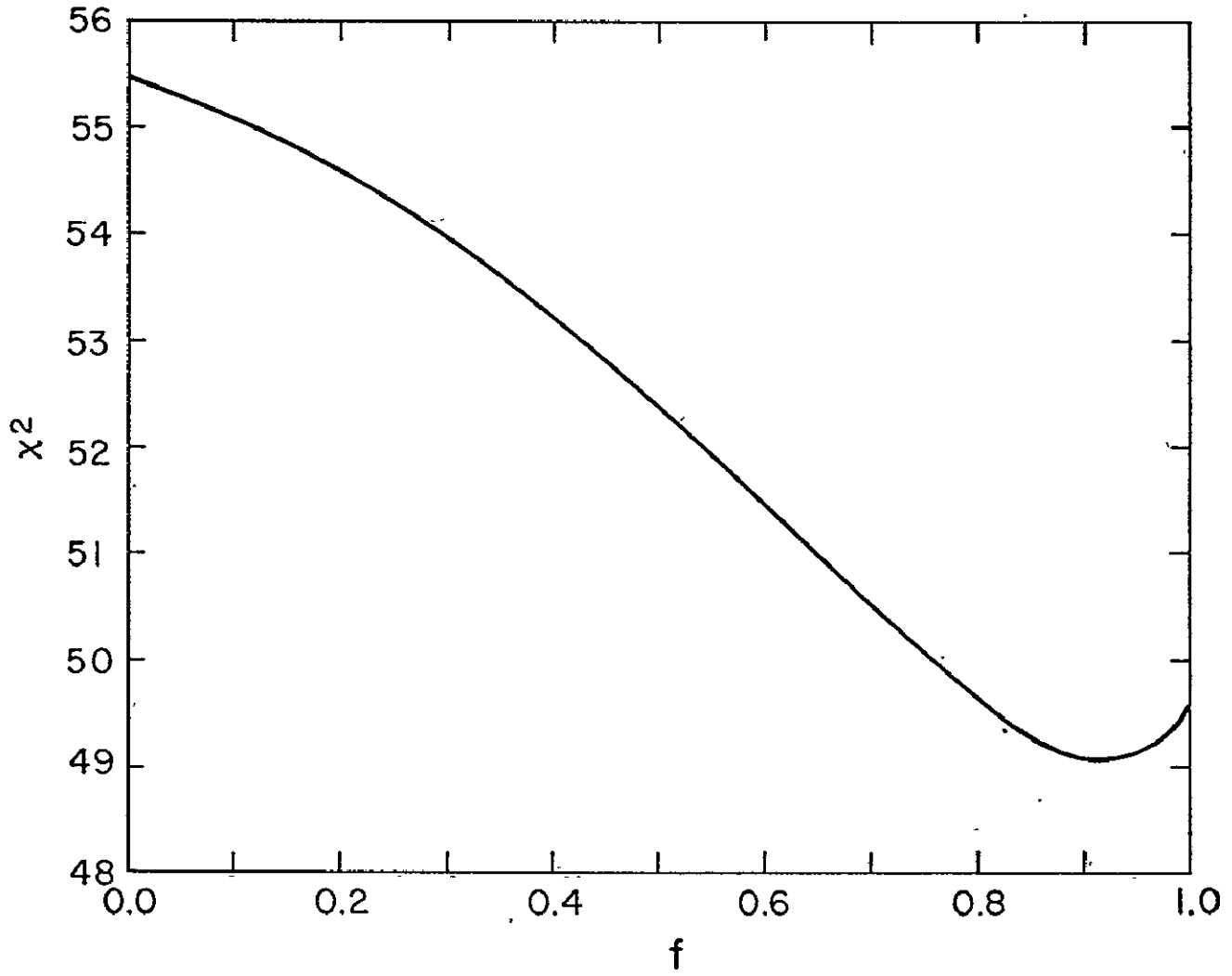
FIGURE 3

THE GALACTIC GAMMA RAY FLUX IN THE 0.06 TO 5 MEV RANGE

D. Gilman, A.E. Metzger, R.H. Parker*
Jet Propulsion Laboratory
California Institute of Technology
Pasadena, Calif. 91103 .

J.I. Trombk,
Goddard Space Flight Center
Greenbelt, Md. 20771

In using the Apollo 16 spacecraft as an occulter, the Apollo Gamma-Ray Spectrometer (AGRS) obtained information on the spectrum of 0.06 to 5 MeV gamma-ray emission from the longitude range $-50° \leq \ell \leq 22°$ of the Galactic plane. Taken with observations of Haymes, et al. (1975), Wheaton (1976), and Imhof and Nakano (1977), the spectrum of Galactic emission near 1 MeV over this range of longitudes is

$$(1.35 \pm 0.45) \cdot 10^{-3} \, (h\nu/1 \text{ MeV})^{-(2.8 \pm 0.1)} \text{ photons/cm}^2 \text{ sec MeV rad.}$$

The agreement with hard X-ray observations of the Galactic central regions suggests that an ensemble of point sources is responsible. A simple power-law connection between the hard x-ray range and the 100 MeV range is not permitted by the Apollo results. Apollo 16 upper limits to the cosmic 4.4 MeV line flux (Trombka, et al., 1977) imply that the ratio of line strength to continuum emission for the region observed by Haymes, et al. (1975) is higher than the Galactic average.

1 INTRODUCTION

Excluding the Crab nebula, it is generally thought that Galactic photons in the energy range 60 keV to 5 MeV come either from discrete sources powered by accretion in binary systems or a diffuse source from the interaction of cosmic ray electrons and matter in the interstellar medium. At X-ray energies of a few keV, emission from the plane is dominated by sources in the Uhuru catalog with luminosities near the Eddington limit. By 60 keV, however, the flux from most of the Galactic Uhuru sources has fallen drastically, leaving only Cygnus X-1 and the Crab nebula as strong point sources (Wheaton, 1976) and a large number of low luminosity sources which may account for virtually all the emission from the plane in the low energy gamma ray range. Alternatively, the emission could come from the

---

*Present address:
ITT, Aerospace Optical Division, Fort Wayne, In. 46803

interstellar medium, in which case the spectrum reveals important information on the shape of the cosmic ray electron spectrum in the few MeV region. The spectrum is too steep to contain a substantial contribution from inverse-Compton scattered starlight or 3° background radiation.

2 INSTRUMENTATION

The primary detector of the AGRS was a thallium-activated crystal of sodium-iodide in the shape of a right circular cylinder 7 cm in diameter and 7 cm long. It was viewed at one end by a photomultiplier tube and surrounded on all other surfaces by a thin charged-particle detector for the rejection of cosmic ray events in the primary detector. The AGRS was sensitive to gamma rays with energies between 60 keV and 10 MeV, depending on the gain setting, and its primary purpose was the detection of gamma rays from the moon for studies of lunar surface composition. A full description of the instrument can be found in Harrington, et al. (1974).

The AGRS had a nearly isotropic sensitivity to gamma rays, and in order to take advantage of the time in cis-lunar space on the return of Apollo 16 from the moon, the boom carrying the AGRS was partially extended so that the spacecraft occulted ~1 rad^2 of the sky as seen by the detector. When the spacecraft was maneuvered so that cosmic sources of gamma rays were occulted, decreases in the count rate were expected, allowing us to obtain angular and spectral information. Figure 1 shows the position of the AGRS relative to the spacecraft in the gamma-ray astronomy configuration.

The detector was kept 2 m from the spacecraft for 34 of the last 39 hours of the mission, and a series of maneuvers was executed so that every part of the sky was eventually occulted. In these maneuvers, the spacecraft rolled about its axis of symmetry, (the X-axis in Figure 1) with a period of 20 minutes almost broadside to the sun, performing the function of passive thermal control (PTC) for the vehicle structure. The four PTCs, their spin axes, and the amount of instrument live-time in each maneuver are listed in Table 1. The zones of occultation by the spacecraft were between 26° and 112° from the spin axis. Energy-dependent partial transmission through the Service Propulsion System (SPS) nozzle modulated zones 112° to 145° from the spin axis.
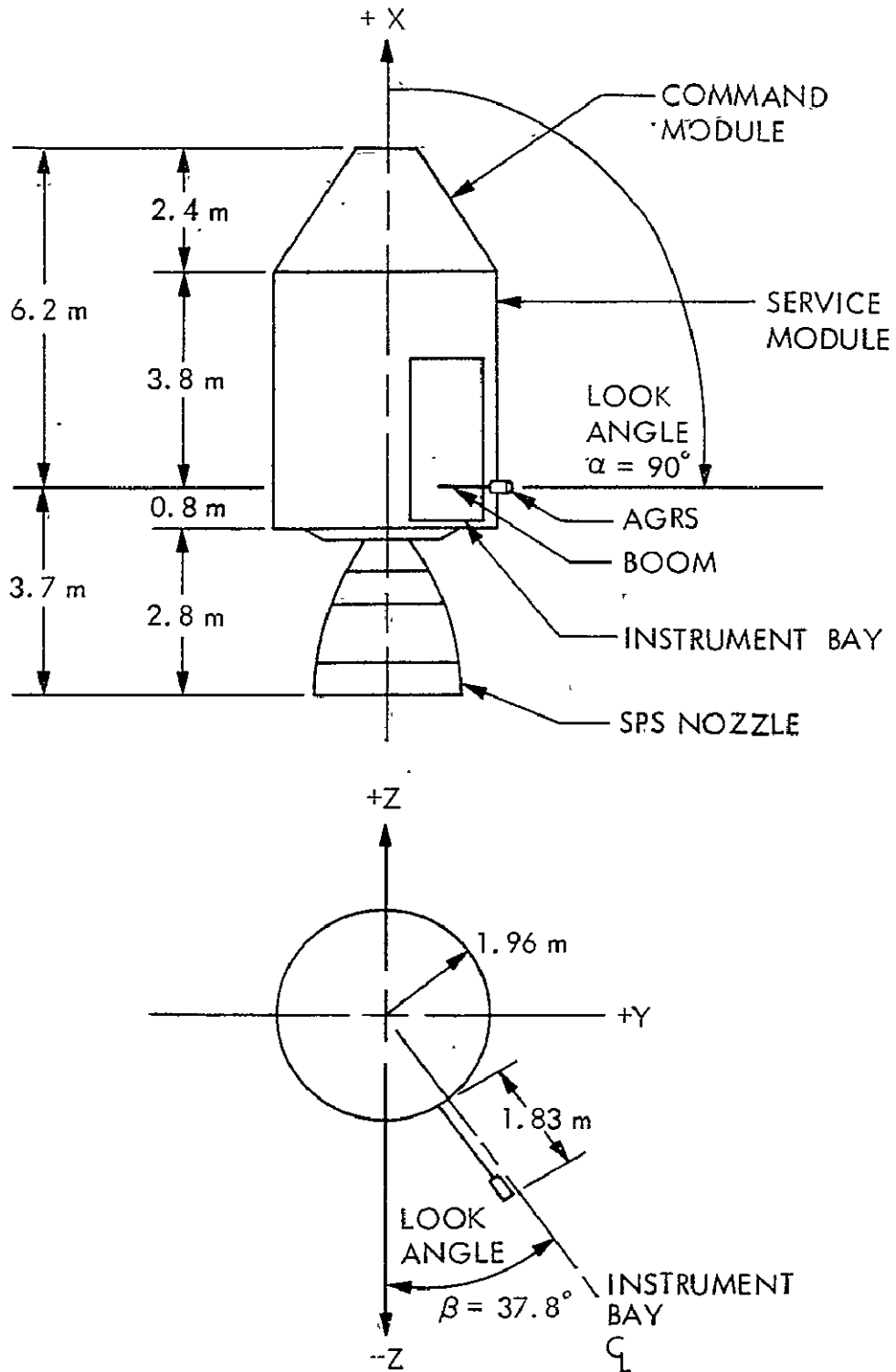
Figure 1. Apollo 16 Command and Service Module showing the Apollo Gamma-Ray Spectrometer (AGRS) in the occultation astronomy position.

Table 1

Live-Time and Spin Axes for the Four Apollo 16 PTCs

Maneuver (PTC)	Spin Axis		Live-Time hours
	α	δ	
Ecliptic	$6^h\ 0^m$,	-66°	3.17
Super-Galactic Auxilliary	$6^h 50^m$,	15°	1.17
Ecliptic Auxilliary	$9^h 20^m$,	50°	0.80
Super-Galactic	$18^h 40^m$,	15°	5.51

3   RESULTS

3.1 Separation of Cosmic from Non-Cosmic Background

The data base is shown in Figure 2. The roll angle, called CDUX, can be thought of as scan phase. The roll angles of mid-occultation for several sources are shown, with occultation extending $\pm 30^{\circ}$ about mid-occultation. The count rate is only modulated by ~5%, and it follows that either there is a strong non-cosmic background.or that the cosmic flux has an intense isotropic component. We find that they contribute almost equally. The non-cosmic background over the energy range 72 to 200 keV is estimated to be 38 ± 7 cps, and the implied count rate for the cosmic flux is 31 ± 7 cps, which agrees with measurements of others (summarized in Silk, 1973). Details can be found in Gilman (1977). We wish to emphasize that the uncertainty is only in separating the isotropic background from the non-cosmic background and does not affect the. significance of the variations seen in Figure 2.

3.2 Spectrum of the Galactic Center

The Galactic center region between -65° and $+30^{\circ}$ longitude was occulted during two PTC maneuvers. The section of Galactic plane occulted varied with roll angle during the two PTCs, as is illustrated in Figure 3, but there was extensive over-lap, especially for the 1/5 of the plane between -50° and $+22^{\circ}$.
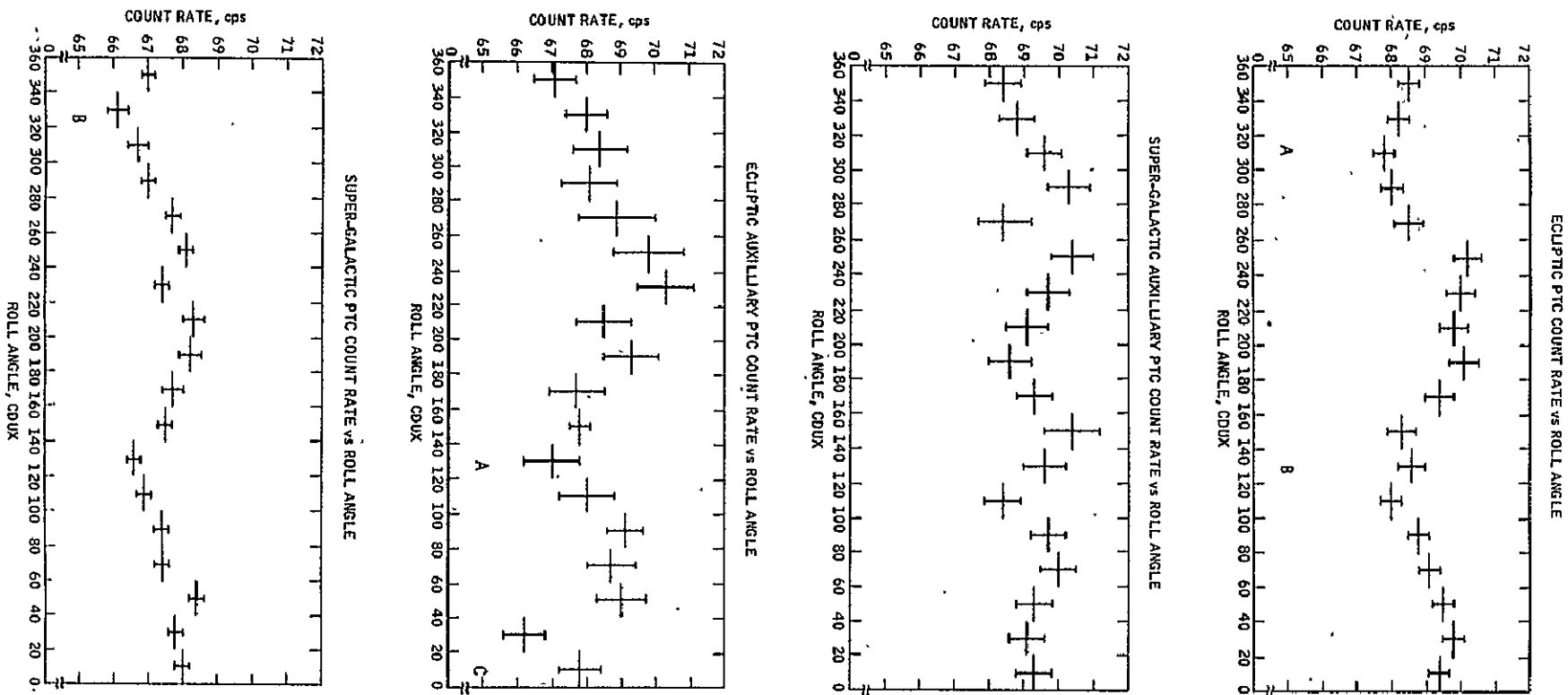
Figure 2.   AGRS count rate, 72 to 200 keV, as a function
of roll angle for the four Passive Thermal
· Control (PTC) maneuvers. 'Dips occur when
bright sources are occulted: A) Crab nebula
B) Galactic center, C) Cygnus X-1. Sources
are occulted for ± 30° about mid-occultation.

194
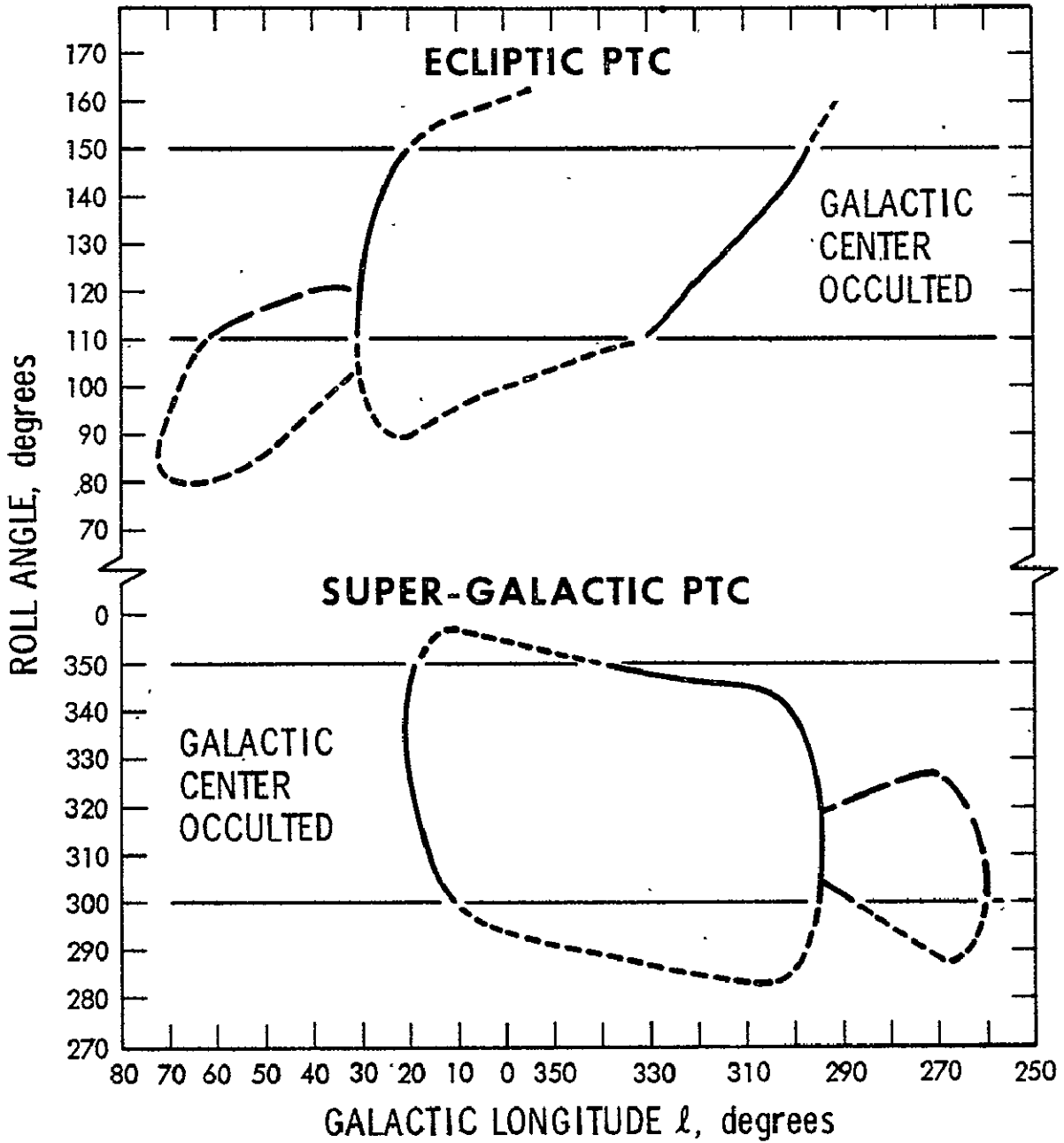
Figure 3. Longitude of occultation as a function
of roll angle. The Service Propulsion
System (SPS) rocket nozzle was completely
transparent to gamma-rays above 150 keV.

Background rates, taken when no part of the Galactic plane was occulted and which should therefore exhibit a higher rate than the Galactic-center-occulted data, were obtained separately for the two PTCs. For the Ecliptic PTC the intervals of roll angle were 10° to 60° (southern hemisphere) and 190° to 260° (northern hemisphere) while for the Super-Galactic PTC the background intervals were 10° to 90° (southern hemisphere) and 190° to 260° (northern hemisphere). See Figure 2; Galactic center occultation can be seen to extend $\pm 30^{\circ}$ about points marked B.

To combine the two spectra into a single energy-loss spectrum, we found the rates r_i in energy bins i which minimized the function

$$q_i(r_i) = (r_i - r_{Ei})^2/\epsilon_{Ei}^2 + (r_i - r_{SGi})^2/\epsilon_{SGi}^2 ,$$

which is related to χ^2. The rates r_{Ei} and r_{SGi} are the differences between background and source-occulted energy-loss rates in energy bin i for the Ecliptic and the Super-Galactic PTCs respectively, while the ϵ_{Ei}^2 and ϵ_{SGi}^2 are the variances. Error bars were found from $r_i' - r$ with r_i' satisfying $q_i(r_i') = q_i(r_i) + 1.0$.

The energy loss spectrum was converted to the photon spectrum shown in Figure 4 by applying attenuation and photo-peak efficiency corrections to the observed count rates. Corrections for high energy photons which Compton scattered in the crystal and escaped were also calculated, but because of the steep spectrum and wide energy bins, we found the correction to be less than 10% in all cases and ignored it.

4   DISCUSSION

Because the Apollo 16 gamma-ray telescope had only the crudest angular resolution, we cannot identify the nature of the emission volume unambiguously; it could be distributed diffusely in the Galaxy or confined to energetic environments in the viscinity of degenerate stars or other compact objects.

Figure 5 is a composite spectrum of the Galactic central region from just below 10 keV to just above 1 GeV, showing this work along with the hard X-ray results from OSO-7 (Wheaton, 1976) and COS-B high energy gamma-ray results (Bennett, et al., 1977), normalized to a per radian basis. No part of this spectrum has been corrected for point source contribution;
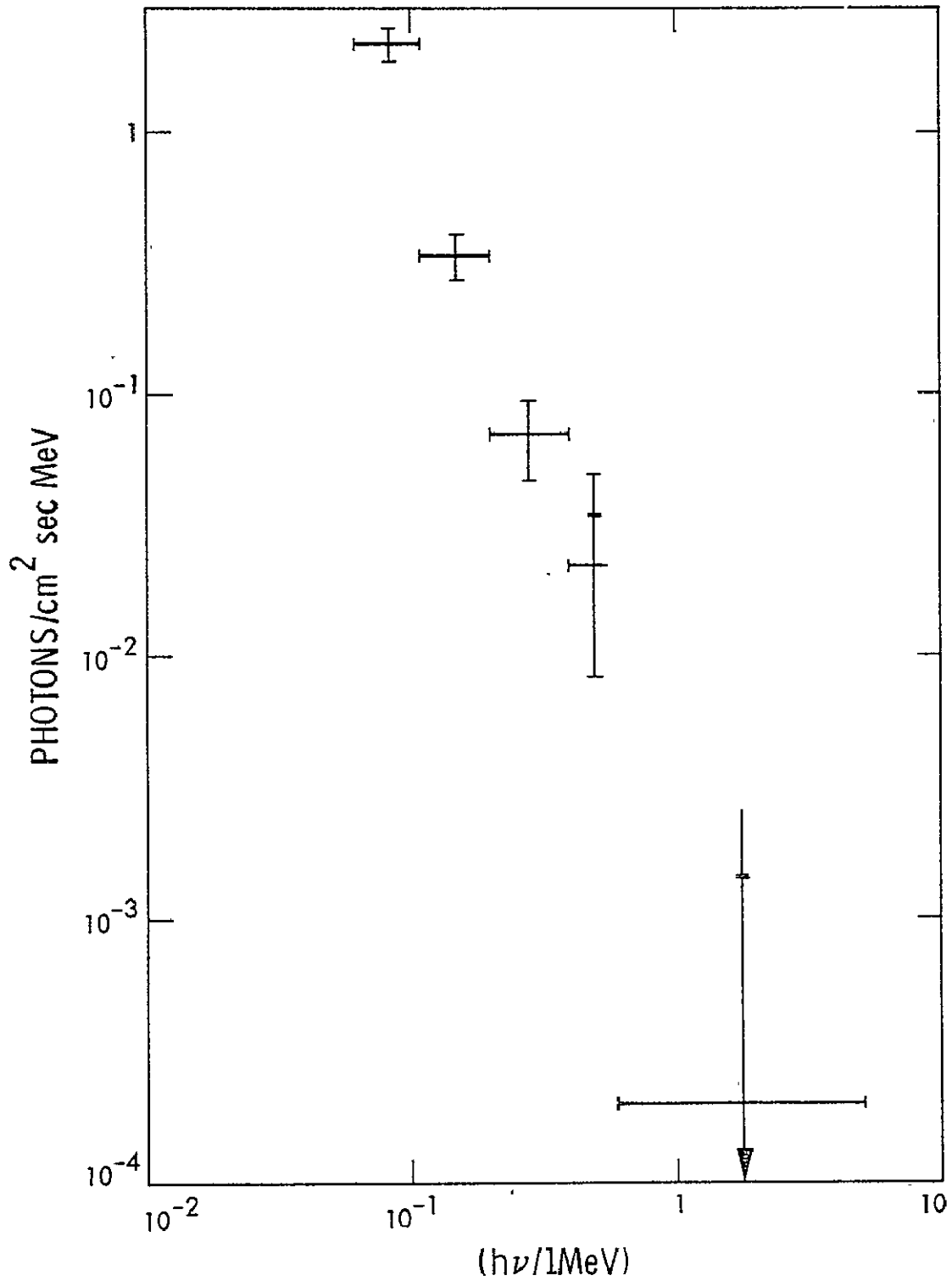
Figure 4. Apollo 16 spectrum of Galactic plane emission, $-50° \leq \ell \leq 22°$. One and two standard deviation marks are shown for the two points above 400 keV.
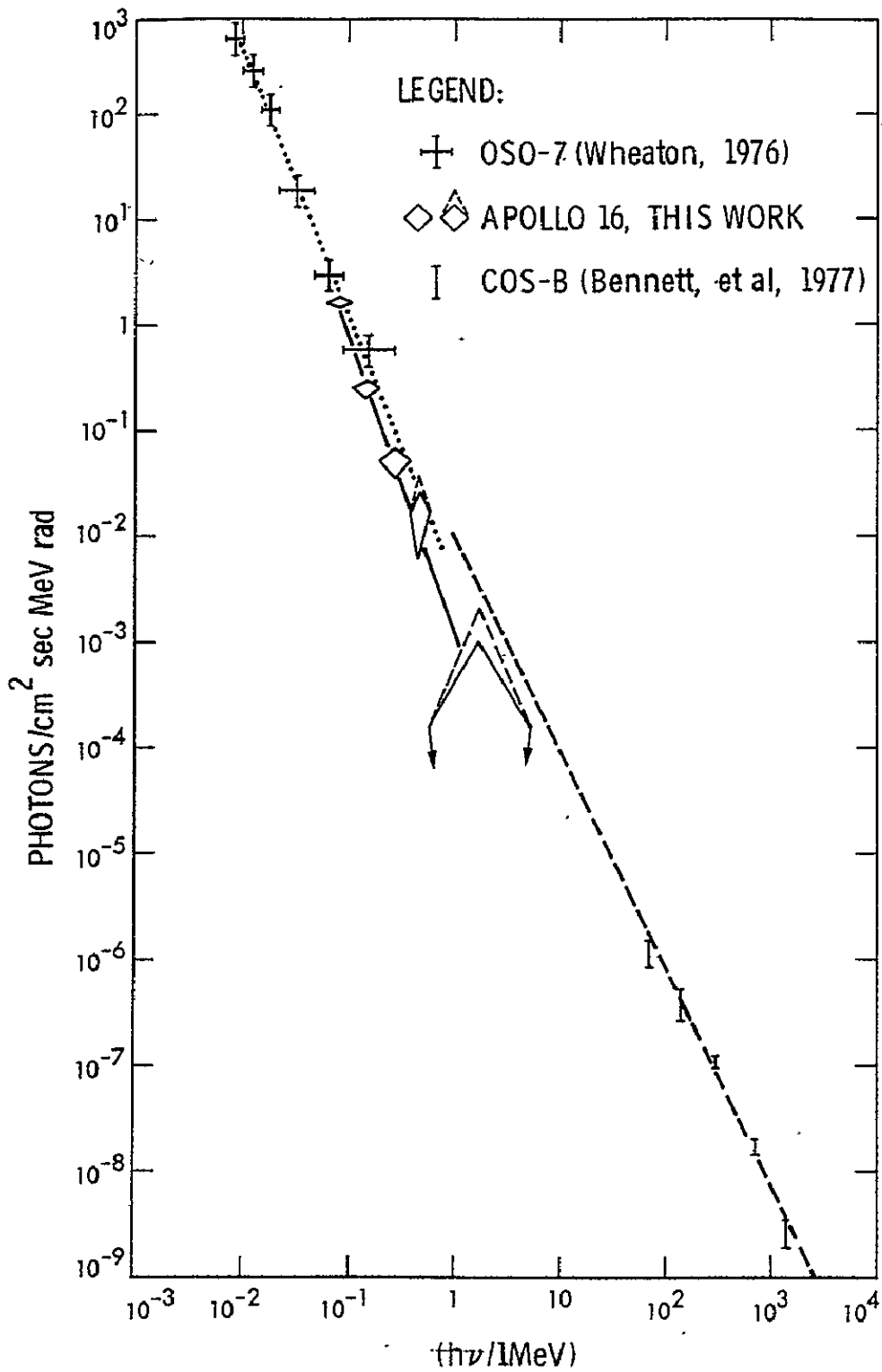
Figure 5. Spectrum of emission from the Galactic plane for longitudes within 50° of the Galactic center, 7 keV to 1 GeV. Point source contributions have not been removed.

rather, it represents the gamma-ray spectrum for the central parts of our Galaxy that might be measured by an observer far from the Galaxy.

The spectrum shows clearly that a simple power law connection between the hard X-rays, ($h\nu$<0.1 MeV) and the high energy gamma rays ($h\nu$>50 MeV) is not allowed by the work we are presenting. This suggests that at least two different emission volumes are contributing. It is well known that hard X-ray emission from the plane comes almost entirely from discrete sources with the possible exception of a faint Galactic background discussed by Wheaton (1976). While it is possible that the high energy gamma-ray emission is also dominated by discrete sources (Hermsen, et al., 1977), diffuse emission from the interaction of cosmic rays with the interstellar medium is still the most attractive hypothesis despite differences between the predicted and the observed spectrum (Paul, et al., 1978).

Figure 5 suggests that the emission in the 0.06 to 5 MeV range observed by Apollo 16 should be identified with hard X-ray sources in the plane because the most extreme power law allowed by the Apollo data would account for less than 15% of the flux from $-50^{o} \leq \ell \leq 22^{o}$ observed above 100 MeV by COS-B; while the low energy gamma-ray and hard X-ray portions can be fit by a single power law.

If discrete sources dominate the emission observed by Apollo 16, it is useful to find the range of thermal bremsstrahlung spectral parameters which fit the data. Good fits to the spectrum of Figure 4 are allowed, and the 70% and 90% confidence contours are shown in Figure 6. We have used the Gaunt factor of Matteson (1972).

It is more common to use power-laws when discussing spectral parameters of emission from the Galactic plane. Good power-law fits to the spectrum of Figure 4 are also permitted, and the 70% and 90% confidence contours are shown in Figure 7, labelled Apollo 16. Also shown are spectral parameter ranges for

1. Hard X-rays observed by OSO-7 (Wheaton, 1976).
   Energy range: 7 keV to 275 keV, longitude range: -40° to 40°
2. Low energy gamma rays observed by balloons.
   a. Johnson and Haymes (1973).
      Energy range: 0.03 to 2.3 MeV, longitude range: -10° to 15°
   b. Haymes, et al. (1975), total emission.
      Energy range: 0.04 to 2.0 MeV, longitude range: -4° to 6°
   c. Haymes, et al. (1975), as in b. but excluding some possible line

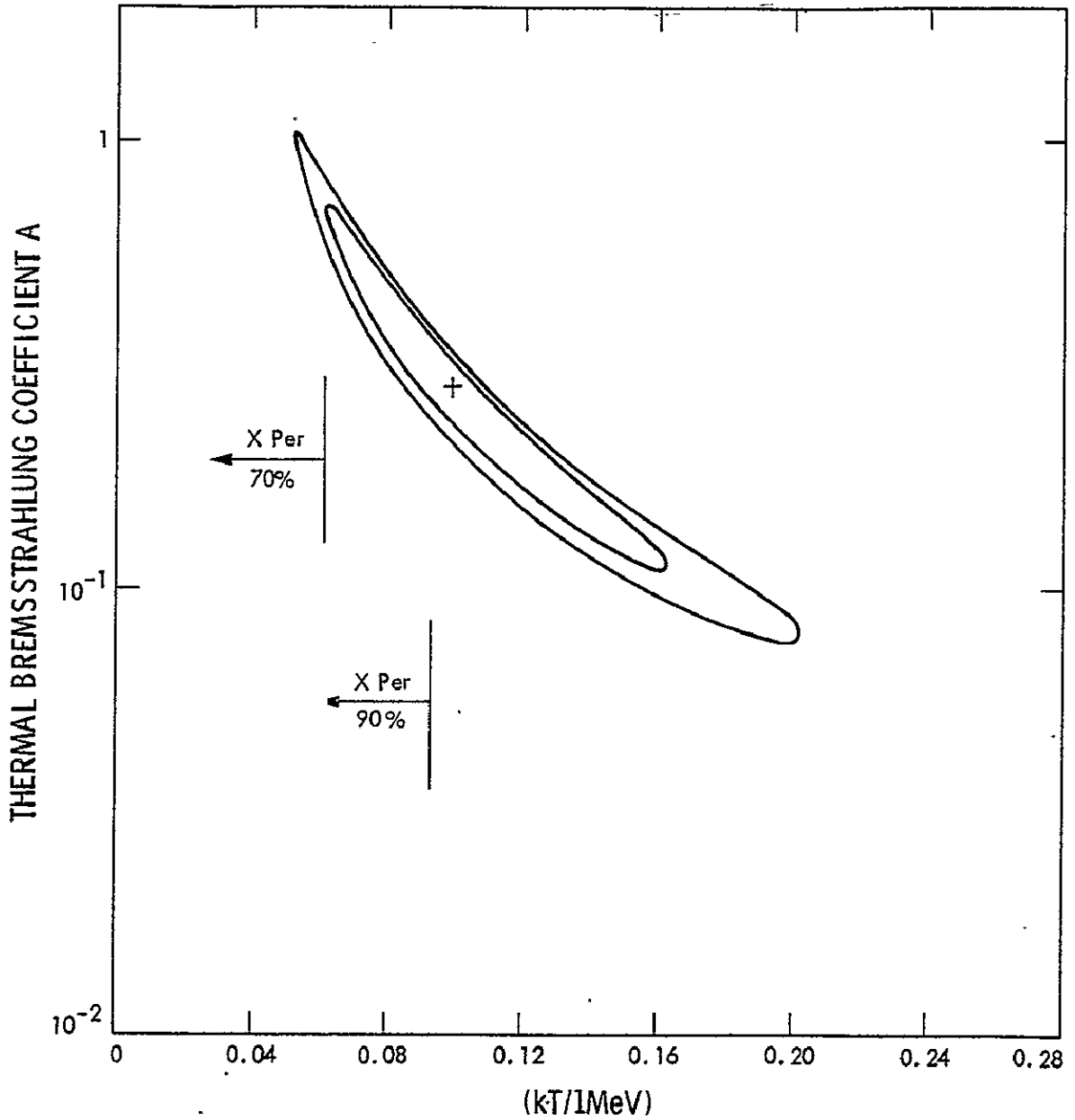$$\frac{dN}{d(h\nu)} = A \frac{g\ (h\nu\ ,\ kT)}{(h\nu/1\ MeV)} EXP\ \{-h\nu\ /kT\}\quad \frac{PHOTONS}{cm^2\ sec\ MeV}$$

Figure 6. Apollo 16 thermal bremsstrahlung spectral
parameters of the Galactic plane emission,
$-50° \le \ell \le 20°$

contributions at 0.5 and 0.9 MeV.

3. Low energy gamma rays observed by the satellite 1972-076B (Imhof and Nakano, 1977).

   Energy range: 38 to 500 keV, longitude range: 255° to 328°.

   Only the range of spectral index was reported for this observation.

4. High energy gamma rays observed by COS-B (Bennett, et al., 1977).

   Energy range: 50 to 1000 MeV, longitude range: 10° to 40°.

   The 70% and 90% confidence contours were found from an analysis of the spectrum given by Bennett, et. al. (1977); however, we note that a single power-law does not fit their spectrum at all well. This is not surprising in view of the shape of the spectrum of Galactic plane emission shown in Figure 5.

Figure 7 shows the good agreement between the Apollo 16 spectrum in Figure 4 and the results of Haymes, et al. (1975) when they fit power laws to their spectrum excluding two bands at 0.5 and 0.9 MeV which may have contained line emission. However, Apollo 16 is also consistent with the power law fits of Haymes, et al. (1975) and of Johnson and Haymes (1973) which were made to the total spectrum between 0.04 and 2 MeV, including contributions from the reported lines. Intensities in Figure 7 are normalized on a per radian basis, and the consistency of the Apollo 16 spectrum for $-50^{\circ} \leq \ell \leq 22^{\circ}$ with the results of the Rice group for $-4^{\circ} \leq \ell \leq 6^{\circ}$ implies a fairly uniform intensity distribution for the whole of $-50^{\circ} \leq \ell \leq 22^{\circ}$. The actual fluxes measured by Haymes, et al. (1975) were a factor of 7 less than the flux measured by Apollo 16, but Apollo 16 occulted a factor of 7 greater range in longitude than the Rice group observed.

A uniform intensity distribution has also been suggested by Matteson (1978) as the basis of consistency between the fluxes of 4.4 MeV gamma rays reported by Haymes, et al. (1975) and that measured by the hard X-ray/soft gamma-ray telescope on HEAO-1. However, Apollo 16 upper limits to the flux of 4.4 MeV gamma rays given by Trombka, et al. (1977) are not consistent with the distribution of 4.4 MeV line intensity being uniform on $-50^{\circ} \leq \ell \leq 22^{\circ}$. More specifically, we can show that the fraction of 0.06 to 5 MeV flux that is in 4.4 MeV photons, averaged over $-50^{\circ} \leq \ell \leq 22^{\circ}$ is significantly less than the fraction found for the inner regions of the Galaxy ($-20^{\circ} \leq \ell \leq 20^{\circ}$) by Haymes, et al. (1975) and Matteson (1978).
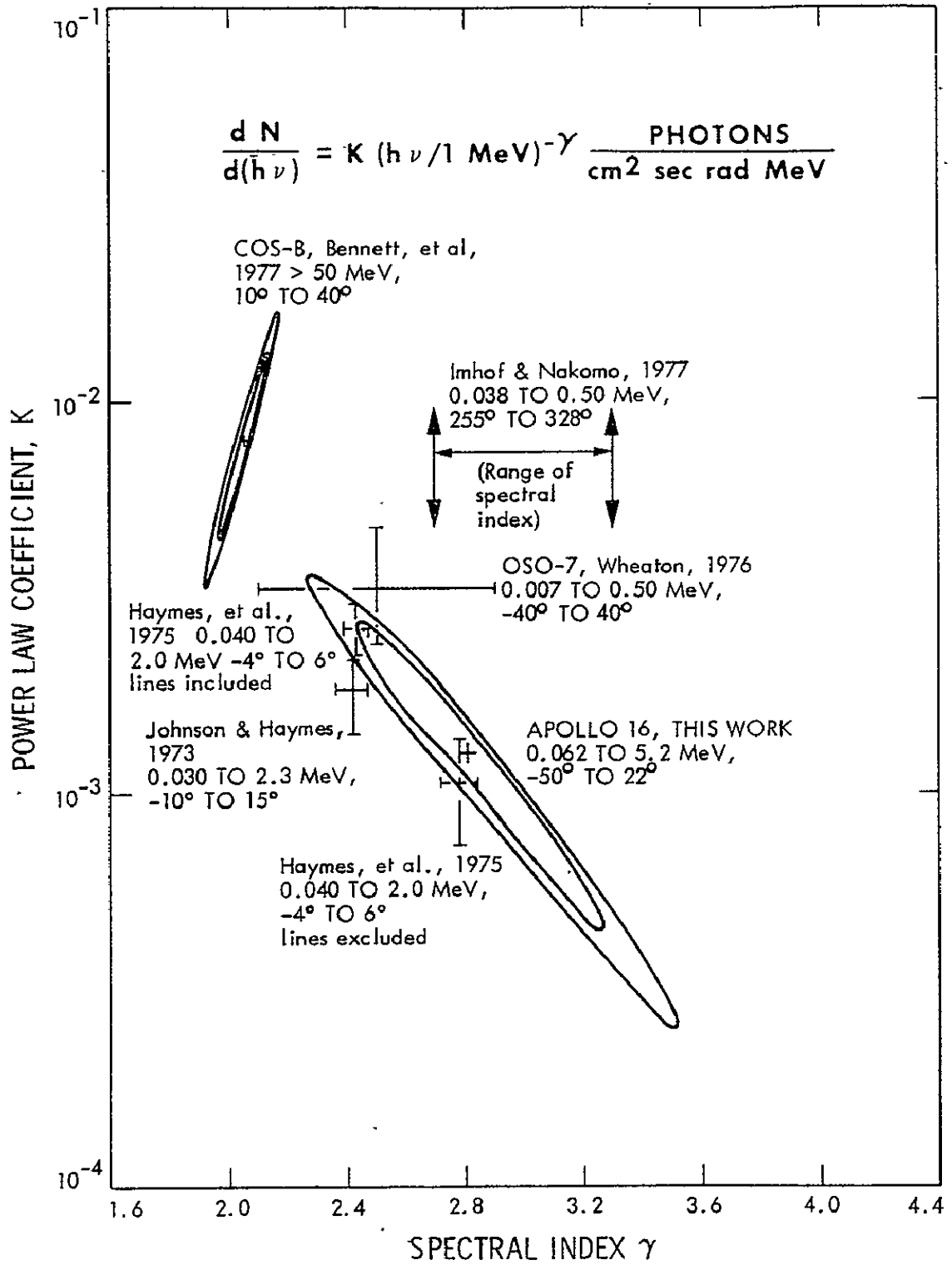
Figure 7. Power law spectral parameters of Galactic plane emission, showing 70% and 90% confidence contours for the Apollo 16 spectrum of Figure 4.

By dividing the lower 70% confidence flux of Apollo by the $+1\sigma$ flux from the Rice group at a given power law index Y, a minimum ratio of the total flux observed by Apollo 16 and the flux observed by the Rice group can be found. If the total 0.06 to 5 MeV emission from $-50°\leq\ell\leq22°$ is made up of a continuum plus lines, then the appropriate spectral index to use is Y~2.4, found by Johnson and Haymes (1973) and by Haymes, et al. (1975) when lines were allowed to affect their estimate of power law parameters. If lines have not significantly affected the Apollo 16 spectrum from $-50°\leq\ell\leq22°$, then the comparison should be made at Y~2.8, found by Haymes, et al. (1975) when lines were not allowed to contaminate the estimates of power law parameters. The minimum ratios of total flux observed by Apollo 16 to that observed by Haymes et al. (1975) are 5.8 and 6.0, respectively, for these two cases.

The Rice group reported a 4.4 MeV line flux of $(9.5 \pm 2.7)\cdot10^{-4}$ photons/cm^2 sec, and if the ratio of 4.4 MeV flux to total flux were constant in $-50°\leq\ell\leq22°$, then Apollo 16 should have seen at least

$$(5.8)\cdot(58 \text{ cm}^2)\cdot(9.5 \pm 2.7)\cdot10^{-4} \text{ photons/cm}^2 \text{ sec} = (0.32 \pm 0.9) \text{ photons/sec}$$

at 4.4 MeV. However, the Apollo 16 2σ upper limit for 4.4 MeV photons is 0.20 photons/sec for contributions from all sources, including the space-craft and detector sources.

Supposing that instrumental effects have been completely eliminated from the balloon and HEAO-1 observations, we conclude that the gamma-ray line at 4.4 MeV is not emitted as a constant fraction of the continuum in the whole of $-50°\leq\ell\leq22°$. Rather, the regions observed by the Rice telescope and by the gamma-ray telescope on HEAO-1 have an enhancement of 4.4 MeV emission.

Following this conclusion further and assuming that Apollo 16 measured emission dominated by a continuum, we note the substantial over-lap in the spectral index ranges of Haymes, et al. (1975) with lines excluded, Wheaton (1976), and Imhof and Nakano (1977) (see Figure 7). Taking the spectral index Y =2.8 $\pm$ 0.1, the intensity range allowed by our work in Figure 7 implies that the emission from $-50°\leq\ell\leq22°$ has the spectrum

$$\frac{dN}{d(h\nu)} = (1.35 \pm 0.45)\cdot10^{-3} \text{ (h}\nu \text{ /1 MeV)}^{-(2.8 \pm 0.1)} \text{photons/cm}^2 \text{ sec MeV rad.}$$

This intensity is clearly consistent with the measurement of Haymes, et al. (1975) with the line contribution removed and is probably also consistent with Wheaton (1976), although the actual shapes of his confidence contours are not given. This supports the finding of our mapping work (Gilman, et al., to be published), that on scales of 20° to 40°, the continuum emission is not sharply peaked at the center of the Galaxy, but instead has a relatively uniform intensity distribution across the Galactic central region. This distribution may extend to $\pm 50^\circ$ in longitude.

REFERENCES

Arnold, J.R., Metzger, A.E., Peterson, L.E., Reedy, R.C., Trombka,
J.I., 1972, Apollo 16 Preliminary Science Report, NASA SP-315,
18.1 - 18.8.

Beale, E.M.L., 1959, Naval Res. Log. Quarterly, 6, 227-243.

Bennett, K., Bignami, G.F., Buccheri, R., Hermsen, W., Kanbach, G.,
Lebrun, F., Mayer-Hasselwander, H.A., Paul, J.A., Piccinotti,
G., Scarsi, L., Soroka, F., Swanenburg, B.N., Wills, R.D.,
1977, Proceedings of the 12th ESLAB Symposium, ESA SP-124,
83-93.

Dyer, C.S., Trombka, J.I., Schmadebeck, R.L., Eller, E., Bielefeld,
M.J., O'Kelley, G.D., Eldridge, J.S., Northcutt, K.J., Metzger,
A.E., Reedy, R.C., Schonfeld, E., Seltzer, S.M., Arnold, J.R.,
Peterson, L.E., 1975, Space Sci. Inst. 1, 279-288.

Fichtel, C.E., Kniffen, D.A., Thompson, D.J., 1977, Proceedings of
the 12th ESLAB Symposium, ESA SP-124, 95-104.

Gilman, D.A., 1977, Ph.D. Thesis, Cornell University, CRSR Report 652.

Harrington, T.M., Marshall, J.H., Arnold, J.R., Peterson, L.E.,
Trombka, J.I., Metzger, A.E., 1974, Nucl. Inst. Methods 118,
401-411.

Haymes, R.C., Walraven, G.D., Meegan, C.A., Hall, R.D., Djuth, F.T.,
Shelton, D.H., 1975, Ap. J. 201, 593-602.

Hermsen, W., Bennett, K., Bignami, G.F., Boella, G., Buccheri, R.,
Higdon, J.C., Kanbach, G., Lichti, G.G., Masnou, J.L., Mayer-
Hasselwander, H.A., Paul, J.A., Scarsi, L., Swanenburg, B.N.,
Taylor, B.G., Wills, R.D., 1977, Proceedings of the 12th ESLAB
Symposium, ESA SP-124, 13-20.

Imhof, W.L., Nakano, G.H., 1977, Ap. J. 214, 38-49.

Johnson, W.N., III, Haymes, R.C., 1973, Ap. J. 184, 103-125.

Katz, J.I., 1977, Ap. J. 215, 265-275.

Lampton, M., Margon, B., Bowyer, S., 1976, Ap. J. 208, 177-190.

Lingenfelter, R.E., Ramaty, R., 1977, Ap. J. (Letters) 211, L19-L22.

Maraschi, L., Treves, A., 1977, Ap. J. (Letters) 218, L113-L115.

Matteson, J.L., 1972, Ph. D. Thesis, UCSD.

Matteson, J.L., paper read at this Symposium.

Metzger, A.E., Parker, R.H., Gilman, D., Peterson, L.E., Trombka,
    J.I., 1974, Ap. J. (Letters) 194, L19-L25.

Mushotzky, R.F., Roberts, D.H., Baity, W.A., Peterson, L.E., 1977,
    Ap. J. (Letters) 211, L129-L133.

Paul, J.A., Bennett, K., Bignami, G.F., Buccheri, R., Caraveo, P.,
    Hermsen, W., Kanbach, G., Mayer-Hasselwander, H.A., Scarsi, L.,
    Swanenburg, B.N., Wills, R.D., 1978, Astron. Ap. 63, L31-L33.

Silk, J., 1973, Ann. Rev. Astron. Ap., 12, 269-308.

Trombka, J.I., Dyer, C.S., Evans, L.G., Bielefeld, M.J., Seltzer,
    S.M., Metzger, A.E., 1977, Ap. J. 212, 925-935.

Wheaton, W.A., 1976, Ph. D. Thesis, UCSD SP 76-01.

D9-93

N78-31980

Low Energy Gamma Ray Observations
with the MPI-Compton Telescope

F. Graml, F.-P. Penningsfeld, and V. Schönfelder

Max-Planck-Institut für Physik und Astrophysik
Institut für extraterrestrische Physik
D-8046 Garching, W-Germany

In October 1977 the new large area Compton telescope of the Max-Planck-Institut was flown for the first time on a balloon. The evaluation of the data from this flight has by far not yet been completed. In this brief talk a report is given on the present status of the data evaluation. Two preliminary results are presented. First, from the measured background spectrum at float altitude the sensitivity of the telescope for the detection of cosmic gamma ray lines is estimated; second, an enhanced gamma ray flux is observed from the direction of the Seyfert galaxy NGC 4151. Its energy spectrum is determined.

A schematic drawing of the telescope is shown in Fig. 1. It consists of two scintillation detectors, an upper one of liquid scintillator and a lower one
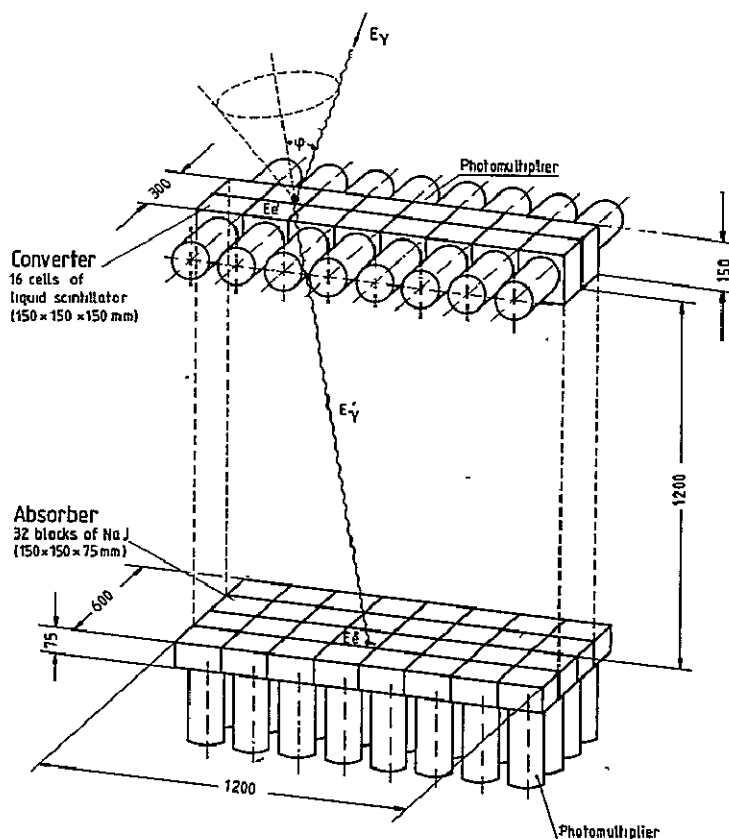
Fig. 1 Schematic drawing of the Compton telescope

of. NaI. Each detector is subdivided into optically separated cells and entirely surrounded by thin anticoincidence plates of plastic scintillator which are not shown in the schematic drawing.

A gamma ray is identified by a first Compton collision in the upper detector and a second interaction in the lower one. The sequence is confirmed by a time-of-flight measurement. In case of a double scattering event the following quantities are measured:

(1) Energy losses E'_e and E''_e in both detectors

(2) Location of the scattering processes in both detectors

(3) Pulse shapes in both detectors

(4) Time-of-flight of the scattered gamma ray

(5) Absolute time of each event

(6) Azimuthal orientation of the telescope

Pulse shape and time-of-flight measurement are performed in order to reject background events: the time-of-flight measurement rejects those events which make a first Compton collision in the lower detector and are then scattered upwards. The purpose of the pulse shape measurement in the upper detector is to reject neutron induced events.

From the energy losses E'_e and E''_e and from the locations of the scattering processes in both detectors the energy E_γ of the infalling gamma ray and its arrival direction can be determined to lie on a cone mantle of half opening angle φ. The projection of this cone mantle onto the sky is called the event circle.

This telescope has imaging properties in the following sense: Imagine, there is a celestial point source within the field of view, then this source can be identified by the intersections of the event circles from different source gamma rays in one point. The event circles from the source will only then intersect in one point if the scattered gamma ray is totally absorbed in the lower NaI-detector. If the scattered gamma ray is not totally absorbed, then the calculated scattering angle φ is not the true one, and therefore, the event will look like a background event. Because only totally absorbed events from a point source are accepted, the energy resolution is automatically good: the Compton tails of gamma ray lines are nearly totally suppressed.

In case of the MPI-telescope the angular resolution is mainly determined by the size of the detector cells: within the broad field of view of typically 40° FWHM, the angular resolution is about 10° FWHM (see Graml et al., 1977). The energy resolution is 10% FWHM at 1 MeV and slightly better at higher energies as can be seen from the later Fig. 6.

Fig. 2 shows a photography of the telescope some days before its launch in Palestine. The size of the upper detector is $1/3$ m^2, and that of the lower detector $2/3$ m^2. The total weight was 1580 kg.

During the flight the balloon reached an altitude of 3.5 g/cm^2 and stayed there for 20.5 hours. The telescope axis always pointed towards the zenith. In Fig. 3 those regions of the sky are shown which were observed during the flight. The typical field of view of the telescope is indicated by a circle.

Sensitivity of the telescope for gamma ray line spectroscopy

With its energy resolution of typically 10% FWHM the telescope has a high sensitivity to detect broadened or integral gamma ray lines. The high sensitivity of the telescope is due to its directional resolution on the one side, and on the other side due to its high background suppression. The advantage of the directional resolution is evident: only events from a certain direction of interest are accepted, the others are not. The background suppression is mainly achieved by the time-of-flight and pulse shape measurement and is illustrated in Fig. 4 and Fig. 5.

Fig. 2 Photographic view of the Compton telescope
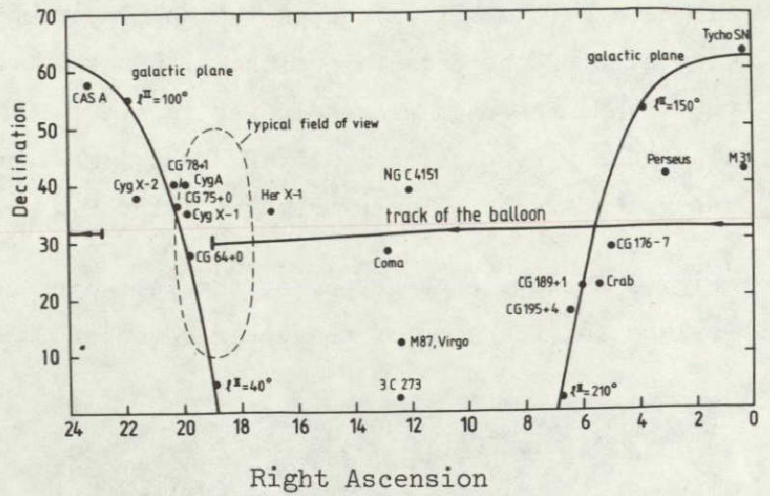
Fig. 3 Track of the balloon during the flight

Right Ascension

Fig. 4 Measured time-of-flight distribution at float altitude (E'_e, $E''_e \geq 1$ MeV). Only events within the shaded area are accepted
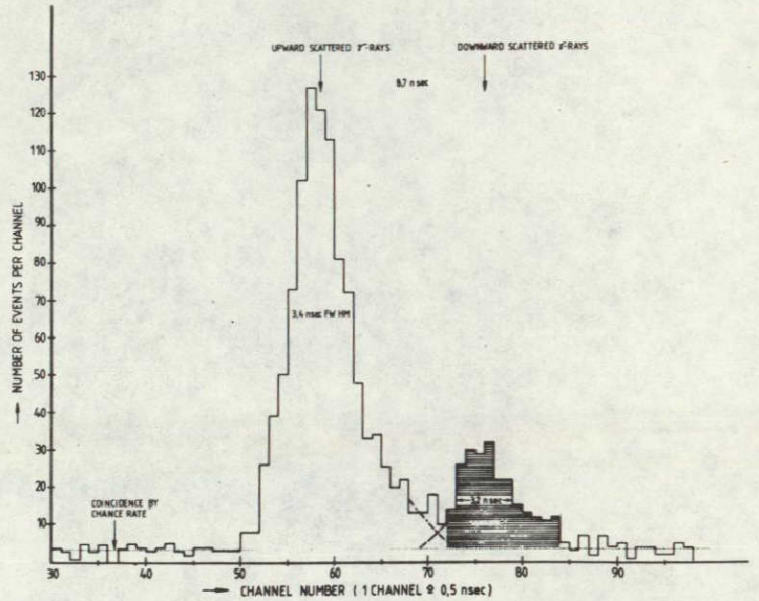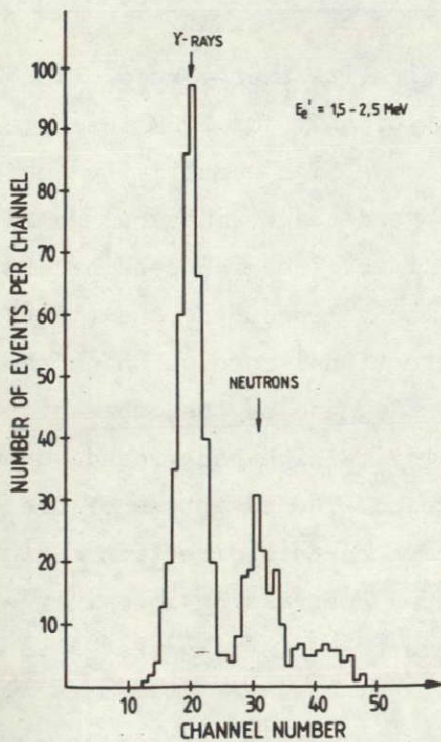

$E_e^+ = 1.5 - 2.5$ MeV

Fig. 5 Measured pulse shape distribution of the upper detector at float altitude. The channel number plotted on the abscissa is an indication for the pulse shape. Gamma ray and neutron induced events are nicely separated

The measured energy spectrum of all accepted events at float altitude, the event circles of which intersect a resolution element of $10°$ FWHM, is plotted in Fig. 6.

As can be seen immediately, there is one strong line in the spectrum at 2.2 MeV, which is an intrinsic detector line and which is produced by deuterium formation from thermal neutron capture in the upper detector. There may be other locally produced features in the spectrum. This will be investigated in more detail. The spectrum of Fig. 6 contains everything: atmospheric, cosmic and locally produced gamma rays.
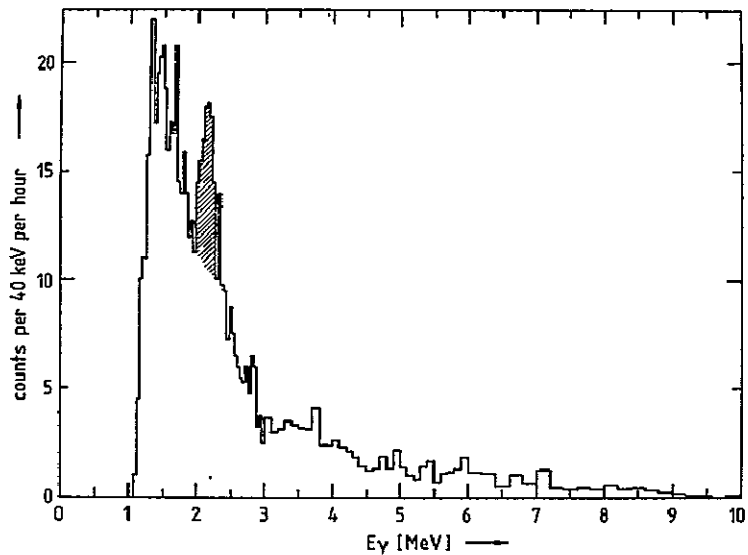
Fig. 6   Energy spectrum of all accepted events at float altitude of 3.5 g/cm²

It has been used to estimate the sensitivity of the telescope for the detection of cosmic gamma ray lines. The result is illustrated in Fig. 7. The gamma ray line fluxes reported by Chupp et al. (1975) during the large solar flare in August 1972 and the gamma ray line fluxes reported by Haymes et al. (1975) from the galactic center region are compared with our 3σ detection limit during 3 hours observation time.

In the very near future a search for gamma ray lines in our data will be performed for those regimes of the sky which were observed during the balloon flight (see Fig. 3).

The energy spectrum of the Seyfert galaxy NGC 4151

A preliminary search for discrete gamma ray sources from the balloon flight data was performed by determining the event rate at float altitude within the total field of view of the telescope ($\approx 40°$ FWHM) as a function of time. So far, the imaging properties of the telescope within its field of view have not yet been used. In Fig. 8 the total (1-20) MeV event rate - normalized to a constant float altitude of 3.5 g/cm² rest atmosphere - is plotted as a function
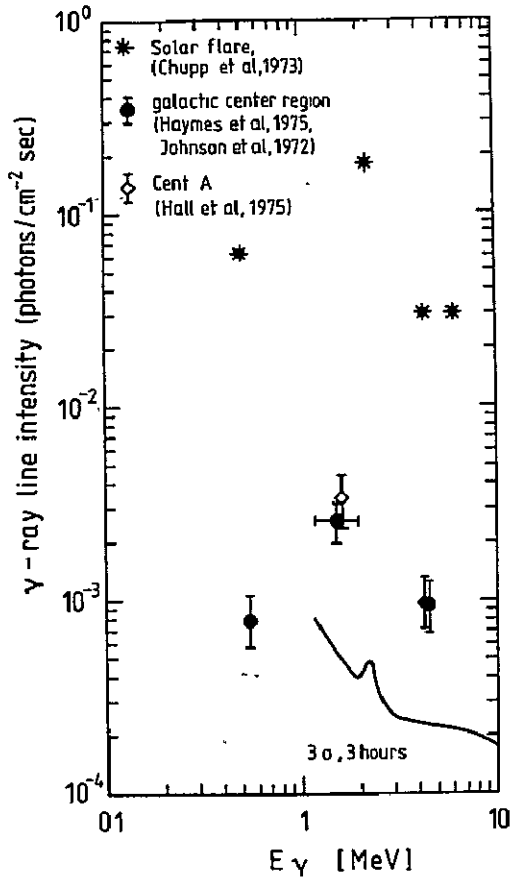
Fig. 7 Sensitivity of the Compton
telescope for the detec-
tion of gamma ray lines

of universal time. Special selection
criteria have been applied to those events
which are accepted (see Graml et al.,
1978). The transit times of some typical
celestial objects are indicated in Fig. 8.
Of course, they must not neccessarily
be identical with gamma ray sources.

First, there is a very significant en-
hancement in the counting rate at the
transit time of the anticenter of our
galaxy: It has a significance of 14
standard deviations. The long duration
of the enhancement seems to indicate that
it is not caused by the Crab alone. In
case of one single source the duration
of the enhancement should last only
about 3 hours. Second, an enhanced gamma
ray emission is also observed during the
transit time of the Seyfert galaxy NGC
4151; this enhancement indeed lasts for
about 3 hours. Its significance is 7
standard deviations above the background
level (6.00 - 8.00 UT and 20.00 - 22.00
UT).

In the next step similar event curves like that shown in Fig. 8 have also
been determined for smaller energy bins between 1-20 MeV (see Graml et al.,
1978). The excess rates during the transit time of NGC 4151 have then been
converted into gamma ray fluxes using the effective geometrical area of the
telescope and taking into account the absorption of gamma rays in the over-
lying atmosphere. The result is shown in Fig. 9, where the energy spectrum

Fig. 8 1-20 MeV event rate
at float altitude
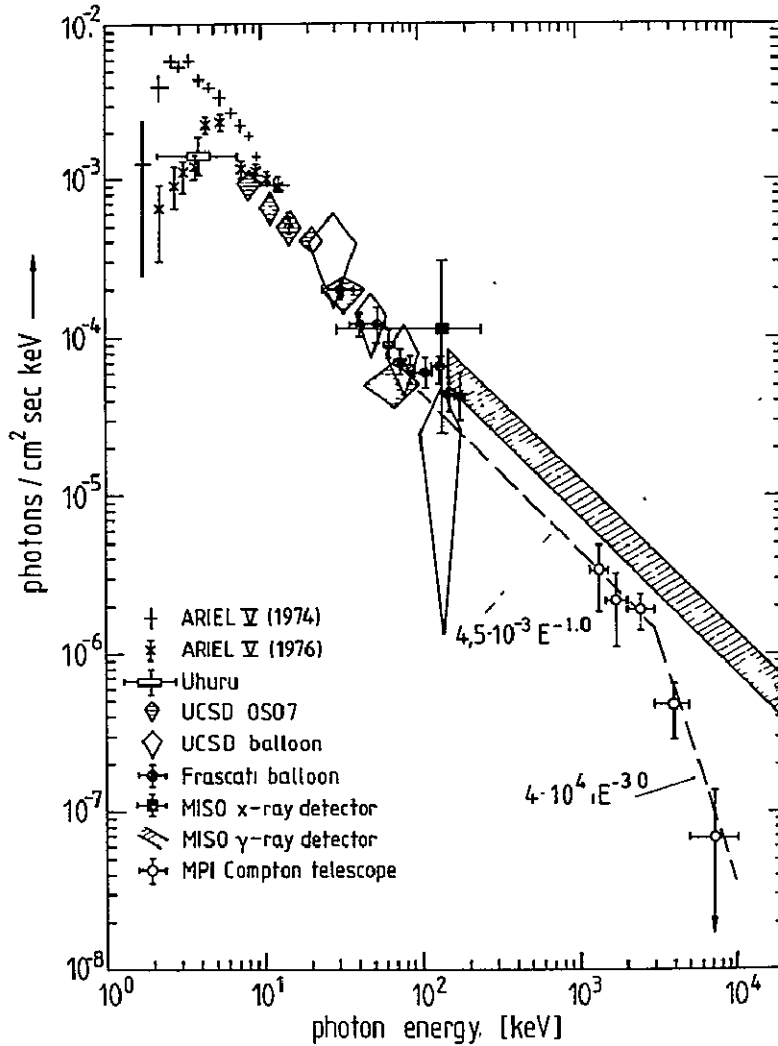within the total
field of view of the
telescope
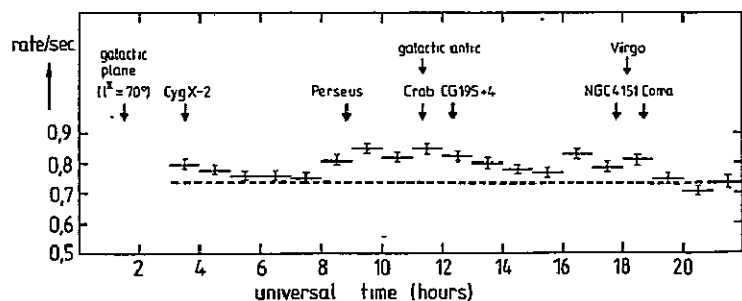
Fig. 9   The energy spectrum of the Seyfert galaxy
NGC 4151. The X-ray results are adopted from
Auriemma et al. (1978)

of NGC 4151 is plotted from 2 keV to 10 MeV. The five measuring points obtained with the Compton telescope are in good agreement with a power law extrapolation from X-ray energies up to about 3 MeV. Above that energy the spectrum is considerably steeper.

Strictly speaking, the measurements with the Compton telescope are only an upper limit, because all excess counts observed during the transit of NGC 4151 through its aperture were attributed to this one source. The consistency of the gamma ray data with the X-ray data, however, may indicate that this procedure is correct. The discrepancy of the MISO gamma ray measurements (Di Cocco et al., 1977) with the present measurements is due to the fact that the former measurements were evaluated without using any spectral information of

their data. In order to convert their excess counting rate above 0.2 MeV into a gamma ray flux, these authors have assumed that the gamma ray spectrum follows an E^{-1}-power law between 0.2 MeV to 20 MeV.

The gamma ray luminosity of NGC 4151 - as determined from our measurements - is extremely high: it is 10^{45} erg/sec below 3 MeV. At X-ray energies between 2-10 keV - for comparison - it is only $10^{42.85}$ erg/sec (Elvis et al., 1978). This powerful energy source seems to be obtained in a small volume of less than $3 \cdot 10^{-3}$ pc size, as can be estimated from the fact that variations in the X-ray luminosity of 3 days duration have been observed (same ref. as above). The origin of the high gamma ray luminosity is not yet clear. It may be produced by high energy electrons via synchrotron self-Compton collision (Bergeron and Salpeter, 1973 and Mushotzky, 1977) or by mass accretion onto a massive black hole in the center of the Seyfert galaxy (Fabian et al., 1976).

NGC 4151 is the first external galaxy the electromagnetic spectrum of which could be measured up to gamma ray energies. It is, therefore, interesting to ask whether the so called diffuse cosmic gamma ray component could be explained as the superposition of many unresolved galaxies of the same type as NGC 4151.

For this purpose the spectrum of NGC 4151 has been fitted by two power laws, one below and one above 3 MeV. Spectra with the same exponents have also been drawn into the measured energy spectrum of the diffuse cosmic gamma ray components (Fig. 10).

As fas as the spectral shape is concerned, galaxies of the same type as NGC 4151 could, indeed, explain the bump at MeV-energies if not the total diffuse flux above 1 MeV. If the spectrum of NGC 4151 could in reality be steeper than $\sim E^{-3}$ above 3 MeV, only the bump could be explained. A spectral shape flatter than $\sim E^{-3}$ would cause difficulties. A definite answer on the spectral shape above 3 MeV will be obtained in the near future, when the COS-B observations from this region have been evaluated. Only if the measured flux at 100 MeV from NGC 4151 would be stronger than that from the Crab, its spectrum would be flatter than $\sim E^{-2.8}$.

In the next step the required density of galaxies has then been estimated that would be necessary to explain the diffuse cosmic gamma ray flux by superposition (Schönfelder, 1978). The answer is that X-ray Seyferts could explain the observed gamma ray flux if nearly all of them have similar power

Fig. 10 The energy spectrum
of the diffuse cos-
mic gamma ray compo-
nent. The power law
fits below and above
3 MeV have the same
spectral index as
the observed energy
spectrum of NGC 4151
(adopted from Schön-
felder, 1978)
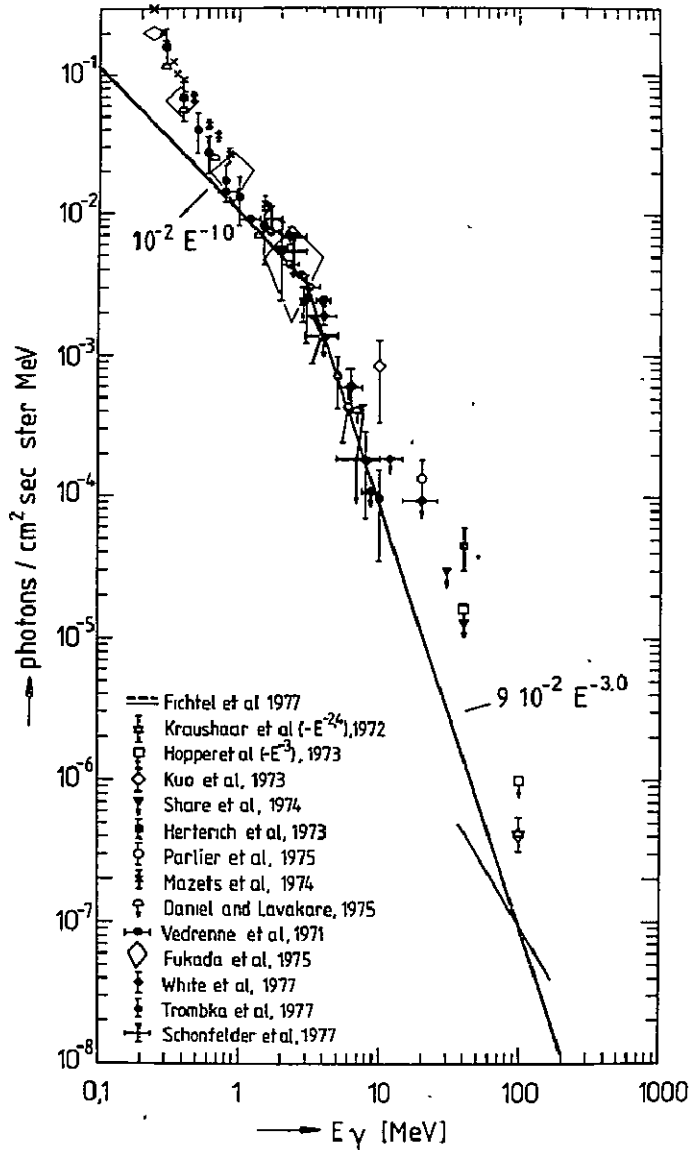
and similar spectra as NGC 4151 at gamma ray energies. If there is propor-
tionality between gamma ray power and X-ray power in some objects, only 13%
of all X-ray Seyferts are needed. For the very early Seyferts the break in
the spectrum at 3 MeV will be redshifted. If, therefore, redshift and (or) -
to a certain extent - evolution are taken into account, the picture will
slightly change; however, the qualitative conclusion will not be changed.
Of course, so far the spectrum of only one single external galaxy has bee
observed at gamma ray energies and more observations are strongly needed.

Auriemma, G., Angeloni, L., Belli, B.M., Bernardi, A., Cardini, D., Costa, E., Emanuele, A., Giovanelli, F., and Ubertini, P., 1978, Hard X-ray spectrum of NGC 4151, Astrophys. J.; 221, L7-L11.

Bergeron, J. and Salpeter, E.E., 1973, Models for extragalactic objects with very high IR and X-ray luminosity, Astron. & Astrophys., 22, 385-406.

Chupp, E.L., Forrest, D.J., and Suri, A.N., 1975, Solar gamma-, X-, and EUV-radiation, IAU Symp. No. 68, D. Reidel Publishing Co., Dordrecht, Holland, p. 341.

Di Cocco, G., Boella, G., Perotti, F., Stiglitz, R., Villa, G., Baker, R.E., Butler, R.C., Dean, A.J., Martin, S.J., and Ramsden, D., 1977, Low energy gamma ray observations of NGC 4151, Nature, 270, 319-320.

Elvis, M., Maccacaro, T., Wilson, A.S., Ward, M.J., Penston, M.V., Fosbury, R.A.E., Perola, G.C., 1978, Seyfert galaxies as X-ray sources, Mon.Not. R. Astr. Soc., 183, 129-157.

Fabian, A.C., Maccagni, D., Rees, M.J., and Stoeger, W.R., 1976, The nucleus of Centaurus A, Nature, 260, 683-685.

Graml, F., Penningsfeld, F.-P., and Schönfelder, V., 1977, The MPI-imaging double Compton telescope for balloon observations of MeV gamma radiation, Proc. 12th ESLAB-Symp. on Recent Advances in Gamma Ray Astronomy, Frascati 24-27 May 1977, ESA SP-124, 301-307.

Graml, F., Penningsfeld, F.-P., and Schönfelder, V., 1978, Low energy gamma ray astronomy at balloon altitudes with the MPI Compton telescope, to be published in Proc. of the ESA Symp. on European Sounding Rocket, Balloon and Related Research, 24-29 April 1978, Ajaccio, Corsica.

Haymes, R.C., Walraven, G.D., Meagan, C.A., Hall, R.D., Djuth, F.T., and Shelton, D.H., 1975, Detection of nuclear gamma rays from the galactic center region, Astrophys. J., 201, 593-602.

Mushotzky, R.F., 1977, Observational consequences of synchrotron self-Compton models of compact extragalactic X-ray sources, Nature, 265, 225-226.

Schönfelder, V., 1978, Origin for MeV excess in the energy spectrum of diffuse cosmic gamma rays found? submitted to Nature.

SEARCH FOR BROAD GAMMA RAY LINES
WITH THE UCR DOUBLE COMPTON SCATTER TELESCOPE

R. Stephen White, James M. Ryan, Robert B. Wilson and Allen D. Zych
Physics Department and Institute of Geophysics and Planetary Physics
University of California, Riverside
Riverside, California   92521
and
Bruce Dayton
Physics Department, California State University, Los Angeles
Los Angeles, California   90032

ABSTRACT. A search for broad gamma ray lines in the anti-galactic center direction is being carried out with the large UCR gamma ray double Compton scatter telescope. Measurements of the energy deposits of the recoil electrons in 2 scintillator cells separated by 1 m and the identification of the 2 cells yield the energy of the gamma ray and its zenith angle. The zenith angle resolution is about 10° HWHM. The energy resolution varies from 24% to 5% HWHM as the angle of the first Compton scatter changes from 10° to 60°. An increase in gamma rays was observed as the galactic anti-center crossed the telescope aperture. Searches for lines from $p(n,\gamma)d$ at 2.2 MeV, $^{12}C^*$ at 4.4 MeV and $^{16}O^*$ at 6.1 MeV and others broadened and perhaps redshifted are under way on data from a 24 hr balloon flight from Palestine, Texas, on May 13, 1975. Measurements of these lines could help identify the processes responsible for the production of celestial gamma rays. Two sigma upper limits for lines in the galactic anti-center direction at 4.4 MeV and 6.1 MeV are 6 and 4×10^{-4} γ/cm^2-s.

I. INTRODUCTION. Today I would like to report our search for broad gamma ray lines from the direction of the anti-galactic center direction. Nuclear line spectroscopy offers great promise for explaining the violent interactions taking place in our universe. The observation of broad gamma ray lines that are also redshifted will give exciting new information about interactions that take place on the surfaces of compact objects. The redshift gives a measure of the mass of the neutron star or black hole and the width of the line gives an estimate of the energies of the colliding nuclear matter.

The search for nuclear gamma ray lines was carried out with the University of California, Riverside (UCR), double Compton scatter gamma ray telescope. The telescope was launched from Palestine, Texas, on May 13, 1975, to a maximum height of 3 g/cm^2 residual atmosphere and floated near this altitude for 24 hr. An increase in the gamma ray flux was observed when the anti-galactic center direction crossed the telescope aperture (Wilson et al., 1977). The measurement of a continuous energy distribution during the transit gave two sigma upper limits for the fluxes of gamma ray lines at energies of 4.4 and 6.1 MeV of 6 and 4×10^{-4} photons/cm^2-s.

II. OBSERVATIONS. The gamma ray telescope used for the observations is shown in Figure 1 (Herzo et al., 1975; Zych et al., 1975). A gamma ray is identified by a scatter in the liquid scintillator S1 followed by a second scatter in S2 with no accompanying signal from anticoincidence shields A1 and A2. The energy deposits of the electrons in S1 and S2, the time of
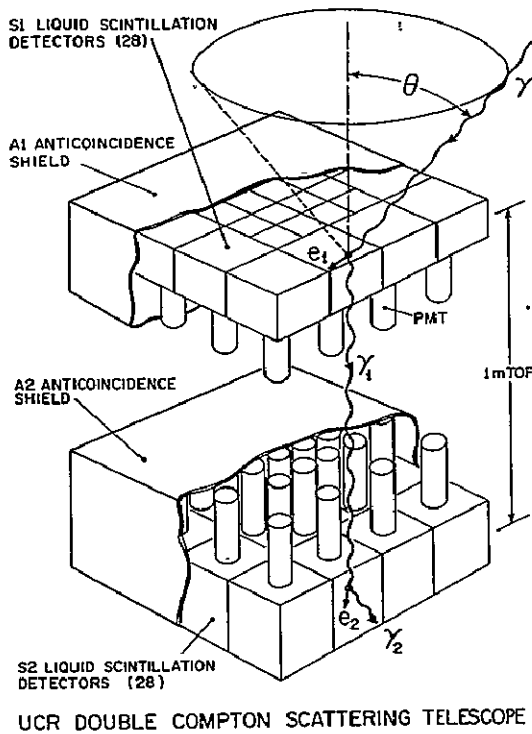
SI LIQUID SCINTILLATION DETECTORS (28)

UCR DOUBLE COMPTON SCATTERING TELESCOPE

Fig. 1. Schematic drawing of the double Compton scatter gamma ray telescope. The incident gamma ray γ enters at angle θ to the vertical direction, scatters from an electron e_1 in liquid scintillator S1, and continues as γ_1 into liquid scintillator S2, where it scatters from electron e_2. The 28 separate cells in S1 and S2 with their individual photomultipliers are shown. The plastic antiscintillator completely surrounds S1 and S2.

flight of the gamma ray between S1 and S2 and the identifications of the cells in S1 and S2 containing the scatters are measured and recorded. This gives the energy and scattering angle of the incoming gamma ray. The scattering angle defines a ring on the sky for the direction of the incident gamma ray. For the analysis of this paper, vertical pairs of cells only are used; then the scattering angle is the zenith angle. Since the telescope is supported by the balloon in a vertical position, the calculated zenith angle is independent of the azimuth angle and the rotation of the telescope is neglected in the data analysis. The telescope aperture is divided into zenith angle intervals of 0°-10°, 10°-20°, 20°-30° and 30°-40° and the fluxes are measured simultaneously in each of these angle intervals. A source is identified by its increasing flux as it passes through the angular intervals of the aperture.

The efficiency of the telescope for vertical cell pairs only is given in Figure 2 as a function of the incident angle for monochromatic gamma rays of 4.4, 6.1 and 12.1 MeV. The monochromatic gamma rays for the laboratory calibrations were obtained by bombarding targets with protons at the California State University Van de Graaff accelerator (Ryan et al., 1977). Analytical and Monte Carlo calculations verify the laboratory calibrations. The energy and angle resolutions were measured for an incident gamma ray energy of 6.1 MeV and are shown in Figure 3. The resolution varies from 24% HWHM for 10° incident angle to 5° HWHM for 60°. The angular resolution is about 10°, nearly constant, independent of the scattering angle from 10° to 60°. The angular resolution appears narrower at 10° only because the telescope efficiency cuts off rapidly below 10°.

III. BACKGROUND REJECTION. The UCR double scatter gamma ray telescope has an exceptionally high background rejection capability. (1) Coincident counts required by S1 and S2 eliminate much of the background measured by single scatter detectors. (2) A high fraction, about 40%, of the telescope mass is in gamma ray detection scintillators S1 and S2, very high compared to other detectors. (3) The anti-scintillators surrounding S1 and S2 veto 99.99% of the charged particles incident on the scintillators. (4) The angular resolution of the telescope of 10° HWHM limits significantly the solid angle for
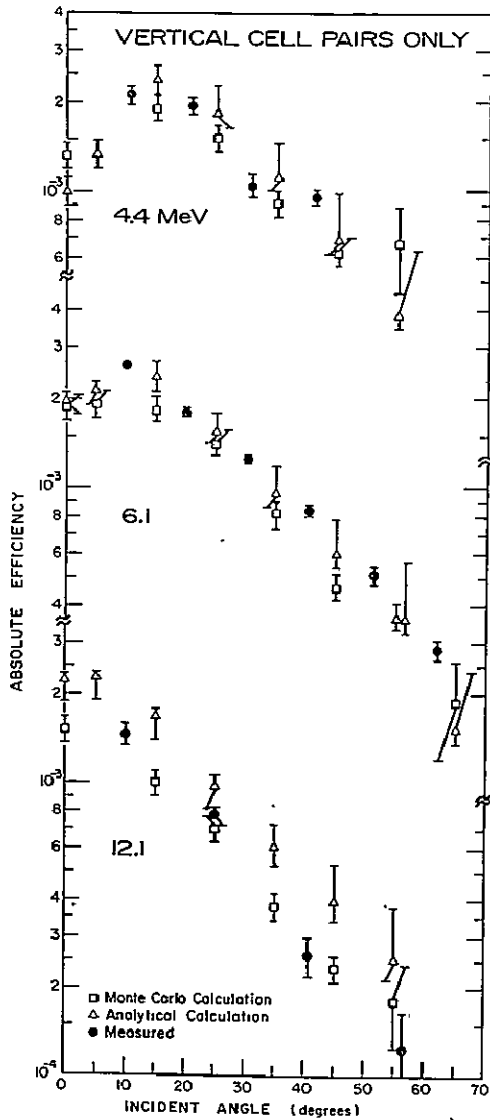
Fig. 2. Comparisons of absolute analytical and Monte Carlo calculated efficiencies with measured efficiencies for vertical cell pairs as a function of the incident gamma ray angle. The incident gamma ray energies are 4.4, 6.1 and 12.1 MeV. The absolute efficiency is the ratio of the detected to incident gamma rays.
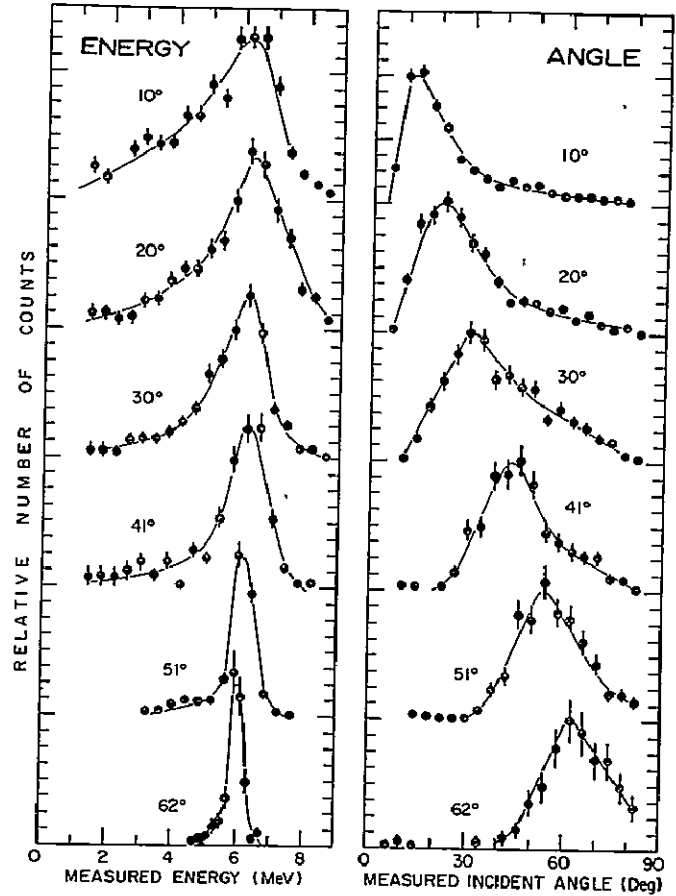

Fig. 3. Measured angle and energy resolutions for vertical cell pairs with 6.1 MeV incident gamma rays. The measured energy distributions for different incident angles given on the left have HWHM values that vary from 24% to 5%. The measured angular distributions on the right have HWHM values that vary from 10° to 12.5°. Curves are drawn through the points to guide the eye.

observation of background gamma rays. (5) Gamma rays traversing the telescope from S2 to S1 and neutrons are eliminated by time of flight. Typical gamma ray time-of-flight distributions obtained on the balloon flight are shown in Figure 4 (Ryan et al., 1977). The upward moving gamma rays can be easily subtracted from the downward moving ones at all altitudes. (6)
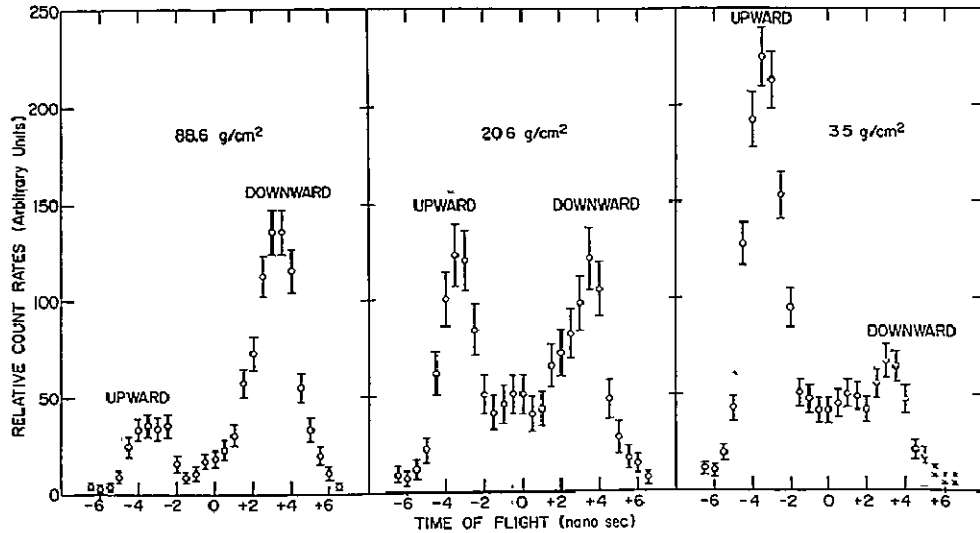
Fig. 4. Time-of-flight resolution. The gamma ray distribution is given at residual atmospheric depths of 88.6, 20.6 and 3.5 g/cm². The upward moving gamma rays are to the left, and the downward moving ones to the right. At atmospheric depths below and above 20 g/cm² the downward and upward moving gamma rays are dominant, respectively.

Gamma rays from radioactive decays of isotopes produced by cosmic ray proton and alpha-particle bombardment of high-Z scintillators are not produced in the hydrogen and carbon of the mineral oil scintillators S1 and S2. (7) The mineral oil scintillator has a high hydrogen/carbon ratio, 1.8 compared to 1.1 of most plastic scintillators. This reduces the fraction of neutron induced gamma rays to less than about 20% of the cosmic diffuse gamma rays for energies up to 10 MeV (White et al., 1977). (8) The gamma rays from neutrons captured by protons are less than about 10% of the cosmic diffuse gamma rays at 2 to 3 MeV and are negligible at higher energies (White et al., 1977).

IV. RESULTS. The gamma ray flux from the anti-galactic center direction is plotted versus time in Figure 5 for angle intervals in the telescope aperture of 0°-10°, 10°-20°, 20°-30° and 30°-40° (Wilson et al., 1977). The time of meridian transit of the Crab Nebula is 2035 UT. The solid lines are the expected fluxes based on the measured telescope angular resolution (Ryan et al., 1977). At the time of local meridian transit, the Crab Nebula passes 11° from the zenith. This coupled with the low telescope efficiency below 10° gives the straight line plotted in Figure 5. The fit of the data to the solid curve for 10° to 20° is quite good and the fits to the broader peak for 20° to 30° and the double humped curve for 30° to 40° with higher backgrounds are reasonable. The source flux is the difference in the flux in the 10° to 40° interval with the source present and with it absent. Four points on the energy distribution are plotted along with the data of other investigators in Figure 6. Comparison of our data with a power law connecting gamma ray fluxes at lower and higher energies enables us to set upper limits on gamma ray lines at 4.4 and 6.1 MeV from the anti-galactic center direction. These upper limits are 6 and 4 × 10⁻⁴ photons/cm²-s at energies of 4.4 and 6.1 MeV.
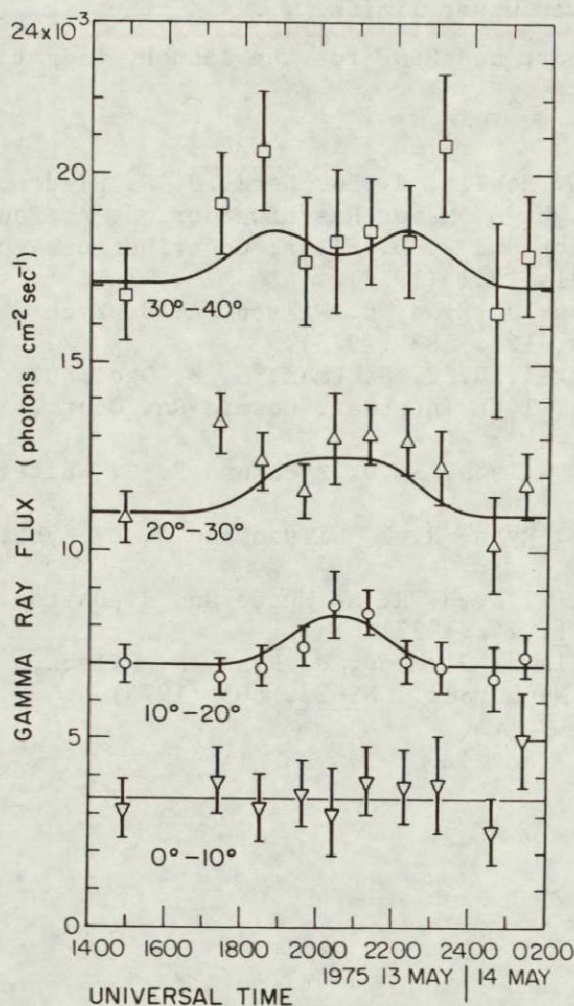
Fig. 5. Total flux from the Crab
Nebula from 2 to 25 MeV during its
passage through the telescope aperture.
Vertical cell pairs only are used. The
flux is shown for four angular apertures
of 0°-10°, 10°-20°, 20°-30° and 30°-
40°. The solid lines are the expected
fluxes on the basis of the measured
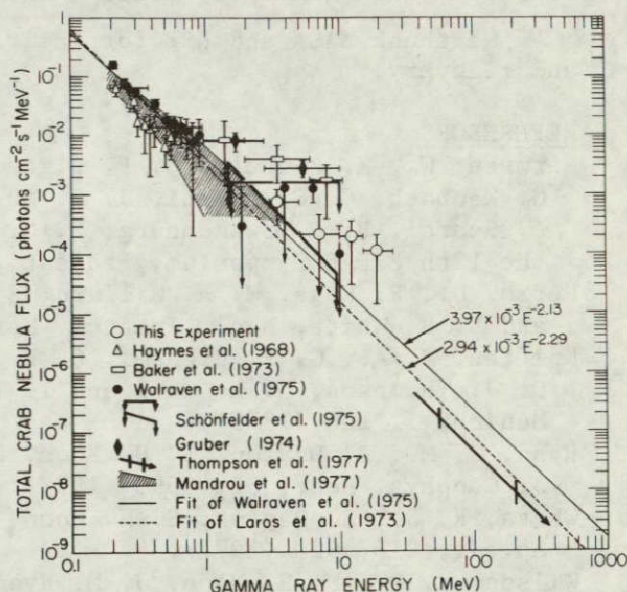angular resolution (Ryan et al., 1977).

Fig. 6. The energy distribution of
the total gamma rays from the Crab
Nebula. Vertical cell pairs only
are used. Our results are compared
with other observations.

The fact that our angular resolution is not sufficient to separate the Crab
Nebula from the source 195, +5 (Kniffen et al., 1975; Hermsen et al., 1977)
means that the upper limits apply to a region that could include more than
one gamma ray source. The upper limits for gamma ray lines also apply
equally well to the period of time from 1400 UT 1975 May 13 to 0200 UT 1975
May 14. This period covered a region of the sky centered at RA of 23^h20^m
to 10^h15^m and declination nearly constant of 32°. In galactic coordinates
the center of the region varied from ℓ^{II} of 102° to 195° and b^{II} of -27° to
+56°. We are currently working to extend the search to lower fluxes to

find the broad gamma ray lines or set lower upper limits.

REFERENCES

Hermsen, W., K. Bennett, G. F. Bignami, G. Boella, R. Buccheri, J. C. Higdon, G. Kanbach, G. G. Lichti, J. L. Masnou, H. A. Mayer-Hasselwander, J. A. Paul, L. Scarsi, B. N. Swanenburg, B. G. Taylor and R. D. Wills, Contributions to the 12th ESLAB Symposium, Frascati, Italy, 3.1 (1977).

Herzo, D., R. Koga, W. A. Millard, S. Moon, J. Ryan, R. Wilson, A. D. Zych and R. S. White, Nucl. Instrum. Methods, 123, 583 (1975).

Kniffen, D. A., G. F. Bignami, C. E. Fichtel, R. C. Hartman, H. B. Ögelman, D. J. Thompson, M. E. Özel and T. Tümer, 14th Internat. Cosmic Ray Conf., Munich, 1, 100 (1975).

Ryan, J. M., B. Dayton, S. H. Moon, R. B. Wilson, A. D. Zych and R. S. White, J. Geophys. Res., 82, 3593 (1977).

White, R. S., B. Dayton, S. H. Moon, J. M. Ryan, R. B. Wilson and A. D. Zych, Ap. J., 218, 920 (1977).

Wilson, R. B., S. H. Moon, J. M. Ryan, A. D. Zych, R. S. White and B. Dayton, Proc. 15th Internat. Cosmic Ray Conf., 1, 24 (1977).

Zych, A. D., D. Herzo, R. Koga, W. A. Millard, S. Moon, J. Ryan, R. Wilson, R. S. White and B. Dayton, IEEE Trans. Nucl. Sci., NS-22, 605 (1975).

RICE UNIVERSITY OBSERVATIONS OF THE GALACTIC CENTER

Charles A. Meegan

In view of the recent results on gamma-ray lines from the Galactic Center (Leventhal, 1978; Matteson, 1978), it is appropriate to summarize here the original Rice observations of this region. The Galactic Center was observed on four balloon flights between the years 1969 and 1974 (Haymes, et al., 1969; Johnson, et al., 1972; Johnson and Haymes, 1973; Haymes, et al., 1975). The most recent, and most sensitive, observation will be emphasized here.

The detector employed in the 1974 observation is shown in Figure 1. It consists of a 6 inch by 2 inch NaI(Tℓ) central detector collimated to ~15° FWHM by a NaI(Tℓ) anticoincidence shield. The shield is at least two interaction mean free paths thick at all gamma-ray energies. The instrumental resolution was ~11 percent FWHM at 662 keV. Pulses from the central detector are analyzed by two 256-channel PHA's covering the energy range ~20 keV to ~12 MeV. The detector is equatorially mounted and pointed by command from the ground. Observations are made by measuring source and background alternately for 10-minute periods. Background is measured by rotating the detector 180° about the azimuthal axis.
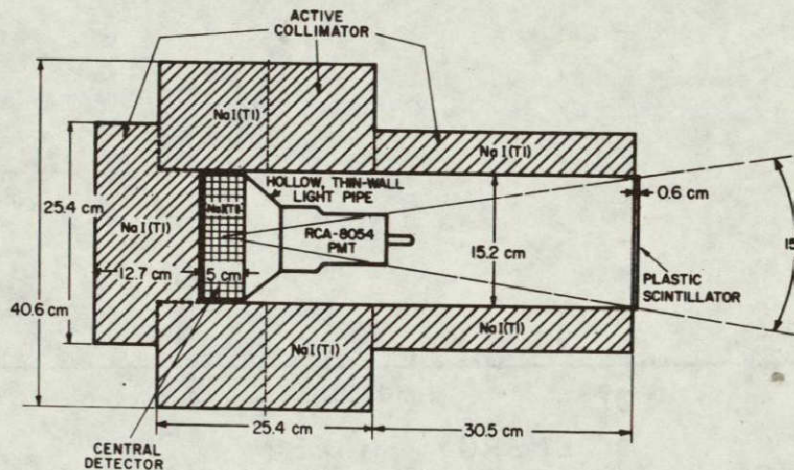

Figure 1. Schematic diagram of gamma-ray detector.

The Galactic Center was observed for 8 hours on a balloon flight launched from Rio Cuarto, Argentina, on April 1, 1974. The float altitude was 4 mbar. Figure 2 shows the background spectrum observed. The total count rate was ~25 counts/sec. The major source of background for this instrument has been shown to be activation (Djuth, 1977).

Figure 3 shows the spectrum determined for the Galactic Center region, centered on the position of GX 1+4. The spectrum is well represented by a power
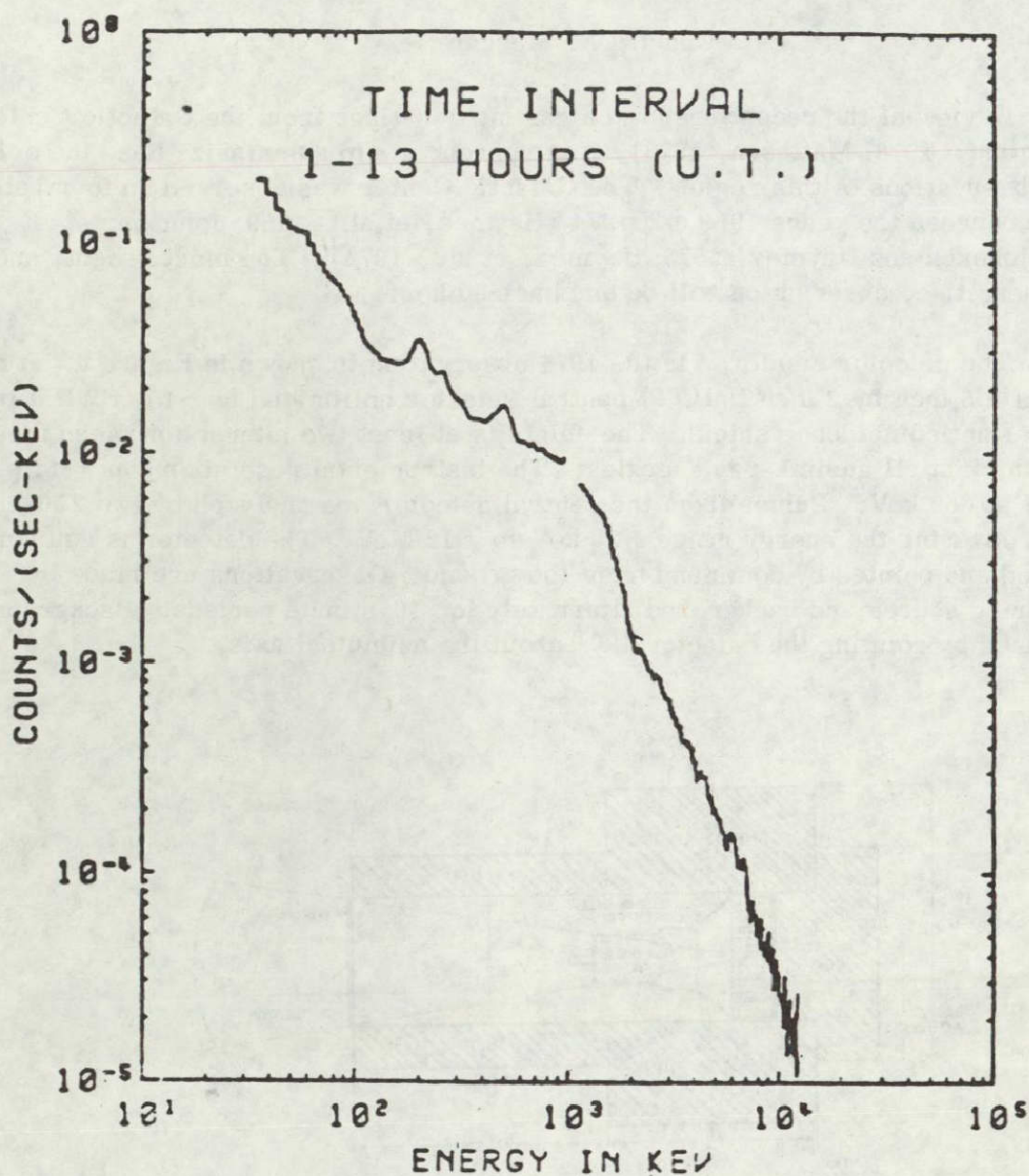
224

Figure 2. Count rate spectrum of background observed
at float altitude.

law plus superposed spectral features at 0. 5 MeV, 1. 2-2. 0 MeV, and 4. 6 MeV. The
features at 0. 5 MeV and 4. 6 MeV are 3. 5 standard deviations above the power law;
the 1. 2-2. 0 MeV feature is 4. 1 standard deviations above the power law. The 0. 5
MeV feature was also seen on both the 1970 and 1971 Galactic Center observations,
which employed slightly different detectors. The combined data from the previous
flights yielded a 5. 3σ excess above the power law at ~476 keV. In the 1974 observa-
tion, however, the peak was at ~530 keV and the intensity about half of that measured
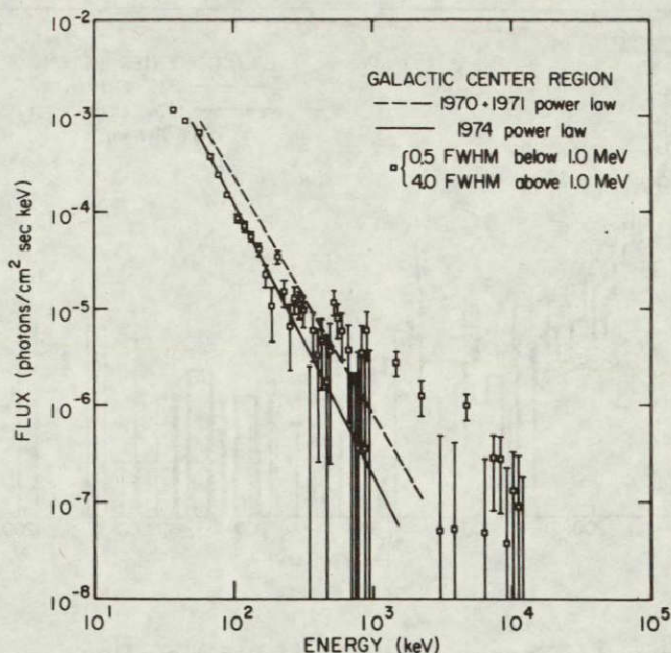previously. Figure 4 shows a comparison of the 0. 5 MeV feature measured in 1974

Figure 3. Energy spectrum of
Galactic Center region.

with that measured in 1970 and 1971. The origin of the apparent shift in energy is
not known. It seems somewhat too large, $\sim 3.4\sigma$, to be caused by statistical fluctua-
tions alone. It is also difficult to attribute the shift to a calibration error, since a
background feature at $\sim$490 keV allows an inflight calibration. Whatever the cause
of the discrepancy, the uncertainty appears to be resolved now with the observation
of the line at 511 keV by Leventhal and McCallum. The lower intensity in the 1974
observation is consistent with the smaller field of view of the instrument used in 1974,
if the source of the line is an extended region.

Figure 5 is a linear plot of the flux above 1 MeV, showing the excess at 4.6
MeV and in the 1.2-2.0 MeV region. Each bin is 1 FWHM resolution width. The
lines are believed to be caused by interactions of cosmic ray nuclei with interstellar
matter. Rygg and Fishman (1973) have calculated the relative intensities of lines to
be expected from this mechanism. The observed lines occur at the energies of the
most intense predicted lines. If the lines rise from this mechanism, the 0.5 MeV
line would be due to positron emitters produced in spallation reactions. The 1.2 to
2.0 MeV excess would be due to inelastic collisions of one or more of the nuclides
Mg^{24}, Ne^{20}, and Si^{28}. The line at 4.6 MeV, which shows evidence of Doppler broaden-
ing, would be due to inelastic collisions of cosmic-ray C^{12}. The observations and
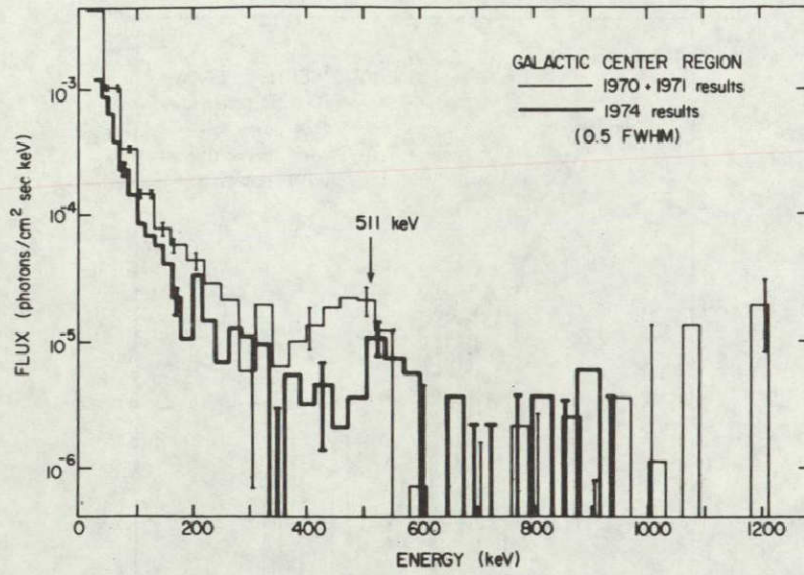possible origins are summarized in Table 1.
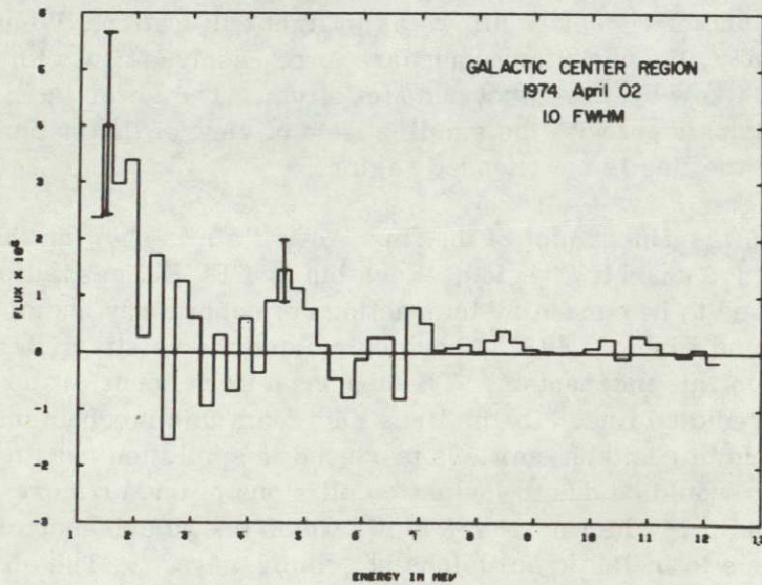
Figure 4.   Energy spectrum of 0.5 MeV line.

Figure 5.   Linear plot of flux above 1 MeV.

OBSERVATIONAL EVIDENCE FOR EXTRATERRESTRIAL GAMMA-RAY LINE SOURCES*

by

A. S. Jacobson, J. C. Ling, W. A. Mahoney and J. B. Willett

Jet Propulsion Laboratory
California Institute of Technology
Pasadena, California

During the 1974 balloon flight of a high spectral resolution gamma-ray telescope, observing in the energy range of about 50 keV to 10 MeV, evidences were gathered for two cosmic sources of gamma-ray lines. These are (1) a 73 keV line feature superimposed on a power law continuum spectrum in the 55 to 300 keV range from the Crab nebula; and (2) a flare-like event lasting about twenty minutes, during which four intense gamma-ray lines were measured at .41, 1.79, 2.22 and 5.95 MeV.

The balloon-borne system we at JPL have been operating for several years has a sensor which consists of a cluster of four Ge(Li) detectors with a present combined volume of 180 cm^3 (Jacobson, et al., 1975). To provide collimation and background reduction, the detectors are surrounded by a CsI(Na) scintillation shield of thickness 6.4 cm defining a solid angle of 0.1 sr. Figure 1 shows the sensor. The shield is in four pieces: a collimator on top with a hole drilled through it above each of the Ge(Li) crystals, defining the aperture, two halves of a split annulus, and a plug in the bottom. The shield is in electrical anticoincidence with the central detectors. The preflight spectral resolution of the Ge(Li) cluster is about 2 keV at 100 keV (2%) and 2.9 keV at 1.33 MeV (.22%). Cooling for the Ge(Li) crystals is provided by a pressurized liquid nitrogen dewar.

Figure 2 shows the balloon gondola. Above the sensor, on a commandable turntable are a ^{133}Ba radioactive calibration source and a 20.3 cm diameter

by 10.2 cm thick NaI(Tℓ) detector used as an active blocking crystal, or
shutter for the sensor. Using the shutter to block the aperture allows us
to study the background properties of the instrument and to modulate an
external source. Each Ge(Li) crystal is operated independently with its
own analog signal chain and 8192-channel pulse-height analyzer. This allows
the processing of simultaneous events and hence the recovery of most events
which involve absorption by the Compton and pair production processes. An
event in any crystal is analyzed, assigned a time tag to 0.017 msec preci-
sion, assigned various I.D. and status bits and telemetered on an event-by-
event basis.

The system was flown on 10 June 1974 to observe the Crab nebula. Due
to a malfunction some weeks before the flight, one Ge(Li) crystal was elec-
tronically eliminated from the system leaving three operational with a com-
bined volume of about 120 cm^3. Some results of this experiment are reported
by Ling, et al. (1977a, 1977b). Figure 3 is the Ge(Li) count-rate record of
that flight in the 65 to 100 keV energy band. The experiment was launched
at about 1205 UT and, after climbing through the Pfotzer maximum, the balloon
reached float altitude of 2.9 mb at about 1520 UT. At 1600 UT, the sensor
aperture was blocked for 45 minutes to study its background properties; and
the sun and the Crab nebula made transits through the aperture at 1845 UT
and 1902 UT, respectively. The point-source viewing technique used is to
fix the alt-azimuth axes of the instrument throughout an observation and
allow the source of interest to drift through the field of view. Since
there are indications that the background varies both with zenith angle
(Ling and Gruber, 1977) and with azimuth angle (Fishman, et al., 1976),
this technique keeps the background more nearly constant during the obser-
vation and minimizes the corrections to the data which have to be made,

although these are still considerable and include, besides the detector properties, atmospheric absorption and altitude and latitude dependent background variations.

Figure 4 shows the net Crab spectrum from 50 keV to 300 keV after subtraction of the background and corrections to the top of the atmosphere. Two curves fit to this spectrum are shown. The dashed line is a power law of the functional form $\phi = 25E^{-2.28}$ photons/cm^2-sec-keV. This fit gives $\chi^2 = 42$ for 27 degrees of freedom. The probability of getting such a poor fit is 3.5%. 32% of the χ^2 value is contributed by the possible line feature in the 71-76 keV bin. If we add a Gaussian-shaped line feature to the power law, i.e.,

$$\phi = 10.1E^{-2.1} + 1.13 \times 10^{-3}e^{-(E-73.3)^2/3.6}, \qquad (1)$$

we get $\chi^2 = 42$ for 37 degrees of freedom with 25% probability. The inset in the figure shows the spectral region containing the possible line on a single 1 keV wide channel basis. This feature appears in the spectrum measured by each of the three Ge(Li) crystals. Figure 5 shows the count rate response in the spectral region around the line during the transit of the source. The dashed curve represents the expected count rate in three energy bins vs time if the Crab nebula has a pure power law spectrum, and the solid line represents the expectation if the spectrum is a power law plus a line at 73.3 $^{\pm 1}$ keV. As can be seen, the dashed curve adequately describes the response in the 66-71 keV channel and the 76-81 keV channel, but the response in the 71-76 keV channel is better described by the solid curve. The dot-dashed curve represents the expected response from a solar line which, while not reasonably reconcilable with our knowledge of the sun, cannot be definitely ruled out.

Figure 6 shows our measured spectrum compared to other recent measure-
ments of the Crab nebula. We are in close agreement with these other measure-
ments, except for the line discussed above. The flux in the line is (4.0 ±
1.1) x 10^{-3} cm^{-2}-sec^{-1}, and its width is < 4.9 keV. No pulsation was detected.
The 1σ upper limit on the pulsed fraction for the line component is 25%. It
is possible that, like the 58 keV Her X-1 line reported by Trumper, et al.
(1976), it too is associated with cyclotron radiation at the surface of the
neutron star. If it is the first harmonic, and is red-shifted by Z = .2, it
represents a magnetic field strength of $\sim$ 8 x 10^{12} Gauss over the emitting
region. If the line width is a measure of non-uniformity of this field, then
over the emitting region, the field must vary by no more than $\frac{\Delta H}{H}$ = .05.
Though probably only fortuitous, it is also of interest to note that the
line, both in energy and width, is fit quite well by the spectrum of x-rays
from Pb. Such x-rays could result from the radioactive decay of large quan-
tities of trans-Bismuth elements. The energy in the line is 2 x 10^{35} ergs/
sec, and if connected with radioactive decays, would represent 2 x 10^{42}
decays/sec, resulting in an energy release of about 10^{38} ergs/sec at the
nebula.

Analysis of the spectrum above 300 keV is not complete, but we have
looked at the region around 400 keV in the hopes of seeing the line reported
by Leventhal, et al. (1977). Figure 7 shows the results of this search.
The top part of the figure shows both our source spectrum, and our source
plus background spectrum. Below it are shown the equivalent spectra from
the paper referenced above. We do not see a line at 400 keV and estimate
it should have appeared with a statistical significance of about 3.9σ in
our measurement. Our 3σ upper limit on such a line is 1.75 x 10^{-3} cm^{-2}-sec^{-1},
while the reported flux is (2.24 ± 0.65) x 10^{-3} cm^{-2}-sec^{-1}. The observations

were separated by two years, so we cannot rule out the possibility that the line might be a time varying feature.

Toward the end of this same flight, we observed a transient event during which four intense lines appeared in the measured spectrum. Figure 8 shows the Ge(Li) count rate, during the same balloon flight, in three adjacent 100 keV wide energy bands centered at 1710 keV, 1810 keV and 1910 keV. At about 2020 UT, there was an increase of about 45 percent in the rate of the 1810 keV band with no corresponding increase in the adjacent bands. The increased rate lasted for ~ 20 minutes after which it returned to its background value until the experiment was cut down at 2210 UT. The duration of the increase was too short to be a point source transit. Estimates indicated that if the increase represented the response to a transient event, it would be measurable in the scintillation detectors on board.

We found that the scintillator count rates did indeed register an increase coincident with the increased Ge(Li) rate in the energy band around 1.8 MeV. The integral rates >150 keV and >4 MeV are sampled every 9 seconds in each of the shield pieces and the blocking crystal. The collimator rate >150 keV shows a >5σ increase; the blocking crystal had a >3σ increase; the shield halves rates increased by ~ 2.5σ and the plug showed no significant deviation from its background rate. Figure 9 shows the collimator >150 keV rate sampled at 90 second intervals. Also shown for reference is the pertinent portion of the 1.8 MeV Ge(Li) rate. The shield rates were used to determine the time intervals over which Ge(Li) spectral data were accumulated and analyzed. This approach led to the detection of the four spectral features, of greater than 3σ significance, shown in Figure 10. Table I gives the information that has been developed to date on these features. The background spectrum was measured before and after the transient event. The time

intervals are those which maximized the statistical significance of the line and can be taken as a rough measure of the onset and end of the event. In the case of the line around 6 MeV, the onset seems to be earlier than for the other three lines by about 10 minutes. The strongest feature was at about 1790 keV and is within 1.8σ of the energy of the most prominent line of $^{28}Si^*$ and 3.2σ from that of $^{26}Mg^*$. The 2220 keV line is less than 1σ from the energy of the deuterium formation line. There are no such obvious associations for the remaining two lines. It must be pointed out that if the 1.8 MeV line were to be considered a red-shifted component of the 2.2 MeV line (and both were emitted in the source region), the red-shift factor of 0.24 would shift the .511 MeV line to within 1σ of the observed line at .413 MeV. The corresponding non-red-shifted component at 0.511 MeV would be unobservable because of our high background in that line (Ling, et al., 1977a). The red-shift factor is typical of the surface of a neutron star of $\sim 1.2\ M\odot$.

Our information on the direction of this source is highly uncertain at this time. In principle, the relative rates of the various shield pieces and the Ge(Li) crystals could provide reasonably good directional information, but they were not designed for this function and hence the data they do provide are incomplete. It is clear, however, that the transient source is not distributed like the background environment counted by these crystals, but is concentrated in the upper hemisphere of the sensor. Because of the large difference between the relative solid angles viewed by the Ge(Li) crystals and the collimator crystal, the relative count rates rule out a source extended to a solid angle greater than about 0.1 sr. These arguments lead to the conclusion that the source is probably extraterrestrial.

Preliminary indications are that it is close to the detector axis but this is by no means a firm result.

Figure 11 shows the portion of the sky viewed during the event. The concentric curves are the FWHM fields of view at the energies of the lines detected. Within this field are the planets Mercury and Saturn; the SN-remnant IC443 and the pulsar PSR 0611+22 which may be associated with it; and the high energy gamma-ray source γ195+5 observed by both SAS-2 (Fichtel, et al., 1975) and COS-B (Bennett, et al., 1976). Not shown is a γ-ray burst source in the region reported recently by Cline, et al. (1978). At the edge of the field was the Crab nebula and the sun. The numbered dots are stars within 6 pc. of the earth. The closest is number 3, Procyon at 3.5 pc. Number 5 is the flare star YZ Canis Minor. The duration of the event, about 20 minutes, is typical of flare events. If this event had originated in YZ CMi at a distance of 6 pc., the energy in the lines would be $\sim 10^{36}$ ergs. This is more than the largest optical flare observed from that star which was $\sim 10^{35}$ ergs over 4 hours (Gershberg, 1970). The Sun is rather far off our detector axis to be considered a likely source of this event, but it cannot definitely be excluded. The duration is similar to that of the solar flare lines observed by Chupp, et al. (1973) where the event lasted about 10 minutes. Most of the lines, however, associated with the event reported here were not seen in the solar flare observations. Nor was a continuum observed in this event as it was in the solar flare. If the ratio of line-to-continuum flux had been the same as for the observed solar flares, we would have detected a strong continuum. Although relatively rare, x-ray flares of about this duration have also been observed (Markert, et al., 1976).

The fact that this event was observed during 6.5 hours of balloon observing time indicates it could be quite common. They can, however, be easily overlooked in the data analysis, and must be carefully searched for. The scintillator shields, or isotropically sensitive detectors are sensitive to the events but the peak rate increase in the one reported here was less than 1% of the mean background rate, and typically, variations in background for such detectors, are of this order. In the spectra measured by shielded detectors, the events are easily missed if time averaging is not just right to enhance the lines. We urge experimenters to carefully search their data for corroborating events of this nature.

REFERENCES

Bennett, K., Bignami, G. F., Boella, G., Buccheri, P., Burger, J. J.,
Cuccia, A., Hermsen, W., Higdon, J., Kanback, G., Koch, L., Lichti, G. G.,
Masnou, J., Meyer-Hasselwander, H. A., Paul, J. A., Scarsi, L., Shukla, P.
G., Swanenburg, B. N., Taylor, B. G., and Wills, R. D. (1976) Proc. of 2nd
Int. Gamma-Ray Symposium, GSFC X-662-76-154.

Carpenter, G. F., Coe, J. M., and Engel, A. R. (1976) Nature, 259, 99.

Chupp, E. L., Forrest, D. J., Higbie, P. R., Suri, A. N., Tsai, C., and
Cumphy, P. P. (1973) Nature, 241, 333.

Cline, T. L., Desai, U. D., Pizzichini, G., Spizzichino, A., Trainor, J. H.
(1978) Paper KH9 Bulletin of the APS, 23, 632.

Dolan, J. F., Crannell, C. J., Dennis, B. R., Frost, K. J., Maurer, G. S.,
and Orwig, L. E. (1977) Ap. J., 217, 809.

Fichtel, C. E., Hartman, R. C., Kniffen, D. A., Thompson, D. J., Bignami, G.
F., Ogelman, H., Ozel, M. D., and Tumer, T. (1975) Ap. J., 198, 163.

Fishman, G. J., Watts, Jr., J. W., Meegan, C. A. (1976) JGR, 81, 6121.

Gershberg, R. E. (1970), "Flares of Red Dwarf Stars" transl. by D. J. Mullan,
Armagh Observ., N. Ireland.

Gruber, D. E. and Ling, J. C. (1977), Astrophys. J., 213 802-814.

Jacobson, A. S., Bishop, R. J., Culp, G. W., Jung, L., Mahoney, W. A. and
Willett, J. B. (1975) Nucl. Instr. & Methods, 127, 115.

Jacobson, A. S., Ling, J. C., Mahoney, W. A. and Willett, J. B. (1976), Bull.
on AAS, 8, 528

Leventhal, M., MacCallum, C. and Watts, A. (1977) Nature, 266, 696.

Ling, J. C. and Gruber, D. E. (1977) JGR, 82, 1211.

Ling, J. C., Mahoney, W. A., Willett, J. B. and Jacobson, A. S. (1977a) JGR,
82, 1463.

Ling, J. C., Mahoney, W. A., Willett, J. B. and Jacobson, A. S. (1977b)
Nature, 370, 36.

Markert, T. H., Backman, E. E. and McClintock, J. E. (1976) Ap. J., 208,
L115.

Toor, A and Seward, F. D. (1974) Astrophys. J., 79, 995.

Trumper, J., Pietsch, W., Reppin, C., Sacco, B., Kendziorra, E. and Staubert,
R. (1976) Proc. of VIII Texas Symp. on Rel. Astrophysics.

FIGURE CAPTIONS

Figure 1   An exploded view .of the JPL Ge(Li) balloon-borne spectrometer.

Four Ge(Li) crystals with a present combined volume of 180 cm^3

is shielded and collimated by 6.35 cm of CsI(Na). Cooling is

provided by liquid nitrogen (from Jacobson, et al., 1975).

Figure 2   A diagram of the JPL gamma-ray spectrometer gondola. It is a

108 cm cube and constitutes a payload weight of 580 kg. The

turntable above the sensor allows a calibration source or a

blocking·crystal to be positioned by command over the aperture

(from Jacobson, et al., 1975).

Figure 3   Count rate records in the 65-100 keV range for the 10 June 1974

balloon flight. At around 1600 UT, the aperture was blocked by

an 20.3 cm diameter x 10.2 cm thick NaI(Tℓ) detector. There

was a transit of the aperture by the sun 17 minutes before the

Crab nebula transit. During the Crab nebula transit, the mean

count rate in this interval increased by 27 percent.

Figure 4   The net photon spectrum from the Crab nebula in the energy

range of about 50 keV to 300 keV, measured on 10 June 1974.

The solid and dashed curves indicate, respectively, power law

fits to the data, with and without a Gaussian shaped line at

73.3 keV. The inset shows details of the fit in the vicinity

of the possible line on a channel-by-channel basis.

Figure 5   Details of the Crab nebula transit as measured in a 5 keV wide

channel containing the possible line feature, as well as those

5 keV wide channels directly adjacent to it. The expected

response for power law spectra with and without a line feature

are also shown. The power law, without a line feature, is clearly a poor fit to the data measured in the 71-76 keV range. Curves are shown for a line emitted from both the sun and the Crab nebula. Each adequately describes the observation so that the sun cannot be ruled out as a possible source of the feature on the basis of the data.

Figure 6   The net Crab nebula photon spectrum measured on 10 June 1974. Except for the significant deviation around 73 keV, the data agrees with other recent measurements reported.

Figure 7   Comparison of differential count spectrum of the Crab nebula measured in the energy range of 388 to 414 keV by Jacobson, et al. (1976) and Leventhal, et al. (1977). The line at 400 keV reported by Leventhal, et al., was unobserved in the 10 June 1974 flight.   (Ling, et al., 1977b).

Figure 8   The count rate record of the 10 June 1974 balloon flight in three adjacent 100 keV wide energy bands. A 45 percent increase in the 1760-1860 keV range occurred at about 2020 UT, and signals a transient event manifested by four significant gamma-ray lines and count rate deviations in several scintillators on board.

Figure 9   Integral count rate >150 keV measured in the CsI(Na) shield collimator crystal, sampled at 90 second intervals. These rates are not corrected for dead time. Also shown for reference is a portion of the rates shown in Figure 11. A significant count rate deviation occurred in coincidence with the increase around 1.8 MeV. Such deviations also occurred in coincidence with the increase around 1.8 MeV. Such deviations also occurred in several other scintillation counters on board.

Figure 10   Those portions of the spectrum containing the lines measured

during the transient event of 10 June 1974.   All of these lines

are greater than the resolution width·of the instrument.

Details of the lines are given in Table I.

Figure 11   The instrument field of view at the mid-time of the transient

event of 10 June 1974.   The concentric curves represent the FWHM

fields of view at three energies, corresponding approximately

to the observed lines.   Some interesting objects in and near

the field are shown.   The numbered dots represent stars closer

than 6 pc.

GAMMA-RAY LINES OBSERVED
DURING THE
10 JUNE 1974 TRANSIENT EVENT

LIVE ENERGY (keV)	COUNT RATE $(SEC)^{-1}$	FLUX* $(CM^2 - SEC)^{-1}$	FWHM (keV)	TIME INTERVAL SPANNED (U.T.)
413.2 ± 1.8	$(5.5 \pm 1.6) \times 10^{-2}$	$(7.0 \pm 2.0) \times 10^{-3}$	15	2020 - 2041
1789.7 ± 6.0	$(6.78 \pm 1.55) \times 10^{-2}$	$(3.15 \pm 0.74) \times 10^{-2}$	95	2026 - 2041
2218.6 ± 6.3	$(2.67 \pm 0.87) \times 10^{-2}$	$(1.51 \pm 0.49) \times 10^{-2}$	70	2020 - 2041
5946.5 ± 3.7	$(7.06 \pm 2.18) \times 10^{-3}$	$(1.47 \pm 0.46) \times 10^{-2}$	25	2006 - 2041

*ASSUMES SOURCE ON THE DETECTOR AXIS

TABLE 1

1 mm ALUMINUM WINDOW

CsI COLLIMATOR

CsI RIGHT HALF ANNULUS

LN$_2$ DEWAR

Ge(Li) CRYSTALS

COPPER ROD

DETECTOR CRYOSTAT

CsI PLUG

CsI LEFT HALF ANNULUS

VACUUM JACKET

SAPPHIRE DISKS

DETECTOR PREAMPS AND BIAS HV FILTER

⊢ 10 cm ⊣

Ge(Li) BIAS SUPPLY

10 cm

SENSOR ASSEMBLY

FIGURE 1

BLOCKING CRYSTAL

TURNTABLE

SHIELD ELECTRONICS

SERVO DRIVE ELECTRONICS

CALIBRATION SOURCE

LOW VOLTAGE POWER CONVERTER

DIGITAL DATA SYSTEM

Ge(Li) PREAMPS (4)

BATTERIES

EXTERNAL INTERFACE CONNECTORS

BATTERIES

8192-CHANNEL ADC (4)

PULSE SHAPING AMPLIFIERS (4)

FIGURE 2

CRAB NEBULA SPECTRUM - TOTAL EMISSION
10 JUNE 1974 BALLOON FLIGHT
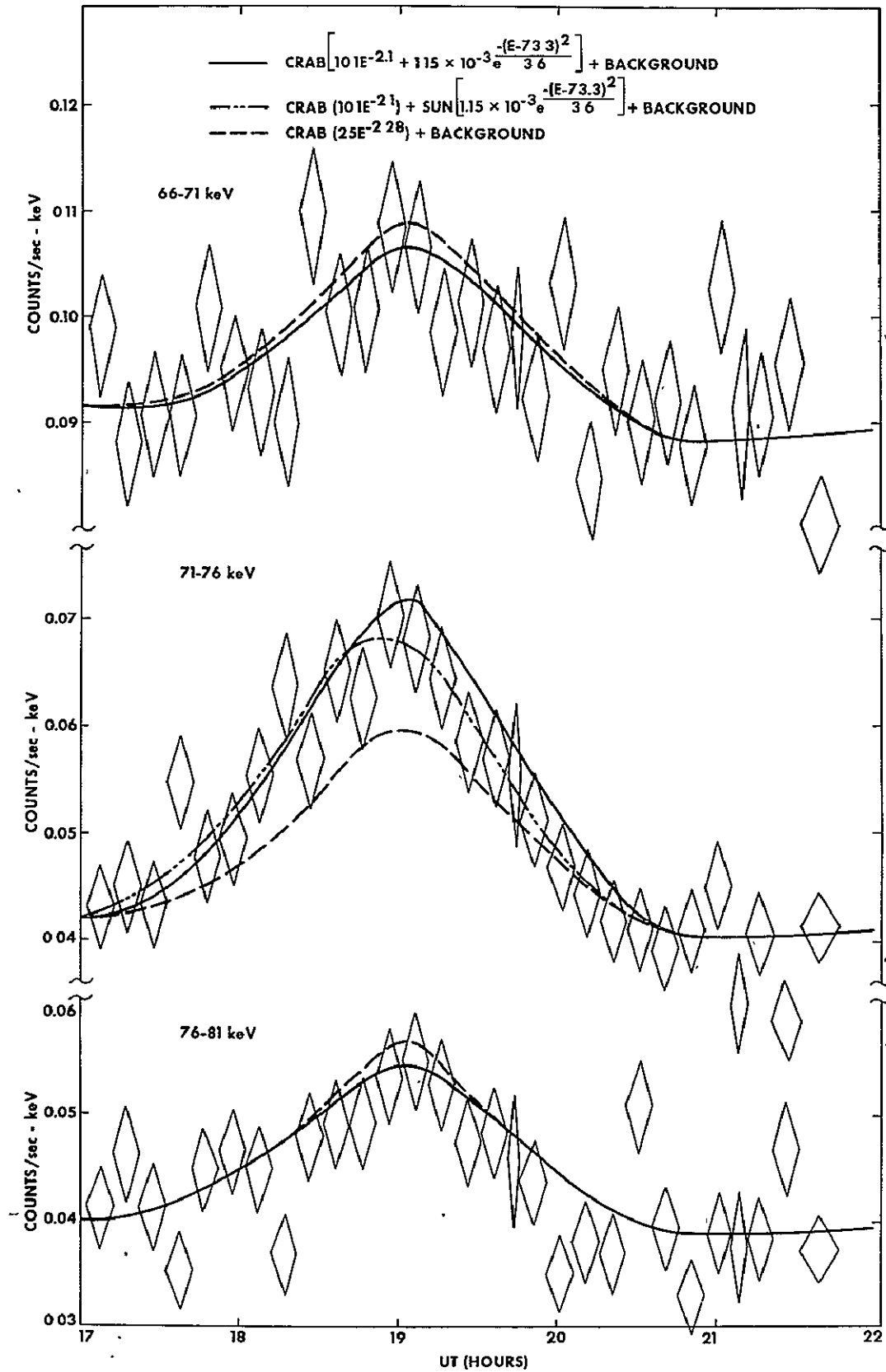### PALESTINE, TEXAS
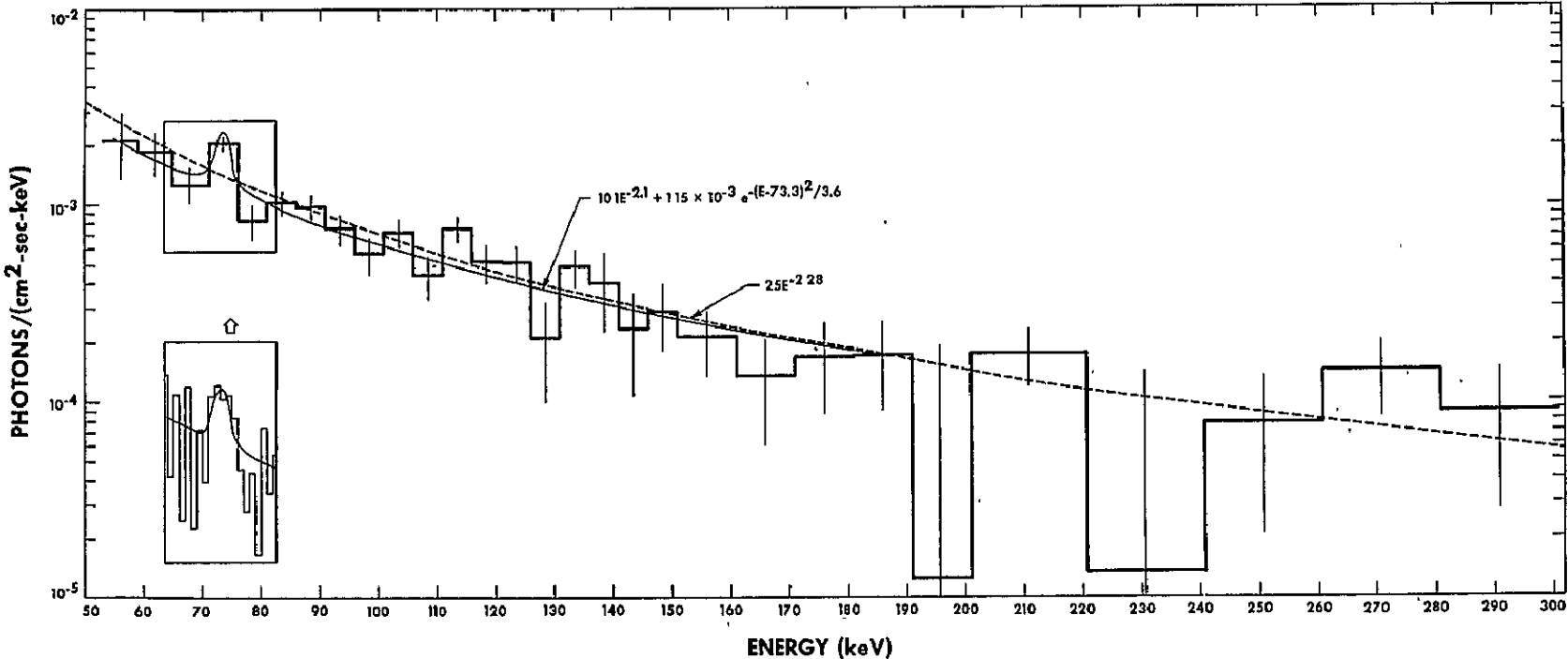
FIGURE 4

COUNTING RATE vs TIME

FIGURE 5

CRAB NEBULA SPECTRUM
TOTAL EMISSION

$9.7E^{-2.1}$

PRESENT MEASUREMENT - 10 June 1974
TOOR AND SEWARD (1974)
CARPENTER et. al. (1976)
GRUBER AND LING (1977)
DOLAN, et. al. (1977)
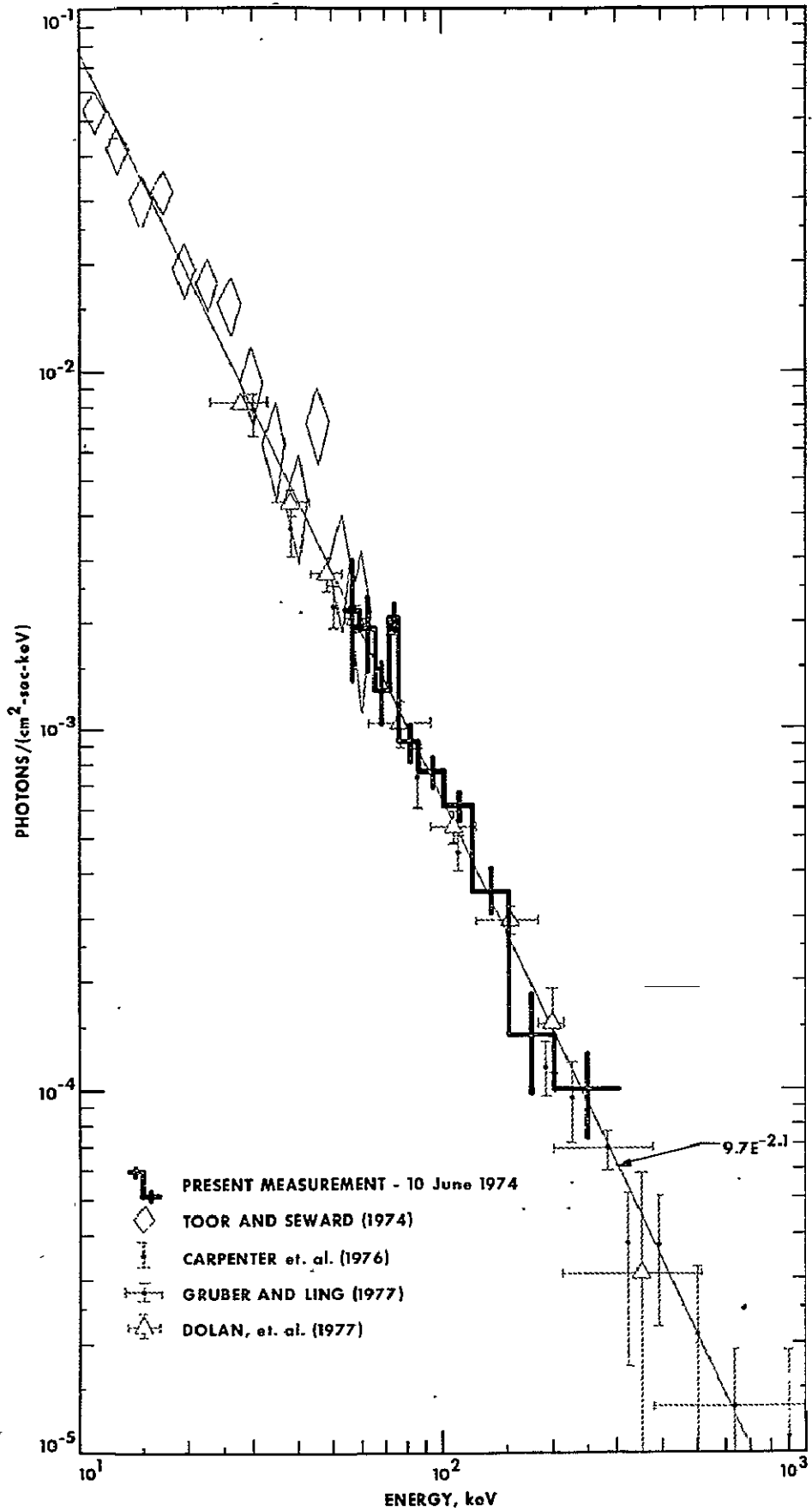
PHOTONS/(cm²-sec-keV)

ENERGY, keV

FIGURE 6
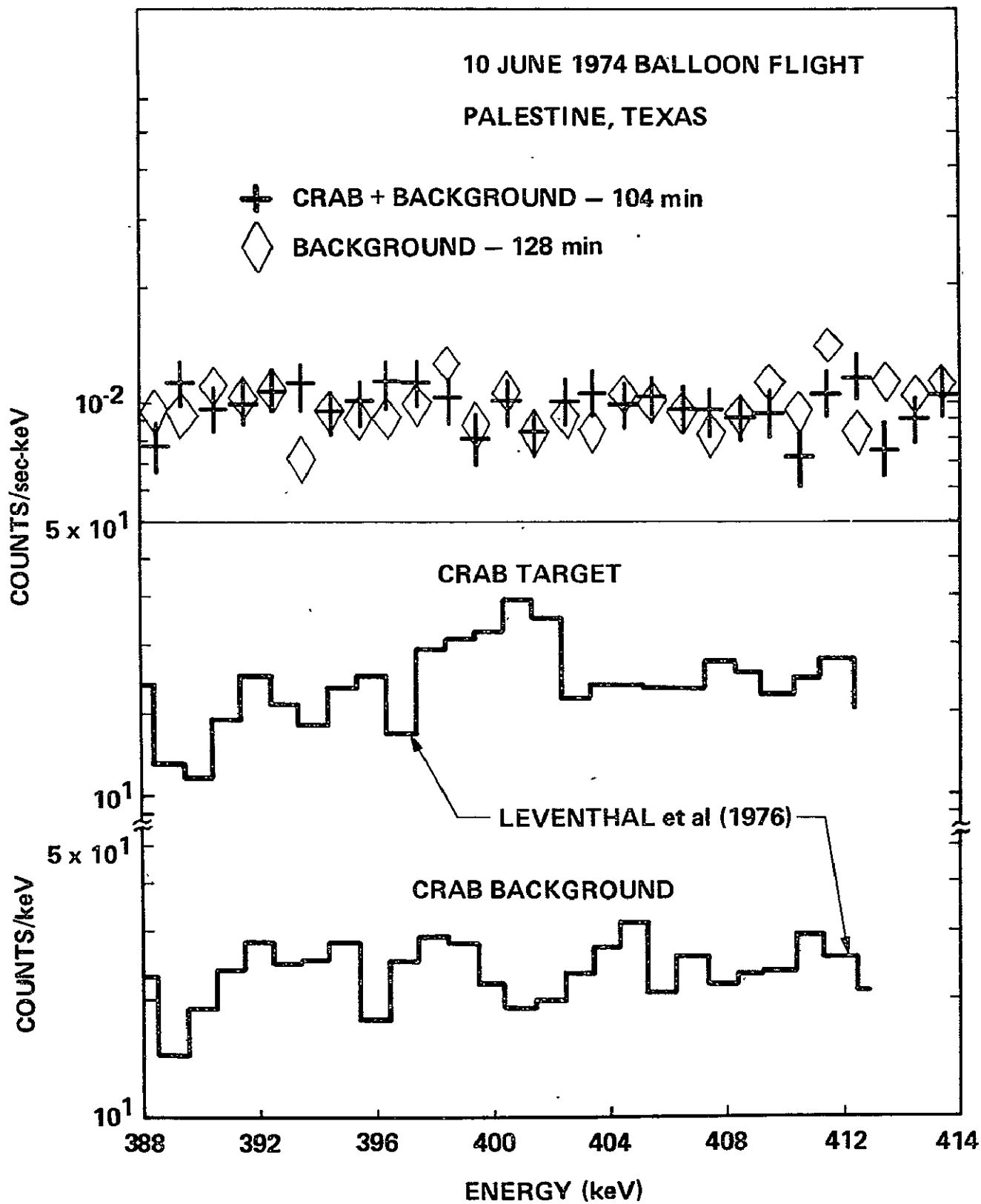
ENERGY LOSS SPECTRA

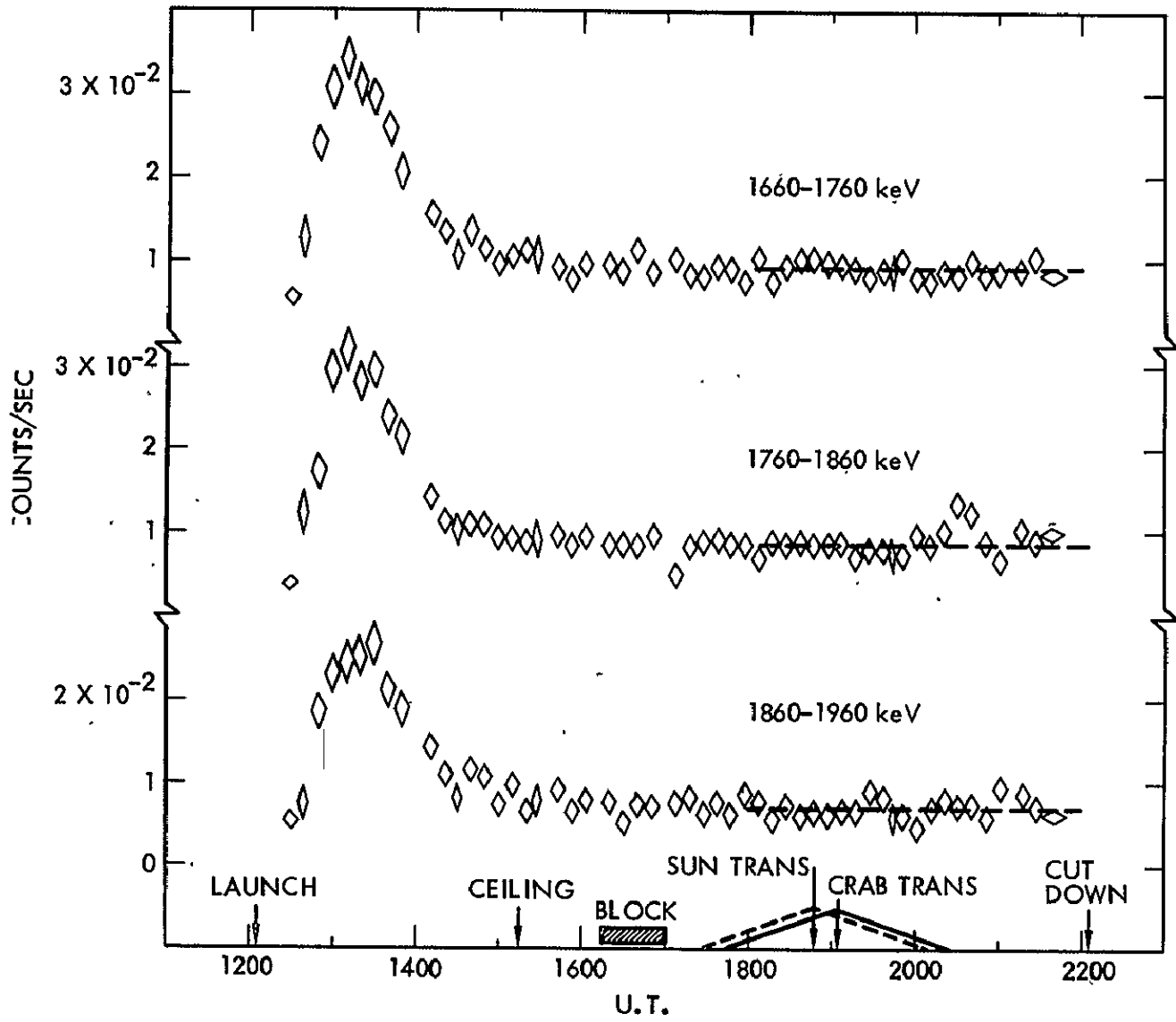FIGÚRE 7

Ge(Li) 1.8 MeV COUNT RATE vs TIME
10 JUNE 1974

FIGURE 8

248

COLLIMATOR RESPONSE TO 10 JUNE 1974
TRANSIENT EVENT

Ge (Li)
1.8 MeV LINE
(REF.)

COLLIMATOR INTEGRAL
RATE > 150 keV
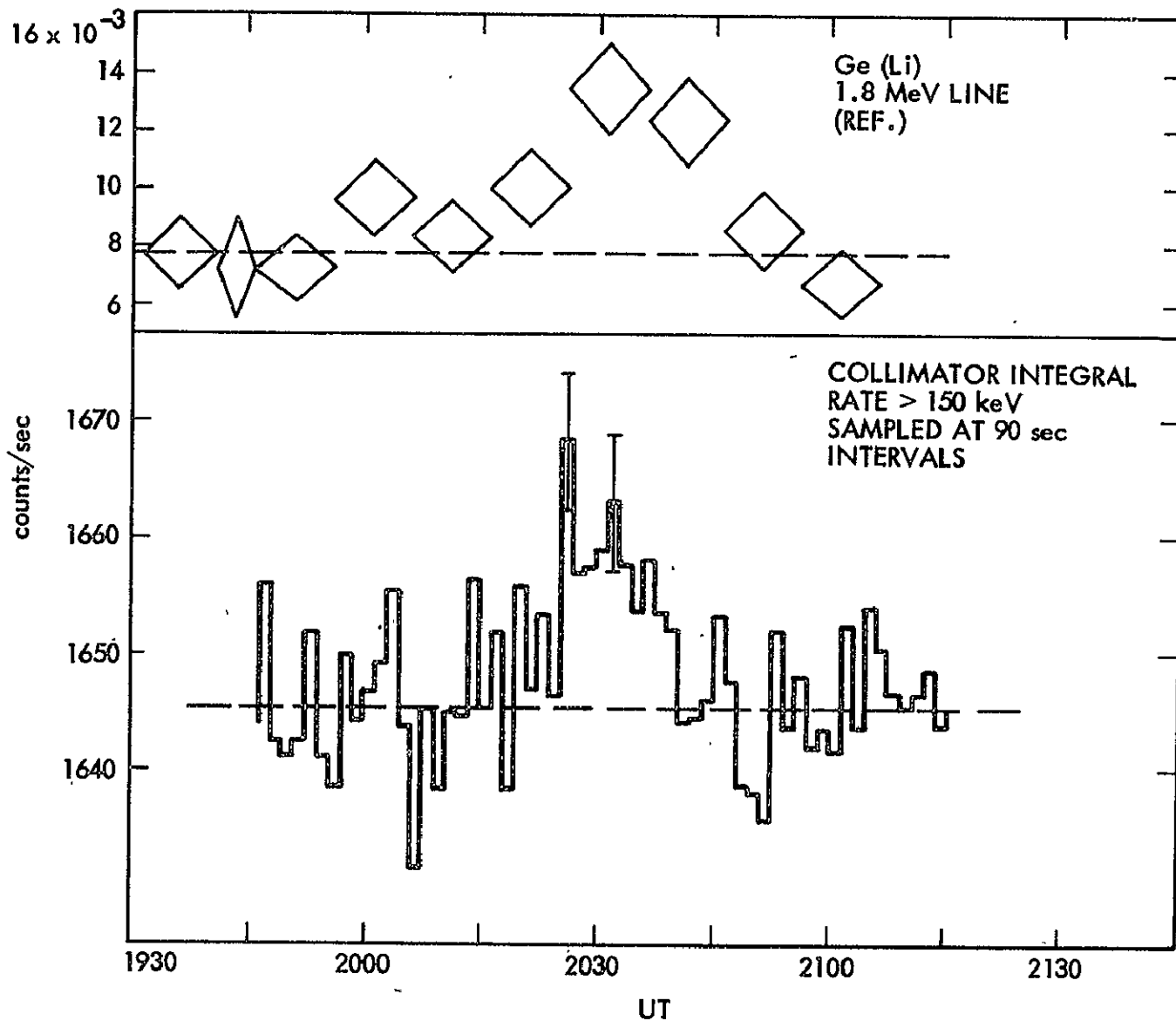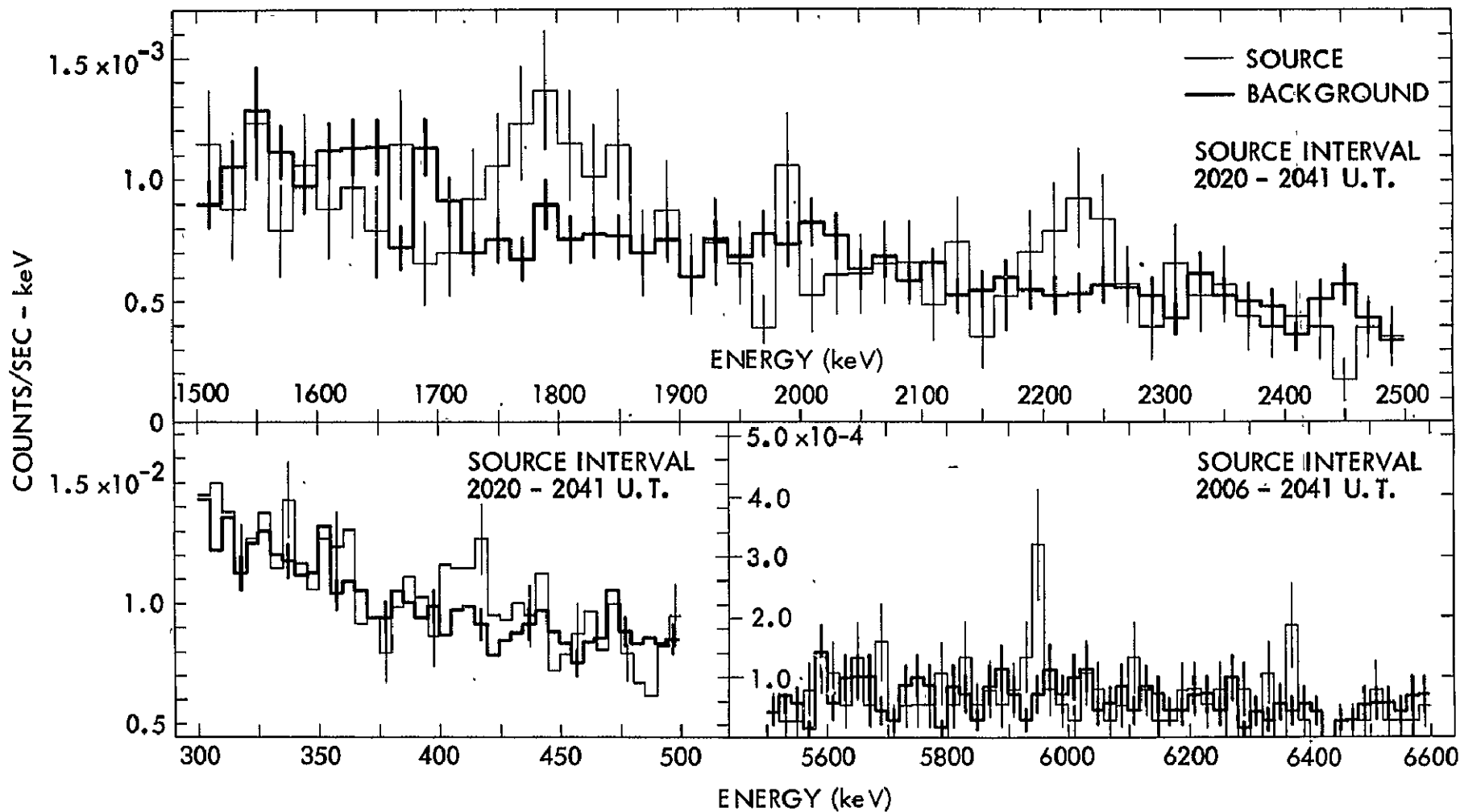SAMPLED AT 90 sec
INTERVALS

FIGURE 9

249

10 JUNE 1974 TRANSIENT EVENT — OBSERVED LINES

FIGURE 10

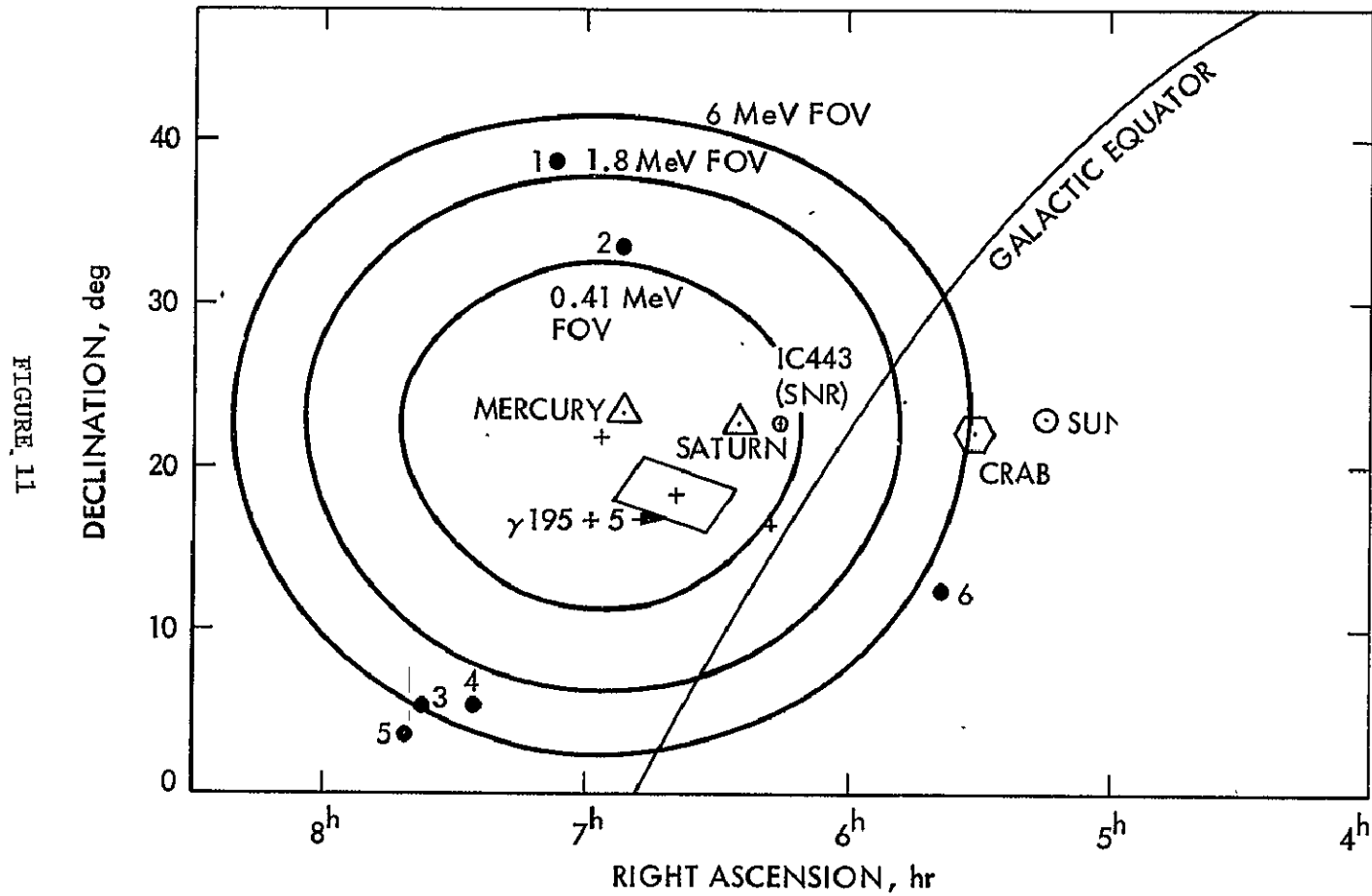# FIELD OF VIEW 10 JUNE 1974 TRANSIENT EVENT
(2033:30 UT)

FIGURE 11

NUCLEAR GAMMA RAYS FROM COMPACT OBJECTS

R. E. Lingenfelter*

Dept. of Astronomy, Univ. of California, Los Angeles

J. C. Higdon**

Planetary Sciences Dept., Univ. of Arizona, Tucson

R. Ramaty

Lab. for High Energy Astrophysics, Goddard Space Flight Center, Greenbelt, Md.

ABSTRACT

We discuss why accreting compact objects in general may be important gamma ray line sources and how such sources may explain recent observations of celestial gamma-ray line emission from a transient source in the direction of the galactic anti-center, from the Galactic Center, and possibly from the radio galaxy Centaurus A. The identification of the lines from the transient source requires a strong redshift. Such a redshift permits the identification of these lines with the most intense nuclear emission lines expected in nature, positron annihilation, and neutron capture on hydrogen and iron. We propose that they are produced as a result of nuclear interactions in accreting gas around a neutron star. The gamma-ray line emission from the Galactic Center and possibly Centaurus A appears to have a surprisingly high luminosity, amounting to perhaps as much as 10% of the total luminosity of these sources. We suggest that such high gamma-ray line emission efficiencies could result from nuclear interactions in accreting gas around a massive black hole.

INTRODUCTION

We shall focus on two questions relative to nuclear gamma-ray line emission from compact objects: first, why accreting compact objects in general might be important gamma-ray line sources and second, how such sources may explain some of the recent observations of celestial gamma-ray line emission.

In order to answer the first question, we must look at what conditions are necessary for the observation of nuclear gamma-ray lines. Most simply stated, for a line to be resolvable above the continuum for practical observing times, the nuclear line emissivity of a source must be at least of the order of the continuum emissivity of that source over the line width. Assuming overall charge neutrality for the energetic ions and electrons, this in turn requires that for nuclear lines at an MeV or more, to be observable above the attendant electron bremsstrahlung continuum, the mean nucleon or ion energy, $\overline{E}_{ion}$ must be greater than ~ 1 MeV and the mean electron energy, $\overline{E}_e$, must be less than that energy,

$$\overline{E}_e < 1 \text{ MeV} < \overline{E}_{ion} \; ,$$

or for two-temperature quasi-thermal distribution,

$$T_e < 10^{10} K < T_{ion} \; .$$

If the mean energies or temperatures of the electrons and ions are equal, the bremsstrahlung emissivity greatly exceeds the nuclear line emissivity for nearly all lines and all compositions.

Much higher mean ion energies than electron energies are expected from an acceleration process such as gravitational accretion. Since $\overline{E}_i \approx \frac{m_p}{m_e} \overline{E}_e$ in this

process, nearly all of the energy initially goes into the ions. Gravitational acceleration of matter accreting around a compact object, such as a neutron star or a black hole, can accelerate ions to about a hundred MeV while electrons are accelerated to less than a MeV. Thus accretion around compact objects, previously proposed as X-ray sources, may also be important sources of resolvable nuclear gamma-ray line emission.

The principal nuclear gamma-ray lines expected from energetic particle interactions in general have been reviewed most recently by Lingenfelter and Ramaty (1978). These include the 6.129, 4.438, 2.313, 1.779, 1.634 and 1.369 MeV lines from deexcitation of excited ^{16}O, ^{12}C, ^{14}N, ^{28}Si, ^{20}Ne and ^{24}Mg respectively, the 0.511 MeV line from annihilation of positrons from decay of radioisotopes and the 2.223 MeV line from capture on hydrogen of neutrons, all produced in inelastic collisions. Depending on the composition, lines at 7.632 and 7.646 MeV from neutron capture on ^{56}Fe may also be important. By way of illustration Figure 1 shows the calculated (Higdon and Lingenfelter, 1977) emissivity of the 4.438 MeV line resulting from thermonuclear reactions at ion temperatures $\gtrsim 10^{10}$K in a plasma of solar composition.

Several of these lines have been observed from celestial sources by balloon and satellite borne gamma-ray detectors. These observations, summarized in Table 1, were reviewed by Chupp (1978) at this symposium and the newer results were presented here by Jacobson et al. (1978), Leventhal, MacCallum and Stang (1978) and Matteson and Peterson (1978).

TRANSIENT LINE EMISSION FROM NEUTRON STARS

We shall discuss in detail two of these observations of line emission which are particularly exciting as they appear to show strong evidence of coming from a compact source. These are the transient event of 10 June 1974 reported by

Jacobson (1977) and Jacobson et al. (1978) and the observation of 10-11 May 1976 by Leventhal, MacCallum and Watts (1977). As pointed out by these authors, the identification of the lines alone almost certainly requires a strong redshift which suggests gravitationally redshifted emission from a compact object. Certainly in the transient event, which also included an unshifted 2.2 MeV line, the redshift could not be cosmological. We suggest that the transient event resulted from episodic accretion around a neutron star from a binary companion. As we shall show, such a model is consistent with all of the observed properties of the event. Moreover, since the observations of 10-11 May 1976 and of the transient event of 10 June 1974 included much of the same field of view and would require the same surface redshift, we also suggest that both may be observations of the same neutron star.

The suggested identification of the lines observed in these two measurements is given in Table 2 together with the required average redshift and the redshift range which could account for the line width. The lines at ~0.4 and ~5.95 MeV cannot be identified with any unshifted lines since all contenders are coupled with stronger companion lines which were not observed. All of these lines however can be identified with lines from the most intense nuclear emission processes expected in nature, positron annihilation and neutron capture on hydrogen and iron, if we assume a self-consistent range of gravitational redshift. In particular the 5.935-5.960 MeV line in the transient event can be identified with the two strongest lines from neutron capture on the iron crust of a neutron star having a surface gravitational redshift of $z \approx 0.285$. Because it has the maximum binding energy per nucleon ^{56}Fe is expected to be the dominant constituent of neutron star crusts and the relative intensity of this line compared to the hydrogen capture line requires enormous enrichment in iron compared to solar abundances. This line alone strongly suggests a neutron star source for the transient emission on 10 June 1974.

The 0.40-0.42 MeV and the 1.74-1.86 MeV lines can similarly be identi-
fied as the positron annihilation and neutron capture in a hydrogen atmos-
phere of density $n_H > 10^{16}$ H/cm^3 from the surface z of 0.285 up to an
altitude corresponding to a z of about 0.2. Such an atmosphere is pre-
sumably a temporary feature formed by infall of gas from an accretion disk.
This minimum hydrogen density is required in order that a significant fraction
of the neutrons are captured before they decay. The width of the ~0.4 MeV
line also places a limit on the average temperature of this atmosphere of
$<2 \times 10^6$ K. The unshifted (z = 0+.02) line at 2.22 MeV requires a comparable
high density region well above the neutron star surface and can be under-
stood as neutron capture in an accretion disk at a distance corresponding to
z < .02 and in the atmosphere of a binary companion.

A surface redshift of ~ 0.285 implies a neutron star mass of about 1.4
to 1.8 M$_\odot$ and a radius of 10 to 13 km, depending on the assumed equation
of state (Börner and Cohen, 1974). The observed 25 KeV full width of the
~ 5.95 MeV line reduced by the instrumental broadening of 5 KeV and the red-
shifted ^{56}Fe doublet separation of 10 KeV gives an emitted width of 10 KeV.
If the line is produced uniformly over the surface of the neutron star, this
width gives a lower limit for the rotation period $P > \frac{E\gamma}{\Delta E_\gamma} \frac{4\pi r \sin\theta}{c} = \frac{\sin\theta}{4}$ sec,
where θ is the angle between the rotation axis and the direction of observa-
tion. Observation of the ~5.95 MeV and ~1.8 MeV lines from the surface of
the neutron star also place an upper limit on the surface magnetic field
of $< 10^{12}$ gauss, since pair production by these gamma rays in the magnetic
field would greatly attenuate emission from the surface if the field were
much stronger (Erber, 1966).

We suggest that the neutrons and positrons which were captured and
annihilated in the vicinity of the neutron star and its binary companion were

all produced by nuclear reactions occurring when gas, flowing episodically from the companion, was gravitationally accelerated to an energy of > 1 MeV and collided with gas in the outer part of the accretion disk around the neutron star. This is shown schematically in Figure 2.

In addition to the observed lines we would also expect other line and continuum emission as indicated in Figure 2, but the expected intensities are not inconsistent with other observations. From calculations of the ratio of the emissivities of the strongest deexcitation line, that at 4.4 MeV from ^{12}C, to the neutron emissivity shown in Figure 3, we find that the expected intensity of the 4.4 MeV line from $^{12}C^*$ would have been below the measured upper limit for this line of ~2 x 10^{-2} photons/cm^2 sec for ion temperatures $\geq$ 6 x 10^{10} K . An unshifted positron annihilation line roughly comparable in intensity of the unshifted 2.2 MeV line should also have been produced, but a 0.511 MeV line of this intensity could not be detected because of the large detector background at that particular energy. We should also expect continuum emission from electron bremsstrahlung at energies somewhere below a few tenths of an MeV. The total power in this continuum can be estimated from the neutron capture line intensity assuming that the continuum luminosity is equal to the rate of energy loss by the ions, which as we noted above carry most of the energy. The calculated ratio of the neutron production rate by thermonuclear inter-actions of hot ions (T_{ion} > few times 10^{10} K) to the energy loss rate of the ions to cooler electrons (T_e < 10^{10} K) is $\leq$ 2 x 10^3 neutrons/ergs, depending primarily on the electron temperature. The ratio is relatively independent of the abundance of ions of atomic charge > 2, since proton interactions with helium are the principal source of neutrons. The observed neutron capture gamma-ray line intensity of ~6 x 10^{-2} photons/cm^2 sec thus implies a continuum flux of $\geq$ 3 x 10^{-5} ergs/cm^2 sec. Such a flux was not observed in the JPL

detector but its energy range extended down to only about ~0.05 MeV, so that

if the bulk of the continuum radiation was emitted below that energy it could

not have been detected. Unfortunately there were no other wide angle X-ray

detectors being flown at that time which might have covered this energy range.

Lastly we should note that, since the sum of the neutron capture gamma-

ray line intensities for the transient event of 10 June 1974 was ~ 3×10^{-7} ergs/

cm^2 sec, the neutron capture line luminosity of the source $L_{n,\gamma}$ (erg/sec) $\approx$

3×10^{37} D^2(kpc). Assuming a maximum neutron yield of $< 2 \times 10^3$ neutrons/erg,

discussed above, and an average neutron capture photon energy of ~ 3 MeV, the

total source luminosity L (erg/sec) must have been $\geq 3 \times 10^{39}$ D^2(kpc).

We have described a model for neutron and positron production in an accretion

disk because alternative sites for their production seem less likely. Although

one might imagine that it should not be hard to find ways of generating neutrons

directly on the surface of a neutron star, the observation of the unshifted

neutron capture line on hydrogen would require that the average energy of the

neutrons produced at the neutron star surface must be ~ 150 MeV, equal to the

escape energy from the star, so that a significant fraction could escape to a

lower z region to be captured. There is no obvious process for generating

such energetic neutrons. The possibility that the neutrons and positrons might

have been produced in nuclear reactions in a flare on the binary companion also

seems exceedingly unlikely from energetic considerations. Calculations presented

at this symposium by Colgate (1978) of the yield of gamma-ray lines from giant

stellar flares would suggest that the 2.2 MeV line from neutron capture rate

on hydrogen in flares is roughly proportional to the total energy released in

the flares and that this proportionally is of the same order as that observed

for the 4 August 1972 solar flare ~ 10^{-5} photons/sec erg at 2.2 MeV. The

transient flux of 1.5×10^{-2} photons/cm^2 sec at 2.2 MeV would thus require a

stellar flare on the binary companion of the neutron star to release a total

energy W(ergs) $\approx 10^{41}D^2$(pc) where D is the distance of the star from the earth.

For any reasonable distance this would require a flare energy many orders of

magnitude larger than the 10^{36} ergs which Colgate calculated for the total

energy of even the largest stellar flares.

The observation by Leventhal et al. (1977) of a possible redshifted positron

annihilation line at ~ 0.400 MeV from the general direction of the Crab Nebula

on 10-11 May 1976 may also be variable emission from the same source as the 10

June 1974 event, since the two observations had overlapping fields of view and

the identification of the lines in both observations implied essentially the

same neutron star surface redshift. The average intensity of the ~ 0.400 MeV

line on 10-11 May 1976 was only about 0.3 of that from the 0.40 to 0.42 MeV

line during the 10 June 1974 event (Table 1). Since the 0.400 MeV line emission

was not observed (Ling et al.,1977) during the detector scan across the Crab

Nebula on 10 June 1974 prior to the transient event, it must also be considered

variable. We should also note that if the 10-11 May 1976 and 10 June 1974 line

emission is for the same source, then the limit on the rotation period P(sec) >

0.25 sin θ for the 10 June 1974 source effectively rules out the Crab pulsar

with a period of 0.033 sec as the source.

We suggest that a similar process of nuclear interactions in episodic ac-

cretion of matter falling onto an accretion disk could be responsible for the

10-11 May 1976 emission but at a lower accretion rate than that during the 10

June 1974 event. Depending on the ion temperature the ratio of neutron to

positron production, shown in Fig. 3, could vary from ~ 0.1 to ~ 10 for T_{ion}

ranging from a few times 10^{10} to a few times 10^{11}K. The narrow width of the

line, < 5 KeV, would require that the positron annihilation occur primarily

at the neutron star surface, excluding any significant atmosphere at that time.

Thus the only other line emission expected from the neutron star surface would

be the redshifted line at ~ 5.95 MeV from neutron capture on iron. Unfortunately

this line was out of the energy range of the detector. An essentially unshifted line at 2.2 MeV from neutron capture on hydrogen in the accretion disk and in the atmosphere of the binary companion, however, should also be expected. The intensity of this line, scaled from the 10 June 1974 event, assuming an ion temperature of 10^{11}K for the latter, should have ranged from $\sim 5 \times 10^{-5}$ to $\sim 5 \times 10^{-3}$ photons/cm^{2}sec for ion temperatures of a few times 10^{10} to a few times 10^{11}K in the accretion disk. Such emission is not inconsistent with the upper limit of 1×10^{-3} photons/cm^{2}sec at 2.2 MeV on 10-11 May 1976, if the ion temperature was in the range $10^{10} < T_{ion} < 10^{11}$ K.

A more detailed discussion of our model of this source together with a discussion of the possible identification of the source with known objects will be given in a forthcoming paper. But we would like to emphasize here that quite independent of the particular model, we believe that the general arguments discussed above very strongly suggest that these are the first observations of the gravitational redshift of a neutron star.

LINE EMISSION FROM BLACK HOLES

Next, we want to call attention to another surprising characteristic of some of the reported gamma-ray line observations; that is their apparently enormous line emission efficiency. Defining such an efficiency as that fraction of the total luminosity radiated in nuclear lines, L_i/L_{rad}, we find (Table 3) that the persistent non-solar sources may have line efficiencies at 4.4 MeV as high as $\sim 10\%$. Not only is such an efficiency surprisingly large in itself, but it is all the more surprising when compared to the efficiencies of $\sim 10^{-7}$ for the same line in the solar flare of 4 August 1972. The efficiency of the Galactic Center source, however, may be only $\sim 10^{-4}$ if the line emission is from an extended region of angular diameter $\sim 3^\circ$. Future gamma-ray observations with $\lesssim 1^\circ$ angular resolution will hopefully resolve this ambiguity.

The basic problem that such high gamma-ray line emission efficiencies present is that the energy radiated in the 4.438 MeV line, for example, is at most only about 10^{-3} of the total energy loss·rate of hot ions to cooler ($T_e < 10^{10}$K) electrons, assuming roughly solar abundances for the ions. This can be seen in Figure 4 which shows the calculated 4.4 MeV line emission efficiency $\dot{w}_{4.4}/\dot{w}_{rad}$ for a two temperature ($T_e < T_{ion}$) plasma, assuming that radiation from electrons is the dominant energy losses process for the medium and that the radiation loss rate $\dot{w}_{rad}$ is equal to the rate of transfer of energy from the ions to the electrons (e.g. Spitzer 1962):

$$\dot{w}_{ion} \approx 1.0 \times 10^{-12} \; n^2 (T_{ion} - T_e)(T_{ion} + 1836 \; T_e)^{-3/2} \cdot ergs/cm^3 sec.$$

A 4.4-MeV line emission efficiency much greater than 10^{-3} would thus require either a greatly increased CNO/H abundance compared to solar values or a nonradiative loss that is the dominant energy loss process for the medium. In the first case a line emission efficiency of ~ 10^{-1} would require an increase of about 10^2 in the CNO/He ratio compared to solar abundances, leading to a medium in which CNO makes up roughly half of the mass. Such conditions may in fact be approximated in the expanding nebulae of supernovae. This possibility will be discussed in detail in a subsequent paper.

In the present discussion, however, we shall consider the alternative possibility that nonradiative losses are dominant in disposing of the bulk of the ion energy before it can be radiated and we shall focus specifically on that ultimate nonradiator - a black hole. Nonradiative losses will dominate in spherical accretion around a black hole if $t_{ff} < t_{eq} < t_{rad}$, where the three times are the free fall time of accreting matter to the event horizon, energy equipartition time between accreting ions and electrons, and the radiation time required for the electrons to radiate away the released gravitation energy of the accreting

matter.

The first inequality, $t_{ff} < t_{eq}$, implies that only a fraction, $\sim t_{ff}/t_{eq}$, of the total gravitational energy released in accretion is transferred from the ions to the electrons, so that the bulk of this energy is carried over the event horizon still in the ions. Taking the free fall time to the event horizon from some distance $< 2 \times 10^3 \, GM/c^2$ at which the ion temperature starts to exceed 10^{10}K but the electron temperature is still $< 10^{10}$K, it can be shown that $t_{ff} < t_{eq}$ requires a column density of matter above the event horizon $N < 6 \times 10^{26}$ H/cm^2. Since the attention length for 4.4 MeV gamma-rays in hydrogen is $\sim 10^{25}$ H/cm^2, the upper limit on the column density above the event horizon places no added constraint on the thickness of the emission region.

The second inequality, $t_{eq} < t_{rad}$, implies that most of the energy transferred to the electrons goes into thermal energy, heating them up, since they can radiate away only a fraction, $\eta \approx t_{eq}/t_{rad}$, of that energy. Assuming that continuum bremsstrahlung emission is the principal radiative loss process for the electrons, the fraction of energy radiated may be rewritten $\eta \approx \dot{w}_{brem}/\dot{w}_{ion}$. For $\dot{w}_{brem}/\dot{w}_{ion} < 1$ requires that $T_e^2/(T_{ion} - T_e) < 10^{10}$ which is in fact always satisfied by the condition, $T_e < 10^{10}$K $< T_{ion}$, which was already required in order to observe the 4.4 MeV gamma-ray line above a bremsstrahlung continuum.

The 4.4 MeV line emission efficiency $\dot{w}_{4.4}/\dot{w}_{rad} = (\dot{w}_{4.4}/\dot{w}_{ion})/\eta$ thus becomes $\dot{w}_{4.4}/\dot{w}_{brem}$ for such cases. The dependence of this line emission efficiency on the ion and electron temperatures is shown in Figure 4. As can be seen, the line emission efficiencies of the order of 0.1 apparently required by the Galactic Center and Centaurus A observations can thus be achieved by spherical accretion around a black hole of plasmas of roughly solar composition, if $T_e \lesssim 10^9$K. The abundance of CNO relative to hydrogen in interstellar gas in the Galactic Center, however, may be at least half an order of magnitude greater than the solar value, because of apparent abundance gradients (e.g. Peimbert, 1975) of these elements in the galaxy. For accretion of such matter, line emission efficiences of ~ 0.1

could be achieved with $T_e \lesssim 10^{10}$K.

We have made preliminary calculations, following Shapiro (1973), of the 4.4 MeV gamma-ray line profile for emission from spherical accretion, around a black hole, of plasma that is optically thin to such radiation. These calculations show that the expected width of the 4.4 MeV line is much larger than the observed line widths of ~ 1 MeV from the Galactic Center (Haymes et al. 1975) and ~ 0.3 MeV from Centaurus A (Hall et al. 1976). Narrower widths such as those observed, however, could be achieved, if the accretion is optically thick so that the bulk of the line emission comes only from an optically thin shell well above to event horizon and/or, if the accretion is not spherically symmetrical so that most of the emission comes from matter accreting in some solid angle Ω.

We consider a simple model to maximize the line emission from such asymmetrical accretion around a black hole, assuming the bulk of the accretion is in a solid angle Ω, that the radial dependence of the density of the accreting plasma is proportional to $r^{-3/2}$, and that the plasma ion temperature exceeds ~ 3 x 10^{10}K at a radius $r_* \lesssim 3 \times 10^2 r_g$, where r_g is the Schwarzschild radius $2GM/c^2$. Then taking the 4.4 MeV line luminosity to be

$$L_{4.4} \approx E_{4.4} \; q_{4.4} \; n_*^2 \; r_*^3 \; \Omega \; \text{erg/sec,}$$

where the photon energy $E_{4.4}$ is in ergs and the line emissivity $q_{4.4} \lesssim 10^{-18}$ photons/cm^3 sec n^{2-} is taken to be three times that given in Figure 1, assuming roughly threefold enrichment of CNO in the gas in the Galactic Center relative to solar abundances. If we further maximize the emission, assuming that the accreting plasma becomes optically thick to 4.4 MeV gamma-rays at a distance of ~ $r_*/2$, so that $r_* n_* \lesssim 0.3 \times 10^{25}$ H/cm^2, we find that the maximum 4.4 MeV line luminosity from optically thick asymmetrical accretion on a black hole is

$$L_{4.4} \lesssim 10^{34} \frac{M}{M_\odot} \Omega \text{ ergs/sec.}$$

If the 4.4 MeV line emission observed (Haymes et al., 1975) from the Galactic Center is produced by thermonuclear interactions in matter accreting onto a black hole then the line luminosity of 8×10^{37} ergs/sec (Table 3), implied by the observed intensity, would require a minimum black hole of mass $\gtrsim 10^3$ $M_\odot$ for $\Omega \approx 1$ ster. The possibility of a much larger $\sim 10^6$ to 10^7 $M_\odot$ black hole in the Galactic Center has been discussed (e.g. Oort, 1977). Such a black hole could produce the necessary line luminosity with optically thin asymmetrical accretion. With the required accretion rate, $\dot{M} = m_p c\, n_* r_*^{3/2} r_g^{1/2} \Omega \simeq$ $(16\, L_{4.4}\, \Omega\, M/M_\odot)^{1/2}$ in gm/sec, or 3×10^{-3} $M_\odot$/yr for a 3×10^6 $M_\odot$ black hole, such a black hole could have accumulated over a period of the order of 10^9 years.

Observations of possible time variations could provide one possible test for such a model. Fluctuations in the emission might be expected on time scales of the order of the free fall time in the gamma-ray line emission region, t_{ff} $\lesssim 0.5 \frac{M}{M_\odot}$ sec, which for a black hole of anywhere between 10^3 and 10^7 $M_\odot$ should be between ten minutes and a couple months.

If similar accretion is responsible for the 4.4 MeV line emission observed (Hall et al., 1976) from Centaurus A, the line luminosity of 1.5×10^{43} ergs/sec (Table 3) would require a black hole of at least $10^9 M_\odot$, assuming optically thick, asymmetrical accretion predominantly in a solid angle Ω of the order of a steradian, which would be required to account for the narrow line width of ~ 0.3 MeV. Variations in the gamma-ray line and continuum luminosity might also be expected on time scales comparable to the free-fall time through the emission region of order of ~ 10 years or less. The luminosity of Centaurus A is, in fact, observed (Beall et al., 1978) to vary on times of the order of several years, which would be consistent with such a model. A black hole of mass $\gtrsim 10^7 M_\odot$

in Centaurus A has been proposed (Fabian et al., 1976) to account for the X-ray emission by spherical accretion.

Thermonuclear reactions could also lead to the other lines observed from the Galactic Center and Centaurus A (Table 1). The intensity of the 0.5 MeV line from the Galactic Center compared to that of the 4.4 MeV line is consistent with the calculated ratio of positron production to 4.4 MeV emissivity (Figure 3) for $T_{ion} > 10^{10}$ K, if $\leq 2/3$ of the positrons annihilate via positronium. The 1.2 - 2 MeV feature observed from the Galactic Center and Centaurus A could result from the combined deexcitation emission from $^{14}N^{*}$, $^{20}Ne^{*}$, $^{24}Mg^{*}$ and $^{28}Si^{*}$.

Thus we see that simple models of thermonuclear reactions in matter accreting around massive black holes in the Galactic Center and in Centaurus A suggest that such processes could provide the observed gamma-ray line emission. We are currently making more detailed models of these processes.

REFERENCES

Beall, J. H., W. K. Rose, W. Graf, K. M. Price, W. A. Dent, R. W. Hobbs, E. K. Conklin, B. L. Ulich, B. R. Dennis, C. J. Cranell, J. F. Dolan, K. J. Frost, and L. E. Orwig, 1978, Ap. J., 219, 836.

Börner, G., and J. M. Cohn, 1973, Ap. J., 185, 959.

Chupp, E. L., D. J. Forrest, P. R. Higbie, A. N. Suri, C. Tsai, and P. P. Dunphy, 1973, Nature, 241, 333.

Colgate, S., 1978 this Volume, p. 149.

Erber, T., 1966, Rev. Mod. Phys., 38, 626.

Fabian, A. C., Maccagni, D. Rees, M. J., and Stoeger, W. R., 1976, Nature, 260, 683.

Hall, R. D., C. A. Meegan, G. D. Walraven, F. T. Djuth, and R. C. Haymes, 1976, Ap. J., 210, 631.

Haymes, R. C., G. D. Walraven, C. A. Meegan, R. D. Hall, F. T. Djuth, and D. H.
    Shelton, 1975, Ap. J., 201, 593.

Higdon, J. C., and R. E. Lingenfelter, 1977, Ap. J., 215, L53.

Jacobson, A. S., 1977, Bull. Am. Phys. Soc., 22, 643.

Jacobson, A. S., J. C. Ling, W. A. Mahoney and J. B. Willett, 1978 (this symposium).

Leventhal, M., C. MacCallum and A. Watts, 1977, Ap. J., 216, 491.

Leventhal, M., C. J. MacCallum and P. D. Stang, 1978 (this symposium).

Lin, R. P., and H. S. Hudson, 1976, Solar Phys., 50, 153.

Ling, J. C., W. A. Mahoney, J. B. Willett, and A. S. Jacobson, 1977, Nature,
    270, 36.

Lingenfelter, R. E., and R. Ramaty, 1978, Phys. Today, 31, 40.

Matteson, J. L., and L. E. Peterson, 1978 (this symposium).

Oort, J. H., 1977, Ann. Rev. Astron. Astrophys., 15, 295.

Peimbert, M., 1975, Ann. Rev. Astron. Astrophys., 13, 113.

Shapiro, S. L., 1973, Ap. J., 180, 531.

Spitzer, L., 1962, Physics of Fully Ionized Gases, New York, Interscience
    Publisher.

Table 1

GAMMA RAY LINE OBSERVATIONS

Source	Line Energy (MeV)	Line Intensity ($\gamma/cm^2 sec$)	Reference
TRANSIENT SOURCES			
Solar Flare 4 Aug 1972	0.51	6.3×10^{-2}	Chupp et al. 1973
	2.2	2.8×10^{-1}	
	4.4	3×10^{-2}	
	6.1	3×10^{-2}	
Solar Flare 7 Aug 1972	0.51	3×10^{-2}	" "
	2.2	6.9×10^{-2}	
Anti-center transient 10 June 1974	0.41	7×10^{-3}	Jacobson 1977 and Jacobson et al. 1978
	1.8	3.2×10^{-2}	
	2.2	1.5×10^{-2}	
	5.95	1.2×10^{-2}	
Crab pulsar transient? 10-11 May 1976	0.40	2.2×10^{-3}	Leventhal et al. 1977 and Ling et al. 1977
PERSISTENT SOURCES			
Galactic Center	~0.5	8×10^{-4}	Leventhal et al. 1978 Haymes et al. 1975 Matteson & Peterson 1978
	1.2 – 2	2.6×10^{-3}	
	~4.5	9.5×10^{-4}	
Centaurus A (NGC 5128)	1.2 – 2	3.4×10^{-3}	Hall et al. 1976
	~4.5	9.9×10^{-4}	

Table 2

IDENTIFICATION OF GAMMA RAY LINES OBSERVED

DURING THE 10 JUNE 1974 TRANSIENT EVENT

AND ON 10-11 MAY 1976

EMISSION PROCESS	EMITTED LINE ENERGY (KeV)	MEAN* LINE ENERGY (KeV)	MEAN REDSHIFT $\bar{z}$	LINE ENERGY RANGE	MAXIMUM REDSHIFT RANGE z
		10 June 1974			
$e^+ + e^- \rightarrow 2\gamma$	511	413.2$\pm$1.8	.237$\pm$.005	400–420	.28–.22
^{1}H(n,γ)	2223	1789.7$\pm$6.0	.243$\pm$.009	1740–1860	.28–.20
^{1}H(n,γ)	2223	2218.6$\pm$6.3	.002$\pm$.003	2180–2260	.00–.02
^{56}Fe(n,γ)	7632 7646	5946.5$\pm$3.7	.284$\pm$.001	5935–5960	.29–.28
		10-11 May 1976			
$e^+ + e^- \rightarrow 2\gamma$	511	400$\pm$1	.278$\pm$.004	397.5–402.5	.29–.27

* From Table 1 of Jacobson et al. (1978) and from Leventhal et al. (1977).

** Estimated from Figure 10 of Jacobson et al. (1978) and Figure 5a of Leventhal et al. (1977).

Table 3

OBSERVED LINE EMISSION EFFICIENCY

Source	Distance	Line Energy (MeV)	Line Intensity (γ/cm^2sec)	L_i Line Luminosity (erg/sec)	L_{rad} Source Lumimosity (erg/sec)	L_i/L_{rad} Line Emission Efficiency
Solar Flares 4 Aug 1972	1 AU	4.4	3×10^{-2}	6×10^{20}	2×10^{28} (a)	3×10^{-8}
4 Aug 1972	1 AU	2.2	2.8×10^{-1}	3×10^{21}	2×10^{28} (a)	1.5×10^{-7}
7 Aug 1972	1 AU	2.2	$>6.9 \times 10^{-2}$	$>7 \times 10^{20}$	1×10^{28} (a)	$>7 \times 10^{-8}$
Transient 10 Jun 1974	<3 kpc	2.2	1.5×10^{-2}	$<5 \times 10^{39}$	(b)	
Galactic Center	10 kpc	4.4	1×10^{-3}	8×10^{37}	10^{39} (c)	0.8×10^{-1}
					10^{42} (d)	0.8×10^{-4}
Centaurus A	4.4 Mpc	4.4	1×10^{-3}	1.5×10^{43}	10^{44} (e)	1.5×10^{-1}

(a) Lin and Hudson (1976)

(b) There are no observational limits on the continuum emission ≤ 0.1 MeV for this event.

(c) Based on the 10-20 micron luminosity from discrete sources in the central core of the galaxy.

(d) Based on the 100 micron luminosity of the extended source ($\sim 3^{\circ}$ diameter) in the nucleus of the galaxy.

(e) Hall et al. (1976

FIGURE CAPTIONS

Figure 1.   The 4.438 MeV line emissivity resulting from thermonuclear reactions
            in a plasma of solar composition.

Figure 2.   Schematic model of nuclear interactions in accreting gas around a
            neutron star from a binary companion, leading to the gamma ray line
            emission observed in the 10 June 1974 transient event.

Figure 3.   The calculated ratios of neutron and positron production rates to
            the 4.438 MeV gamma ray line emissivity for thermonuclear reactions
            in a plasma of solar composition.

Figure 4.   The 4.438 MeV line emission efficiency $\dot{w}_{4.4}/\dot{w}_{rad}$ calculated for
            thermonuclear reactions in a two temperature plasma of solar
            abundance, assuming that the radiation loss rate of the plasma
            $\dot{w}_{rad}$ equals either the rate of energy transfer from the ions to the
            electrons $\dot{w}_{ion}$, on the electron bremsstrahlung emissivity $\dot{w}_{brem}$.
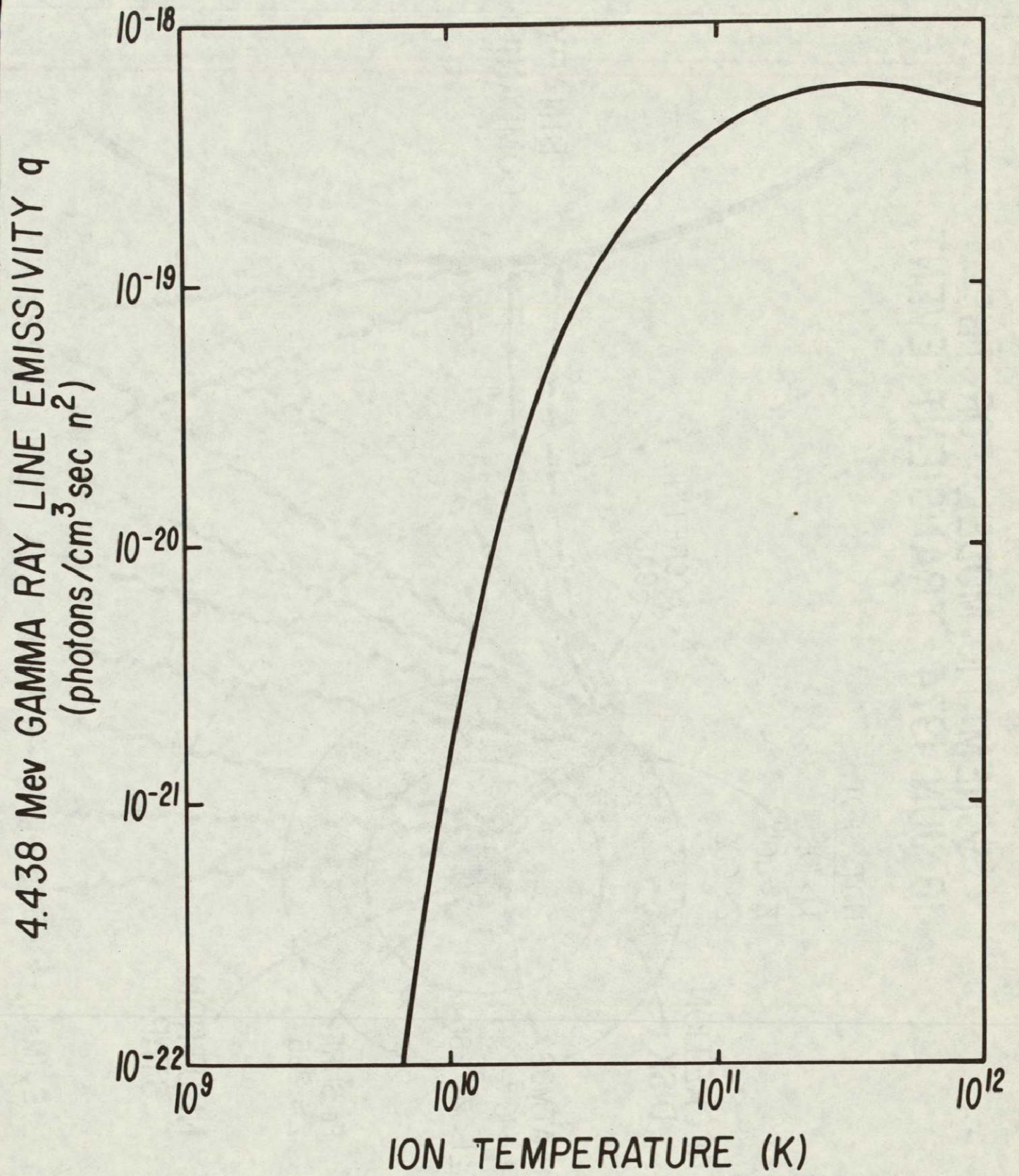
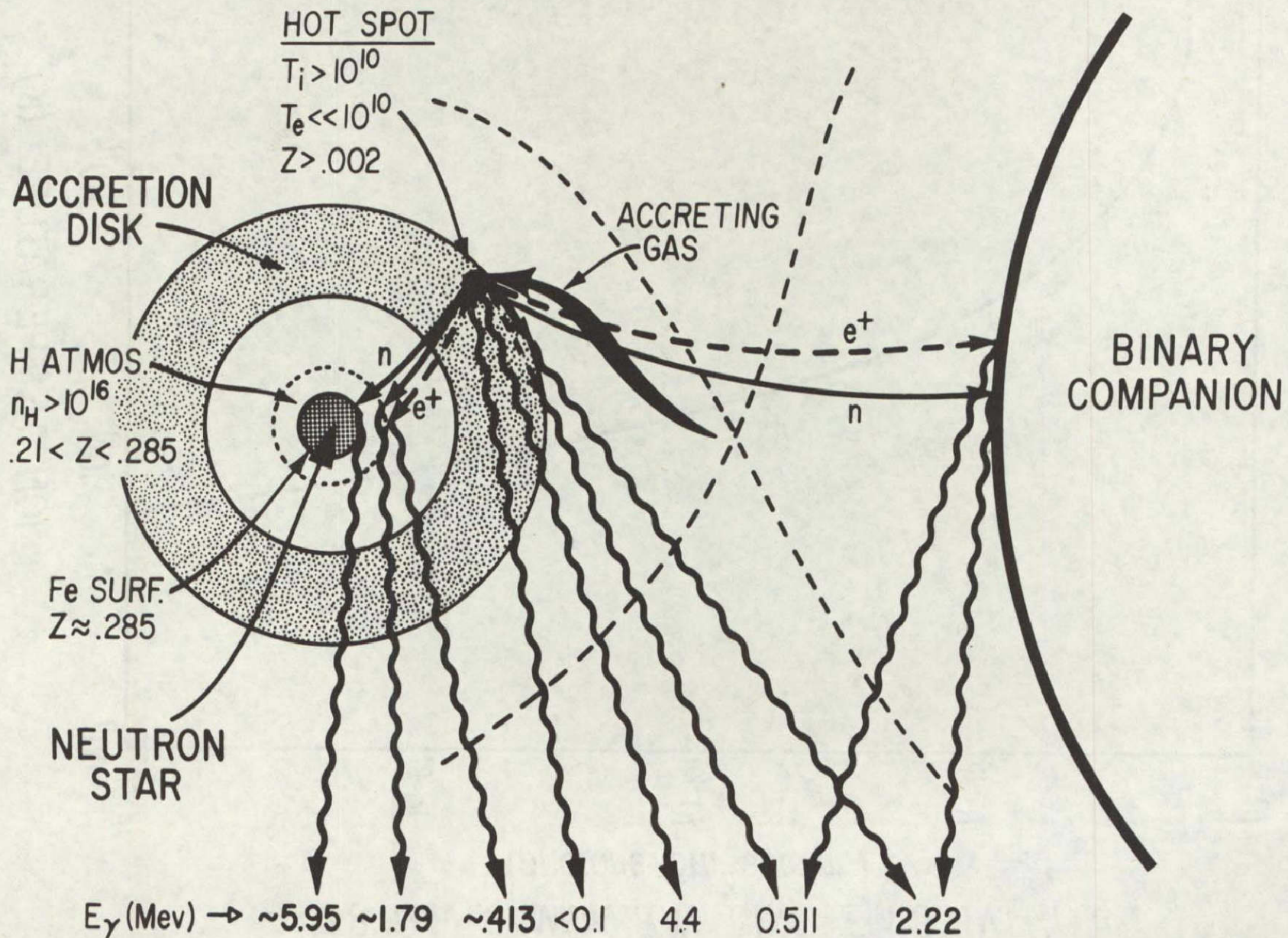Fig. 1

SCHEMATIC MODEL FOR THE 10 JUN 1974 TRANSIENT EVENT

Fig. 2

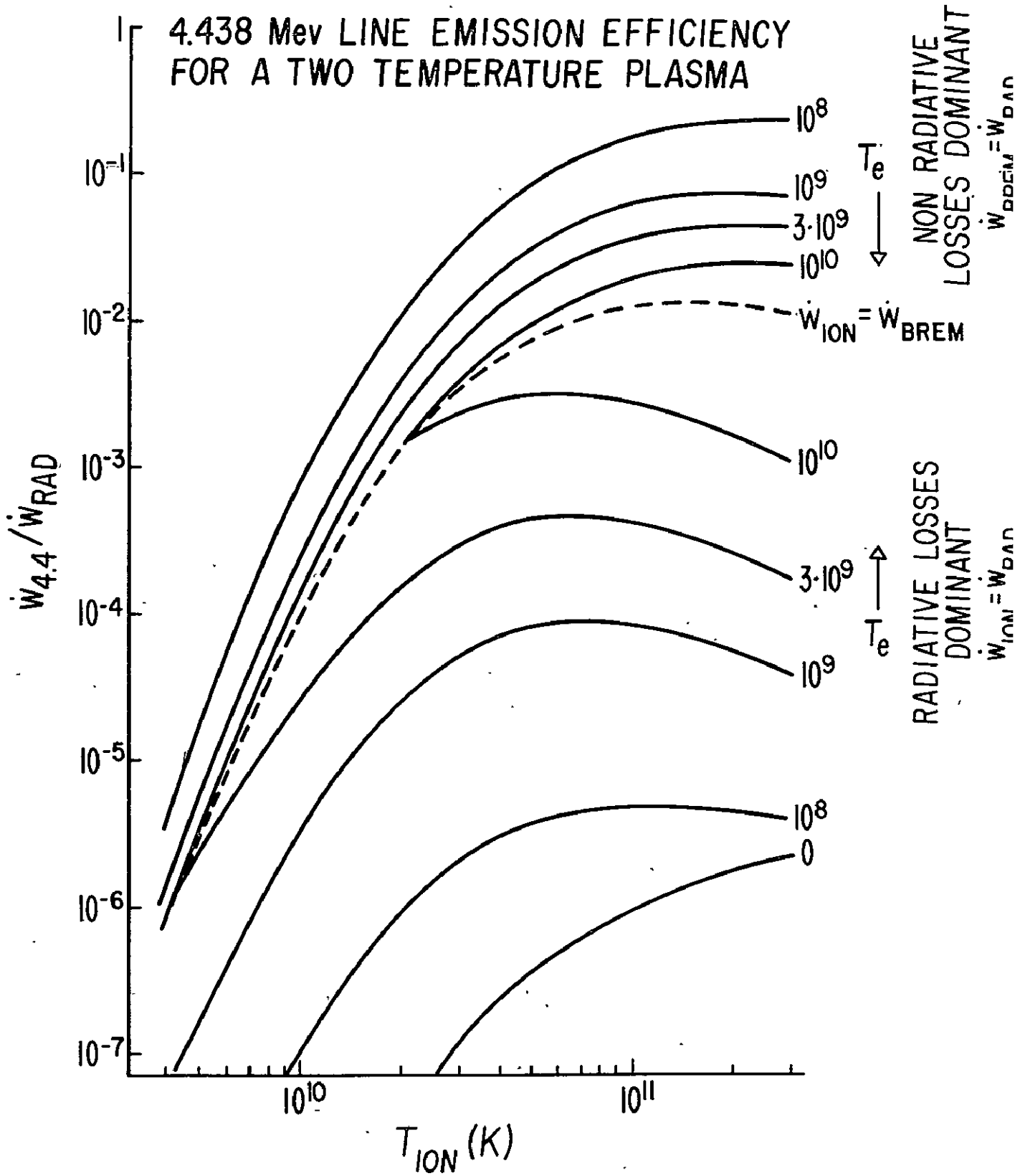4.438 Mev LINE EMISSION EFFICIENCY FOR A TWO TEMPERATURE PLASMA

Fig. 4

N78-31985

GAMMA-RAY LINES FROM NEUTRON STARS

AS PROBES OF FUNDAMENTAL PHYSICS

Kenneth Brecher

Department of Physics
Massachusetts Institute of Technology, Cambridge, MA 02139

ABSTRACT

The detection of gamma-ray lines produced at the surface of neutron stars will serve to test both the strong and gravitational interactions under conditions unavailable in terrestrial laboratories. Observation of a single redshifted gamma-ray line, combined with an estimate of the mass of the star will serve as a strong constraint on allowable equations of state of matter at supernuclear densities. Detection of two redshifted lines arising from different physical processes at the neutron star surface can provide a test of the strong principle of equivalence. Expected fluxes of nuclear gamma-ray lines from accreting neutron stars have been calculated, including threshold, radiative transfer and redshift effects. The most promising probes of neutron star structure are the deuterium formation line and the positron annihilation line. Detection of sharp redshifted gamma-ray lines from x-ray sources such as Cyg X-1 would argue strongly in favor of a neutron star rather than black hole identification for the object.

INTRODUCTION

Astrophysical gamma-ray spectroscopy has the potential for providing the same information about neutron stars that optical spectroscopy provides for main sequence stars: namely information about the surface gravity and composition (both surface and internal). Because of the high surface temperature expected for neutron stars even after a relatively long time (e.g. 10^6 °K after 10^6 years) no optical emission or absorption line from the surface is to be expected. However, gamma-ray lines, produced either by accretion or

by pulsar action, can be expected. Accretion of mass onto a neutron star in binary systems (or from interstellar space) can give rise to the deuterium formation line, (at 2.22 MeV) the positron annihilation line (at 511 KeV) and also the nuclear excitation lines of species such as carbon, oxygen, nitrogen and other abundant nuclei. Pulsars might also be expected to produce the positron annihilation line. Detection of such lines can yield valuable information about conditions at the surface of the radiating neutron star not derivable in any other way.

NEUTRON STAR STRUCTURE AND EQUATION OF STATE

Unlike normal nuclear burning stars, whose properties are determined by their chemical compositions, opacities, con-vection rates, etc., the gross macroscopic properties of neutron stars $\underline{only}$ depend on their equation of state $p=p(\rho)$. In parti-cular, for a given equation of state, one can compute the mass and radius for each assumed central density. The surface red-shift expected is then given by

$$\text{if} \quad z \equiv \frac{\Delta\lambda}{\lambda} = (1-2GM/Rc^2)^{-1/2}-1.$$

Thus if a spectral line arising from the surface of a neutron star can be identified, constraints can be placed on the mass of the star. Shown below are the mass-redshift curves expected for sev-eral equations of state (from Brecher, 1977), derived assuming general relativity to be valid. Quite different curves can arise in other theories of gravity. Essentially all of the other "realis-tic" model equations of state produce curves lying in the region between the models labeled "nuclear" and "Quark Bag".
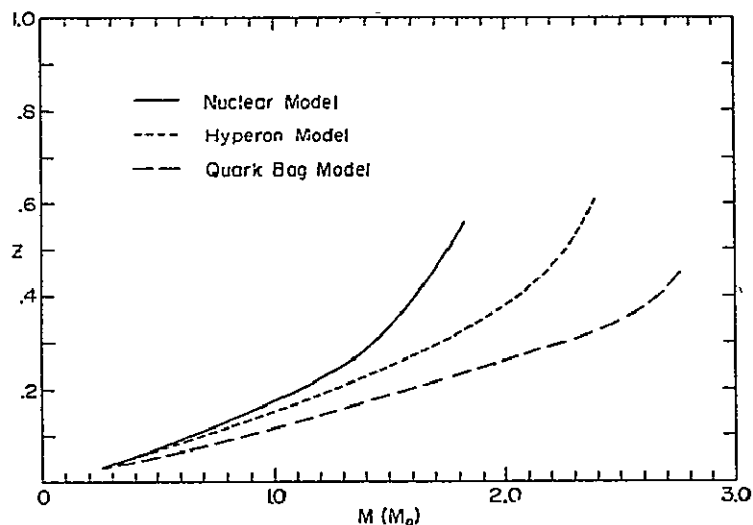
Figure 1. Surface redshift as a function of mass M
(in solar masses).

Since the above curves represent realistic limits on the
allowable equations of state consistent with current physical ideas
about nuclei, hyperons and quarks, the observation of a line from
even a single neutron star (not in a binary system) can prove of
value. For example, M. Leventhal et. al. (1977) and M. Yoshimori
(private communication to M. Leventhal) have found a possible
gamma-ray line at 400 keV from the Crab Nebula. Identifying this
as the redshifted positron annihilation line gives a redshift
$Z \simeq .28$, the above model calculations suggest that the mass of the
Crab pulsar lies in the range $1.4 - 2.4 M_\odot$, considerably higher than
the often stated $0.5 M_\odot$.

Even more exciting is the prospect of detecting gamma-ray
lines from a neutron star in a binary star system. By combining
the redshift with a mass determination from the orbital elements,
one can begin to try to establish the nature of matter in neutron
stars - whether it behaves as neutrons, quarks, or some other state
of matter-from its location in the M-Z plane.

To reiterate, the detection and identification of a <u>single</u>
gamma-ray line arising from the surface of a neutron star can pro-
vide valuable information about the mass and composition of the
underlying star.

STRONG PRINCIPLE OF EQUIVALENCE

The general theory of relativity is founded on the prin-
ciple of equivalence. However, only the "weak" principle has been
tested experimentally, showing that the ratio of the inertial to
gravitational mass (for materials ranging from aluminum to gold) is
a constant (and defined equal to unity). The "strong" principle,
however, states that the local laws of physics are the same in or
out of a gravitational field. It is in fact the strong principle
which must be valid for one to apply a known stress tensor in the
field equations of general relativity.

The detection of gamma-ray lines arising from two different
physical processes near the surface of a neutron star can provide
support for the strong principle (Brecher, 1978). In particular,
consider the deuteron with a binding energy $E_D = 2.22$ MeV and the
positron or electron with rest mass energy $E_e = .511$ MeV. Then the
detection of gamma-ray lines from a neutron star surface produced
by deuterium formation and from positron annihilation <u>with the same
redshift</u> serves as a test of the strong principle of equivalence.
It would say that the physics of strong interactions (which determines
E_D) and the physics of electromagnetic interactions (which presu-
mably predominantly contributes to E_e) remain unchanged, at least
relative to one another, in a strong gravitational potential

M/Rc² as high as .3-.4). That is E_D/E_e = constant, independent
the gravitational field.

Such a result may already have been provided by the transient
mma-ray event of 10 June 1974 observed by Jacobsen (1977). A
riety of gamma-ray lines seem to have been detected in this event,
th energies of .413, .511, 1.79, 2.22 and 5.95 MeV. Lingenfelter
978) suggests that the .413 and 1.79 MeV lines are redshifted
sitron annihilation and deuterium formation lines, respectively,
th redshifted by z = .24 ± .01. Assuming the lines arise from
e surface of a neutron star with redshift .24, this result pro-
des direct support for the strong principle of equivalence with
accuracy of about 4%.

PECTED GAMMA-RAY LINE FLUX FROM ACCRETING NEUTRON STARS

The final question we must address is: does one expect
produce a detectable gamma-ray line flux from neutron stars? Two
ssibilities come to mind. For single radio pulsars (e.g. the Crab
lsar), it is possible to envision the production of a positron flux
ising directly from the pulsar radiation mechanism. In the ab-
nce of a working pulsar emission model, an expected flux is dif-
cult to estimate. For accreting neutron stars, however, the prob-
m is well defined and calculable. We have examined the problem
gamma-ray emission from gas with normal cosmic abundance accret-
g spherically symmetrically onto a rigid neutron star surface. Details
the calculations will appear elsewhere, (Brecher and Burrows, 1978).
e results represent essentially an upper limit to the expected yields
cause they assume free streaming of particles onto the star (with no

energy loss on the way down). The gamma-ray line fluxes expected as a function of accreted proton energy E_p or, equivalently, stellar surface redshift z are given in figure 2. They are given relative to the continuum x-ray flux primarily produced as a result of accretion.
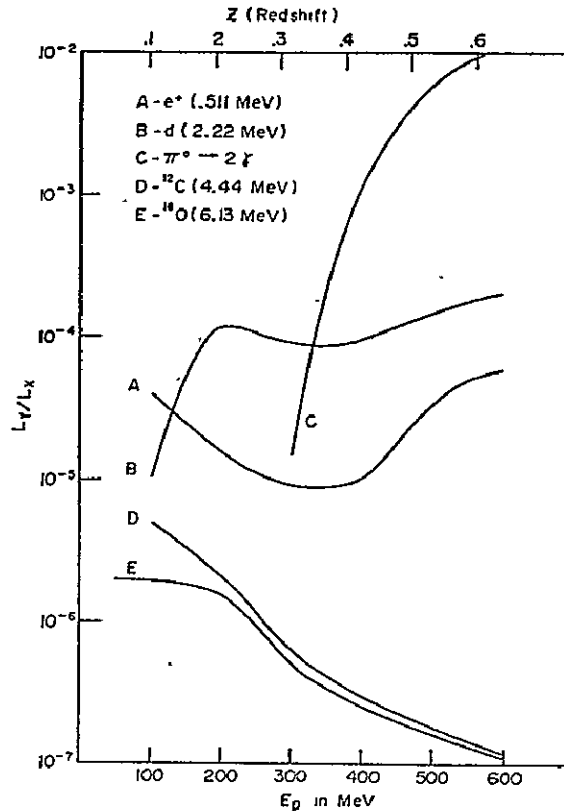

Figure 2. Expected gamma-ray line fluxes as a function of neutron star redshift z or accreted proton energy E_p.

As can be seen from figure 1, we expect reshifts greater than .2 for neutron stars more massive than about one solar mass. The deuterium line is then expected to be the strongest detectable gamma-ray line. (The pion decay flux can be large, but does not give rise to a narrow line.)

Turning to specific known x-ray sources, if they are assumed to be powered by accreting neutron stars, we may estimate the expected line fluxes at Earth for a given accretion energy E_p. For Sco X-1, for example, with $E_p = 300$ MeV, one expects $L_{e^+-e^-} \simeq 4 \times 10^{-6}$ phot cm^{-2} sec^{-1} and $L_D \simeq 1.5 \times 10^{-5}$ phot cm^{-2} sec^{-1}. These fluxes should be just detectable by the proposed Gamma-Ray Observatory, though they are indeed a factor of 10^2 below current (balloon) sensitivities.

Finally, the nature of the x-ray emitting object Cygnus X-1 is still unclear. If the system contains a black hole, it is highly unlikely that it can produce (narrow) gamma-ray line emission with a well defined redshift. Thus detection of sharp gamma-ray lines from this object would be strong support for a neutron star identification. Similarly, systems such as AM Her which have been suggested to contain an accreting white dwarf would not be expected to give rise to gamma ray line emission.

SUMMARY

Gamma-ray line spectroscopy offers a tool for the study of collapsed objects. It can allow tests of the strong and gravitational interactions under extreme conditions. It can make a distinction between the various possible compositions of the radiating object. It can also serve to distinguish between different underlying astrophysical systems. Overall, gamma-ray lines appear to be a promising tool for the study of collapsed astronomical objects.

REFERENCES

Brecher, K. 1977, Ap. J. (Letters), 215, L17.

Brecher, K. 1978, Ap. J. (Letters), 219, L117.

Brecher, K. and Burrows, A., 1978, in preparation.

Jacobsen, A.S., 1977, preprint.

Leventhal, M., MacCallum, C. and Watts, A., 1977, Ap. J., 216, 491.

Lingenfelter, R.E., Higdon, J. C. and Ramaty, R. 1978, this Volume, p. 252.

GAMMA RAY ASTRONOMY AND THE ORIGIN OF THE LIGHT NUCLEI :

Hubert Reeves - CEN Saclay - I.A.P. Paris

Nuclear reactions induced by the collisions of the protons and alphas

of the galactic cosmic ray with heavy nuclei of the interstellar gas are

responsible for the continuous production of the light elements lithium,

beryllium, and boron in the galaxy (Meneguzzi, Audouze, Reeves 1971)

(Reeves 1974) (Reeves and Meyer 1978) (RM). To better than one order of

magnitude, the observed ratios of these abundances to hydrogen abundance

and the nuclidic abundance ratios between themselves are accounted

for by simply considering the effect of fast protons and alphas with a

flux and an energy spectrum as observed in galactic cosmic rays, for

a period comparable with the life of our galaxy ($\sim 10^{10}$y).

However, when more accurate agreement is sought with the increa-

singly accurate data, some difficulties appear, which require a better

understanding of the real situation. It is in this endeavour that gamma

ray astronomy may play a crucial role.

A) The Boron isotopic ratio and low energy "carrots"

We consider first the $^{11}B/^{10}B$ ratio. The observed isotopic ratio

on the earth-moon-meteorites is 4 ± 0.4. The value computed from

galactic cosmic ray bombardment of interstellar matter is 2.4, close

enough to the observed ratio to be of relevance. The accuracy with which the important cross sections involved in the production of these isotopes (p + ^{12}C, p + ^{16}O, etc,) are measured has been constantly improving over the years (Epherre 1972) (Raisbeck and Yiou 1975) (Bodansky et al 1975) (King et al 1977) and is now good enough to make it clear that there is a discrepancy between observations and calculations.

It has been known for many years (Bernas et al 1967) that, in view of the shape of the excitation functions for these reactions, an higher ^{11}B/^{10}B ratio would be generated if one considered a flux of low energy protons and alphas (around a few tens of MeV per nucleon, i.e. close to the energy thresholds). Assuming a flux with an energy spectrum in power law of kinetic energy ($E^{-\gamma}$), with an exponent γ of 3 or more, one could easily reach the isotopic ratio of four.

There were also some reasons to think that such flux of low energy particles might possibly exist in space, in addition to the observed galactic cosmic rays. First of all, the effect of the solar modulation, which essentially chase away from the solar system cosmic rays with less than a few hundred MeV/n, would easily explain why we do not detect these fluxes with our satellites. Nevertheless some low energy particles are actually observed; the spectrum of observed low energy protons has a "turn up" around twenty MeV (fig 1) going up rather steeply with decreasing energy (what we call a low energy "carrot"). A number of people have interpreted this carrot as a feeble echo, enormously damped by solar modulation, of a much larger carrot pervading space. Mc Donald et al (1977) considering how the helium carrots gets bigger and bigger

Fig. 1

The dashed curve labeled "observed" shows the observed galactic cosmic ray flux at earth's orbit and solar minimum modulation. The fluxes labeled "max demodul" and "min demodul" are upper and lower limits to the mean flux in space at solar orbit around the galaxy. The dashed curve labeled Alpha's is the interstellar low energy turn up proposed by Mc Donald et al (1977) from their observations on Pioneer 10. The curves labeled E^{-5} and E^{-3} below 10^2 MeV are our "carrots" fitted to account for the boron isotopic ratio.
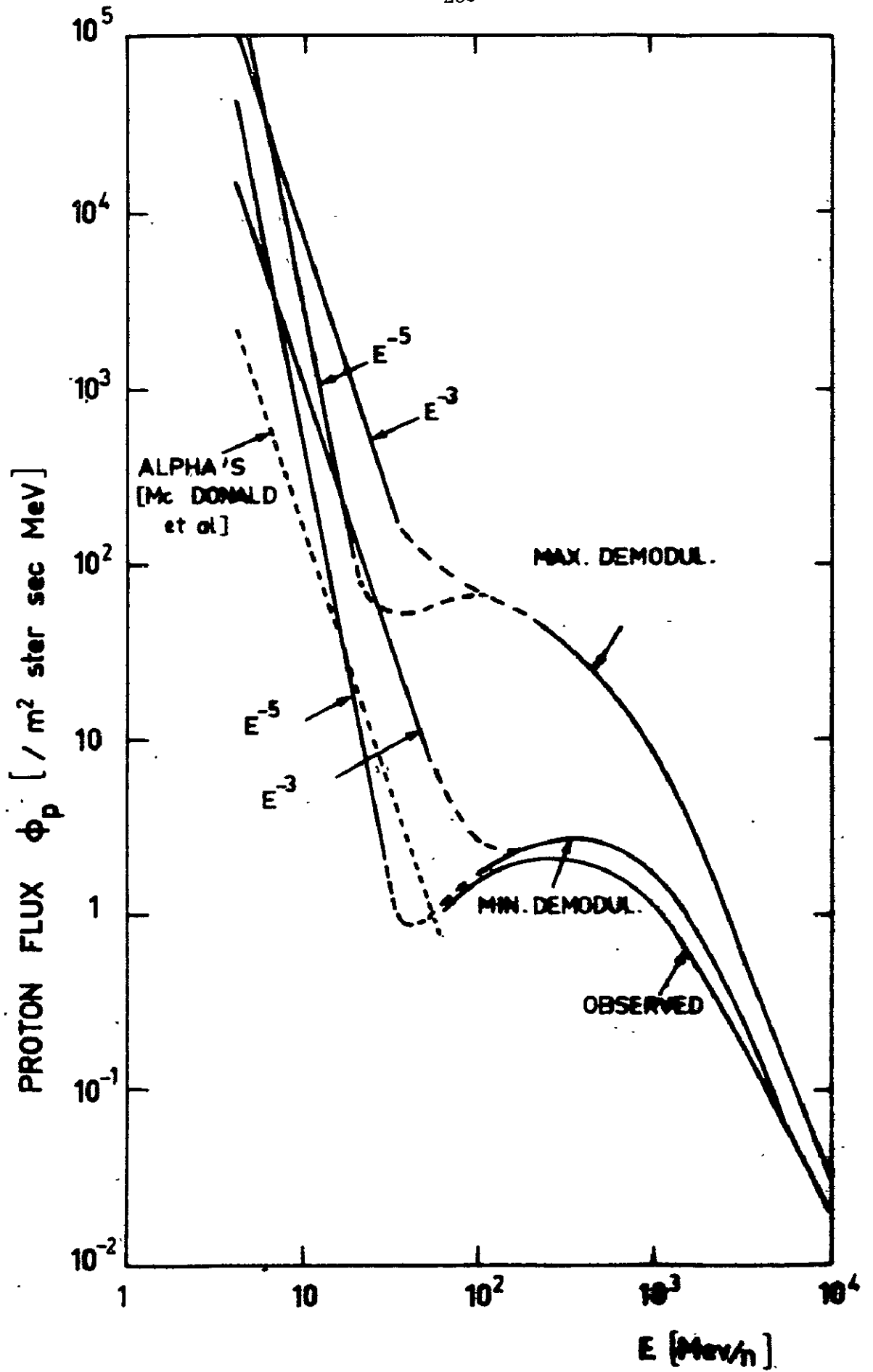
as one moves away from the sun (following the Pioneer 10 experiment) have tried to extrapolate it to outside of the solar system. Their "reconstituted" carrot is shown in fig. 1.

The strategy for the theorist is then to compute the boron isotopic ratio resulting from the sum of the properly demodulated galactic cosmic ray flux plus a low energy carrot. There are two complications 1) as we shall discuss later, the problem of choosing the appropriate high energy mean flux is far from being solved 2) carrots require two parameters: the intensity and the exponent γ

In Fig 1 we take two extreme values for the mean flux outside of the solar system and two exponents: 3 and 5. All these fluxes are tailored to reproduce the observed boron isotopic ratio. For each value of γ larger than 3 one could plausibly find an appropriate amplitude to match this ratio. The values of 3-5 are reasonable in view of their resemblance with solar flare exponent values.

Returning to the Mc Donald et al's extrapolation and taking into account a proton to alpha ratio of ~ 10 one notices the interesting similarity, both in amplitude and in shape, with our hypothetical carrots.

Furthermore we should consider the possibility of low energy carrots existing in localized volumes of space, for instance in supernovae remnants or around active stars. Because of their limited range against deceleration by electronic collisions, these particles do not necessarily pervade the whole of the galactic volume, as higher energy (GeV) particles do. Light nuclei would be generated there at an higher rate

than elsewhere in the galaxy and would later be mixed by galactic gas motions.

All these arguments (extrapolation of galactic cosmic ray; boron isotopic ratio) make it reasonable to assume the existence of low energy carrots but do not prove their existence.

As discussed in Meneguzzi and Reeves 1975 (MR) their actual existence would be revealed by the observations of nuclear gamma ray lines, in particular by the 4.4 MeV line from ^{12}C. The cross sections for formation of these lines by bombardment of p and α are particularly large around a few MeV per nucleon i.e just in the range of the carrots. Because of the large gamma ray background due to electron bremstrahlung emission, it would not be possible to detect the lines produced by carrots diffusely pervading the whole space. However the contribution of confined sources of fast particles could be detected, given appropriate energy and space resolution. Numbers are given in fig (2) from MR. Detection of gamma ray lines in selected regions of space would give important information on the flux of low energy particles; for instance the ratios of line intensities would give information on the energy exponent. It would also give us a better estimate on the present rate of formation of the light nuclei.

B) The Beryllium to Hydrogen ratio, or " Are we living in an open galaxy"?

One other difficulty appeared when we (RM) tried to compare the stellar values of Be/H with the present rate of formation of Be nuclides computed from the present galactic cosmic ray flux. It appeared

Fig. 2

Source function for the nuclear gamma ray lines produced by the interaction of interstellar gas with a flux of particles consisting in the sum of the galactic cosmic rays plus a low energy carrot capable of generating the observed boron isotopic ratio. The background of electron produced bremstrahlung photons has not been included.
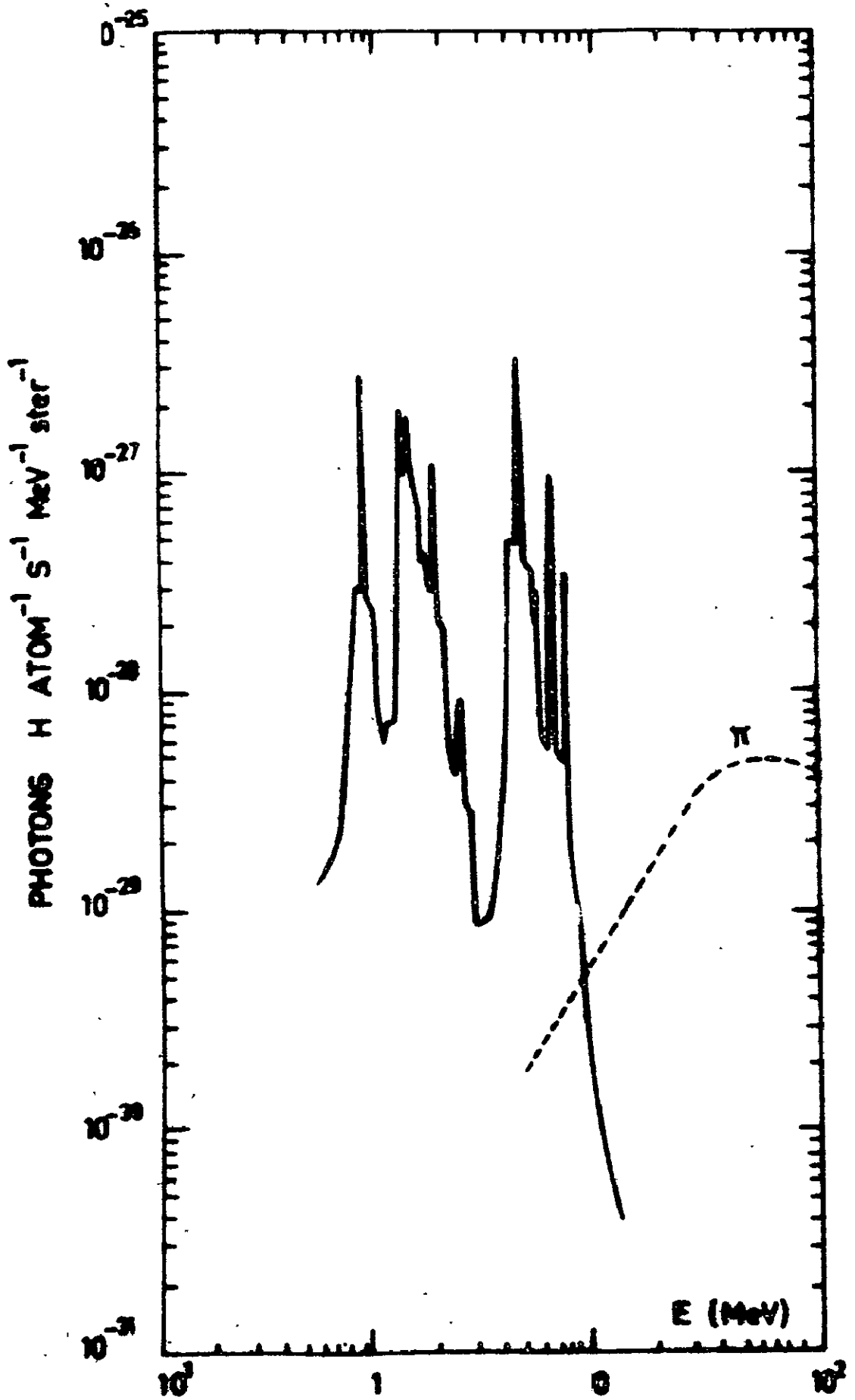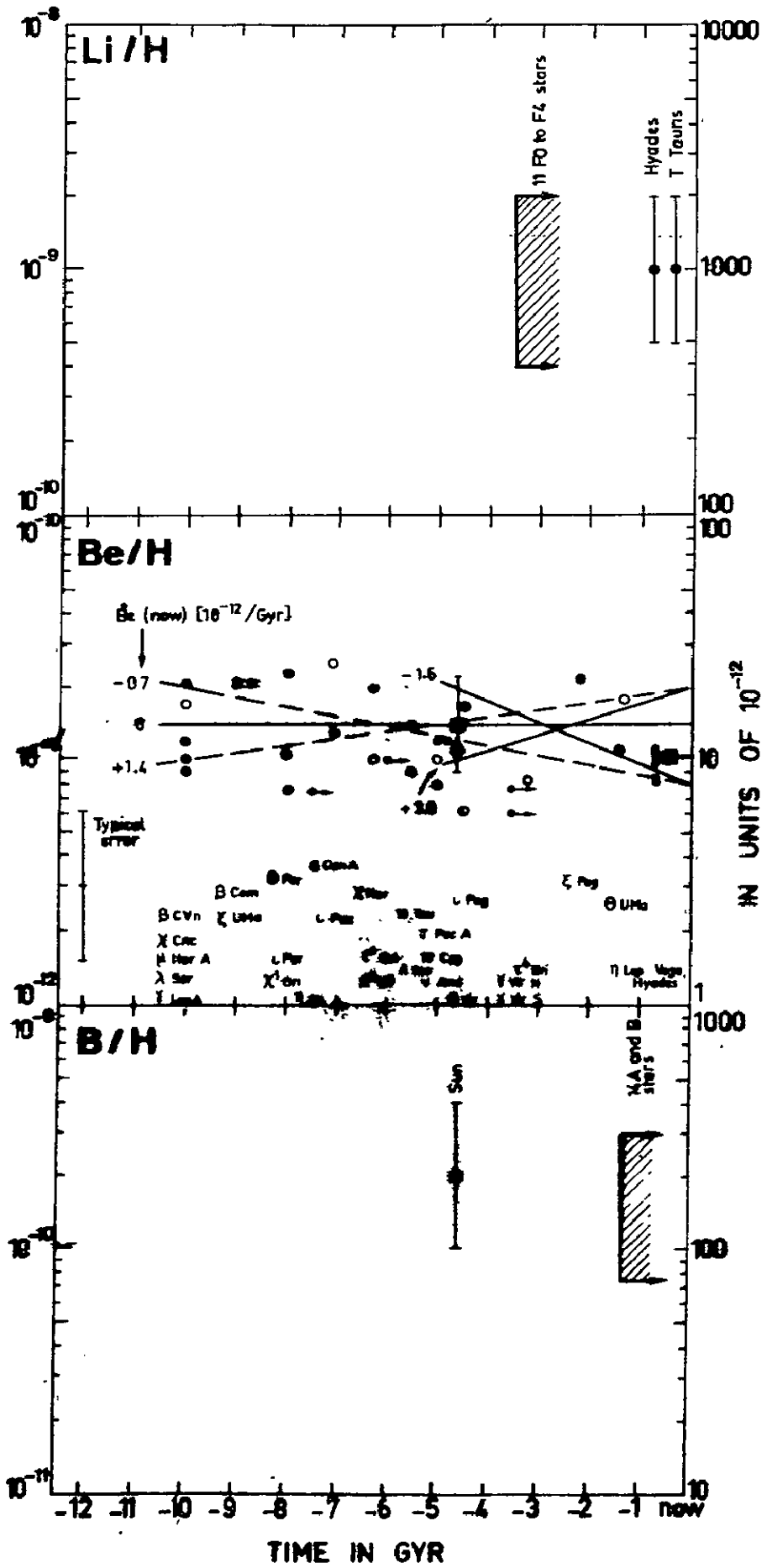
Fig. 3

Evolutionnary abundance curves for Li, Be and B. The abundance

data are the solar and stellar data quoted in the text. We now give more

details about beryllium. Dotted square: adopted solar Be abundance from

the non-LTE study of Chmielewski, Müller and Brault (1975); dotted circle:

solar abundance from the LTE analysis of Boesgaard (1976b), on which most

stellar abundances are based. The stellar data are from Boesgaard (1976b),

Boesgaard and Chesley (1976), Dravins and Hultqvist (1977), Boesgaard,

Heacox and Conti (1977), and Boesgaard et al. (1974). The full square plotted

for Vega indicates that the assumption of LTE is completely valid for this

star. The typical error on each abundance determination is a factor of 2

each way. Except for the Hyades, the stellar age determinations are from

Perrin et al. (1977) and Perrin (private communication). Full circle: good

age determination ($\pm$ 30%, relative to other stars); open circle: rougher

determination (lower metallicity [Fe/H]$\approx$- 0.50, or star close to main

sequence   Perrin et al. 1977] ; or temperature deduced only from colour

analysis [Perrin, private communication]). The uncertainties on the

whole scale is about $\pm$ 50%, but we certainly have quite a few stars signi-

ficantly older than the Sun. The age upper limits given for a few stars are

the main sequence lifetimes corresponding to their spectral types (after

check that their metallicity is about solar, [Perrin private communication]).

We have also indicated our adopted limits to the observed variation of the Be

abundance based, either on the last 5 Gyr only (full), or on the last 10 Gyr

(dashed), and the corresponding limits to the present-day Be (now), assuming

a smooth exponential variation. (See Reeves and Meyer 1978 for the references

quoted in this caption).

TIME IN GYR

that the stellar abundance (Be/H~1.4 x 10^{-11}) (Boesgaard 1976)

could be generated in approximately 3 x 10^9 years...while the

galaxy is· 15 x 10^9 years !

The problem became worst when we plotted the stellar Be/H

ratio as a function of stellar ages (fig 3). Within an uncertainty of

about two, the Be/H has not varied in the last 10^{10} years (good argu-

ments can be given that stellar destruction of Be cannot be large

enough to save the situation). Reeves and Meyer (1978) have argued that

the most likely explanation is the effect of infall, into our galaxy, of

extragalactic matter (essentially hydrogen and helium and no Be). ·

(A similar argument can be made for lithium and boron, but the obser-

vations are not as good).

Matter infall has been discussed from other grounds..It could

come from. the motion of our galaxy, sweeping the extragalactic gas of

our local cluster of galaxies (Hunt and Sciama 1972, Hunt 1975);it could

be late-comer matter from the initial collapse giving birth to our galaxy

(Larson 1976). The rate of infall needed to account for the low value

and constancy of the stellar Be/H ratio is of about two solar masses per

year in the whole galaxy (with rather large uncertainties), quite compa -

rable to the rate computed from these other grounds. RM gives an

equation which relates the rate of matter infall to the present rate of

formation of Be/H. This last rate is uncertain on several grounds:

uncertainties on the importance of the solar modulation effects, uncer-

tainties on the galactic radial and azimuthal variation of the galactic

cosmic rays at the solar orbit around the galactic center, uncertainties on the contribution of localized production of Be in confined acceleration regions. Here we come back to a problem mentioned in section A; light elements are made in a large volume of space and time; they represent the average effect of cosmic rays throughout those space and time, while we observe cosmic rays only here and now. The space variations, at least, can be studied through gamma ray astronomy both from the 100 MeV rays issued from $(p+p \to \gamma)$ reactions, for the higher energy particles, and from the gamma ray lines, mainly from low energy particles. The first task (γ decay) is already well on its way, from the SAS 2 and COS B satellites (Stecker et al 1978) (Fichtel et al 1977) (Paul, Cassé, Cesarsky 1976), while the second task is just starting. We expect from their combined results to improve the estimate of the matter infall in the galaxy, to improve the modulation theory, together with obtaining most valuable information on where and how cosmic rays are accelerated...

C) The contribution of gravitationnaly contracting stars to the acceleration of galactic cosmic rays .

In this respect, Reeves and Cesarsky (1977) have recently worked on the idea that a part at least of the galactic cosmic ray flux could originate from the conversion of gravitational energy to rotational energy and eventually to magnetic energy during the contraction of a gas cloud into a star. It was shown in this paper that the amount of gravitational energy released per unit time by all contracting stars in our solar neighborhood is appreciably larger that the power needed to keep the cosmic ray alive against galactic escape and electronic deceleration.

The efficiency required for the transformation of gravitational

energy into fast particles is a few percent, if one wants to account

for the whole of the cosmic rays in this manner. If only a fraction

of the galactic cosmic ray flux originate this way, the efficiency required

would be proportionally smaller.

It is not yet possible to compute with any degree of accuracy

what a reasonable value of the efficiency should be. Again here, obser-

vations of gamma ray lines in location of stellar births would give us

a magnificent handle on this problem...

D) Deuterium and the active center of our galaxy.

When deuterated molecules (DCN) were detected in the center of our

galaxy (Penzias 1976), we realized that this was a sign that something

funny was going on out there (Audouze et al 1976).

The ratio DCN/HCN of 10^{-3} was not really different from ratios

of deuterated molecules found in nearby molecular cloud (Jefferts.et al

1973), These values are usually understood as arising from equilibrium

molecular exchanges at low temperature (Reeves and Bottinga 1972) (Watson

1975) from a pool of hydrogen atoms with isotopic ratio D/H of a few x 10^{-5}

(York and Rogerson 1976) (Vidal Madjar et al 1977) (Laurent 1978). The

deuterium atoms are believed to have originated in the Big Bang. After

a mild degree of destruction by passing through stars (at most fifty

percent of the original atoms have disappeared (Reeves and Johns 1976)

(Audouze and Tinsley 1976)) the left-over D atoms have taken advantage

of the law of mass- action to increase their representation in the three-body molecules by almost two orders of magnitude.

Why cant we use a similar explanation to account for the molecular ratios of deuterated molecules in the center of our galaxy? Because there, we have good reasons to believe that the fraction of surviving D atoms must be considerably less than elsewhere in the galaxy. The ratio of interstellar gas mass to stellar masses is, there, less than 10^{-3}, while in the solar neighborhood and in general it is about ten per cent. This is usually interpreted as meaning that the rate of stellar activity (formation and destruction) is vastly faster there than elsewhere. A detailed model (Vigroux 1977) (which does not include the simplifying but unjustified assumption of "Instant Recycling") has shown that the fraction of surviving D isotopes is probably only of the order of 10^{-6} (i e $D/H \sim 10^{-11}$). To account for the DCN/HCN ratio of 10^{-3} one would require a exchange enhancement of 10^{+8}, which is certainly not realistic. There lies the problem.

Audouze et al (1976) have considered two possible solutions A) Infall of extragalactic matter with pristine D/H, somewhat along the lines discussed before, and B) a faster rate of galactic cosmic rays, continuously producing D from the $[p + \,^{4}He \rightarrow \,^{3}He + D]$ reaction.

The hypothesis of an increased rate of galactic cosmic rays in the galactic center (the flux needed is $\sim 10^{3}$ larger than the local flux) was not without fondation. Haymes et al (1975) had already reported the detection of the 4.4 MeV gamma ray line from excited carbon originating from this direction. This report has been confirmed recently by the

(1978)

HEAO satellites (Leventhal and Mac Callum).Combining the data

from the 4.4 MeV line with the flux of ~100 MeV gamma rays line,

we showed (in Audouze et al 1976) that the fast particles responsibl

for the gamma ray lines could also build up a D/H ratio of 10^{-5} in a

period of time comparable to the mean life of the galactic center gas

against astration (2×10^8 years). The concommitant ^{3}He, Li, Be

B are yet below detectability.

Therefore we now have two acceptable solutions; infall and

increased flux of galactic cosmic rays. Clearly, better data on the

volume extension of the source of the gamma ray lines will help

to discriminate between both mechanisms.

E) Boron and quasars

Baldwin et al (1977) have recently fiven an upper limit of ~ 0.10

for the ratio of Boron to Carbon in the photosphere of the quasar 3 C 273.

This upper limit is already problematic for our (poor) understanding

of quasar's dynamics. Why?

One popular picture of the machinery of quasars is that fluxes of

fast particles (electrons and presumably also protons) are ejected

from the nuclei of quasars. These particles travel until they reach the

double radio sources, where, circulating around the lines of forces of

the localized magnetic field, they emit enormous fluxes of synchrotron

radiation.

In their way from the active nuclei of the quasar to the radio

sources, these particles must most probably traverse the photospheric

regions where quasar optical line emission is taking place. In a

simple-minded estimate made by Baldwin et al, the protons and electrons

should induce enough spallation reactions to generate an observable

. B/C ratio (larger than the upper limit quoted above). One can of course

appeal to rather special conditions of propagation in order to avoid the

problem but this may not be totally satisfactory. Here again it is imme-

diately visible that the detection of nuclear gamma ray lines from

quasars would help in untangling these difficulties and would give us a

better understanding of the machiney of quasars, yet a most baffling subject...

Audouze J., Lequeux J., Reeves H. and Vigroux L., 1976, Ap.J.Letters, 208, L51 " Implications of the presence of deuterium in the galactic center".

Audouze J. and Tinsley B.M., 1976, Ann.Rev.Astr.Ap., 14, 43. " Chemical evolution of galaxies".

Baldwin J., Boksenberg A., Burbidge G., Carswell R., Cowsik R., Perry J. and Wolfe a., 1977, 15th Int.Cosmic Ray Conf., Plovdiv, 2, 357. " Cosmic-ray spallation effects in QSO's".

Bernas R., Gradstajn E., Reeves H. and Schatzman E., 1967, Annals of Physics, 44, 426. " On the nucleosynthesis of lithium, beryllium and boron".

Bodansky D., Jacobs W.W. and Oberg D.L., 1975, Ap.J., 202, 222. " On the production of lithium, beryllium and boron at low energies".

Boesgaard A.M., 1976a, Pub.A.S.P., 88, 353. "Stellar abundances in lithium, beryllium and boron".

Epherre M., 1972, Thèse Université Paris-Sud. " Etude expérimentale et semi-empirique de la spallation des noyaux légers; application à la nucléosynthèse des éléments Li, Be et B ans la galaxie".

Fichtel C.E., Simpson G.A. and Thompson D.J., 1977, Goddard Space Flight Center, preprint. "Diffuse gamma radiation".

Haymes R.C., Walraven G.D., Meegan C.A., Hall R.D., Djuth F.T. and Shelton D.H., 1975, Ap.J., 201, 593. " Detection of nuclear gamma rays from the galactic center region".

Hunt R., 1975, M.N.R.A.S., 173, 465. " Accretion of intergalactic gas by a realistic model of the galaxy and its implications".

Hunt R. and Sciama D.W., 1972, M.N.R.A.S., 157, 335. " Soft X-ray emission from intergalactic gas in the neighbourhood of the galaxy".

Jefferts K.B., Penzias A.A. and Wilson R.W., 1973. Ap.J.Letters, 179 L 57. " Deuterium in the Orion nebula".

King C.H., Austin S.M., Rossner H.H. and Chien W.S., 1977, Preprint.

Larson R.B., 1976, M;N.R.A.S., 176, 31. "Models for the formation of disc galaxies".

Laurent C., 1978, Thèse Université de Paris VII. "Abondance du deuterium interstellaire à partir du satellite Copernicus et ses implications astrophysiques".

Leventhal M. and Mc Callum C., 1978, Goddard Conf. on Gamma Ray Lines.

Mc Donald F.B., Lal N., Trainor J.H., Van Hollebeke M.A.I. and Webber W.R., 1977, Ap.J., 216, 930. " Observations of galactic cosmic-ray energy spectra between 1 and 9 AU".

Meneguzzi M., Audouze J. and Reeves H., 1971, Astr.Ap., 15, 337 (Mar) " The production of the elements Li, Be, B by galactic cosmic rays in space and its relation with stellar observations".

Meneguzzi M. and Reeves H., 1975, Astr.Ap., 40, 91. " Nuclear gamma ray production by cosmic rays".

Paul, J., Cassé, M., and Cesarsky C., 1976, Ap.J., 207, 62. " Distribution of gas, magnetic fields, and cosmic rays in the galaxy".

Penzias A.A., Wannier P.G., Wilson R.W. and Linke R.A., 1977. Ap.J. 211, 108. " Deuterium in the galaxy".

Raisbeck G.M. and Yiou F., 1975, 14th Int.Cosmic Ray Conf., Munich, 2, 502. "Cross sections for nuclear reactions induced by high energy alpha particles and the influcence of interstellar helium in cosmic ray propagation".

Reeves H. and Bottinga Y., 1972, Nature, 238, 326. " The D/H ratio in Jupiter's atmosphere".

Reeves, H., and Meyer J.P., 1978, Ap.J. (in press) "Cosmic ray nucleosynthesis and the infall rate of extra galactic matter in the solar neighborhood".

Reeves H. and Johns O., 1976, Ap.J., 206, 958. " The long lived radioisotopes as monitors of stellar, galactic and cosmological phenomena".

Reeves H., 1974. Ann.Rev.Astr.Ap., 12, 437. "On the origin of the light elements".

Reeves H. and Cesarsky C.J., 1977, 15th Inter.Cosmic Ray Conf., Plovdiv, 2, 15, "Cosmic rays from pre-main sequence stars".

Stecker F. W. , 1978, Goddard preprint "Gamma ray astronomy and the origin of cosmic rays".

Vidal- Madjar A. , Laurent, C. , Bonnet R. M. and York D. G. , 1977, Ap. J. , 211 , 91. "The ratio of deuterium to hydrogen in interstellar space. III; the lines of sight to Zeta Puppis and gamma Cassiopeiae".

Vigroux L. , 1977, Astr. Ap. , 56, 473. " On the iron abundance in clusters of galaxies".

Watson W. D. , 1975. Ecole d'Eté de Physique Théorique, les Houches, 1974: Physique atomique et moléculaire et matière interstellaire. Ed. par Roger Balian, Pierre Encrenaz et James Lequeux, North-Holland Publ. Co. , Amsterdam, 1975.

York D. G. and Rogerson J. B. Jr, 1976, Ap. J. , 203 , 378. " The abundance of deuterium relative to hydrogen in interstellar space".

GALACTIC CENTER IRON LINE EMISSION

D.M. Worrall[*], E.A. Boldt, S.S. Holt,
S.H. Pravdo[*], and P.J. Serlemitsos

Laboratory for High Energy Astrophysics
NASA/Goddard Space Flight Center
Greenbelt, Maryland 20771

ABSTRACT

Data from the Goddard Space Flight Center experiment on HEAO 1 have been examined for galactic centre iron line emission. Evidence for a 6.8 keV line from the summed flux within 10^{0} longitude and 10^{0} latitude of the galactic centre has been found. We cannot put firm limits on the intrinsic line width. If the line emission is diffuse and cosmic-ray-induced, the calculations of Bussard et al. (1978) yield an upper limit to ^{12}C 4.44 MeV line emission, which is not inconsistent with the results of Haymes et al. (1975). We cannot, however, rule out significant contributions to the iron line from discrete sources.

[*]Also Department of Physics and Astronomy, Univ. of Maryland

I. INTRODUCTION

Reports of gamma-ray line emission from the galactic centre (Haymes et al. 1975; Matteson et al. 1978, these proceedings) have motivated a search for X-ray iron line emission from the region. The detection of the ^{12}C nuclear deexcitation line at 4.44 MeV implies the presence of subrelativistic cosmic rays and the line arises from interactions of cosmic ray ^{12}C with interstellar H and He and from cosmic ray H and He with interstellar ^{12}C. Such cosmic rays are expected to be the source of spectral features from processes other than nuclear interactions and, consequently, in wavebands other than the gamma ray. Bussard et al. (1978) have investigated the X-ray line strength expected from cosmic ray iron undergoing collisional excitation and charge exchange with the interstellar medium. These authors calculate an emissivity ratio for the iron and ^{12}C lines, assuming solar abundances for the interstellar medium and an extrapolation of measurements above 300 MeV/nucleon for cosmic-ray abundances at the energies of importance for iron line production ($\sim$ 10 meV). The iron line is produced by a combination of hydrogen and helium-like ions and as such has a mean energy of $\sim$ 6.8 keV, Doppler broadened to a width of roughly 2.4 keV.

II. MEASUREMENTS

Since the opening angle of the gamma-ray detector of Haymes et al. (1975) is 13^0 (FWHM) and that of Matteson et al. (1978; these proceedings) 40^0 (FWHM), we have taken an extended region around the galactic centre and have summed X-ray spectra within 10^0 galactic longitude and 10^0 latitude of the centre. Data are from the Goddard Space Flight Center experiment on board the HEAO 1 spacecraft. Details of

the experiment are described elsewhere (Rothschild et al. 1978). The data discussed here were collected when the experiment was in its normal scanning mode in which the spin axis always points towards the sun and therefore precesses 1^O per day, so that the experiment, oriented perpendicular to the spin axis, scans a great circle of sky about once every 30 minutes. We therefore have roughly uniform coverage of our galactic centre region. Summed spectra, using a 32 channel pulse height analyzer, have been obtained from one of our three higher energy xenon multiwire proportional counter detectors, which is sensitive between about 2 and 80 keV, and from our argon detector, which is sensitive to the lower energy range between 1½ and 20 keV. The satellite movement is such as to complete a full sky coverage in 6 months. These results are from our first coverage of the galactic centre region in September 1977. In March 1978 we observed the same region with twice the number of pulse height channels and these data will soon be available for analysis.

The diffuse high latitude background X-ray flux found by this experiment (Marshall et al. 1978) has been subtracted from the observations. The internal detector background is eliminated by subtracting fluxes observed in the two halves of each detector, where each half is designed to have the same internal background but a different collimator size and therefore different amount of sky flux. For the detector whose results are discussed here, the collimator sizes are 3° x $1\frac{1}{2}^O$ (FWHM) and 3° x 3° (FWHM). We can demonstrate that the preponderance of photons measured from the 20° x 20° galactic center region arise from a number of bright discrete sources.

The differential photon spectra are derived by an automated procedure which inputs an assumed incident spectrum through the detector

response, compares with observed counts, and iterates the incident spectrum until a minimum χ^2 is found. The summed flux is found to be significantly better fit by a thermal bremsstrahlung continuum than a power law, the required temperature being between 4.8 and 6.3 keV. The continuum was fit with an acceptable χ^2.

The large accumulation of data has presented us with excellent statistics. When a line with energy, width and intensity as free parameters was included in the model, a preferred energy for a line of 6.8 keV was found, but the sensitivity to width was poor. The energy was then fixed at 6.8 keV, and a line width fixed at 2.4 keV gives the results in Table 1. Only one extra degree of freedom enters the model and therefore our confidence of an iron line being present is greater than 95%.

III. DISCUSSION

Our results indicate iron line emission from a summed region within 10^0 longitude and latitude of the galactic centre. However, we are not able to definitely say that the iron line is broadened, because the number by which χ^2 is reduced for a narrow line (< 1 keV) in the model is comparable with that for a broad line.

Applying the calculations of Bussard et al. (1978) to the values in Table 1 gives an upper limit to the broad ^{12}C feature of 4 10^{-3} $cm^{-2} s^{-1}$. This is above and therefore consistent with the value of Haymes et al. (1975) ($(9.5 \pm 2.7) \times 10^{-4}$ $cm^{-2} s^{-1}$). Our main problem in such an analysis is the uncertainty as to how much of this iron line emission is from the bright galactic centre sources themselves. There have been reports of broad iron features in the spectra of some bright sources thought to be in a class similar to several of those contained in the galactic centre region (Swank 1977). In addition,

some spectral iron lines have been reported by Parsignault and Grindlay (1978), from a survey of the brightest galactic centre sources. To date, September 1977 scanning data from the HEAO experiment have been analysed for only three of the sources in the region, results for which are given in Table 2. Since we were in a scanning mode at this time and source confusion is a problem, the statistics are poor. Although we found no definite evidence for iron lines from these sources, the 2.6 sigma upper limits to the equivalent widths for broad lines are rather high, clearly above the equivalent width for the summed flux iron line.

In summary, we have found evidence for iron line emission from a region within 10° longitude and latitude of the galactic centre. We cannot as yet rule out contributions from discrete sources in the region, but we expect to be able to deduce reliable values for these with additional data. Our value for the iron line flux must therefore be considered an upper limit. It is not inconsistent with that expected from relationship with the ^{12}C 4.44 MeV gamma-ray line of Haymes et al. (1975).

The extent of the ^{12}C emission region is not well established. If it is found to be large enough, a pointed observation may allow limits to be set on the iron line emission in a galactic centre direction which does not include known point X-ray sources. However, contamination from low luminosity unresolved sources with iron line features in their spectra may still be a problem. For example, SS Cygni, at a distance of about 200 pc has an X-ray luminosity (2-15 keV) of $\sim$ 5 10^{32} erg s^{-1} and an iron line flux of $\sim$ 4 10^{-4} cm^{-2} s^{-1} (Swank, private communication). Assuming this source to be typical of a class, we estimate

that the density of similar sources must be less than $\sim 6 \times 10^{-7}$ pc^{-3} for the summed iron line flux from this class alone to be less than the lower limit to the X-ray line flux predicted by Bussard et al. (1978) for the region contained by the Haymes et al. (1975) experiment. Deeper surveys of these weak sources should soon provide us with a density function for their iron line emission. We can then decide whether or not we will ever be able to conclude that iron line emission seen in a region void of resolved sources is uncontaminated by emission from faint unresolved sources.

REFERENCES

Bussard, R. W., Omidvar, K., and Ramaty, R., 1978, Ap. J. 220, 353.

Haymes, R. C., Walraven, G. D., Meegan, C. A., Hall, R. D., Djuth, F. T., and Shelton, D. H., 1975, Ap. J. 201., 593.

Marshall, F. E., Boldt, E. A., Holt, S. S., and Serlemitsos, P. J. 1978 in preparation.

Parsignault, L. R., and Grindlay, J. E., 1978, Ap. J., in the press.

Rothschild, R. E., Boldt, E. A., Holt, S. S., Serlemitsos, P. J., Garmire, G., Agrawal, P., Riegler, G., Bowyer, S., Lampton, M. 1978, submitted to Space Science Instrumentation.

Swank, J. H. 1977, Bull. of the APS 22, 588.

TABLE 1: Results of the inclusion of a 2.4 keV wide, 6.8 keV energy iron line in fits to the summed photon spectrum for $|l| < 10^0$, $|b| < 10^0$

DETECTOR	x^2 WITHOUT LINE	x^2 WITH LINE	LINE FLUX $cm^{-2} s^{-1}$	EQUIVALENT WIDTH (eV)	^{12}C PREDICTED LINE FLUX $cm^{-2} s^{-1}$
Argon	28	21	0.13	247	$4 \ 10^{-3}$
Xenon	32	19.5	0.10	142	$3 \ 10^{-3}$

TABLE 2: 2.6 sigma upper limits to the equivalent widths of broad iron lines for three bright galactic centre sources.

SOURCE	EQUIVALENT WIDTH (eV)
3U1735-44	917
3U1728-16 (GX9+9)	611
3U1820-30	903

GAMMA LINE RADIATION FROM SUPERNOVAE

W. D. Arnett
Enrico Fermi Institute
University of Chicago
Chicago, IL 60637

ABSTRACT

Recent calculations of core collapse of massive stars result in explosive ejection of the mantle by a "reflected shock". These new hydrodynamic results are important for predictions of explosive nucleosynthesis and gamma-ray line emission from supernovae. Previous estimates, based on simple parameterized models of the nucleosynthesis in an "average" supernova, are compared with the new results.

At present the theory of the production of gamma-ray line emitters in supernovae has dealt with two idealizations: (1) the representation of an exploding star as a few (usually three or four) homogeneous zones, and (2) the "average" supernova event (see Clayton 1973, for example). To go beyond this exploratory stage it would be desirable to deal instead with the distribution of conditions throughout a more realistic stellar model, and with a variety of presupernova models corresponding to the variety of observed supernova remnants. As a step in this direction, this paper will discuss recent hydrodynamic and nucleosynthesis calculations appropriate to stars of roughly 12 and 22 solar masses. Such objects might resemble, respectively, the more numerous events and the events most typical of nucleosynthesis (see Arnett 1977b for further details). The evolution of these stars through the exhaustion of silicon burning is described in Arnett(1977a). The collapse of the iron core occurs at such high density that the neutrinos formed by electron capture are trapped by the matter and are carried along

with it (see Arnett 1977c and references therein). This implies that an enormously simplifying approximation can be made: the collapse is roughly adiabatic. Van Riper and Arnett(1978) have examined such abiabatic core collapse for a variety of conditions.

In order to examine the nucleosynthesis and possible mass ejection a series of hydrodynamic calculations has been made. From the adiabatic collapse results, shock waves of several energies were taken, at a time when they had propogated beyond the neutrino "photosphere" but not yet to the silicon-burning snell, and grafted on to stellar structure models which were well into core collapse. The zone above the neutrino photosphere was the taken to be a rigid boundary; at present it is difficult to suggest a boundary condition which is clearly more realistic.

Several points can be made:

(1) The amount of matter ejected is very sensitive to the energy of the explosion (i. e., the reflected shock). For the 22 solar mass case ($m_\alpha = 8$ $M_\odot$), an energy of several times 10^{51} ergs can even eject neutron rich material from the pre-collapse iron core, and cause an embarrassment from over- abundance. With an energy of 2×10^{50} ergs however, much of the nuclearly-processed matter is slowed so much by running into the mantle that it falls back onto the hot neutrino star. An energy of about 10^{51} ergs is suggested by light curves of type I and II supernovae and by x-ray and radio observations of supernova remnants; this would eject the matter outside the original iron core, leaving a remnant of about 1.5 to 2 $M_\odot$.

(2) The conditions for nucleosynthesis are promising. It appears that silicon and oxygen burning occur on an explosive time scale much like the older parameterized results suggested. Carbon burning appears to be more complex, with a previous stage of hydrostatic burning in a convective shell determining the ejected abundances (see Arnett and Wefel 1978).

(3) The lower mass star ($M = 12$ $M_\odot$, or $M_\alpha = 4$ $M_\odot$) requires less energy to eject the matter above the old iron core, but there is less synthesized matter in these regions of these stars. Such objects are therefore less effective in making freshly synthesized matter to eject and be seen by gamma-ray astronomers.

The results are summarized in Table 1. In these events Ni56, and probably Co56, decay before these ejecta expand enough to be transparent to gamma rays. Ni57(Co57) is a better prospect, provided we have the right sort of galactic supernova. Clayton (1974) has discussed this case in an interesting way. Ti44(Sc44) might also be seen in a galactic event. Perhaps the best prospect is detection of

the "steady state" emission in the interstellar medium from the Al26 decay. The event rate should be roughly

$$F_{ss}(Al^{26}) \simeq t(decay) \; F(event)/t(sn)$$
$$\simeq n * (2 \times 10^{-5} \, cm^{-2} s^{-1}),$$

where t(decay) is the mean life for radioactive decay, F(event) is the initial number flux (in cgs units) per supernova (at 10 Kpc; see table 1), t(sn) is the mean time interval between galactic supernovae which are massive enough to make Al26 this way, and n is the number of such supernovae which occur in the Galaxy during one century. Unfortunately there are uncertainties of the order of a factor of 5 in this estimate due to inadequate nuclear data alone (see Arnett and Wefel 1978). Further note that the estimate is based upon the M = 22 $M_{\odot}$ star (M_{α}= 8 $M_{\odot}$); such objects can represent only a fraction of the supernovae. Finally, the possibility that the synthesized matter is not ejected by a "weak" explosion makes firm prediction difficult.

These models are still in an exploratory stage. So far no significant production of Na22 or Fe60(Co60) has been found, but the basic agreement with the earlier work of Clayton is good, especially considering the very different methods used.

AKNOWLEDGEMENTS

TABLE 1. ESTIMATES OF
GAMMA LINE RADIATION FROM NUCLEOSYNTHESIS

NUCLEUS (HALF-LIFE)	SOLAR ABUNDANCE BY MASS	ATOMS PER AVERAGE SN (DDC)	ATOMS EJECTED (IN CALC.)	MAX. FLUX AT 10 KPC	GAMMA LINES IN MEV (%)
NI56 (6.1D)	1.3(-3) (AS FE56)	3(54)	0 TO 1(55) 6(54)		
CO56 (77D)				5(+1) OPAQUE?	.511(40%) .847(100%)
NI57 (36HR)	3.1(-5)	7(52)	0 TO 2(53) 1.4(53)		
CO57 (270D)				4(-1)	.122(89%)
CR48 (23HR) V48 (16D)	2.3(-6) (AS TI48)	6(51)	0 TO 2(52) 1(52)	OPAQUE	---
TI44 (48YR)	1.9(-6) (AS CA44)	6(51)	0 TO 2(52) 1(52)		
SC44 (3.92HR)				4(-4) (?)	.511(188%) 1.159(100%)
AL26 (7.3(5) YR)	8.6(-5) (AS MG26)	---	7(50) TO 4(51)	2(-9) TO 1(-8)	.511(170%) 1.81(100%)
FE60 CO60	---	4(52)	NONE?		
NA22	---	?	NONE?		

"FLUX" MEANS NUMBER FLUX PER SQUARE CM PER SEC

REFERENCES

Arnett, W. D. 1977a, Ap. J. Suppl. 35, 145.
————————— 1977b, Ap. J. 219, 1008.
————————— 1977c, Ap. J. 218, 815.
Arnett, W. D. and Weiel, J. 1978, Ap. J. Lett., in press.
Clayton, D. D. 1973, Explosive Nucleosynthesis, ed. D. Schramm and W. D. Arnett, (Univ. Texas Press: Austin), p. 263.
————————— 1974, Ap. J. 188, 155.
Van Riper, K. and Arnett, W. D. 1978, submitted for publication.

GAMMA RAY LINES FROM NOVAE

by

James W. Truran
Department of Astronomy, University of Illinois

Sumner G. Starrfield
Department of Physics, Arizona State University

Warren M. Sparks
Goddard Space Flight Center, N.A.S.A.

INTRODUCTION

The past decade has witnessed considerable theoretical activity directed

toward identifying the mechanisms responsible for the eruptions characterizing

the cataclysmic variables. Building upon the defining work by Kraft (see, for

example, Kraft 1963), all such studies are concerned with close binary systems,

the properties of which are dominated by the presence of mass transfer from a

late-type star onto a white dwarf via an accretion disk. Within this frame-

work, theories for the outbursts vary in their identification of the eruption

mechanism with either gravitational or nuclear energy sources. Existing models

for the dwarf novae invoke a dynamical instability in the envelope of the red

star which triggers episodic Roche lobe overflow and a concomitant increase in

the rate of mass transfer (Osaki 1974; Bath, Evans, Papaloizou and Pringle

1974; Gorbatskii 1975); the outbursts are then associated with an increase in

the accretion luminosity liberated in the disk.

In contrast, the most successful theoretical models for common nova events

involve thermonuclear runaways proceeding in accreted hydrogen envelopes on

the white dwarf components of these systems. It is the characteristics of

such runaway events -- which can give rise to detectable gamma ray fluxes --

to which we direct our attention in this paper. Salient features of existing

runaway models are briefly reviewed. Specific predictions concerning gamma

ray fluxes follow.

THE THERMONUCLEAR RUNAWAY MODEL

Continued accretion of hydrogen-rich matter onto the white dwarf component

of a nova binary system must inevitably give rise to the initiation of nuclear

burning. Hydrostatic studies (Giannone and Wiegert 1967; Taam and Faulkner

1975) have demonstrated that envelope masses $\sim 10^{-4}$ - 10^{-3} $M_\odot$ on white dwarfs

of masses $\sim$ 0.5 - 1 $M_\odot$ are sufficient to ensure ignition of the hydrogen fuel.

The runaway lifetimes are of course dependent upon such other factors as the

white dwarf mass and luminosity (Truran et al. 1977). However, given the mass

transfer rates $\sim 10^{-10}$ - 10^{-8} $M_\odot$/yr. characteristic of nova systems, it follows

that runaway conditions can be achieved relatively early in the lifetimes of

these systems.

Hydrodynamic calculations of thermonuclear runaways leading to nova erup-

tions have recently been reviewed by Starrfield, Sparks and Truran (1976). All

studies to date are concerned with hydrogen thermonuclear runaways, the dominant

hydrogen-burning reactions being those involving carbon, nitrogen and oxygen

(CNO) nuclei. We have emphasized the important role played by the concentra-

tions of these nuclear species in defining the characteristics of the runaway.

Substantial enrichments of the envelope matter in CNO nuclei are required if

the runaway is to give rise to a fast-nova-like outburst (Starrfield et al.

1972; 1978); in fact, for some of our models the CNO concentrations approached

50 percent by mass of the ejecta. Heating of the outer regions of the enve-

lope by radiative decay of the positron-unstable isotopes ^{13}N, ^{14}O and ^{15}O

plays a significant role in mass ejection. The required large CNO enrichments

are consistent with abundance determinations for the ejecta of Nova Cygni 1975

(Ferland and Shields 1978). In contrast, thermonuclear runaways proceeding in

matter of solar composition give rise to slow-nova-like outbursts (Prialnik et al. 1978; Sparks et al. 1978). The epoch of thermonuclear burning is rather entended for slow novae, with mass ejection being effected by radiation pressure at the prevailing high luminosities. Again, observational support for this view is provided by the determination that the ejecta of the slow nova HR Del 1967 is solar in composition (Robbins and Sanyal 1978), although the high carbon concentration determined for DQ Her (Williams et al. 1978) presents problems. These considerations are extremely relevant to questions concerning the magnitudes of gamma ray fluxes, as will be shown below.

<div align="center">PREDICTED GAMMA-RAY FLUXES</div>

Within the framework of the thermonuclear runaway theory for the common novae, there arise several possible sources of gamma rays. These include: (1) the 1.275-MeV gamma ray line resulting from the decay of ^{22}Na; (2) annihilation radiation following the positron decay of ^{13}N, ^{14}O and ^{15}O; and (3) gamma ray fluxes which result when an outgoing shock wave (realized in some models) reaches the surface. We note that all of these sources have been identified and discussed previously (Clayton and Hoyle 1974; Brown, Starrfield and Waller 1976). In the following, we briefly review the predicted fluxes from each of these distinct sources in the light of recent calculations of nova explosions.

(1) <u>Gamma rays from ^{22}Na decay</u>. The thermonuclear processing of nova ejecta is expected to give rise to the production of the relatively long lived ^{22}Na. This represents perhaps the most promising avenue for detection of gamma rays from novae. The expected flux of 1.275 MeV gamma rays may generally be written in the form

$$F_{1.275} = 8 \times 10^{-5} \text{ cm}^{-2} \text{ s}^{-1} \left[\frac{(M_e/10^{-4} M_\odot) \cdot e^{-t/3.75 \text{ yr}}}{D^2 \text{(kpc)}} R_{22} \right]$$

where M_e is the mass of the ejecta in solar masses, D is the distance in kilo-parsecs, t is the time following the event in years, and R_{22} is the ratio of the initial ^{22}Na concentration in the ejecta to the solar abundance of ^{22}Ne (2 x 10^{-4} by mass). The crucial parameters to be specified are the mass of the ejecta and the ^{22}Na concentration.

The current observational situation regarding the mass of material expelled in nova events has recently been reviewed by Gallagher and Starrfield (1978). Estimates for individual events can vary widely. They note, for example, that the well studied (slow nova) HR Del remnant has mass determinations 1.8 x 10^{29} g (Anderson and Gallagher 1977), 5 x 10^{29} g (Malakpur 1973), and 2.9 x 10^{30} g (Robbins and Sanyal 1978). Our theoretical studies suggest that the typical mass ejected by fast novae may be somewhat less than that for slow novae, but there certainly exists no observational evidence for systematic correlations between speed class and ejected mass. Our adopted value $\sim 10^{-4}$ $M_\odot$ represents a reasonable estimate in view of current theoretical and observational considerations, although it may ultimately be shown to be somewhat high.

The most substantial uncertainty associated with any prediction of a ^{22}Na gamma-ray flux involves the abundance of ^{22}Na. Significant ^{22}Na production can accompany a hydrogen thermonuclear runaway at sufficiently high temperatures by the reactions

$$^{20}Ne(p,\gamma)^{21}Na(e^+\nu)^{21}Ne(p,\gamma)^{22}Na$$
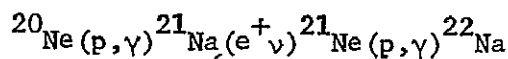
If all initial ^{20}Ne, assumed present in solar proportions ~ 1.5 x 10^{-3} by mass (Cameron 1973), were transformed to ^{22}Na in this manner, the corresponding value of $R_{22} \sim 8.25$. Clayton and Hoyle (1974) utilized this value of R_{22} and an ejected mass 1.7 x 10^{-4} $M_\odot$ to arrive at the very promising estimate

$$F_{1.275} = 1.1 \times 10^{-3} \text{ cm}^{-2} \text{ s}^{-1} \left[\frac{e^{-t/3.75 \text{ yr.}}}{D^2 (\text{kpc})} \right]$$

If we take D = 1.1 kpc for the specific case of Nova Cygni 1975, we arrive at a predicted flux $\sim 8 \times 10^{-4}$ cm^{-2} s^{-1}, which is almost exactly the upper limit quoted by M. Leventhal and C. J. MacCallum in these proceedings. This would suggest that observations of nova remnants with instrumentation of higher sensitivity can provide important information guiding theoretical studies of nova events.

Predictions of the ^{22}Na concentrations formed in nova explosions are extremely model dependent. The lifetime of the slowest reaction in the sequence noted above (the ^{21}Ne(p,γ)^{22}Na reaction), for a proton mass density of 10^4 g cm^{-3}, becomes comparable to the hydrodynamic expansion timescale ~ 10 seconds for a temperature $\gtrsim 200$ million degrees: significant ^{22}Na production cannot occur at much lower temperatures. The required high temperatures are not realized in our recent models relevant to fast nova eruptions (Starrfield, Truran and Sparks 1978), for which lower envelope masses were utilized than in previous work. The peak temperature achieved is dependent upon the initial degree of degeneracy at the base of the hydrogen envelope, which itself is a sensitive function of both the white dwarf mass and the envelope mass. Predictions based upon these models typically give $R_{22} \lesssim 1$. Somewhat higher values may characterize slow novae, which burn at high temperatures on a longer timescale. The choice $R_{22} = 1$, for an ejected mass 10^{-4} M$_\odot$, yields our estimate of the initial 1.275 MeV flux, $F_{1.275} \sim 8 \times 10^{-5}$ cm^{-2} s^{-1} for a nova at a distance of one kpc. We therefore wish to emphasize that even an upper limit on the flux in the range $\sim 10^{-4}$ cm^{-2} s^{-1} can provide useful information concerning the characteristics of nova events. We call attention to the fact that Ferland and Shields (1978) have determined that the ejecta of the fast

nova Nova Cygni 1975 is considerably enriched in neon, a result which is not explained by existing theoretical calculations. Gamma ray observations at increases sensitivities may shed important light on this and related questions.

An additional source of gamma ray lines from novae is provided by the decay of ^{7}Be. Starrfield, Truran, Sparks and Arnould (1978) have estimated that the concentration of ^{7}Li in nova ejecta might be enhanced by a factor ~ 1000 following the decay of ^{7}Be formed in thermonuclear burning sequences. Novae thus represent a potential source of the ^{7}Li in galactic matter. However, the predicted gamma-ray flux for a nova at one kiloparsec is significantly less than 10^{-5} cm^{-2} s^{-1}.

(2) Annihilation radiation. A further prediction of the thermonuclear runaway model of novae is that significant concentrations of the proton-rich positron-unstable isotopes ^{13}N, ^{14}O and ^{15}O will exist in the envelope during and immediately following peak nuclear burning; following decay, the isotopic compositions of carbon and nitrogen can be severely distorted. Clayton and Hoyle (1974) have noted that for fast nova models, for which large enrichments of carbon, nitrogen and oxygen are required in the envelope to ensure mass ejection at high velocities, a substantial gamma ray flux can be generated. The observable lines would be the annihilation radiation following upon positron decay of these isotopes. Basing their estimates upon the published characteristics of model J of Starrfield et al. (1972), they have determined that about 7 cm^{-2} annihilation photons from ^{13}N are to be expected from a nova at one kpc. These would arrive over a ~ 10 minute period approximately half an hour after the peak of the runaway. Given the much larger CNO enrichments characteristic of our current fast nova models, their estimate can be revised to ~ 20 cm^{-2} annihilation photons from this source.

(3) Shock induced gamma ray fluxes. Brown et al. (1976) have calculated

the time and spectral dependence of the gamma rays emitted from the $^{12}C(p,\gamma)$ $^{13}N(p,\gamma)^{14}O$ and $^{13}C(p,\gamma)^{14}N(p,\gamma)^{15}O$ reactions for the specific case of Model 2 of Starrfield, Truran and Sparks (1975). The four lines at 1.944, 4.626, 7.293 and 7.550 MeV are superposed on a Compton continuum, which they determined can be quite accurately described as a power law of spectral index 1.1 between photon energies 7.55 MeV and 10 keV. The peak gamma ray luminosity was found to be approximately 10^{38} erg s^{-1}, falling by two orders of magnitude within the ~ 0.02 seconds required for the shock to break through the surface. The pulse shape was found to be controlled by photon transport properties rather than the photon production rate.

While such a gamma flux may be realized in a particularly violent nova-like runaway event, it is certainly not expected to characterize novae. The model in question produced the strongest shock we have encountered in any of our models and shock ejection of $\sim 10^{29}$ grams moving with speeds up to 90,000 km s^{-1} resulted. This is certainly not typical of novae. Our most promising models for both slow and fast novae involve runaways which do not give rise to shocks.

In conclusion, we emphasize that future gamma ray observations of novae can impose important boundary conditions upon theories of nova outbursts, particularly at a sensitivity of 10^{-5} cm^{-2} s^{-1}. Detection of gamma rays from ^{22}Na decay would constitute a strong confirmation of the thermonuclear runaway model.

References

Anderson, C. M. and Gallagher, J. S. 1977, Publ. Astron. Soc. Pac., 89, 264.

Bath, G. T., Evans, W. D., Papaloizou, J. and Pringle, J. E. 1974, M.N.R.A.S., 169, 447.

Brown, R. T., Starrfield, S. G. and Waller, G. W. 1976, B.A.P.S., 21, 587.

Cameron, A. G. W. 1973, Space Sci. Rev., 15, 121.

Clayton, D. D. and Hoyle, F. 1974, Ap. J. Letters, 187, L101.

Ferland, G. J. and Shields, G. A. 1978, Ap. J., in press.

Gallagher, J. S. and Starrfield, S. G. 1978, Ann. Rev. Astr. Ap., in press.

Giannone, P. and W igert, A. 1967, Zs. f. Astrophys., 67, 41.

Gorbatskii, V. G. 1975, Soviet Astr. Letters, 1, 11.

Kraft, R. P. 1963, Adv. Astron. Astrophys., 2, 43.

Malakpur, I. 1973, Astron. Ap., 28, 393.

Osaki, Y. 1974, Publ. Astron. Soc. Japan, 26, 429.

Prialnik, D., Shara, M. M. and Shaviv, G. 1978, Astron. Astrophys., 62, 339.

Robbins, R. R. and Sanyal, A. 1978, Ap. J., 219, 985.

Sparks, W. M., Starrfield, S. G. and Truran, J. W. 1978, Ap. J., 220, 1063.

Starrfield, S. G., Truran, J. W., Sparks, W. M. and Kutter, G. S. 1972, Ap. J., 176, 169.

Starrfield, S. G., Truran, J. W. and Sparks, W. M. 1975, Ap. J. Letters, 198, L113.

Starrfield, S. G., Sparks, W. M. and Truran, J. W. 1976, In Structure and Evolution of Close Binary Systems. IAU Symp. 73, ed. P. Eggleton, S. Mitton and J. Whelan, p. 155, Dordrecht: Reidel.

Starrfield, S. G., Truran, J. W., Sparks, W. M. and Arnould, M. 1978, Ap. J., 222, 600.

Starrfield, S. G., Truran, J. W. and Sparks, W. M. 1978, Ap. J., in press.

Taam, R. E. and Faulkner, J. 1975, Ap. J., 198, 435.

Truran, J. W., Starrfield, S. G., Strittmatter, P. A., Wyatt, S. P., and Sparks, W. M. 1977, Ap. J., 211, 539.

Williams, R. E., Woolf, N. J., Hege, E. K., Moore, R. L. and Kopriva, D. A. 1978, Ap. J., in press.

GAMMA–RAY LINE EMISSION ABOVE 8 MeV

C. J. Crannell

Laboratory for Astronomy and Solar Physics

NASA–Goddard Space Flight Center

H. Crannell

Department of Physics

The Catholic University of America

ABSTRACT

Gamma-ray line emission above 8 MeV may provide a sensitive diagnostic tool for determining the spectra of energetic nuclei within astrophysical sources. Excited states which can be produced by inelastic scattering, charge exchange, and spallation reactions in the abundant nuclear species have been considered in order to identify nuclear lines which may contribute to the γ-ray spectrum. The cross sections for production of most high-energy states are sparsely measured. Those which have been determined are comparable to the cross section for production of the 15.11-MeV level in ^{12}C, with few exceptions. The branching ratios for γ-ray and particle emission are, however, better known. Of those states considered, 44 have measured branching ratios greater than 40% for emission of a γ-ray with energy above 8 MeV. For twelve more states the branching ratios have not been determined but are expected to be small. The γ-ray emission from other individual nuclear states is not likely to be as great as that for the 15.11-MeV state in ^{12}C.

GAMMA-RAY LINE EMISSION ABOVE 8 MeV

I. INTRODUCTION

While discrete line spectra at x-ray and optical wavelengths give evidence of electromagnetic processes, γ-ray lines give evidence of energetic nuclear interactions. Discrete γ-ray lines can be used to identify the emitting nuclear species and to study the kinetic environment of the γ-ray source. Pairs of γ-ray lines, from the same nuclear species but resulting from the de-excitation of nuclear levels with widely separated thresholds, proved a unique measure of the spectra of high-energy particles within their source.

One of the well-studied γ-ray transitions, which is also one of the strongest, is produced by decay of the 15.11-MeV state in ^{12}C. The flux of 15.11-MeV γ rays relative to the flux of 4.44-MeV γ rays has been calculated from measured cross sections and branching ratios as a function of the spectrum of the exciting protons (Crannell, Ramaty and Crannell 1978). This flux ratio may be as high as 0.03 for a relatively flat proton spectrum. Background due to the γ-ray continuum above 8 MeV was estimated and found to be relatively small, enhancing the observability of high-energy γ-ray lines.

Gamma-ray line emission below 8 MeV has been reviewed recently by Ramaty, Kozlovsky, and Lingenfelter (1978). The work reported here is a search for nuclear processes which may lead to emission of additional γ-ray lines with energies greater than 8 MeV. Since even the 15.11-MeV line will be difficult to detect with present instrumentation, consideration is restricted to those lines which are expected to have a relative intensity of approximately 5% of the 15.11-MeV line. Production of these high-energy lines is limited by the scarcity of high-energy γ-ray transitions associated with the small number of relatively abundant isotopes. In the present work, excited states which can be produced by inelastic scattering, charge exchange, and spallation reactions in the abundant nuclear species have been considered.

II. NUCLEAR STATES WITH GAMMA-RAY TRANSITIONS ABOVE 8 MeV

Three factors are fundamental in determining the relative strengths of nuclear γ-ray lines: the relative abundance of the target nuclei, the cross section for producing the excited state, and the branching ratio for electromagnetic decay of the excited state to a suitable level. For most nuclei, cross sections for production of any of the high energy states are known only at a few selected energies, if at all. Those inelastic scattering cross sections which have been determined are within a factor of three of the cross section for producing the 15.11-MeV state in ^{12}C. Spallation and charge exchange cross sections are generally smaller. For purposes of this investigation, therefore, it is assumed that none of the unknown cross sections are significantly greater than that for

the 15.11-MeV state in ^{12}C, and hence only those nuclei with moderate abundances relative to ^{12}C have been considered. The nuclear species with abundances greater than 1% that of ^{12}C and their relative abundances in the solar photosphere (Trimble 1975) are presented in Table 1.

In order for an excited state to exhibit a significant γ-ray branching ratio, it must be particle stable. Thus all states above the single nucleon threshold have been ignored. States above the alpha-particle threshold also were ignored unless alpha decay is forbidden by isospin considerations. The list of excited states is further restricted to those which can be excited by relatively simple reactions with the abundant nuclei listed in Table 1. These are (p,p'), (p,2p), (p,d), (p,p'α), (p,n), (α,α'), and (α,γ). Hydrogen has no excited nuclear states below the delta resonance at 294 MeV. This resonance does decay by γ-ray emission 0.6% of the time but does not produce line emission because of its intrinsic width of 115 MeV. The excited states in helium are all above the particle disintegration threshold. Furthermore γ-ray transitions from the first three excited states, which lie in the energy range 19 to 23 MeV, are either forbidden or inhibited by the spin and the parity of the nuclear states. In oxygen and iron there are no particle-stable nuclear levels above 8 MeV.

In Table 2 a list of the energies of strong γ-ray transitions together with the excited nuclei and the γ-ray branching ratios (Ajzenberg-Selove 1972, 1975, 1976, 1977; Ajzenberg-Selove and Lauritsen, 1974; Auble, 1977; Endt and Van der Leun 1973; Fiarman and Hanna 1975; Fiarman and

Table 1
Nuclear Species Considered

	ABUNDANCE RELATIVE TO ^{12}C IN %
^{1}H	25 x 10^4
^{4}He	2 x 10^4
^{14}N	30
^{16}O	160
^{20}Ne	10
^{24}Mg	8
^{28}Si	10
^{32}S	4
^{56}Fe	6

Table 2

Gamma-Ray Transitions Above 8 MeV

γ – RAY ENERGY IN MeV	EMITTING NUCLEUS	MEASURED BRANCHING RATIO	STRENGTH FACTOR
8.05	^{27}Al	100	
8.13	^{32}S	84	4
8.29	^{32}S	60	3
8.31	^{15}N	79	
8.32	^{20}Ne	90	10
8.33	^{28}Si	59	6
8.36	^{23}Na	53	
8.43*	^{28}Si	50	6
8.44	^{24}Mg	80	8
8.49	^{28}Si	100	10
8.53*	^{28}Si	50	6
8.56	^{11}B	56	
8.59	^{20}Ne	90	10
8:65	^{23}Na	100	
8.67	^{23}Na	100	
8.69*	^{24}Mg	100	9
8.76*	^{28}Si	100	11
8.89*	^{28}Si	100	11
8.90	^{28}Si	59	6
9.00	^{24}Mg	55	5
9.05	^{15}N	92	
9.15	^{14}Mg	45	4
9.15	^{15}N	100	
9.17*	^{28}Si	85	9
9.36*	^{24}Mg	48	4
9.48	^{28}Si	100	11
9.50	^{28}Si	76	8
9.76	^{15}N	82	
9.83*	^{24}Mg	85	7
9.84*	^{24}Mg	83	7
9.93	^{15}N	78	
9.97	^{24}Mg	90	8
10.07	^{15}N	96	
10.31	^{28}Si	50	6
10.59	^{28}Si	100	11
10.62	^{20}Ne	100	11
10.67*	^{12}C	2	3
10.72	^{28}Si	100	11
10.73	^{24}Mg	40	4
10.90	^{28}Si	68	8
11.23	^{20}Ne	100	11
11.45	^{28}Si	100	11
12.61	^{12}C	2	2
15.11	^{12}C	91	100

Meyerhof, 1973) are presented. For the most part the γ-rays are the result of transitions from an excited nuclear state to the ground state of that nucleus. In a few cases, those marked with an asterisk, the dominant transition is to the first excited state of the nucleus. The last column labeled "strength factor" gives the product of the γ-ray branching ratio with the relative abundance of the target nucleus, normalized to a value of 100 for the 15.11-MeV transition in ^{12}C. If the total (p,p') cross sections were the same for each of these states, the relative intensities of the γ-ray emissions would be directly proportional to the strength factors listed. The cross sections for the spallation reactions, on the other hand, are generally more than an order of magnitude lower than the inelastic scattering cross sections. Strength factors for these transitions would, therefore, be misleading in relationship to the γ-ray flux. For this reason, strength factors for those transitions produced by spallation reactions are not listed in Table 2. It is not expected that the γ-ray flux from any of the transitions listed in Table 2 will exceed 30% of that of the 15.11-MeV line.

Two additional lines, with branching ratios less than 40%, are included in Table 2 because both are produced by transitions in ^{12}C and because their intensities relative to the 15.11-MeV line are well·known. The 15.11-MeV state decays to the 4.44-MeV state, producing a line at 10.67 MeV with a flux 3% that of the 15.11-MeV line. The state at 12.61 MeV, (1$^+$, T=0) is known to decay electromagnetically to the ground state 2% of the time. The cross sections for the production of this state, while not well measured, are a factor of from 2 to 4 times the cross section for the production of the 15.11-MeV state. Thus this state will produce a line with approximately 5% of the strength of the 15.11-MeV line.

III. CONCLUSIONS

A summary, indicating the number of γ-ray transitions by energy and by excited nuclear species, is presented in Table 3. It is readily seen that the total number of lines is a decreasing function of energy, with most of the transitions having energies less than 10 MeV. The density of possible γ-ray lines in the energy interval 8 to 10 MeV, all with similar strength factors, will increase the difficulty of resolving and identifying the individual lines. Accurate predictions of the relative strengths of these lines will require a much better knowledge of the important cross sections. The large number of γ-ray emitting levels will certainly make a significant contribution to the continuum between 8 and 10 MeV. Other possible sources of γ-ray line emission at energies characterizing the nuclear binding energy, 8 MeV, are reactions involving thermal neutron capture. These (n,γ) reactions have not been considered in this work, but are known to be powerful diagnostics in remote sensing (Trombka et al., this symposium).

Table 3
Number of γ-Ray Lines Above 8 MeV

EXCITED NUCLEUS	PRODUCTION REACTIONS	8-9 MeV	9-10 MeV	10-11 MeV	11-12 MeV	12-13 MeV	>13 MeV
^{11}B	^{12}C(p,2p)	1					
^{12}C	^{12}C(p,p') ^{16}O(p,p'α)			1*		1	1
^{15}N	^{16}O(p,2p)	1	4				
^{20}Ne	^{20}Ne(p,p')	2*		1*(1)	1	(2)	
^{23}Na	^{24}Mg(p,2p)	3(1)				.	
^{24}Mg	^{24}Mg(p,p')	1,1*	4,2*(1)	1			
^{27}Al	^{28}Si(p,2p)	1(6)					
^{28}Si	^{28}Si(p,p')	2,5*	2,1*(1)	4	1		
^{32}S	^{32}S(p,p')	2			.		
TOTALS		19(7)	13(2)	8(1)	2	1(2)	1

In Table 3, the asterisks designate the numbers of lines in each interval which result from a transition to an excited state rather than to the ground state. The parenthesis designate the numbers of possible additional lines based on excited states for which the γ-ray branching ratios have not been measured.

The only known γ-ray line above 13 MeV is the well resolved and isolated transition due to the 15.11-MeV state in ^{12}C. The Giant Dipole Resonance (GDR) states in all nuclear species considered here lie above 15 MeV. While preliminary measurements indicated the γ-ray flux due to the GDR in ^{12}C might be significant, further measurements have shown this not to be the case (Lapides et al., this symposium).

Because of its relative strength and its isolation, the 15.11-MeV line from ^{12}C remains the best candidate for detection above an energy of 8 MeV. Other high-energy states are expected to be more difficult to detect. When positive detection of any of these states is achieved, interpretation in an astrophysical context will require more accurate and detailed knowledge of the production cross sections.

REFERENCES

Ajzenberg-Selove, F. 1972 Nucl. Phys. A190, 1.

Ajzenberg-Selove, F. 1975 Nucl. Phys. A248, 1.

Ajzenberg-Selove, F. 1976 Nucl. Phys. A268, 1.

Ajzenberg-Selove, F. 1977 Nucl. Phys. A281, 1.

Ajzenberg-Selove, F., and Lauritsen, T. 1974 Nucl. Phys. A227, 1.

Auble, R. L. 1977 Nucl. Data Sheets 20, 253.

Crannell, C. J., Ramaty, R., and Crannell, H. 1977 Proc. 12th ESLAB Symposium, 213.

Endt, P. M., and Van der Leun, C. 1973 Nucl. Phys. A214, 1.

Fiarman, S., and Hanna, S. S. 1975 Nucl. Phys. A251, 1.

Fiarman, S., and Meyerhof, W. E. 1973 Nucl. Phys. A206, 1.

Lapides, J. R., Crannell, C. J., Crannell, H., Hornyak, W. F., Seltzer, S. M., Trombka, J. I., and Wall, N. S. 1978 this Volume, p. 502.

Ramaty, R., Kozlovsky, B., and Lingenfelter, R. E. 1978, to be published.

Trimble, V. 1978 Rev. Mod. Phys. 47, 887.

Trombka, J. I., Crannell, C. J., Evans, L. E., Bielefeld, M. J., and Metzger, A. E. 1978 this Volume, p. 97.

IV. CYCLOTRON LINE EMISSION

D20-93

CYCLOTRON LINES FROM HER X-1 N78-31991

J. Trümper

Max-Planck-Institut für Physik und Astrophysik
Institut für extraterrestrische Physik
8046 Garching, West Germany

1. Introduction

Cyclotron lines from accreting neutron stars are interesting for
a number of reasons.

First of all, their detection provides a unique method of determining
neutron star magnetic field strengths. An accurate knowledge of
these fields is important not only in the context of stellar
magnetism in general and with respect to neutron star field origin
and decay. It is also clear that the interaction of neutron stars
with the accretion disks or accretion winds as well as the flow of
accreted material towards the stellar surface is largely controlled
by the neutron star magnetic fields.

Moreover, cyclotron line spectroscopy may become an important tool
for the diagnostics of the X-ray emitting hot plasma. In particular,
cyclotron line widths, equivalent line widths and line intensity
ratios are of interest in this context.

In this talk I want to summarize the present observational evidence.
In doing so, I can concentrate on the work done in Germany since
almost all the other observers (or non-observers) will talk after
me. I also want to discuss briefly what we can learn from the
experimental data without going too much into theoretical problems,
some of which will be dealt with by subsequent speakers.

2. Observations

The German hard X-ray balloon programme is a collaborative effort
of the Astronomisches Institut of the University of Tübingen (E.
Kendziorra and R. Staubert) and MPI Garching (W. Pietsch, C. Reppin,

J. Trümper, W. Voges). In total we had 4 balloon flights during
which pointed observations of Her X-1 were performed for typically
a few hours each.

The first of these flights on May 3, 1976 (5 days after turn-on
of the 35 day cycle, binary phase 0.77) lead to the discovery
of a strong spectral feature at 58 keV in the pulsed flux
Trümper et al., 1977) exceeding the steep continuum spectrum
by~5 standard deviations (Fig. 1). This line feature contained
~ 4% of the X-ray luminosity and it was immediately clear that
it could not be produced by atomic or nuclear processes. On
the other hand, a magnetic origin of the feature seemed to us
not only possible, but also very plausible. Interpreting the
58 keV feature as first harmonic cyclotron emission line

$$h\nu = \frac{eH}{mc} = 11.6 \text{ keV } \frac{H \text{ (Gauss)}}{10^{12}}$$

the corresponding magnetic field strength is 5.3×10^{12} G,
uncorrected for gravitational red-shift.

The immediate question was whether it would be possible to detect
higher harmonic cyclotron features which (in nonrelativistic
approximation) should appear at multiples of the fundamental
frequency. A relativistic treatment yields

$$E_n = mc^2 \left[\left\{ 1 + \left(\frac{p_z}{mc}\right)^2 + (2n + s + 1)\frac{H}{H_{cr}} \right\}^{1/2} - 1 \right]$$

where p_z is the electron momentum in magnetic field direction and
$H_{cr} = 44.14 \times 10^{12}$ Gauss.

There was a possibility to tackle this question using the data
of the May 3, 1976 flight: During the ~ 4 hours of observation
the Her X-1 total and pulsed flux underwent a decrease by a factor
of ~ 2.5 seen independently in both telescopes which were looking
parallel. Since the background remained almost constant,
the signal-to-noise ratio was highest at the beginning and we
took the first 45 minutes in order to search for the second
harmonic. Fig. 2 shows the raw data spectra for the pulsed flux

(POP = Pulse minus Off Pulse) and for the pulse phase (POS = Pulse minus Off Source). The corresponding signals at the position of the second harmonic are at 2.2 and 3.3 σ (Trümper et al., 1978). Since the signals appear at the predicted energies (110 keV) the corresponding confidence levels are 97% and 99.9%. Using the POS spectrum we derived the primary photon spectrum correcting for atmospheric absorption and detection efficiency/resolution. This spectrum is shown in Fig. 3 (Trümper et al., 1978).

At this point we felt that the most urgent problem was to improve the statistical quality of the data. Therefore we built a much larger (factor 6.5) Phoswich detector of ~ 800 cm^2 collecting area (Reppin et al., 1978). Fig. 4 depicts its characteristics.

The energy resolution of this detector is ~ 21% at 60 keV. It is superior to present day satellite instruments not only in terms of area and resolution, but also with respect to background since the activation of detector materials plays no role for balloon instruments.

This detector has been flown successfully three times from Palestine, Texas, in September/October 1977 and a number of sources were looked at (Her X-1, AM Her, DQ Her, Cyg X-1, Cyg X-2, Cyg X-3, Sco X-1, Aqu X-1, Coma Cluster, Virgo Cluster). The flights covered three interesting phases of the Her X-1 35-day cycle:

    Sep 3, 1977   on-state   (phase[+] 0.12)
    Sep 20, 1977   short on-state (phase 0.61)
    Oct 18, 1977   off-state   (phase 0.41)

Her X-1 was detected at all phases at energies > 20 keV (Voges et al., 1978) and in the following I want to present a few pre-liminary and unpublished data from the on-state flight on Sep 3.

Fig. 5. shows the corresponding light curves for different energy bands in comparison with the results of May 3, 1976. The improvement in statistical quality is obvious. The pulsed count rate spectrum derived from this data is depicted in Fig. 6. Around 55 to 65 keV a clear excess is present. This spectral excess is a persistent feature during the whole observation time and for all four detector modules having 200 cm^2 area each. There are two properties

---

[+]measured with respect to "turn-on".

of this feature which are indicative of a line. (1) Around 45 keV
a notch appears in most of the spectra, although it is not that
pronounced as in the 1976 data. (2) Above ~ 65 keV there is a
steep flank. Both attributes make it very difficult to fit a
second continuum spectrum (thermal bremsstrahlung, blackbody
or power law) through the data. If we fit a thermal bremsstrahlung
+ Gaussian line to the data correcting at the same time for
atmospheric transmission and detection effects, we get the primary
spectrum shown in Fig. 7. The corresponding spectral parameters
are

$$\text{line flux} \quad 1.7 \times 10^{-3} \text{ cm}^{-2} \text{ sec}$$
$$\text{line energy} \quad 55.4 \text{ keV}$$
$$\text{line width} \quad 11.5 \text{ keV (FWHM)}$$

We note two major differences if we compare the new data with the
May 3, 1976 results:

(1) The continuum flux and the line flux are a factor $\geqslant$ 2 lower
than at the beginning of the May 3, 1976 flight; we note that the
Her X-1 intensity at 20-50 keV was roughly the same on Sep 3,
1977 and at the end of the May 3, 1976 flight.

(2). We are unable to detect the second harmonic in the Sep 3,
1977 data.

3. Discussion

Summarizing, our new data provide strong support for the existence
of a spectral line feature at 54 to 58 keV, while the existence
of the second harmonic remains unconfirmed. Since it is very
difficult to explain the observed feature by a second continuum
spectrum or by atomic and nuclear processes, an interpretation
in terms of a cyclotron line seems the most likely one. In
principle, there are two different possibilities

1. There may be a cyclotron _emission_ line at ~ 58 keV, and a
    possible second one at 110 keV.

2. There may be a cyclotron _absorption_ feature at ~ 42 keV, and
    a possible second one at ~ 80 keV. In particular, there may

be a rather broad absorption feature between the spectral break (25 keV) and ~ 40 keV.

On the basis of the experimental results we cannot distinguish between both alternatives (Trümper et al., 1978). This statement is based on the fact that a continuum + absorption line fit to our May 3, 1976 data gave an equally good χ^2. We have not yet examined the new (1977) data in this respect.

The possible occurrence of cyclotron emission lines has been suggested by Gnedin et al. (1974) and Basko et al. (1975), while an interpretation of the observed spectral feature in terms of cyclotron absorption was first pointed out by Daugherty at al. (1977).

The answer to the question whether the cyclotron resonance manifests itself in absorption or emission will depend on the detailed distribution of density and temperature in the skin layers of the emitting plasma. It is clear that the region emitting hard X-rays is rather small and close to the neutron stellar surface such that the cyclotron resonance corresponds to the surface magnetic field and is rather narrow.

However, we have no self-consistent picture yet which describes how the kinetic energy of the infalling material is dissipated, how the radiative energy transfer in the plasma looks like and how the radiation pressure affects the plasma flow.

Our final conclusions have to await the solution of these problems.

Finally, I would like to illustrate what we can learn from the observational data in the case of the emission line interpretation. According to Gnedin et al. (1974) and Basko et al. (1975), cyclotron emission lines should reach the blackbody intensity while the bremsstrahlung continuum should remain well below it. We then can use the intensity ratio of the first and second harmonic in order to derive the blackbody temperature and find kT ~ 20 keV. Another information can be derived from the observed line widths: Our data yield $\frac{\Delta E}{E}$ ~ 0.2 FWHM for the in-

trinsic line width. This width may be due to different mechanisms of which magnetic broadening, Doppler broadening and self-absorption broadening are supposed to be the most important.

In the case of magnetic inhomogeneities over the emission region we find $\frac{\Delta H}{H} = \frac{\Delta E}{E} = .2$ and for a dipole field ($H \sim r^{-3}$) it follows $\Delta r/r \leqslant .07$, and with $r \sim 10$ km, $\Delta r \leqslant 700$ km. This figure is entirely consistent with estimates of the radiation surface A from the observed luminosity and temperature (A $\ll$ 1 km^2).

Another broadening mechanism is Doppler broadening which is anisotropic since the thermal agitation of electrons in a strong magnetic field is only parallel to the field lines:

$$\frac{\Delta E}{E}\bigg|_{Doppler} = \sqrt{8\ln 2 \frac{kT}{mc^2}} \cos \theta \ [FWHM] \leqslant .2$$

where θ is the angle between the line of sight and the magnetic field lines. Using kT = 20 keV we find $\theta \geqslant 70^{\circ}$. This means that during pulse maximum (where we derived our spectrum) the polar angle of the line of sight is large, corresponding to a fan beam.

It has been shown by Meszaros (1977) that self-absorption broadening is also $\sim \cos \theta$ and imposes even stronger restrictions on viewing angles.

References

Basko, M.M., and Sunyaev, R.A., 1975, Astr. Ap., 42, 311.

Daugherty, J.K., and Ventura, J., 1977, preprint.

Gnedin, Yu.N., and Sunyaev, R.A., 1974, Astr. Ap., 36, 379.

Meszaros, P., 1977, preprint.

Reppin, C., Pietsch, W., Trümper, J., Voges, W., Kendziorra, E., and Staubert, R., 1978, Proceedings of the Symposium on European Sounding Rocket, Balloon and Related Research, Ajaccio, April 1978.

Trümper, J., Pietsch, W., Reppin, C., Sacco, B., Kendziorra, E., and Staubert, R., 1977, Texas Symposium on Relativistic Astrophysics (Boston, 1976), Ann. NY Acad. Sci., in press, (Paper I).

Trümper, J., Pietsch, W., Reppin, C., Voges, W., Staubert, R., and Kendziorra, E., 1978, Astrophys. J., 219, L105.

Voges, W., and Pietsch, W., 1978, IAU Circular No. 3184, March 7.

Figure Captions

Fig. 1   First pulsed spectrum derived from the May 3, 1976
        balloon flight (Trümper et al., 1977).

Fig. 2   Count rate spectra derived from the beginning of the
        May 3, 1976 balloon observation, where the source inten-
        sity was highest (Trümper et al., 1978).

Fig. 3   Deconvoluted spectrum of Her X-1 derived from the POS-
        spectrum shown in Fig. 2 (Trümper et al., 1978).

Fig. 4   Cross section of the large MPI/AIT Phoswich detector
        flown in September/October 1977 (Reppin et al., 1978).

Fig. 5   Comparison of light curves obtained during the May 3, 1976
        and September 3, 1977 balloon flights.

Fig. 6   Pulsed count rate spectrum obtained during the Sep 3, 1977
        flight. The error bars are at 1σ, the upper limits are
        2 σ. The dotted line represents a thermal bremsstrahlung
        + Gaussian line fit through the data.

Fig. 7   Deconvoluted pulsed spectrum of Her X-1 derived from the
        count rate spectrum shown in Fig. 6.

Fig. 1

HER X-1
P-OP SPECTRUM
MAY 3, 1976
MPI / AIT

a

HER X-1
P-OS SPECTRUM
MAY 3, 1976
MPI / AIT

b

CYG X-1
MAY 3, 1976

MPI / AIT

c

COUNTS·/cm² sec KEV

PHOTON ENERGY IN KEV

Fig. 2
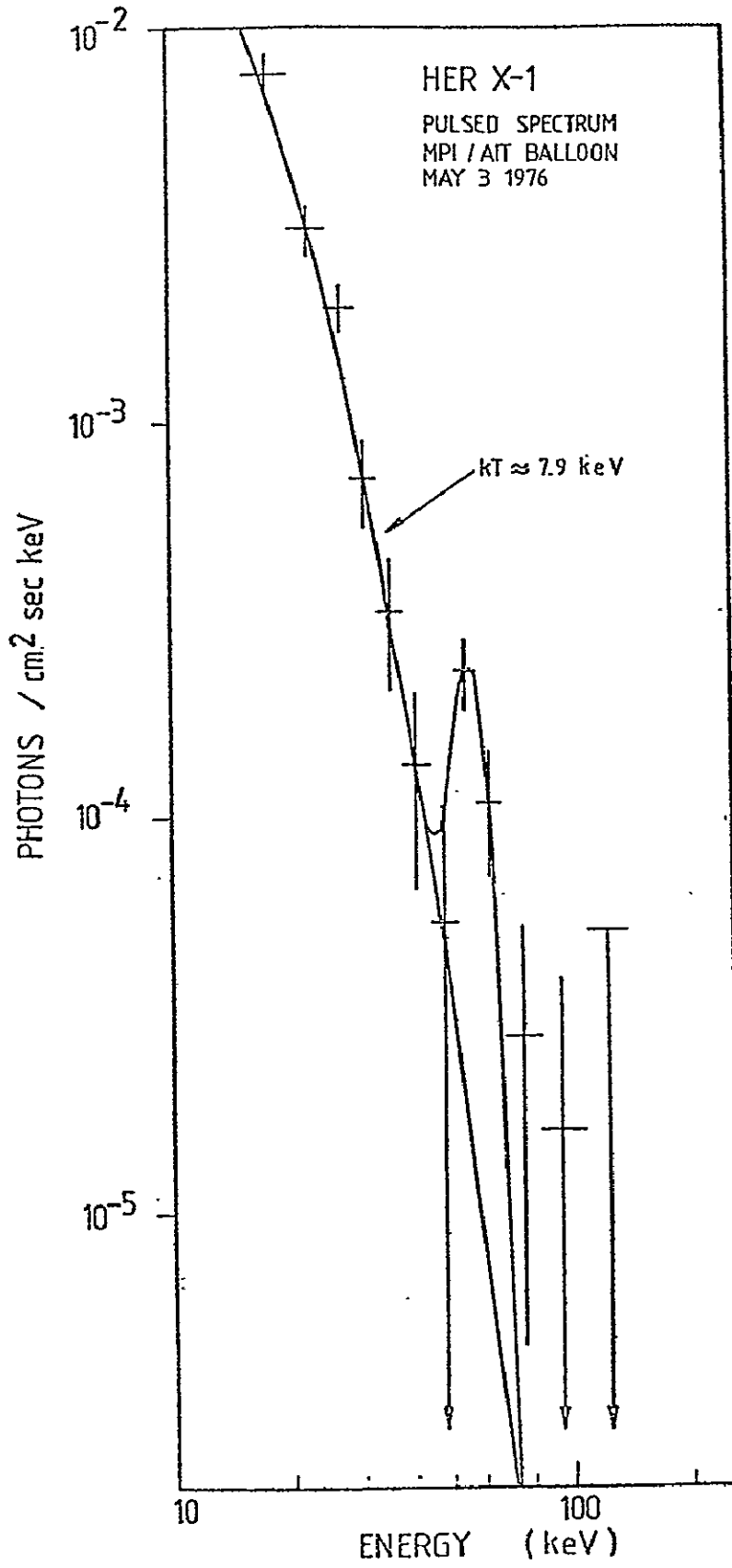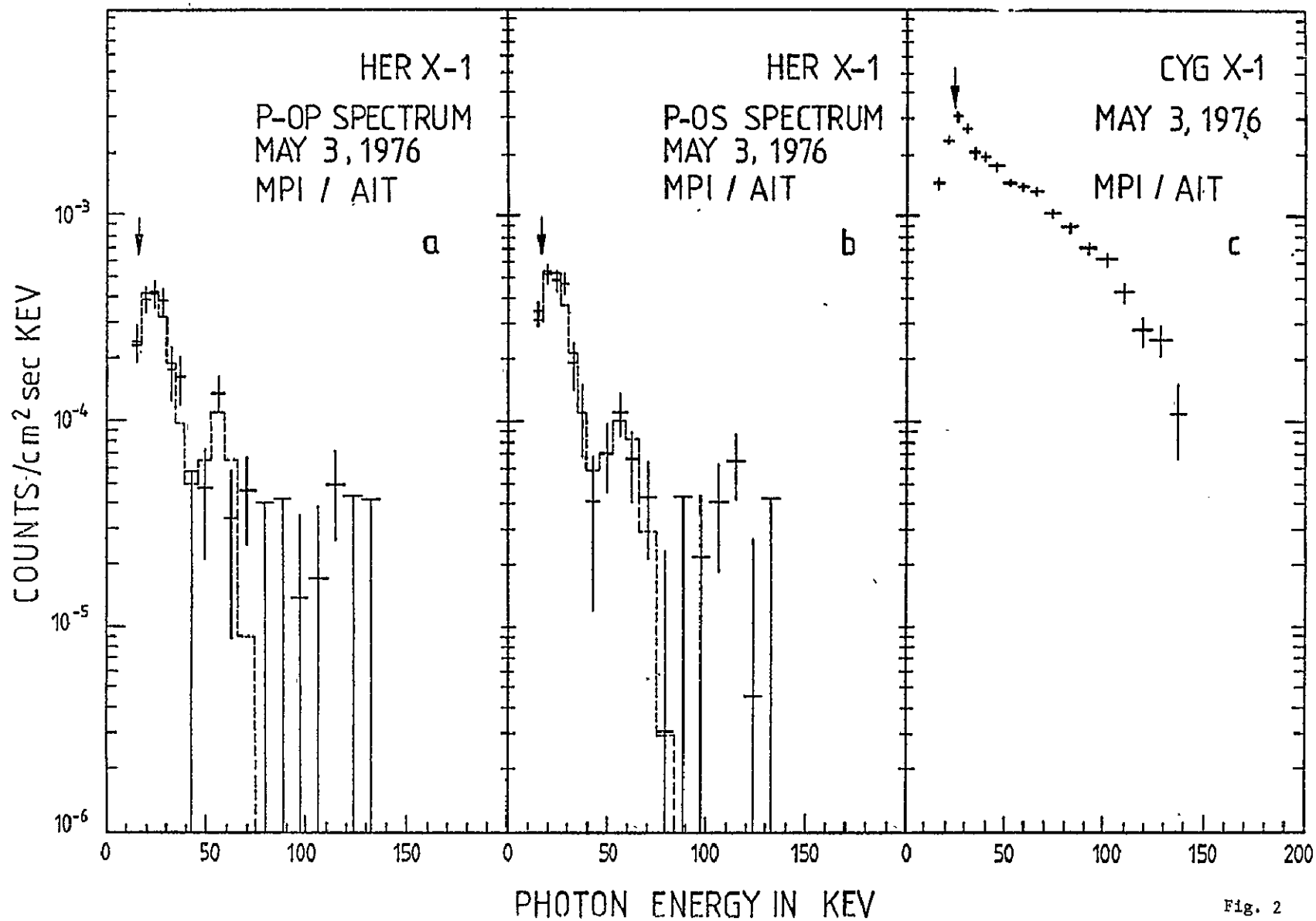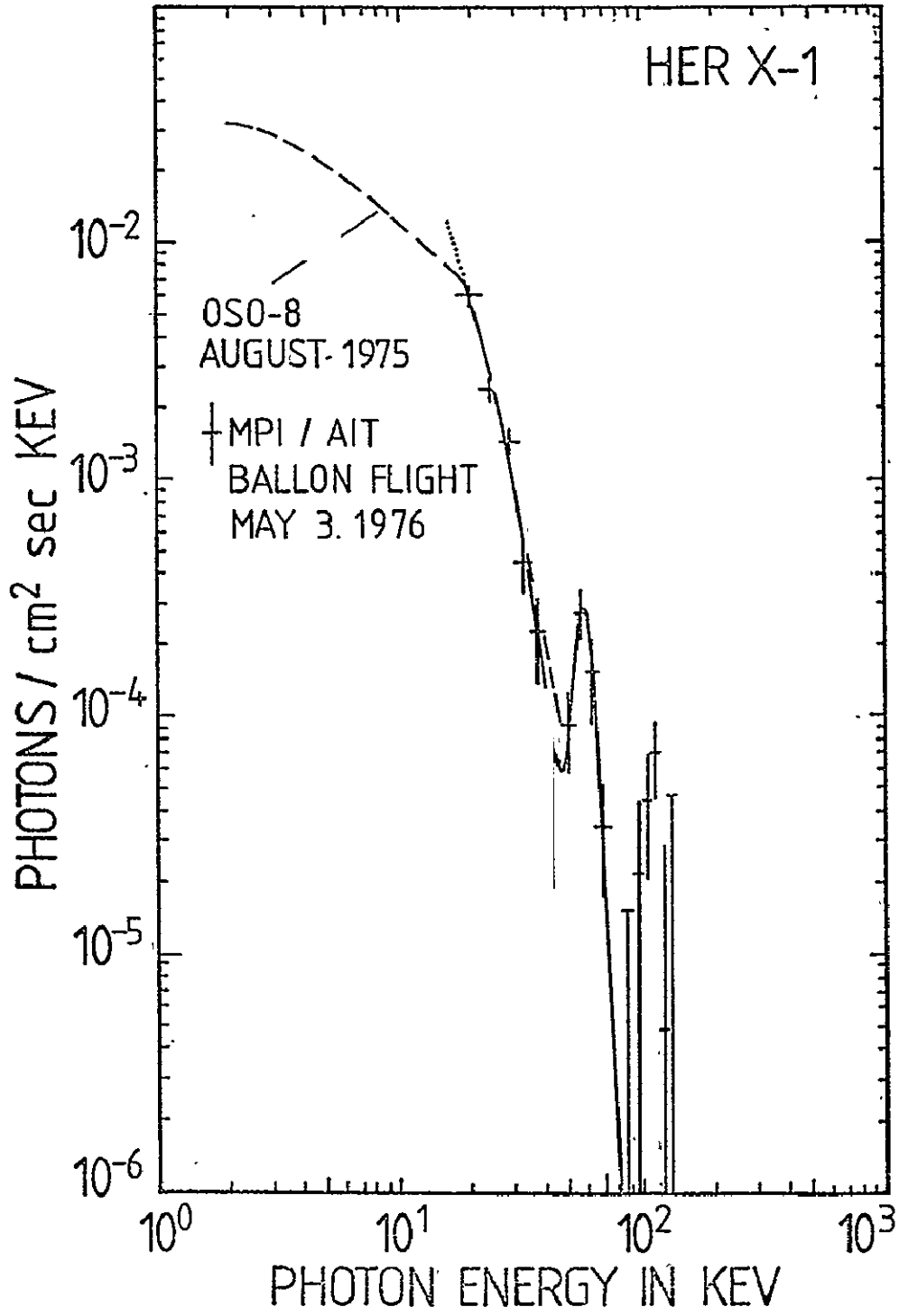
Fig. 3

X-RAY BALLOON EXPERIMENT

PLASTIC-ANTICOINCI-
DENCE·

PASSIVE SHIELDING
(3MM LEAD, 2MM TINN
1MM BRASS)

GRADED SHIELD
SLAT COLLIMATOR
$3° \times 3°$

Cd^{109} CALIBRATION
UNITS

4-PHOSWICH DETECTORS·
$14,4 \times 14,4 \, CM^2$
0,3 CM Na I (Tl)
5 CM Cs I (Tl)

5"-PHOTO TUBE FOR
PHOSWICH DETECTOR

WEIGHT : 160 kg
EFFECTIVE AREA :
730 CM^2
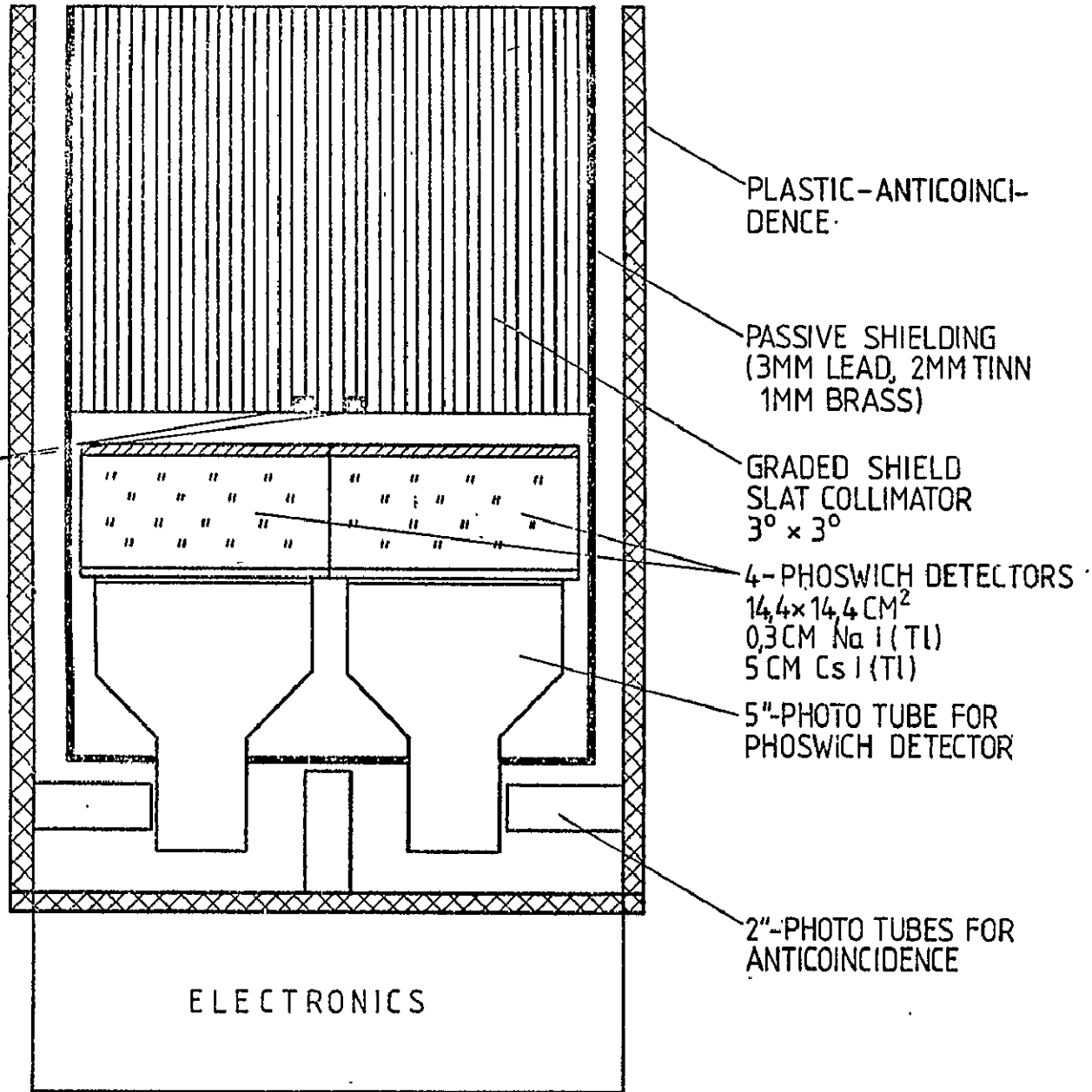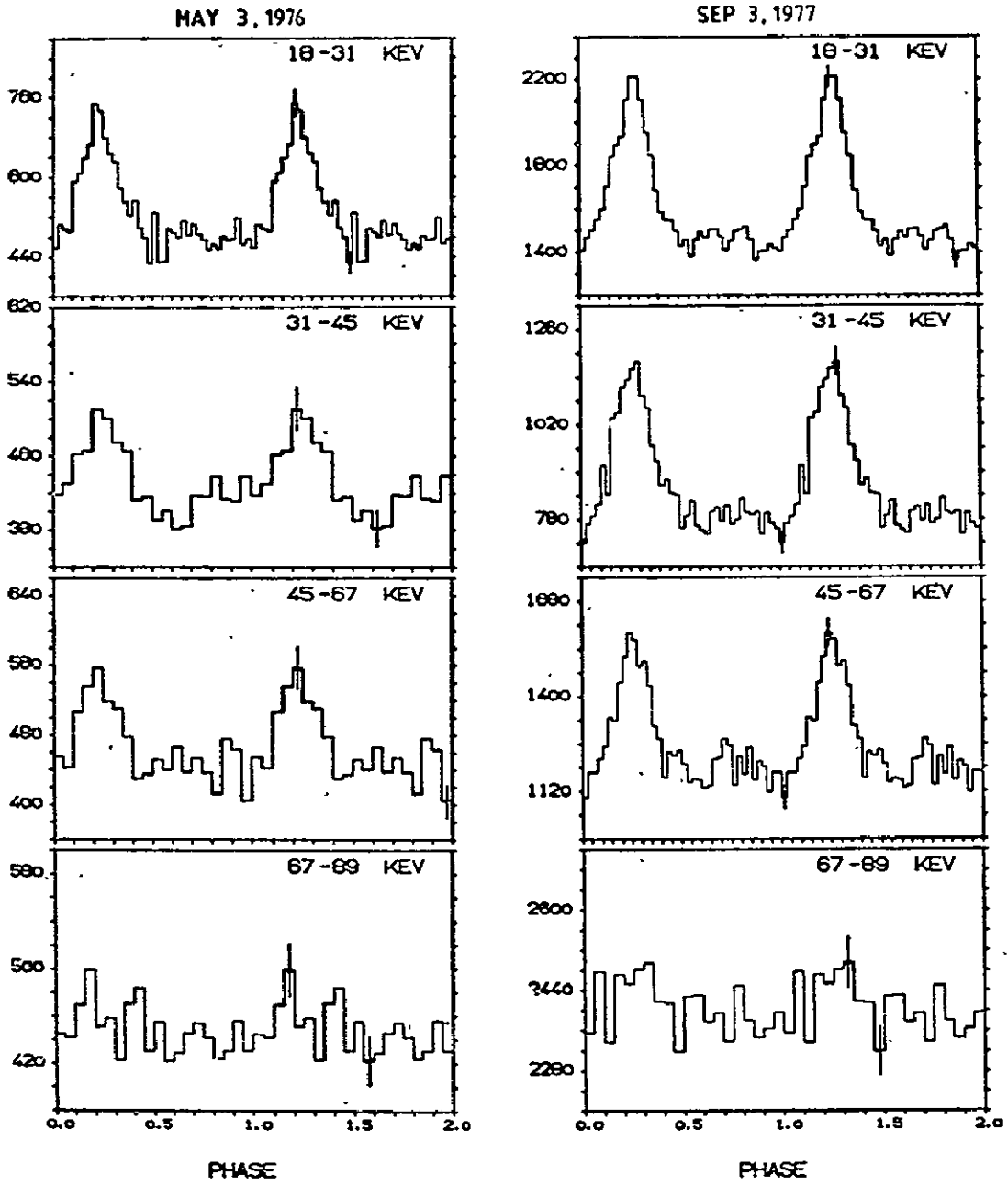
2"-PHOTO TUBES FOR
ANTICOINCIDENCE

ELECTRONICS

10 CM

342

Fig. 4

HER X-1

MAY 3, 1976   SEP 3, 1977

Fig. 5

HER X-1

MPI / AIT BALLOON
SEP 3 1977
PULSED SPECTRUM
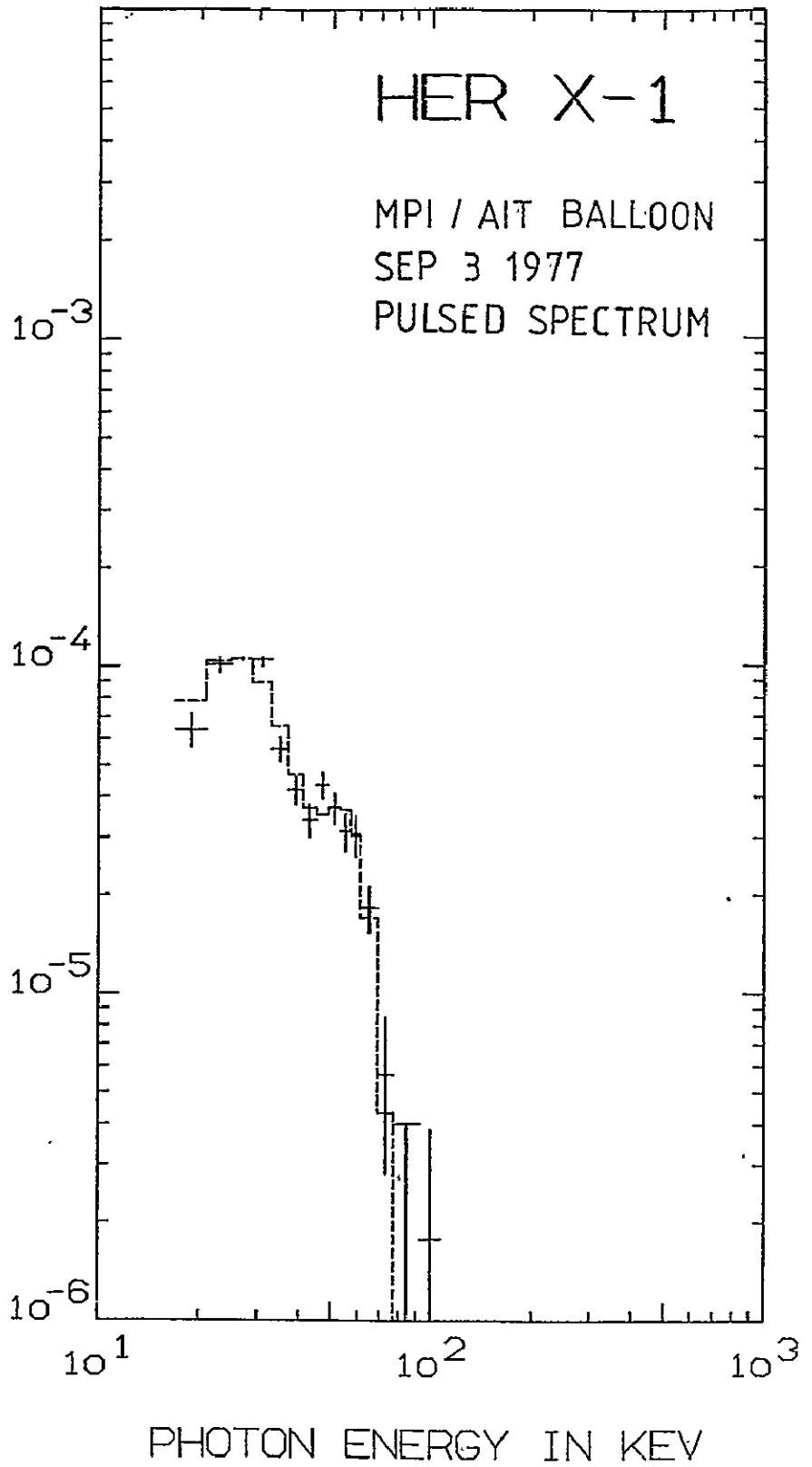
Fig. 6
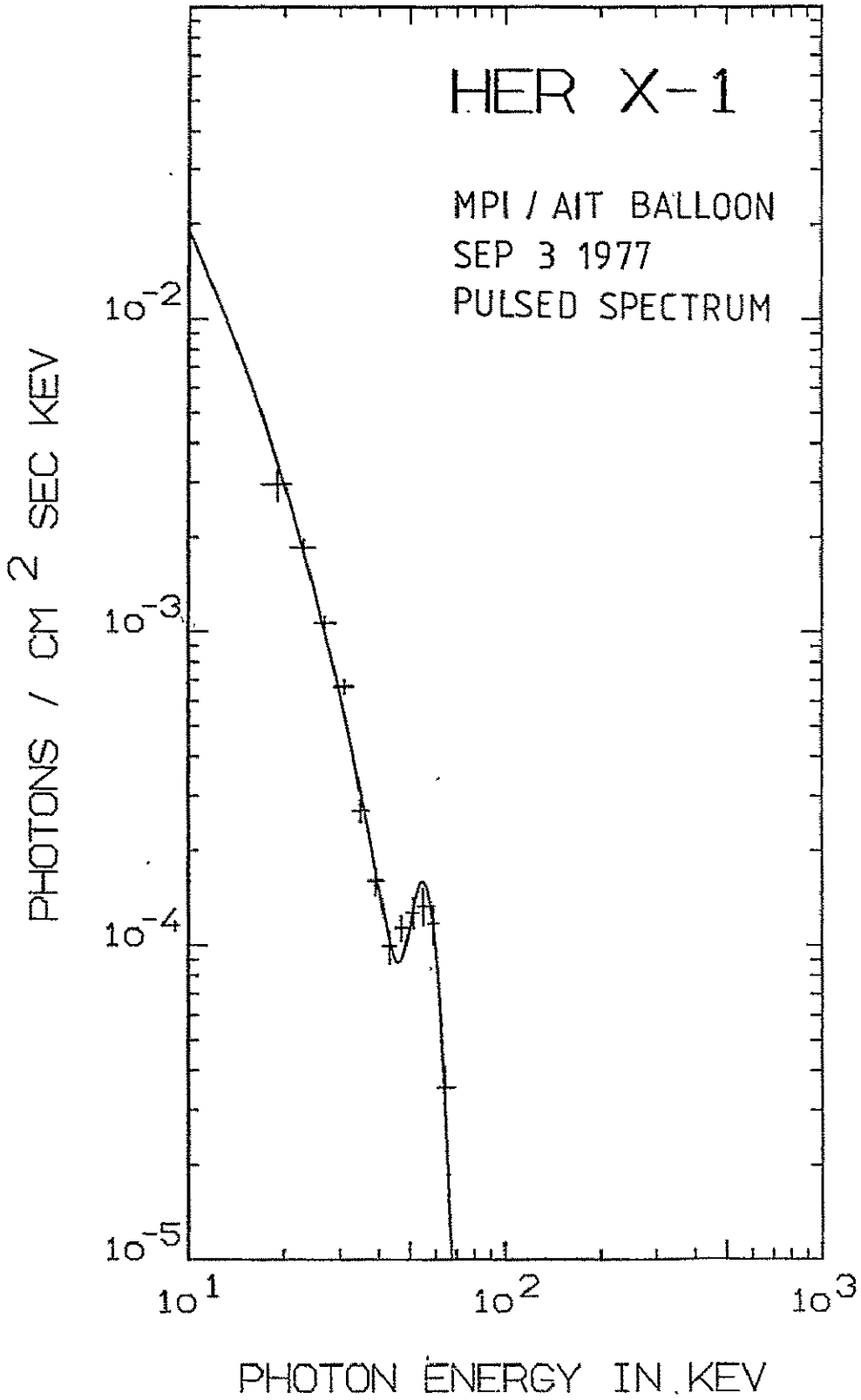
Fig. 7

CONFIDENCE ABOUT LINE FEATURES

IN HER X1 SPECTRUM

Ph. DUROUCHOUX, D. BOCLET, R. ROCCHIA

Centre d'Etudes Nucléaires de Saclay

(France)

347

ABSTRACT

A balloon borne X-ray telescope was flown from Aire-sur-l'Adour (France) on May 14 - 15, 1975 to search for pulsation of the X-ray source HER X1.

We monitored the source for about 3500 s with a relative exposure larger than 0.75 and noticed the detection of features at 57.5 ± 7.5 keV and 135 ± 10 keV in the spectrum.

Nevertheless, we carefully reanalysed our data in terms of possibility of gain shift encoder.

We show, in the present paper, the very strong dependence of the line features on such a shift.

I - INTRODUCTION

When we decided the present experiment, only low energies data about HER X1 pulsation were obtained (Tananbaum et al.[1], Giacconi et al.[2], Doxsey et al.[3], Holt et al.[4]).

They gave information about light curve and percentage of pulsation up to 35 keV.

So, the Saclay X-ray spectroscopy experiment (Source) was aimed to the observation of HER in the high X-rays energy range.

Recently, Trümper et al.[5] and Kenziorra et al.[6] reported the detection of two lines in the HER X1 spectrum, respectively at 58 keV and 110 keV.

Coe et al.[7] claimed also the detection of an excess in the flux of HER X1 at 64 ± 6 keV, consistent with the Trümper' results.

This paper presents the temporal and spectroscopic results of HER X1 in 15 - 150 keV energy range.

II - INSTRUMENTATION

a) Detector and shield (fig. 1)

The detector consists of a 229 mm diameter NaI(Tl) crystal, 25 mm thick, covered by a beryllium window 1 mm thick. A passive collimator (Pb, Cd) gives to the telescope a field of view of 10° in the NS direction, and 8° in the EW direction at F.W.H.M.

The telescope is surrounded by an active guard scintillators (plastic) viewed by four photomultiplier tubes, the outputs of which are electronically connected in anticoincidence with the central detector's output.

A passive shield (Fe, Cd, Pb) reduce the background due to neutron activations. The energy resolution (F.W.H.M.) of the NaI detector is 25% at 59.5 keV as shown on fig. 2.

b) Electronics

The pulse given by the crystal (corresponding to the photon energy loss) which satisfies the conditions imposed by the event selection logic, is amplified, shaped, and sent into a 128 channel ADC's. The linearity of the whole electronic system is checked before and after the flight.

The total number of bits (of 120 μs) allocated to each event is 13, including start and stop flags.

Four temporary buffers, with an interrogative frequency ajustable from 1/16 s to 1 s used to monitor the count rates of the central crystal and the surrounding plastics. The time resolution is 1 ms.

c) <u>Gondola</u>

The gondola consists of a duralumin cubic frame, 120 cm on a side, where the spectrometer, electronics, stabilization telemetry and telecommand are attached ; the entire system represents a payload of 200 kg.

d) <u>Azimuth servosystem</u>

Azimuth stabilization locks the payload with respect to the Earth magnetic field by mean of a magnetometer which drives the suspension bearing.

The accuracy is ± 0.5 degree.

Corrections are performed at frequent intervals according to the local magnetic declination along the balloon trajectory.

Moreover the angle between the payload and the magnetic North can be modified by the rotation of the magnetometer operated by telecommand.

e) <u>Telemetry-Telecommand</u>

Information is sent to the ground via a FM/FM telemetry using 8 IRIG standard channels. Telecommand allows the transmission to the gondola of 9 different orders used for scientific servitudes.

f) <u>Pressure sensors</u>

Two sensors are mounted on board (Albin-Springer type, modified CEA) indicating the residual atmospheric pressure during the ascent of the balloon with a precision of ± 2 mb and the pressure at the floating altitude with a precision of 0.1 mb.

g) Analog multiplexer

A housekeeping analog multiplexer gives the possibility to transmit at regular intervals of 30 seconds, the housekeeping parameters.

Among them, we can mention :

. low voltage monitoring

.. attitude parameters

. temperature of electronics

. test of telecommand orders concerning the speed and the

. direction of the rotation of the spectrometer

h) Inflight calibration

In an effort to better determine the energy of any spectral features observed during the flight, a X-ray calibration source was flown.

Upon radio command a 10 μc ^{241}Am radioactive source was removed from its 5 mm-thick lead container for about 1 minute.

III - THE EXPERIMENT

Experiment was carried out at Aire-sur-l'Adour, France, longitude 1° East, latitude 43°43' North.

The observations were conducted on May 14 and 15, 1975 (JD 2442547). The balloon reached its ceiling altitude at 23.43 UT

and remained at atmospheric depths between 2.4 and 2.7 mbars until the flight was command terminated at 05.16 UT.

The inflight calibration gives a maximum of the radioactive 59.5 keV peak at the 25th channel (2.43 keV/channel) at the departure of gondola and the 24th channel (2.53 keV/channel) at the end of the flight as mentioned on the table below.

Inflight calibration time	Max peak channel	Energy/channel	Shift in gain %
22.00 UT	25	2.43	0
22.55 UT	24.5	2.48	2
02.27 UT	24	2.53	4
03.25 UT	24	2.53	4
04.22 UT	24	2.53	4
04.59 UT	24	2.53	4

The part of the flight used as background reference was 23.25 UT to 00.25 UT whereas HER X1 was monitored from 01.32 UT to 02.26 UT.

The pointing errors during the period are believed to be less than 1° from the nominal aiming point, and the mean efficiency of the collimator over this period of tracking of HER X1 was 78.3% as shown on fig. 3.

The launching date (JD 2442547) was choosen taking into account the predicted eclipses of HER X1 in May 75 due to orbital period (fig.4) i. e. at the beginning of the 11 day "on" cycle ($\emptyset = 0.9$) between orbital phases 0.39 and 0.43.

IV - RESULTS AND DISCUSSION

a) Temporal analysis

Fig. 5 shows χ^2 values by degree of freedom for 3434 s data of HER X1 versus analysis period. We adopted for best apparent period P = 1.237508 s.

Table 1 summarizes χ^2 values by degree of freedom for different energy ranges.

For 23 degrees of freedom, χ^2 value corresponding to 1% reliability level is 1.81/d.o.f., so, only results up to 30 keV are statistically significant.

Fig. 6 is an histogram of the HER X1 light curve folded modulo 1.237508 s pulse period.

The profile exhibits a double peaks structure : a main pulse with a statistical significance of 3.28 standard deviation and an inter-pulse at 1.17 standard deviation. F.W.H.M. of the two pulses are about 60° and separation 150°. The main pulse is apparently more intense than the interpulse which seems to exhibit much steeper a spectrum. Let us call $\emptyset_s$ the phase of the maximum of the main pulse :

$$\phi_s = 1975 \text{ May } 15, \ 017 \ 653512 \pm 0.000000578$$

To estimate the pulsed fraction, we determine the continuum level as the mean value of the lowest six bins in the 12 bins light curve, i.e. half a period. We calculated that pulsed X-ray radiation fraction is $54 \pm 12\%$ in $12.5 - 25$ keV energy range.

Fig. 7 and 8 show light curves in $20 - 30$ keV and $30 - 37.5$ keV energy range.

Comparing to low energies values (80% Tananbaum et al.[1], 60% Doxsey et al.[3], 66% Holt et al.[4], 55% Pravdo et al.[7]) and similar energies (Kendziorra et al.[6]: $58 \pm 8\%$ in the $18 - 31$ keV interval) one can give a mean value of 60% for the pulsed fraction of HER X1 in $2 - 25$ keV energy range taking into account statistical errors (fig. 9).

b) Spectral analysis

We have plotted on fig. 10 the raw spectrum of background just corrected for dead time, and the total spectrum for corresponding time observation when HER X1 is in the field of view of the detector.

One can easily see a significant difference (HER X1 + BKG) -(BKG) at energies lower than 35 keV, and also near 55 and 135 keV.

On the same figure we have plotted this difference in terms of standard deviations versus energy. Two significant lines at 57.5 keV and 137.5 keV are detected respectively at 7σ, 2.95σ and our data are consistent with the feature given by Trümper et al.[5] which has been tentatively interpreted as representing the first and second cyclotron harmonic in a neutron star magnetic field of about 5.10^{12} Gauss.

As shown in fig. 11, we observe a lack of detection of pulsation in the 52.5 - 67.5 keV range and 127.5 - 147.5 keV range, corresponding to the first and second harmonic. This result is in conflict with Kendziorra et al.[6] who detected a pulsed fraction of 51 ± 14% in the 31 - 88 keV range, but which could be due to the highest signal to noise ratio of their experiment.

In fig. 12 are plotted χ^2 values versus energy. It does not show any evidence for pulsation in the X-ray flux above 40 keV.

Following a remark made by Dennis[8], we tried to determine the influence of a possible drift in gain in the electronics on the line features. Fig. 13 shows the variation of the standard deviation versus energy for three different background spectrum derived from the measured one, and whose the calibration has been slightly drifted. This operation was conducted in computer and the shifts were respectively 0.2 and 0.4 channel on the calibration reference.

Its corresponds to 0.8% and 1.6% in the gain variation.

One can see that a low gain change is sufficient to smooth the bumps and decrease the confidence in the line observation.

The incertitude due to statistics in our inflight periodical calibration ($\sim 1.6\%$) does not allow us to be conclusive about line detection whose identification is doubtful in our data.

To obtain decisive line features in no-pulsed X-ray emission of binary systems, an observation with an improved energy resolution (with solid state detectors) seems to be highly desirable.

FIGURE CAPTIONS

Fig. 1 Diagram of the NaI (Tl) scintillation detector system

Fig. 2 Energy resolution of the NaI detector

Fig. 3 Efficiency of collimator (5° x 10° F. W. H. M.) used for the observation of HER X1

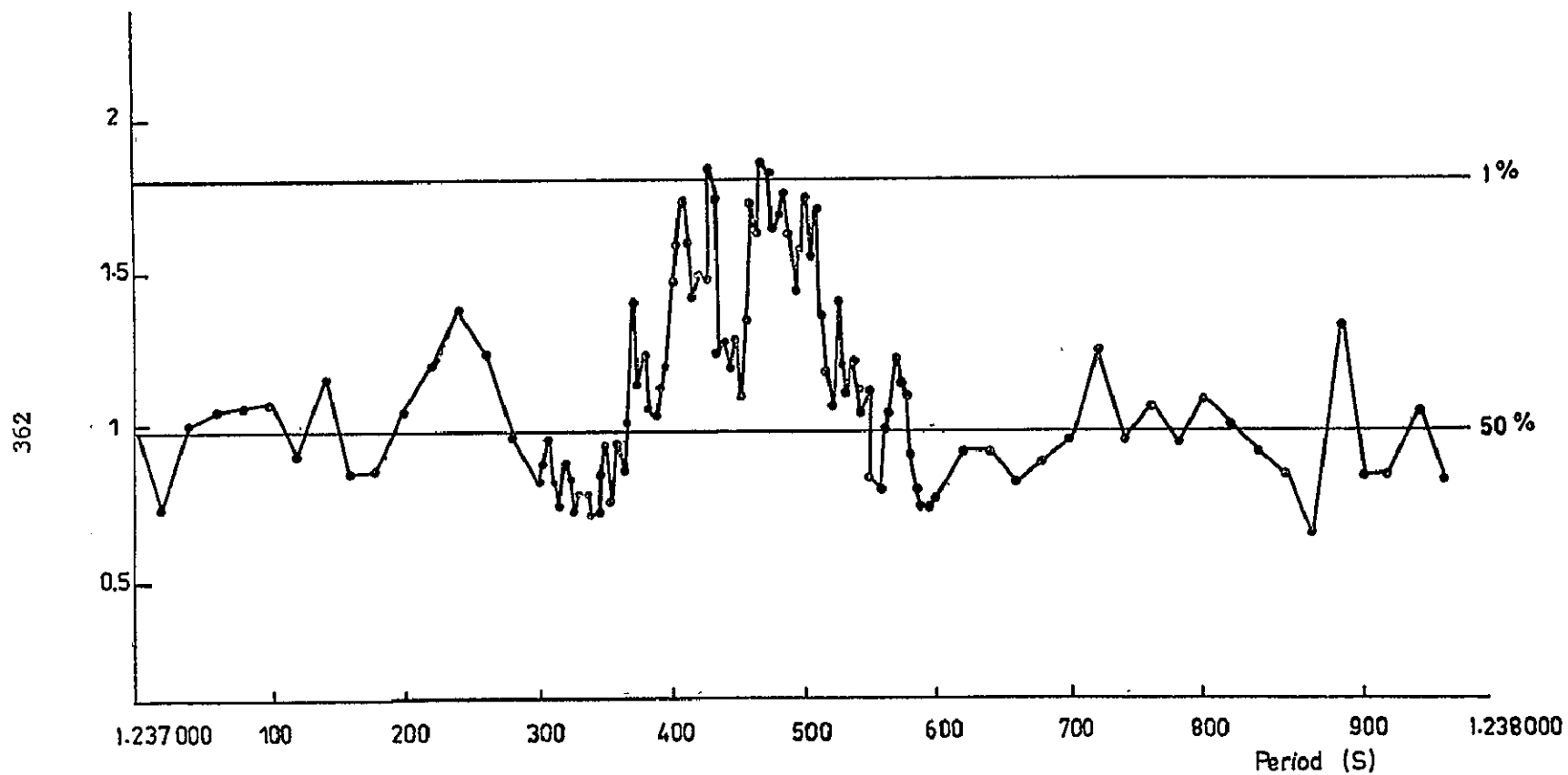Fig. 4 The predicted eclipses of HER X1 in May 1975 due to the orbital period

Fig. 5 χ^2 values for 3434 s data of HER X1 versus analysis period (23 d. o. f.)

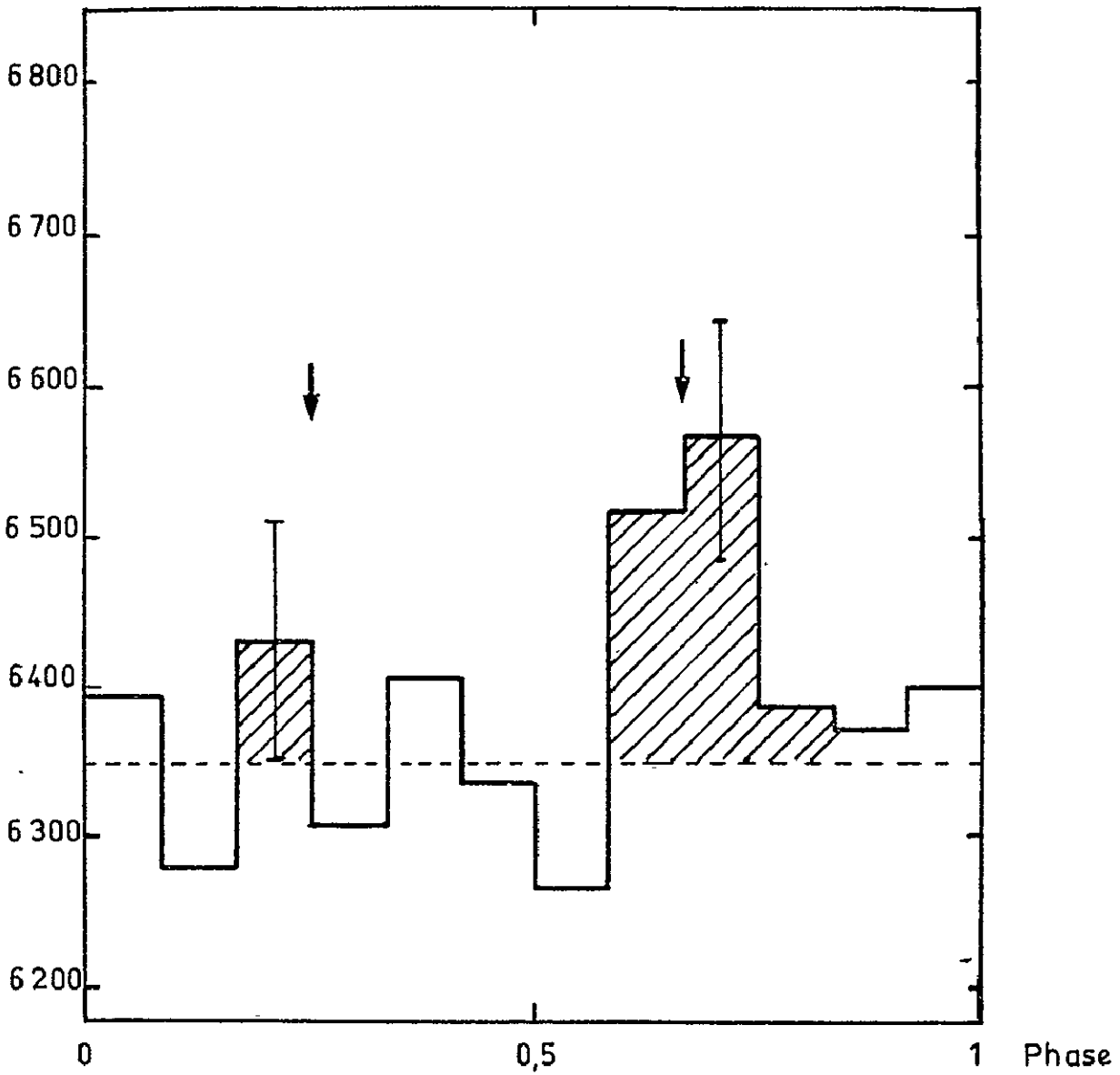Fig. 6 HER X1 light curve P = 1.237508 s (3434 s of analysis) 15 - 25 keV energy range
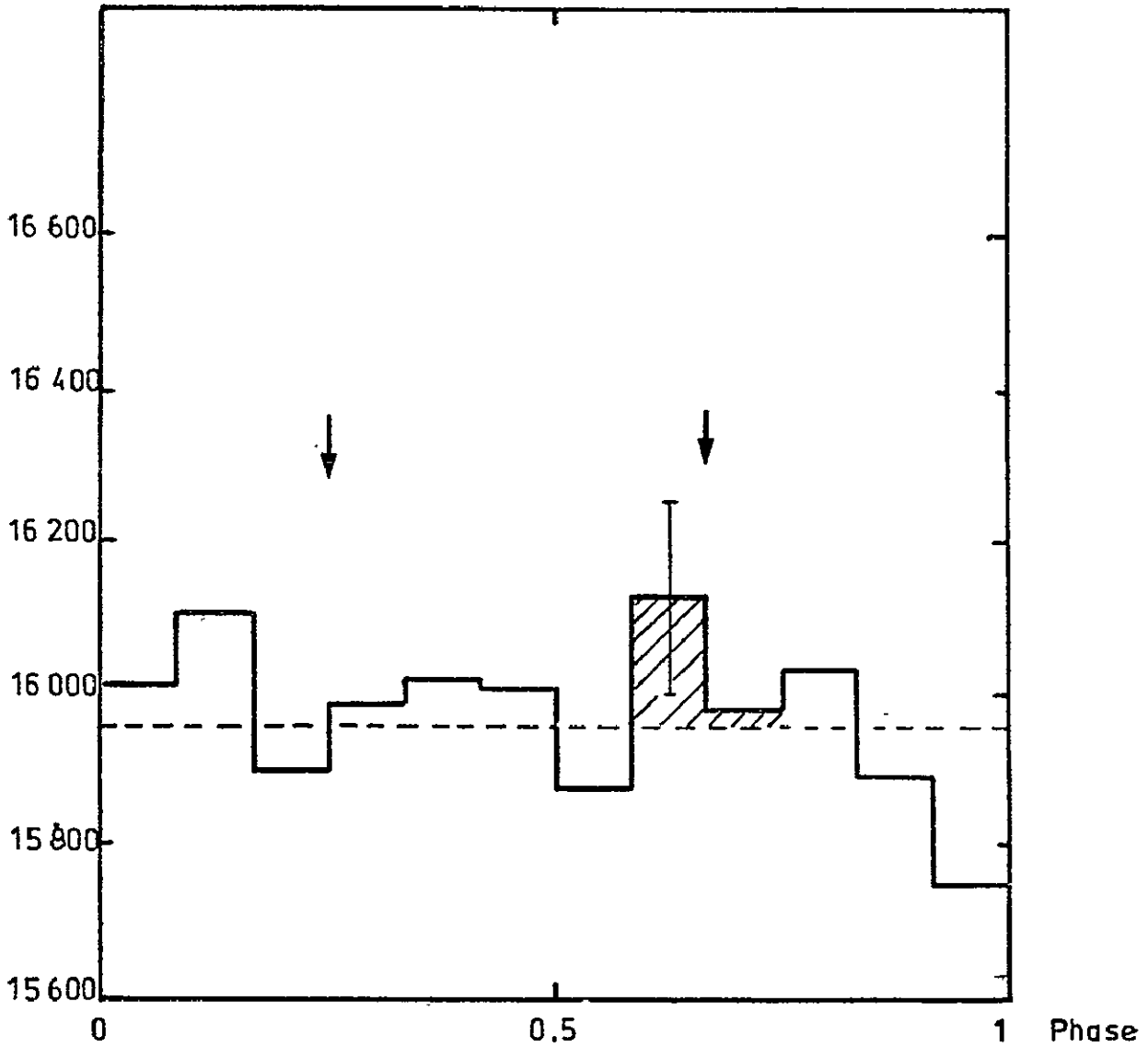
Fig. 7 HER X1 light curve 20 - 30 keV energy range

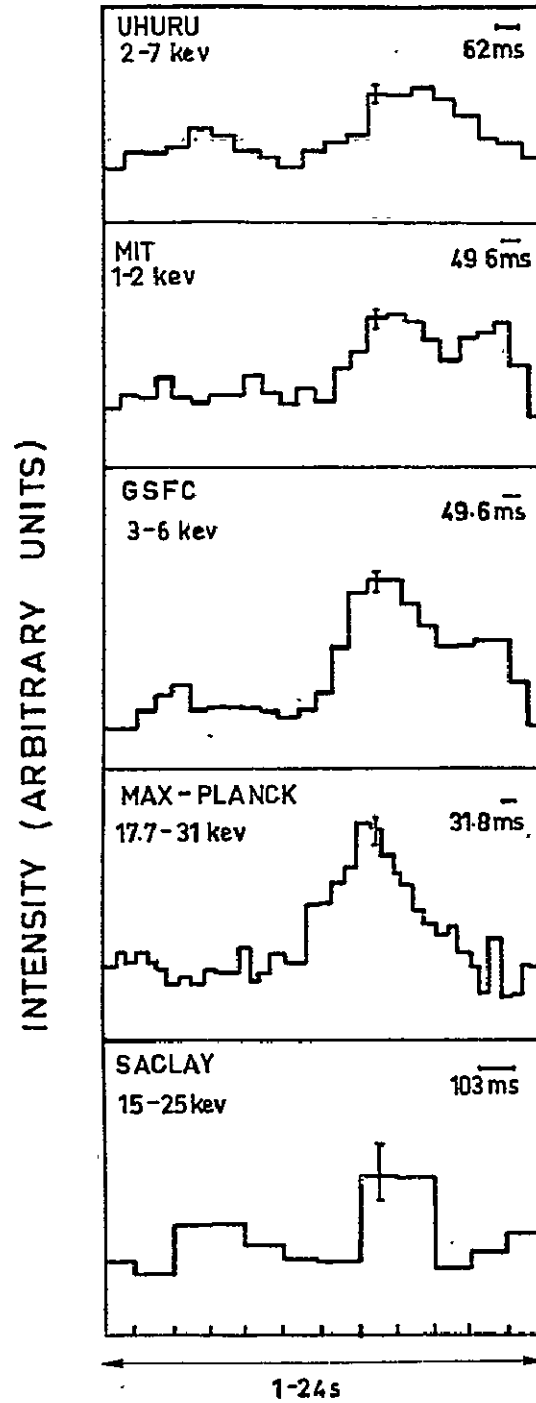Fig. 8 HER X1 light curve 30 - 37.5 keV energy range

Fig. 9 The X-ray light curve of HER X1 observed by different groups

Fig. 10 HER X1 and background spectra. Difference in terms of standard deviations versus energy

Fig. 11 The X-ray light curve of HER X1 shown in different energy ranges
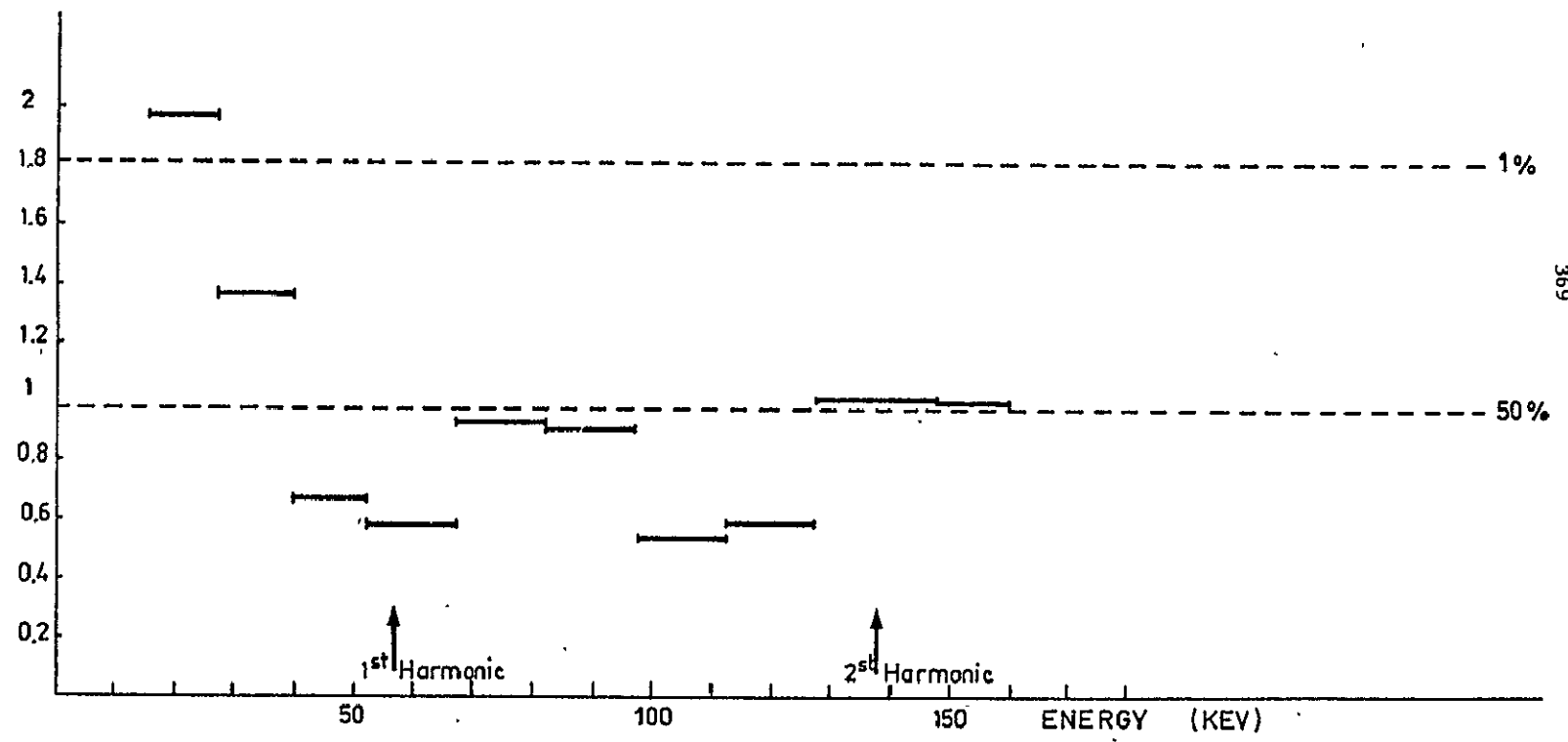
Fig. 12 HER X1 pulsation represented in terms of χ^2 versus energy

Fig. 13 HER X1 contribution versus energy for three possible calibration shifts (0%, 0.8%, 1.6%)

REFERENCES

1. Tananbaum, H., Kellog, E., Gursky, H., Murray, S., Schreir, E., and Giacconi, R. Ap. J. (Letters) <u>165</u>, L 37 (1971).

2. Giacconi, R., Gursky, H., Kellog, E., Levinson, R., Schreir, E., Tananbaum, H. Ap. J. (Letters) <u>184</u>, L 227 (1973).

3. Doxsey, R., Bradt, H. V., Levine, A., Murphy, S., Rappaport, S., Spada, G. Ap. J. (Letters) <u>182</u>, L 25 (1973).

4. Holt, S., Boldt, E., Rotschild, R., Saba, J., Serlemitsos, P. Ap. J. (Letters) <u>190</u>, L 109 (1974).

5. Trümper, J., Pietsch, W., Reppin, C., Voges, W., Staubert, R., Kendziorra, E. Ap. J. (Letters) <u>219</u>, L 105 (1978)

6. Kenziorra, E., Staubert, R., Pietsch, W., Reppin, G., Sacco, B., Trümper, J. Ap. J. (Letters) <u>217</u>, L 93 (1977).

7. Coe, M., Engel, A., Quenby, J., Dyer, C. Nature <u>268</u>, 508 (1977).

8. Dennis, B. private communication, March 24, 1978.

PHOTOMULTIPLIER RTC
X P 1010

PLASTIC
SCINTILLATOR

LIGHT PIPE

PHOTOMULTIPLIER
TYPE 8054

ACTIVE SHIELD :
PLASTIC SCINTILLATOR

20

LIGHT PIPE

9" dia x 1" thick NaI (Tl) CRYSTAL

1mm thick
BERYLLIUM
WINDOW

19

100

Cd
Pb
STAINLESS
STEEL
PASSIVE
SHIELD

SHOCK
ABSORBER

APERTURE
10° x 20°
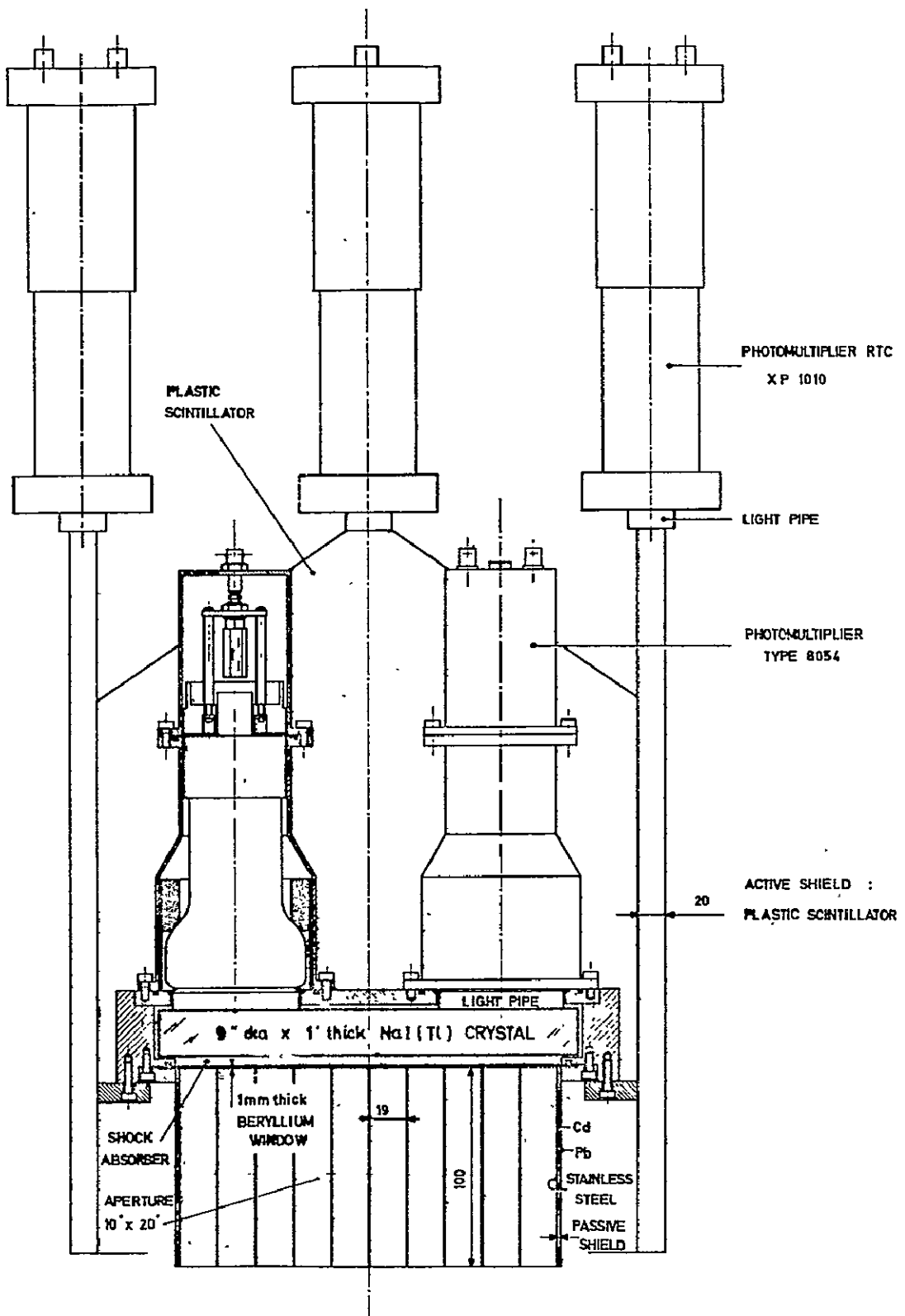
Fig. 1 _ LOW ENERGY DETECTOR (12.5 _ 150 keV)
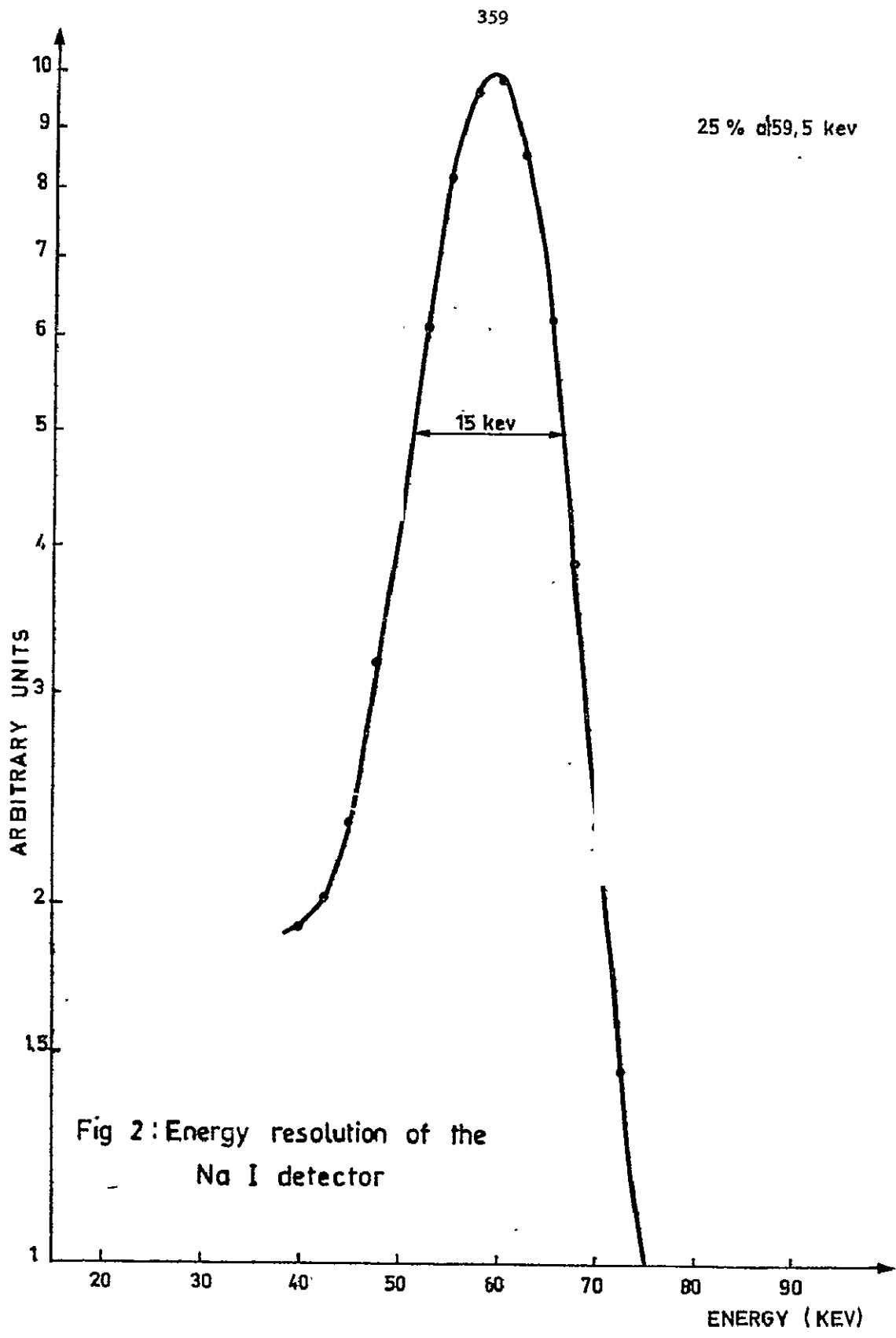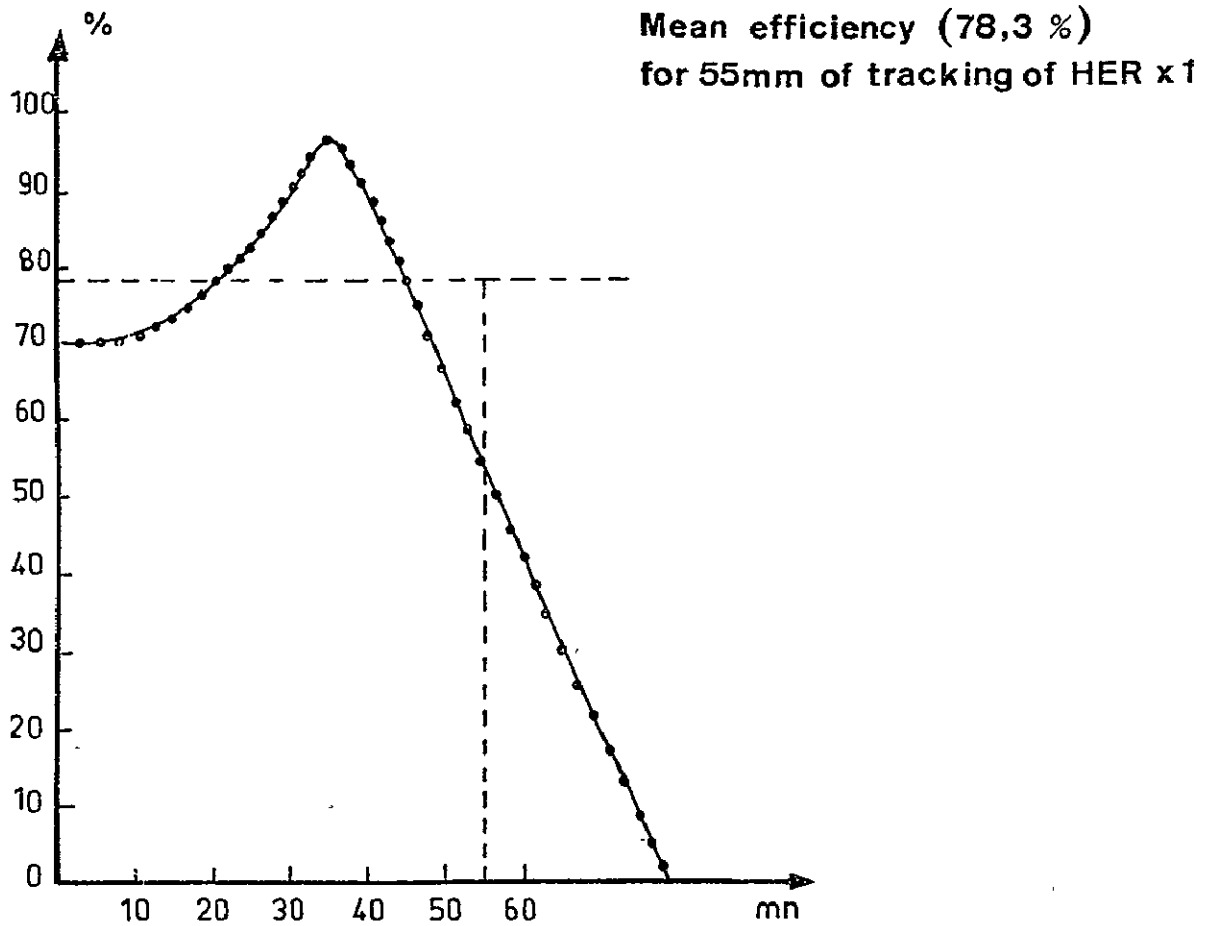
Fig 2 : Energy resolution of the
Na I detector

25 % at 59,5 kev

15 kev

Fig 3 ; Efficiency of collimator (5°x10° FWHM) used for the observation of HER x1
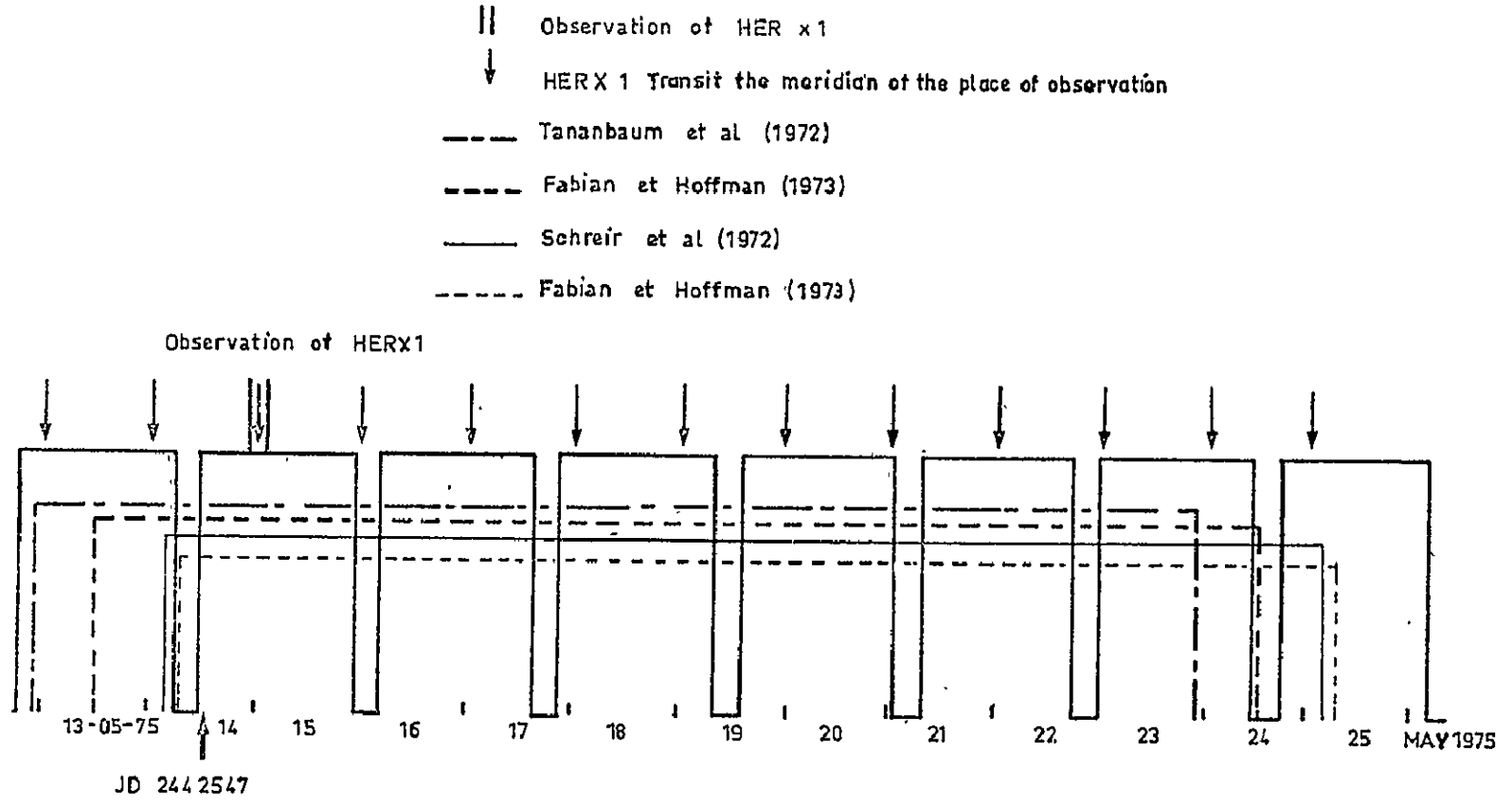
Fig 4 : The Predicted eclipses of HER x 1 in MAY 1975 due to orbital period

Fig 5; X^2 Values for 3434 s data of HER X1 versus analysis period (23 d.o.f.)
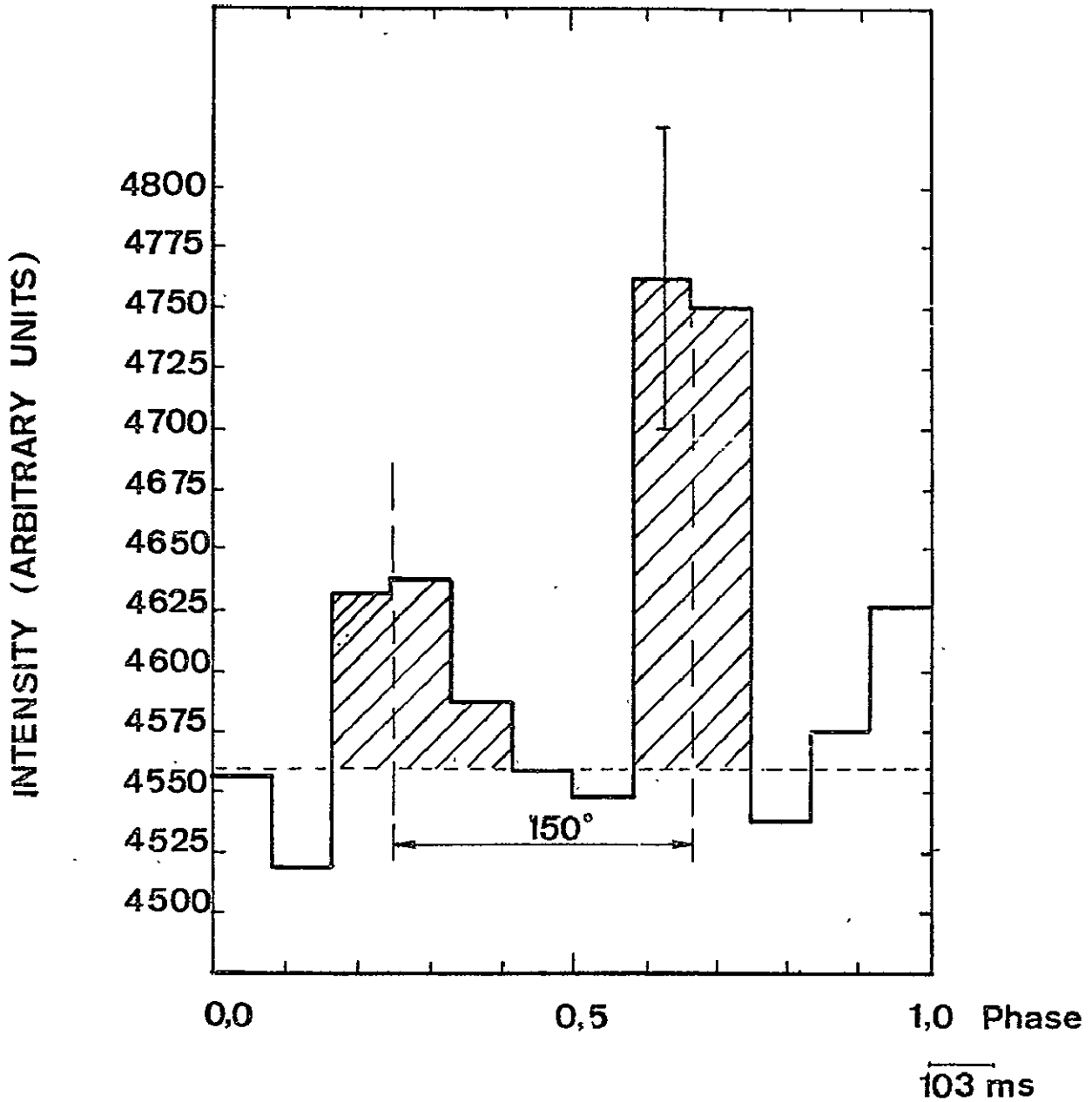
Fig 6 ;HER X1   light curve P=1.237508 s.

3434 s. of analysis   15-25 KeV Energy range

Fig 7   HER x 1 light curve - 20-30 kev Energy range

Fig 8 ; HER x1 light curve 30-37,5 kev Energy range

Fig 9 ; HERX1 light curve observed by different groups

Fig 10 : HER X1 and background spectra. Difference in terms of standard deviations versus energy
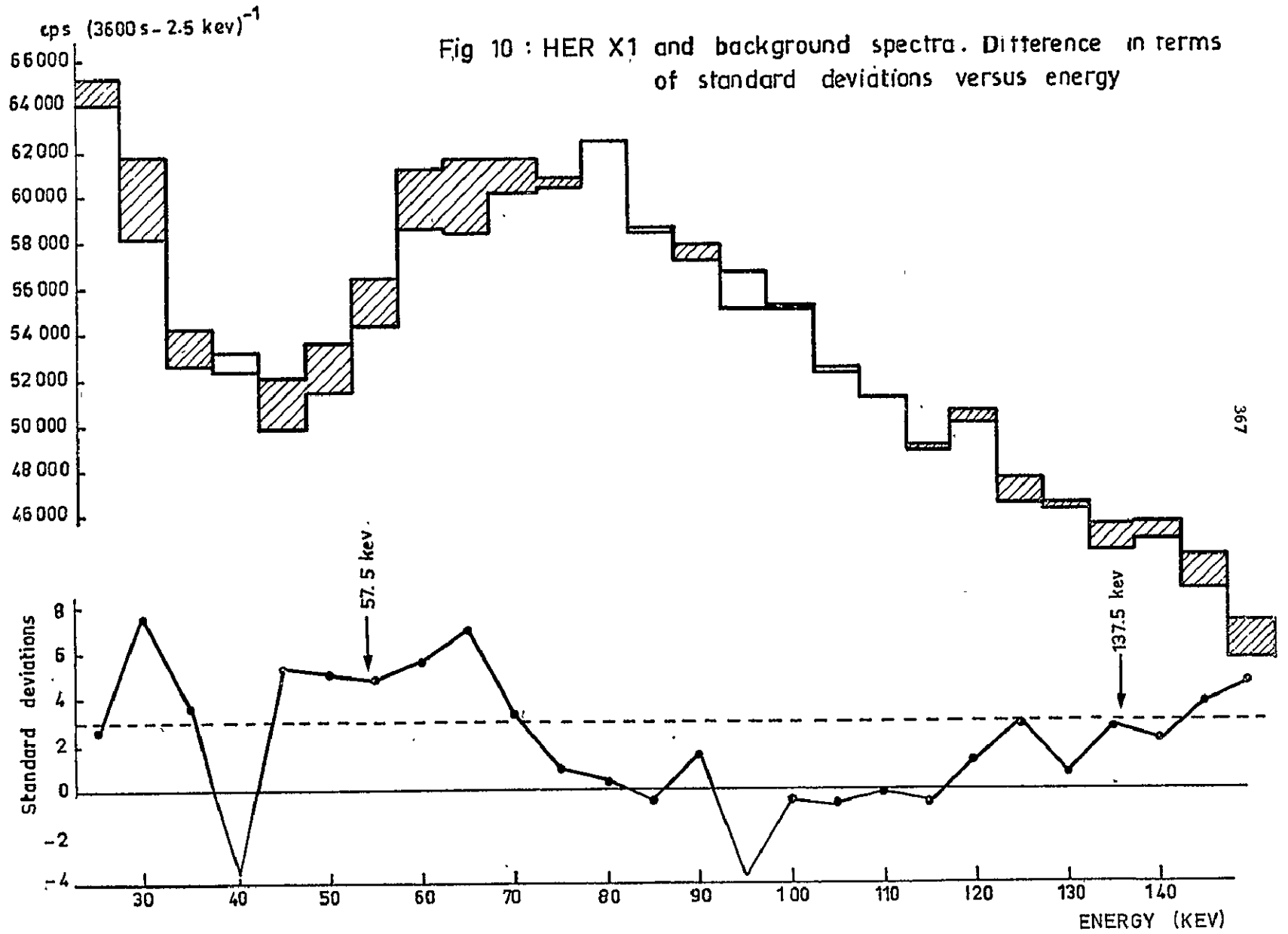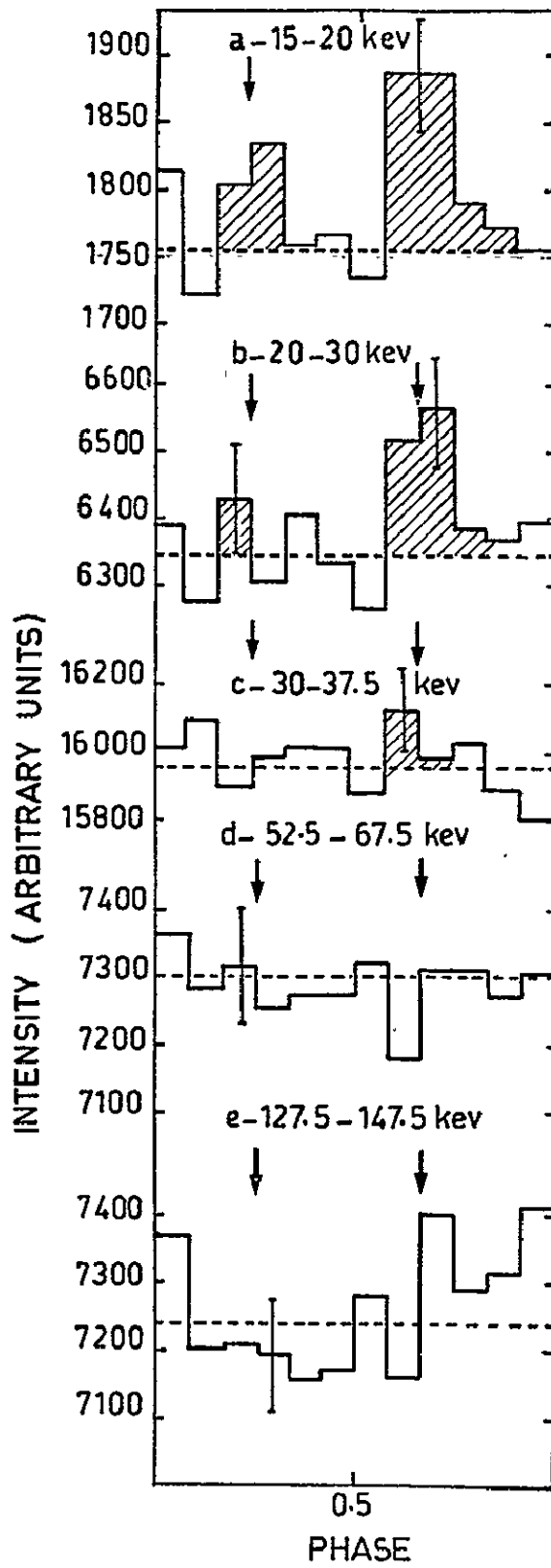
Fig 11 ; HER X1   light   curves
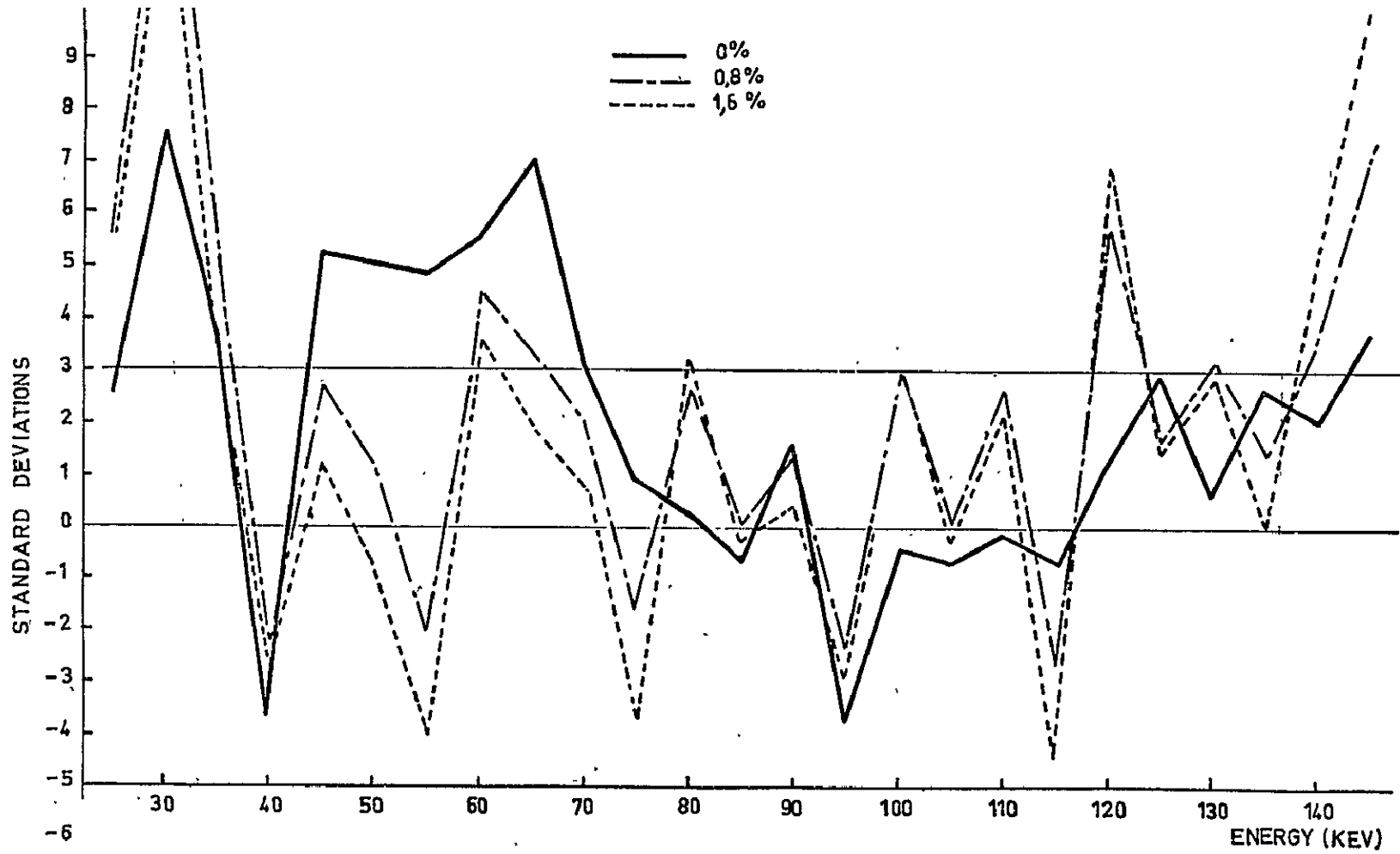
Fig 12; HER X1 pulsation represented in terms of x^2 versus energy

Fig 13 : HER X1 contribution versus energy for three possible calibration shifts

$\mathcal{D}_{22}-93$

N78-31993

UPPER LIMITS ON THE CYCLOTRON LINES
FROM Her X-1 AS OBSERVED WITH OSO-8

B. R. Dennis, G. S. Maurer*, E. P. Cutler**, C. J. Crannell,

J. F. Dolan, K. J. Frost and L. E. Orwig

Laboratory for Astronomy and Solar Physics, Code 684

Goddard Space Flight Center, Greenbelt, MD, U.S.A., 20771

ABSTRACT

Observations of Her X-1 were obtained during its ON-state in September, 1977, with the high-energy X-ray detector on board OSO-8. Upper limits on the line fluxes at 60 and 135 keV based on these observations are above, and hence consistent with, the positive results reported by Trümper et al. from a balloon flight during the same time interval. A detailed analysis of the time-variable background spectrum suggests that the line emission, especially in the time-averaged spectrum of Her X-1 previously reported by other workers at 25, 60, and 135 keV, is due to instrumental effects. The spectrum obtained with OSO-8 in September, 1977, is considerably steeper than that observed in pre-1976 balloon flights. These results are consistent with the results obtained by Trümper showing a decrease in the effective temperature of Her X-1 between May, 1976, and September, 1977.

UPPER LIMITS ON THE CYCLOTRON LINES
FROM Her X-1 AS OBSERVED WITH OSO-8

1.0 INTRODUCTION

The discovery by Trümper et al.[1,2] of a strong, narrow line at (58 ±5)keV and a possible second line at 110 keV in the X-ray spectrum of Her X-1 has rivetted the attention of the astrophysics community onto this highly variable X-ray source. The two high-energy X-ray lines have been interpreted as quantized electron cyclotron emission in the intense magnetic field of the rotating neutron star. The 58-keV line is believed to be produced by electron transitions from the first excited state to the ground state, and the 110-keV line is produced by transitions from the second excited state to the ground state. The observed energies are those predicted on the basis of this model, originally developed by Gnedin and Sunyaev,[3] and Basko and Sunyaev,[4] for a magnetic field strength of 5.3×10^{12} gauss. If the transitions take place near the surface of the neutron star as expected, then the gravitational redshift results in a corrected field strength of $5.8 - 7.3 \times 10^{12}$ gauss.

The evidence for the existence of the 58 keV line is very strong. The line intensity observed during a balloon flight on May 3, 1976, is reported to be 3×10^{-3} photons cm^{-2} s^{-1} or $5-6\sigma$ above the extrapolated continuum. This significance level has, however, been questioned by Brecher and Ulmer.[5] Further balloon observations by the same group on September 3, 1977, show the line at a significance level of $\geqslant 10\sigma$.[6,7] The credibility of the line is greatly enhanced by the fact that it is observed to pulse with the same 1.24s period as that determined at lower energies. The measured intensity of the 110 keV line during the 1976 observations was $1.4 - 2.6 \times 10^{-3}$ photons cm^{-2} s^{-1} or $2.3 - 3.3\sigma$ above zero and it was also observed in the pulsed spectrum.

No other X-ray observation of Her X-1 has been made with the sensitivity, energy resolution and time resolution required to confirm the existence of these lines. The results of the observations which have been made are summarized in Table 1. Unless otherwise indicated, the tabulated values are the fluxes averaged over the 1.24-s period, or they are 3σ upper limits. Coe et al.[8] observed Her X-1 in February, 1977, with an X-ray detector on Ariel V and report a line feature in the time-averaged spectrum centered at (64 ±6) keV with an intensity of (1.7 ±0.7) x 10^{-2} photons cm^{-2} s^{-1}. This is consistent in energy with the line observed by Trümper et al., but somewhat higher in intensity. Confirmation of the pulsed nature of the line could not be made. Brecher and Ulmer[5] report a feature also in the time-averaged spectrum but at 25 keV with an intensity of (2.4 ±1.2) x 10^{-2} photons cm^{-2} s^{-1} from observations made on OSO-7 in 1972. They point out, however, the more probable interpretation of the feature as being related to the peak in the detector background spectrum. No

Table 1

Reported X-Ray Line Fluxes from Her X-1 in Photons cm^{-2} s^{-1}

VEHICLE	OBSERVERS	25 keV	60 keV	110 keV	135 keV
BALLOON	TRÜMPER et al.[1,2] 1976	—	$(2.9^{+3.0}_{-1.0})$ x 10^{-3} PULSED	(1.4 ± 0.6) x 10^{-3} PULSED	—
BALLOON	TRÜMPER[7] 1977	—	(1.1 ± 0.1) x 10^{-3} PULSED	$<10^{-3}$	—
ARIEL V	COE et al.[8] 1977	—	(1.7 ± 0.7) x 10^{-2}	(1.7 ± 0.6) x 10^{-3} * 70—280 keV	
OSO-7	BRECHER AND ULMER[5] 1972	(2.4 ± 1.2) x 10^{-2}	—	—	—
BALLOON	DUROUCHOUX et al.[21] 1975	—	<6 x 10^{-3}	—	< 4 x 10^{-3}
OSO-8 (PROPORTIONAL COUNTER)	PRAVDO (PRIVATE COMMUNICATION)	—	<9 x 10^{-3} PULSED	—	—
OSO-8 CsI (Na)	THIS PAPER TIME-AVERAGED	—	<4 x 10^{-3}	—	< 2 x 10^{-3}
OSO-8 CsI (Na)	THIS PAPER PULSED	—	<2 x 10^{-3} PULSED	—	< 1 x 10^{-3} PULSED

*Coe, private communication.

such feature at this energy has been reported by other more recent observations[9] made with proportional counters having greater sensitivity and better energy resolution than the NaI(Tl) scintillation counters used to obtain the Brecher and Ulmer data. Results from the high-energy X-ray detector on HEAO-1 presented at this symposium by Matteson[10] indicate a pulsed excess above the extrapolated low-energy spectrum consistent with the 1977 flux in the 58 keV line reported by Trümper.[7]

Many observations were made of the high-energy spectrum of Her X-1 before the discovery of the narrow lines. Manchanda[11] has summarized the results obtained prior to 1976. He finds that the data from 1 to 10 keV can be fit by a power law with an index of ~1.5, while beyond 25 keV the spectrum steepens and a power-law index of ~2.7 is required. He attributes the considerable scatter in the observed flux values to the different observing times during the 11-day "ON" cycle, in which the source exhibits a triangular intensity profile. The break in the spectrum at ~20 keV has been interpreted by Boldt et al.[12] in terms of the energy dependence of the anisotropic scattering of photons from a highly magnetized plasma. The existence of the break in the spectrum has been confirmed with improved statistics by Becker et al.[9] They have fitted their "HIGH-STATE" data from 25–60 keV with a spectral form which can be approximated by a power law with an index of ~5.3 i.e. considerably steeper than the mean value of ~2.7 obtained by Manchanda.[11] Trümper et al.[1,2] obtain an index of ~4 when their data above 20 keV are fitted to a power law spectrum. Thus, there appears to be some considerable evidence that the shape of the spectrum above the break varies significantly during the 11-day ON state or from one 35-day cycle to another.

The available evidence on the pulsed fraction of the high energy X-ray flux, also suggests variability. On a balloon flight in December, 1973, Iyengar et al.[13] obtained an upper limit to the pulsed fraction of 10% for the energy band from 20-45 keV. In May, 1976, Kendziorra et al.[14] observed pulsing up to 88 keV with a pulsed fraction of $(58 \pm 8)\%$ from 17.7–31 keV and $(46 \pm 15)\%$ from 31–45 keV. Joss et al.[15] obtained a pulsed fraction of $(35 \pm 11)\%$ from 19–30 keV. Kurfess and Crosa[16] report a 2σ upper limit of 3.4×10^{-3} photons cm^{-2} s^{-1} for the pulsed emission from 0.1 to 10 MeV in February, 1972. It is clear from the previous results that there is a need for long-term observations of Her X-1 throughout its 35 day cycle. In particular it is important to determine if there are systematic variations in the high-energy spectrum and in the pulsed fraction during the 11-day ON-state.

We report here the results of a 12-day observation of Her X-1 during its ON-state in September, 1977.[17] The observations were made with the high-energy X-ray detector on OSO-8 and cover the energy range from 15–280 keV. Statistically significant energy spectra were obtained for each of six 1.7-day binary periods during this time interval, and the 1.24s pulsed fraction was also determined

in each case. Because of the unique modulation of the source signal resulting from the ten-second rotation of the satellite, it was possible to subtract the relatively large detector background arising mainly from induced radioactivity, and also to correct for a small change in detector gain between the on-source and the off-source observations. We show how such a gain change of the order of 1% can, as a result of the shape of the detector background spectrum, simulate source line features at 25, 60 and 135 keV. We caution against the interpretation of such lines as being of cosmic origin.

2.0 OBSERVATIONS WITH OSO-8

The high-energy X-ray detector on OSO-8 used to obtain our data has been described in detail by Dennis et al.[18] It is an actively shielded CsI(Na) scintillation detector with a sensitive area of 27.5 cm^2. The field of view is circular with a full width at half maximum (FWHM) of 5°. The time resolution for each recorded photon is 0.3125 ms. The energy resolution of the central detector as measured before launch is well represented by the expression FWHM $= 1.45E^{0.7}$ keV, where E is the X-ray photon energy in keV. This corresponds to a FWHM of 25 keV at 60 keV. Some slight degradation may have occurred in orbit as indicated by the widths of the features in the background spectrum. However, for the purposes of the data analysis, we used energy bins each chosen to be the width of the detector resolution ($1\sigma = 0.425$ FWHM) at the mid-point energy. The X-ray detector is mounted in the wheel section of OSO-8 such that the axes of the collimation holes are offset by 5° from the anti-spin axis of the spacecraft. With this orientation the signal for any X-ray source 5° away from the anti-spin axis is modulated as the wheel rotates once every 10 s.

The data reported here were recorded when Her X-1 was in the ON-state of its 35-day cycle between August 31 and September 12, 1977. During this time the anti-spin axis of the satellite was oriented towards a point on the celestial sphere 5° away from Her X-1. This point gradually moved around the source but was maintained at an angular separation of 5° from Her X-1. Thus, during this whole period, except in parts of the orbit when the earth filled the detector aperture, Her X-1 passed through the detector field of view once every 10 s. This modulation allows the source energy spectrum to be determined even in the presence of the large and variable detector background spectrum. The method of analysis used to obtain the energy spectrum of Her X-1 is basically the same as that previously described by Dolan et al.[19] to determine the energy spectrum of the Crab Nebula. For each energy bin the counting rate of the X-ray detector is first accumulated as a function of the angular separation between the detector axis and the direction to the source. The counting rate attributable to the source is calculated from this distribution by first assuming that the detector background remains independent of the angular separation between the source and the detector axis, although it may vary slowly during the data accumulation time. The known, approximately

triangular, detector response as a function of angular separation is then used to calculate the least-squares-fit source strength and the average detector background rate. Finally, the source counting rate spectrum is unfolded through the detector response function taking into account the detector-efficiency and resolution, K-escape photons, and the sensitive area. The resulting source fluxes in the 20 energy bins are the best representation of the source spectrum obtainable from the data and can be fit to any trial source spectrum.

When this analysis procedure was used on the full set of Her X-1 data, the spectrum shown in Figure 1 was obtained. Two significant features are apparent, one at ~60 keV and the other at ~140 keV. The intensities of the lines are 1.6×10^{-3} photons cm^{-2} s^{-1} at 60 keV and 4.3×10^{-3} photons cm^{-2} s^{-1} at 140 keV. Two things seemed suspicious about these lines, however. First of all, several energy bins showed apparently negative source strengths. These can clearly be seen in Figure 2 where the flux is plotted on a linear instead of a logarithmic scale. These negative values are shown as 1σ upper limits in Figure 1. None of the negative source strengths in any energy bin is greater than 2σ below zero but the trend indicates that a systematic error exists. The second problem is that attempts to detect a pulsed flux at the apparent line features proved unsuccessful. With the time resolution of 0.3125 ms, the 1.24s pulses at energies below 33 keV are readily resolved as indicated in Figure 3, but the pulsed flux at the energies of the apparent line features are less than the 3σ upper limits given in Table 1.

2.1 Instrumental Effects

The cause of the features in the calculated spectrum of Her X-1 and of the negative fluxes is now believed to be a small change in the gain of the photomultipliers (RCA·C31016F) as the spacecraft rotates. This change of gain, of the order of 1% or less, is believed to result from the changing orientation of the photomultipliers in the earth's magnetic field. A cylinder of 4 mil CO-NETIC magnetic shielding (Perfection Mica Company) was put around each photomultiplier but a residual variation of gain with magnetic field remains. This is presumably because it was not possible to extend the magnetic shield one diameter beyond the photocathode as recommended by RCA, the manufacturer of the photomultiplier.

As a result of this gain change, the detector background spectrum is shifted slightly with respect to pulse-height-analyzer channel number. When the gain is high, the same rate is measured in a higher channel and vice-versa. Consequently, the counting rate in each channel is observed to vary approximately sinusoidally each wheel rotation. The amplitude and phase of the variation is dependent on the shape of the background spectrum and on the strength of the magnetic field and its orientation with respect to the axis of the spacecraft. Since the conversion from channel number to
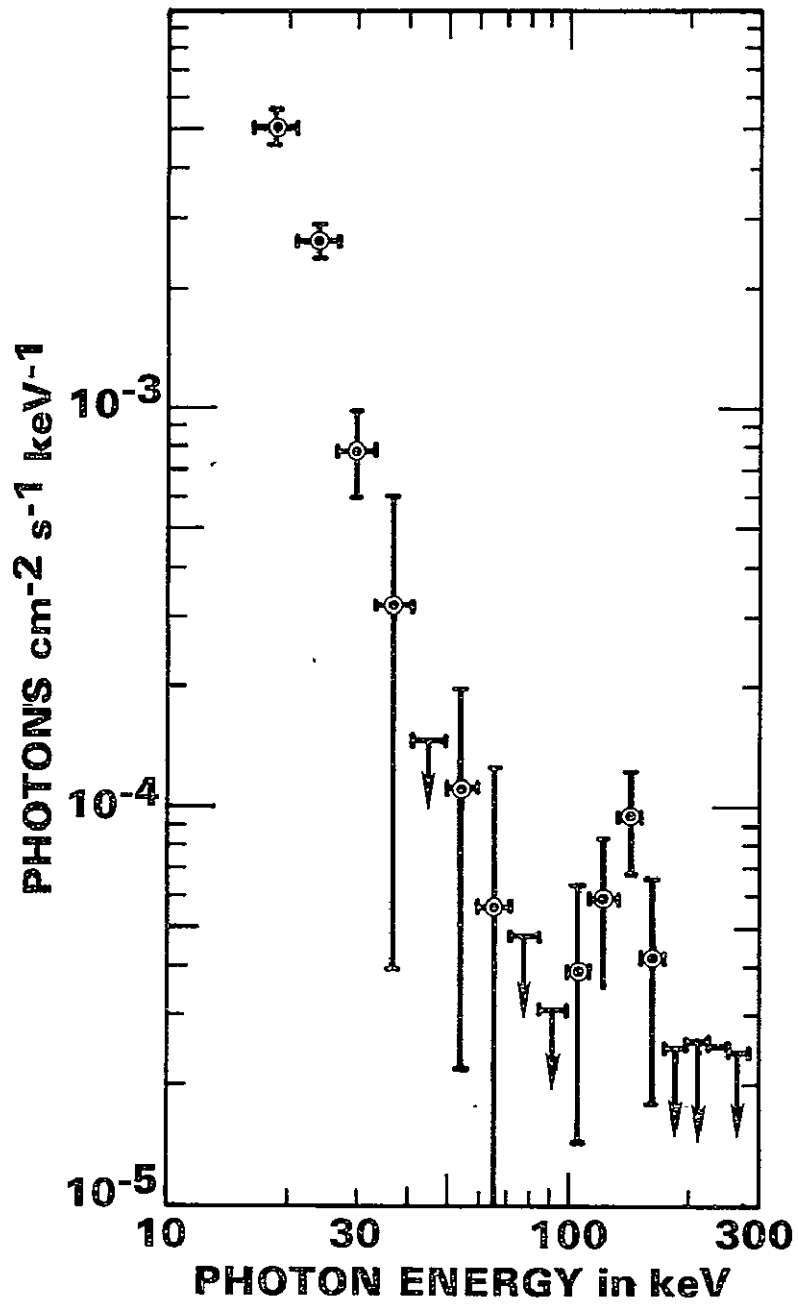
Figure 1. The calculated energy spectrum of Her X-1 determined for the total observing time from August 31 to September 12, 1977. The detector resolution has not been unfolded and negative values of the calculated source strengths are plotted as 1σ upper limits.
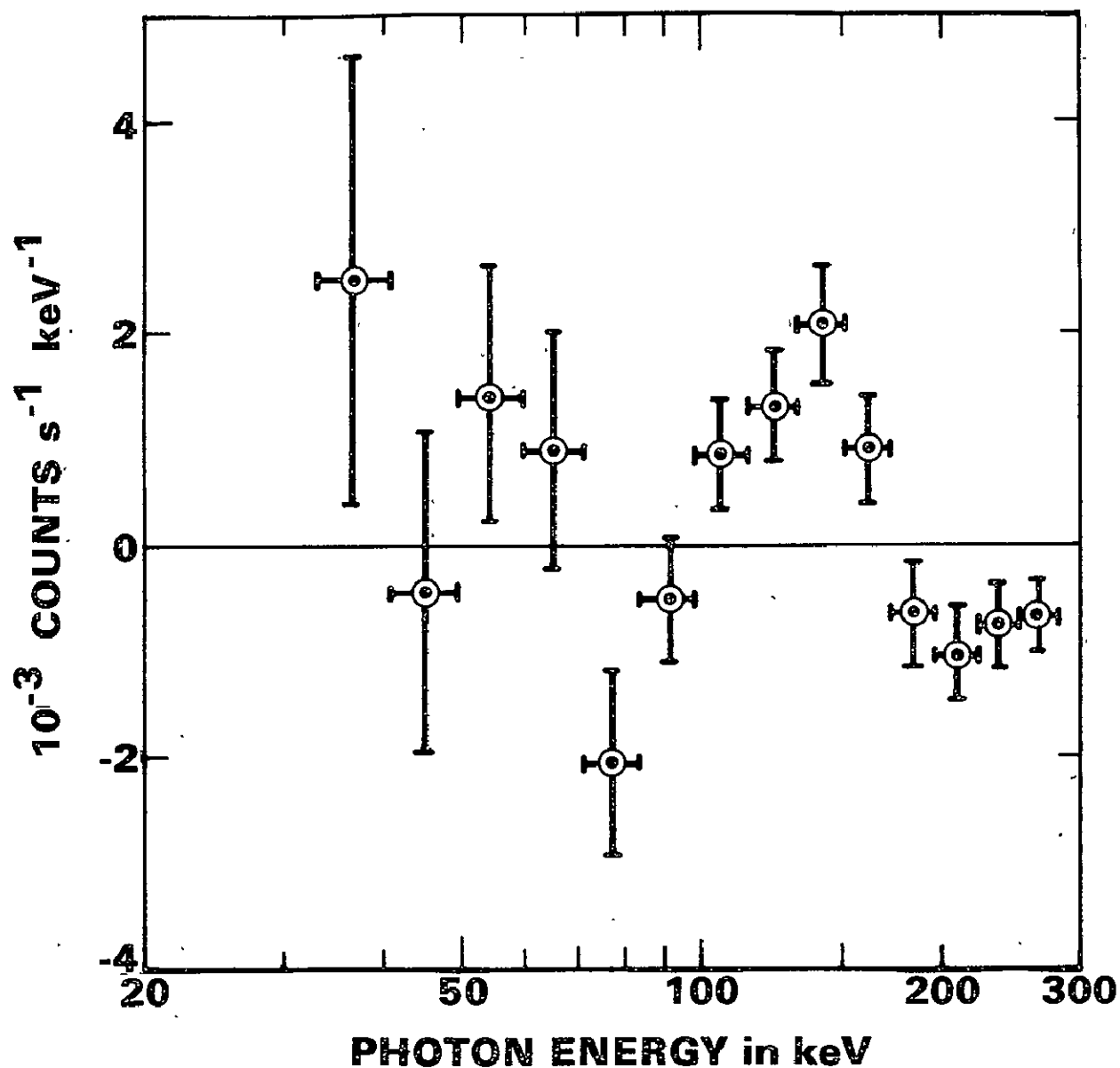
Figure 2. The calculated counting rate spectrum of Her X-1 determined for the total observing time from August 31 to September 12, 1977. The spectrum is plotted on a linear rate scale to show the negative calculated fluxes at 45keV, 70-100keV and > 170keV and also the apparent line features centered at ~ 60keV and ~ 135keV.
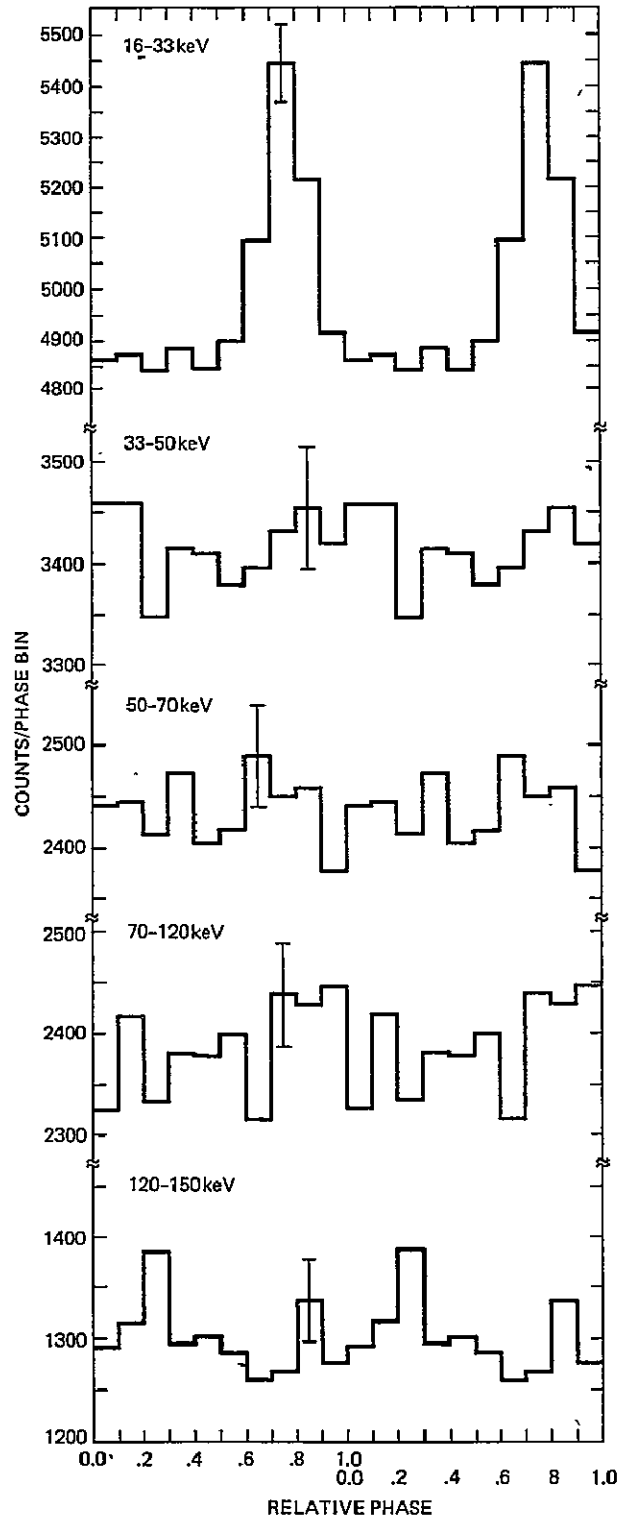
Figure 3. The phase distribution of Her X-1 in
five energy ranges from 16-150keV for the four
binary orbits from August 31 to September 6,
1977. The data were folded modulo the period
given by Pravdo et al.[20] with adjustments to the
photon detection times to allow for the motion
of the satellite with respect to the source.

energy loss in the CsI(Na) crystal is calculated with a constant calibration factor, this sinusoidal variation is also present in each of the energy bins used in the analytic procedure. In the absence of any real source flux, the calculated apparent source strength is, thus, the difference between the average background rate when the source is in the detector field of view and the average background rate when the source is out of the field of view. For small changes in gain, ΔG, this difference in background rate, D, is given by the following expression

$$D(E) = \frac{R_2 C_2 - R_1 C_1}{C_2 - C_1} \cdot \Delta G$$

where R_1 is the counting rate and C_1 is the channel number at the lower edge of the energy bin and R_2 and C_2 are the rate and channel number at the upper edge. In Figure 4, the average background spectrum observed during the Her X-1 observation is shown together with the difference, D, calculated from this spectrum using the above equation with ΔG = 1%. The origin of the features in the calculated Her X-1 spectrum at 60 keV and 135 keV can now be clearly seen as can the negative source strengths obtained at 45, 80 keV and above 170 keV. It is also interesting to note that a third positive feature exists at ∼27 keV as previously reported by Brecher and Ulmer[5] although, in our measurements, such an excess is lost in the statistics of the real source flux at that energy.

2.2 Determination of the Source Spectrum

The true spectrum from Her X-1 can be rather simply determined from the calculated source spectrum and the variation of D with energy. This is possible in spite of the rather complicated variations in the strength and direction of the magnetic field as seen by the satellite as it orbits the earth. The shift in the background spectrum each wheel rotation will always result in an apparent source spectrum given by some fraction of D providing only that the shape of the background spectrum does not change significantly. By restricting the data to that collected well out of the South Atlantic Anomaly, this condition is easily satisfied to the accuracy required. Consequently, the calculated source spectrum can be corrected for the effects of the gain changes by subtracting the background difference spectrum for some mean value of the gain change, ΔG. The mean value of ΔG can be most easily determined by a least-squares technique in which significant negative source strengths are removed. The background difference spectrum for a given value of ΔG is subtracted from the calculated source counting-rate spectrum and the resulting spectrum unfolded to obtain a source spectrum in photons cm^{-2} s^{-1} keV^{-1}. This is then fitted with a trial function such as power law or a thermal spectrum and a value of χ^2 is obtained. The process is repeated with different values of ΔG until a minimum value of χ^2 is obtained. The spectrum of Her X-1 obtained in this way for the
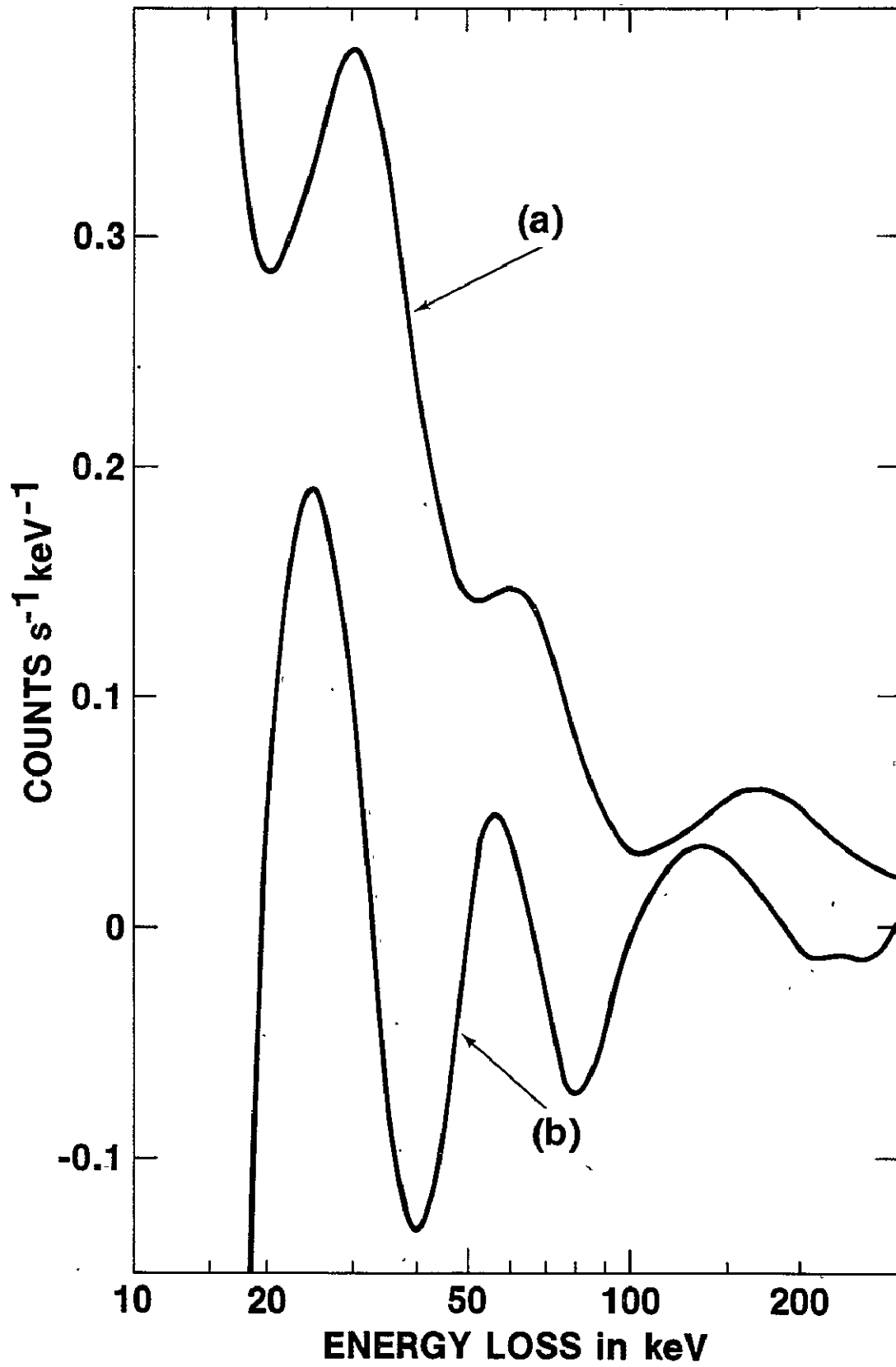
Figure 4. Curve (a) – Detector background spectrum for the Her X-1 observing time.
Curve (b) – The difference (x25) between two background spectra measured with a gain difference of 1%.

period from August 31 to September 6, 1977, excluding the eclipse time, is shown in Figure 5. The source intensity was highest during this time interval covering four binary orbits. The spectrum can be fitted by a power law of the form $(2.4 \pm 0.4) \times 10^{-3}$ $(E/25)^{-(4.9 \pm 0.7)}$ photons cm^{-2} s^{-1} keV^{-1} or by a thermal bremsstrahlung spectrum of the form $1.6 \exp [-E/(8 \pm 2)] \cdot E^{-1}$ photons cm^{-2} s^{-1} keV^{-1}. No significant line features are evident in this spectrum at any energy with the 3σ upper limits indicated in Table 1.

3.0 CONCLUSIONS

We have, thus, obtained an understanding of features observed in our time-averaged spectrum of Her X-1 in terms of small changes in gain of our X-ray detector. Such changes in gain can produce apparent line features in the spectrum at energies which have been previously reported in the literature. Brecher and Ulmer[5] have pointed out the probable relation to the detector background of the 1.5 sigma feature at 2.5 keV in the OSO-7 spectrum of Her X-1. Durouchoux et al.[21] have shown that a small change in gain can explain the apparent line features at 57.5 keV and 137.5 keV in their time-averaged Her X-1 spectrum obtained on a balloon flight in May, 1975. Coe et al.[8] report a line feature at (64 ± 6)keV in the time-averaged Her X-1 spectrum from the high-energy X-ray detector on Ariel V. Attempts to explain their result in terms of a gain change have not been successful since the detector background spectrum does not have the required shape.[22] Our 3σ upper limit at 60 keV is, however, considerably below their measured line flux and suggests that the line strength is variable from one 11-day ON-state to another. The much steeper spectrum ($E^{-4.9}$) which we obtain compared to the average spectrum ($E^{-2.7}$) obtained from pre-1976 balloon flights[11] also supports the idea that the flux above $\sim$40 keV had decreased in September, 1977, to a level well below its previous value. This agrees with the result obtained by Trümper[7] that the flux in the 58 keV pulsed line decreased by a factor of $\sim$2.6 between May, 1976, and September, 1977, and that the effective temperature of the spectrum had also decreased between these two dates.

In addition to the time-averaged spectrum discussed above, we also obtained a spectrum of the pulsed flux. We detected significant pulsed flux up to an energy of 33 keV and obtained the 3σ upper limits on any pulsed line feature given in Table 1. These upper limits are consistent with the results of Trümper et al.[1,7,14] They do show that the line features are not significantly stronger at any time during the high state than during the relatively short interval of a balloon flight observation.

In summary, we have shown how a fraction of a percent change in gain can produce data which can simulate line features or breaks in a source spectrum. The features generated depend on the magnitude of the gain change and the shape of the detector background spectrum. We suggest that such
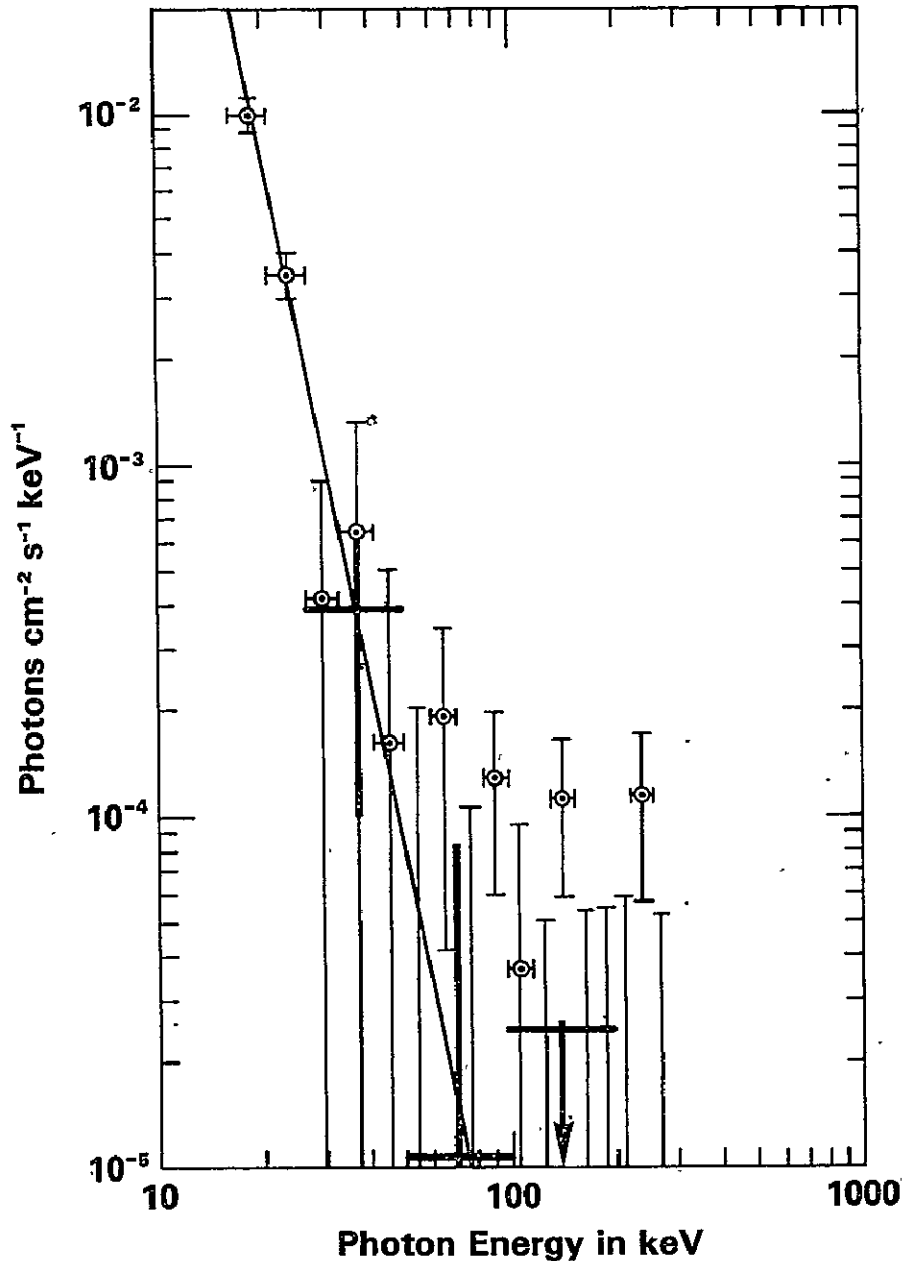
Figure 5. The time-averaged spectrum of Her X-1 for the period August 31 to September 6, 1977, during which the intensity was at its highest level. The count-rate spectrum for this period was corrected for an average change in gain of 0.7% and unfolded through the detection efficiency, K-escape.probability and detector resolution using the method given by Dolan et al.[19]. The best fit power law indicated is of the form $(2.4 \pm 0.4) \times 10^{-3} \, (E/25)^{-(4.9 \pm 0.7)}$ photons cm^{-2} s^{-1} keV^{-1}. The circled points are for energy bins each the width of the detector resolution (1σ at that energy. Consequently, any real line feature would appear in at least two adjacent bins. The heavy lines show the source flux averaged over the wider energy intervals indicated. The vertical lines indicate 1σ statistical uncertainties or 1σ upper limits.

a change in gain can account for previously reported lines particularly in the time-averaged spectrum of Her X-1. The line at 58 keV reported by Trümper et al. remains highly credible, however, because of its pulsed nature. This makes it largely immune from most systematic effects. Confirmation of this line by different observers and measurements with improved energy resolution to determine the true line width remain highly desirable objectives.

REFERENCES

1. Trümper, J., Pietsch, W., Reppin, C., Sacco, B., Kendziorra, E., and Staubert, R., Proc. 8th Texas Symposium, 538 (1977).

2. Trümper, J., Pietsch, W., Reppin, C., Voges, W., Staubert, R., and Kendziorra, E., Astrophys. J. 219, L105 (1978).

3. Gnedin, Yu. N., and Sunyaev, R. A., Astron. and Astrophys. 36, 379 (1974).

4. Basko, M. M., and Sunyaev, R. A., Astron. and Astrophys. 42, 311 (1975).

5. Brecher, K., and Ulmer, M. P., Nature 271, 135 (1978).

6. Voges, W., Pietsch, W., Reppin, C., Trümper, J., Staubert, R., and Kendziorra, E., Central Bureau for Astronomical Telegrams, Circular No. 3184 (1978).

7. Trümper, J., Proc. of Symp. on Gamma-Ray Spectroscopy in Astrophysics, Goddard Space Flight Center, Md., U.S.A., April 28-29, 1978 (to be published).

8. Coe, M. J., Engel, A. R., Quenby, J. J., and Dyer, C. S., Nature, 268, 508 (1977).

9. Becker, R. H., Boldt, E. A., Holt, S. S., Pravdo, S. H., Rothschild, R. E., Serlemitsos, P. J., Smith, B. W., and Swank, J. H., Astrophys. J. 214, 879 (1977).

10. Matteson, J., Proc. of Symp. on Gamma-Ray Spectroscopy in Astrophysics, Goddard Space Flight Center, Md., U.S.A., April 28-29, 1978 (to be published).

11. Manchanda, R. K., Astrophys. and Space Sci. 50, 179 (1977).

12. Boldt, E. A., Holt, S. S., Rothschild, R. E., and Serlemitsos, P. J., Astron. and Astrophys. 50, 161 (1976).

13. Iyengar, V. S., Manchanda, R. K., Durgaprasad, N., Gokhale, G. S., Kunte, P. K., and Sreekantan, B. V., Nature 251, 292 (1974).

14. Kendziorra, E., Staubert, R., Pietsch, W., Reppin, C., Sacco, B., and Trümper, J., Astrophys. J. 217, L93 (1977).

15. Joss, P. C., Li, F. K., Wang, Y.-M., and Hearn, D. R., Astrophys. J. 214, 874 (1977).

16. Kurfess, J. D., and Crosa, L., Nature, 245, 116 (1973).

17. Dennis, B. R., Maurer, G. S., Cutler, E. P., Crannell, C. J., Dolan, J. F., Frost, K. J., and Orwig, L. E., Submitted to Nature (1978).

18. Dennis, B. R., Frost,.K. J., Lencho, R. J., and Orwig, L. E., Space Science Instrumentation $\underline{3}$, 325 (1977).

19. Dolan, J. F., Crannell, C.J., Dennis, B. R., Frost; K. J., Maurer, G. S., and Orwig, L. E., Astrophys. J. $\underline{217}$, 809 (1977).

20. Pravdo, S. H., Becker, R. H., Saba, J. R., Serlemitsos, P. J., and Swank, J. H., Central Bureau for Astronomical Telegrams, Circular No. 3116 (1978).

21. Durouchoux, Ph., Boclet, D., and Rocchia, R., Proc. of Symp. on Gamma-Ray Spectroscopy in Astrophysics, Goddard Space Flight Center, Md., U.S.A., April 28-29, 1978 (to be published).

22. Engel, A. R., and Coe, M. J., Space Sci. Inst. $\underline{3}$, 408 (1978).

HEAO-1 OBSERVATIONS OF HER X-1 AT ENERGIES ABOVE 13 keV

IN FEBRUARY 1978

J.L. Matteson and D.E. Gruber
Department of Physics
University of California, San Diego

and

J.A. Hoffman[*]
Department of Physics and Center for Space Research
Massachusetts Institute of Technology

ABSTRACT

Results from preliminary analysis of HEAO-1 pointing observations of Her X-1 on three days in February 1978 are presented. Pulsed flux is detected up to ~70 keV with a clear indication of emission at ~60 keV which is above the continuum spectrum extrapolated from lower energies. If this excess emission is interpreted as a spectral line, its intensity varies from (1.2 ± 0.2) x 10^{-3} to (0.2 ± 0.2) x 10^{-3} ph/cm^2-sec with a time scale of one day. A factor 2 decrease in the low energy continuum is associated with the decrease in the excess emission.

INTRODUCTION

Her X-1 is among the brightest of the X-ray binaries. Its intensity varies with periodicities of 1.24 sec, 1.70 days and 34.9 days respectively, in the form of pulsations, binary eclipse and unexplained long period variability (1). Regular intensity dips of a few hours duration also occur. Spectral variability occurs during the pulsation, the intensity dips and the 34.9 day period (2,3). The spectrum and its variability contain the signature of the geometry and physical processes of the accretion and emission regions of Her X-1. Therefore sensitive spectral observations at all intensity phases and X-ray energies are of primary importance. In the ~2 to ~30 keV range the observational picture is reasonably complete. However, the low flux at higher energies, due to the steepening spectrum of Her X-1 (4), requires sensitive instruments which have become available in only the last few years.

In May 1976 a Max Planck/Tübingen balloon observation of Her X-1 sensitive above ~20 keV (hereafter MPT-76) confirmed the spectral steepening and revealed a pulsed spectral excess at ~58 keV which was interpreted as cyclotron line emission in the ~10^{12} gauss field of the neutron star in the Her X-1 system (5). A line flux of $(2.9 + 3.6, -1.2)$ x 10^{-3} ph/cm^2-sec was required to fit the observation. Emission interpreted as the second harmonic of the cyclotron line was detected at 3.3σ significance at ~110 keV with a flux of ~2.6 x 10^{-3} ph/cm^2-sec. A UCSD balloon observation in June 1975 placed an upper limit on line emission

---

[*]Present address: Astronaut Office, Johnson Space Center

at 57 keV of 1.1 x 10^{-3}ph/cm^2-sec (95% confidence) (6). In order to confirm the reported line emission, clarify its variability and extend the observations of Her X-1 at high energies to additional intensity phases, a series of HEAO-1 pointing observations of Her X-1 were conducted in February 1978 with the UCSD/MIT Hard X-ray and Low Energy γ-ray Experiment, A4. In this paper we present preliminary results based on quick-look data from these observations.

OBSERVATIONS

The results presented here were obtained with one of the two Low Energy Detectors of the A-4 instrument. Results from both detectors will be published later. These phoswich type scintillation counters have 3 mm thick NaI (Tl) detectors, each with an effective area of 103 cm^2, and operate from ~13 to ~200 keV. Their energy resolution is weakly dependent on energy because of the dominance of light collection nonuniformities. It is 28% FWHM at 22 keV and 25% at 60 keV. Each detector is collimated to 1.7° x 20° FWHM with graded-Z slats and a CsI(Na) active anticoincidence shield annulus. Background in the 15-200 keV range is ~5 c/sec. Gain variations, which occur in some A-4 detectors on 30 min time scales, were <2% over the periods of observation. Energy losses which satisfied the anticoincidence condition were pulse-height-analyzed into 64 channels with ~3 keV/channel. A maximum of 81 pulse-height/sec could be telemetered. Live-time corrections were telemetered each 0.08 sec. Table I presents details of the observations. The day 59 observation was chosen to be as close as possible to the phases of the MPT-76 observation. All observations were straight pointings at Her X-1 with no off-source data taken during the observation.

RESULTS

The presence of pulsed emission was determined by testing the data against the hypothesis of no pulsation at the barycenter over a range of periods which bracketed the expected period. In all observations pulsed emission was clearly indicated. The Doppler shift of these periods is in agreement with the Her X-1 binary ephemeris. Light curves were constructed using the measured periods. Since the event rate was always <60/sec, and typically ~30/sec, the 0.08 sec live-time corrections had only a slight effect on the light curves, which are shown in Figure 1. Pulsed emission is clearly indicated up to pulse heights equivalent to ~64 keV and includes the energy range of the reported cyclotron line. However, at ~110 keV, the energy expected for the cyclotron harmonic, no pulsation is apparent. That the day 59 pulsed emission is weaker than that of the other days is likely due to an intensity dip in Her X-1 since scanning data (30-min period) indicates the average intensity around this time was ~0.75 of that on days 55 and 58. Additional analysis of scanning data will be required to verify the presence of an intensity dip.

Pulse height spectra of the pulsed emission were obtained as the difference between the "pulsed" and "non-pulsed" parts of the light curve (see Figure 1). The resulting spectra are shown in Figure 2. Multiparameter fits to each day's spectrum were performed with a model consisting of a power law below

2

a break energy, an exponential above the break and a spectral line with intrinsic width. Corrections for detector efficiency, energy resolution, K X-ray escape and absorption in the overlying material were included in the fitting. The same model was used in the MPT-76 analysis. Our analysis corresponds to the Pulse minus Off-Pulse MPT-76 analysis. Best fit values occurred at the x^2 minimum. Standard errors for the best-fit parameters were estimated from the method of Bevington (7).

The model and the results of the fitting are given in Table II. On days 55 and 58 a satisfactory fit requires the line component. Its intensity on each of these days is in agreement with the average for these days, (1.16 ± 0.15) x 10^{-3} ph/cm^2-sec. The day 59 spectrum has a fitted line flux of (0.21 ± 0.17) x 10^{-3} ph/cm^2-sec, a factor > 2.4 (95% confidence) below that measured one day earlier and consistent with no line component. On all days the fitted line energy is consistent with the average value of 60.0 ± 1.3 keV. The intrinsic width of the line is poorly determined because of the relative insensitivity of x^2 to it which is partly due to the low flux in the line. The fitted value of kT on all days is consistent with the average value of 7.36 ± 0.31 keV. The exponential spectral component at 30 keV is constant on days 55 and 58, but is a factor 2.0 lower on day 59.

DISCUSSION

Significant high-energy variability of Her X-1 is indicated by these observations. The fitted continuum and line decreased a factor ~2 in one day. This is not surprising, in view of the short time scales (hours) of the intensity dips of Her X-1. The fitted kT remained constant through the variation, suggesting that the mechanism responsible for the apparent temperature is uncoupled from that producing the luminosity changes. Our observation of the constancy of the 20 to 40 keV spectrum shape is in agreement with previous observations (3). The MPT-76 fitted line strength is $(2.9 + 3.6, -1.2)$ x 10^{-3} ph/cm^2-sec, a factor 2.6 above our values for day 55 and 58, the fitted kT is $7.3 + 2.4, -3.8$ keV, in agreement with our observations, and the exponential continuum at 30 keV agrees with our day 59 value. When combined with our results, these indicate a change in fitted line strength from 2.9 x 10^{-3} (MPT-76, to <0.5 x 10^{-3} ph/cm^2-sec (day 59, 95% confidence) while the exponential component's intensity and kT value remained essentially constant

CONCLUSION

The HEAO-1 observations reported here clearly indicate pulsed emission from Her X-1 at energies above 50 keV which is in excess of the pulsed spectrum extrapolated from lower energies. This excess is fitted by spectral line emission at 60.0 ± 1.3 keV with a flux of (1.16 ± 0.15) x 10^{-3} ph/cm^2-sec on 1978 day 55 and 58 and (0.21 ± 0.17) x 10^{-3} on day 59. The data do not require a spectral line to explain the excess. Other spectral shapes are possible. The fitted continuum below 50 keV was observed to decrease a

factor 2.0 in one day while the fitted line decreased a factor > 2.4 (95% confidence) and the fitted kT remained constant at 7.36 ± 0.31 keV. These results and the April 1976 observation indicate a factor > 6 variability in the fitted line. The fitted line and continuum variations have not yet been time-resolved. Additional analysis of the present data and that taken during the HEAO-1 observations planned for August and September 1978 should clarify the spectral variability of Her X-1.

ACKNOWLEDGEMENTS

TABLE I - HEAO-1 Pointing Observations of Her X-1

Day of 1978	Pointing Interval (UT)	Analyzed Data Interval (UT)	1.7 Day Phase	Days After 34.9 Day Turn-on*
55	1452-1809	1459-1628	0.30-0.34	3.9
58	1547-1845	1459-1747	0.09-0.14	6.9
59	1620-1937	1840-1937	0.74-0.77	8.1

TABLE II - Best-Fit Parameters from Model* Fitting

	Day 55	Day 58	Day 59
Line Parameters:			
I_o (10^{-3} photons/cm^2-sec)	1.20 ± 0.21	1.11 ± 0.21	0.21 ± 0.17
E_o (keV)	59.6 ± 1.8	60.0 ± 1.6	61.4 ± 6.8
FWHM[†] (keV)	15 ± 15	$10 ^{+15}_{-10}$	$3 ^{+30}_{-3}$
Continuum Parameters:			
N_o[‡] (photons/cm^2-sec-keV)	3.32 ± 0.78	2.49 ± 0.74	1.08 ± 0.53
kT[‡] (keV)	6.96 ± 0.44	7.56 ± 0.49	7.76 ± 0.83
E_b (keV)	28.4 ± 0.9	28.2 ± 0.8	29.5 ± 1.5
s[‡]	1.17 ± 0.25	0.16 ± 0.25	0.92 ± 0.29

$$ *\varphi(E) = \begin{cases} N_o\exp(-E/kT)/E \times \dfrac{.937 I_o}{FWHM} \exp\left\{-2.67\left(\dfrac{E-E_o}{FWHM}\right)^2\right\}, & E \geq E_b \\ N_o\exp(-E_b/kT)/E_b \times (E/E_b)^{-S} & , E \leq E_b \end{cases} $$

[†] χ^2 weakly dependent on this parameter.

[‡] These parameters highly correlated. Holding other parameters fixed gives N_o errors ~ 0.025 of those given in Table II

REFERENCES

1. Giacconi, R., Gursky, H., Kellog, E., Levinson, R., Schreier, E., and Tananbaum, H., Ap. J., 184, 227 (1973).

2. Pravdo, S.H., Boldt, E.A., Holt, S.S., and Serlemitsos, P.J., Ap. J., (Letters), 216, L23 (1977).

3. Becker, R.H., Boldt, E.A., Holt, S.S., Pravdo, S.H., Rothschild, R.E., Serlemitsos, P.J., Smith, B.W. and Swank, J.H., Ap. J., 214, 879 (1977)

4. Holt, S.S., Boldt, E.A., Rothschild, R.E., and Serlemitsos, P.J., Ap. J. (Letters), 190, L109 (1974).

5. Trumper, J., Pietsch, W., Reppin, C., Voges, W., Stanbert, R. and Kendziorra, E., Ap. J. (Letters), 219, L105 (1978)..

6. Paciesas, W.S., "Hard X-ray Variability in Binary X-ray Sources," Ph.D Thesis, University of California, San Diego, UCSD SP 78-02 (1978).

7. Bevington, P.R. "Data Reduction and Error Analysis for the Physical Sciences," McGraw-Hill pp 153-154 (1969).

FIGURE CAPTIONS

Figure 1. Observed light curves of Her X-1. The pulsed spectra, Figure 2, are formed from the difference of the average spectra of the "Pulse" and non-"Pulse", i.e. off-Pulse, phases. 1σ error bars are indicated. The dashed lines are background rates from 1 day earlier or later when HEAO-1 was in the same geomagnetic environment and scanning source-free regions. These rates were not used in the analysis reported here.

Figure 2. Pulsed spectra of Her X-1 and model fits. 1σ error bars and 2σ upper limits are indicated. The heavy dots represent the best fit model after folding through the instrument's response. They are connected for convenience. The day 55 spectrum and best fit are similar to those of day 58.
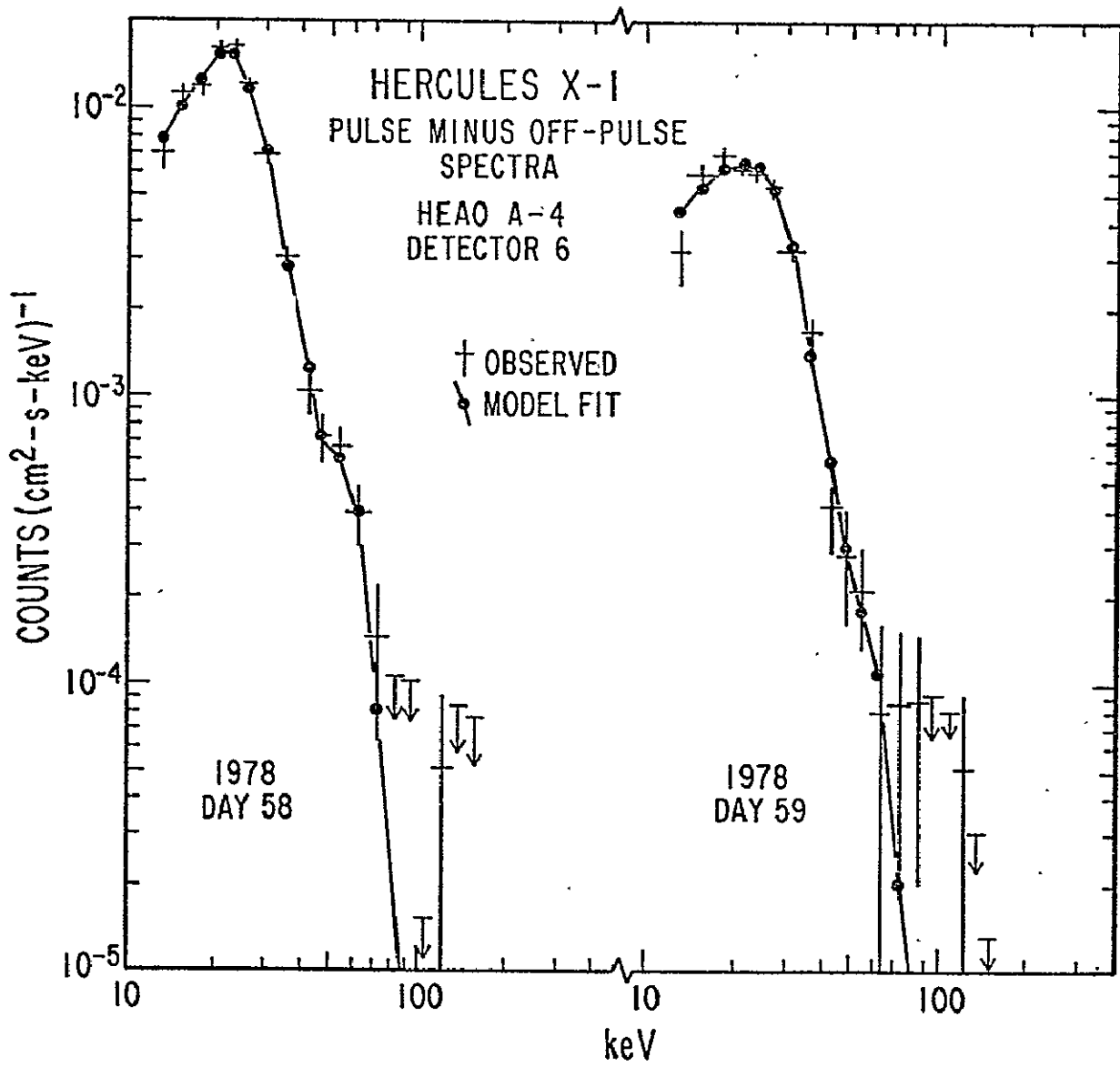
HERCULES X-1 PULSATION, HEAO-1
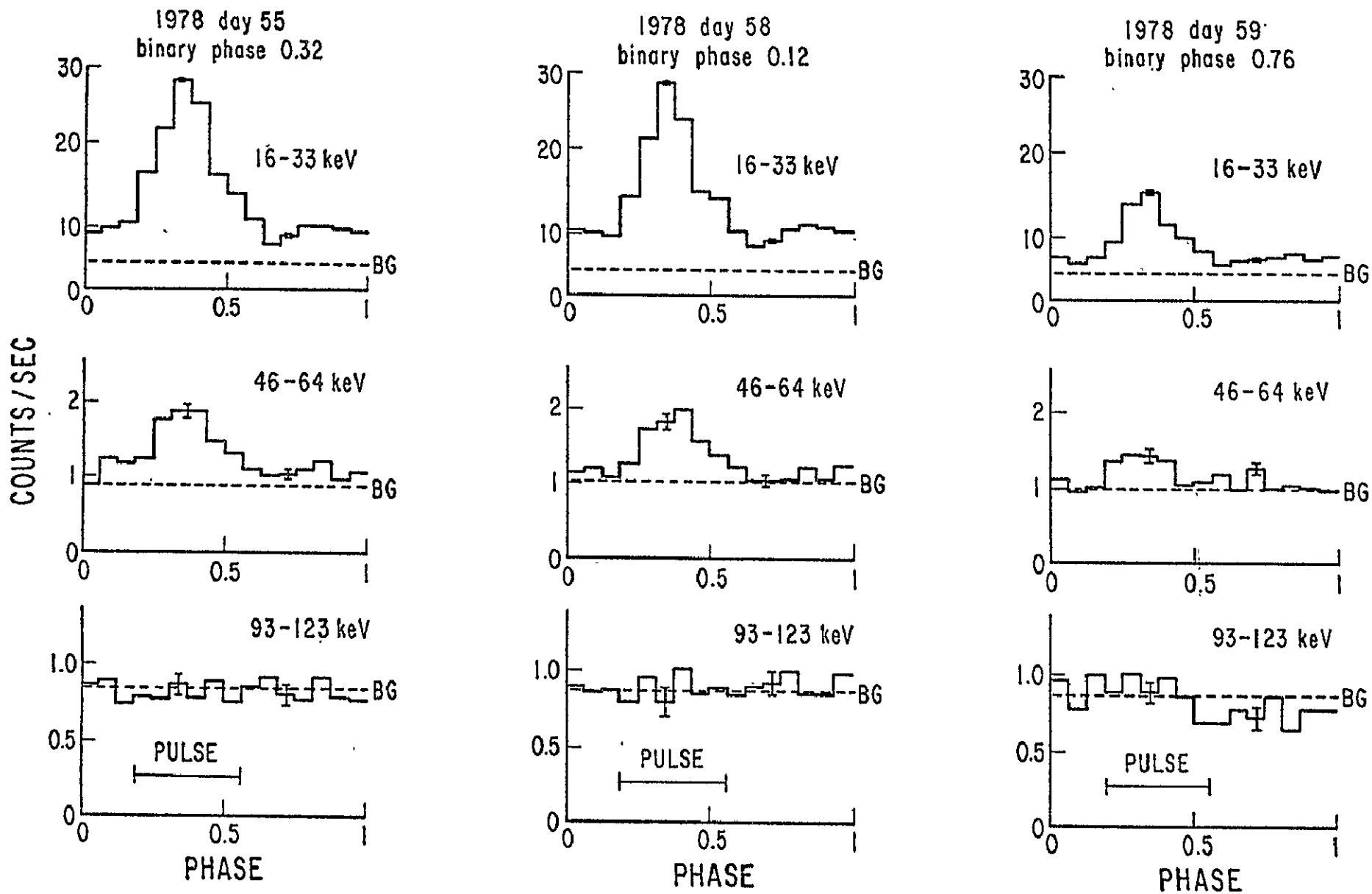
Figure 1

Figure 2

Cyclotron Emission in Neutron Star Magnetospheres

J. K. Daugherty
Durham, NC

Kinematic aspects of cyclotron emission in superstrong magnetic fields are reviewed to suggest characteristic features which might be useful in confirming the nature of the reported line feature near 50 keV in the spectrum of Her X-1. The role of the inverse process of cyclotron absorption is also discussed.

I. Introduction

The reported line feature near 50 keV in the pulsed Her X-1 spectrum (Trümper et al. 1978) has been tentatively interpreted by its discoverers as cyclotron emission in the intense magnetic field of an accreting neutron star. If their result is confirmed, its actual identification with cyclotron emission would be extremely significant, and in fact might well constitute the closest possible approach to a direct measurement of the field strength near the surface of a neutron star. Hence the reported measurements have already prompted efforts to predict characteristic spectral features which might confirm this interpretation (Daugherty and Ventura 1977). A short discussion of possible higher harmonics and kinematic effects (line shapes due to

Doppler broadening, splitting of multiple first harmonics) was presented at this conference and will be summarized below. However, it also appears worthwhile in these proceedings to add a brief discussion of the equally significant inverse process of cyclotron absorption (Daugherty and Ventura 1978) and its influence on the spectrum of Her X-1 (Pravdo et al. 1978) and similar objects.

Two concluding remarks have also been inserted, concerning both the construction of detailed models of X-ray pulsars in general, and also the precise relation of cyclotron emission line energies to the actual stellar magnetic field strengths.

II. The Emission Process

Cyclotron emission in a superstrong, macroscopically varying magnetic field must be treated as a first-order QED interaction described by the S-matrix element

$$S_{fi} = ie \int d^4x \; \overline{\psi_{final}(x)} \; a_\mu(x) \gamma^\mu \psi_{initial}(x)$$

where the initial and final states of the radiating electron satisfy the Dirac equation in the prescribed (classical) magnetic field. The potential a_μ describes the radiation field alone and here corresponds to the emission of a single photon during the transition. It is worthwhile to note that the relativistic Dirac equation should be used

either if the longitudinal velocities of the electrons
are relativistic, or if the field strength is significant
compared to the critical value $B_{cr} = \dfrac{m^2 c^3}{e\hbar} = 4.414 \times 10^{13}$ G.
Only for conditions of both low velocities and low field
strengths can the Dirac equation be safely replaced by its
nonrelativistic Schrödinger limit.

The dynamics of the cyclotron emission process have
already been discussed elsewhere in the nonrelativistic
case (Canuto and Ventura 1977, Daugherty and Ventura 1977),
and the lifetimes of excited states in the relativistic
case have been found by Daugherty and Ventura (1978).
These treatments, which are concerned with the transition
rates and angular distributions of the emission, are too
involved to be discussed here. However, the kinematic
aspects of the emission process are both straightforward
enough and of sufficient interest to be described briefly.

The relativistic energy-momentum conservation equations
for an emission event may be written in the form

$$E_j = E_k + \hbar \omega_{jk} \qquad \text{(1a)}$$

$$q = p + \frac{\hbar \omega_{jk}}{c} \cos \theta \qquad \text{(1b)}$$

where the radiating electron of initial energy E_j and
longitudinal momentum q emits a photon of energy $\hbar \omega_{jk}$ at
an angle θ with respect to the field direction B, and
thereby drops to a lower state E_k with longitudinal

recoil momentum p. The electron energy in the magnetic field

has the form $E_j = \left(q^2 + m^2(1+2j\frac{B}{Bc})\right)^{1/2}$, corresponding to the

quantization of the transverse motion. The most striking aspect

of the conservation equations given above is that the transverse

momentum is not included, since the field lines themselves can

absorb an arbitrary transverse momentum exchange.

Onc immediate consequence of eq. (1) is that distinct

transitions j→k such

that j-k=1 have differing

energies whose separations

depend on field strength,

as shown in Fig. 1. This

splitting effect is also

angle-dependent, as may be

seen from a comparison of

the values for θ = 0 and

$\theta = \frac{\pi}{2}$.

Fig. 1a and b. Splitting of the first harmonic with increasing external magnetic field. At fields of less than 10^{12} Gauss the individual components corresponding to the various $\Delta n=1$ transitions tend to merge in agreement with the predictions of the nonrelativistic limit

The conservation equations may also be used immediately

to derive the Doppler line shape $\zeta_{jk}(\omega)$ corresponding to

an arbitrary distribution of radiating electrons denoted by

$\eta(q)$. If both distributions are normalized to unity, the

result is

$$\zeta_{jk}(\omega) = \sum_{i=1}^{2} \eta(q_i) \left| \frac{dq_i}{d\omega} \right|$$

where the two discrete momenta q_i are those initial values

which will produce an emitted photon of the exact energy ω

(Note that recoil as well as Doppler effects are automatically

taken into account by equations 1a, 1b, which are used to derive the values q_i.)

The implications of these equations may be seen in Fig. 2 and 3. Fig. 2 shows the line shapes due to transverse (relativistic) Doppler broadening at $\theta = \frac{\pi}{2}$. The relative heights of the distinct harmonics here correspond to a black-body emission region with an arbitrary temperature $T=5 \times 10^8 K$. The relation used to determine the relative intensities is simply

$$\frac{I_{20}}{I_{10}} = \frac{n_2 R_{20}}{n_1 R_{10}} = exp\left[\frac{-(E_2-E_1)}{kT}\right] \frac{R_{20}}{R_{10}} \text{, etc.}$$

where n_1 and n_2 are the population numbers of the electron levels and the R's are the individual transition rates.

Finally, Fig. 3 shows the more severe broadening of the emission line as θ is decreased from $\frac{\pi}{2}$. If the observed
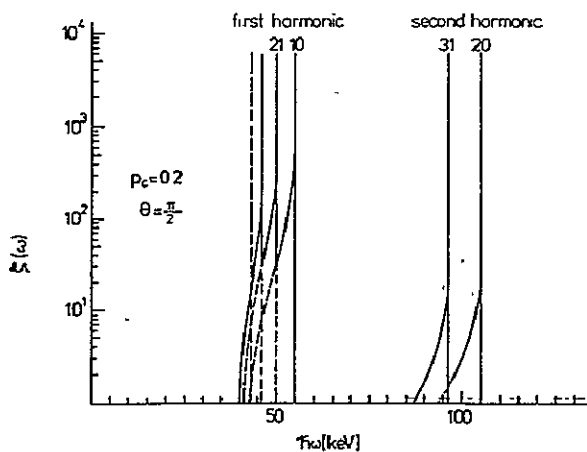
Fig. 2. The Doppler-broadened intensity profile of the individual emission lines tends to show a strong asymmetry at angles near $\pi/2$ with respect to the B field. The relative intensities shown correspond to a thermal electron distribution at $5 \cdot 10^8$ K
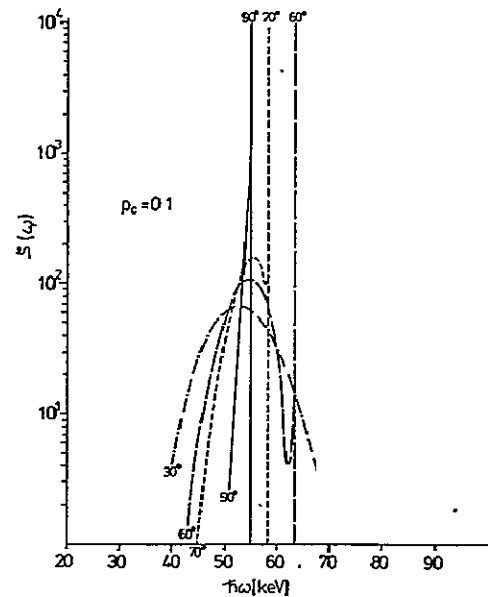
Fig. 3. The asymmetric behavior of the intensity profile $\zeta(\omega)$ persists at angles smaller than $\pi/2$, but becomes more complex showing two distinct maxima, one at $\omega_0(\theta)$ corresponding to the peak of the distribution function and another at the frequency $\omega=\omega_0(\pi/2)/\sin\theta$, at which the denominator in Equation (10) vanishes

X-ray pulsations from Her X-1 are indeed due to the sweep of the magnetic axis past the line of sight, then the line broadening should exhibit a similar dependence on pulse phase.

III. Cyclotron Absorption

As might be expected, the inverse process of cyclotron absorption is equally dependent on the motion of the absorbing electrons. Most of the kinematic effects of absorption are due to the longitudinal motion alone, however, since for temperatures $kT < E_1-E_0$ a majority of the electrons at any given instant occupy only the lowest allowed orbital. Thus for all values of $kT < 50$ keV in the case of Her X-1, it is entirely sufficient to calculate the absorption coefficients for photons traversing a pure ground-state electron gas.

Under the above assumption, the general form of the absorption coefficients for polarized photons of energy $\hbar\omega$ propagating at an angle θ with respect to the field $\underline{B}$ may be written in the form (Daugherty and Ventura 1978)

$$K(\omega,\theta) = \frac{\pi^2 \alpha \hbar^2 c^2 n_0}{(\hbar\omega)^2} e^{-Z} \sum_{j=1}^{\infty} \sum_{i=1}^{2} \zeta(p_i) \cdot \frac{2}{|E_0 \cos\theta - c p_i|}$$

$$\left\{ \frac{1}{j!} Z^j D_1 \left[E_0 E_j - m^2 c^4 + c p_i (c p_i + \hbar\omega\cos\theta) \right] \right.$$

$$+ \frac{1}{(j-1)!} Z^{j-1} D_2 \left[E_0 E_j - m^2 c^4 - c p_i (c p_i + \hbar\omega\cos\theta) \right]$$

$$\left. - \frac{2\sqrt{2}}{(j-1)!} Z^{j-\frac{1}{2}} D_3 \sqrt{\frac{B}{B_{cr}}} mc^2 \cdot c p_i \right\}$$

where $\eta(p)$ is the normalized distribution function for
the longitudinal electron momenta and n_0 is the spatial
electron density. The dimensionless parameter Z is given
by the equation

$$Z = \frac{1}{2}\left(\frac{\hbar\omega}{mc^2}\right)^2 \frac{B_{cr}}{B}\sin^2\theta$$

and the quantities D_i are polarization coefficients
defined in Table 1 below for both linear $(1,2)$ and circular $(\pm)$
polarizations. (The labels are here chosen so that
$\hat{\epsilon}_1 \times \hat{\epsilon}_2 = \hat{k}$, $\hat{\epsilon}_2 \cdot \underline{B} = 0$, $\hat{\epsilon}_\pm = \frac{\mp 1}{\sqrt{2}}(\hat{\epsilon}_1 \pm i\hat{\epsilon}_2)$.   ).

<u>TABLE 1</u>

Polarization:	(1)	(2)	($\pm$)
D_1	$\sin^2\theta$	0	$\frac{1}{2}\sin^2\theta$
D_2	$\cos^2\theta$	1	$\frac{1}{2}(\cos\theta \pm 1)$
D_3	$\sin\theta\cos\theta$	0	$\frac{1}{2}\sin\theta(\cos\theta \pm 1)$

The above expressions for the absorption coefficients
are approximate in that they assume no dispersive effects
for the photons, although for the density regimes expected
in the case of Her X-1 such an approximation should be
quite valid. In any event, the proper inclusion of dispersive
effects is made quite formidable by the fact that the
radiating plasma is almost certainly not homogeneous.

The above expressions have been used by Pravdo <u>et al</u>.
(1978) to fit detailed observations of spectral features,
notably cutoff energies, in the lower continuum emission
of Her X-1. Their results appear to be in good agreement
with a simple power law emission spectrum with superimposed

absorption features. In addition, the absorption process must also play a direct role at the energies associated with any emission features, since numerical estimates based on equation (2) demonstrate that the emission region should be opaque throughout most of its volume. This fact also happens to be necessary in order to produce the high luminosity of the reported line feature. However, a complete model consistently treating both the cyclotron emission and absorption effects, as well as the other possible radiation mechanisms, remains to be developed.

IV. Discussion

In discussions of models for Her X-1 and other pulsating X-ray sources which have appeared to date, it is unfortunately difficult to find detailed calculations which consistently recognize that the deep magnetosphere of the accreting neutron star is an extremely exotic environment dominated completely by the presence of the superstrong magnetic field. The quantizing effects of the field become quite drastic long before the accreting material has reached a height of several stellar radii from the surface. In particular, all the transverse energy of the infalling electrons is lost through rapid magnetic bremsstrahlung. In the increasing field at even lower depths, the plasma remains a one-dimensional gas, and only the intense heating near the surface by Coulomb excitation and photon absorption can manage to raise a fraction

of the electrons back into the first excited orbital at any instant.

As noted above, the field also profoundly changes both the kinematic and dynamic aspects of the interactions between particles. Since the microscopic particle interactions underlie all macroscopic plasma effects, these too must be profoundly modified. Under these conditions it should be obvious that the classical descriptions of Coulomb excitation, cyclotron emission and absorption, Doppler and other broadening effects, as well as large-scale plasma effects, have little or no validity. Consistent quantum-mechanical treatments of all these processes will be required before a quantitative model for objects like Her X-1 is possible.

A second, more specific remark is that even in the context of a quantized treatment of cyclotron emission, the connection between an observed line energy and the actual surface field strength is not entirely unambiguous. In particular, a knowledge of the velocity distribution of the radiating electrons is essential (though non trivial to determine), since any remaining net downward motion in the emitting region will result in a corresponding Doppler shift of the line. It has also been pointed out already (Trümper et al. 1978) that a gravitational red-shift correction of order 10-20% is necessary, although its actual value would require a knowledge of both the stellar mass and radial distance of the emitting region. Further complications may be expected if temperatures become so high that additional harmonics in the spectrum are significant.

In this case, unresolved multiple "first" harmonics (single-step transitions between higher excited states) would also tend to shift the apparent line energy downward from its fundamental value. Whether these several effects can be untangled to arrive at a reliable value for the field strength will depend both on further observations and the development of more refined theoretical models.

Acknowledgements

References

Canuto, V., and Ventura, J., Fundamentals of Cosmic Physics 2, 203 (1977)

Daugherty, J., and Ventura, J., Astron. Astrophys. 61, 723 (1977)

Daugherty, J., and Ventura, J., Phys. Rev. D, 1978 (in press)

Pravdo, S. H., Bussard, R. W., Becker, R. H., Boldt, E. A., Holt, S. S., Serlemitsos, P. J., and Swank, J. H., NASA/Goddard Space Flight Center preprint (1978)

Trümper, J., Pietsch, W., Reppin, C., Voges, W., Staubert, R., and Kendziorra, E., Astrophys. J. 219, L105 (1978)

The Excitation of Electronic Transverse Energy Levels

in an Intense Magnetic Field

Roger W. Bussard[*]
Laboratory for High Energy Astrophysics
NASA/Goddard Space Flight Center
Greenbelt, Maryland 20771

*Also, Department of Physics and Astronomy, University of Maryland

I. Introduction

Recent observations of the X-ray pulsar Hercules X-1 have shown a line emission feature at about 60 keV, which has been interpreted as the fundamental electron cyclotron line in a magnetic field of around 6×10^{12} gauss (Trümper et al. 1978, Coe et al. 1977). In this interpretation, the line radiation results from transitions between transverse energy levels, which are quantized by the field. This paper calculates the expected line luminosity from the excitation of these levels by protons which are falling into the polar cap of a neutron star. They are assumed to attain kinetic energies up to around 200 MeV, the gravitational potential energy at the surface. In section II, we calculate the cross sections for high energy Coulomb encounters between small pitch angle protons and electrons in a strong field. In section III, these cross sections are used to calculate the energy loss rate of the infalling protons. This rate, together with the rate of elastic nuclear proton collisions, is then used to calculate the number of line photons an infalling proton can be expected to produce, directly or indirectly. Finally, in section IV, we apply the results to Hercules X-1.

II. Coulomb Encounters

The solution of the Dirac equation for an electron in an intense magnetic field B yields total energy (W) eigenvalues

$$W^2 = p^2 c^2 + m_e^2 c^4 (1 + 2jB/B_q) \qquad j = 0,1,2,\ldots \qquad (1)$$

where P is the electron momentum parallel to the field, c is the speed of light, m_e is the mass of the electron, and

$$B_q = m_e^2 c^3/(eh) = 4.414 \times 10^{13} \text{ gauss.} \qquad (2)$$

The radiation we are primarily considering is emitted when an electron makes a transition from the first excited state (j=1) to the ground state (j=0). In normal astrophysical situations, the electron Lorentz factors are much larger than B/B_q, so that the electrons occupy states of high quantum number and have

large parallel momenta. In this case, they radiate mostly the first harmonic ($\Delta j=1$), but the Doppler shifts resulting from the large parallel velocities broaden the radiation into a synchrotron spectrum. However, even for mildly relativistic electrons ($\gamma \leqslant 1.1$) in fields greater than 10^{12} gauss, the quantum nature of the radiation must be taken into account. Discrete cyclotron line emission rates and absorption cross sections have been calculated for intense fields by Daugherty and Ventura (1977 and 1978). The lifetime they obtain for an electron in an excited state is of order 10^{-16} seconds, much shorter than collisional time scales for reasonable densities implying that relatively cool ($kT_e \leqslant \hbar eB/m_e c$) electrons will spend most of their time in the ground state.

In a Coulomb collision, the momentum transfer prefers to occur perpendicular to the relative velocity. For energetic protons with small pitch angle colliding. with an electron in the ground state of an intense field, the transfer of energy to the electronic plasma is inhibited (Basko and Sunyaev 1975). However, under energetically favorable conditions, the proton can transfer transverse momentum to the electron by excitation of the quantum levels. In addition, head-on or knock-on collisions can occur, in which the electrons are not excited, but are reflected along their field line. We have calculated the cross sections for these processes as a function of the electron energy in the proton's rest frame, E_e^*, by a first order quantum electrodynamic approximation. The results are shown in Figure 1, where the dashed lines represent the results of the calculation, which because of a breakdown in the approximation, become infinite at the thresholds of excitation. We have arbitrarily smoothed these infinities as shown by the solid lines. The index j labels the final state: j=0 represents a knock-on collision, j=1 represents an excitation from the ground state to the first excited state, and so on. For the energies under consideration, excitation of the 1st excited state dominates all other Coulomb processes above its threshold. Analytically, the

cross section σ_j for excitation of the jth state from the ground state in a Coulomb collision with an ion of charge Ze with zero pitch angle is given in the ion's rest frame by

$$\sigma_j(p) = \frac{\pi\,B_q}{B}\,\frac{Z^2 r_e^2}{c^2(E+2m_ec^2)}\sum_{\pm}\left|\frac{1}{p\,p'_\pm}\right|\left\{\delta_{s',-\frac{1}{2}}\frac{1}{j!}\left[2(E+m_ec^2)(E+2m_ec^2)+c^2(p'_\pm-p)p\right]^2\right.$$
$$\left.+\,\delta_{s',\frac{1}{2}}\frac{2}{(j-1)!}\frac{B}{B_q}m_e^2c^4\,p^2c^2\right\}\,\epsilon_j\left(\frac{B_q}{2B}\frac{(p'_\pm-p)^2}{m_e^2c^2}\right)\tag{3}$$

where r_e is the classical electron radius, 2.82×10^{-13} cm, p and p' are the initial and final momenta parallel to the field respectively, of the electron, E is the electron kinetic energy, and s' is its final spin. There are two possible values of the final momentum, given by $p'_\pm = \pm\sqrt{p^2 - 2m_e^2c^2\,B/B_q\,j}$, and these are summed over in equation (3). Finally the ϵ_j are defined by

$$\epsilon_j(x) = \int_x^\infty \frac{dt}{t^2}\,e^{-(t-x)}(t-x)^j.\tag{4}$$

The first three are given here in terms of the exponential integral:

$$\epsilon_0(x) = 1/x - e^x E_1(x)$$
$$\epsilon_1(x) = e^x(1+x)\,E_1(x) - 1$$
$$\epsilon_2(x) = 1+x - (x^2+2x)\,e^x E_1(x)$$

III. Line production by infalling protons

Using the results of the previous section for the Coulomb cross sections σ_j, in an intense magnetic field, we have calculated the energy loss rate per unit matter traversed for a proton with zero pitch angle by Coulomb processes:

$$dE/dX = 1/(m_p v)\sum_{j=0}^\infty \int_{-\infty}^\infty dp\; f_e(p)\,v_{rel}(E,p)\,\sigma_j(E,p)\,\Delta E_j(E,p),\tag{5}$$

where m_p is the proton mass, v is the proton velocity, p is the electron parallel momentum, f_e is the electron distribution function in p, v_{rel} is the relative

velocity between the particles in the encounter, and ΔE_j is the energy lost in the collision. The results, assuming a relativistic one dimensional thermal distribution of electrons, are shown in Figure 2 for four temperatures. For comparison the energy loss rate in a non-magnetized gas of temperature 35 keV is shown by the dotted line (Book and Ali 1975). For $T_e = 0$, there is a sharp discontinuity at the threshold for excitation, but this disappears when the electrons take on a thermal distribution, and at $T_e = 35$ keV, dE/dx is relatively constant in energy.

Figure 3 shows the Coulomb mean ranges for the temperatures discussed above. As Basko and Sunyaev (1975) pointed out, for high enough energies elastic proton-proton nuclear scattering has a mean free path smaller than the Coulomb range ($X_{p-p,elas} \sim 50$ gm/cm^2). In an elastic scattering, the proton is deflected from zero pitch angle, and then the energy can be given up rapidly to ambient electrons, via the excitation of plasma waves, for example. Thus, the equation for the energetic proton distribution function in a steady state atmosphere can be written

$$\frac{\partial \Phi}{\partial X} - \frac{\partial}{\partial E} \left(\Phi \frac{dE}{dX} \right) = - \sigma_{pp}/m_p \; \Phi(E,X),$$

(6)

where E is the proton energy, X the amount of matter traversed (in gm/cm^2 for example), Φ is the differential (in energy) flux of protons, and σ_{pp} is the cross section for a nuclear collision with an ambient proton. The solution to this equation with the boundary condition that injection occurs at the top of the atmosphere, (X=0) with flux $\varphi_0 \delta(E-E_0)$ is

$$\Phi(E,X) = \varphi_0/(dE/dX) \; \exp \left[- \int_E^{E_0} \frac{\sigma_{pp}(E')}{m_p \, dE/dX(E')} \, dE' \right]$$

(7)

To evaluate the line productivity of the protons in a one dimensional thermal gas, we have integrated the flux given by equation (7) with the cross sections for knock-on and excitation collisions. An excitation to the jth level is

assumed to yield j line photons since the electrons tend to deexcite in single step transitions (Canuto 1977, Daugherty and Ventura 1977). A knock-on was assumed to produce as many line photons as was energetically possible by Coulomb collisions with ambient ions. It is important to note that we neglect energy losses of the knock-ons to continuum photons by resonant absorption (Pravdo et al. 1978) which results in the conversion of these photons to line photons. The results for the multiplicity of line photons produced under our assumptions are shown for the four temperatures in Figure 4a, and Figure 4b shows the fraction of the proton's energy put into line photons as a function of the injection energy. For Figure 4b, we assume a line photon has an average energy equal to the energy of the 1st excited state with p = 0.

In order to investigate the production of cyclotron line photons by the high energy tail of a one dimensional thermal electron distribution in collisions with ambient protons, we have integrated the cross-section for the excitation of the first excited state with such a distribution function. The resulting line production rate per unit gas density, α_1, is given by

$$\alpha_1(T) = \int dp \; f_T(p) \; \sigma_1(p)v \; , \tag{8}$$

where T is the temperature of the medium, v is the velocity of an electron with momentum p , σ_1 is the cross section for the transition from the ground state to the first excited state, and $f_T(p)$ is given by

$$f_T(p) = \exp(-c\sqrt{p^2+m^2c^2}/kT)/(2mc \; K_1(mc^2/kT)) \tag{9}$$

where $K_1(x)$ is the modified Bessel function (Abramowitz and Stegun 1965). The results for temperatures of 1 to 100 keV are shown in Figure 5, for field values of 10^{12} and 6×10^{12} Gauss. As can be seen, the line production coefficient α_1 rises quite dramatically as kT approaches $\hbar eB/(m_e c)$ and flattens somewhat at higher temperatures.

IV. Application to Hercules X-1

If we assume that radiative transfer has little effect on the ratio of line energy to total energy released, the calculations of the preceding section may be compared with observations of the X-ray pulsar Her X-1. From a recent observation of a feature near 60 keV, Trumper et al. (1978) have estimated a luminosity in line photons of $2x10^{35}$ ergs/sec. There are two observed components of continuum radiation, hard (2 to 20 keV) and soft (.1 to 1 keV) X-rays, with roughly comparable luminosities of 1 to $2x10^{37}$ erg/sec (Giacconi et al. 1973, Schulman et al. 1975, Catura and Acton 1975). The infalling protons are generally assumed to power both components, so at most, only 1/2 to 1 percent of the energy comes out in the line. Since the effective hard X-ray temperature is $\geqslant 20$ keV (Pravdo et al. 1977), we see from Figure 4b that this fraction is consistent with infall proton energies of 140 MeV to 180 MeV.

On the other hand, Compton scattering of the line by electrons in a relatively cool $(T \sim 10^{6}K)$ shell of material at the Alfven radius may reduce the line luminosity considerably. Such a shell has been proposed to account for the soft X-ray flux mentioned above (McCray and Lamb 1976, Basko and Sunyaev 1976). In addition, the reported width of the ~ 60 keV feature implies that its emission occurs at angles close to 90 degrees with the magnetic field direction (Trumper et al. 1978) where the Alfven shell is expected to be the thickest. The Compton scattering depth is estimated to be from 2 to 4 in this region. Using the calculations of Weaver (1978), who finds that the luminosity in a narrow feature at 60 keV is reduced by $2 \exp(-\tau_{c})$ by a shell of Compton depth $\tau_{c} \sim 3$ we see that if the Alfven shell exists, the observed ratio of line luminosity to total (soft and hard X-ray) luminosity is inconsistent with our calculations by about an order of magnitude or more. However, it can be argued that a large amount of the accretion energy goes into unobservable channels. In this case, we can estimate an accretion rate as a function of the Compton depth of the Alfven shell. For an infalling proton energy of 150 MeV into a gas at a temperature of 35 keV, the accretion rates required under our assumptions are $3.4x10^{17}$, $1.2x10^{18}$, $3.4x10^{18}$, and $9.3x10^{18}$ gm/sec for τ_{c} of 0, 2, 3, and 4 respectively.

References

Abramowitz, B. and Stegun, I. A., Handbook of Mathematical Functions, Dover, New York, (1965).

Basko, M. M. and Sunyaev, R. A., Astron. and Astrophys. 42, 311 (1975).

Basko, M. M. and Sunyaev, R. A., M.N.R.A.S., 175, 395 (1976).

Book, D. L. and Ali, A. W., A Collection of Plasma Physics Formulas and Data, NRL Memorandum Report 2898 (1975).

Canuto, V. and Ventura, J., Fundamentals of Cosmic Physics, 2, 203 (1977).

Catura, R. C., and Acton, L. W. , Ap. J. Letters, 202, L5 (1975).

Coe, M. J., Engel, A. R., Quenby, J. J., and Dyer, C. S., Nature, 268, 508 (1977).

Daugherty, J. K., and Ventura, J., Astron. and Astrophys. 61, 723 (1977).

Daugherty, J. K., and Ventura, J., Phys. Rev. D, (in press).

Giacconi, R., Gursky, H., Kellogg, E., Levinson, R., Schreier, E., and Tananbaum, H., Ap. J. 184, 227 (1973).

McCray, R., and Lamb, F. K., Ap. J. Letters, 204, L115 (1976).

Pravdo, S. H., Bussard, R. W., Becker, R. H., Boldt, E. A. , Holt, S. S., Serlemitsos, P. J., and Swank, J. H., submitted to Ap. J.

Schulman, S., Friedman, H., Fritz, G., Henry, R. C. and Yentis, D. J., Ap. J. Letter 119, L101 (1975).

Trumper, J., Pietsch, W., Reppis, C., Voges, W., Staubert, R., and Kendziorra, E., Ap. J. Letters, 219, L105 (1978).

Weaver, R. P., Nature, in press (1978).

Figure Captions

1. The Coulomb cross-sections for excitation and knock-on collisions in a field of 6×10^{12} G as a function of the electron energy in the proton rest frame (bottom scale) or the proton energy in the electron rest frame (top scale). The electrons are initially in the ground state and the protons have zero pitch angle; j labels the final transverse energy state.

2. The Coulomb energy losses suffered by zero pitch angle protons per unit matter traversed for several temperatures in a field of 6×10^{12} G, as a function of the proton energy. Also shown are the losses in a non-magnetized gas of kT = 35 keV.

3. The Coulomb range of fast protons with zero pitch angle, without taking nuclear collisions into account, in gases at several temperatures.

4. a) The multiplicity of line photons produced as a result of Coulomb interactions with infalling protons as a function of the initial energy of the proton.

    b) The fraction of the proton kinetic energy going into line radiation as a function of the initial proton energy.

5. The coefficients for thermal excitation of the first excited state in fields of 1 and 6×10^{12} G, as functions of the gas temperature.

Figure I

COULOMB ENERGY LOSS, $B=6\times10^{12}$ G

T=35 keV, B=0

T=5 keV

0

15

35

$\langle dE/dx \rangle$ (MeV CM^2/GM)

E_p (MeV)

Figure 2

COULOMB RANGE, B≈6×10¹²G
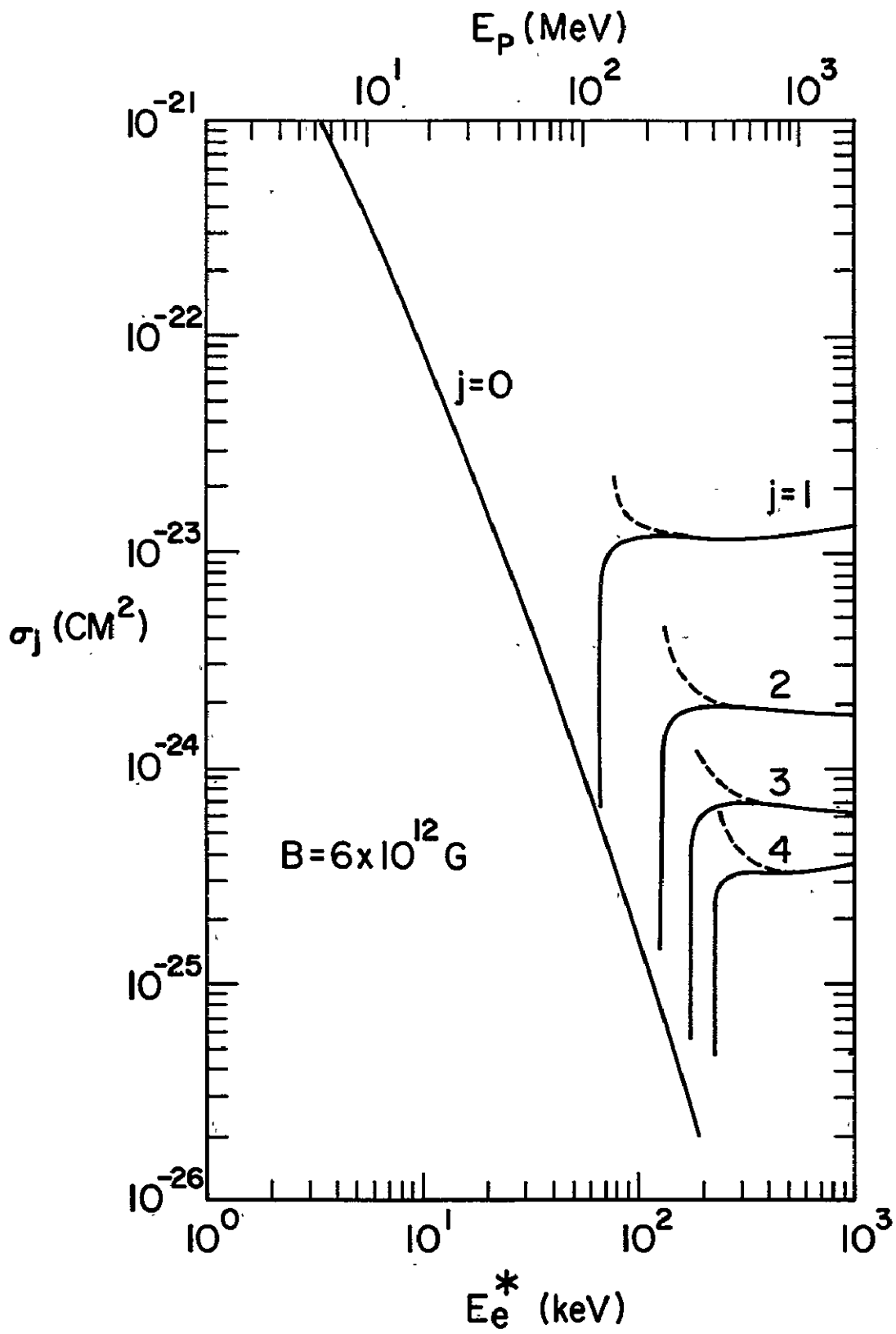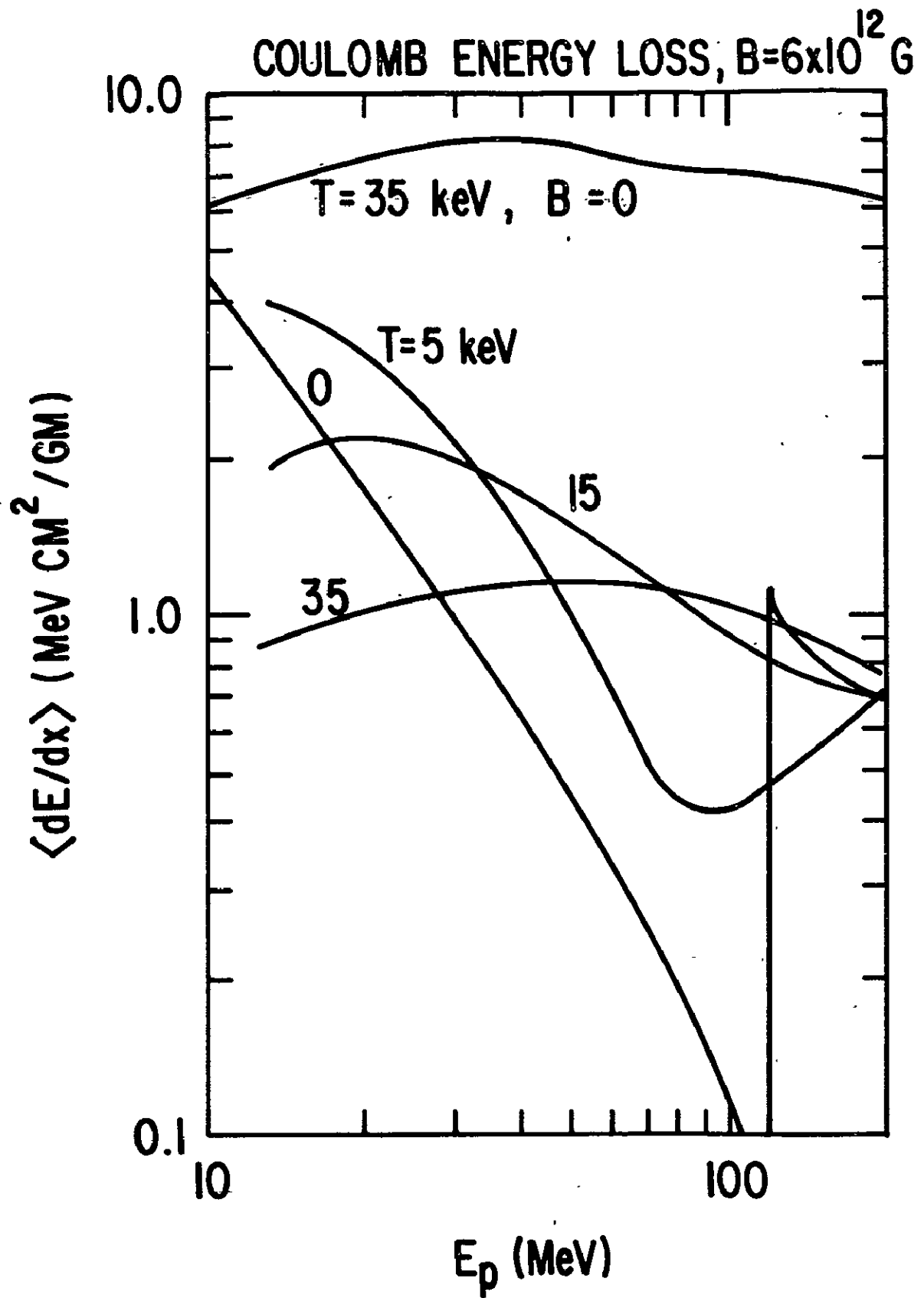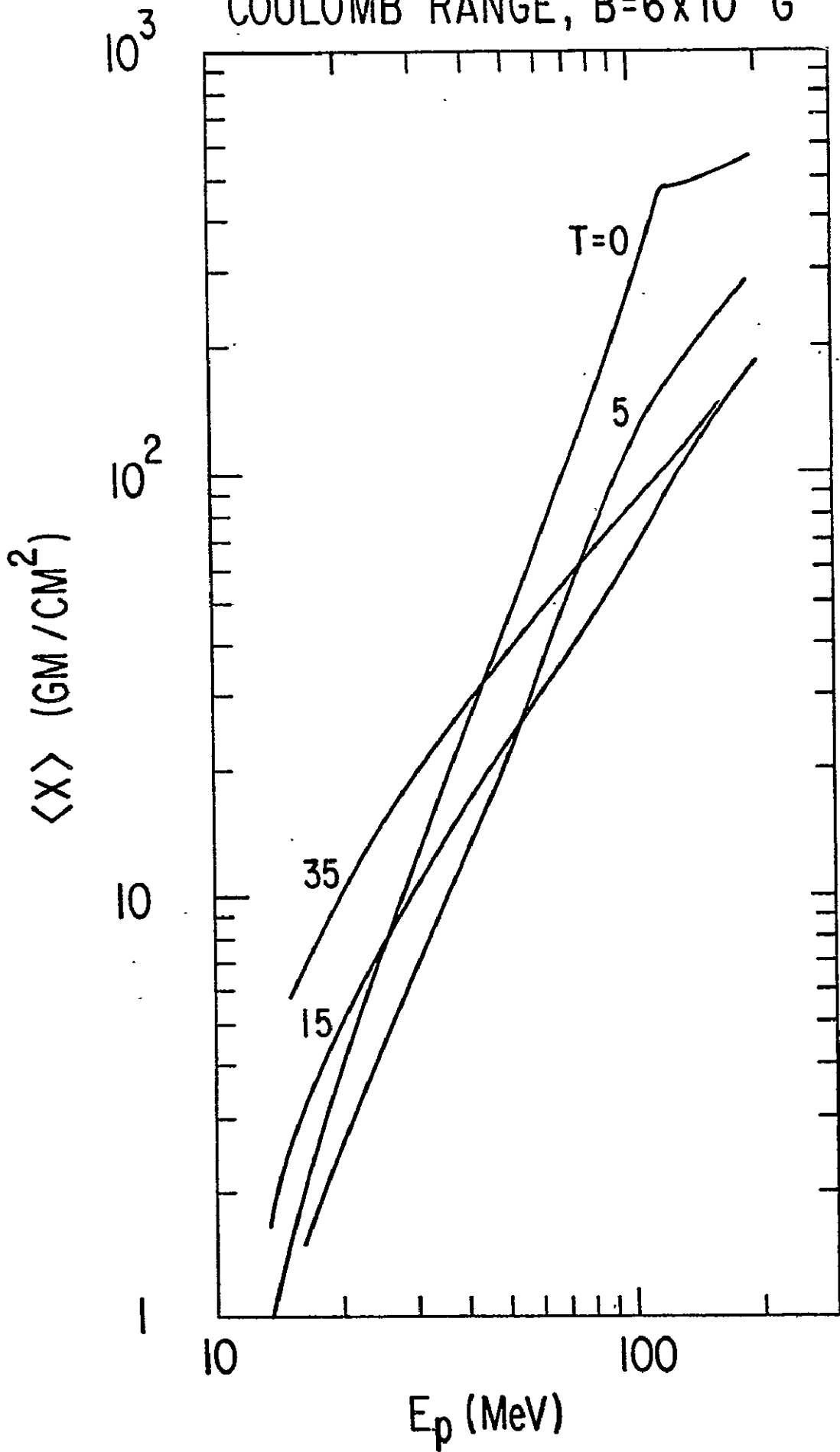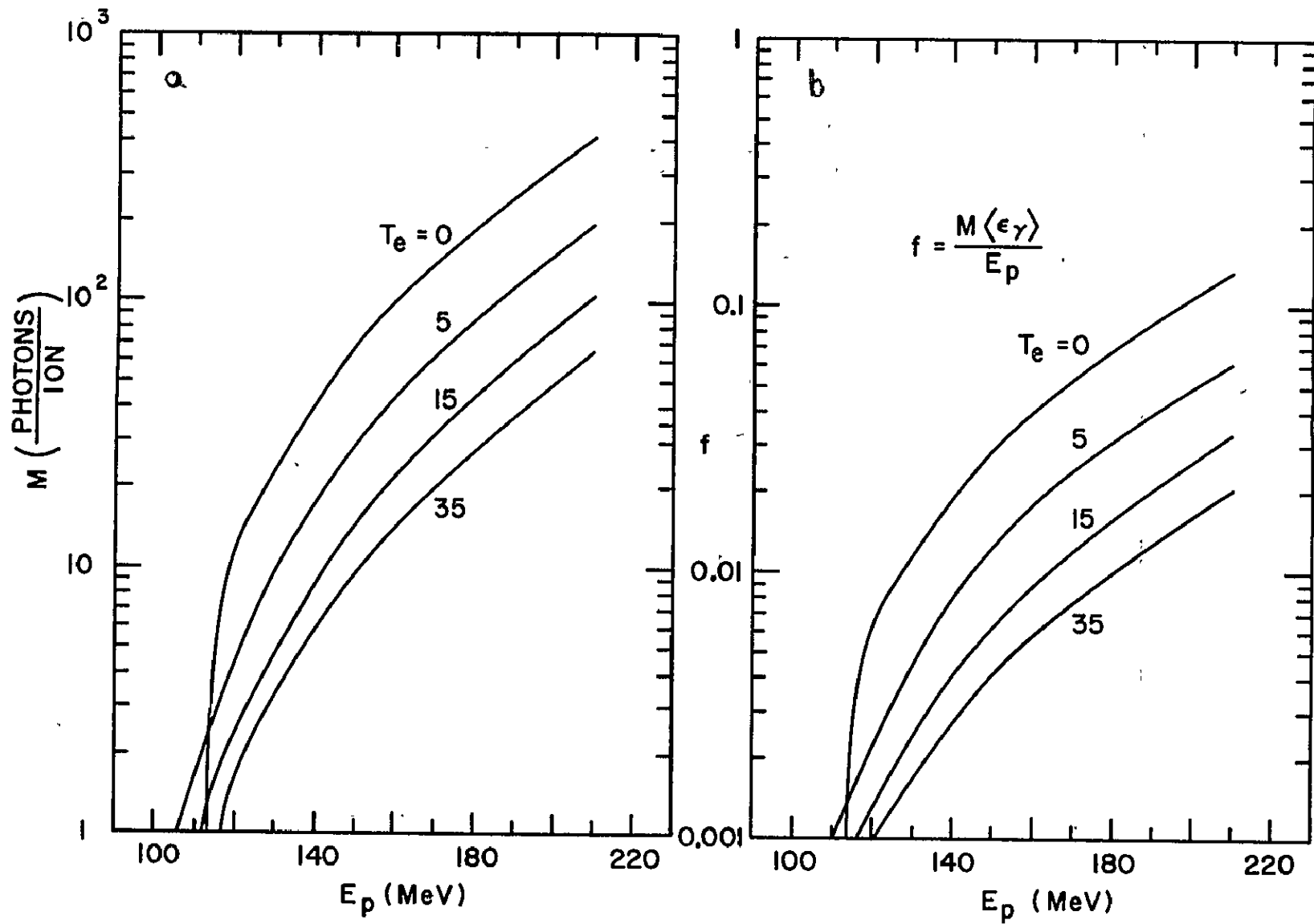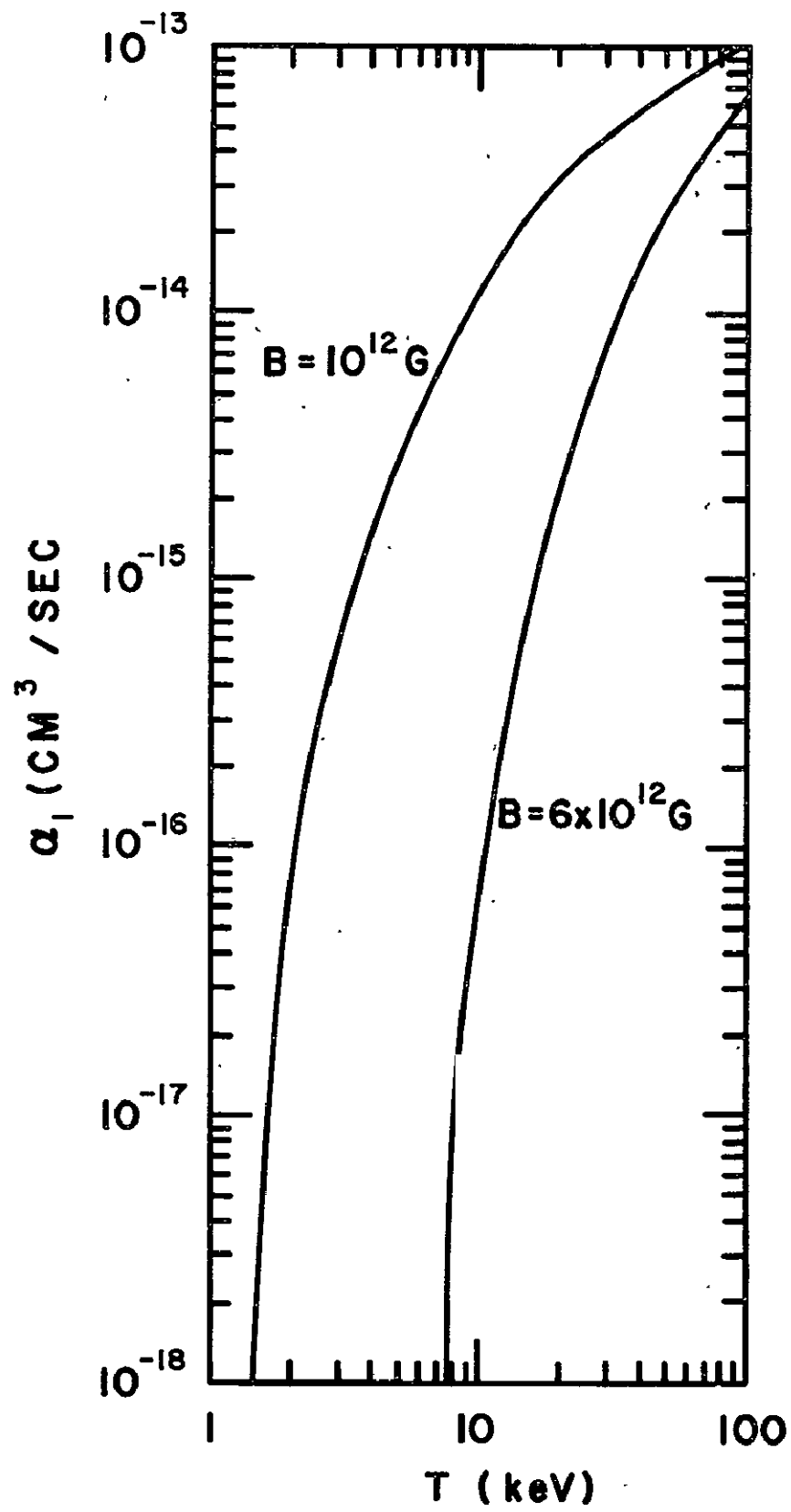
Figure 3

igure 4

Figure 5

The Transfer of Cyclotron Lines through the Magnetospheric Shell of Hercules X-1

Robert P. Weaver
Laboratory for High Energy Astrophysics
Goddard Space Flight Center
Greenbelt, Maryland   20771

1. INTRODUCTION

A line feature has been observed in the hard X-ray spectrum of the neutron star Hercules X-1 (Trumper, et al. 1978; Voges, et al. 1978). In this volume, Professor Trumper has presented an excellent case for the identification of this feature as cyclotron emission from a strong magnetic field ($B \approx 5 \times 10^{12}$ G). If this interpretation is indeed correct, and one accepts the model wherein the 1.24 second hard X-ray pulse is due to the occultation of a more isotropic X-ray flux by an opaque magnetospheric shell (McCray and Lamb 1976; Basko and Sunyaev 1976), then these observations can be used to place strict limits on the total source luminosity of the cyclotron emission. Here, I shall consider the obser-vational fate of cyclotron line photons that have emerged from the region near the neutron star surface ($R \approx 10^{6}$ cm), but have yet to encounter an opaque shell at the magnetosphere ($R \approx 10^{8}$ cm). It is shown that if a narrow line is incident on such a shell, then a residual narrow feature can emerge from the shell.

The important feature of the observations described by Professor Trumper is that the lines are narrow. The observed FWHM is $\leqslant$ 12 keV (Trumper, et al. 1978), with a total observed luminosity in the line of approximately 1% of the total X-ray luminosity. Furthermore, the line seems to be pulsed in phase with the 1.24 second hard X-ray pulse (Kendziorra, et al. 1977). This width of $\leqslant$ 12 keV is narrow for a line centered near 58 keV if the line photons have Compton scattered.

The conditions on the surface of the neutron star ($T \approx 15$ keV and $B \approx 10^{12}$G) seem to favor the production of a significant flux of cyclotron radiation. In this case, the fundamental cyclotron harmonic can be excited either by collisions or by blue shifted photons. The physics of this excitation and subsequent re-emission are discussed in this volume by J. Daugherty and R. Bussard. From their results, it is not presently clear whether we understand how a narrow emission line can be emitted by this source region near the neutron star surface. However the fundamental result of these studies is that if a narrow line is emitted by the source region, then it is emitted in a narrow beam directed almost perpendicularly to the magnetic field lines.

2. The Magnetospheric Shell

It was the discovery of a luminous soft X-ray flux ($E < 1$ keV) by Catura and Acton (1975) and Shulman, et al. (1975) that lead Basko and Sunyaev (1976) and McCray and Lamb (1976) to propose that there is an opaque magnetospheric shell surrounding Hercules X-1. The key observational result was the total luminosity of the soft X-rays. Even if the soft source emitted as a blackbody, the minimum surface area that could account for the observed luminosity is given by a sphere with radius $R \approx 10^8$ cm. For simple estimates of the properties of the neutron star, this radius corresponds well with that expected for the termination of the neutron star magnetic field. Thus the accreting gas should be delayed somewhat at this "magnetosphere," since the magnetic pressure at this radius is sufficient to counterbalance the ram pressure of the infalling gas.

McCray and Lamb (1975) estimate that the magnetospheric shell formed by this process should be opaque to Compton scattering, with $\tau_{es} \approx$ few. Furthermore, this shell should not be of uniform thickness in magnetic latitude. As the gas can accrete more freely towards the magnetic poles, the flow speed is enhanced (over that at the magnetic equator) and from continuity arguments one

finds that the shell should become transparent in some region surrounding the direction of the magnetic poles. Thus, the narrowest cyclotron line that can emitted by the source region is directed at the thickness part of the magnetospheric shell.

3. Effects of Incoherent Compton Scattering

Most of the $\approx$ 58 keV line photons will be removed (in energy) from the narrow line core by incoherent Compton scattering. One can produce simple estimates for the redistribution effects of the scattering. The angle averaged energy shift per scattering for a zero temperature gas (a good approximation for conditions in the shell since $E_{line} \approx$ 58 keV) is $< \Delta E > = - E^2/ m_e c^2 = - 5$ (E/50 keV)^2 keV. Also, there are two effects that tend to broaden an initial delta function in energy (even for $T_e = 0$). First, for a given scattering depth, the photons which emerge from the scattering medium at a particular time will have a distribution in their number of scatterings. Second, every photon will not scatter through the same angles, and since the actual energy shift depends on these angles, the emergent distribution will be broadened. The combination of these two dispersion effects tend to broaden an initial delta function by approximately the same amount as it was shifted in energy. For example, for a τ_{es} = 4 shell, one would expect that an average photon will scatter about τ_{es}^2 = 16 times; thus, even a delta function at 60 keV will be shifted into a broad peak centered near 20 keV and having a width of 2 $\sigma \approx$ 30 keV!

The question then is, how can there be a narrow feature at 58 keV, if these photons have scattered through a magnetospheric shell? For a uniform spherical shell, the only way photons can escape in a narrow feature is if the unscattered or primarily forward scattered photons are strong enough to be seen above this broad "continuum" of scattered line photons. Whether a

line can be seen or not depends critically on the total scattering depth

of the medium the photons have traversed and on the initial energy of the line.

4. Results and Discussion

These simple considerations can be shown to be correct. I have developed

a Monte Carlo X-radiation transfer code in order to study the scattering of

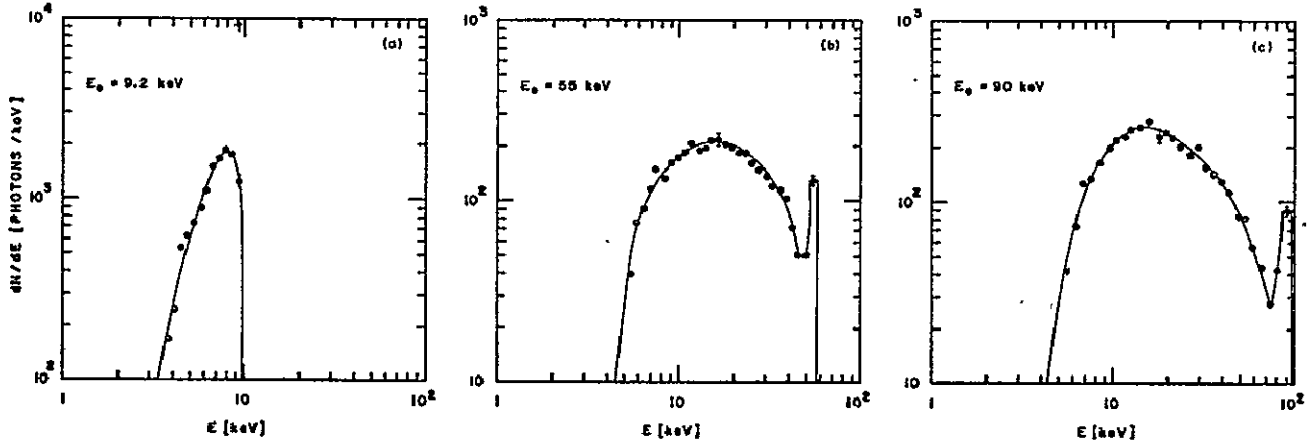narrow lines in the X-ray regime (1 keV < E < 100 keV). Figure 1 shows

Figure 1. The Comptonized distribution of photons that have scattered through a uniform $\tau_{es} = 3$ spherical shell. The shell is cold ($T_e = 0$). Monoenergetic photons were incident normally on the inner surface of the shell.

the results of a typical calculation. Monoenergetic photons were injected

into a $\tau_{es} = 3$ spherical shell at three energies: 9.2 keV (figure 1a); 55 keV

(figure 1b); and 90 keV (figure 1c). As the energy of the initial photons

increases a typical photon will lose more energy per scattering. The final

distribution will be correspondingly broader for a fixed scattering depth.

As a result the Comptonized distribution for low energy photons (figure 1a)

engulfs the narrow peak of unscattered or primarily forward scattered photons.

However above about 20 keV, the scattered continuum is sufficiently reduced

(due to down scattering) at the initial line energy so that this narrow

residual peak can be seen above the continuum (for the same resolution of

the line and continuum). Note that for photons at 90 keV, the energy loss

per scattering is so large (with the total scattering depth essentially un

changed) that the broad peak of the scattered distribution is nearly at the same energy as that from photons which started at 55 keV.

Thus, even if there is an opaque shell at the neutron star magnetosphere, a narrow line can be seen at $\approx$ 60 keV if the scattering depth is not too large. For large depths ($\tau_{es} > 5$), the number of photons that do not scatter is sufficiently small that the scattered distribution always overwhelmes them. Note that in this model, the line would appear to be 180° out of phase with the hard X-ray pulse. The line photons emerge from the shell near $\theta \approx 90°$, while the photons in the hard X-ray pulse must leave the system near $\theta \approx 0°$ if the pulse is due to the variable opacity of the shell (θ is the angle to the pole direction).

Clearly, a more self-consistent model would allow line photons to escape through the "holes" in the shell where the hard X-ray pulse originates. To this end, and following Langer, Ross and McCray (1978), I have used a uniformly thick ($\tau_{es} = 3$) spherical shell with symmetrically placed holes over the magnetic poles. These holes remove 25% of the surface area of the shell (see Langer, et al. 1978). Monoenergetic photons ($E_0 = 56$ keV) are still injected at $\theta = 90°$; however, there are now two escape routes for these photons. They can escape through the shell itself (as before) or if they backscatter through the inner wall of the shell and are moving in the right direction, they can escape through one of the holes.

The spectral results for this model are shown in figure 2. Figure 2a shows the spectrum of the total radiation that escaped through the shell. As before, a narrow feature remains at the initial energy of the line. Figure 2b shows the spectrum of the total radiation that escapes through the holes. Again there is a narrow feature in the spectrum. The energy of this feature corresponds exactly to the energy of a once backscattered photon $E' = E_0/$

$(1 + 2E_0/m_ec^2)$. For this backscattered feature to be present, the shell

scattering depth need only be $\tau_{es} > 1$ (with no upper limit).
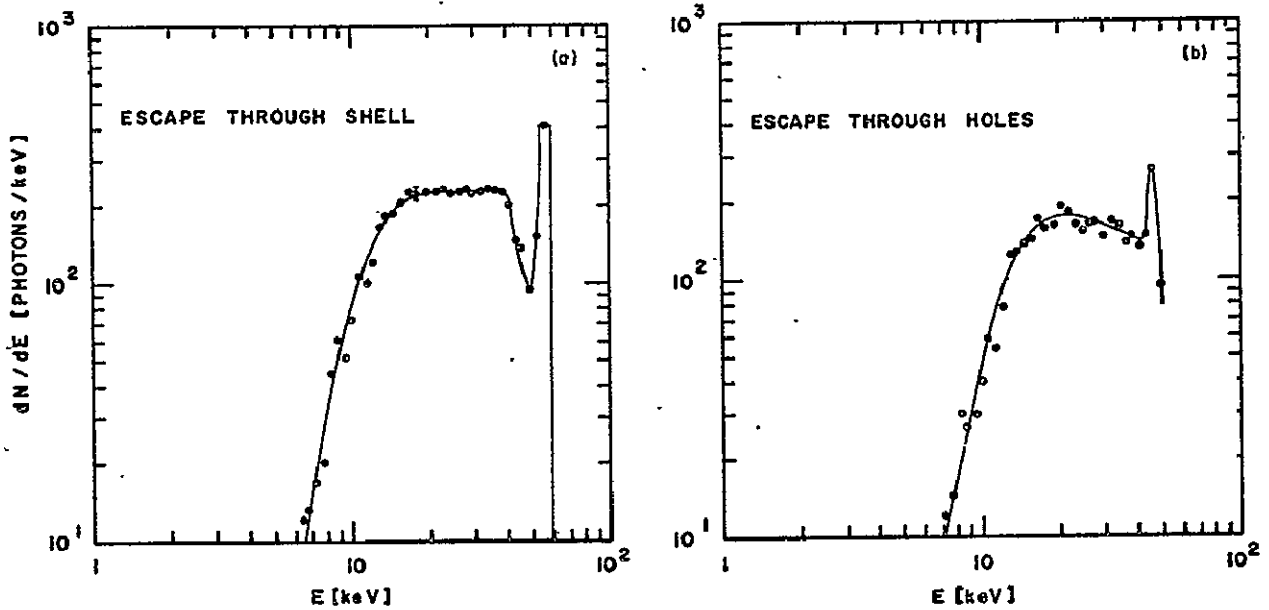

Figure 2. The spectrum of the total radiation that escapes through a $\tau_{es} = 3$ spherical shell with holes over the magnetic poles. Monoenergetic photons ($E_0 = 56$ keV) were directed towards $\theta = 90°$; they were followed until they escaped through the shell or through one of the holes.

Notice that in any case where there is a scattering medium surrounding the cyclotron source region, most of the photons will be removed from the original narrow feature. In other words, the observed luminosity of the line in this model is only a small fraction of the total source luminosity. Only 5% of the total source luminosity escapes in the narrow feature through the holes, while 11% escapes in the narrow feature through the shell. The amount that escapes through the holes depends only on the size of the holes, while that which escapes through the shell depends strongly on the total scattering depth through the shell. Thus, if one observes a narrow feature near 60 keV and there is an opaque magnetospheric shell surrounding the source of line photons, then some fraction greater than 10% of the available gravitational energy in the accretion is being transformed into cyclotron emission. Since the observed line seems to be pulsed in phase with the hard X-rays (Kendziorra, et al. 1977), it seems reasonable that the observed emission is cyclotron

line radiation that has backscattered and escaped through a more-or-less

transparent region of the magnetospheric shell.

REFERENCES

Basko, M. M., and Sunyaev, R. A. 1976, M.N.R.A.S., 175, 395.

Cature, R. C., and Acton, L. W. 1975, Ap. J. (Letters), 202, L5.

Kendziorra, E. Staubert, R., Pietsch, W., Reppin, C., Sacco, R., and
     Trumper, J. 1977, Ap. J. (Letters), 217, L93.

Langer, S. H., Ross, R. R., and McCray, R. 1978 Ap. J., in press.

McCray, R., and Lamb, F. K. 1976, Ap. J. (Letters), 204, L115.

Shulman, S., Friedman, H., Fritz, G., Henry, R. C., and Yentis, D. J.
     1975, Ap. J. (Letters), 199, L101.

Trumper, J., Pietsch, W., Reppin, C., Voges, W., Staubert, R., and
     Kendziorra, E. 1978, Ap. J. (Letters), 219, L105.

Voges, W., Pietsch, W., Reppin, C., and Trumper, J. 1978, IAU Circular
     No. 3184/

Theory of the accretion column
and cyclotron radiation in X-ray pulsars

by

P. Mészáros

ax-Planck-Institut für Physik und Astrophysik,
Föhringer Ring 6, 8000 München 40, F.R. Germany

Abstract

The energetics of the decelerating matter in the accretion column of X-ray pulsars is considered, in particular the Coulomb process. A two zone model is presented to account for the continuum and cyclotron line emission, incorporating a fan-beam radiation scheme, which appears able to explain the observed properties.

The most straightforward interpretation for the line feature

observed around 53 KeV in Her X-1 is that it is a cyclotron emission

line, corresponding to a field B $\sim$ 4x10^{12} Gauss, seen in emission

(e.g. Trümper et al. 1977, Mészáros 1978), the argument being that

at the line the opacity is so high that the intensity reaches the

Planck value. A very complete model of the accreting column has been

discussed by Sunyaev and Trümper (1978). The model discussed here,

while producing a roughly similar geometry and temperature structure,

is based on different physical processes.

If the line is thick, one can estimate the surface area required

to produce a line luminosity L_L $\sim$ few x 10^{35} erg s^{-1} to be

$$A_L = L_L (2\pi \ I_L)^{-1} \simeq 10^7 \ cm^2 \qquad (1)$$

The continuum, on the other is probably somewhat below the Planck

value, due to comptonization (the main opacity being Thomson,

τ_T $\sim$ 5-10). The area required to produce the observed L_c $\sim$ 10^{37}

erg s^{-1} is, at an estimated kT_c $\sim$ 4-8 KeV,

$$A_c > 10^9 \ cm^2 \qquad (2)$$

What may determine the characteristic dimensions of these

areas? The radius of the polar caps, estimated on the basis of

a dipole pattern and an Alfven radius where $B^2/8\pi$ $\sim$ ρv^2 of

infalling matter, is a_o $\sim$ 10^5 cm. The height along the accret-

ing column of the emitting regions l_c and l_L of the continuum

and line (see Fig. 2) must be given by the deceleration process

of the matter. A radiation pressure shock (Basko and Sunyaev

1975) is only marginally important, if the matter fills the

whole volume of the column and we consider Thomson scattering

mainly (the critical luminosity above which radiation pressure

is important turns out to be $L* = 10^{37}$ $(a_o/10^5$ cm) $(R/R_*)^{3/2}$
(σ_T/σ) erg s^{-1} $\simeq L_c$). Using reduced Thomson cross sections
$\sigma \sim \sigma_T (v/v_H)^2$ due to magnetic field effects would increase
L*, on the other hand including cyclotron opacities might de-
crease it (the cyclotron luminosity is however also smaller).
If the column were not filled by matter totally, but only a
shell, or wall on the outside of it, this would reduce the
area and decrease L*, but whether such a configuration arises,
or is stable in the presence of instabilities present in a shock,
is unclear, and a more or less filled column is probably the
safest assumption. Two stream instability-type collisionless
shocks are another possibility, but there is uncertainty as
to whether the instabilities really develop to the non-linear
stage in the situation envisaged (Alme and Wilson 1973, Shapiro
and Salpeter 1975). We consider now deceleration of the in-
falling ions, which carry most of the accretion energy, by
coulomb collisions with the electrons of the stationary plasma
in the lower part of the column. The energy loss per unit path
length is

$$\frac{dE}{dz}\bigg|_{B=0} = - \omega_{pe}^2 \ e^2 \ V_o^{-2} \ \ln \ [2\zeta^{-1} \ \rho_D/\rho_{min}] \ \propto \frac{1}{E} \tag{3}$$

where $\omega_{pe}^2 = 4\pi n e^2/m_e$, V_o = proton velocity, ρ_D = debye length
and $\rho_{min} = \hbar/mV$. In a strong $B \neq 0$, the corresponding stopping
length $l_o = E(dE/dz)^{-1}$ has to be multiplied by a factor (Pavlov
and Yakovlev 1975)

$$\delta = 2\Lambda_o \Lambda_\perp^{-1} \ \{\ln[4/(\theta_o^2 + \beta)] - 2\} \tag{4}$$

where $\beta = (1 + \Lambda_{\parallel}/\Lambda_{\perp}) \; (m/M)$, $\Lambda_{\perp} = (1 + \rho_D/\rho_L)$,

$\Lambda_{\parallel} = \ln\{(\rho_D/\rho_{min}) (1 + \rho_D/\rho_L)^{-1}\}$, $\Lambda_0 = \Lambda_{\parallel} + \Lambda_{\perp}$, and ρ_L = electron

larmor radius. The value of l_o turns out to be

$l_o \sim 10^4 \; (n_e/10^{20})^{-1}$ cm, and the correction $\delta \sim 16$, so that

taking into account some increase of density as the matter

decelerates,

$$l_B = E(dE/dz)_B^{-1} \sim 10^4 - 10^5 \text{ cm} \qquad (5)$$

Now the rate of slowing of the proton increases as $1/E$, so

most of the heating occurs towards the end of its stopping

length. Moreover, the slowing down is caused by many distant

encounters, which gradually increase the mean square angular

deviation of the proton, until at $l \sim l_B$ the proton has changed

its original momentum by 90°, i.e. it has a large $p_{\perp}$, c.f.

Fig. 1, and one would on this account also expect a greater

likelihood of exciting the cyclotron line (i.e., imparting

to the electrons a larger $p_{\perp}$) in this region, at the base of

the column. The geometry of the emitting regions would be then

as in Fig. 2, the larger part of the column (height $l_c \sim l_B$)

providing the continuum radiation, while the bottom section

of height l_L would be responsible for the line emission. The

ratio of continuum to line luminosity is 1/20, and integrating

equation (3), one sees that if we denote by l_L the end part

of the stopping length l_c, where the last 1/20 of the initial

energy E_0 is spent, the ratio of characteristic heights comes

out naturally to be $(l_L/l_c) \sim (l_{1/20}/l_{tot}) \sim (1/4 \times 10^2)$, so that

$$l_L \sim l_B \times (l_{1/20}/l_{tot}) \sim 2 \times 10^1 - 2 \times 10^2 \qquad (6)$$

A larger area $A_c \sim a_o \times l_c \sim 10^9 - 10^{10}$ cm^2, with average

temperature $T_c \sim$ 4-8 KeV would emit a continuum, consisting

of downscattered (and smeared) cyclotron photons, as well as

photons from collective processes and bremsstrahlung. The

increased temperature of the base, especially the increased

$p_\perp$ expected from the Coulomb process, would then make visible

the cyclotron line itself from the outer surface of a smaller

area $A_L \sim a_o \times l_L \sim 2\ 10^6 - 2\ 10^7$ cm^2 at the base of the column.

What would be the directionality of the radiation emitted?

The observed width of the cyclotron line ($\Delta E/E < 0.3$) imposes

some restrictions on the possible types of beaming, since in

a magnetic field, the broadening of a line can depend on the

angle θ between photon direction $\vec{k}$ and magnetic field vector

$\vec{B}$. Of the possible broadening mechanisms, the collisional and

radiative broadening are negligible, while the relativistic

change of mass only imposes the restriction T < 170 KeV. The

Doppler broadening $\Delta E/E = (8.\ln2.kT/mc^2)^{1/2} \cos\theta < 0.3$ al-

ready requires $\theta > 40^\circ$ if T > 15 KeV. Incoherent Compton

scattering ($\Delta E/E \sim kT/mc^2$) imposes the restriction that the

line must arise from a skin depth of Thomson optical depth

$\tau_T < 1$. The most important broadening effect should in fact

be due to the self-saturation of the line (Mészáros 1978),

since $\tau_{cy} \gg \tau_T > 1$. The absorption coefficient is

$$\mu(\nu) = B(\theta).\omega.(zc\beta_{th})^{-1} \exp(-z_j^2/2) \tag{7}$$

where $\beta_{th}^2 = kT/mc^2 \ll 1$, $z_j = (1-\nu_H/\nu)/(\beta_{th} \cos\theta)$, and the

angular factor averaged over polarizations is

$B(\theta) = (8\pi)^{-1/2} n_e e^2 \nu^{-2} (1+\cos^2\theta)|\cos\theta|^{-1}$, both for quasilongi-

tudinal and quasitransverse propagation. The width is determined by letting $\nu-\nu_H$ be the value for which $\tau_{cy}(\nu) \sim \mu_{cy}\, d \lesssim 1$, and this imposes, for $T > 15$ KeV the rather severe restriction

$$\theta \gtrsim 75^\circ \tag{8}$$

All indications therefore point towards emission strongly concentrated in the plane perpendicular to $\vec{B}$, i.e. a fan-beam scheme. Because the pulse duty cycles and phases of the line and continuum photons are almost the same, it follows that the beaming properties of the continuum (at least in the band 2-50 KeV) is also fan-beamed. The very soft continuum, $E < 0.5$ KeV, may be radiation emerging from the stellar surface over a larger area around the base of the column, if the emission process is nonthermal, i.e. $T_{ph} < T_{surf}$, a situation which does not appear unlikely. This flux, due to the relative orientation of the emitting surfaces, would then be beamed $\pi/2$ out of phase respect to the harder flux, as observed, c.f. Fig. 2.

References

Alme M L and Wilson J R, 1973, Ap. J. 186, 1015.

Basko M M and Sunyaev R A, 1975, M.N.R.A.S. 175, 395

Mészáros P, 1978, Astron. Astrophys. 63, L19

Pavlov G G and Yakovlev D G, 1975, J.E.T.P. 68, 105

Shapiro S L and Salpeter E E, 1975, Ap. J. 198, 671

Sunyaev R A and Trümper J, 1978 (preprint)

Trümper J, Pietsch W, Reppin C, Sacco B, Kendziorra E
    and Stanbert R, 1977, to appear in Proc. VIII Texas
    Symposium, held Dec 1976, Boston. See also
    Kendziorra et al. 1977, Ap. J. 217, L93, and this
    Volume, p. 331.
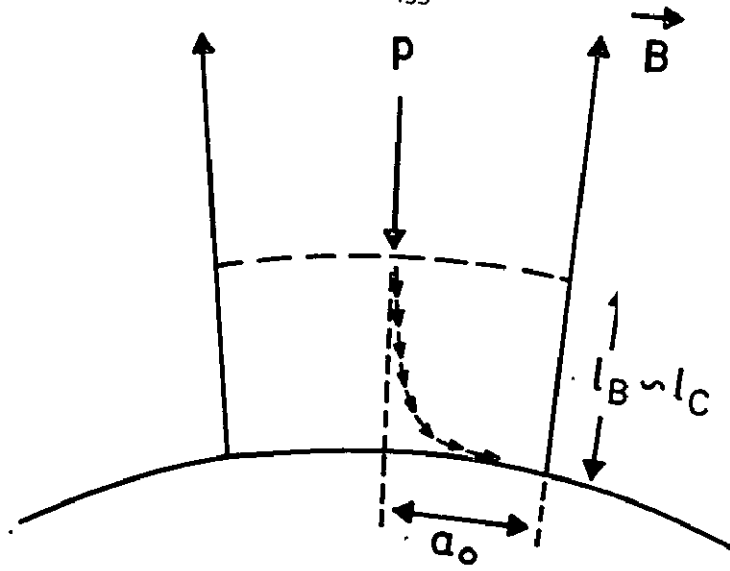
Figure 1
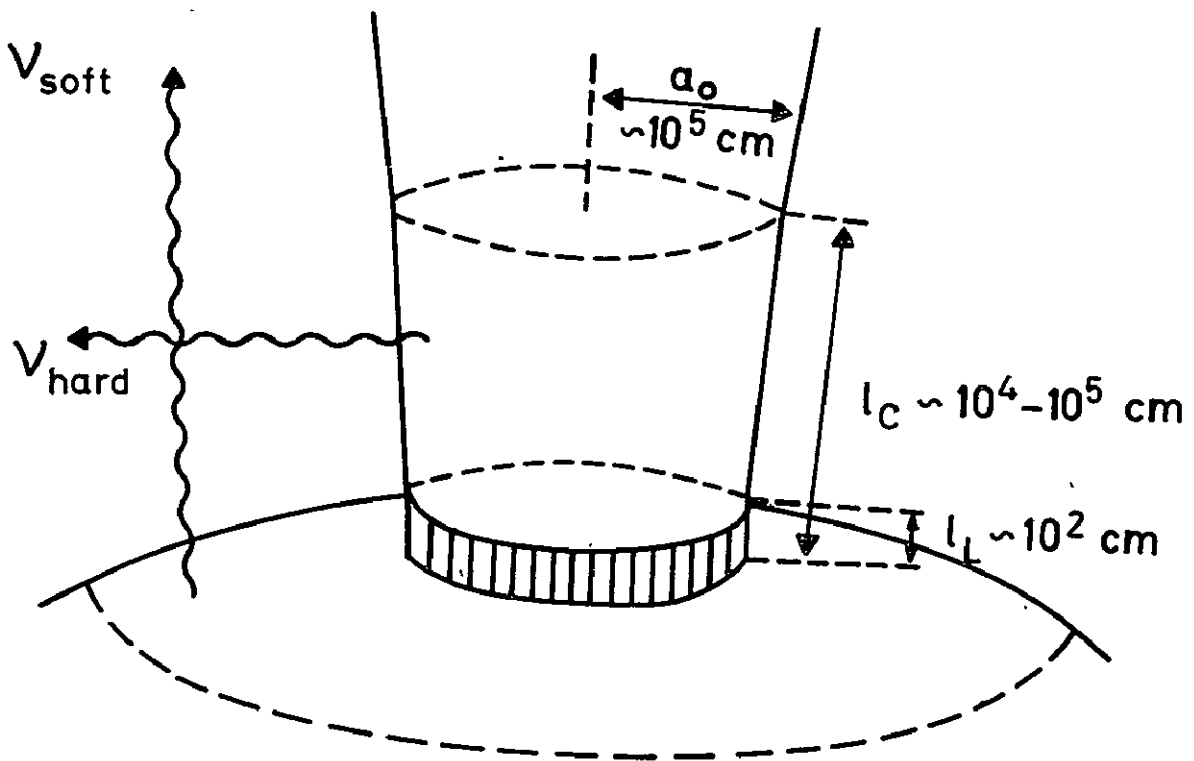
Figure 2

V. DETECTION TECHNIQUES AND NUCLEAR CROSS SECTION MEASUREMENTS

SUMMARY OF THE WORKSHOP ON DETECTOR CAPABILITIES

G. J. Fishman
Space Sciences Laboratory
Marshall Space Flight Center
Huntsville, Alabama 35812

The importance of observations in nuclear gamma-ray astronomy for solving many astrophysical problems is quite clear from theoretical papers presented at this symposium. Experimental work in the field has had a slow and laborious start; there exists today only a few observational results of relatively low statistical significance. A Detector Workshop session was organized to discuss the present detector capabilities and future prospects for more sensitive detectors. Brief talks were given by panelists followed by discussions.

The workshop session began with spirited discussions of the relative merits of scintillation detectors, and germanium detectors, for astronomical line spectroscopy observations. J. Kurfess, Naval Research Laboratory, presented data showing that under certain conditions, large scintillation detectors would have distinct advantages. These conditions included transient events, the observation of doppler-broadened lines, and the limited volume and cost constraints of germanium detectors. J. Willett, Jet Propulsion Laboratory (JPL), presented the current capabilities of germanium detectors with regard to resolution and sensitivity. There seemed to be a consensus that there would continue to be a trend toward experiments with large germanium arrays, but that large scintillation detectors will continue to provide contributions as well. Compton telescopes are expected to have great potential, especially at the higher energies. Their background rejection capabilitie: and ability to simultaneously observe source and background regions where pointed out.

There were a series of discussions on the mechanism and effects of background and radiation damage in detectors. A. Metzger, JPL, showed high resolution spectra of germanium detectors irradiated by 3 GeV protons. Numerous activation lines and their time variations were measured. W. Mahoney, JPL, presented data obtained by a balloon-borne germanium detector, showing the development of activation lines from radiation found at balloon altitudes. In general, the radiation environment producing internal induced radioactivity in detectors is quite complex, consisting not only of cosmic rays and trapped radiation, but locally-produced secondary radiation as well.

R. Pehl, Lawrence Berkeley Laboratory, presented data showing the degradation of resolution of germanium detectors from relatively low fluxes of protons and neutrons. The effects can be greatly reduced by proper choice of detector types and biasing. Annealing of detectors has been shown to reverse the degradation. The effects of radiation on the planned HEAO-C instrument, to be launched next year, are uncertain, since the internal secondary radiation is unknown. G. Nakano, Lockheed, mentioned that no degradation was observed in their germanium satellite instrument.

K. Long, Columbia University, reviewed the polarization characteristics of Compton-scattered gamma rays. He stated that, with proper readout design, arrays of detectors and Compton telescopes could be made sensitive to polarized gamma rays from sources.

Several new and exotic gamma ray detectors were mentioned by participants including: liquid argon counters, gas scintillation detectors and cadmium telluride. R. Haymes, Rice University, described a gamma-ray "correlator" consisting of a large three-dimensional array of small scintillation detectors. Several people stressed the importance of continued laboratory development and balloon flight tests of these new detectors and techniques.

The Detector Workshop provided an excellent forum for the exchange of ideas among representatives of all active experimental groups in the field. It was noted that the Detector Workshop was also attended by many theorists, who will eagerly be awaiting data from upcoming balloon flights, HEAO-1, HEAO-C and from the Gamma Ray Observatory.

The following 6 articles of this volume were presented at the Detector Workshop Session.

N78-31999

GAMMA RAY SPECTROSCOPY IN ASTROPHYSICS:

FUTURE ROLE OF SCINTILLATION DETECTORS

J.D. KURFESS
Naval Research Laboratory
Washington, D.C. 20375

ABSTRACT

The future role of conventional scintillation detector telescopes
for line gamma-ray astronomy is discussed. Although the energy resolution
of the germanium detectors now being used by several groups is clearly
desirable, the larger effective areas and higher efficiencies available
with scintillation detectors is advantageous for many observations. This
is particularly true for those observations of astrophysical phenomena
where significant line broadening is expected.

Subject Headings: Gamma-Ray Astronomy, Gamma-Ray Detectors

After more than a decade of difficult, pioneering efforts in the
gamma-ray spectroscopy of selected astronomical sources, the results
presented at this conference indicate that the field is entering an
exciting and productive era during the next few years. During the
initial phase of gamma-ray astronomy, inorganic scintillators have been
the most widely used detectors. Most of the results presented at this
conference were obtained with scintillation detectors. However, interest

in high resolution measurements has been keen for many years.
Following the pioneering efforts of Jacobson (1968) and Womack and
Overbeck (1970) there are now six or more active gamma-ray astronomy
groups using high resolution germanium detectors. Although these
spectrometers will clearly make significant contributions in the develop-
ment of gamma-ray astronomy, it is the purpose of this paper to point
out that conventional scintillation experiments will continue to play a
major role in the near future.

The scope of this paper will be limited to the relative advantages
and disadvantages of 'conventional' scintillation and germanium experi-
ments. These are the 'actively-shielded' telescopes which have been
utilized almost exclusively in the past and undoubtedly will continue
to be the most widely utilized detectors for many years. There is a
definite need for other developments in detector technology, e.g.,
detectors with much better angular resolution or imaging capabilities,
and detection techniques which suppress instrumental background, such as
the double Compton telescope. Other papers at this conference have
discussed some of these developments; they will not be considered further
in this paper.

A brief introduction to observational techniques is required before
a comparison of scintillation and germanium detectors is discussed.
The 'conventional' detector consists of a central detector element, usually
a NaI(Tl) or germanium crystal surrounded by an inorganic scin-
tillator anticoincidence shield which typically restricts the field-of-
view of the detector to ~10° to 30° FWHM. The intrinsic detector background

due to the local γ-ray environment and to background induced in the central detector by nuclear reactions is rather high, so that the signal to background ratio is generally well below 1:1. Therefore, some technique for subtracting background from possible source contributions is required. This usually involves alternating source observations with background measurements in which the detector is offset from the source by some angle greater than the detector's field-of-view. This technique has been used for most balloon observations. Another technique is to allow the source to drift through the field-of-view. This scanning technique has been utilized by most satellite experiments and has also been used by some balloon groups.

When comparing scintillator and germanium experiments it might be assumed that a detector with much better energy resolution would clearly be the detector of choice. A recent article in the popular literature emphasizes the importance of high resolution measurements (Lingenfelter and Ramaty, 1978). However, other factors must also be considered. The energy resolution, full energy peak efficiencies, and detector area are all parameters which directly enter into the γ-ray line sensitivity. Table 1 lists typical values for the photopeak efficiency and the energy resolution for both an 8"-diameter x 4"-thick NaI(Tl) crystal and a 100 cm^3 germanium detector for several energies in the 0.1-10 MeV region. For the size detectors which are currently available NaI(Tl) has a much higher detection efficiency throughout most of this energy interval. The superiority of the germanium detector with respect to energy resolution is also evident.

Table 1

| Energy | Full Energy Efficiency | | Energy Resolution (keV) | |
	NaI 8"x4"	Germanium* 100 cc	NaI 8"x4"	Germanium 100 cc
0.1 MeV	.95	0.70	20	2
0.5 MeV	.85	0.30	45	2
1.0 MeV	.65	0.15	65	3
2.0 MeV	.47	0.08	95	4
5.0 MeV	.30	0.05**	150	5

* germanium efficiency data kindly provided by J. Willett

** sum of full energy peak and first 0.51 MeV escape peak

The 3σ line γ-ray sensitivity for an experiment is given by the following.

$$S(3\sigma) = \frac{3 \times 1.31}{\varepsilon} \left[\frac{2 \cdot B \cdot \Delta E}{A \cdot T}\right]^{1/2}$$

where: A = detector area
   T = source exposure time = background exposure time
   ε = photopeak efficiency at energy E
   B(E) = background rate (cts/cm^2-s-MeV) at energy E
   ΔE = energy resolution (FWHM)

The factor 1.31 arises because only 76% of the counts in the peak fall within the 'full-width-half-maximum, E (a gaussian peak is assumed). For optimum sensitivity to a weak line, equal source and background periods are required.

Generally, detector systems must be designed within some cost and weight restrictions. In practice, the larger detection areas and higher efficiencies which can be realized with scintillators offset the poorer energy resolution so that better sensitivity can be obtained with a scintillator experiment for many applications. More importantly, many of the γ-ray lines produced in astrophysical sources are expected to exhibit broadening. Broadening is certainly a significant factor for many lines produced in solar flares or by cosmic ray interactions with the interstellar medium. Line broadening can also be expected in supernovae and novae where shell expansion velocities of up to 10^4 km/sec will result in Doppler broadening of up to ~5%. Even line emission from compact objects may be broadened because of variations of the gravitational or magnetic fields in the production region. Whenever significant broadening occurs, the relative sensitivity of the scintillation detector is improved.

As an example, Figure 1 shows the emitted γ-ray spectrum calculated by Lingenfelter and Ramaty (1978) for cosmic rays interacting with the interstellar medium. Both the cosmic rays and the interstellar medium were assumed to have normal cosmic abundance. A rich spectrum is observed, and the clear implication is that high resolution observations are necessary to investigate γ-ray emission from the interstellar medium. However, this figure is somewhat misleading when viewed from the detectability of these various features. For a medium energy resolution detector such as NaI(Tl) the integrated line intensity (i.e., $γ/cm^2$-sec in the line)
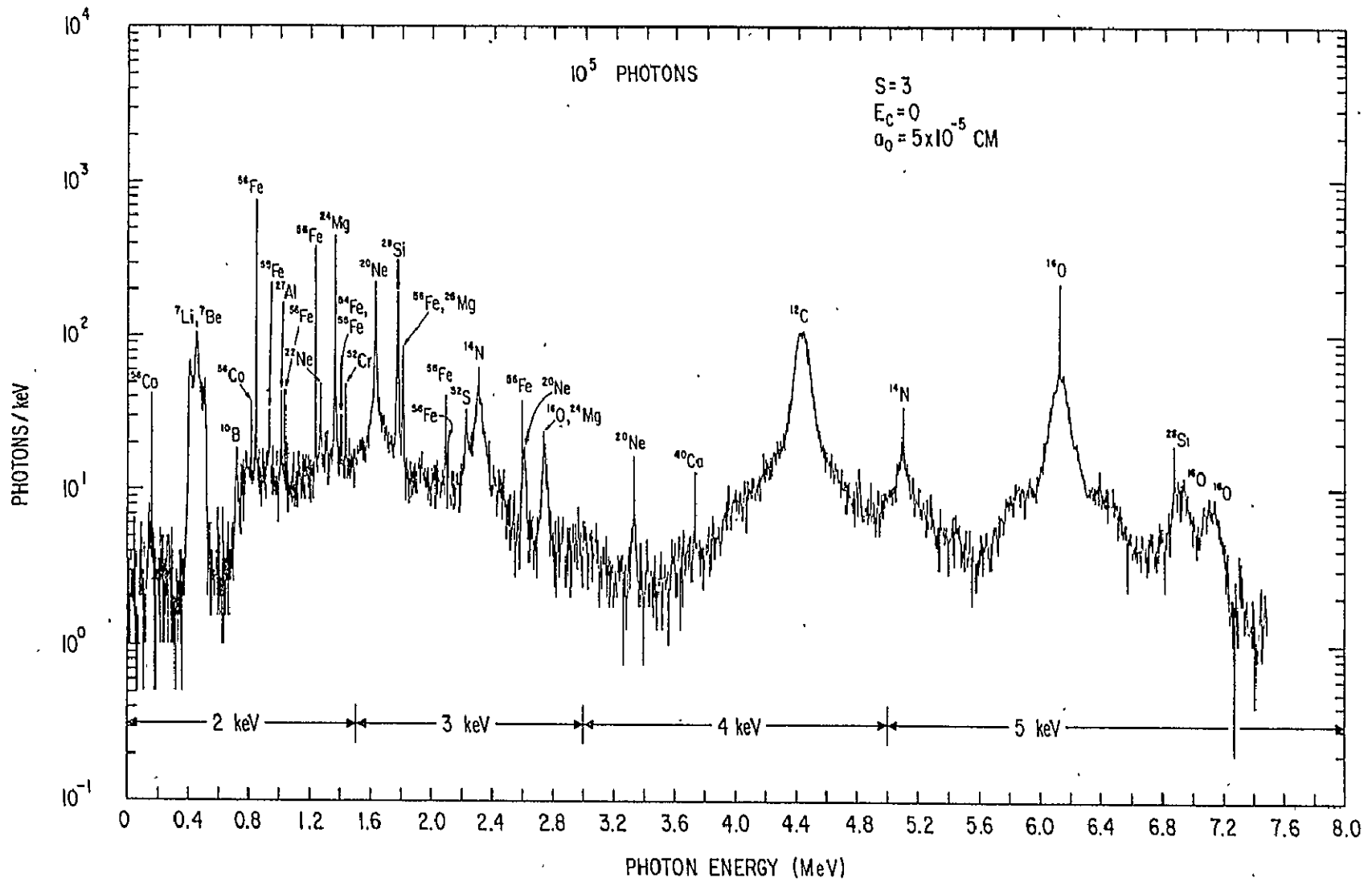
Figure 1. Calculation by Lingenfelter and Ramaty of the γ-ray emission produced by cosmic rays interacting with the interstellar medium.
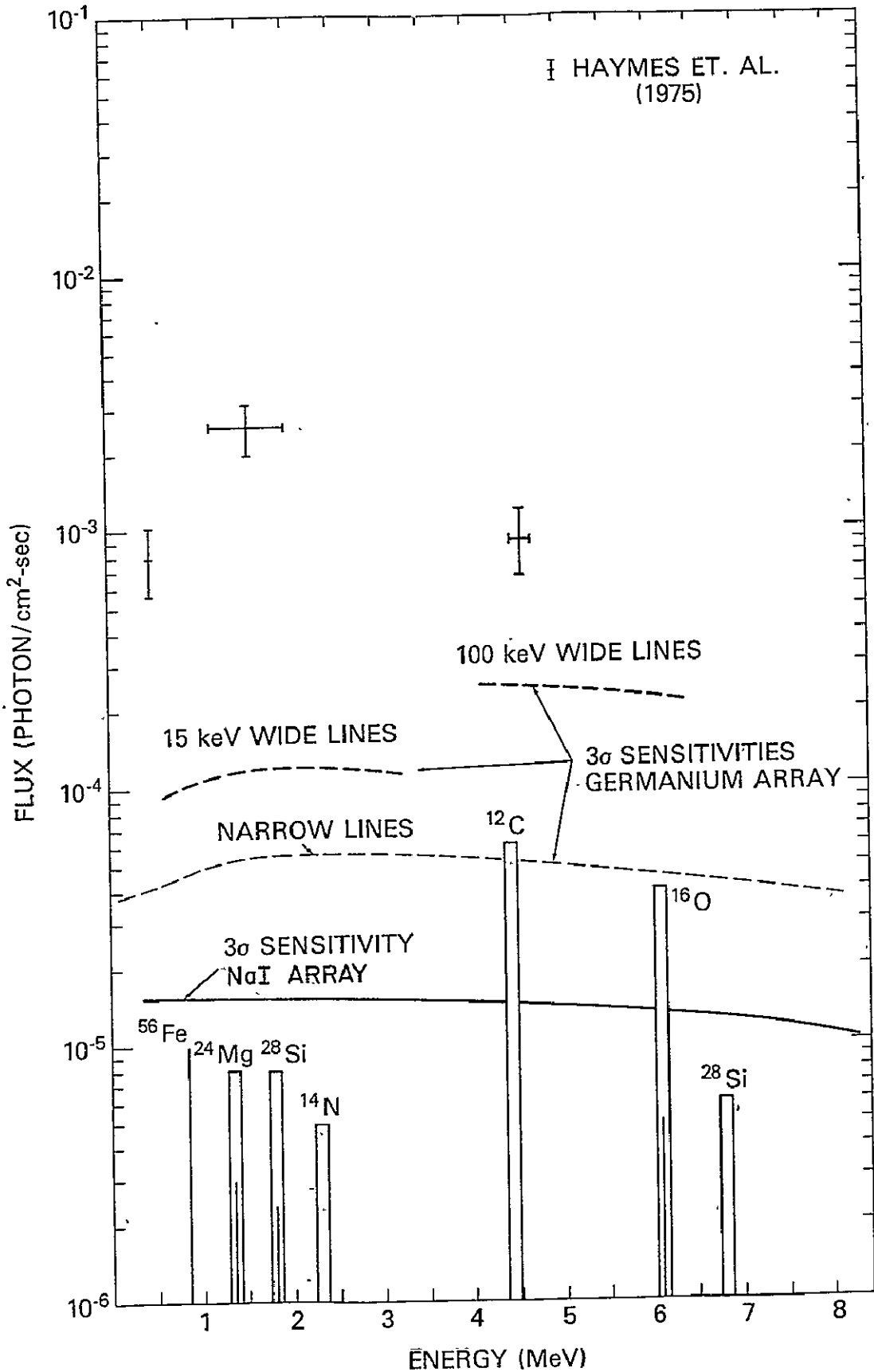
Figure 2. The most intense features in Fig. 1 plotted as integrated line intensities expected from the galactic center region assuming a low-energy cosmic-ray energy density of 4 eV/cm³. The sensitivities of large NaI and germanium detector arrays is also shown (see text). For comparison, the reported features by Haymes et al. (1975) are included.

is a measure of the detectability. Therefore, the line intensities

of the stronger features in Figure 1 are reproduced in Figure 2, but

plotted in γ/cm^2-sec. The flux values have been normalized to those

expected for an observation of the galactic center region, assuming

the energy density of low-energy cosmic rays to be 4 eV/cm^3. The broadened

lines are represented by bars, while narrow features are indicated as

lines. Notice that now the most intense features are seen to be the ^{12}C

and ^{16}O lines, each of which is expected to be broadened by ~100 keV.

Also included in Figure 2 are the limiting sensitivities for both

medium and high energy resolution experiments which might be typical

of the next generation of large γ-ray astronomy instruments. Both

experiments were assumed to utilize a large, actively-shielded configuration.

A NaI array with an effective area of 2000 cm^2 'and a germanium array of

twenty 100 cm^3 diodes were studied. An observation period of 10^6 seconds

equally divided between source and background intervals, was assumed.

The background rates for the NaI array were based on a study conducted

at NRL of a large area phoswich γ-ray detector using an estimated back-

ground environment for the Space Shuttle. A spallation contribution to

the background, assuming a 28° inclination, 225 n.m. orbit was also

included (Dyer 1976). The background rates in the germanium array were

based on the balloon results of Jacobson et al. (1977). A spallation con-

tribution was also included below ~1 MeV for the germanium array under the as-

sumption that the spallation activity per gram is approximately the

same for germanium and NaI when exposed to a similar high-energy proton

environment.

Notice in Figure 2 that only the ^{12}C and ^{16}O features would be detectable in this case, and those would be detected by the scintillator experiment. The narrow line features are all well below the sensitivity of the high resolution experiment.

This comparison is not meant to indicate that high resolution experiments are not important. Indeed, for strong lines or complex spectra, high resolution experiments will clearly provide capabilities that scintillators cannot provide. However, it is equally clear that during this developing phase of γ-ray astronomy, improved sensitivity is very important, and there are many observations which require large scintillator arrays. This is particularly true when line broadening is considered. In Figure 2 it is seen that for the ^{12}C and ^{16}O lines the scintillator experiment is ~10 times more sensitive.

Scintillation detectors also provide an advantage for those observations where the time-integrated photon flux in the feature of interest is low. Solar flares and γ-ray bursts are examples. Figure 3 indicates the energy spectra which would have been observed during the 4 Aug 1972 flare by a single 8" x 4" NaI detector and a single 100 cm^3 germanium detector, typical of the detectors currently in use. The intensities of the solar line gamma rays were taken from the observations of Chupp et al. (1973) or from the calculations of Ramaty, Kozlovsky and Lingenfelter (1975). As in the previous example, the detectors used equivalent actively-shielded configurations. Many features are seen by both detector systems, however a limitation of the high resolution experiment can be seen by the paucity of detected photons in the 4.4, 6.1 and 7.1 MeV features.
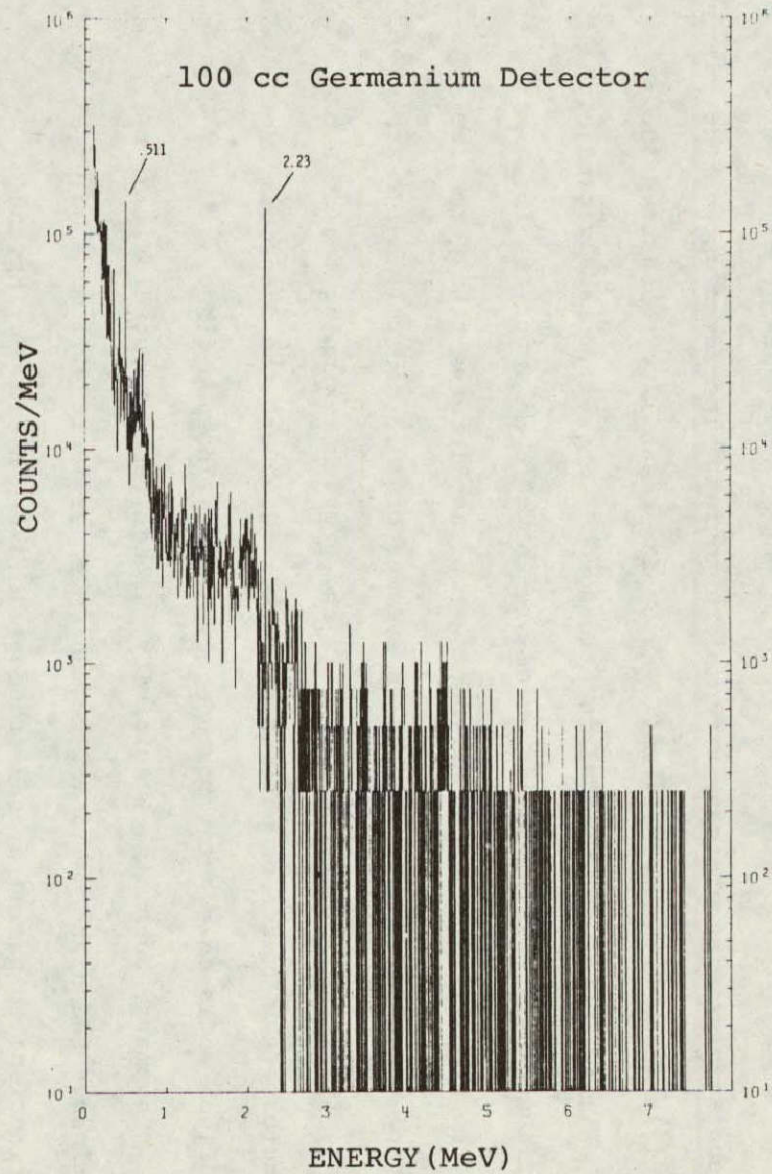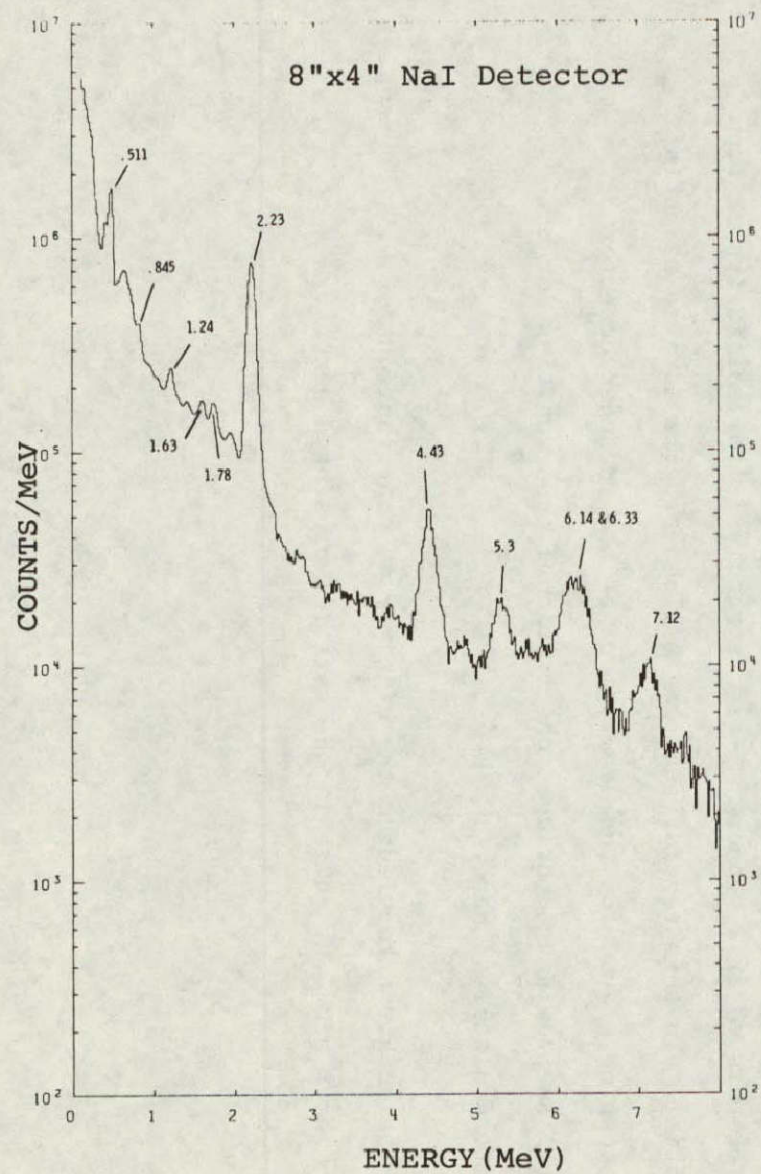
Figure 3. Calculated responses of an 8" x 4" NaI detector and a 100 cc germanium detector to the 4 Aug 1972 flare.

These lines are very important for observing the time dependence of the
nucleon acceleration process in the flare region. The advantage of the
scintillator experiment is exemplified by its capability to observe the
4.4 MeV line ^{12}C at the 8σ level in a 10-second interval, thereby providing
significant data on time scales which are known to be important for
electron acceleration processes. During the same interval the germanium
detector would have only detected an average of ~0.3 counts! Large arrays
of detectors, similar to those used in the previous example, could be used
to increase the number of photons detected. However, the identical
comparison would then occur for a somewhat less intense flare.

In summary, both high sensitivity, medium resolution scintillator
experiments and high resolution germanium experiments will make major
contributions to gamma-ray spectroscopy in astrophysics during the
forseeable future. An aggressive program utilizing both types of
detectors, and using both satellite and balloon-borne instrumentation
must be pursued if low-energy γ-ray astronomy is to realize its maximum
potential. In this regard, a strong balloon program is also essential
as a testing ground for the development of the advanced detectors,
as well as providing continued observational opportunities for the
detectors discussed here.

CAPABILITIES OF GERMANIUM DETECTORS *

J. B. Willett, J. C. Ling, W. A. Mahoney and A. S. Jacobson

Jet Propulsion Laboratory
California Institute of Technology
Pasadena, California

Abstract

·The gamma-ray detection efficiency and energy resolution of germanium detectors is reviewed. A general sensitivity equation for gamma-ray detectors is presented and calculated sensitivity curves are shown for a large volume balloon-borne spectrometer using germanium detectors. Improvement anticipated from a planned satellite experiment using germanium detectors is discussed.

C-6

Germanium detectors have begun to make significant contributions to gamma-ray spectroscopy in astrophysics. In many cases the small size of these detectors is more than offset by their high spectral resolution. This paper discusses the importance of high spectral resolution and its impact on the sensitivity of a gamma-ray spectrometer.

A comparison of linear attenuation coefficients for gamma rays in both germanium and cesium iodide, as indicated in Figure 1, shows that the inherent full energy detection efficiency of a germanium detector is the same as that of a cesium iodide detector of the same dimensions provided these dimensions are greater than about 3 cm. At low energies the mean free path of a photon is small compared with detector dimensions and at higher energies the energy collection process is dominated by multiple Compton scattering followed by photoelectric absorption. However, while scintillator crystals can be made with many 100's of cm^2 front surface area, the largest germanium crystals currently available are on the order of 30 cm^2. To get equivalent detection area many germanium detectors must be grouped together. Yet germanium spectrometers have one great advantage over their scintillating cousins; high spectral resolution. A typical germanium detector can attain a spectral resolution full width at half maximum varying from 1 keV to 6 keV over the energy range from 0.1 to 10 MeV. The corresponding scintillator resolution varies from 20 to 200 keV over the same energy range. Currently, it is only the germanium crystal spectrometer that can resolve the complex structure of gamma-ray lines which arise from closely spaced multiplets, or which have undergone Doppler distortion or gravitational redshift. In addition, a germanium detector allows measurement of line energies to a small fraction of a keV. There are several examples presented in this conference of the need for high spectral resolution in astrophysical

measurements. The value of the germanium spectrometer is aptly demonstrated in the presentation by Leventhal and MacCallum (1978) on the measurement of a 0.511 MeV line flux from the galactic center region.

An equation for calculating the minimum gamma-ray flux detectable in a spectrometer is given in Figure 2. This equation is general, applying to both point and diffuse sources as well as line and continuum fluxes. Gaussian statistics are assumed in the derivation which is given in Appendix A. For line fluxes, G is the fraction of the line flux within energy band ΔE. In the presence of background ΔE is set to 1.2 times the full width at half maximum (FWHM) for a gaussian line shape to optimize the signal to background ratio. For diffuse sources the integration over the transmission term is valid when the source distribution is uniform. For continuum sensitivity, G is replaced by ΔE in order to convert sensitivity to a per keV basis. If source count statistics are insignificant when compared with background effects, the equation for a point source line flux reduces to the simplified form shown in Figure 2. To improve sensitivity, the observation time, detector area and efficiency, and photon transmission into the instrument may all be increased, while detector FWHM and background should be decreased. It must be pointed out that an increase in area also increases the background, and thus area impacts the sensitivity approximately as the square root of itself. Scintillator spectrometers achieve maximum sensitivity by means of large area detectors, while germanium spectrometers depend on a small FWHM contribution. For measurement of narrow gamma-ray line fluxes a scintillation detector must have from 15 to 30 times the effective area to match the sensitivity of a germanium detector.

Figure 3 shows the 3 sigma minimum detectable flux for both an unbroadened line flux and a continuum flux as might be measured by one of the larger balloon borne, CsI shielded, Ge spectrometers. Typical observation

times for balloon measurement are on the order of 10^4 seconds. The continuum measurement drops off at high energies due to the band width definition. Sensitivity is strongly affected by photon attenuation in the 50 to 100 keV energy region. Above 200 keV background leakage through the shield becomes an important factor degrading instrument sensitivity. Above 1 MeV the background drops significantly, improving sensitivity, but above 5 MeV the detector efficiency drops sharply causing the turn-up at the end.

Figure 4 shows the 3 sigma sensitivity curves for diffuse sources, both cosmic and atmospheric, for the same balloon borne spectrometer. These have the same characteristics except that the large drop at high energy is due to shield leakage of source photons, making the instrument behave more isotropically.

For satellite instruments the observation time can be increased by an order of magnitude, and in the case of the HEAO C-1 instrument the detector area is nearly doubled over the balloon case just discussed. The sensitivity of the HEAO C-1 instrument to narrow lines should look like the corresponding curve for the balloon instrument shown in Figure 3, but it is expected to be down in the 1 to 2 x 10^{-4} photons/cm^2-sec range.

Germanium detectors have brought to the field of spectroscopy in astrophysics the capability of performing high spectral resolution measurements which are essential to the understanding of many astrophysical processes. In view of the exciting results which have been presented in this symposium it is apparent that germanium detectors will make a new class of very challenging observations possible in the field of gamma-ray astronomy.

Appendix A

Gamma-Ray Line Detectability

In the presence of a given background flux, the minimum gamma-ray line flux which can be detected in any given source and background observation time periods and with any given detector parameters is derived below.

Let F_m photons/cm^2-s be a line flux at energy E_o. Passage through any absorptive material and into the detector will result in an observed count rate of

$$R_m = F_m \alpha \epsilon A \quad \text{counts/s,}$$

where α is the transmission of the absorption layers and ϵA is the full-energy-peak detection effective area.

If the chosen pass-band, or channel width is $\Delta E(E_o)$, centered about E_o, then, after Gaussian resolution spreading of the line, the measured rate within this channel is:

$$R_m = \frac{\alpha \epsilon A F_m}{\sqrt{(2\pi)}\,\sigma} \int_{E_o - \frac{1}{2}\Delta E}^{E_o + \frac{1}{2}\Delta E} \exp\left[-\frac{(E' - E_o)^2}{2\sigma^2} \right] dE' ,$$

or, letting:

$$G(x) = \frac{1}{\sqrt{(2\pi)}} \int_{-x}^{x} \exp\left(-\tfrac{1}{2}t^2\right) dt,$$

$$R_m = \alpha \epsilon A F_m G\left(\frac{\Delta E}{2\sigma}\right) \quad \text{counts/s.} \tag{1}$$

To be detectable, this flux must be k standard deviations above the background rate R_b in counts/s keV. The variance in the subtraction of the background is:

$$\sigma^2 = \frac{\alpha \epsilon A F_m G + R_b \Delta E}{T_s} + \frac{R_b \Delta E}{T_b} \qquad (2)$$

where T_s and T_b are the respective observing times on the source and the background. The condition for $k\sigma$ detection significance is:

$$R_b = \alpha \epsilon A F_m G = k\sigma \qquad (3)$$

Solving for F_m an expression for the minimum-detectable line flux is obtained.

$$F_m = \frac{k}{2\alpha\epsilon AG} \left\{ \frac{k}{T_s} + \left[\left(\frac{k}{T_s} \right)^2 + 4R_b \Delta E \left(\frac{1}{T_s} + \frac{1}{T_b} \right) \right]^{\frac{1}{2}} \right\} \qquad (4)$$

References

Leventhal, M., MacCallum, C., and Stang, P. D. (1978) this Volume, p. 169.

FIGURE CAPTIONS

Figure 1   Linear attenuation coefficients for both Ge and CsI. Both

photoelectric and total (photoelectric + Compton + pair)

attenuation curves are shown. Multiple Compton scattering fol-

lowed by photoelectric absorption dominates the energy collec-

tion process for characteristic detector dimensions of more than

a couple of centimeters.

Figure 2   Sensitivity equation for a gamma-ray spectrometer. Gaussian

statistics have been assumed. The k/T_s terms reflect source

count statistics and the R_b term represents the background

statistics contribution. The simplified version assumes a

background dominated spectrum of a line flux from a point

source.

Figure 3   3 sigma minimum detectable flux from a point source. The upper

curve represents the instrument sensitivity to a very narrow

line flux from a point source. The lower curve shows the sensi-

tivity to a continuum flux, assuming the sampling band width

to be 0.1 times the energy.

Figure 4   ~3 sigma minimum detectable flux from a diffuse source. The

upper curve represents the instrument sensitivity to a very

narrow line flux from an isotropic diffuse cosmic source. The

lower curve shows the sensitivity to a very narrow line flux

from the atmosphere. The large source solid angles and shield

transparency accounts for the great sensitivity above 1 MeV.

LINEAR ATTENUATION COEFFICIENTS
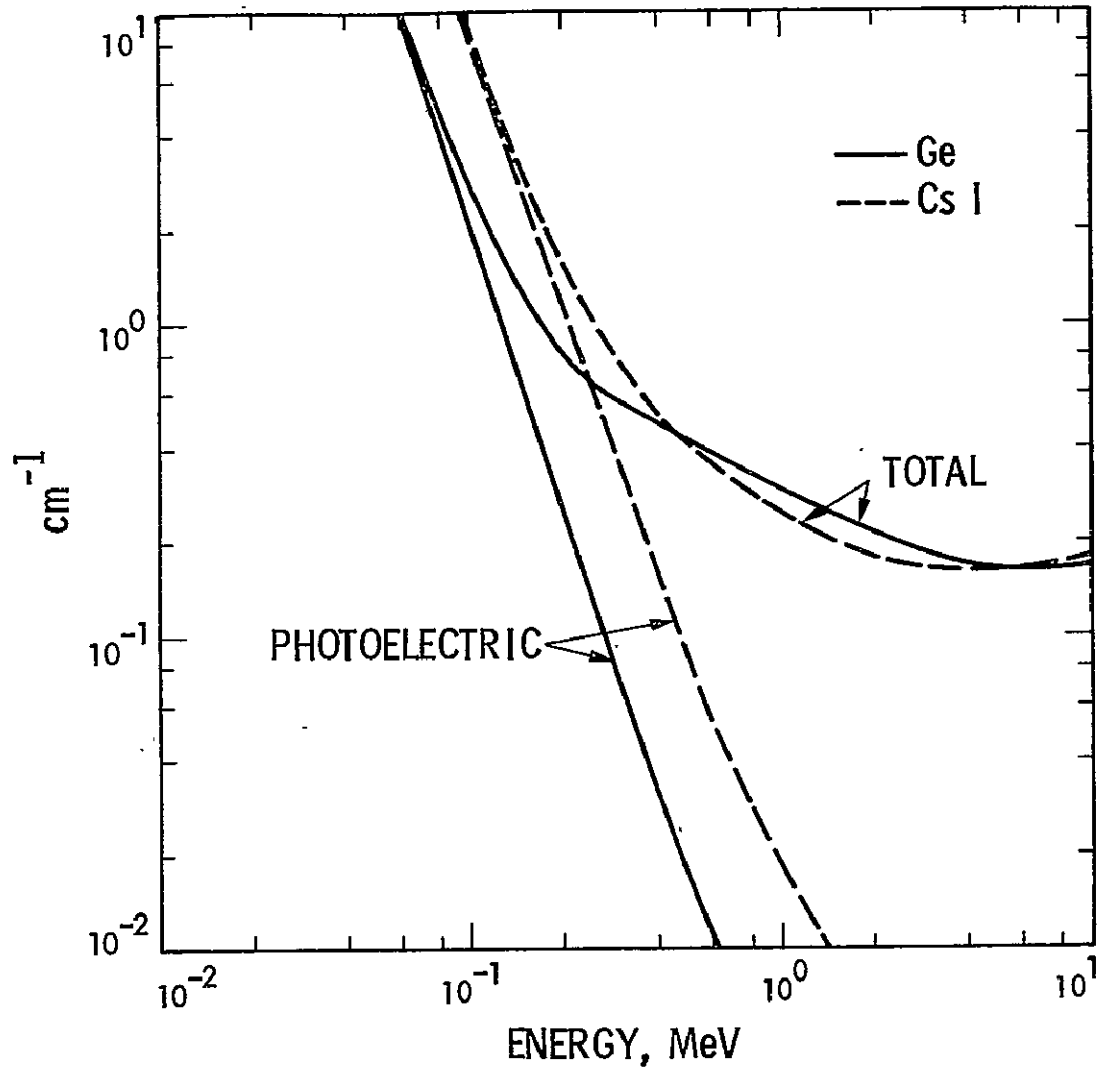
Figure 1

SENSITIVITY EQUATION

$$F_m = \frac{K}{2 \epsilon A\, G \int \alpha\, d\Omega} \left\{ \frac{K}{T_s} + \left[\left(\frac{K}{T_s}\right)^2 + 4 R_B \Delta E \left(\frac{1}{T_s} + \frac{1}{T_b}\right) \right]^{\frac{1}{2}} \right\}$$

WHERE

F_m = MINIMUM DETECTABLE FLUX, PHOTONS/cm^2-sec, OR PHOTONS/cm^2-sec-KeV

K = # SIGMA

ϵ = EFFICIENCY

A = AREA, cm^2

α = PHOTON TRANSMISSION FACTOR

$d\Omega$ = SOLID ANGLE, INTEGRATING OVER SOURCE

T_s = OBSERVING TIME ON SOURCE, INCLUDING DEADTIME CORRECTIONS, sec

T_b = OBSERVING TIME ON BACKGROUND, INCLUDING DEADTIME CORRECTIONS, sec

R_b = DETECTOR BACKGROUND, COUNTS/sec-KeV

ΔE = ENERGY BANDWIDTH, KeV

1. CONTINUUM

$$G = \Delta E$$

2. LINE FLUX, OPTIMIZED FOR GAUSSIAN LINE SHAPE IN PRESENCE OF BACKGROUND

$$G = 0.84, \text{ INTEGRATE TO } 1/e$$

$$\Delta E = 1.2 \left(\omega_\ell\right), \text{WHERE } \omega_\ell = \text{FWHM}$$

SIMPLIFIED VERSION - POINT SOURCE - LINE FLUX

$$F_m = \frac{2K}{\epsilon A \alpha} \sqrt{0.425\ R_b\left(\omega_\ell\right)\left(\frac{1}{T_s} + \frac{1}{T_b}\right)}$$

Figure 2

3σ MINIMUM DETECTABLE FLUX
POINT SOURCE
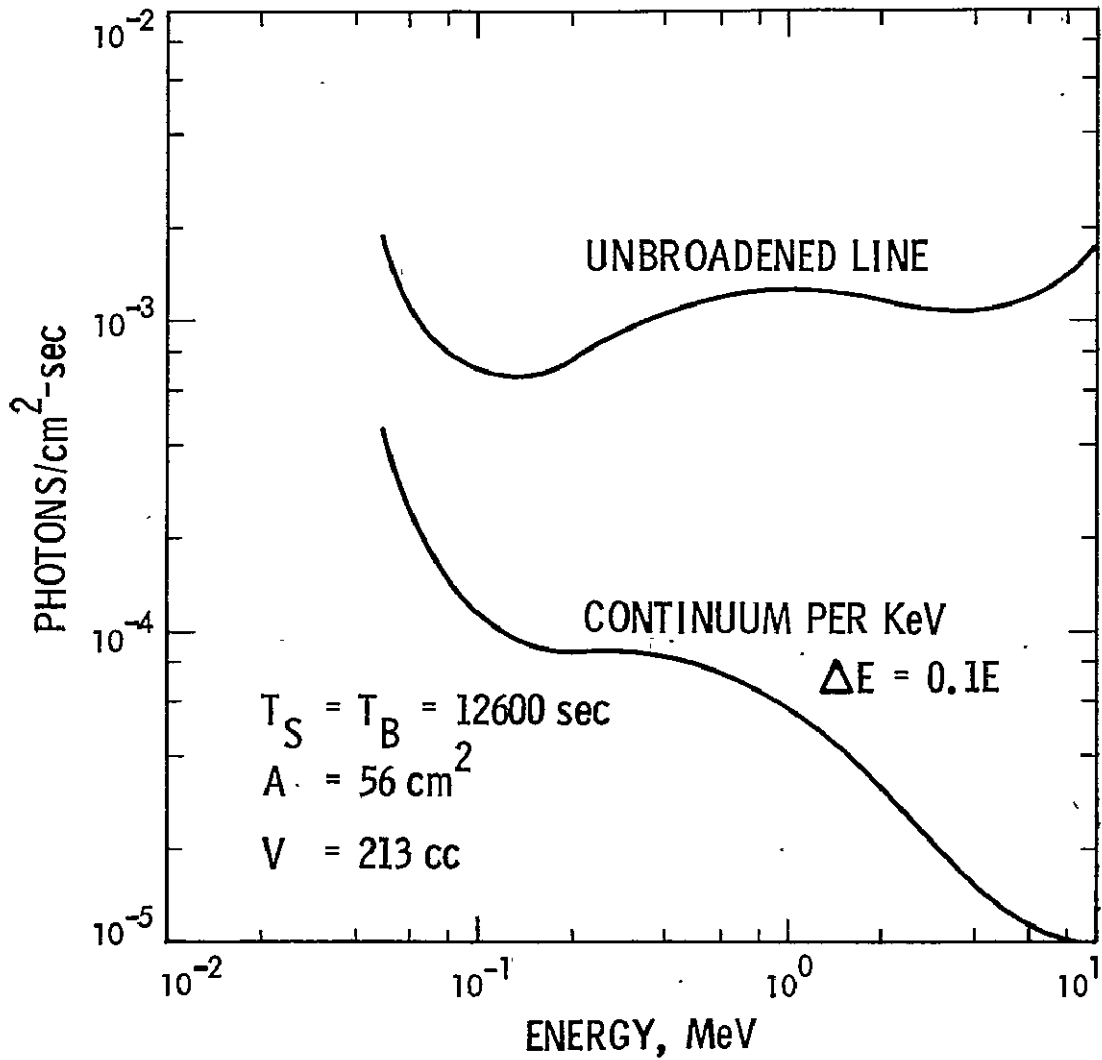
Figure. 3

3σ MINIMUM DETECTABLE FLUX
DIFFUSE SOURCE
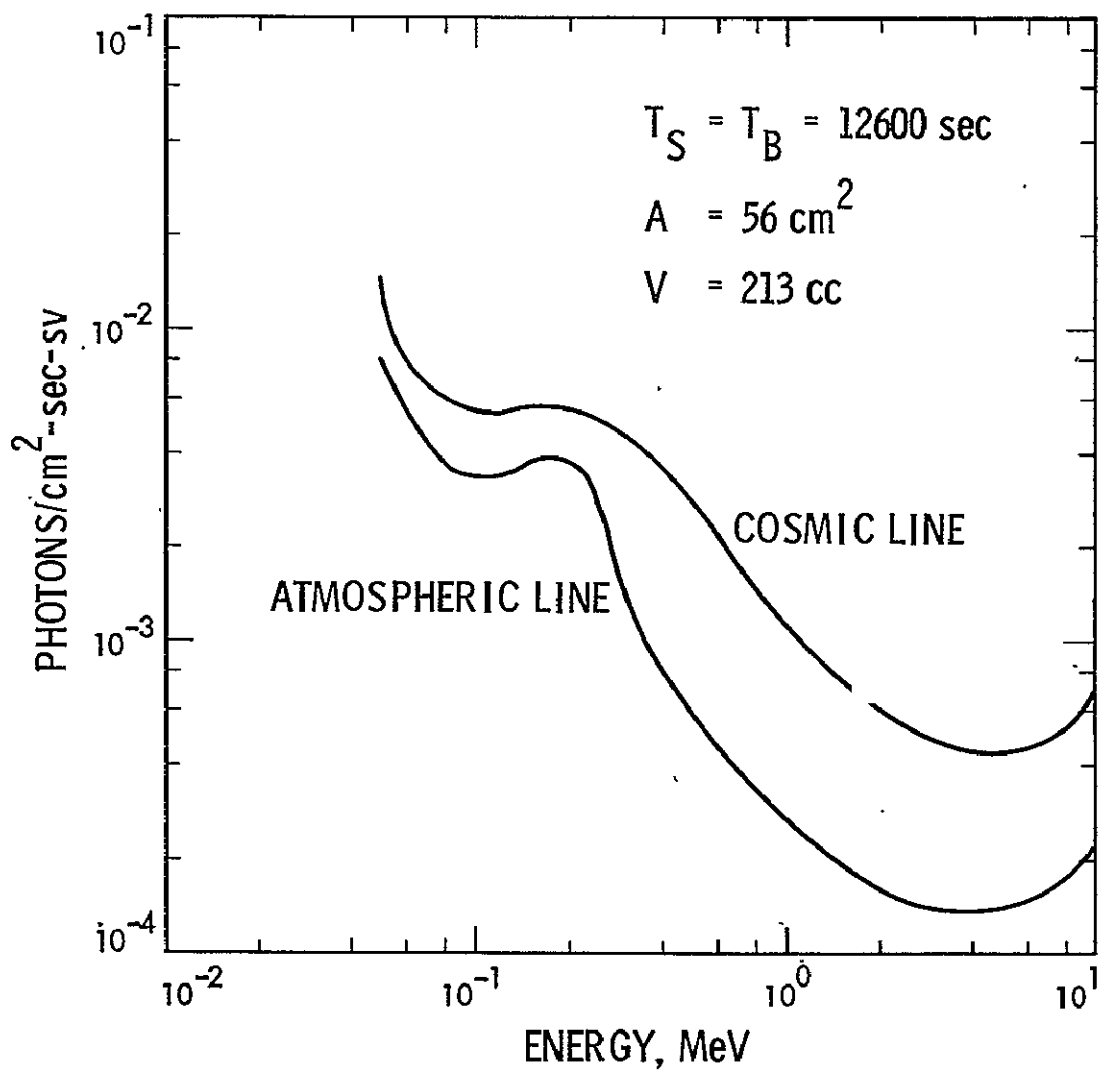
Figure 4

Background of a Shielded Ge(Li) Spectrometer at Balloon Altitudes

W. A. Mahoney, J. C. Ling, J. B. Willett and A. S. Jacobson

Jet Propulsion Laboratory
California Institute of Technology
Pasadena, California   91103

ABSTRACT

The background data obtained from an actively shielded Ge(Li) spectrometer flown on a balloon have been analyzed and a preliminary model has been developed to explain background features including the intensity and time profile of line emission. It is found that these features can be explained by a combination of secondary radiation originating in the CsI shield and atmospheric secondary radiation leaking through it.

On 10 June 1974 a balloon flight was conducted from Palestine, Texas with a shielded Ge(Li) gamma-ray spectrometer. In addition to astronomical observations reported earlier (Ling et al., 1977a and 1977b, and Jacobson et al., 1976) and elsewhere in this volume, a vast quantity of information was obtained on the background counting rates of Ge(Li) detectors in the atmosphere. This information is important not only in assessing the performance of the instrument during the balloon flight and in interpreting cosmic observations, but it is also used as the basis for either modifying our current system to improve performance, or designing new instruments which will have to operate in high radiation and particle flux environments such as, those encountered during balloon and satellite flights. Therefore, we have been studying in some detail the background spectrum of shielded Ge(Li) detectors measured during a balloon flight.

The instrument consists basically of four approximately 40 cm^3 Ge(Li) crystals in a single cryostat and cooled by liquid nitrogen (Jacobson et al. 1975). Prior to the flight, one of the detectors failed leaving three operational. Surrounding the cryostat is a 6.4 cm thick CsI(Na) shield with a collimator aperture of about 20° FWHM. The shield functions actively in anticoincidence with the Ge(Li) detectors with veto time constants of 6 μsec for shield events with 150 keV < E < 4 MeV and 55 μsec for larger events with E > 4 MeV. Each Ge(Li) detector has its own preamplifier, shaping amplifier and 8192 channel pulse height analyzer. All valid events are encoded in a 36 bit word which includes a time tag accurate to 17 μsec and each event is telemetered individually. The instrument operates in the energy range of about .050 to 10 MeV and has an energy resolution of about 2.9 keV at 1.33 MeV.

The background counting rate shown in Figure 1 illustrates the highlights of a typical balloon flight. Shown is the time profile of the counting rate in the energy range 65-100 keV. The main features are a rapid rise

after launch at 1205 UT, followed by a peak counting rate at Pfotzer maximum. Pfotzer maximum is the region at a depth of about 100 g/cm^2 where the secondary radiation due to primary cosmic ray interaction in the atmosphere reaches a maximum. Following Pfotzer maximum, the counting rate drops by a factor of roughly three as the balloon rises to float at an atmospheric depth of about 3 g/cm^2. During float, the counting rate remains reasonably constant except for a 45 minute interval during which a 20 cm diameter by 10 cm thick blocking crystal was moved in front of the aperture, and during the Crab nebula transit.

Figure 2 is an energy spectrum which shows numerous lines superimposed on a rather strong continuum. Most of these lines can be attributed to particle interactions resulting in excited levels in the Ge(Li) detectors or in the materials inside the CsI shield. This spectrum is rather complex because there are five naturally occurring Ge isotopes and numerous materials inside the shield. Since the particular isotope responsible for each line can generally be identified by its energy, we proceeded by first identifying these lines and then studying their time history. Table 1 gives the strong background lines together with their strength and origin, if known. The time profiles of these lines were plotted and as an example the 140 keV line time profile is shown in Figure 3. All line intensities were determined by a spectral analysis program called HYPERMET (Phillips and Marlow, 1976). The time profile of the 140 keV line is noticeably different from that of the continuum shown in Figure 1. The line intensity increases to a maximum at about Pfotzer maximum, but remains high as the balloon continues to rise to float altitude.

The 140 keV line arises from proton and neutron interactions in Ge resulting in ^{75m}Ge which decays to ground with a 48 sec half-life. At Pfotzer maximum, the strength of the 140 keV line can be explained by the measured

atmospheric proton and neutron fluxes taking into account attenuation in the shield. The (n,γ) reaction accounts for 75% of the intensity mostly from resonance neutrons (~ 100 eV) and the rest results from $(n,2n)$ and (p,pn) reactions on ^{76}Ge.

The isotropic atmospheric fluxes of neutrons and > 100 MeV protons drop by a factor of several, depending upon the particle and upon energy, between Pfotzer maximum and float (Armstrong, et al., 1973 and McDonald and Webber, 1959). Thus it is at first surprising that the 140 keV line strength does not also drop. However, since the lifetime of the ^{75m}Ge level is much longer than the shield veto time constants, any gamma-rays following excitation of this level due to secondary radiation produced in the shield will not be vetoed. Thus for excitation of this level, the shield acts like a slab of inert material approximately 35 g/cm^2 thick which produces secondary radiation. To a first approximation, the secondary radiation produced in CsI is the same as that produced at an equivalent atmospheric depth of air so even at float the Ge(Li) detectors are at an equivalent atmospheric depth of approximately 40 g/cm^2 as far as production of the 140 keV line is concerned.

The time profiles of other lines were studied and found to depend upon the lifetime of the excited state, and the reaction responsible for the line. They can be grouped into the following categories:

1. Lines originating from metastable levels formed in Ge with lifetimes $\geqslant 10$ µsec. These include the lines at 54, 67, 175, 198 and 439 keV and all have the same general shape as that of the 140 keV line shown in Figure 3.

2. Short lived states ($\leqslant 10$ µsec) in Ge that were excited by a reaction that did not cause a shield veto. These include the lines at 596 and 691 keV resulting from (n,n') reactions. In this case, neutrons formed in the CsI shield do not contribute to the line because of the shield veto. These two lines have a large high energy tail (~ 20 keV) corresponding to the

recoil energy of the excited isotope. The time profile of these lines is similar to that of the continuum and it is consistant with the atmospheric fast neutron fluxes.

3. Lines originating in materials other than Ge inside the CsI shield. These include the 844, 847 and 1014 keV lines from inelastic neutron scattering in Aℓ and Fe which also have a profile similar to the continuum.

4. Naturally occurring radioisotopes in the gondola such as ^{40}K which results in a line of constant intensity at 1461 keV.

5. Complex lines originating from more than one isotope such as the annihila-. tion line (Ling et al., 1977a) and the 93 keV line.

The results of a preliminary analysis of all these lines is consistant with the model discussed for the 140 keV line. Although the contributions from different reactions varies, the strength of each line can be explained by the interaction of neutrons and protons in the Ge(Li) detectors and in other materials in the gondola. The particles are a combination of atmospheric secondary radiation and secondary radiation produced in the gondola and in particular in the CsI shield. The fractional contribution from these two sources depends on the lifetime of the resulting state and on the method of excitation.

REFERENCES

Armstrong, T. W., K. C. Chandler and J. Barish (1973) JGR, 78, 2715.

Jacobson, A. S., R. J. Bishop, G. W. Culp, L. Jung, W. A. Mahoney and J. B. Willett (1975), Nucl. Instr. and Meth., 127, 115.

Jacobson, A. S., J. B. Willett, W. A. Mahoney and J. C. Ling (1976), Bulletin Am. Astron. Soc., 8, No. 4, 528.

Ling, J. C., W. A. Mahoney, J. B. Willett and A. S. Jacobson (1977a), JGR, 82, 1463.

Ling, J. C., W. A. Mahoney, J. B. Willett and A. S. Jacobson (1977b), Nature, 370, 36.

McDonald, F. B. and W. R. Webber (1959) Phys. Rev., 115, 194.

Phillips, G. W. and K. W. Marlow (1976), Nucl. Instr. and Meth., 137, 525.

FIGURE CAPTIONS

Figure 1   The time profile of the count rate between 65 and 100 keV during the balloon flight.

Figure 2   The energy loss spectrum for the three operating Ge(Li) detectors summed together and measured during the float portion of the balloon flight.

Figure 3   The time profile of the intensity of the 140 keV background line. The intensity and error for each point were determined by HYPERMET.

BACKGROUND LINES OBSERVED
DURING 10 JUNE 1974 BALLOON FLIGHT

Measured Energy	True Energy	Origin	Half Life	Intensity at Float (Counts/sec x 10^{-3})
53.	53.53(6)	^{73m}Ge	–	550*
66.	66.70(1)	^{73m}Ge	.53(3)s	225*
93.3	93.32(2)	^{67}Ga ^{67m}Zn	78.26(7)h 9.1(3)μs	14(4)
139.66	139.69(5)	^{75m}Ge	48.3(6)s	243(10)
159.2	–			12(3)
175.08	174.88(5)	^{71m}Ge	–	28(5)
184.8	–			10(2)
198.30	198.31(14)	^{71m}Ge	21.9(1)ms	479(10)
212.6	–			8(3)
239.2	–			10(4)
438.5	438.634(18)	^{69m}Zn	14.0(3)h	6.5(1.6)
443.4	442.91(7)	^{128}I	24.99(2)m	7.4(1.7)
472.0	472.32(15)	^{24m}Na	20.12(11)ms	12.7(2)
497.5	–			10(2)
511.27	511.0034(14)	Annihilation		125(5)
595	595.88(4)	^{74}Ge	11.8(11)ps	27
661.4	–			7.1(2.5)
695	691.2(2)	^{72}Ge	.43(2)μs	33(5)
844.2	843.76(3)	^{27}Al	30.5(35)ps	12.2(1.5)
847.2	846.751(19)	^{56}Fe	5.5(9) ps	3.3(1.1)
1015.2	1014.46(4)	^{27}Al	1.32(14)ps	6.4(1)
1460.87	1460.81(4)	^{40}K	1.277(8) x 10^9y	7.1(1)

*Measured with detector 1 only and scaled by 1./.292 which is the 3 detector total to detector 1 ratio of the volume, the front surface area and the total count rate, all of which are nearly equal.

Table 1

Ge(Li) RATE vs TIME

10 JUNE 1974
PALESTINE, TEXAS
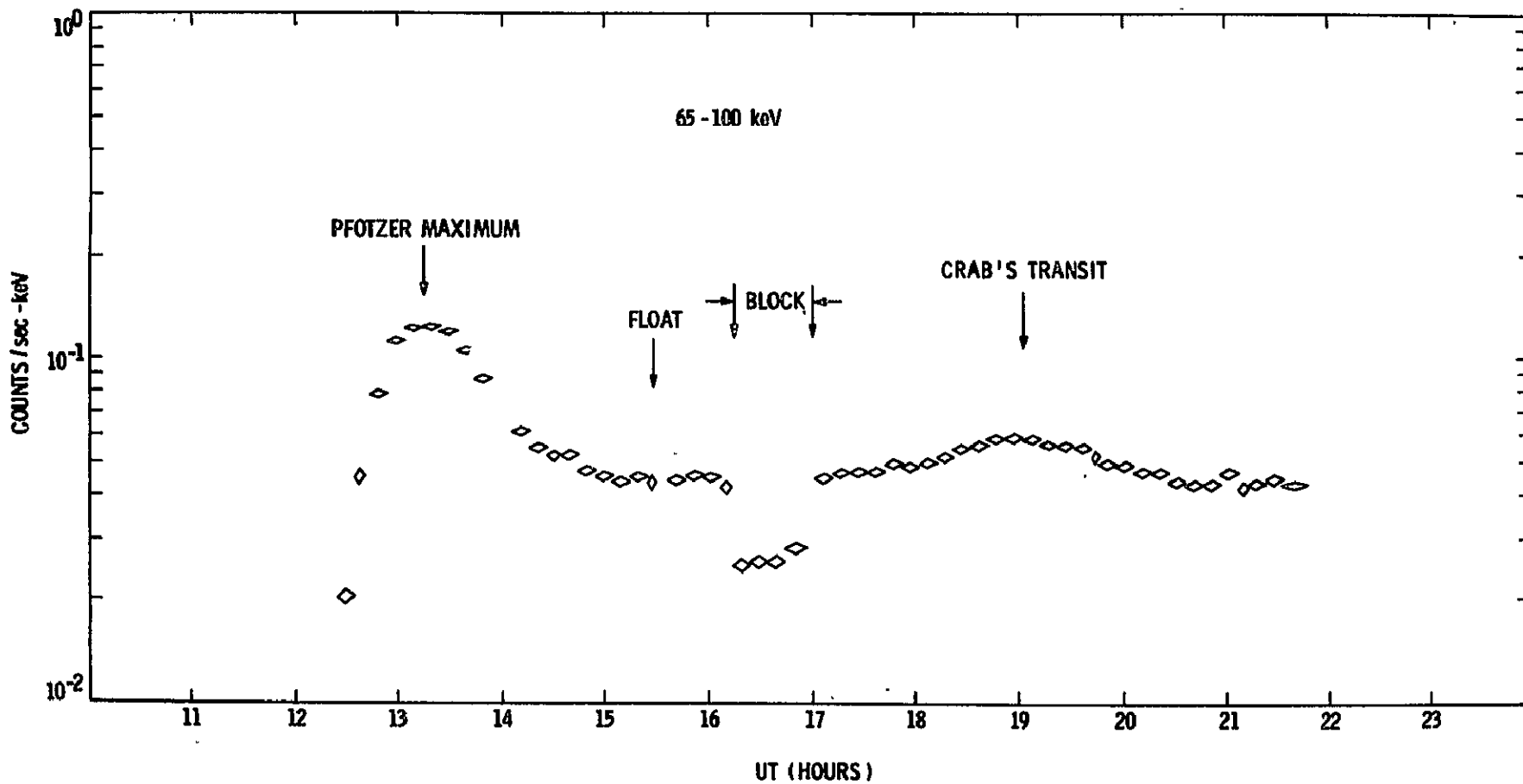
Figure 1

ENERGY LOSS SPECTRUM — Ge(Li) SPECTROMETER
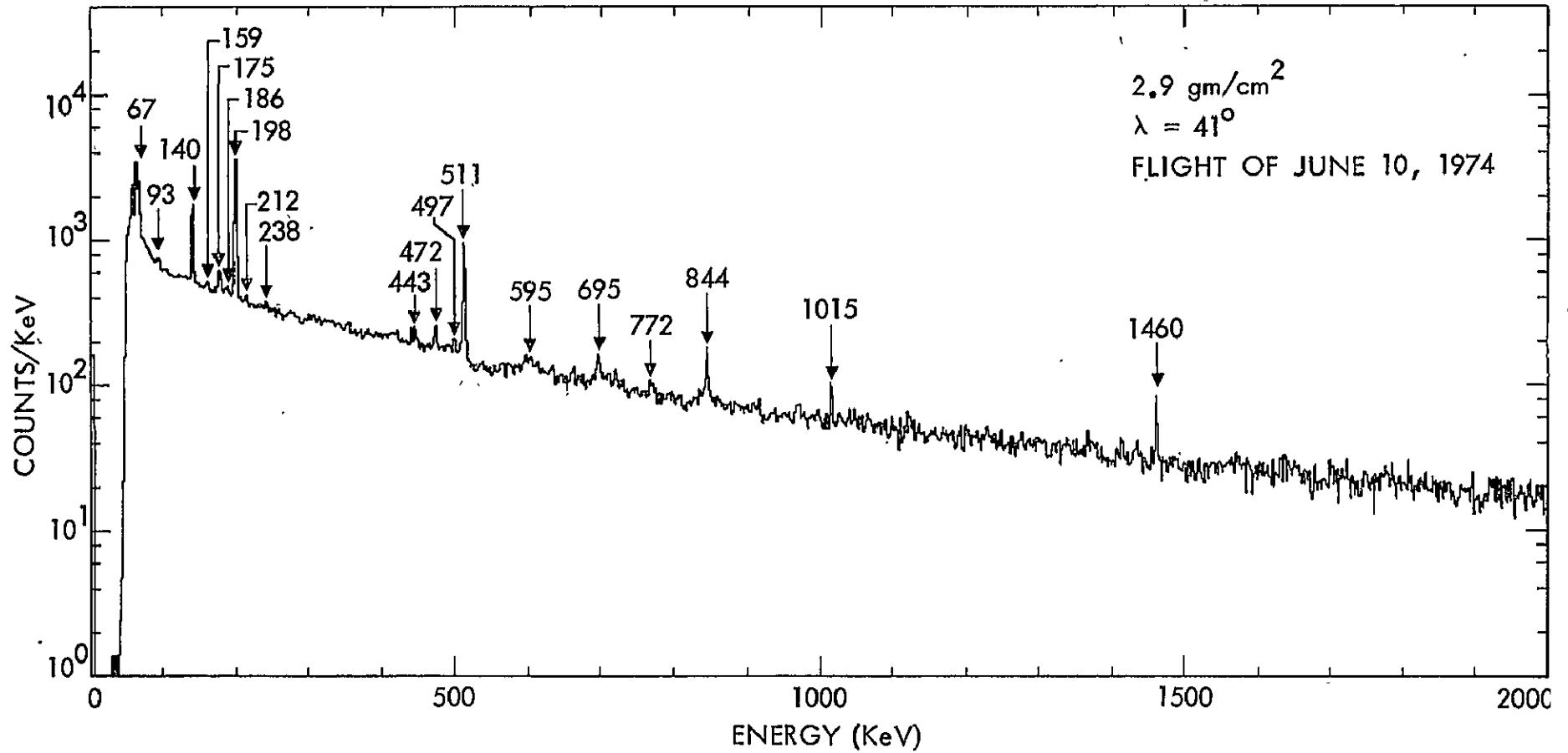
Figure 2

3 DETECTOR SUM – 140 KEV LINE – 10 JUNE 1974 BALLOON FLIGHT

Figure 3

472
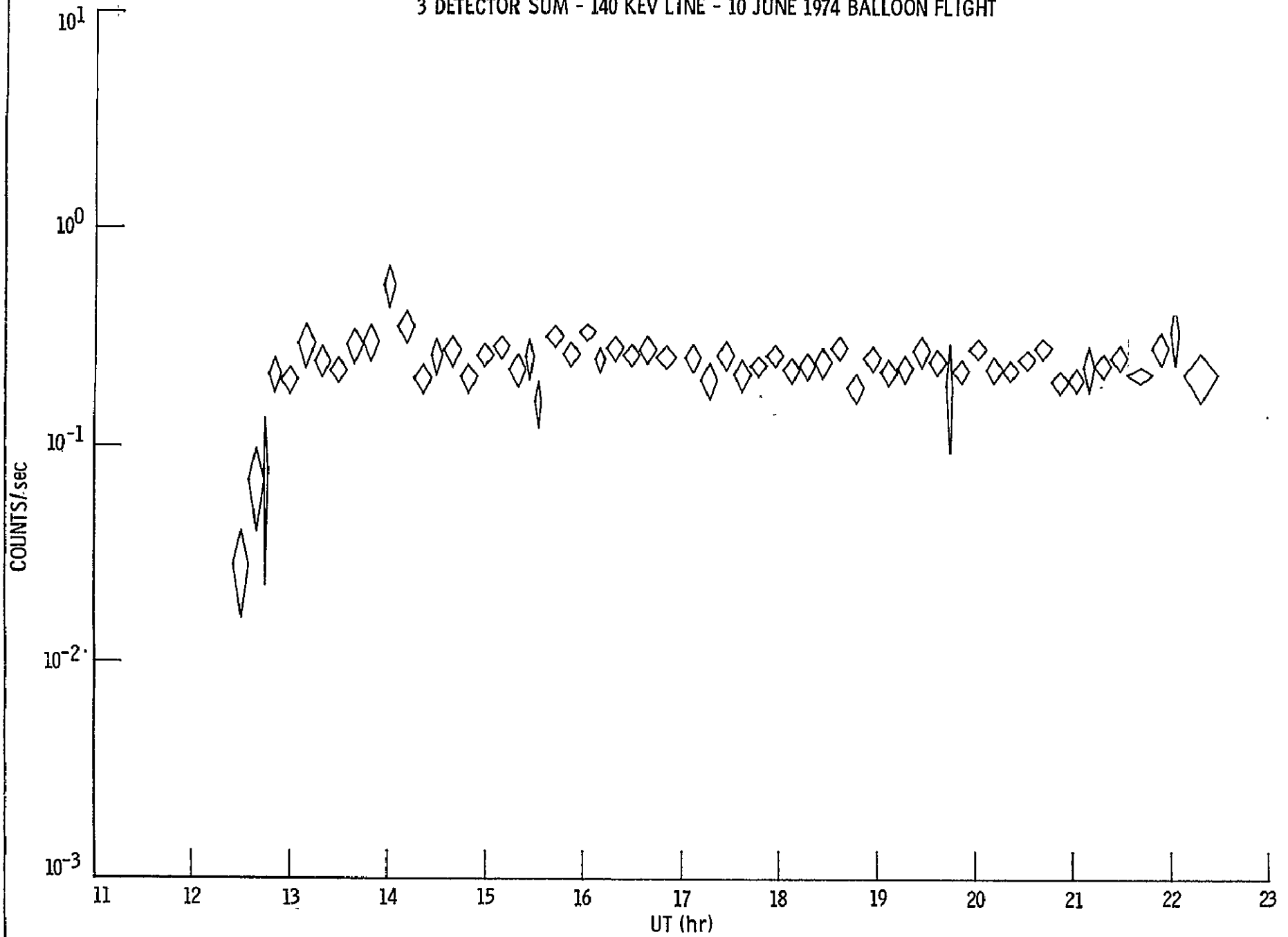
N78-32002

RADIATION DAMAGE OF GERMANIUM DETECTORS*

Richard H. Pehl
Lawrence Berkeley Laboratory
University of California
Berkeley, California 94720

Energetic particles can produce interstitial-vacancy pairs (a Frenkel defect) in a crystal by knocking the atoms from their normal positions. Detectors are unique among semiconductor devices in depending on very low concentrations of electrically active impurities, and also on efficient transport of holes and electrons over relatively large distances. Because the dense regions of damage produced by energetic particles may result in donors and/or acceptors, and also provide trapping sites for holes and electrons, detectors are very sensitive to radiation damage. (Compared to fast neutrons and charged particles, the damage caused by electrons and gamma rays is negligible and will not be discussed here.) In addition to these effects occurring within the detector, radiation may also change the characteristics of the exposed surfaces causing unpredictable effects on the detector leakage current. Fortunately, radiation-induced surface degradation has rarely, if ever, been observed for germanium detectors.

It has been known for a number of years that fast neutrons generate predominantly hole trapping centers in germanium detectors. This fact leads to a consideration of the possibility of minimizing hole trapping in charge collection by the use of a high-purity germanium coaxial detector configured with the p^+ contact on the coaxial periphery. As depicted in Fig. 1, the holes then make only a short traversal from the outer portions of the detector (where most interactions occur) to the contact of collection. To establish high electric fields at the periphery one would want to use n-type germanium.

Fig. 1 Charge collection direction in germanium coaxial detectors.

XBL 787-9757
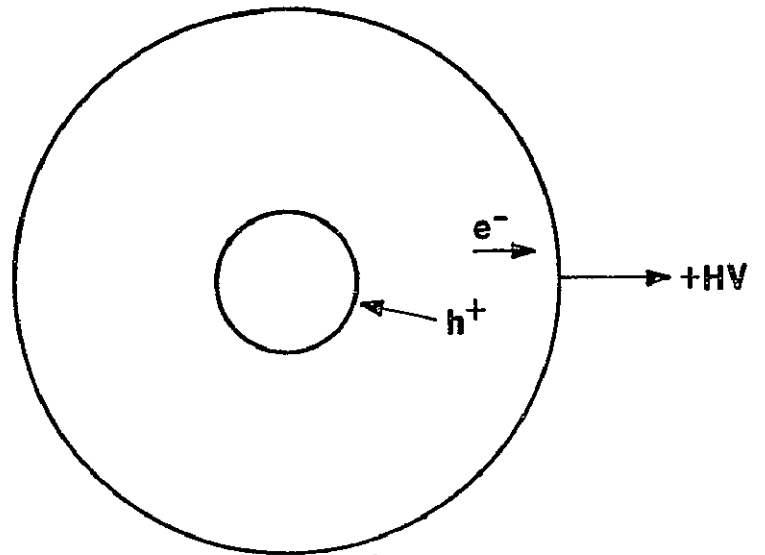
Although this hypothesis had not been tested—at least not directly—it was generally accepted that typical coaxial detectors (conventional electrode configuration) were considerably more vulnerable to neutron damage than were planar detectors.[1] However, no controlled experiments were done. (By controlled one means directly comparing a planar and coaxial detector made from the same germanium crystal to the same neutron irradiation. In light of the range of radiation damage sensitivities among detectors made from different crystals,[2] it is important that comparisons be made from detectors made from the same crystal.) Nevertheless, it is safe to say that a typical moderate size coaxial detector is at least 20 times more sensitive to neutron damage than is a 1 cm thick planar detector.

In the course of a continuing study of the proton damage of germanium detectors, (Reference 3, which reports the first experiment in this study, provides a far more extensive discussion of proton damage and subsequent annealing of germanium detectors than will be attempted in the present paper. Reference 4 also provides some pertinent general background on the subject.) a reverse electrode configuration coaxial detector that had been fabricated at Lawrence Berkeley Laboratory (LBL) five years ago—and a 1 cm thick planar detector made from the same crystal were irradiated with 5.1 GeV protons in a recent experiment by L. S. Varnell, R. H. Parker, B. D. Wilkins, L. Finnin, M. Fong and myself. These detectors were irradiated simultaneouly—there were actually a total of five detectors in line.

As shown in Fig. 2, the coaxial detector was considerably less sensitive to the high-energy proton damage than was the planar detector. These data indicate a factor of ~3. This would imply a factor of ~60 when comparing coaxial detectors having the opposite electrode configuration. Although additional experiments must be done, the evidence is now quite strong that coaxial germanium detectors having the n^+ contact on the coaxial periphery should not be used in any situation subject to significant radiation damage such as on an extended mission in space. To illustrate the problem, the anticipated resolution as a function of proton flux is plotted in Fig. 3 which one can then translate to days in orbit by making some estimates. Carefully studied proton irradiations of germanium detectors have been made only at 5.1 GeV, consequently the dependence of radiation damage on proton energy has not been established.
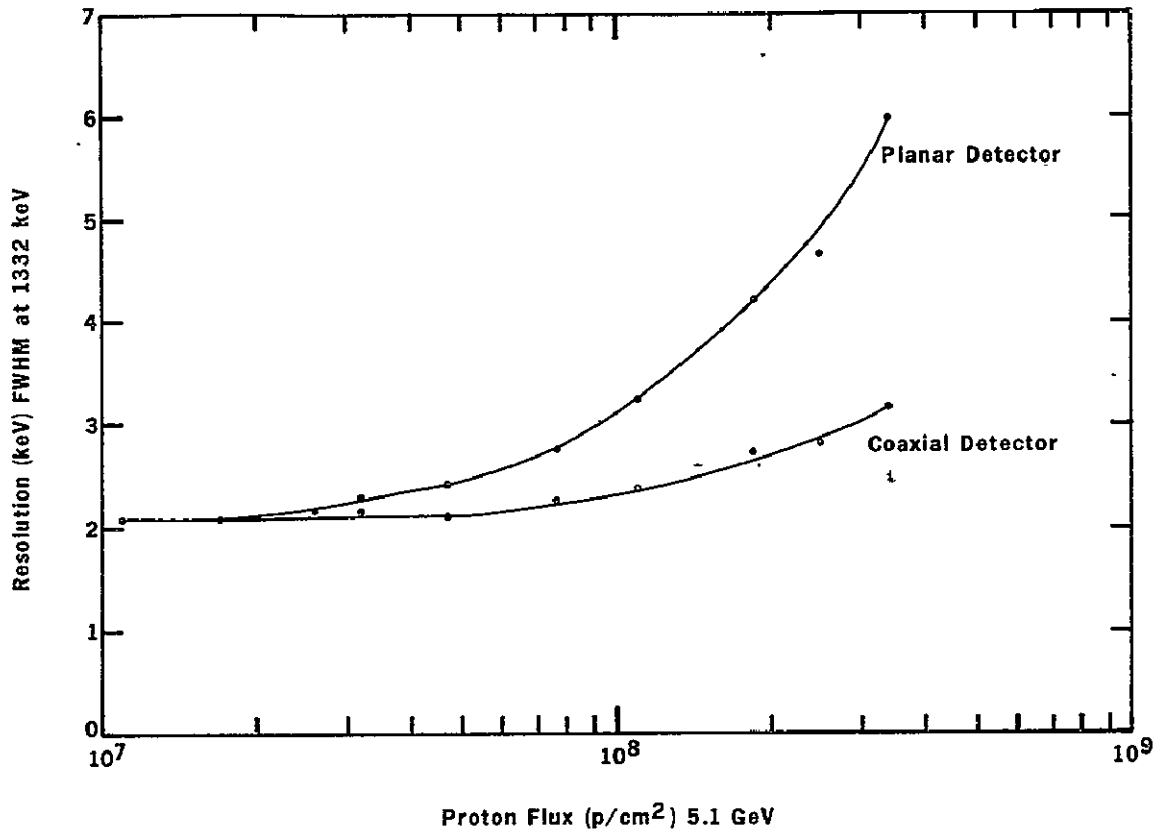
Fig. 2 Effect of proton flux on energy resolution. Electronic noise has not been subtracted but is equal in both systems.
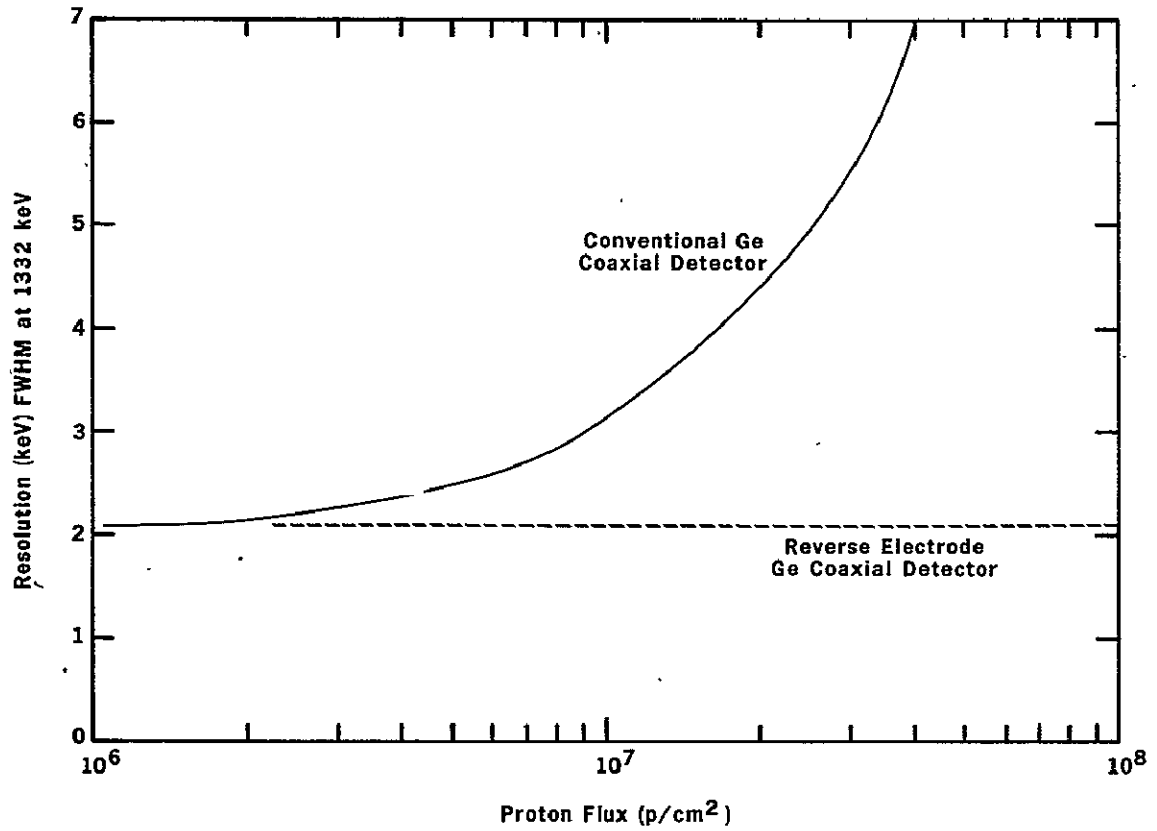
XBL 787-9758

Fig. 3   Predicted effect of proton flux on energy resolution of germanium coaxial detectors.,

Thus the predictions presented in Fig. 3 include an allowance (best guess) for this factor. Although heavy ions are known to produce more damage per particle than protons, this cosmic-ray component has been ignored in the predictions presented in Fig. 3.

Our conclusion is that large germanium-coaxial detectors are much more viable for extended space missions than many people thought several years ago-- at least as far as radiation damage is concerned. Unfortunately, some of the early experiments scheduled to fly germanium coaxial detectors for an extended time in space are presently planning to use detectors having the improper electrode configuration. Their anticipated difficulties should not diminish interest in the use of germanium coaxial detectors in the future.

Acknowledgments

References

1. P. H. Stelson, A. K. Dickens, S. Raman, R. C. Trammell, Nucl. Inst. Meth., 98, 481 (1972).

2. H. W. Kraner, R. H. Pehl, E. E. Haller, IEEE Trans. Nucl. Sci., NS-22, 149 (1975).

3. R. H. Pehl, L. S. Varnell, A. E. Metzger, IEEE Trans. Nucl. Sci., NS-25, 409 (1978).

4. R. H. Pehl, Physics-Today, 30, 50 (1977).

THE NUCLEAR RADIATION MONITOR FOR THE SPACELAB/SHUTTLE

G. J. Fishman[*]
Astrophysics Division
NASA Headquarters
Washington, D.C.   20546

Abstract

The Nuclear Radiation Monitor (NRM), planned for the
Spacelab 2 mission, is designed to make quantitative measurements
of the neutron and gamma-ray environment in the Shuttle payload
bay. The detector is a 5" x 5" NaI(Tl) scintillation crystal
with a charged-particle shield. It is mounted near the center of
the orbiter bay, and has nearly omnidirectional response.

[*]Permanent address: Space Sciences Laboratory,
                       NASA Marshall Space Flight Center
                       Huntsville, AL   35812

The ultimate sensitivity of future gamma-ray astronomy experiments depends to a large extent on the background radiation environment they encounter. From papers presented at this symposium, and other recent results, it has been shown that induced radioactivity and secondary neutrons constitute a major fraction of the observed background in the energy range of interest to gamma-ray spectroscopy, 0.1 to 20 MeV. Measurements of induced radioactivity in detector and spacecraft materials have been made on numerous spacecraft and on manned missions (Ref. 1-4). Since the Spacelab/Shuttle vehicle is expected to carry many high-energy astronomy experiments and developmental instruments, a detailed measurement of the radiation environment in the payload bay on an early mission is highly desirable.

￼ At orbital altitudes, background due to prompt interactions with charged particles, both from trapped radiation and cosmic rays, can be reduced by shielding, anticoincidence techniques and/or pulse shape discrimination. However, the neutron and gamma radiation, and the induced radioactivity cannot be adequately shielded against, nor can they be accurately predicted prior to launch. These sources of background radiation depend, in a complex way on the geometry and composition of surrounding materials, and on the detailed production and transport of the radiation in these materials.

Figure 1 shows the various sources of what is termed nuclear radiation: primary nuclei, neutrons and gamma rays produced by
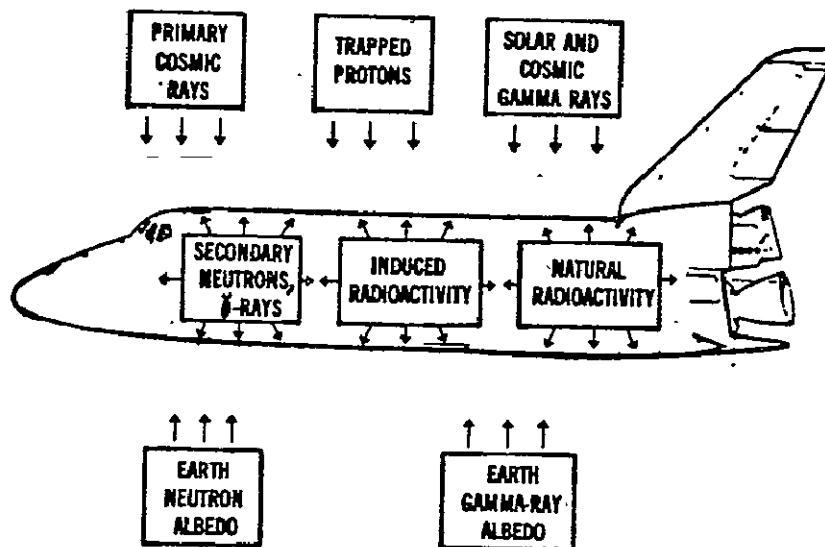

Figure 1: Shuttle/Spacelab Nuclear Radiation Environment

nuclear processes. The Nuclear Radiation Monitor (NRM) is designed to measure the sum total of this radiation in the payload bay, although seperating the individual components will be more difficult. The incident, external fluxes have been measured and modeled by other satellite and balloon measurements. The natural radioactivity of materials in the Spacelab/Shuttle can be measured prior to flight. The induced radioactivity may be identified by its characteristic spectral and temporal decay characteristics. A measurement of this radiation, along with the secondary neutron and gamma rays, is the primary objective of the Nuclear Radiation Monitor.

The main detector is a 5" x 5" diameter sodium iodide, NaI(Tl), scintillation crystal viewed by a 5-inch photomultiplier tube. Original plans for a high resolution germanium detector had to be abandoned due to programmatic constraints. However, the NaI(Tl) detector should be capable of identifying many of the stronger, seperated gamma-ray lines. The expected energy resolution is 8% FWHM at 662 keV. The detector will operate in an energy range from 0.1 to 20 MeV. A charged-particle anticoincidence shield, consisting of a 1 cm-thick plastic scintillator viewed by three 2-inch photomultiplier tubes, covers the crystal detector. The entire detector is designed to have nearly omnidirectional response.

Induced radioactivity will be produced in the detector as well as all other components in the Spacelab/Shuttle. The seperation of internal induced radioactivity from external radioactivity may be accomplished by the detection of individual gamma-ray lines, and by preflight irradiation of similar detectors at a nuclear accelerator.

The ambient charged particle flux near the detector will be monitored by the plastic scintillation detector and by several small silicon detectors. Neutron fluxes may be determined by observing discrete gamma-ray lines that are emitted from materials following neutron capture, inelastic scattering or the decay of a radioactive isotope produced after an (n,p) reaction. The latter gamma rays are particularly informative since they are only produced by neutrons with energies above a known threshold energy. Data from several threshold reactions may be unfolded to derive a neutron spectrum in the MeV region.

Analog electronics and high voltage power supplies will
be located on the supporting structure as shown in Figure 2.
The digital electronics will accumulate spectra in various
formats under the control of a micro-processor. High resolution
(1024 channel) spectra will be accumulated every 10 seconds;
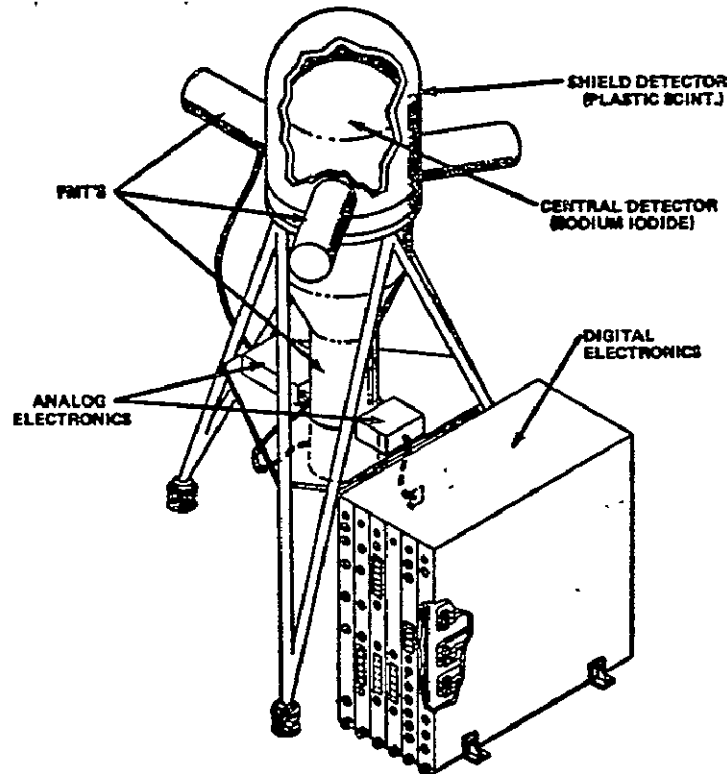lower resolution data will be sampled more frequently.

Figure 2: Nuclear Radiation Monitor

The NRM is scheduled to fly on the Spacelab 2 mission in 1981
as part of the Spacelab verification and testing instrumentation.
It will be located on a pedestal near the center of payload bay.
The need for the NRM and other instruments to monitor the Shuttle/
Spacelab induced environment was recognized in early Spacelab
planning (Ref. 5). The NRM will operate before, during and after
the nine day mission, in order to measure the natural radioactivity
the on-orbit radiation environment, and the post-flight induced
radioactivity. These measurements are expected to be of great
value to experimenters on future Shuttle/Spacelab missions.

REFERENCES:

1. Wasson, J. T., "Radioactive Cobalt and Manganese in Discover XVII Stainless Steel," _J. Geophys. Res., 67_, p. 3513, 1972.

2. Peterson, L. E., "Radioactivity Induced in Sodium Iodide by Trapped Protons," (OSO-1), _J. Geophys. Res., 70_, p. 1762, 1965.

3. Fishman, G. J., "Neutron and Proton Activation Measurements from Skylab," _Progress in Astronautics and Aeronautics, 48_, p. 397, 1976.

4. Trombka, J. I., et al, "Crystal Activation, Experiment MA-151," Apollo-Soyuz Test Project: Summary Science Report, Vol. 1, p. 101, NASA SP-412, 1977.

5. Naumann, R. J., "STS Contamination Control: Requirements for Induced Environment," Report of the NASA Shuttle Contamination Requirements Definition Group, 1974.

D33 - 93

N78-32004

GAMMA RAY POLARIMETRY*

K. S. Long and R. Novick

Columbia Astrophysics Laboratory
Departments of Astronomy and Physics
Columbia University
New York, New York 10027

As illustrated by the following examples, polarization measurements

of gamma ray sources are astrophysically important, allowing characteriza-

tion of basic emission mechanisms which are impossible using other tech-

niques:

(1) Compton and synchrotron models have been proposed to explain

emission from the active radio galaxy Cen A, one of the most intense of

the known gamma ray sources (JC Perola and M Terenghi 1971). Since

synchrotron emission characteristically exhibits large linear polarization

in contrast to inverse Compton scattering models, a polarization experi-

ment sensitive to polarization of a few per cent would permit a resolution

of this question.

(2) Detailed models of pulsed gamma emission from pulsars in the

Crab and Vela supernova remnants are being proposed by various theoreticians,

including Cheng and Ruderman (1977) and Sturrock (1971). Because coherent

radiation is required to explain the high radio brightness temperatures

observed from these sources, large polarization is a common feature in

these models. However, in the Cheng and Ruderman model in which the gamma

---

rays are produced via curvature radiation, the polarization vector at

1 MeV and at 1 eV should be parallel in contrast to the Sturrock model in

which the polarization vectors in the two regimes would be perpendicular.

Since the polarization in the optical band is well known, a positive

detection of polarization at 1 MeV would invalidate one of these models.

(3) Cygnus X-1 is widely inferred to be a binary X-ray system

containing a black hole. This conclusion is primarily based on indirect

evidence concerning the mass of the compact object. Polarization is

anticipated in this source due to the anisotropic nature of the X and

gamma-ray emitting regions. Recently, Stark and Connors (1977) have

predicted that if the black hole were rapidly rotating the polarization

vector would rotate as a function of energy. If this is so, it would be

one of the few directly observable signatures of a black hole in a binary

system. Polarization sensitivities of 1% or less are required, however,

since the emission is of thermal origin. If polarizations exceed 10%,

it is unlikely that the Cygnus X-1 system can contain a black hole at all.

To recapitulate, fundamental questions about the nature of cosmic

gamma ray sources can be answered if high sensitivity polarization

measurements can be made. But why bring that question up at a symposium

devoted to gamma ray spectroscopy? Because spectroscopic instruments

currently being proposed may possess polarimetric capabilities which should

be nurtured and if possible enhanced.

Two processes, Compton scattering and pair production, have been used

to detect the polarization of high energy (E > 50 keV) photons in labora-

tory experiments. The differential scattering cross-section for Compton

scattering is given by the Klein-Nashina formula:

$$\frac{d\sigma}{d\Omega} = \frac{r_o^2}{4} \left[\frac{E'}{E}\right]^2 \left[\frac{E}{E'} + \frac{E'}{E} - 2 + 4(\hat{e}' \cdot \hat{e})^2\right]$$

where r_o is the classical electron radius, and E and E' are the initial and final photon energies respectively (Jauch and Rohilick 1955). The polarization dependence of Compton scattering arises from the last term which involves the dot product of the incident electric vector $\hat{e}$ and the final electric vector $\hat{e}'$.

The usefulness of a polarimeter is determined by its photon sensitivity and modulation factor. The modulation factor is defined as the apparent polarization recorder by the device when it is exposed to a beam of 100% polarized radiation. If I_{max} and I_{min} are the maximum and minimum intensities recorded when the polarimeter is rotated about a beam of 100% polarized photons then the modulation factor is given by,

$$M = \frac{I_{max} - I_{min}}{I_{max} + I_{min}}$$

The largest modulation factor obtainable is therefore 1, and a process with no sensitivity to polarization would have a modulation factor of 0. Modulation factors for Compton scattering are indicated in figure 1, as a function of scattering angle for several energies. At low energies, the Thomson limit, the modulation factor is 1 at a scattering angle of 90°. The modulation factor for a 2.5 MeV photon is at best 0.25, large enough to be useful for polarimetric purposes. At higher energies, the modulation factor continues to decrease.

One can imagine a Compton scattering polarimeter consisting of a cluster of detectors, perhaps made of intrinsic Germanium. Any two members

of the cluster defines an angle with respect to the sky. Compton events would be those which trigger two detectors, in coincidence, corresponding to a photon which Compton scattered in one detector and was then photoabsorbed in another. Polarization would be detected in terms of the difference in counting rates in different pairs of detectors.

A Compton scattering polarimeter is a broad-band device which makes up somewhat for the fact that the number of photons which will be detected is small, compared to those available at lower energies. The maximum energy which can usefully be detected is determined by the declining modulation factor and will typically be about 10 MeV. The minimum energy would be determined by the competing process – namely photoabsorption. In Germanium, the photoabsorption cross-section equals the Compton scattering cross-section at about 200 keV.

In conjunction with Marvin Leventhal, Ian Strong, Crawford MacCallum and Tom Green, we have considered the polarization properties of a specific detector system which would consist of 19 Germanium crystals in a close packed array. The polarization detectable at 99% confidence level by any polarimeter is given by

$$S(99\%) = 4.29 \ R/(M\sqrt{N})$$

where R is the ratio of signal plus background rate to signal rate, M is the modulation factor and N is the total number of signal plus background counts. In the detector system we considered, Cen A would produce about 15 counts per second in the energy range 0.1 to 10 MeV. A Monte Carlo calculation revealed that for spectral parameters appropriate to Cen A,

the modulation factor for the elements of the array would be about 0.5, about 3% of the events being detected as Compton events. Thus assuming the signal is source dominated, about 45,000 Compton events would be detected in a 10^5 second observation, and the polarization sensitivity at 99% confidence would be approximately 4%, probably sufficient to resolve the question of the emission mechanism in that source.

A Compton scattering polarimeter like the one just described possesses considerable advantages over conventional Thomson scattering polarimeters which have been constructed at Columbia and elsewhere to observe polarization at X-ray wavelengths. In those systems the scattering block is not a detector but a block of inert low Z material, typically lithium. (1) The Germanium polarimeter records the entire energy of the event. The polarimeter serves the secondary purpose of operating as a high purity Germanium spectrometer for those sources in which you do not detect polarization. (2) In systems with a separate scattering block the percentage of the total aperture occupied by the scattering block is usually rather small, whereas in a Germanium system a large fraction of the aperture is utilized. (3) Compton scattered events have a well defined signature, hence background rates are likely to be very low, just as they are in existing double Compton telescopes. This is particularly true since many types of background have associated gamma ray lines, regions which can be avoided in the data analysis.

The possibility of using pair production to detect polarization of high energy gamma rays was first suggested by Berlin and Madansky (1950). The modulation factors associated with pair production are quite complicated since in general two particles are produced, but substantial modulation can theoretically be obtained at much higher energies than are practical using

Compton scattering. One can use a wide variety of signatures for valid

events. For example, you can examine the total electron distribution, those

events in which the electron and positron have the same transverse momentum

and so on. Recently, the first practical laboratory polarimeter, used to

detect linear polarization from coherent bremstrahlung of 1 MeV electrons,

was constructed by Kondo et al. (1974). However, it is unlikely that pair

production polarimeters can be adapted to any astrophysical application

in the near future. The central difficulty is that the typical opening

angle of the electron or positron direction with respect to the incident

photon aircitron is small, of order E/mc^2. On the other hand, multiple

scattering in the material used to convert the photons to an electron

positron pair causes deviations in the direction of the electron and

positron. The deviation is roughly given by

$$\sqrt{(\theta^2)_{av}} = \left(\frac{E_s}{E}\right)\sqrt{\frac{t}{2}}$$

where t is the depth of the scatterer in radiation lengths and E_s is of

order 20 MeV (Rossi and Greisen 1941). In order to have a high conversion

efficiency the depth of the scatterer must be approximately 1 radiation

length. But in that case, the average deviation of the electron deviates

from the photon direction. For the experiment of Kondo, et al., an acceler-

ator was used and a target with a depth of 10^{-4} radiation lengths was adequate.

This would be impossible in an astrophysical experiment.

In conclusion, while pair production polarimeters do not appear prac-

tical in the forseeable future, polarimeters which utilize Compton scattering

can be constructed. In some instances, instruments which have polarimetric

capabilities are unlikely to be constructed for other reasons, such as

the Germanium spectrometer system we have discussed. If so, it is obvious

that the instruments should be designed to optimize their polarimetric

capability.

REFERENCES

Perola, J.C., and Terengli, M., 1971, Astron. and Astrophys., 24, 461

Cheng, A., and Ruderman, M.A., 1977, Astrophys. J. (Letters), 216, 865

Sturrock, P.A., 1971, Astrophys. J. (Letters), 164, 529

Stark, R.F., and Connors, P.A., 1977, Nature Vol. 266, 429 and 430

Jauch, J.M., and Rohilick, F. The Theory of Photons and Electrons (1955: Addison Wesley: Cambridge, Ma.) P233

Bulin, T.H. and Madansky, L., 1950, Physics Rev., 78, 623

Kondo, K., Mayachi, T., Ukai, K., Yamamato, A., Gotow, K., Yoshida, H., Inaba, S., Kurokawa, S., Muramotsa, H., Sasoa, N., Suzoki, S., Kobayashi, M., and Iwata, S., 1974, Nuc. Inst. and Meth., 114, 315

Rossi, B., and Greisen, K., 1941, Rev. of Mod. Phys., 13, 240
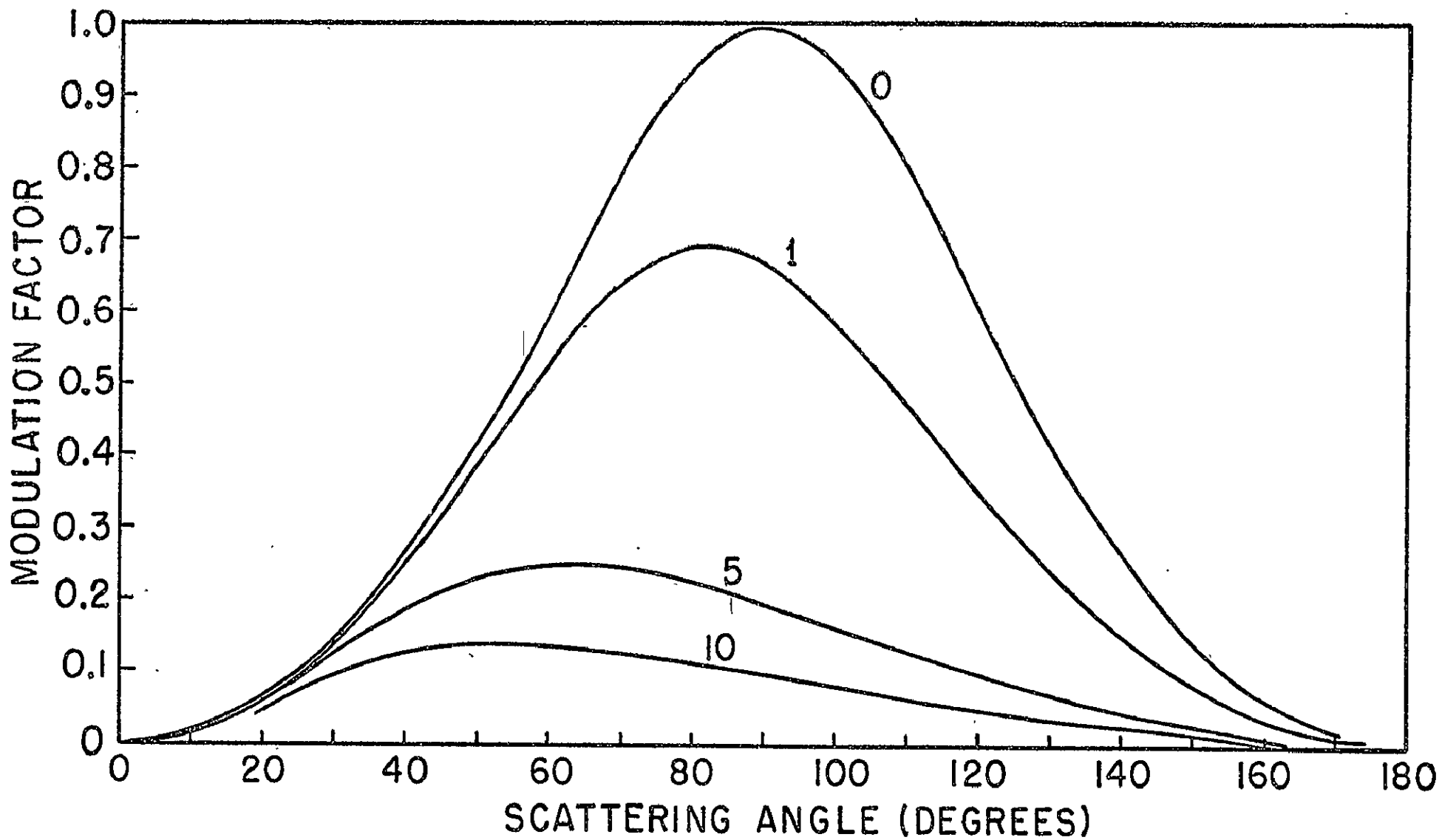
Figure 1: The modulation factor for a Compton polarimeter as a function of scattering angle for several photon energies. The photon energies are given in units of E/mc^2.

FUTURE DIRECTIONS IN EXPERIMENTAL GAMMA RAY ASTRONOMY

R.C.Haymes[+]

Max-Planck-Institut für Physik und Astrophysik
Institut für extraterrestrische Physik
D-8046 Garching, West Germany

During this Symposium, we have been priviledged to see a new
branch of astronomy come firmly into existence. Gamma ray
spectroscopy, as we have been seeing, adds a whole new dimension
to our investigations into astrophysics and cosmology, because
of the nuclear and other information that it uniquely conveys.
While we now know that detectable fluxes of gamma ray spectral
lines that have cosmic origins do in fact exist, there are
experimental needs that must be met, if this field is to develop
its full potential. These needs may be divided into two parts,
a need for better vehicles and a need for better instruments.
Better vehicles: (a) We will need long-term observations of
selected sources, both to measure variability and to achieve
the highest sensitivity. Without sensitive data on variability
of the sources of low energy gamma rays, we may miss important
clues as to the nature of the sources. We now have observing
periods measured in hours; the next step would logically be
periods measured in days or weeks to acquire variability in-
formation. (b) We will need access to the entire sky, not just
a part of it, both to observe the many various sources predicted
to exist, and to measure the energy spectrum and map the isotropy
of the cosmic gamma ray background. Taken together, this and
item (a) suggest that a spacecraft with several years operating
life is needed. (c) Increased sensitivity is a must, for future
observational work. Only the cosmic source that was theoretically
expected to be among the very brightest sources of nuclear gamma
rays, the galactic center region, has been definitely confirmed
at this point, by the existing observations. To measure the other
sources, experiments with larger collecting areas will be needed.

[+]On leave from Rice University, Houston, Texas, U.S.A.

We presently have instruments with collecting areas of order
100 cm^2; the next step would logically be to geometric areas
of the order of a square meter, to get a factor of ten reduction
in the random errors. This step inevitably means heavy experi-
ments; experiments likely weighing a thousand kilograms or more,
will be needed.

Putting items (a), (b) and (c) together, we see a clear scienti-
fic need for the Gamma Ray Observatory (G.R.O.). The projected
G.R.O. would fill the scientific requirements.

But the G.R.O. is not the only vehicle needed, for the development
of this fledgling branch of astronomy that promises so much
enrichment of our understanding of the cosmos. As will be dis-
cussed later, a vigorous, on-going program in scientific ballooning
must also be maintained, for the scientific development of the
field.

Better instruments: Nuclear gamma rays have energies that range
from about 0.1 MeV to about 20 MeV. Future instruments should
each cover this entire energy range. At present, the various
experiments each only cover portions of the range; trying to piece
together a single spectrum from such experiments, each of which
has a different amount of systematic error (frequently unknown)
is at best difficult and may be misleading.

The present-day experiments seem to have reached a sensitivity
"floor" of about 10^{-3} photons cm^{-2} sec^{-1}, for gamma ray spectral
lines. According to the results of astrophysical theory, the
sensitivity must be improved, to 10^{-4} photons cm^{-2} sec^{-1} or better
to measure the many cosmic sources expected to exist, and to see
the wealth of spectral lines expected from the bright sources
already found.

Conventional instruments produce data that are ambiguous; as dis-
cussed further later-on, absolute fluxes of spectral lines from
discrete or diffuse cosmic sources, and the absolute flux and iso-
tropy of the cosmic background, are uncertain. There therefore
appears to be good reason for new approaches to astronomical gamma
ray instruments, in order to eliminate the ambiguities.

The energy resolution needed in future instruments should be
"as good as feasible", providing that sensitivity is not sacri-

ficed. This means 10% FWHM, or better. Good energy resolution
helps in measuring closely-spaced lines and in improving the
sensitivity to narrow spectral lines. Spectral lines of various
widths are expected from the different astrophysical environments.
Therefore a continuing need will exist for both scintillation-
counter instruments (high efficiency, moderate energy resolution)
and solid-state instruments (moderate efficiency, high energy
resolution).

Finally, in this list of desirable features for future instru-
ments, an angular resolution of one degree or better is desirable.
There are discrete X-ray sources in the galactic center region
that are spaced about this much apart, and it seems not un-
reasonable that some of them may additionally be sources of
nuclear gamma rays. In the same sky region, the spectrum of inter-
stellar nuclear gamma rays may have a spatial gradient, which
should be measured.

Astronomical nuclear gamma ray instruments for the 1980's may
be divided into two categories, the conventional and the un-
conventional. Among the conventional instruments, we will likely
see the further development of actively collimated detectors,
some of which have scintillation counter primary detectors,
with about one-square-meter geometric collecting area, and some
of which have arrays of germanium primary detectors with
0.003 MeV or better energy resolution. We will likely also see
further development of double Compton instruments, which reduce
some but not all of the systematic errors that are presently
a problem.

It may be that we have been very lucky, thus far, in that the
error bars due to random fluctuations have hidden the systematic
errors in the observations. It is to eliminate the systematic errors
as well as to increase the sensitivity of the measurements, that
unconventional instruments should be explored. For actively col-
limated instruments, the systematic error sources include induced
radioactivity and offset background pointing. Particle bombardment
induces radioactivity in the instrument's crystals and other
components. The counting rates due to this instrumental background
are typically a full order of magnitude greater than even the

galactic center fluxes of nuclear gamma rays from cosmic rays alone. This instrumental background, even if it were stable in time, makes impossible actively-collimated measurements of the cosmic background's spectrum and isotropy.

To measure a cosmic source, an actively collimated instrument must be pointed away from the source, to measure the background. But, where should it be pointed for background observations? The gamma radiation from the sky has galactic and extragalactic components, so its flux depends upon direction. The sky brightness of the sky area chosen for the background observations may or may not have the same brightness as the sky area that includes the source. Because of the induced radioactivity problem mentioned above, the background observations should be made simultaneously with the cosmic measurements. This is not the case with actively collimated instruments. The fluxes and indeed the line energies of nuclear gamma ray lines from cosmic discrete and diffuse sources may therefore appear different, when measured with different actively collimated instruments, especially if they select different sky areas for background observations.

Double Compton instruments also suffer from systematic errors. Some photons recoil out of a double Compton instrument, after having caused correct-signature pulses in both of the two detector layers. This distorts the measured energy spectrum. Corrections for these energy losses may be calculated and applied, but there is no independent check on their sufficiency.

Another problem experienced with double Compton instruments is that their energy range is incomplete. Double Compton instruments have a lower energy threshold that is typically somewhere in the (1-2) MeV energy interval. Therefore they do not accurately measure the spectrum around one MeV, nor any of the lower energy photons of the nuclear energy range. As noted previously, it is desirable to cover the entire nuclear energy range with a single instrument.

There have also been other problems associated with past versions of double Compton instruments. These include sensitivity to neutrons, and crude energy resolution and angular resolution..

These problems of the conventional instruments make exploration of alternative, unconventional concepts worthwhile. One such concept is called the gamma ray "correlator". The correlator statistically synthesizes the absolute energy spectrum of the sky photons, through a correlation of the various total energy deposition spectra measured by the many independent gamma ray detectors that comprise the system, with the skyward vector solid angles viewed by the detectors, throughout the nuclear energy range. Much instrumental background is rejected by the system, but the spectrum of the remaining instrumental background is measured at the same time as is the sky spectrum, through a correlation of the measured spectra with non-skyward look-directions. No offset pointing is used; the sky background, which correlates with detector look-direction and solid angle magnitude, is measured simultaneously with the source, from the sky area surrounding the source, so that measurements of the cosmic background's absolute spectrum and isotropy are byproducts of measurements of cosmic sources.

No doubt, there are other unconventional instruments, in addition to the correlator. If the G.R.O. should gain approval, it will be in the exploration and development of unconventional approaches that there will remain a need by nuclear gamma ray astronomy, for scientific balloons. New instrument development is essential for the future health of the field. Scientific balloons are also valuable academically, and as quick reaction vehicles, for new, unexpected phenomena.

Without the G.R.O., the development of nuclear gamma ray astronomy will depend heavily on balloons and on Spacelab, although existing versions of neither of these vehicles would meet the scientific needs as fully as would the G.R.O.

Laboratory Accelerator Workshop

N. S. Wall

A Workshop on Laboratory Accelerator Measurements was held on April 29, 1978. There were five papers presented illustrating the sort of data which can be obtained in such measurements. These papers also demonstrated the techniques used in such measurements. Two of the papers suggested a number of experiments which are of interest to those currently working with gamma-ray line spectra.

The papers presented were:

1. Cross Section Measurements Relevant to Gamma Ray Astronomy - P. Dyer, et al.

2. Measurement of 15.11 MeV γ-Ray Flux in the Reaction $^{12}C(p,p')^{12}C*$ and $^{16}O(p,p'''\alpha'')^{12}C*$ - J. Lapides, et al.

3. Needed Measurements in Simulated Condensed Mass Systems - A. Metzger, et al.

4. Needed Measurements for γ-Ray Astronomy - R. Ramaty

5. University of Maryland Gamma Ray Facilities - W. F. Hornyak

Following these presentations the characteristics and accessibility of accelerators at the University of Washington and the University of Maryland were briefly discussed. Anyone desiring the use of these accelerators should contact Prof. J. G. Cramer at Seattle and Prof. N. S. Wall at Maryland.

The session was chaired by Prof. N. S. Wall of the University of Maryland.

Cross Sections Relevant to Gamma Ray Astronomy[†]

P. Dyer

University of Washington, Seattle, WA   98195
and
Michigan State University, East Lansing, MI   48824

D. Bodansky

University of Washington, Seattle, WA   98195

D.R. Maxson

University of Washington, Seattle, WA   98195
and
Brown University, Providence, RI   02912

We have measured gamma-ray production cross sections relevant to gamma-ray line astronomy for protons and alpha particles incident on targets consisting of nuclei of high cosmic abundance: ^{12}C, ^{14}N, ^{16}O, ^{20}Ne, ^{24}Mg, ^{28}Si, and ^{56}Fe.

Solid or gaseous targets were bombarded by monoenergetic beams of protons and alpha particles, and gamma rays were detected by two Ge(Li) detectors. The proton energy for each target was varied from threshold to about 24 MeV (lab); for alphas the range was from threshold to about 27 MeV. For most transitions, it was possible to measure the total cross section by placing the detectors at $30.5°$ and $109.9°$, where the fourth-order Legendre polynomial is zero. For the case of the ^{16}O ($E_\gamma = 6.13$ MeV, multipolarity E3) cross sections, we measured yields at four angles. Absolute cross sections were obtained by integrating the beam current and by measuring target thicknesses and detector efficiencies. The Ge(Li) detector resolution was a few keV (although the peak widths were greater, due to Doppler broadening).

An overview of the measured gamma-ray cross sections for incident protons is presented in Fig. 1, where the cross section and energy of the most prominent gamma-ray line for each target are displayed for several proton energies. Except for ^{16}O, these lines correspond to the de-excitation of the first excited state of the target nucleus; for ^{16}O the transition is from the second excited state to the ground state. If the energy spectrum of the interacting particles is known, the cross sections can be used to deduce relative nuclear abundances at the gamma ray source. The abundance analysis will be somewhat complicated by the multiplicity of channels opened up as the incident energies increase. For example, for protons above about 13 MeV, the 4.44-MeV gamma rays from the first excited state of ^{12}C can be produced in the $^{16}O(p,p\alpha)^{12}C$ reaction, as well as in the $^{12}C(p,p')^{12}C$ reaction.

The multiplicity of lines from a given target can also be useful. Of special interest are cases where the different gamma-ray lines have different excitation functions, for example the 0.847-MeV gamma rays produced in $^{56}Fe(p,p')^{56}Fe$ reactions and the 0.812-MeV gamma rays produced in $^{56}Fe(p,n)^{56}Co$ reactions. The relative yield in such cases can provide insight into the energy spectra of the interacting particles.
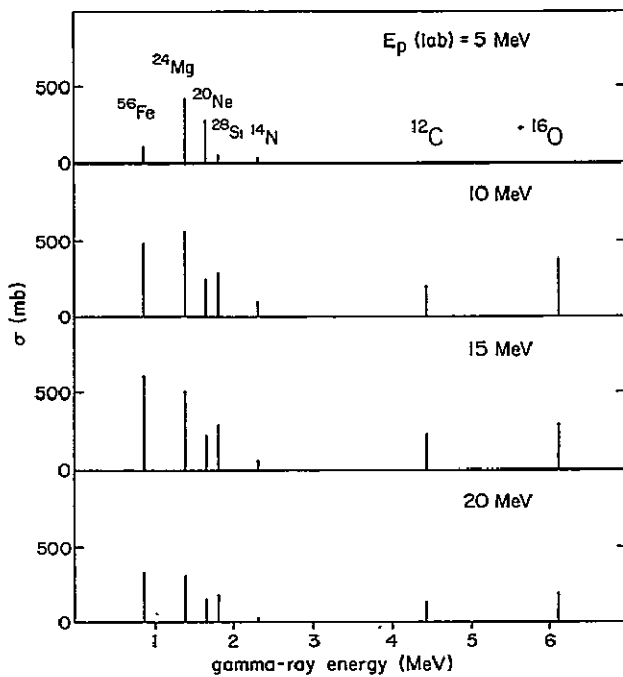
Fig. 1. Cross sections for the most prominent lines produced by protons.
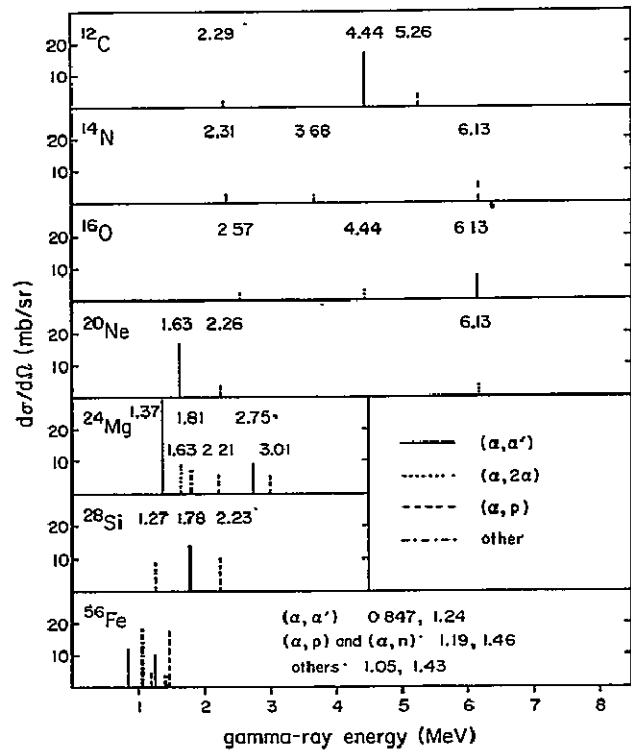

Fig. 2. Approximate differential cross sections at 90° for lines strongly excited by 24-MeV alpha particles.

For alpha particles, a slightly different sort of overview is presented in Fig. 2, where approximate differential cross sections at 90° are shown for some of the lines strongly excited in bombardments at 24 MeV. As with protons, lines from the de-excitation of the lowest excited state of the target nucleus (or next lowest, in the case of ^{16}O) are prominent.

A further feature is the prominence of lines from nuclei produced in reactions where only one or two nucleons are emitted from the compound nucleus, especially (α,p) reactions. While these lines are strongly excited for all the targets other than ^{14}N, they are particularly interesting in the case of ^{56}Fe. The A = 58 and A = 59 lines can only be formed in proton bombardments if the target is above A = 56. In view of the precipitous drop in nuclear abundances above A = 56, these lines may prove to be a characteristic signature for alpha-particle interactions. For 24-MeV alpha particles, relatively strong peaks are seen which are interpreted as corresponding to the following lines: the 1.050-MeV line from ^{58}Co, the 1.190 MeV line from ^{59}Co or ^{59}Ni, the 1.428-MeV line from ^{59}Ni (to the first excited state), and unresolved lines at 1.454 MeV from ^{59}Ni and at 1.459 MeV from ^{59}Co. As to be expected, the A = 59 lines are found to be strongest below 20 MeV, and the A = 58 lines are strongest above 20 MeV.

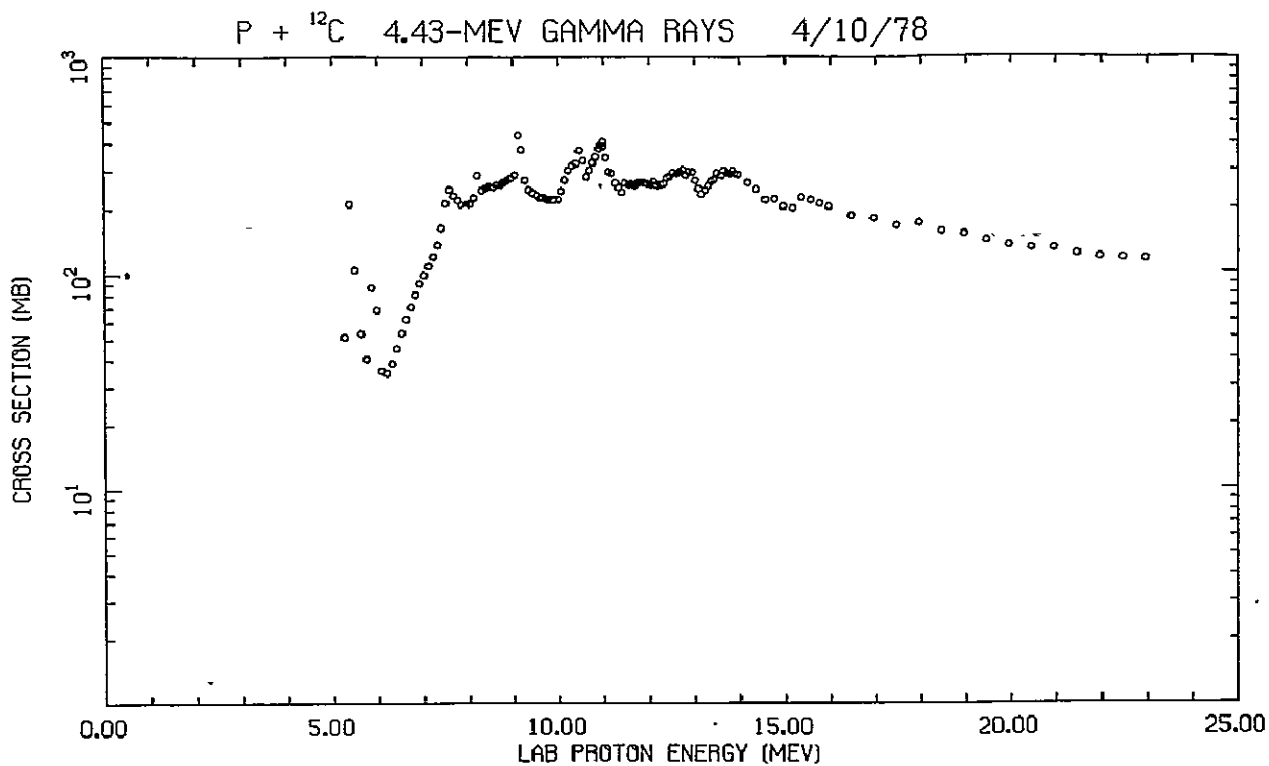P + ^{12}C   4.43-MEV GAMMA RAYS   4/10/78

Fig. 3. Cross sections for production of 4.44-MeV gamma·rays produced by protons incident on a carbon target.

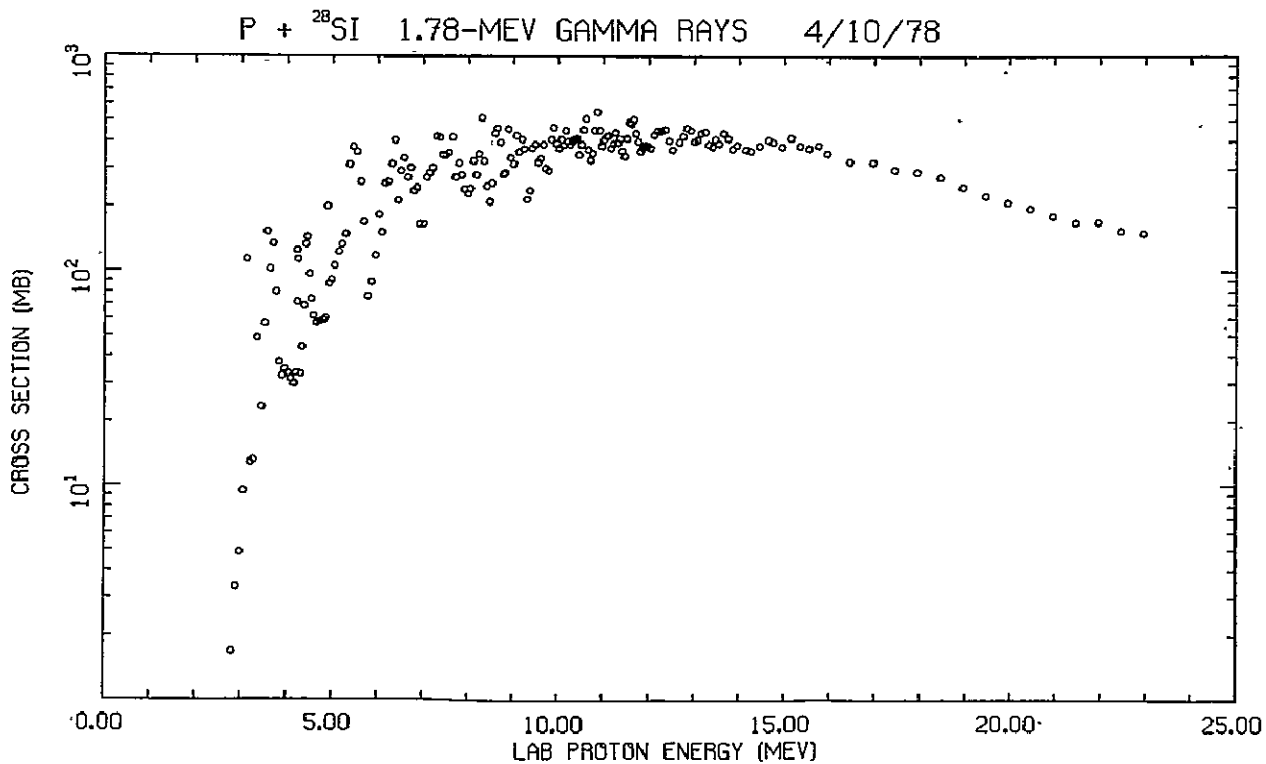P + ^{28}SI   1.78-MEV GAMMA RAYS   4/10/78

Fig. 4. Cross sections for production of 1.78-MeV gamma rays produced by protons incident on a silicon target.

Examples of the results of our measurements are given in Figs. 3 and 4. The excitation functions presented are for 4.44-MeV gamma rays produced by protons incident on a carbon target and for 1.78-MeV gamma rays produced by protons incident on a silicon target.

The present data, from some perspectives, cover only a small region in proton energies. However, it is quite possible that the bulk of the gamma rays from astronomical sources will be produced at these low energies. For example, for a proton spectrum characterized by a power law in kinetic energy, E^{-s}, the fraction of the 4.44-MeV gamma rays attributable to the measured energy interval (threshold to 23 MeV) is about 93% for s = 2 and over 99% for s = 4. In making this estimate, the cross sections up to 23 MeV are those of Fig. 3, and at higher energies are taken from Ramaty et al.[1]

In addition to cross section measurements, we have measured Doppler-broadened lineshapes for protons and alpha particles incident on ^{12}C and ^{16}O targets, at intervals of a few MeV, and at five gamma-ray angles. These data, now under analysis, may be useful for measurements of the directions of particles in astrophysical sources. Sample spectra, for p + ^{12}C, are shown in Fig. 5. The double peak at the higher bombarding energies arises from the increasing Doppler

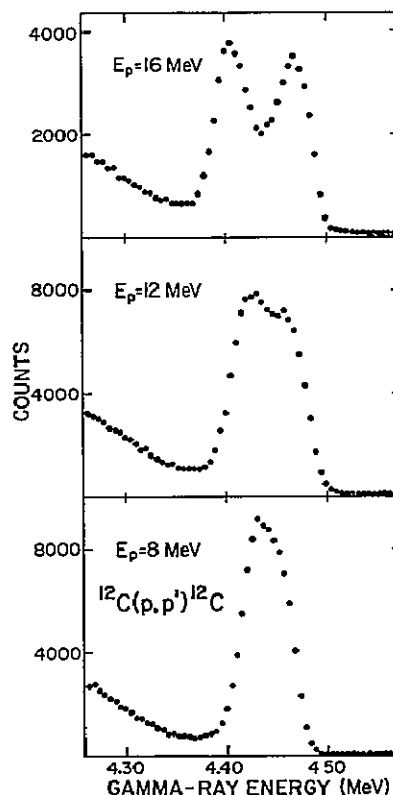

Fig. 5. Doppler-broadened lineshapes for 4.44-MeV gamma rays detected at 90° from the $^{12}C(p,p')^{12}C$ reaction.

broadening and non-uniform population of magnetic substates of the 4.44-MeV, 2^+ state, resulting from low spin-flip probabilities for the proton scattering.

In the case of 6.13-MeV gamma rays produced by protons and alpha particles incident on an oxygen target, we observed Doppler-broadened lines for a gas target and sharp lines for a solid target (silicon oxide). Since the 6.13-MeV state of ^{16}O is relatively long-lived, most ^{16}O atoms recoiling in a solid target are stopped before decaying, whereas those recoiling into a gas decay in flight. As pointed out by Lingenfelter and Ramaty, astrophysical observation of this sharp line might provide evidence for interactions in interstellar grains.

References:

1. Ramaty, R., B. Kozlovsky, and R.E. Lingenfelter, preprint (1978).

2. Ramaty, R. and C.J. Crannell, Ap. J. 203, 766 (1976).

3. Lingenfelter, R.E. and R. Ramaty, Ap. J. (Letters) 211, L19 (1977).

N78-32007

MEASUREMENTS OF 15.11-MeV γ-RAY FLUX PRODUCED IN THE REACTIONS

$^{12}C(p,p')^{12}C^{*(15.11\ MeV)}$ and $^{16}O(p,p'\alpha)^{12}C^{*(15.11\ MeV)}$
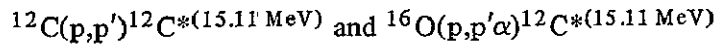
J. R. Lapides,[1,2] C. J. Crannell,[1] H. Crannell,[3]

W. F. Hornyak,[2] S. M. Seltzer,[4] J. I. Trombka,[1] N. S. Wall[2]

Institutional Affiliations:

1. Laboratory for Astronomy and Solar Physics, NASA Goddard Space Flight Center.

2. Department of Physics, University of Maryland.

3. Department of Physics, The Catholic University of America.

4. Center for Radiation Research, National Bureau of Standards.

MEASUREMENTS OF 15.11-MeV γ-RAY FLUX PRODUCED IN THE REACTIONS

$$^{12}C(p,p')^{12}C*^{(15.11\ MeV)} \text{ and } ^{16}O(p,p'\alpha)^{12}C*^{(15.11\ MeV)}$$

J. R. Lapides,[1,2] C. J. Crannell,[1] H. Crannell,[3]

W. F. Hornyak,[2] S. M. Seltzer,[4] J. I. Trombka,[1] N. S. Wall[2]

ABSTRACT

The flux of 15.11-MeV γ rays relative to the flux of 4.44-MeV γ rays, which are emitted from the corresponding states of ^{12}C, are a sensitive measure of the spectrum of exciting particles in solar flares and other cosmic sources. Emission of 15.11-MeV γ rays may result not only from the direct excitation of ^{12}C but also from the interaction $^{16}O(p,p'\alpha)^{12}C*^{(15.11\ MeV)}$. Although the cross sections for the direct reaction has been studied extensively, the cross section for the spallation interaction with ^{16}O is not reported in the literature. Preliminary measurements have demonstrated the feasibility of measuring the production of 15.11-MeV γ rays by proton interactions with ^{16}O using the University of Maryland cyclotron facility. For both carbon and oxygen targets the flux of 15.11-MeV γ rays is being measured relative to the flux of 4.44-MeV γ rays. The γ-ray emission from de-excitation of the Giant Dipole Resonances also is being measured.

Institutional Affiliations:

1. Laboratory for Astronomy and Solar Physics, NASA Goddard Space Flight Center.

2. Department of Physics, University of Maryland.

3. Department of Physics, The Catholic University of America.

4. Center for Radiation Research, National Bureau of Standards.

MEASUREMENTS OF 15.11–MeV γ–RAY FLUX PRODUCED IN THE REACTIONS

$$^{12}C(p,p')^{12}C*^{(15.11\ MeV)} \text{ and } ^{16}O(p,p'\alpha)^{12}C*^{(15.11\ MeV)}$$
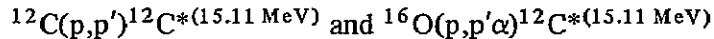
I. INTRODUCTION

Gamma-ray emissions yield information about energetic particle reactions and abundances of nuclear species in astronomical sources as well as in laboratory sources. The measurement of the ratio of the fluxes in two γ-ray lines which are well separated in energy is sensitive to the particle spectrum which excites the γ-ray emitting nuclei. The thresholds for producing the γ rays depend on the energies of the nuclear levels from which they are emitted. The ratio of the γ-ray fluxes from the two levels depends on the relative fluxes of energetic particles above the respective thresholds. The 4.44-MeV and 15.11-MeV γ rays resulting from ground state transitions in ^{12}C have been suggested as a promising astrophysical possibility for this type of study (Crannell, Ramaty, and Crannell 1977). In order to be able to extract particle spectra from γ-ray data, it is necessary that the cross sections for producing these γ rays be well known both as a function of energy and of angle. The major nuclear reactions which contribute to excitation of these states are listed in Table 1. Excitation of the 15.11-MeV state in ^{12}C by (α,α') reactions is only weakly allowed due to isospin considerations. All significant cross sections have been measured with the exception of the spallation reaction $^{16}O(p,p'\alpha)^{12}C*^{(15.11\ MeV)}$. It is the purpose of this paper to report preliminary measurements of the ratio of the fluxes of the 15.11-MeV and 4.44-MeV γ rays from the reaction $^{16}O(p,p'\alpha)^{12}C*$.

II. INSTRUMENTATION

The incident proton beam at an energy of 65-MeV was obtained with the University of Maryland cyclotron. A BeO foil was employed for the oxygen measurements and a CH_2 foil was used for a measurement of the γ-ray spectrum produced by proton scattering from carbon. The carbon measurements were performed to check the instrumentation as well as for calibration purposes. An unshielded right cylindrical 12.7 cm x 12.7 cm NaI(Tl) scintillation crystal was used as the γ-ray detector. It was placed at 90° to the incident proton beam at a distance of 50 cm from the CH_2 target and 70 cm from the BeO target. Plastic, 2.5-cm thick, was placed between the target and the detector to absorb scattered protons in the carbon measurements. In the oxygen measurements, the plastic absorber was only 1.2-cm thick so that additional background due to protons is present at about 25-MeV in the oxygen results. The total charge, Q, was measured with a Faraday cup. The instrumentation is summarized in Table 2.

Table 1

Contributing Nuclear Reactions

4.44 MeV	15.11 MeV
$^{12}C(p,p')^{12}C*$	$^{12}C(p,p')^{12}C*$
$^{12}C(p,2p)^{11}B*$	$^{16}O(p,p'\alpha)^{12}C*$
$^{16}O(p,p'\alpha)^{12}C*$	$^{12}C(\alpha,\alpha')^{12}C*$
$^{12}C(\alpha,\alpha')^{12}C*$	
$^{12}C(\alpha,\alpha'p)^{11}B*$	

Table 2

Experimental Parameters

ACCELERATOR:	UNIVERSITY OF MARYLAND CYCLOTRON
INCIDENT BEAM:	65-MeV PROTONS
DETECTOR:	RIGHT CYLINDRICAL 12.7cm x 12.7cm NaI(Tℓ)
ANGLE:	90°
TARGETS:	CARBON - CH_2, POLYETHYLENE FOIL
	0.012 $g\,cm^{-2}$ THICK
	OXYGEN - BeO FOIL
	0.082 $g\,cm^{-2}$ THICK
TOTAL CHARGE:	CARBON - 1.5 μ COLOUMB
	OXYGEN - 1 μ COLOUMB

III. RESULTS

The γ-ray spectrum from protons incident on ^{12}C is presented in Figure 1. The 4.44-MeV line, as well as its first and second escape peaks are easily seen. The 15.11-MeV line can also be seen to be quite strong. At this energy the total energy absorption peak is decreased relative to the escape peaks and the features are blended by the Doppler broadening and the actual energy resolution of the detector. The additional flux above 15.11 MeV may be due in part to the de-excitation of the Giant Dipole Resonance (Buenerd et al. 1974).

The γ-ray spectrum from protons incident on ^{16}O is shown in Figure 2. The 4.44-MeV line is again visible and the 6.13 MeV line of ^{16}O appears to be present also although it is not well resolved. Most important, an excess over the background in the 15-MeV region of the spectrum indicates the presence of the 15.11-MeV line.
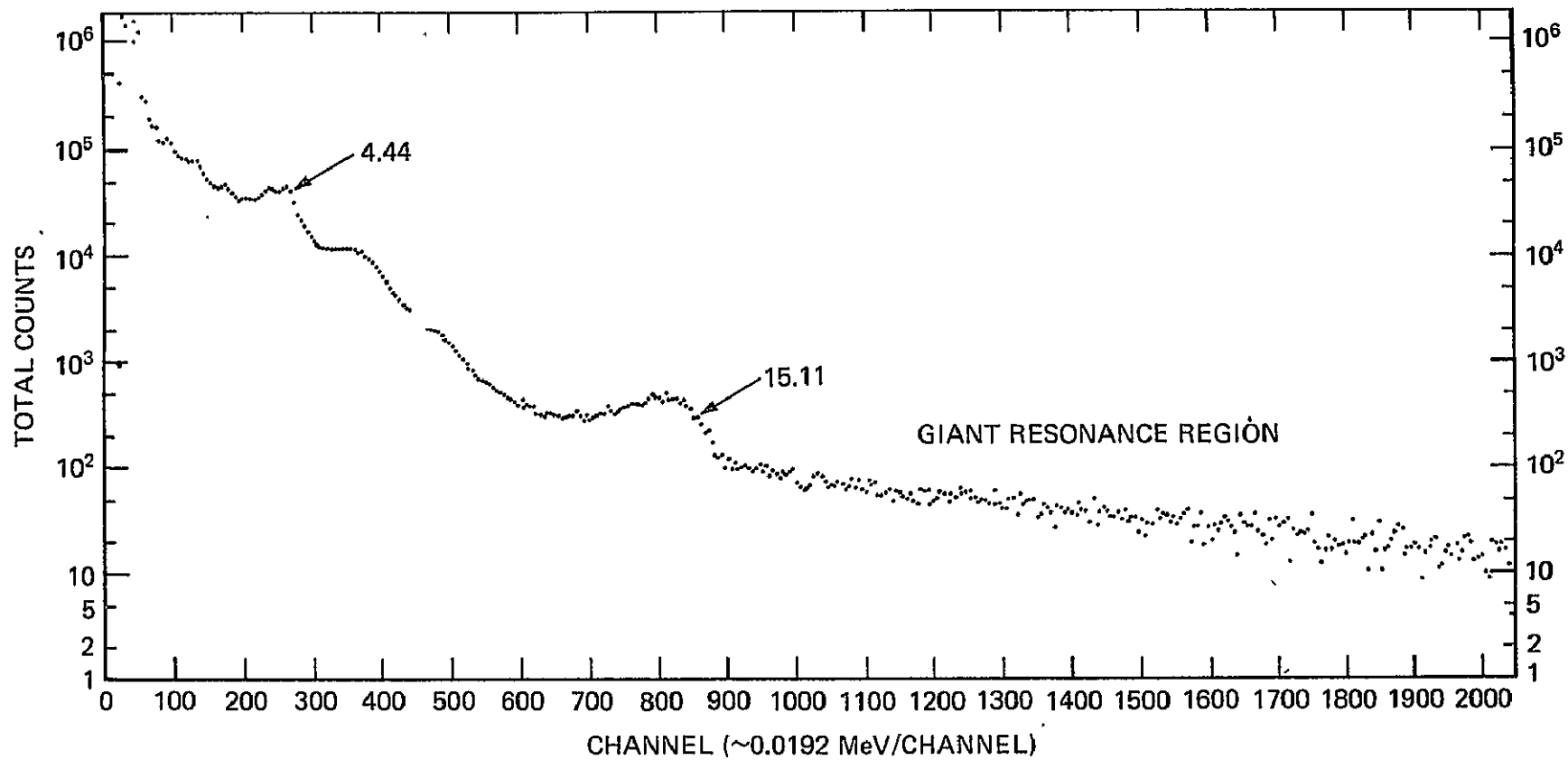
Figure 1. γ-Ray Differential Energy-Loss Spectrum at 90° 65-MeV Protons Incident on Carbon Target
12.7cm x 12.7cm Right Cylindrical NaI(Tℓ) Detector
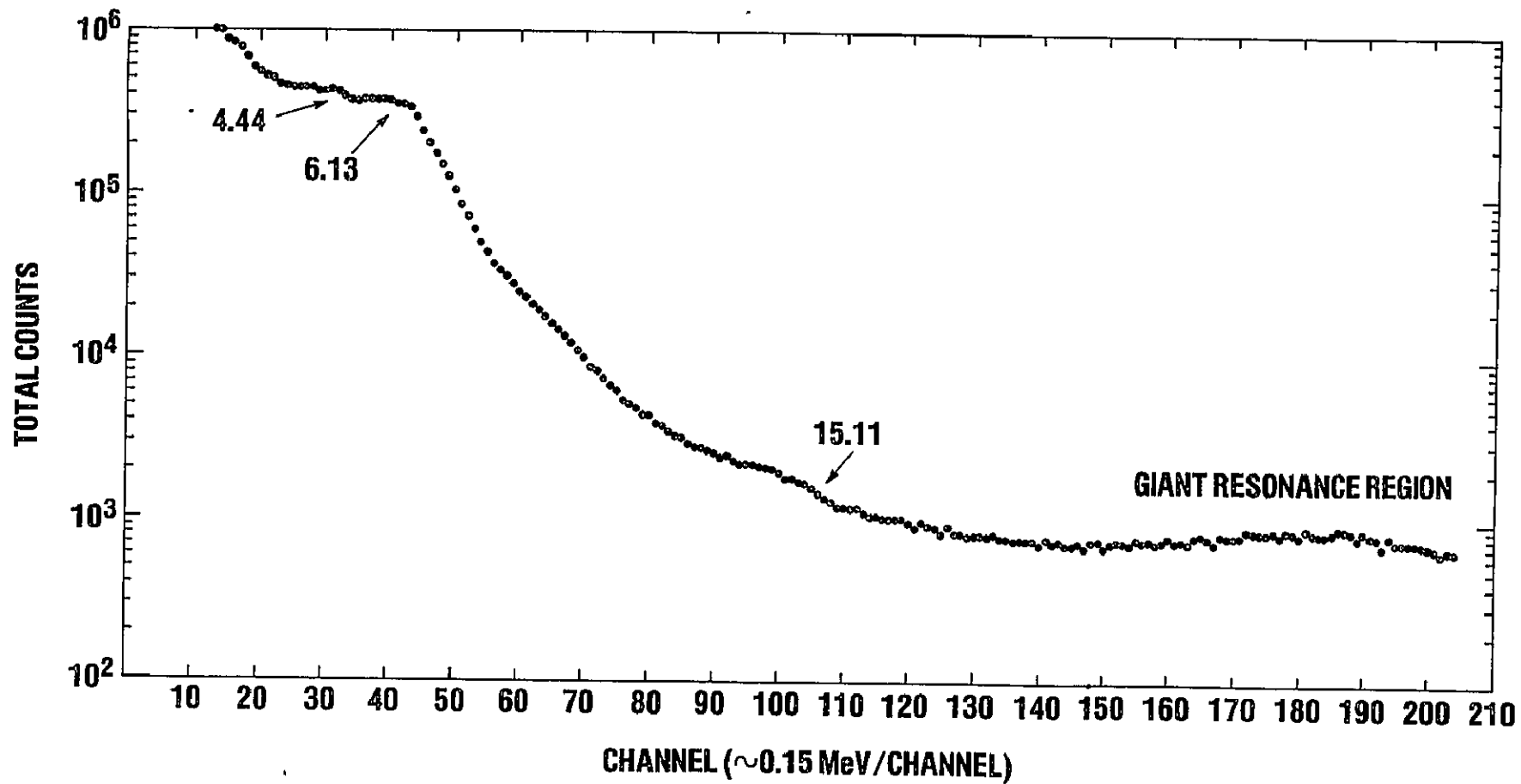Each data point represents the sum of 5 channels

Figure 2. γ-Ray Differential Energy-Loss Spectrum at 90° 65-MeV Protons Incident on Oxygen Target
12.7cm x 12.7cm Right Cylindrical NaI(Tℓ) Detector

IV. DATA ANALYSIS

Analysis of the measurements described in this paper is still in progress. We can, however, report some preliminary results on the ratio of the fluxes in the 15.11-MeV and 4.44-MeV lines. Preliminary analysis indicates that the ratios are the same, within a factor of 2 for both the reaction $^{12}C(p,p')^{12}C^*$ and the reaction $^{16}O(p,p'\alpha)^{12}C^*$ at the incident proton energy of 65-MeV and at an angle of 90°. We stress, however, that this result is for only one energy and angle and that the cross sections are expected to depend strongly on these variables. The threshold for production of each state is different, and at high proton energies the γ-ray flux is peaked forward due to the kinetic recoil of the excited nucleus.

In order to calculate the cross section for producing the 15.11-MeV line from $^{16}O(p,p'\alpha)^{12}C^*$ accurately, we must transform the energy loss spectrum shown in Figure 2 to the desired photon energy spectrum. This cannot be accomplished by a simple efficiency transformation for the case of 15.11-MeV γ rays as is usually done for widely-separated, lower-energy γ rays of a few MeV or less.

The physical considerations are illustrated in Figure 3. This figure shows the results of calculations (Berger and Seltzer 1972) of the energy-loss spectrum of a broad beam of mono-energetic γ rays incident on a cylindrical 7.6 cm x 7.6 cm NaI(Tℓ) detector. An intrinsic resolution of 7.5% for the 661-keV line was assumed. The curves obtained from these calculations will be referred to as response functions. The response function for 2-MeV γ rays shows the familiar features: a total absorption peak followed by the Compton distribution. In addition, the two escape peaks are just visible as the pair production cross section begins to be important. The next response function at 4-MeV is in the pair production dominated region. We see the total absorption peak and the two escape peaks. The continuum is due to Compton scattering. The broadening of the first escape peak and the second escape are the result of the Compton edges from the total absorption peak and the first escape peak respectively. At higher energies, the escape peak structure becomes blended by the increase in the actual peak width. In addition, electrons scattered in the crystal have enough energy to occasionally leak out the edge of the crystal. This has the effect of broadening the peak as well as shifting the maximum to lower energies. At the highest energy shown, no escape peaks are visible and the shift of the maximum is more evident. This effect is evident in our data on the 15.11-MeV line. Based on our calibration, the maximum is at an energy of 14.8 MeV. Figure 4 shows a response function and experimental data (Kockum and Starfelt 1959) for 20.3-MeV γ rays produced in the reaction $^3He(p,\gamma)$. It is seen that the calculation agrees quite well except at lower energies for which background problems become acute.
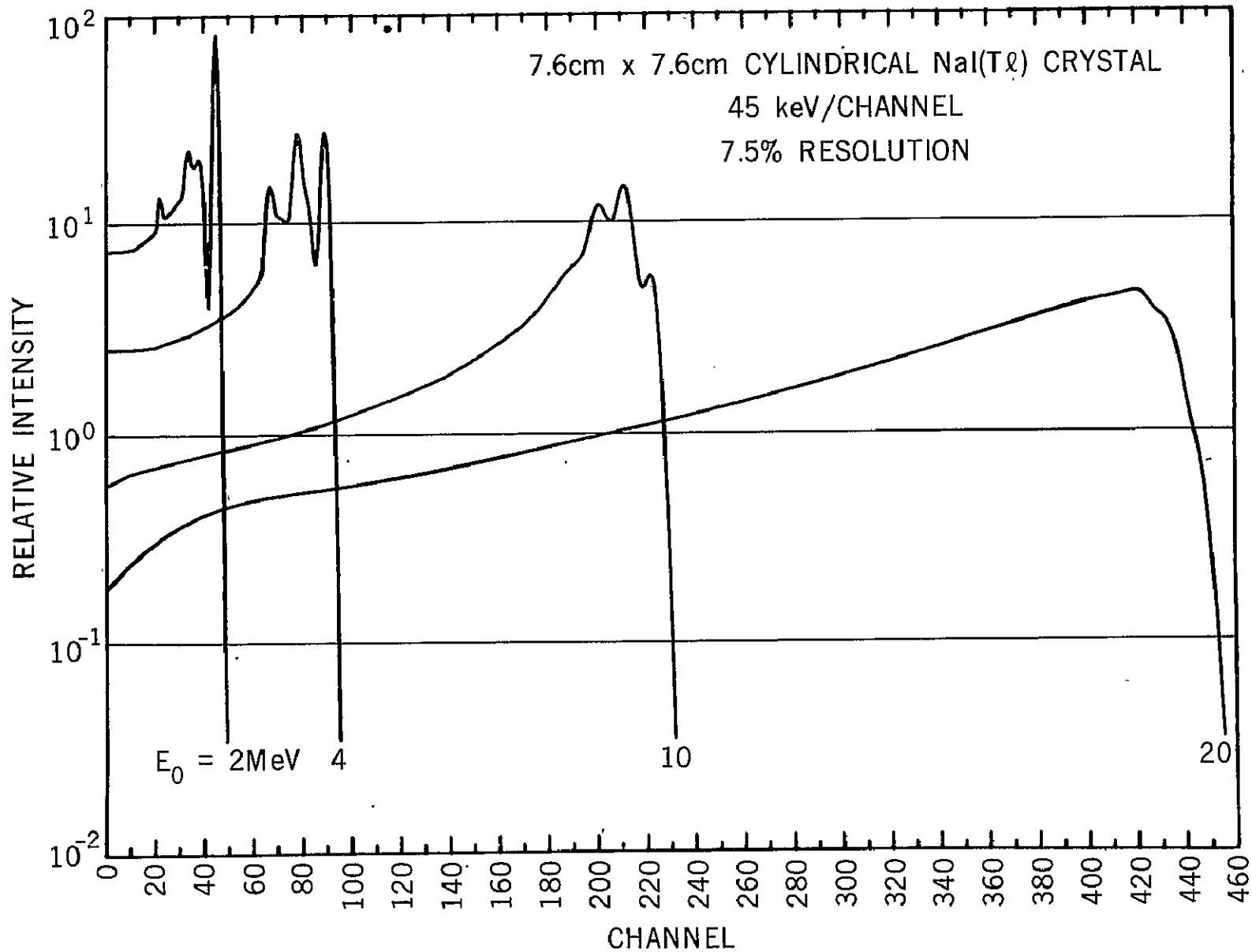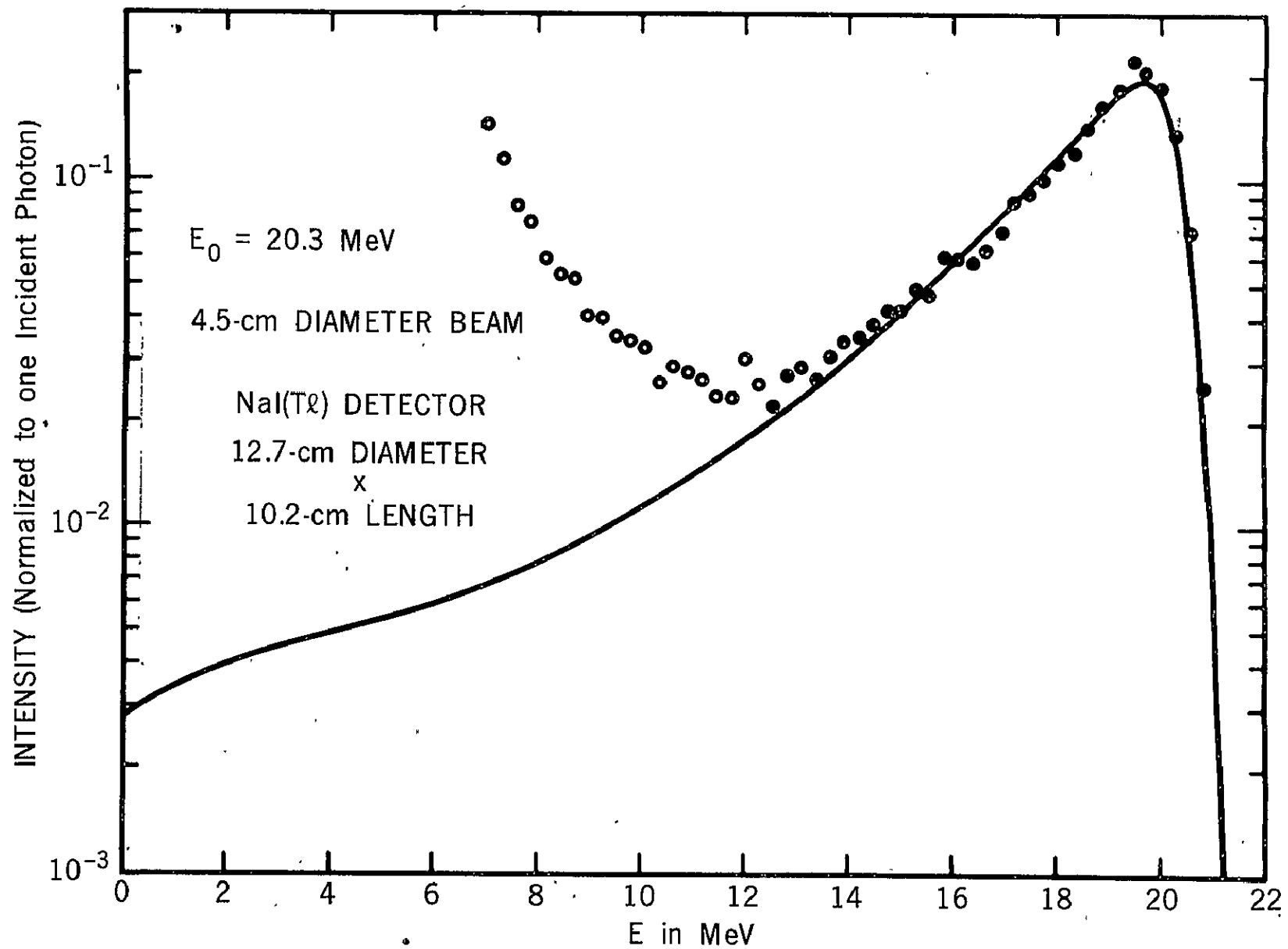
Figure 3. Broad Parallel Beam Response Functions

The figure contains the following labels:

Y-axis: RELATIVE INTENSITY, with values 10^2, 10^1, 10^0, 10^{-1}, 10^{-2}

X-axis: CHANNEL, with values 0, 20, 40, 60, 80, 100, 120, 140, 160, 180, 200, 220, 240, 260, 280, 300, 320, 340, 360, 380, 400, 420, 440, 460

Text in plot: 7.6cm x 7.6cm CYLINDRICAL NaI(Tℓ) CRYSTAL
45 keV/CHANNEL
7.5% RESOLUTION

E_0 = 2MeV   4   10   20

Figure 4. Response Function and Experimental Data for 20.3-MeV γ Rays

The figure shows a plot with the following labels:

- Y-axis: INTENSITY (Normalized to one Incident Photon), ranging from 10^{-3} to above 10^{-1}
- X-axis: E in MeV, ranging from 0 to 22

Text within the plot:

$E_0 = 20.3$ MeV

4.5-cm DIAMETER BEAM

NaI(Tℓ) DETECTOR
12.7-cm DIAMETER
x
10.2-cm LENGTH

It should be noted that the higher energy response functions are quite asymmetrical because the asymmetrical Compton distributions are blended with the absorption peaks. The asymmetry is enhanced by energy dependent background under the 15.11-MeV line in the carbon data. The response functions may be utilized in line-broadening studies. Once the background has been removed, additional width in the peaks beyond that calculated, can be attributed to physical processes such as Doppler broadening which are not associated with the detector.

Numerical least square iterative techniques have been developed (Adler and Trombka 1970) which utilize the response functions to properly transform the data in energy loss space to photon energy space. These methods have been employed successfully in the analysis of the Apollo 15 and 16 γ-ray spectra obtained to study lunar surface composition. Elemental abundances derived from this analysis agree well with lunar samples returned to earth, illustrating that the use of the response functions is a reliable technique. These techniques are presently being used to analyze the ^{12}C and ^{16}O data and to obtain a good understanding of the response functions for our detector.

V. CONCLUSION

The ratio of the fluxes in the 15.11-MeV and 4.44-MeV γ-ray lines has been found to be the same within a factor of 2 for both the reaction ^{12}C(p,p')^{12}C* and the reaction ^{16}O(p,p'α)^{12}C* for an incident proton energy of 65-MeV and at an angle of 90°. We have demonstrated the feasibility of measuring the ^{16}O(p,p'α)^{12}C*$^{(15.11\ MeV)}$ cross section with the instrumentation discussed in Section II. We will, however, utilize additional detector shielding to minimize the background flux for the rest of our measurements. In addition, we will employ the numerical methods (Adler and Trombka, 1970) mentioned in Section IV to transform accurately the energy-loss spectra to photon energy spectra.

REFERENCES

Adler, I., and Trombka, J. I., 1970, "Geochemical Exploration of the Moon and Planets," Physics and Chemistry in Space, 3 (Berlin, Heidelberg and New York: Springer Verlag).

Berger, M. S., and Seltzer, S. M., 1972, Nucl. Instr. and Methods, 104, 317.

Buenerd, M., de Saintignon, P., Martin, P., and Loiseau, J. M., 1974, Phys. Rev. Letters, 33, 1233.

Crannell, C. J., Ramaty, R., and Crannell, H., 1977, Proc. of the 12th ESLAB Symposium, Frascati, 213.

Kockum, J., and Starfelt, N., 1959, Nucl. Instr. and Methods, 4, 171.

D37-14   N78-32008

Gamma Ray Facilities at the University of Maryland Cyclotron

W. F. Hornyak[*]

The purpose of this communication is to describe the on line or in situ gamm-ray facilities available at the University of Maryland cyclotron. A special beam line has been set up in a separate shielded experimental room to provide a low background station for gamma-ray measurements. All active beam defining slits and stops are located externally to this shielded area. The transmitted beam leaving the target is gathered in by a magnetic quadrupole lens located 1.8m further downstream and focused on a Faraday cup located on the far side of the 2.5m-thick concrete shielding wall of the experimental room. In general target thicknesses up to $10mg/cm^2$ may be used with most beams giving negligible interception by the 10 cm-diameter beam tube of the downstream target scattered beam. A beam spot size on targets of order 2 x 2 mm is readily achieved.

A software computer program has been developed that permits timing information to be obtained using the cyclotron beam fine structure as a time reference for the observed gamma-ray events. Measurements indicate a beam fine structure width (for the generally obtainable single turn extraction) of less than 1.2 nanoseconds repeated, for example, in the case of 140MeV alpha-particles every 90 nanoseconds. Twelve contignous time channels of adjustable width may be set as desired with reference to the RF signal. In effect this allows the creation of 12 separate 8192 channel analyzers. A number of these time windows are generally set covering the undelayed or prompt gamma-ray events that occur within a peak having a time width of 4 nanoseconds (FWHM). Some windows may be set fairly broad and delayed to obtain information on events such as those due to radioactivity, decay of long-lived meta-stable states and neutron induced secondary reactions. Fig.1

* Department of Physics and Astronomy, University of Maryland.

shows a typical on-line time spectrum obtained with a 10% Ge(Li) coaxial detector for an ^{27}Al target and 140 MeV alpha-particles. Fig. 2 shows the high energy prompt spectrum. The weak 6246-keV line in ^{24}Mg shows that cross sections as low as 350 microbarns may be observed under these reduced background conditions. Fig. 3 shows a portion of the low energy spectrum; some lines Doppler broadened. Note the absence of the usual neutron-induced secondary lines from Ge ordinarily appearing as strongly asymmetric broad peaks at E =596 keV from ^{74}Ge(n,n') and E =693 keV from ^{72}Ge(n,n').

All of the time gated data may be accumulated and stored on tape, with the IBM 360/44 on-line computer. Data striping for peak locations, widths, areas and their errors may be obtained by use of a light-pen interactive program PEAK 2. The user may intercede in various ways between the usual automatic find program routine and the fit program routine. Lines found in the find-routine may be vetoed or added to prior to the fitting sequence. Backgrounds may be totally, partially or automatically defined. As many as seven overlapping lines may be treated simultaneously with either locked-in or to-be-fitted parameters on either peak location, width, height, or any combination of these.

CHARACTERISTICS OF BEAMS AVAILABLE FROM THE UNIVERSITY OF MARYLAND CYCLOTRON

ENERGIES

Protons	10 to 100 MeV
Deuterons	10 to 82 MeV
He^3-ions	20 to 200 MeV
Alpha-Particles	20 to 165 MeV

INTENSITY

Extracted Beams: to 3 µA
Beams on Target: 10 particles/sec to 2 µ A
Extraction Efficiencies: up to 95% for 100 MeV protons
60 to 80% for other energies and particles

DUTY CYCLE

Macroscopic	100%
Microscopic	$\sim$ 1 ns every RF period

ENERGY RESOLUTION

From Cyclotron = 0.1%
After High Resolution Beam Transport System = 0.01%/mm slit width

PHASE SPACE OF BEAM FROM CYCLOTRON = 20 x 30 mm^2 - mr^2
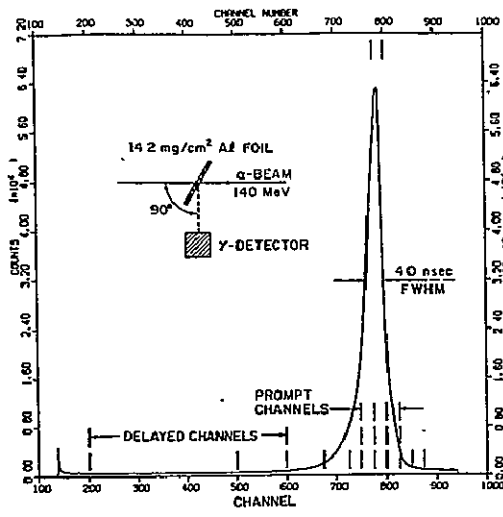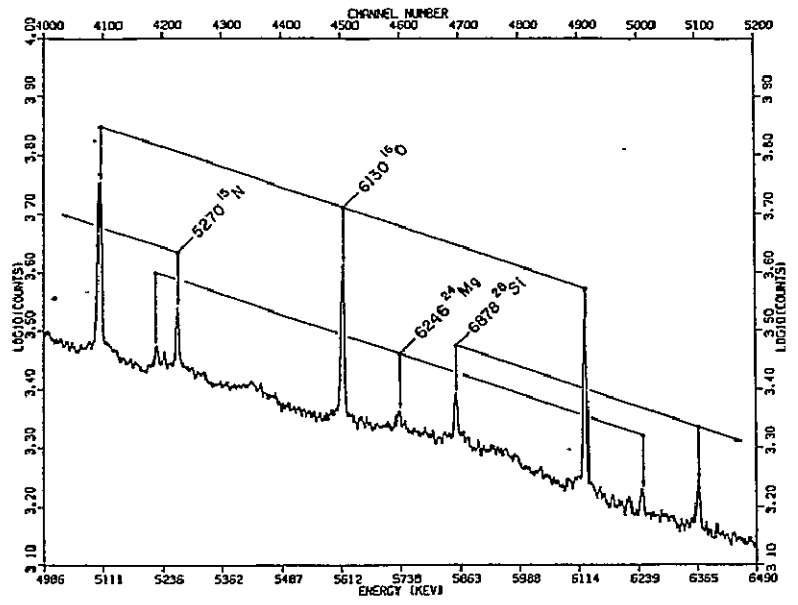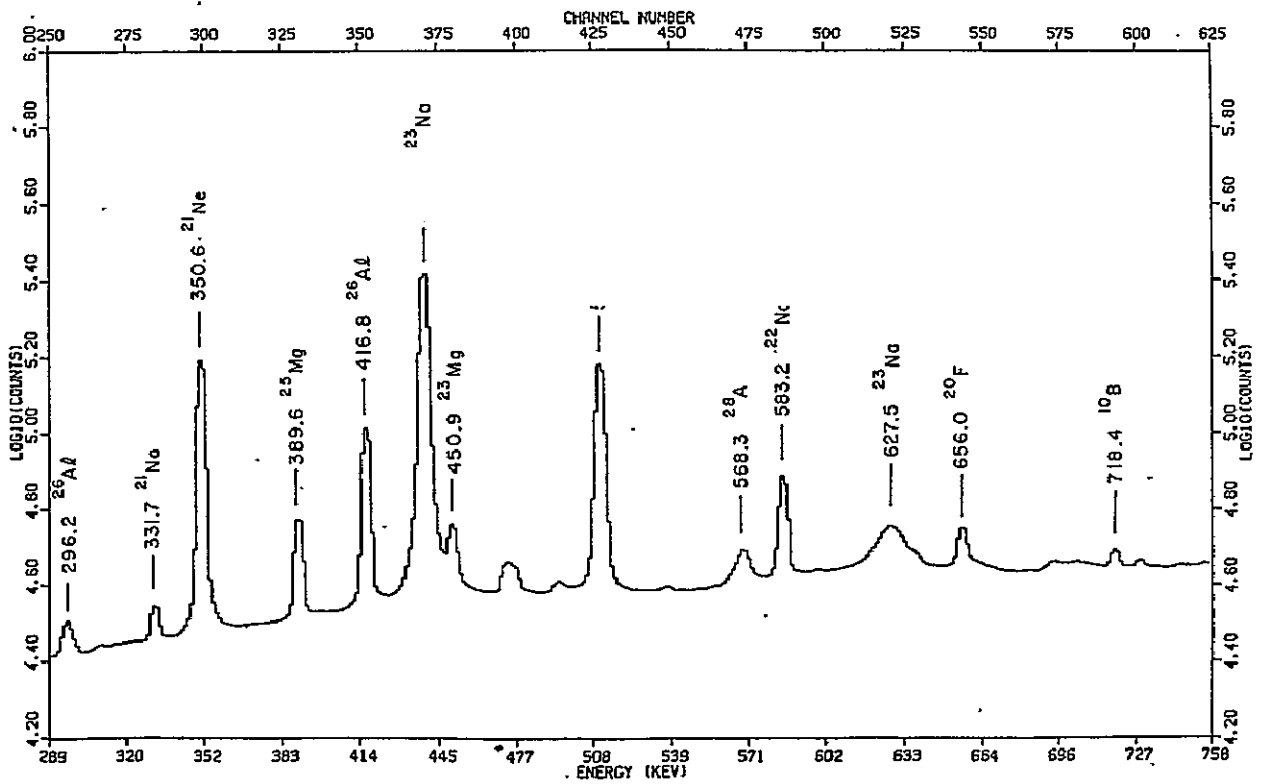
FIG. 1

FIG. 2

FIG. 3

VI. FUTURE SPACECRAFT EXPERIMENTS

THE ISEE-C GAMMA-RAY BURST SPECTROMETER

B. J. Teegarden, G. Porreca, D. Stilwell, U. D. Desai and T. L. Cline
NASA/Goddard Space Flight Center
Laboratory for High Energy Astrophysics
Greenbelt, Maryland 20771

and

D. Hovestadt
Max Planck Institut fur Physik und Astrophysik
Garching b. Munchen, W. Germany

ABSTRACT

This paper describes the technical properties, operation and expected sensitivity of an experiment, to be launched on the ISEE-C spacecraft, that is intended to search for narrow lines in the spectra of gamma-ray bursts. At the heart of the experiment is a radiatively cooled Germanium solid state photon detector. The instrumentation is capable of storing the entire spectrum of all but the largest bursts in the energy range 0.05-6.5 MeV. In addition it analyzes the signals from two CsI detectors in two other experiments on the spacecraft and records event time histories from these to a few millisecond accuracy. A background mode permits spectral analysis during quiet times and will allow the determination of physically interesting upper limits for narrow lines in the diffuse gamma-ray background radiation.

1. Introduction

At the present time gamma-ray lines. are known to exist in two different types of transient events. The first of these, solar flares, have exhibited a family of lines from the 0.511 MeV positron annihilation line to the 6.4 MeV ^{16}O line. (Chupp et al., 1973) The study of these lines has provided valuable new insight into the physical conditions and processes at the flare site. The second type of transient is the mysterious 20 minute duration event observed by the JPL group (Jacobson 1978) in the general direction of the high energy gamma-ray source γ 195+5. This paper will describe a detector system intended to search for narrow gamma-ray lines in a third type of transient event, the gamma-ray burst. The origin of these bursts remains a mystery and the discovery and identification of gamma-ray lines would provide a valuable new clue to. the nature of the physical processes responsible for the burst.

Most of the instrumentation employed thus far in gamma-ray burst studies has had either a very limited spectral capability or none at all. The ISEE-C instrument uses a radiatively-cooled high purity Germanium detector to make precise measurements of the photon energy. It represents a major step forward in the capability for line detection in transient events.

2. Instrument Description

A. The ISEE-C Mission

The ISEE (International Sun-Earth Explorer) Mission is a three-spacecraft series intended to study the spatial and temporal variations of the earth's magnetosphere as influenced by the sun and associated interplanetary conditions. The third spacecraft ISEE-C, to be launched in August 1978, will be in a halo orbit about the Lagrangian point along the earth-sun line 230 earth radii inward towards the sun. It will be spin-stabilized with its axis normal to the ecliptic plane. The spacecraft location and attitude make it an ideal platform for

our experiment from both an engineering and scientific point of view. From

the point of view of thermal performance, the location is far from the earth so

that earth-albedo is not a problem and the spin axis orientation allows for

the optimum orientation of the cooler field-of-view. From a scientific point

of view the location outside the earth's magnetosphere means that the serious effect

of trapped radiation on the instrumental background is avoided.

Our ISEE-C instrument is an augmentation of gamma ray burst instrumentation

developed by us for the ISEE-A mission. This instrumentation is part of the

Hovestadt low-energy charged particle experiment. Figure 1 shows the ISEE-C

spacecraft and the location of the cooler/sensor. Its recessed location

within the lower body of the spacecraft prevents any direct sunlight from

striking the cooler and is generally a favorable situation with regard to its

thermal performance.

B. The Radiatively-Cooled Detector

A cross-sectional view of the Germanium detector mounted in its cooler

is presented in Figure 2. Its basic structure is divided into two parts, an

outer stage and an inner stage. The outer stage is designed to operate at an

intermediate temperature ($\sim 160°K$) and thereby provide a thermal buffer between

the sensor (residing in the inner stage) and the spacecraft. The outer stage

has a basic conical shape to define a field of view (126° full angle) for the

inner stage. This field of view must not contain the sun, earth, or any

significant portion of the spacecraft. The mechanical interface between the

outer stage and the spacecraft is via a support ring, which is in good thermal con-

tact with the spacecraft and will be maintained near room temperature. As the outer

stage radiatively cools (via its radiating surface shown in Figure 1) it will

contract slightly. The support points are designed such that this contrac-

tion causes a break in the thermal path between the support ring and

the outer stage, thereby thermally isolating it from the spacecraft. The inner conical surface of the outer stage is highly polished specular aluminum so that no sunlight can be scattered into the inner stage.

The Germanium crystal is housed in the inner stage of the cooler in a hermetically sealed Magnesium enclosure. The exposed surface is coated with a highly emissive white paint to allow efficient radiation of heat. The inner stage is mechanically supported in a similar fashion to the outer stage so that a second level of thermal isolation is attained. The predicted equilibrium operating temperature of the inner stage is $100°K$ ($-173°C$).

The Germanium crystal itself is 4cm diam. x 3cm depth ($35cm^3$ active volume) and will have an energy resolution of 3-3.5 keV at 1 MeV. It is made from high purity Germanium. The use of this material permits the crystal to be stored indefinitely at room temperature without sustaining any loss in performance. The weight of the cooler/sensor/electronics package is 2.57 · kg. Figure 3 is a photograph of the cooler/sensor.

C. Additional CsI Detectors

In addition to the Germanium detector there are two other detectors on board the spacecraft whose signals we analyze to give us increased sensitivity to gamma-ray bursts. These are CsI crystals located respectively in the Hovestadt and Meyer experiments on the ISEE-C spacecraft. The Hovestadt detector is a small cylindrical CsI crystal from which only time history (count rate) information is obtained. Both count rate and spectral analysis are performed on the Meyer crystal which is much larger and has the shape of a truncated cone. This crystal is also significantly larger than the Germanium crystal, and although it has much poorer resolution, it will provide a more accurate record of the time history of the event.

D. Electronics

A simplified block diagram of the electronics is shown in Figure 4. The Germanium detector signals are amplified and shaped in a charge-sensitive pre-amp and following post-amp. The signals are digitized by a 4096 channel ADC which is identical to one developed for the Caltech-Goddard cosmic ray experiment on the Voyager mission. It covers the energy range .05 to 6.5 MeV. Analysis is initiated when the signal exceeds a ground-programmable threshold which can be set in any of eight different positions between 56 and 440 keV. This same threshold circuit generates those signals that are used for time history analysis.

The CsI crystal located in the Meyer experiment is viewed by a small PMT whose signals are amplified and shaped and then digitized in a 512 channel ADC. A count rate signal and the 512 channel pulse train are both analyzed by our electronics. The smaller Hovestadt CsI crystal provides only a count rate, but is located on the opposite side of the spacecraft from Meyer so that a more complete coverage of the burst time history during the spacecraft rotation cycle can be obtained.

The digital portion of the electronics is physically housed in the Hovestadt experiment. The detection of a burst is accomplished by two independent trigger circuits. These circuits continuously sample the count rate and register a trigger if and when the rate exceeds a value selected by ground command. Any one of three sensors can be connected by ground command to each of the trigger circuits. More precisely, these circuits measure the time interval between the occurrence of N counts, where N is also selectable by ground command and can have any binary value between 1 and 128. Time is measured by counting a clock frequency whose value can also be selected from the ground.

Upon the occurrence of a trigger the burst data is then stored in a 10^5 bit memory. This memory is partitioned into three sections, two of which are devoted to recording the time history of the event. The same technique used to define a burst, i.e. storage of a time interval rather than a count rate, is used to record the event in the memory. Each partition contains 2048 12-bit words so that 2048 xN counts can be stored. It is very unlikely that any burst can exceed the storage capacity of the memory. The third memory partition is devoted to the storage of spectral information. Either the Germanium or the Meyer CsI crystal can be input by ground command into this part of the memory. This section of the memory is organized into 3072 16-bit words. Each word contains 12-bits of pulse height and a 4-bit time vernier tag. Again, the time resolution is selectable by command and will most likely be $\sim$ 30 msec.

After the memory is filled it is slowly read out into the spacecraft telemetry stream. There are two read-out modes 1) automatic, where read-out begins as soon as the memory is filled and 2) manual, where read-out is initiated by ground command.

During quiet times the instrument functions in what is called the Background Mode. In this mode a small fraction of the detected photons are analyzed and stored in a small (36 event) buffer memory. They are then read out in the spacecraft telemetry stream in the same manner as spectral data from a gamma-ray burst. This mode is intended to provide information on the detector calibration and background level. In addition it can potentially allow the determination of meaningful upper limits for narrow lines in the diffuse gamma-ray background.

3. Instrument Sensitivity

Since the gamma-ray burst is a relatively short-lived phenomenon the instrument narrow-line detection threshold will in general be statistics rather than background limited. The electronics is configured such that it can store a fixed maximum number of events. It is most useful to discuss the sensitivity in terms of the

fraction of the total photons in the burst that must appear in the line in order for the line to be detectable. Since over most of its range the background under a narrow line is negligible it is simply a question of how many counts in a narrow window are necessary to define a line. If we rather arbitrarily set this threshold at 5 counts this requires that, for a narrow line at 0.5 MeV, 1-2% of the total photons in the burst must appear in this line. For a typical burst duration of 30 seconds the incident line flux is $5.3 \times 10^{-2} \text{cm}^{-2} \text{sec}^{-1}$.

The detector also has the capability of placing meaningful upper limits on the narrow line flux of photons in the diffuse background spectrum. Because of the extremely low bit rate allocated for gamma-ray burst studies ($\sim$ 1.5 bits/ sec), the instrument can analyze only a small fraction of the total number of photons detected. However, the long anticipated life-time ($\geqslant$ 2 yr.) of the ISEE-C mission will compensate for this. Assuming a 2 year accumulation time the 3σ upper limit for narrow line detection in the background mode is plotted in Figure 5 as a function of energy. The range of values is $\sim 2.5 \times 10^{-4} \text{cm}^{-2} \text{sec}^{-1}$ ster^{-1}. These threshold values are low enough to afford the possibility of determining physically interesting upper limits for narrow lines in the diffuse background.

Acknowledgements

REFERENCES

Chupp, E. L., Forrest, D. J., Higbie, P. R., Suri, A. N., Tsai, C., and

Dumphy, P. P. 1973, Nature, 241, 333.

Jacobson, A. S., et al. this Volume, p. 228.

FIGURE CAPTIONS

1. ISEE-C spacecraft. Mounting location of radiative cooler is shown as well as exploded view of cooler.

2. Cross-sectional view of Radiative Cooler and Germanium Detector.

3. Photograph of Radioactive Cooler

4. Simplified Block diagram of electronics.

5. Sensitivity for narrow line detection in the Diffuse Background Radiation. 3σ threshold isotropic intensity is plotted as a function of incident energy.

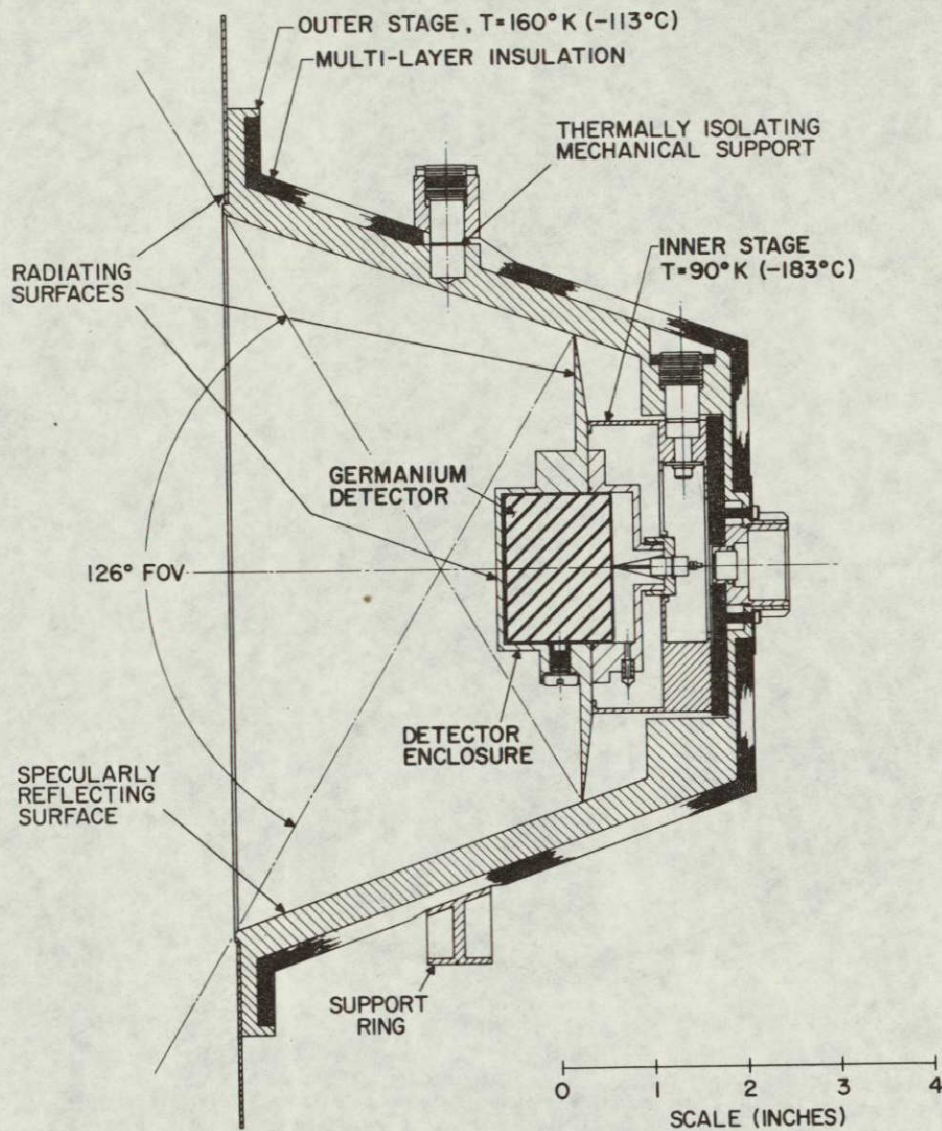# ISEE-C RADIATIVELY COOLED
GERMANIUM GAMMA-RAY BURST DETECTOR

ANALOG
ELECTRONICS

+Z

−Z

RADIATIVE
COOLER

GERMANIUM
DETECTOR

Figure 1

OUTER STAGE, T=160°K (-113°C)
MULTI-LAYER INSULATION
THERMALLY ISOLATING
MECHANICAL SUPPORT
INNER STAGE
T=90°K (-183°C)
RADIATING
SURFACES
GERMANIUM
DETECTOR
126° FOV
SPECULARLY
REFLECTING
SURFACE
DETECTOR
ENCLOSURE
SUPPORT
RING

SCALE (INCHES)
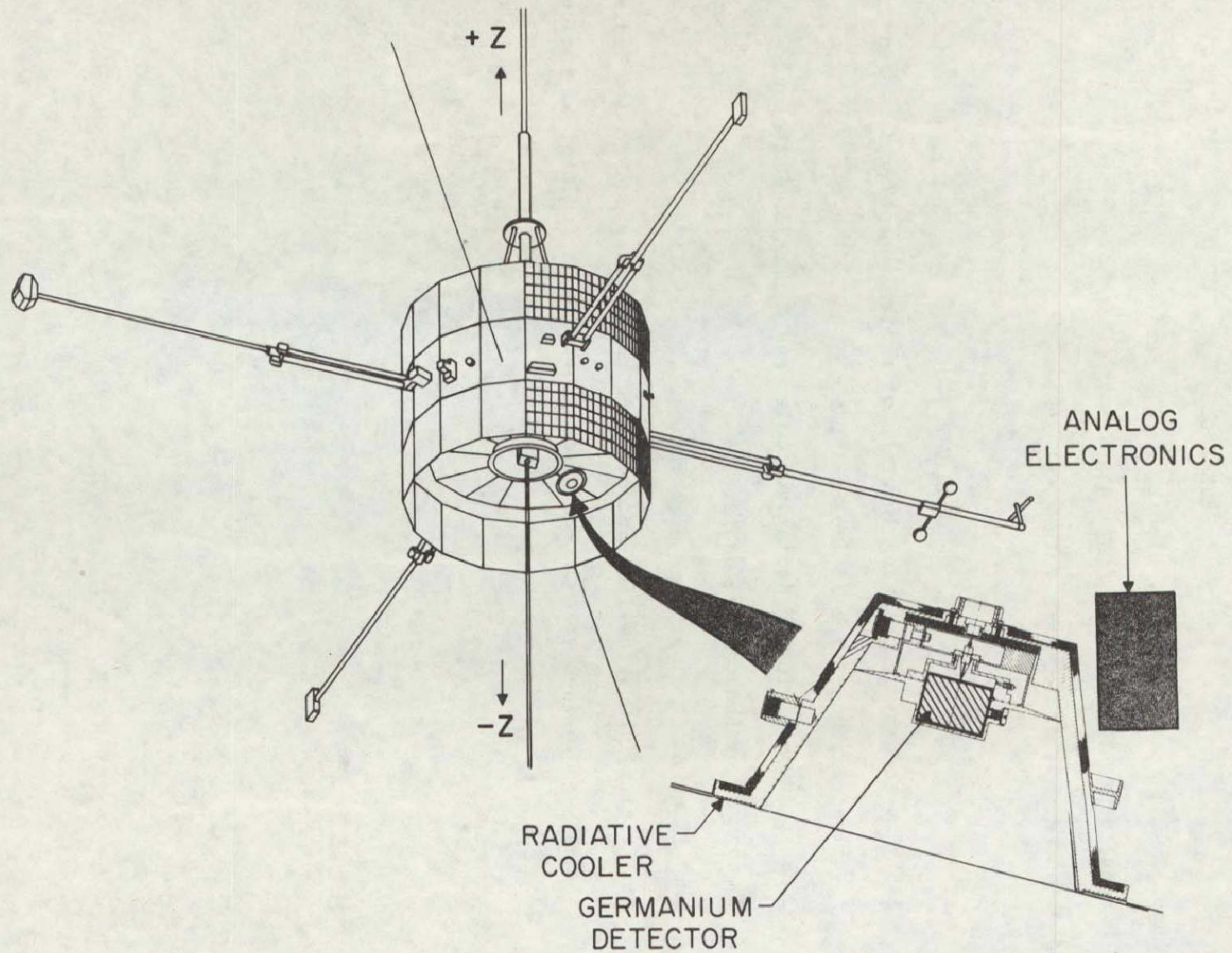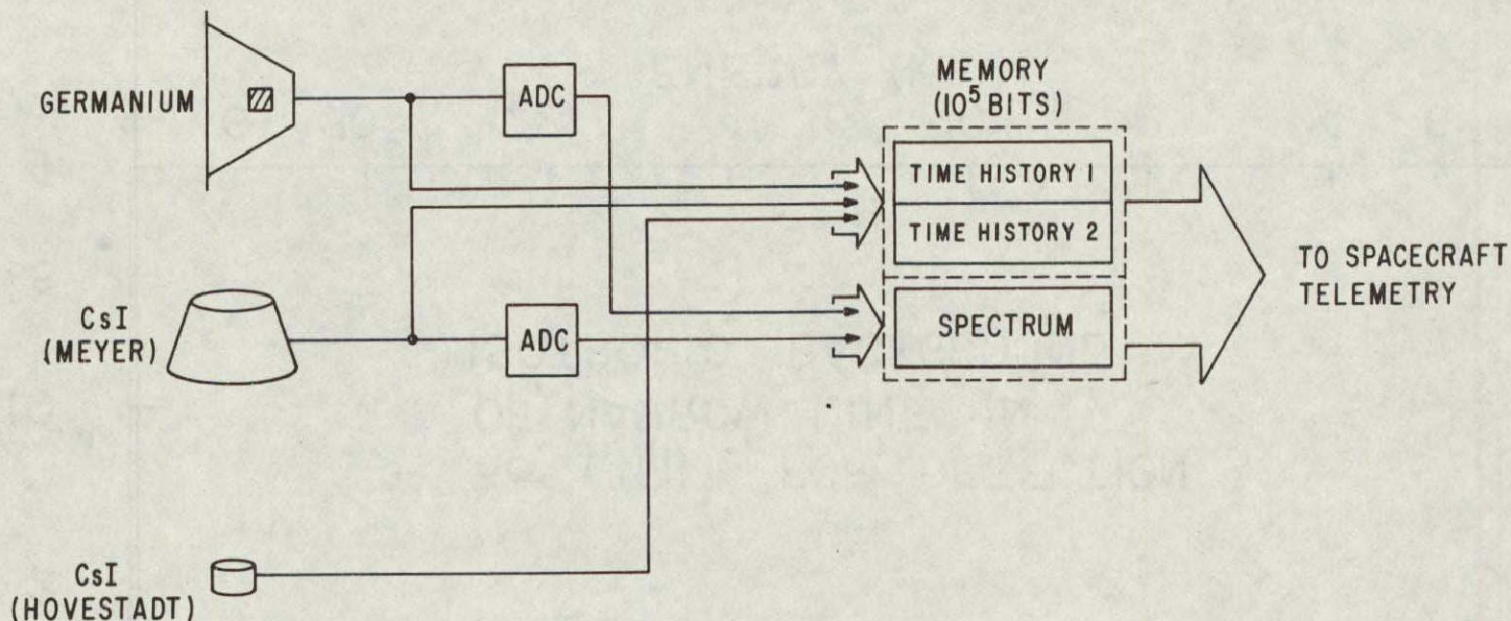
ATD—RADIATIVELY COOLED
GERMANIUM DETECTOR FOR
ISEE—C

Figure 2

526
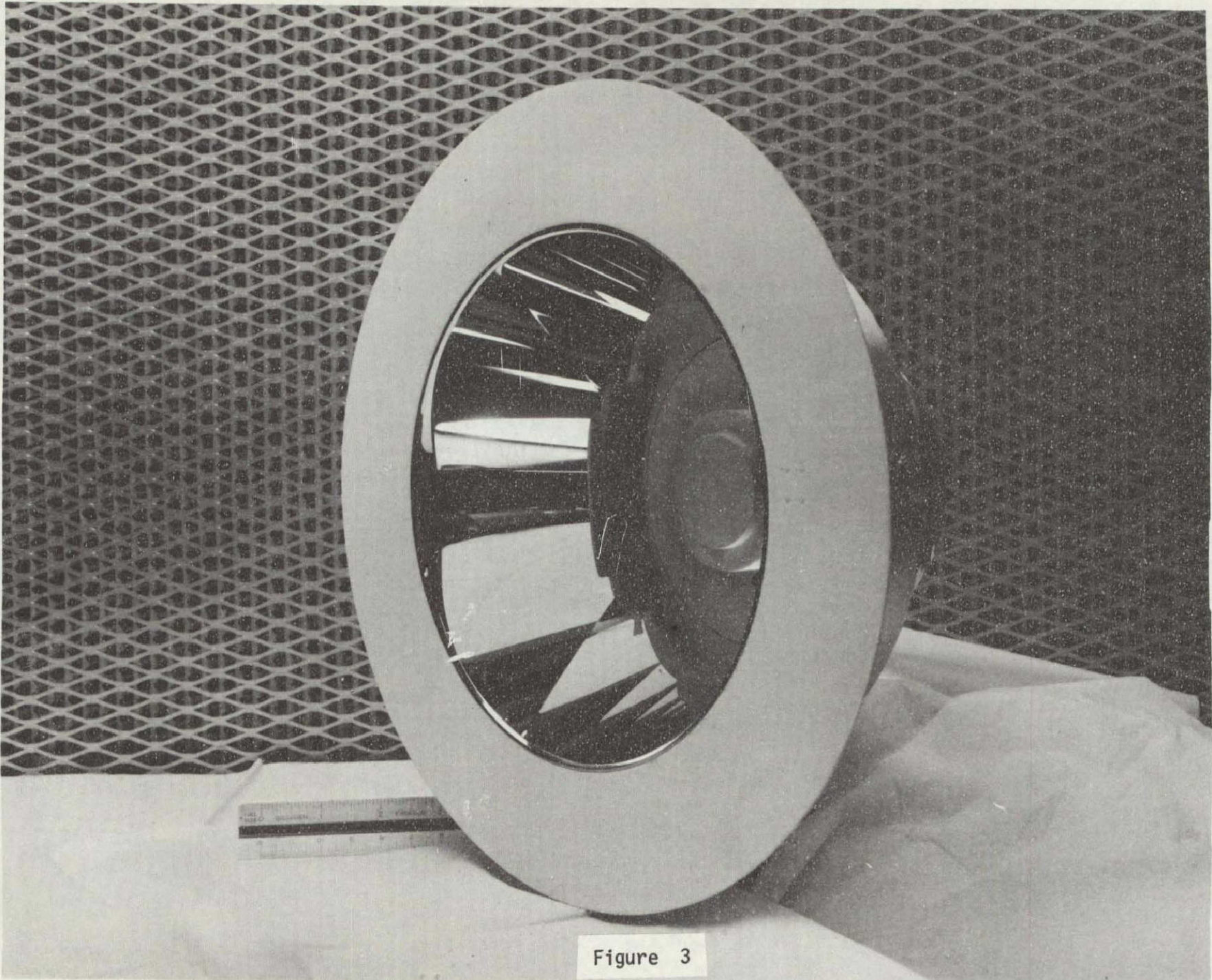
Figure 3

SIMPLIFIED BLOCK DIAGRAM OF
ISEE-C GAMMA RAY BURST INSTRUMENTATION

TIME HISTORY

    TIME HISTORIES ARE STORED VALUES OF ELAPSED TIME FOR
THE OCCURRENCE OF A FIXED NUMBER N COUNTS.
MEMORY CAPACITY IS 2048 x N DETECTOR COUNTS.
ANY OF THE THREE SENSORS CAN BE CONNECTED BY GROUND
COMMAND TO EITHER OF THE TWO TIME HISTORY MEMORIES.

SPECTRUM

    INDIVIDUAL 12 BIT PULSE HEIGHTS + TIME TAGS ARE STORED IN
SPECTRUM MEMORY. MEMORY CAPACITY IS 3000 EVENTS.
EITHER THE GERMANIUM OR THE MEYER CsI CAN BE CONNECTED
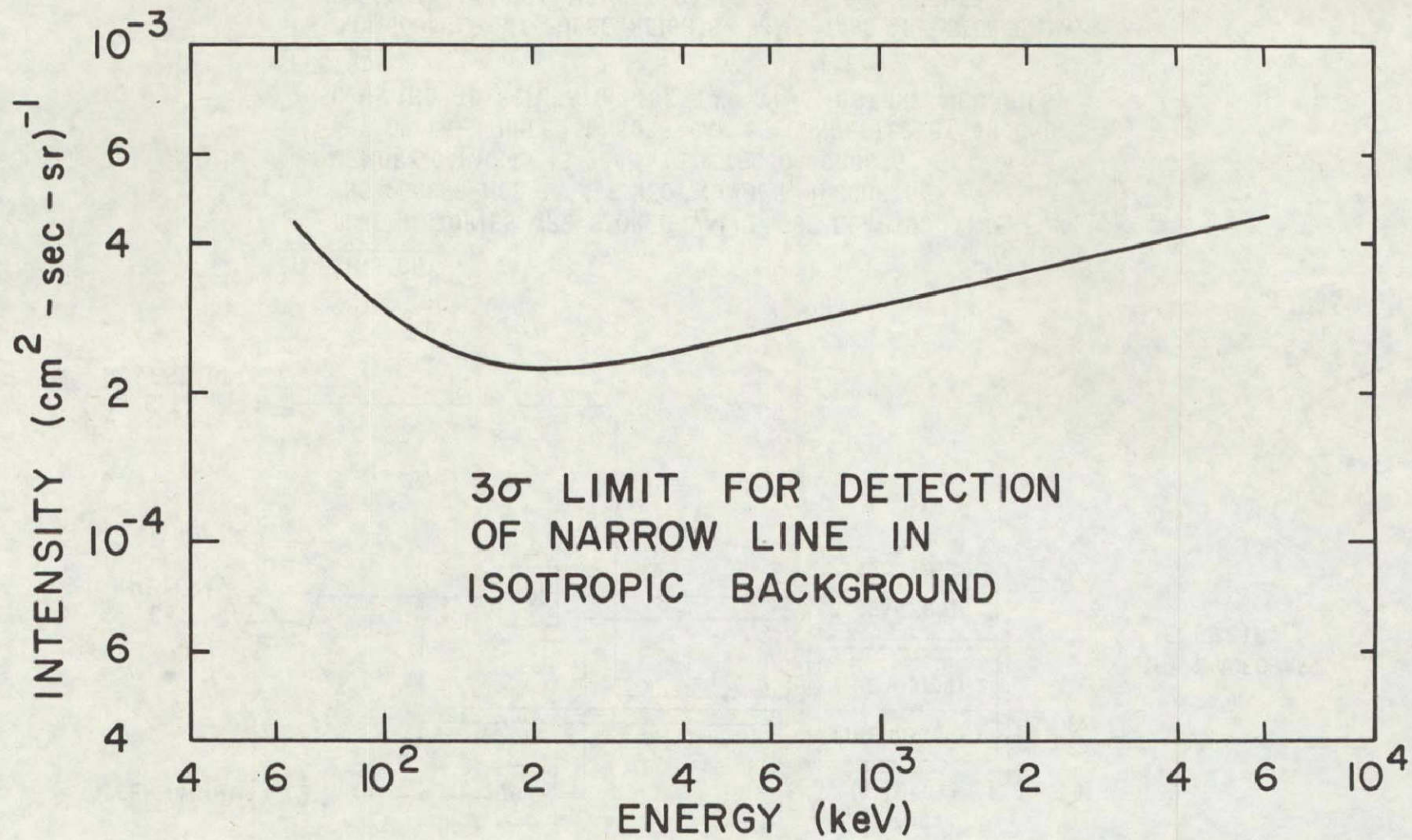BY GROUND COMMAND TO THE SPECTRUM.

Figure 4

Figure 5

D39-93

HIGH RESOLUTION SPECTROSCOPY
FROM LOW ALTITUDE SATELLITES

G. H. Nakano and W. L. Imhof
Lockheed Palo Alto Research Laboratory
Palo Alto, California 94304

I.   INTRODUCTION

Several excellent papers given at this symposium on the observation
of gamma-ray lines and theoretical reviews on the astronomical sources of
line emission have pointed out the unequivocal value and need for high
resolution data. This paper describes a technique to obtain such high
resolution measurements with a satellite-borne cooled germanium spectro-
meter which is scheduled for flight later this year. Some high resolution
data (Imhof and Nakano, 1977) obtained from the first satellite-borne
germanium spectrometer are presented to illustrate the nature of the
on-board background spectrum and the background subtraction technique
employed to yield a net spectrum from a region of the galactic plane.
Different aspects of these data were discussed earlier in this symposium
by E. L. Chupp (1978) and by D. Gilman (1978).

Lithium-drifted germanium, Ge(Li), detectors were developed over
16 years ago (Freck and Wakefield, 1962; Tavendale and Ewan, 1963), and
were first flown on a satellite 10 years later, in 1972, (Nakano et al.,
1973; Imhof et al., 1973) by our group at Lockheed. However, more than
10 years have passed since the technology to pursue high resolution
gamma-ray line astronomy with germanium detectors was first demonstrated
by the pioneering balloon efforts of A. S. Jacobson (1967) and of Womack
and Overbeck (1970). It is worth noting that the level of interest of a
given field goes hand-in-hand with the technology but it often takes an
inordinate length of time for that technology to be appreciated and finally
exploited to yield new and exciting results such as those presented here
and at other recent meetings by A. S. Jacobson (1978) and M. Leventhal (1978).

II.   THE P78-1 HIGH RESOLUTION SPECTROMETER

As part of the primary payload, the P78-1 Satellite will carry two essentially identical high resolution spectrometers each consisting of single ~85 cc intrinsic germanium (IGe) detector. The spacecraft is scheduled for launch late this fall and will be placed into a sun-synchronous polar orbit at an altitude of 550-650 km. The vehicle is an enlarged OSO type satellite which will be spin-stabilized at 11 rpm with the spin vector perpendicular to the sun-synchronous orbit plane. In addition to the two germanium spectrometers, our payload includes a pair of phoswitch scintillators, an array of CdTe detectors and several particle detectors all of which are mounted on the wheel section of the satellite. Some auxiliary instruments from other experimenters are also mounted on the wheel section and on the sail section which will be pointed at the sun during the daylight part of the orbit.

The intrinsic (high purity) IGe detector offers a great advantage over the older Ge(Li) detector in that the former sensor can be stored at room temperature and cycled for operation to cryogenic temperatures an indefinite number of times, whereas the Ge(Li) crystal requires continuous cooling. A major advantage of the IGe detector is that it facilitates the assembly of large and complex detector arrays planned for the next generation of high sensitivity instruments such as those contemplated for the GRO mission.

Figure 1 shows a schematic cross-sectioned view of the high resolution spectrometer which can be divided into four major sub-systems: the sensor-cryostat assembly, the active and/or
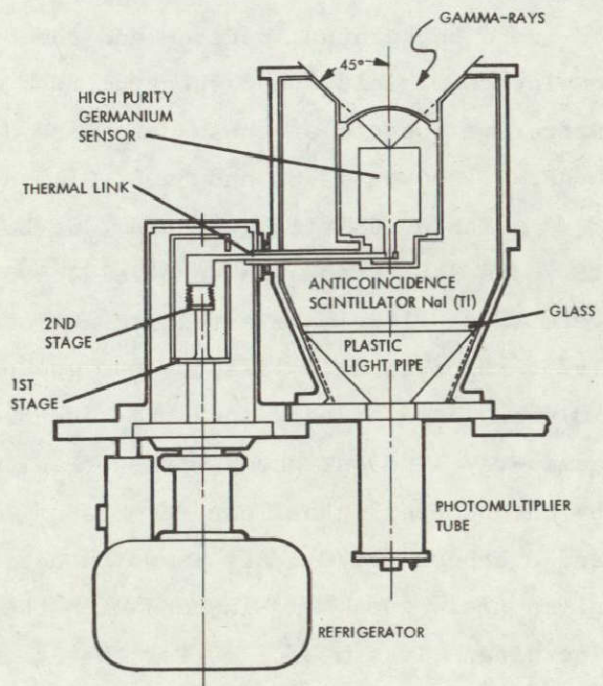

Figure 1.   A schematic cross-section of the ~85 cm^3 IGe spectrometer to be flown on the P78-1 satellite.

passive shield, the cooling system and the electronics system. The instrument design exploits the cyclibility of the large (~85 cc) IGe detector that can be cooled to approximately 80 K by either one of two mechanical Stirling Cycle refrigerators provided for each spectrometer.

The germanium detector is approximately 50 mm diameter by 45 mm in length and its relative peak efficiency at 1.33 MeV is about 20 percent of a standard 3 in. x 3 in. NaI(Tl) measured at a source distance of 25 cm from the face of the detectors. Its intrinsic efficiency in terms of effective area for the detection of the peak photon energy is about 19 cm^2 at 100 keV and decreases to 2 cm^2 at 1.33 MeV. The instrument is sensitive to gamma-rays from ~50 keV to 2.7 MeV in the normal mode. A commandable gain change is included to increase the dynamic range to ~7 MeV, thus, providing the possibility to detect the 6.1 MeV line from ^{16}O expected from interstellar dust grains (Lingenfelter and Ramaty, 1977). A photograph of the high resolution gamma-ray spectrometer is shown in Figure 2. The entire instrument weighs 69.8 kg. Two such instruments, which are completely independent of each other, are mounted in the wheel section of the P78-1 satellite with their central view directions at 75 and 105 degrees from the spin vector.

Another innovation employed in this instrument is the use of an active anticoincidence shield made of ~5 cm thick NaI(Tl) polyscin which defines the aperature to ±45 degrees for the lower energy gamma-rays. The use of the common single crystal NaI(Tl) scintillator has been avoided as a large active shield in space applications because of its mechanical susceptibility to cleave along its principal plane, however, the NaI(Tl) polyscin is an extruded poly-crystalline form providing much greater mechanical strength. Its scintillation and optical properties are identical to that of the single crystal. The decidedly faster light decay times (0.25 μs) in NaI(Tl) than that of the commonly used scintillator shield (~0.7 μs) in CsI(Na) which also exhibits a component with long (~12 μs) decay times are important advantages, particularly in large anticoincidence shield systems where high counting rates can contribute significantly to the dead time. These adverse dead time effects usually force the experimenter to increase the threshold of the anticoincidence signal, thus diminishing the effectiveness of the shield and thereby
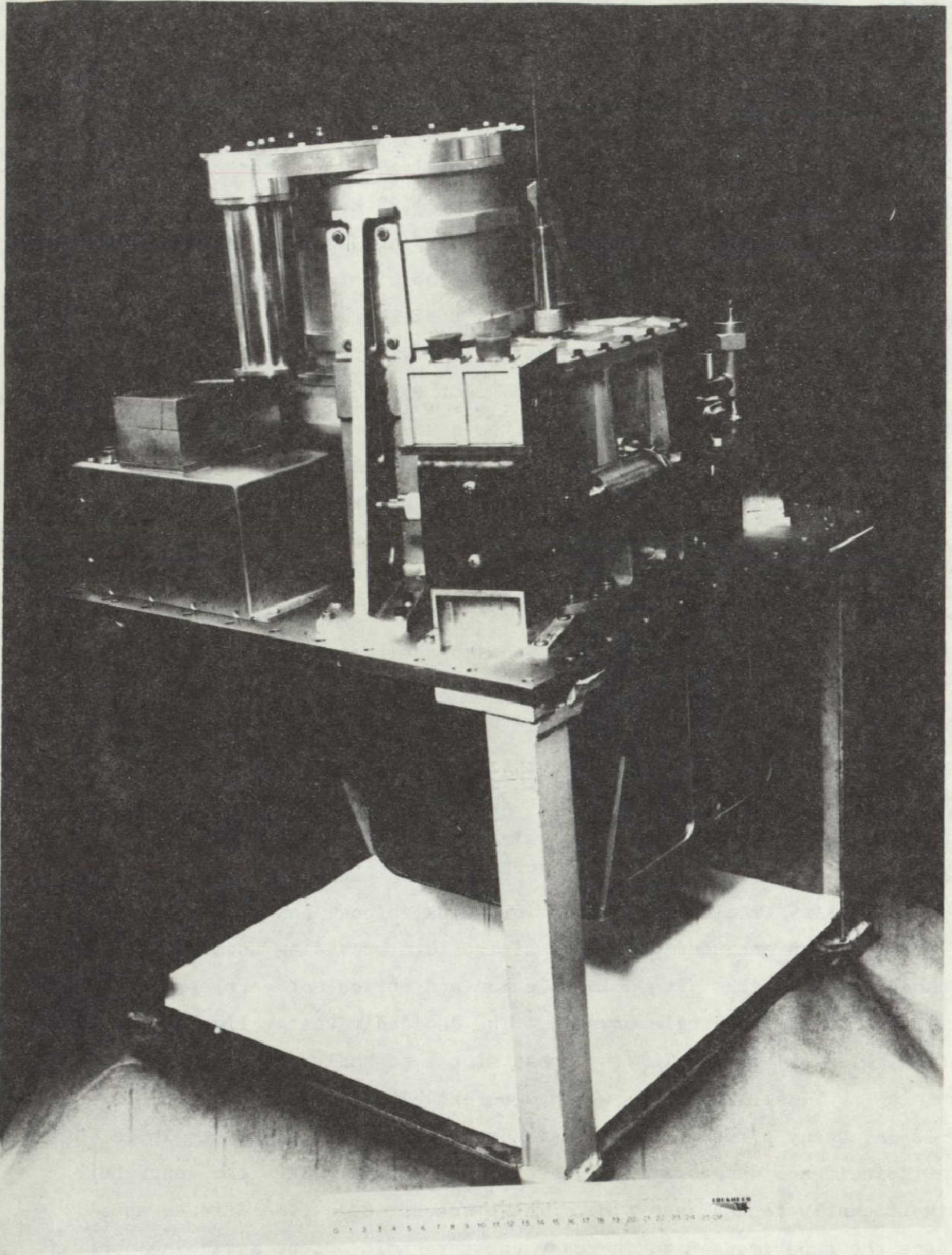
Figure 2.   A photograph of the P78-1 high resolution
gamma-ray spectrometer.

increasing the general background and Compton continuum rates. An important disadvantage in the use of NaI(Tl) is its hydroscopic nature which requires absolute integrity in the hermatic seal complicating the design and assembly of the scintillator housing and of the coupling of the photomultiplier tubes. In our system two photomultiplier tubes are coupled to the main NaI(Tl) shield with a plastic light pipe. The complete instrument was subjected to a series of vibration tests to demonstrate its integrity against the launch environment. The instrument aperature is also shielded against charged particles with a 1.37 cm thick plastic scintillator which is viewed by two additional photomultiplier tubes.

The two Stirling cycle refrigerators in each spectrometer were provided to us by the Johns Hopkins University, Applied Physics Laboratory. The two refrigerators are implemented for redundancy and are coupled to each other and to the central detector. A photograph of the coupled refrigerators is shown in Figure 3. Either refrigerator is capable of cooling the IGe detector from room temperature to 80 K in about 30 hours, expending 25-30 watts of input power at 28 volts and producing approximately 0.3 watts of cooling capacity at the cold stage and about 1.6 watts at the intermediate stage which runs at 155 K at equilibrium. The long cool-down time is partially due to the added heat capacity included in the thermal link so that high resolution data could be obtained with refrigerators turned off. This feature is necessary to eliminate the microphonic noise induced by the operation of the refrigerator which can reduce the systems resolution by factors of two or three. The operational lifetime of small flyable Stirling cycle refrigerators was a factor influencing our decision to include redundant cooling systems. At the beginning of our present program the longest demonstrated lifetime of such refrigerators was about 1000 hours. Since then a lifetime test conducted at APL with a refrigerator that is identical to the flight model has logged more than 8000 hours of operation before the test was terminated.

The electronics is rather straight forward and will not be discussed in detail since it is similar to the system used in our previous flight (Nakano et al., 1974a; Bakke et al., 1974). Apart from the photomultiplier tube circuitry, anticoincidence logic and house-keeping electronics, the

major components involve
the processing of the sig-
nal from the IGe sensor.
The low noise, d.c. coupled
preamplifier incorporates an
optically coupled current
compensation circuit to
correct for leakage currents
which at elevated detector
temperatures would normally
drive the d.c. coupled pre-
amplifier beyond its linear
range of operation. Hence,
this feature allows the spec-
trometer to provide data over
a wide range of temperatures
and still preserve the advan-
tages obtained with the d.c.
coupled configuration.

Pulses from the primary
detector are amplified and
shaped with 2 microsecond
time constants and those sig-
nals that satisfy the anti-
coincidence logic are analyzed
by a 4096 channel pulse height
analyzer. In each instrument

Figure 3. A photograph of two coupled
Stirling cycle refrigerators,
either one of which is capable
of cooling the germanium detec-
tor to ~80 K.

the PHA output address corresponding to the photon energy loss in the IGe
detector is sampled once per millisecond, stored in an on-board tape recor-
der and subsequently telemetered to the ground.

Estimates of the 3σ flux sensitivities at some of the important
gamma-ray line energies are given in Table 1, assuming the lines were not
kinematically broadened, for live times of 600 sec and 10^5 sec. Since the
wheel section of the satellite will be spinning at 11 rpm with the spin
vector perpendicular to the sun-synchronous orbit plane, each instrument
will view the sun once per spin period during the daylight orbit. Should a
flare occur while the germanium spectrometers are working, the 3σ minimum
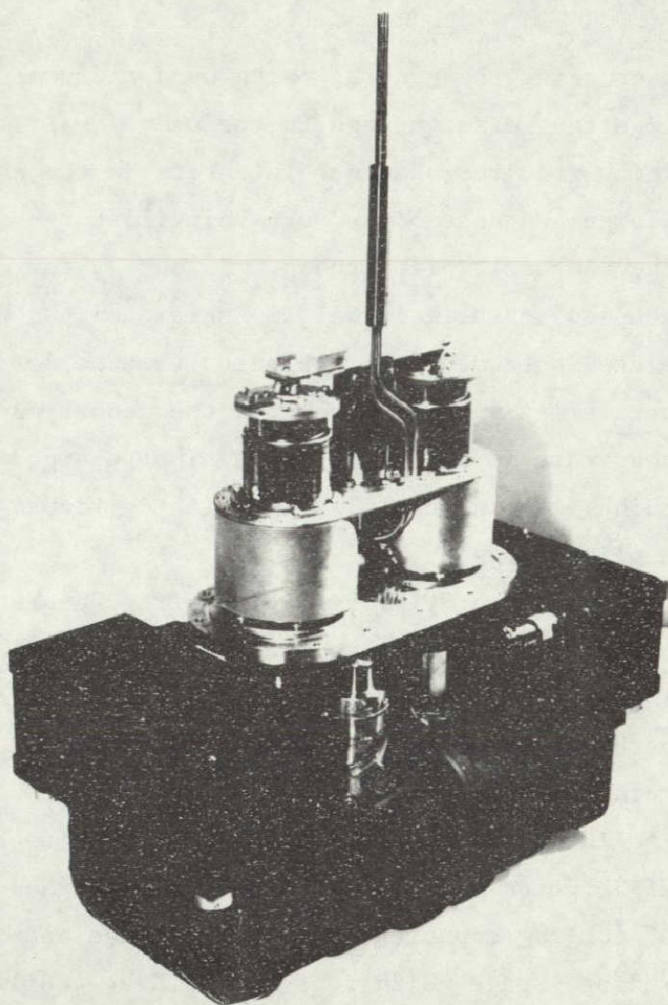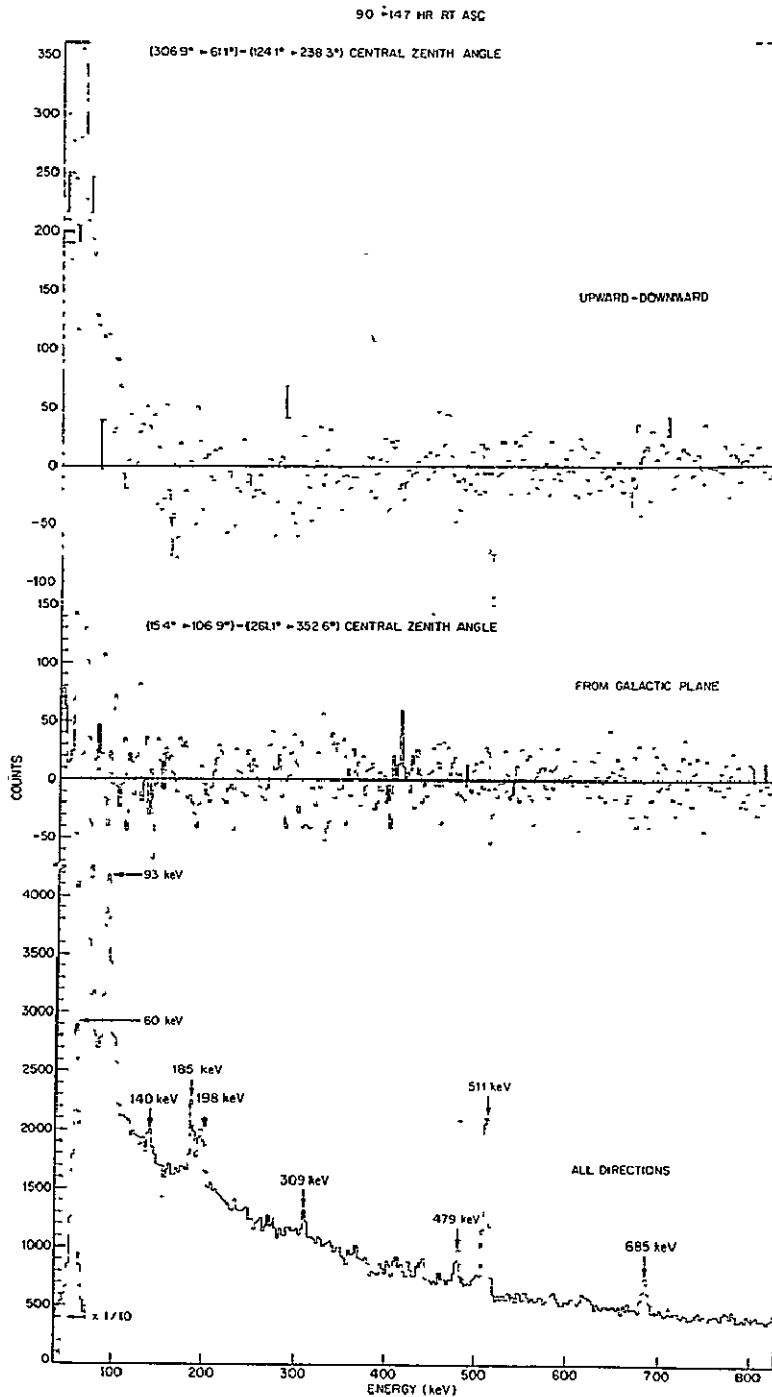
Figure 4a. Energy loss spectra measured during local
noontime passes near the geomagnetic equator
in the period 1972 October 3-12 (from Imhof
and Nakano, 1977). The upper and middle
sections are difference spectra and the lower
section is a composite spectra taken over
all directions. Figures 4a and 4b cover
38-827 keV and 827-2700 keV, respectively.

obtained in space and the techniques used to subtract the backgrounds result-
ing in the net continuum spectrum, shown in Figure 5, emanating from a region
of the galactic plane approximately 60° from the galactic center (longitudes
of 255° to 328°).   Three distinctly different energy loss spectra are
presented in Figures 4a and 4b covering the energy range 38-827 keV and
827-2700 keV, respectively.   These data were taken from local noontime
passes near the geomagnetic equator during the period 3-12 October 1972.
To improve statistics the original 4096 channels in the spectrometer data
have been combined by fours so that each energy bin corresponds to ~2.6 keV.

The spectra in the bottom section of Figures 4a and 4b are data
summed over all zenith angles within a spin of the vehicle. These spectra
are characterized by several prominent lines, the majority of which
are attributed to locally produced background since they are not evident
in any of the difference spectra.   The line at 60 keV is primarily due
to an in-flight [241]Am calibration source.   Some of these lines are

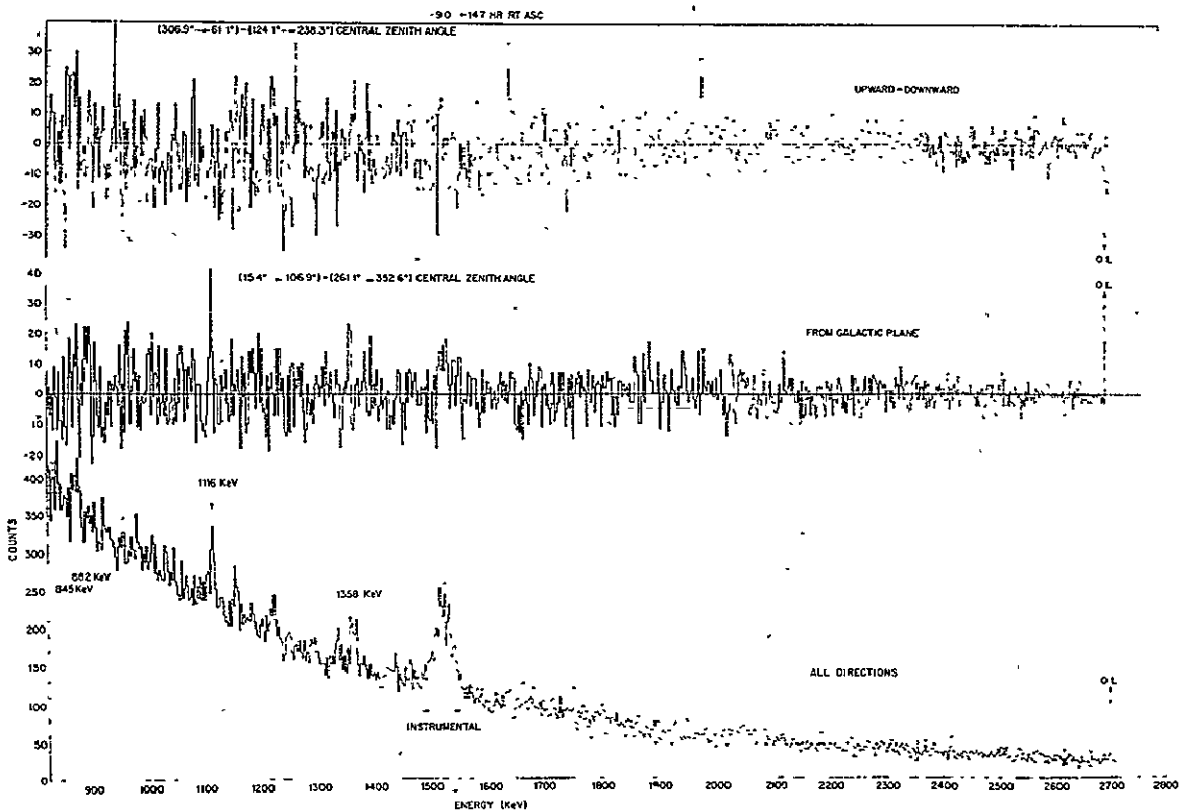
Figure 4b.

associated with isomeric transitions induced in the germanium sensor
itself (Womack and Overbeck, 1970) and with radioactivation in close
lying material (Nakano et al., 1973). Much of the prominent 511 keV line
is generated locally with some additional contribution from atmospheric
interactions which vary with geomagnetic latitude (Nakano et al., 1974;
Imhof et al., 1976).

Data presented in the upper and middle sections of Figures 4a and
4b are the accumulated difference spectra of data taken over equivalent
angular intervals of each spin of the vehicle. The spectra in the upper
sections are the net upward viewing minus the downward viewing spectra.
Hence, the resultant represents a composite of the gamma-ray flux coming
from space in a broad interval of solid angle subtracted by the gamma-ray
flux from the atmosphere over an equiva-
lent interval of solid angle. Note that
at lower energies, below 100 keV, the
diffuse cosmic background dominates the
spectra but at higher energies the atmos-
pheric component becomes stronger as evi-
denced by the slightly negative average
difference above ~150 keV.

The spectra in the middle section
of Figures 4a and 4b are the result of
data taken over an angular interval cover-
ing a region of the galactic plane (long-
itudes of ~255° to ~328°) minus a back-
ground interval over an equivalent solid
angle. The atmosphere was not viewed
in either case. The backgrounds were
taken over angular intervals which were
located symmetrically about the local
zenith direction to that of the signal
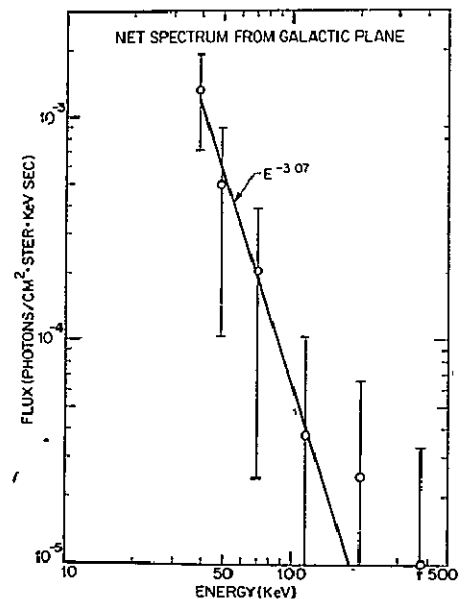and were generally in the direction of

Figure 5. The net continuum
spectrum from a broad
interval spanning the
galactic plane at
longitudes of ~255° to
~328°.

the galactic north pole. This technique provided an accurate spin-by-spin subtraction of the dominant on-board background as attested to by the essentially complete subtraction of almost all the background gamma-ray lines and the net average counts above ~150 keV. There appears to be some residual in the difference spectra at 1116 keV and at 1358 keV suggesting the possible presence of these lines from the galactic plane. Although the statistical evidence for these lines is rather limited, the resulting upper limit intensities averaged over the full fields of view are 0.0152 ± 0.0049 and 0.0140 ± 0.0049 photons $(cm^2 \; sr \; sec)^{-1}$ at 1116 and 1358 keV, respectively. We note that these two lines are within the uncertainty in energy of two gamma-ray de-excitation lines from dust grains considered by Lingerfelter and Ramaty (1976), the 1121 keV line from ^{46}Ti and the 1369 keV lines from ^{24}Mg.

The difference spectrum from the galactic plane also exhibits a significant continuum energy loss spectrum for energies below ~150 keV. In order to derive a net photon spectrum it is necessary to unfold the instrument response function. These response functions were obtained by a series of laboratory measurements of single gamma-ray line profiles which were used to formulate a model gamma-ray line profile parameterized in terms of the peak energy. A more detailed account of this method can be found in Nakano et al. (1976) and in Imhof et al. (1976). The resulting net photon spectrum from a broad region of the galactic plane at longitudes of ~255° to ~328° is presented in Figure 5. A least squares power-law fit to the continuum spectra below ~150 keV resulted in a spectral index of -3.07 ± 0.31.

In summary, these data serve to illustrate the method used to subtract background on the basis of each 5 second spin period. This same technique will be employed on the forthcoming P78-1 satellite flight which will have approximately the same spin period and orbit configuration but at a somewhat lower altitude than the previous flight. Such short interval background subtraction techniques are essential in satellite observations where the characteristics of the background are continually changing as the vehicle traverses through different geomagnetic latitudes and regions of trapped and precipitating energetic particles.

REFERENCES

Bakke, J. C., McDaniel, J. D., Matthews, J. D. and Reagan, J. B., 1974 IEEE Trans., NS-21, 164.

Chupp, E. L., 1978, this Volume, p. 42.

Forest, D. J., Chupp, E. L., Suri, A. N. and Reppin, C., 1973, Gamma-Ray Astrophysics, NASA Report No. SP-339, 165.

Freck, D. V. and Wakefield, J., 1962, Nature, 193, 669.

Gilman, D., 1978, this Volume, p. 190.

Imhof, W. L., Nakano, G. H., Johnson, R. G. and Reagan, J. B., 1977, Gamma-Ray Astrophysics, NASA Report No. SP-339, 77.

Imhof, W. L., Nakano, G. H., and Reagan, J. B., 1976, J. Geophys. Res., 16, 2835.

Imhof, W. L. and Nakano, G. H., 1977, Ap. J., 214, 38.

Jacobson, A. S., 1967, thesis.

Jacobson, A. S., 1978, this Volume, p. 228.

Leventhal, M., 1978, this Volume, p. 169.

Lingenfelter, R. E. and Ramaty, R., 1976, "Structure and Content of the Galaxy and Galactic Gamma-Rays," NASA CP-002, 237.

Lingenfelter, R. E. and Ramaty, R., 1977, Ap. J., 211, L19.

Nakano, G. H., Imhof, W. L., Reagan, J. B. and Johnson, R. G., 1973, Gamma-Ray Astrophysics, NASA Report No. SP-339, 71.

Nakano, G. H., Imhof, W. L. and Johnson, R. G., 1974a, IEEE Trans., NS-21, 159.

Nakano, G. H., Imhof, W. L. and Reagan, J. B., 1974b, Proc. of 9th ESLAB Symposium, ESRO SP-106, 99.

Nakano, G. H., Imhof, W. L. and Reagan, J. B., 1976, Sp. Sci, Instru., 2, 219.

Stecker, F. W., Cosmic Gamma-Rays, NASA SP-249.

Tavendale, A. J. and Ewan, G. T., 1963, NIM, 25, 185.

Womack, E. A. and Overbeck, J. W., 1970, J. Geophys, Res., 75, 1811.

HEAO C-1 Gamma-Ray Spectrometer

W. A. Mahoney, J. C. Ling, J. B. Willett and A. S. Jacobson

Jet Propulsion Laboratory
California Institute of Technolog;
Pasadena, California   91103

ABSTRACT

The gamma-ray spectroscopy experiment to be launched on the third High
Energy Astronomy Observatory (HEAO C) will perform a complete sky search for
narrow gamma-ray line emission to the level of about 10^{-4} photons/cm^2-sec for
steady point sources. The design of this experiment and its performance
based on testing and calibration to date are discussed.

1. INTRODUCTION

The current excitement in gamma-ray spectroscopy in astrophysics has been evident throughout this conference and it has become clear there is great interest in performing a systematic sky survey for gamma-ray line emissions. To perform this task, the HEAO C-1 gamma-ray spectrometer has been developed by JPL under the direction of Principal Investigator Allan S. Jacobson. The experiment consists of an array of 4 high purity Ge detectors in an active CsI shield. It operates in the energy range of 0.05 to 10 MeV and has a three sigma sensitivity for detecting narrow gamma-ray line emission of about 10^{-4} photons/cm^2-sec for steady point sources throughout the energy range. The sensitivity for measuring the continuum emission from point sources varies from about 10^{-5} photons/cm^2-sec-keV at 0.1 MeV to about 10^{-6} photons/cm^2-sec-keV at 10 MeV, assuming the spectrum is broken into bands of width $\Delta E = E$. While scintillation detectors can also be used to detect gamma-ray line emission, we have chosen Ge detectors because of their superior energy resolution. A Ge detector system has better sensitivity to narrow gamma-ray lines than a comparable scintillator experiment, but possibly more important is its ability to better determine the energy of gamma-ray lines which could include measuring small red shifts and its ability to measure complex line structure. HEAO C is basically a scanning mission which is scheduled for launch in September 1979. Thus after 6 months in orbit, it will have completed an entire sky survey for narrow gamma-ray line emission to the level of about 10^{-4} photons/cm^2-sec.

2. SCIENTIFIC OBJECTIVES

A wide variety of scientific objectives may be achieved by observing gamma-ray emission in the energy range 0.05 to 10 MeV. While the primary objective is the detection of gamma-ray line emission from discrete and extende

cosmic sources, the experiment will be sensitive to continuum gamma-ray emission of cosmic origin as well as atmospheric emission. In addition, the CsI shield itself is a crude gamma-ray detector with a large area. It will be used to search for cosmic emission, measure gamma-ray bursts with a temporal resolution of one second, and help interpret or corroborate observations made with the Ge detectors. Specific experiment objectives include:

- An exploratory search for discrete galactic and extragalactic sources of gamma-ray line emission. Such sources could include recent novae and supernovae, interstellar gas and dust clouds and compact objects such as black holes and neutron stars.

- Measurements of spectral details and intensity of the continuum emission from discrete sources.

- Measurements of time variations in the line and continuum emission from discrete sources including pulsating, transient and bursting phenomena.

- Measurement of line and continuum emission from the galactic plane.

- Measurement of the line and continuum spectrum of the diffuse background.

- Measurement of line and continuum atmospheric emission.

3. INSTRUMENT DESCRIPTION

The experiment consists basically of an array of four large volume high-purity germanium detectors in an active CsI shield (Hicks and Jacobson, 1974). Figure 1 is an exploded view of the system. Functionally it is almost identical to our balloon system (Jacobson et al., 1975) which was developed earlier and has served almost as a prototype system for the C-1 experiment.

The four germanium detectors are shown in Figure 2 during transfer to the flight cryostat early in the integration phase. They are high purity closed-end coaxial detectors mounted in individual Al cups and contained in a single

544

vacuum. Each detector is about 54 mm in diameter and about 45 mm in length. The high voltage and signal connections for each detector are provided by feedthroughs in the baseplate of the cryostat. The detectors operate at bias voltages which vary between 1800V and 3900V. Cooling is provided by a two stage solid cryogen cooler with methane and ammonia as the primary and secondary cryogens, respectively. The detectors are now operating at a temperature of about 96K. The lifetime of the cooler is estimated at close to one year.

Surrounding the cryostat is a CsI(Na) anticoincidence shield with a minimum thickness of 66 mm. The shield is in five pieces (Figure 1), four of which together form a well and a fifth which forms the collimator. A hole through the collimator is drilled above each detector to define an aperture of 30°FWHM. Completing a 4π steradian shielding for charged particles is a plastic scintillator 3.3 mm thick in the aperture. Each shield piece is viewed by two RCA C-70132D photomultiplier tubes (with the exception of the collimator which has four). Figure 3 shows the fully integrated system after conformal coating.

The key parts of the instrument electronics are a preamplifier, shaping amplifier and 8192 channel pulse height analyzer for each Ge detector. Each valid Ge' event is processed and transmitted separately as a 32 bit telemetry word. This word consists of a 13 bit pulse height channel number, a 12 bit time tag giving the time of occurrence of the event to 78 μsec, and 7 flag bits indicating the following possible conditions:

1) An event has occurred simultaneously in 2, 3 or 4 Ge detectors. This could represent gamma-rays Compton scattering in one or more detectors and going on to become fully absorbed in another. The true energy of the event could then be recovered by normalizing

each of the simultaneous events and adding the individual detector contributions.

2) An event has been accompanied by one or more .5 MeV events in the shield crystals. At high energies, the largest photon absorption cross-section in Ge is electron-positron pair creation. Following annihilation of the positron, either one or both of the resulting .511 MeV gamma-rays can escape the Ge detector. Normally, these would interact in a shield crystal and cause the event to be vetoed However, shield discriminators around .511 MeV override the shield veto and allow the event to be processed. In this case, the event is tagged with a window flag.

3) An event has occurred simultaneously with a shield event of any energy. This can happen only when the usual shield veto has been disabled by command.

4) The detector ID.

The C-1 telemetry rate is 2.2 kbps including all subcommutated data. The Ge events can be transmitted at a maximum rate of 15.625/sec for each detector. The expected average rate for each detector is about 5/sec.

The CsI crystals, in addition to providing an active shield for the Ge detectors, are gamma-ray detectors themselves. The lower level discriminator (LLD) is set at about 100 keV and provides a 7 μsec veto for Ge events while the upper level discriminator is set at 4 MeV and provides a veto of about 30 μsec. These veto times are nominal. The actual veto time consists of a constant, 5 μsec for the LLD and 20 μsec for the ULD, plus the time the pulse amplitude remains above the corresponding discriminator threshold. The shield LLD rates are read out every 1.28 seconds while the ULD rates, window rates and numerous Ge detector rates are read out every 10.24 seconds. Thus the

shield is a burst detector which will give the time of occurrence of a burst to 1.28 sec and, by analyzing relative rates in the shield pieces, can provide some directional information. In addition, the spectrum of each shield piece, including the charged particle detector, is recorded by a 128 channel roving pulse height analyzer (RPHA). The RPHA can be commanded to read out continuous 40.96 sec spectra from one shield piece or it can cycle sequentially through all six shield detectors. In addition to the RPHA and rate data, numerous housekeeping data such as temperatures and voltages are read out.

Numerous command options are provided for optimizing the instrument performance. These include adjusting the high voltage for both the Ge bias and the PMTs, adjusting discriminator levels for both the Ge and CsI crystals, turning on and off various parts of the experiment and changing the mode of operation of the spectrometer. The experiment weights 230 kg and consumes a maximum power, including heaters, of about 30 watts. The instrument will be mounted at the top of the HEAO C spacecraft and, like all HEAO experiments will point perpendicular to the spin axis.

4. INSTRUMENT PERFORMANCE

The C-1 experiment has been fully integrated and is now operating very well. To date its performance has been determined from extensive testing during integration and from a two week calibration prior to the integration of the CsI shield. Soon the linearity and gain of the Ge and CsI detectors will be measured as a function of temperature during environmental testing. Prior to delivery, an extensive calibration will be performed to characterize the aperture and angular response of the system.

Calibration is being performed with two types of gamma-ray sources. Low energy ($\lesssim$ 3 MeV) calibration lines can be readily obtained with small disks

containing certain long-lived radioisotopes. For lines above 3 MeV, we have

developed a device called a neutron howitzer which allows the use of prompt

gamma-ray emission following thermal neutron capture in Ti and Cr. The how-

itzer, shown in Figure 4, consists basically of a strong Cf^{252} neutron source

in a tank of water which thermalizes the neutrons. A target is placed about

10 cm from the neutron source, and at right angles to the source-target direc-

tion is a port through the water which allows the prompt γ-rays from the target

to travel to the detector nearly unattenuated. In designing the howitzer,

care has been taken to keep the neutron exposure of the Ge detectors to an

acceptable level while maximizing the flux of target γ-rays. Figure 5 shows

a spectrum obtained with a Cr target which gives numerous lines at energies

up to 9.7 MeV. All the lines above about 1.5 MeV occur in triplets with the

highest energy line being the full energy peak and the lines .511 MeV and 1.022

MeV lower in energy corresponding to the single and double escape peak, respec-

tively. At lower energies, there are numerous background lines, including a

very strong one at 2.22 MeV resulting from deuterium formation in the water.

Prior to integration of the CsI shield, a two week calibration was per-

formed to characterize the unshielded detectors. During this period, the

absolute efficiency, the angular response of the unshielded detectors, and the

simultaneous event efficiency of the 4 detectors together were all determined.

The results of a preliminary analysis of the absolute efficiency is shown in

Figure 6 for detector 1 which is typical of all 4. The maximum effective area

reaches about 16 cm^2/detector at 100 keV. The roll off at lower energies is

due to attenuation in the detector dead layer which has a thickness of about

700 μ. At higher energies, the efficiency drops because of a drop in the inter-

action cross sections.

Table I shows the final results of the efficiency measured with an NBS ^{60}Co source. Also shown are the resolutions of each detector at 1.33 MeV measured on two occasions: the first during pre-shield calibration and the second after the complete system had been integrated. Resolution measurements vary by about 0.1 keV from one measurement to the next, but the numbers shown are typical. All the spectral fitting has been done at JPL using a routine called HYPERMET (Phillips and Marlow 1976).

5. CONCLUSION

The HEAO C-1 experiment has now been fully integrated and is functioning very well. During the next four months it will go through environmental testing and a detailed calibration prior to delivery to TRW on 1 October 1978. The mission is currently baselined as a six month sky survey after which we will hopefully be able to answer some of the many questions raised during this conference and elsewhere related to cosmic gamma-ray line emission. The experiment will perform an exploratory complete search for narrow gamma-ray line emission from point sources to the level of about 10^{-4} photons/cm^2-sec, which is approximately an order of magnitude better than current balloon systems are achieving.

REFERENCES

Hicks, D. B. and A. S. Jacobson (1974), IEEE Trans. on Nucl. Sci, <u>NS-21</u>, 169.

Jacobson, A. S., R. J. Bishop, G. W. Culp, L. Jung. W. A. Mahoney and J. B. Willett (1975), Nucle. Instr. and Methods, <u>127</u>, 115.

Phillips, G. W. and K. W. Marlow (1976), Nucl. Instr. and Methods, <u>137</u>, 525.

FIGURE CAPTIONS

Figure 1.   An exploded view of the HEAO C-1 gamma-ray spectrometer

Figure 2.   The four high purity germanium detectors during transfer to the flight cryostat. Each detector is about 54 mm in diameter. Mounted at the base of the cryostat are the bias voltage filters and the signal preamplifiers.

Figure 3.   The fully integrated system after conformal coating.

Figure 4.   The instrument during calibration prior to integration of the CsI shield. The mounting cage was designed to allow the experiment to be rotated to several planes for calibration purposes. To the right is the neutron howitzer used for high energy calibration. In the background is the experiment support and check-out computer system.

Figure 5.   A spectrum obtained with a Cr target in the howitzer. Note the numerous narrow lines in the upper half of the spectrum.

Figure 6.   The effective area (area x efficiency) of detector 1 including the single and double escape peak efficiencies.

EFFICIENCY AND RESOLUTION OF HEAO C-1 GE DETECTORS
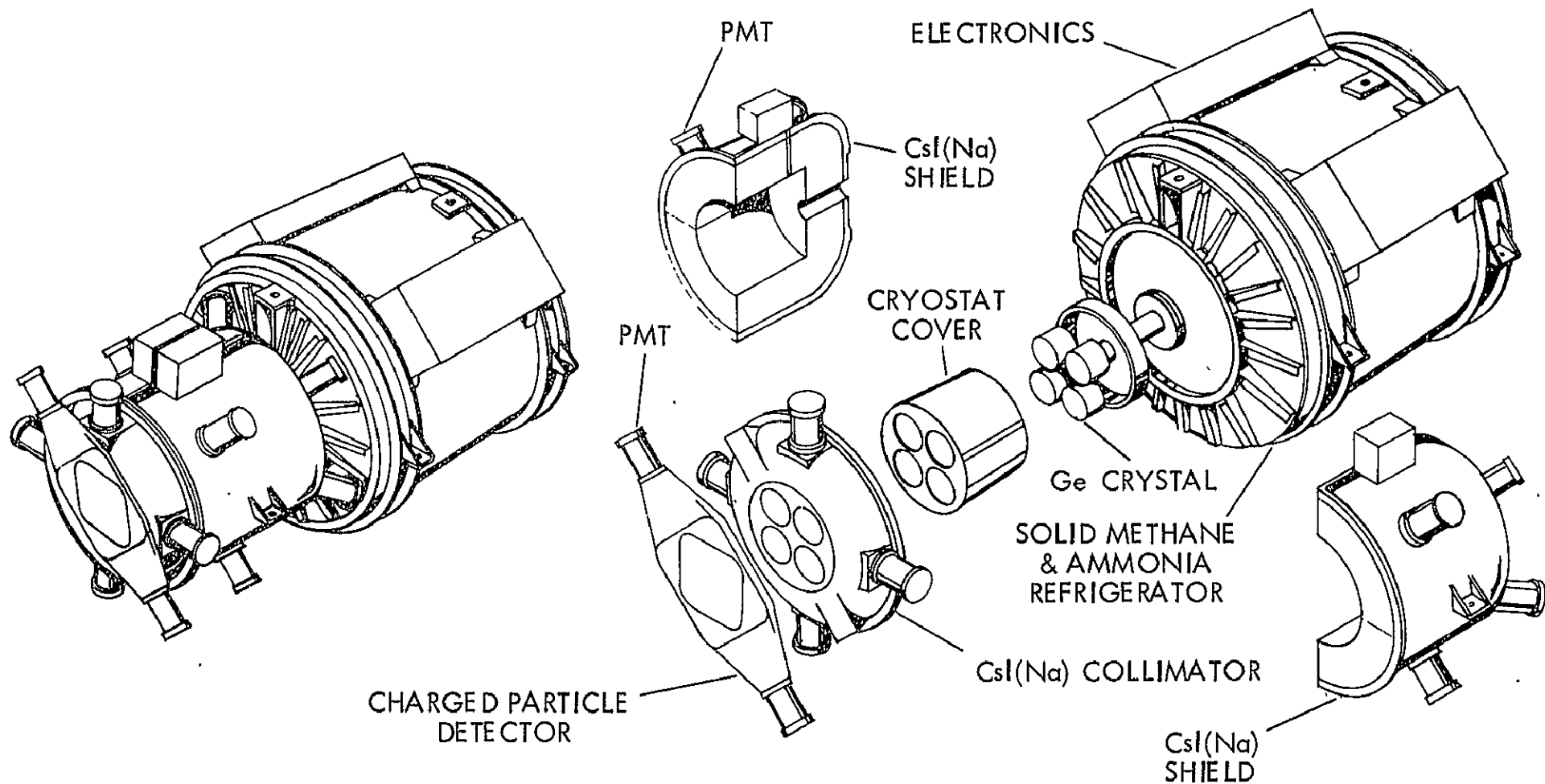
From Analysis of Calibration Data

CHARACTERISTIC		DETECTOR NUMBER			
		1	2	3	4
Resolution – keV (FWHM at 1.33 Mev)	20 Feb 78	2.81 ± .08	3.20 ± .10	2.59 ± .06	2.99 ± .08
	5 May 78	2.81 ± .05	3.05 ± .06	2.58 ± .06	2.83 ± .15
Effective Area (Cm^2 at 1.33 Mev)		2.64 ± .04	2.93 ± .05	2.72 ± .04	2.64 ± .05

Table I

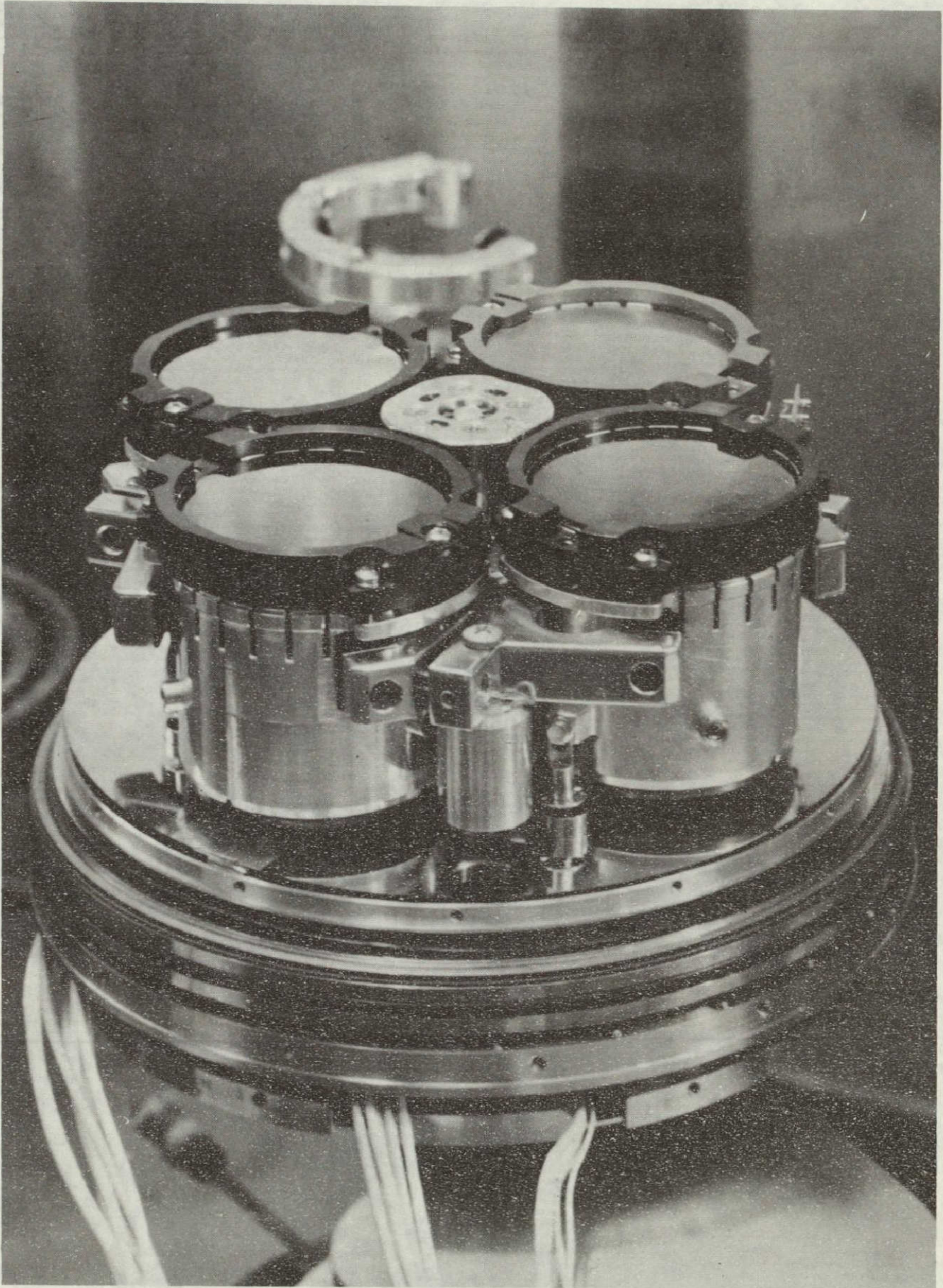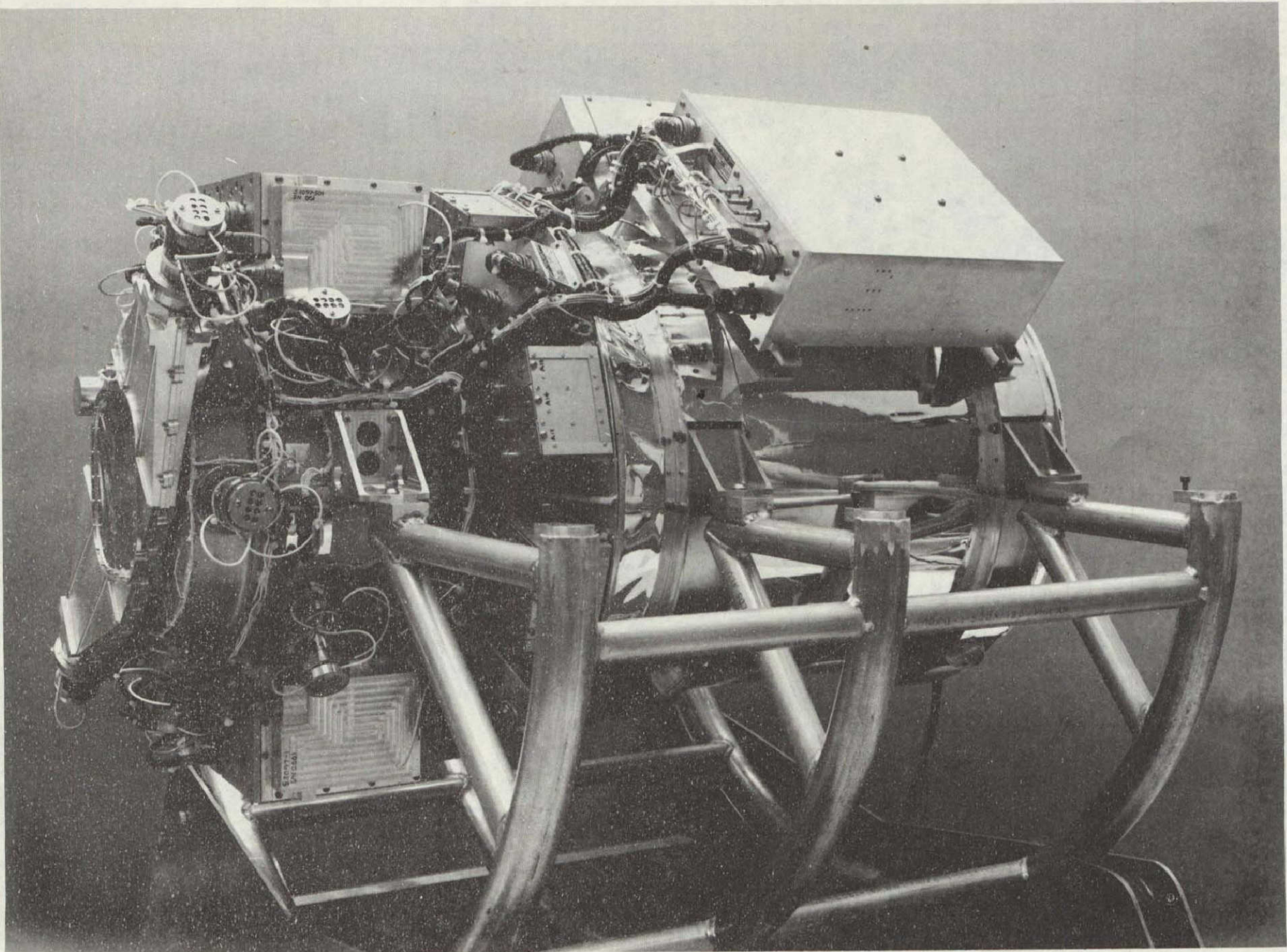# HIGH SPECTRAL RESOLUTION GAMMA-RAY SPECTROMETER

HEAO C-1

PMT

ELECTRONICS

CsI(Na)
SHIELD

PMT

CRYOSTAT
COVER

Ge CRYSTAL

SOLID METHANE
& AMMONIA
REFRIGERATOR

CsI(Na) COLLIMATOR

CHARGED PARTICLE
DETECTOR

CsI(Na)
SHIELD

552
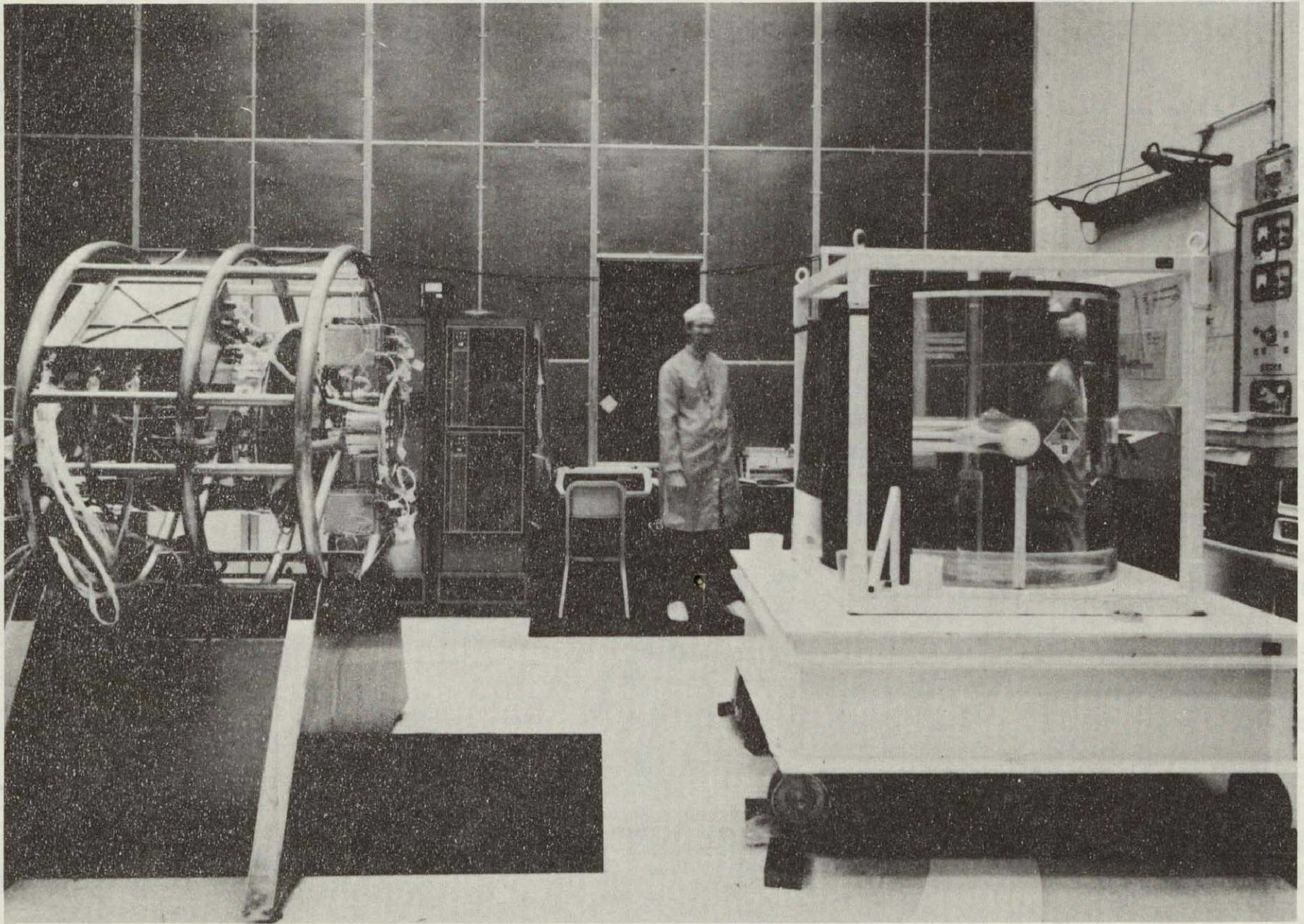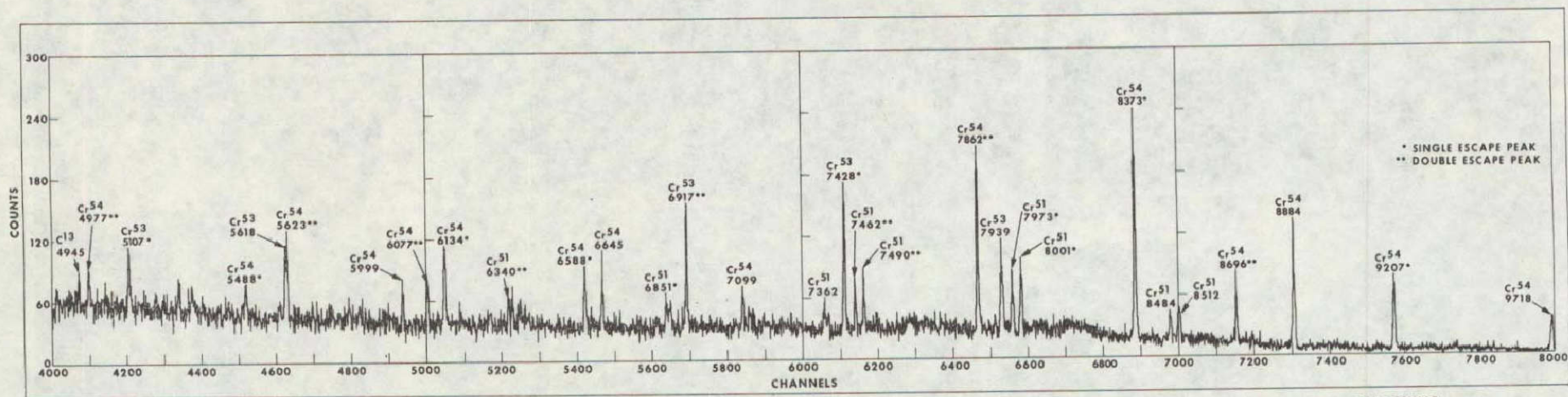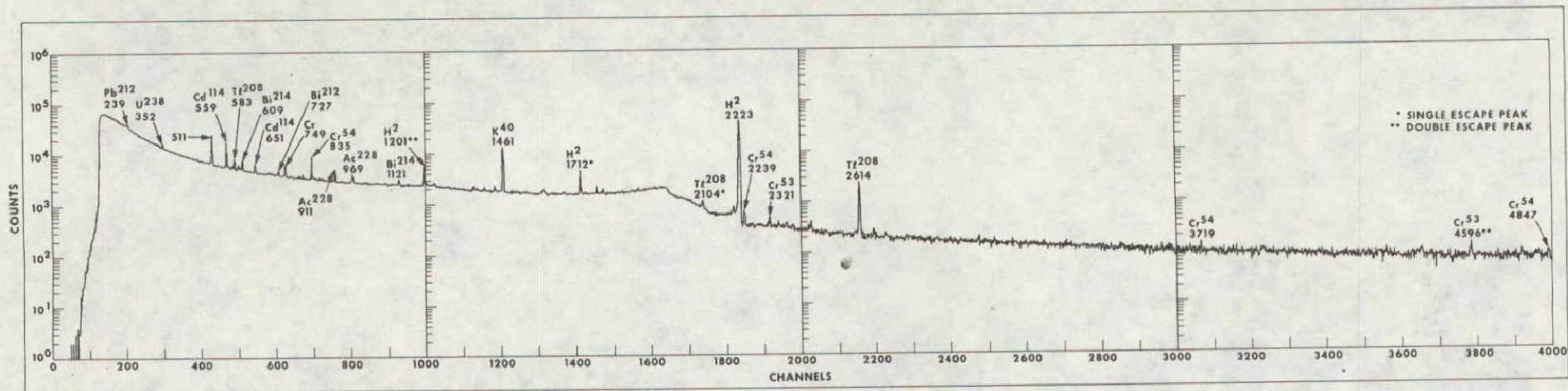
Figure 1

Figure 2

Figure 4

HEAO C JPL GAMMA – RAY SPECTROMETER
PRESHIELD CALIBRATION – THERMAL NEUTRON HOWITZER – Cr TARGET
DETECTOR 1 – 10 HOUR RUN

Figure 5

Solar Gamma Ray Astronomy
On Solar Maximum Mission

D. J. Forrest
Department of Physics
University of New Hampshire
Durham, New Hampshire   03824

ABSTRACT

We present here a summary description of the SMM gamma ray experiment along
with a discussion of the important scientific capabilities of the instrument.
A study has been made of the flare size detectable as a function of spectrum
integration time. A preliminary estimate indicates that a solar gamma ray
line at 4.4 MeV one-fifth the intensity of that believed to have been emitted
on 4 August 1972 can be detected in $\sim$ 1000 sec with a confidence level of 99%.

1. INTRODUCTION

The gamma ray experiment on NASA's Solar Maximum Mission is one of the six

independent but complementary experiments dedicated to the study of solar

flares during the 1979-1980 period of maximum solar activity. The gamma ray

experiment is basically a scaled up version of the University of

New Hampshire NaI gamma ray detector on OSO-7, which first measured solar gamma

ray lines in August 1972. Dedicated solar pointing, increased spacecraft

weight, and telemetry capabilities have allowed an order of magnitude increase

in detection sensitivity and time resolution. These improvements will allow

detailed gamma ray spectroscopy observations during large solar flares.

The fabrication of the solar gamma ray experiment is a joint effort

between the Federal Republic of Germany (FRG) (under the supervision of

DFVLR[†]) and the USA [under the supervision of the Goddard Space Flight Center

(GSFC), which has the overall responsibility for the Solar Maximum Mission

program]. The scientific and engineering program is carried out by

---

[†]Deutsche Forschungs- und Versuchsanstalf fur Luft- und Raumfahrt.

scientists from the Max-Planck Institute, Garching, and engineers from the firm Messerschmitt-Bölkow-Blohm (MBB), Munich. In the USA the collaborating scientists are from the University of New Hampshire, the Naval Research Laboratory, and the Jet Propulsion Laboratory of the California Institute of Technology, with engineering support supplied by American Science and Engineering in Cambridge, Massachusetts. The University of New Hampshire, through the Principal Investigator, has overall scientific and technical responsibility for the program. Table 1 shows a summary of all scientific personnel involved and their specific responsibilities as well as the overall institutional responsibilities for the various phases of the program. Launch for the SMM satellite is scheduled for October 1979. Only a brief summary of the experiment will be given here; detailed descriptions of the instrument will appear elsewhere (cf. Forrest et al., 1979; Seiple et al., 1979).

2. EXPERIMENT DESCRIPTION AND INSTRUMENT PROPERTIES

The heart of the gamma ray detector consists of seven high resolution 7.6 cm x 7.6 cm NaI(Tℓ) integral line detectors which form the main channel detector. Each of the detectors has an energy resolution that is better than 7% (FWHM) at 0.662 MeV. Together they form a gamma ray line spectrometer operating between 0.3 and 9 MeV. The gain of each of the seven units is automatically and continuously corrected to a common (and command selectable) position via an electronic servo loop. In order to achieve the correct gain, the servo loop utilizes gamma rays from three ^{60}Co calibration sources (cf. Forrest et al., 1972) and the corresponding digital output of the main channel pulse height analyzer to continuously trim the high voltage on each detector. Hence all seven detectors are forced to a common gain so that their analog signals can be summed and digitized with a common pulse height analyzer. The digitized signals from the seven main channel detectors are stored in two memories. One of the memories accepts only events associated with any single detector (singles mode) while the second memory accepts only events associated with two or more of the seven detectors (multiple mode). Since the gain or energy-to-pulse-height conversion is the same in both memories, which are read into simultaneously, they can be processed separately or added together. The accumulation time for both of these spectra is 16.38 sec.

Table 1

Solar Gamma Ray Experiment

for the

Solar Maximum Mission

University of New Hampshire

- Durham, N. H. -

(American Science and Engineering)*

E.	Chupp	Principal Investigator	Program Management
D.	Forrest	Project Scientist	Scientific Direction
M.	Cherry	Co-Investigator	Flight Electronics
J.	Ryan	Co-Investigator	Gamma Ray Calibration
I.	Gleske	Data Manager	Data Analysis

Max-Planck Institute for Physics and Astrophysics

- Garching, F.R.G. -

(Messerschmitt-Bölkow- Blohm)*

K.	Pinkau	Co-Investigator	Detector Assembly
C.	Reppin	Co-Investigator	Mechanical Structure
E.	Rieger	Co-Investigator	Gamma Ray Calibration
G.	Kanbach	Co-Investigator	Data Analysis

Naval Research Laboratory

- Washington, D.C. -

J.	Kurfess	Co-Investigator	Monte Carlo Calculations
W.	Johnson	Co-Investigator	Gamma Ray Calibration
R.	Kinzer	Co-Investigator	Data Analysis
G.	Share	Co-Investigator	

Jet Propulsion Laboratory
California Institute of Technology

- Pasadena, Calif. -

A.	Jacobson	Co-Investigator	Scientific Consultation

* Subcontractor

Auxiliary detectors, which have been incorporated into the instrument, are a
thick CsI(Na) crystal, behind the NaI spectrometers, for use in a high energy
detector for gamma rays with energies greater than $\sim$ 10 MeV and two NaI(Tℓ)
X-ray detectors covering the energy range 10-180 keV. The complete high energy
detector consists of the seven main channel NaI detectors and the large 25 cm x
7.6 cm CsI back detector. Events in the 10 MeV to $\sim$ 100 MeV range occurring in
either the NaI or CsI crystals are analyzed by separate four channel pulse height
analyzers and then accumulated in a 5 x 5 matrix where the row and column posi-
tions correspond to the energy bins of the pulse height analyzers. Certain
elements of this matrix are associated with gamma rays interacting in a single
high energy detector (i.e., NaI or CsI) while other elements are associated with
gamma rays which shower and interact in more than one detector. The accumulation
time for the high energy events is 2.05 sec.

The two 8 cm^2 x 0.6 cm NaI X-ray detectors both cover the energy range 10-180 keV
with four channels of pulse height information. The detectors are identical
except that one has an Aℓ filter, whose 50% transmittance energy is $\sim$ 10 keV,
and the other has an Aℓ-Fe filter so the 50% transmittance is $\sim$ 35 keV. The
detector with the higher 50% transmittance energy allows observations to be
made during intense X-ray events with minimum spectral distortion due to pulse
pileup. The accumulation time for these detectors is 1.02 sec.

Figures 1 and 2 are top and side views of the gamma ray detector, respectively.
Shown in Figure 1 are the seven main channel NaI detectors and the three [60]Co
stabilizing sources, all surrounded by the 2.5 cm thick CsI anticoincidence
annulus shield. Also shown are the outlines of the top 1 cm thick plastic
scintillator shield and the two X-ray detectors with their associated [241]Am
calibration source. Figure 2 is a cross-sectional side view; it shows the
large CsI back detector, which is used both as an anticoincidence shield for
the main channel detectors for the 0.3-9 MeV spectroscopy mode and as one of
the detector elements in the high energy mode. The hemispherically shaped
1 cm thick back plastic which acts as an anticoincidence shield is also shown.

The basic operation of the gain stabilization system, mentioned above, can be
understood by reference to Figure 3, which shows a typical ^{60}Co calibration
spectrum in a single 3". x 3" NaI(Tℓ) crystal. A separate photomultiplier
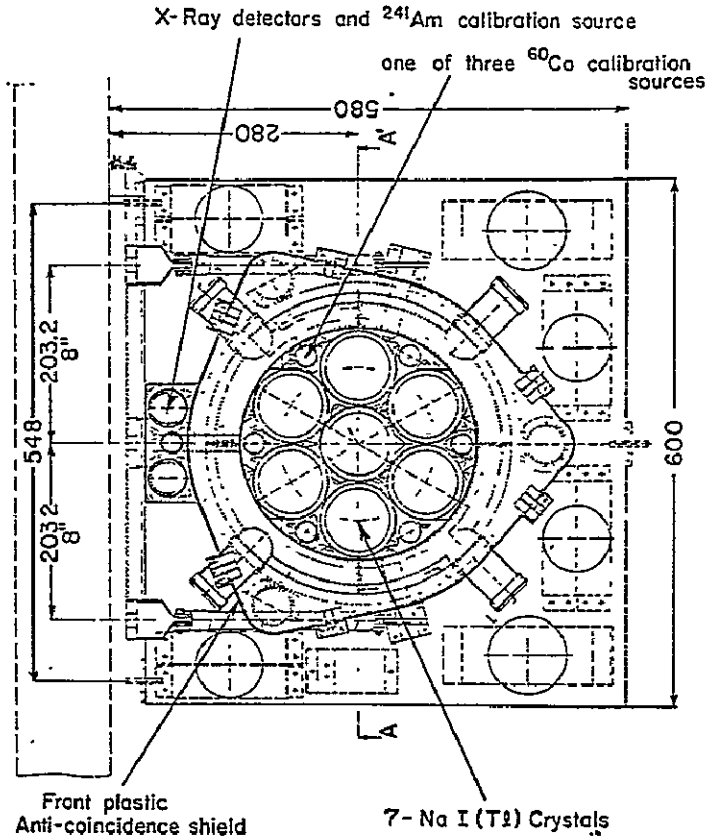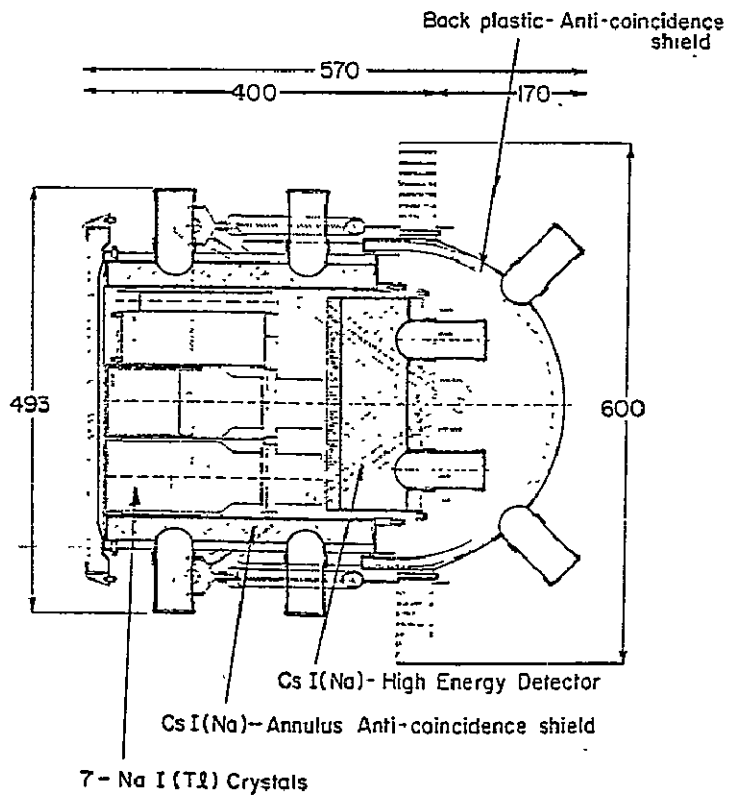
Figure 1. Detector - Top View*

X- Ray detectors and ^{241}Am calibration source

one of three ^{60}Co calibration sources

Front plastic
Anti-coincidence shield

7- Na I (Tℓ) Crystals

Figure 2. Detector - Side View*

Back plastic- Anti-coincidence shield

Cs I(Na)- High Energy Detector

Cs I(Na)—Annulus Anti-coincidence shield

7- Na I (Tℓ) Crystals

ORIGINAL PAGE IS
OF POOR QUALITY

All dimensions are in millimeters.

detects the β^- emission from the ^{60}Co source, which itself is contained in a small plastic scintillator, thereby giving a logic pulse to identify the prompt emission of coincident 1.17 and 1.33 MeV gamma rays. All seven main channel photomultiplier tubes have their gains adjusted to a common value by the stabilizer circuitry. Main channel events occurring in a single detector in coincidence with a ^{60}Co β^- decay are analyzed digitally to see if their energy falls within the bounds set by ground command. Events whose pulse height is above a mid-level (gain) threshold, *decrement* the high voltage for that detector,

Figure 3. Typical ^{60}Co calibration spectrum and gain stabilizer operation (see inset).
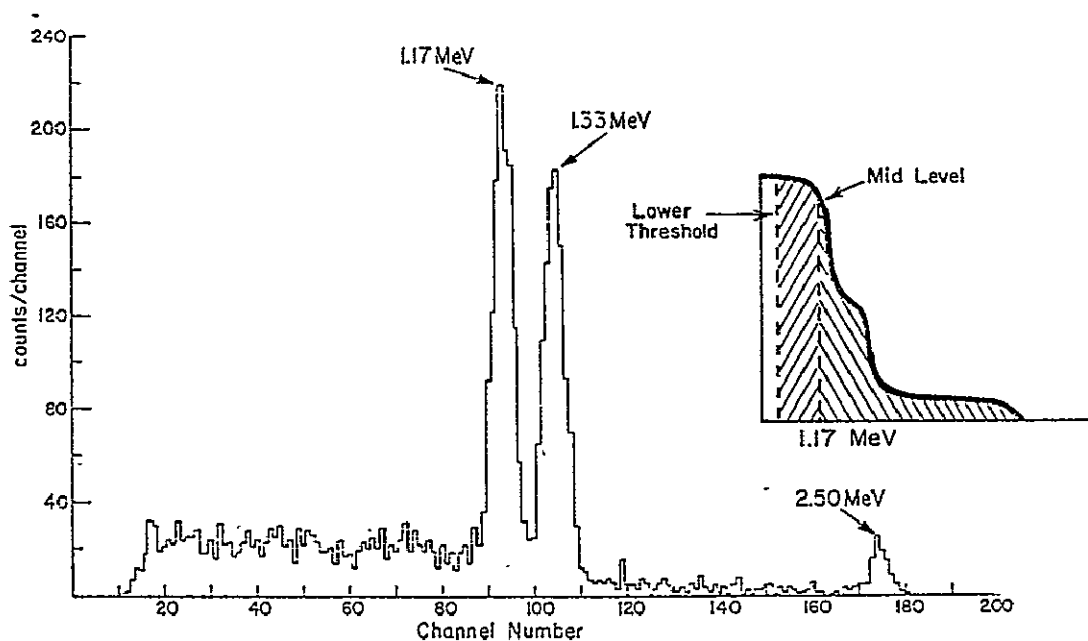

while events below this threshold, and above a lower threshold, *increment* the high voltage. The mid-level gain threshold is chosen to correspond to the pulse height given by the central photopeak energy for the 1.17 MeV ^{60}Co gamma ray. Each decrement or increment changes the high voltage by $\sim$ 50 mV, which changes the system gain by $\sim$ 0.04%. The net effect of this active stabilization system, with a proper setting of the lower threshold, is to continuously insure the equality of the average ^{60}Co rate above and below the mid-level threshold (1.17 MeV). This is illustrated in the inset of Figure 3, which shows the integral counting rate spectrum for the ^{60}Co source where the two regions,

oppositely cross hatched, have equal areas. Gain stabilizer events and main channel ^{60}Co gamma ray events are rejected if an event occurs in any of the anticoincidence shield elements or in a second main channel detector. This insures that prompt multiple events from charged cosmic ray interactions anywhere in the detector will not confuse the stabilizer.

The energy resolution properties of the main channel detectors are illustrated in Figures 4 and 5. Figure 4 shows the spectrum obtained with a ^{137}Cs source

Figure 4. Single detector ^{137}Cs pulse height spectrum.
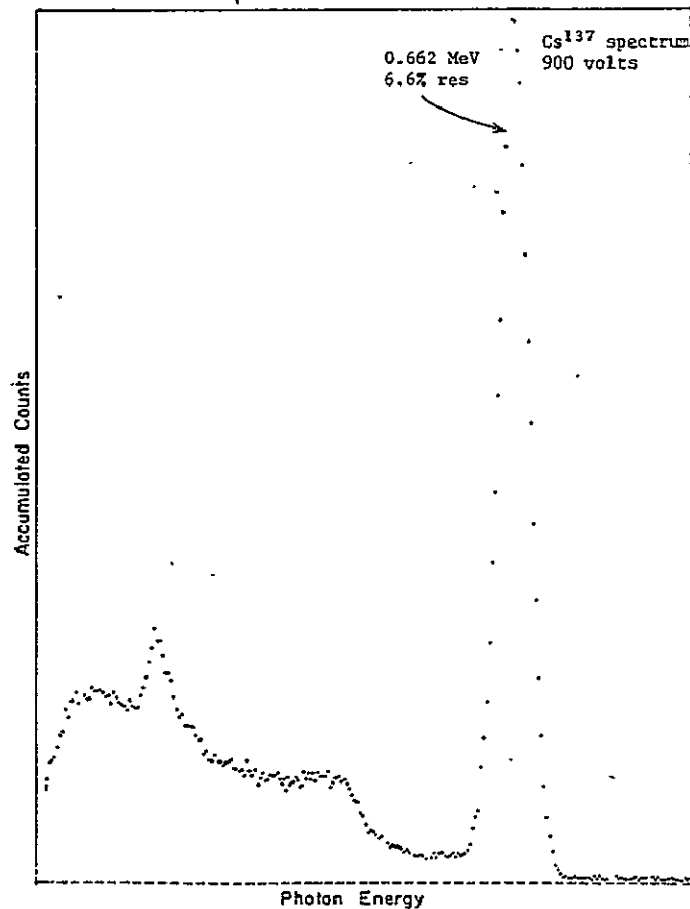
with a gamma ray line at 0.662 MeV, the energy standard used for specifying the resolution of a NaI(Tℓ) spectrometer. The FWHM energy resolution of this particular detector is (6.6 ± 0.1)% and is representative of the seven main channel detectors, the poorest of which has a standard resolution less than (6.9 ± 0.1)%. Under gain stabilizer operation the main channel detector energy

Figure 5. Single detector pulse height spectrum obtained using a ^{241}Am-Be source.
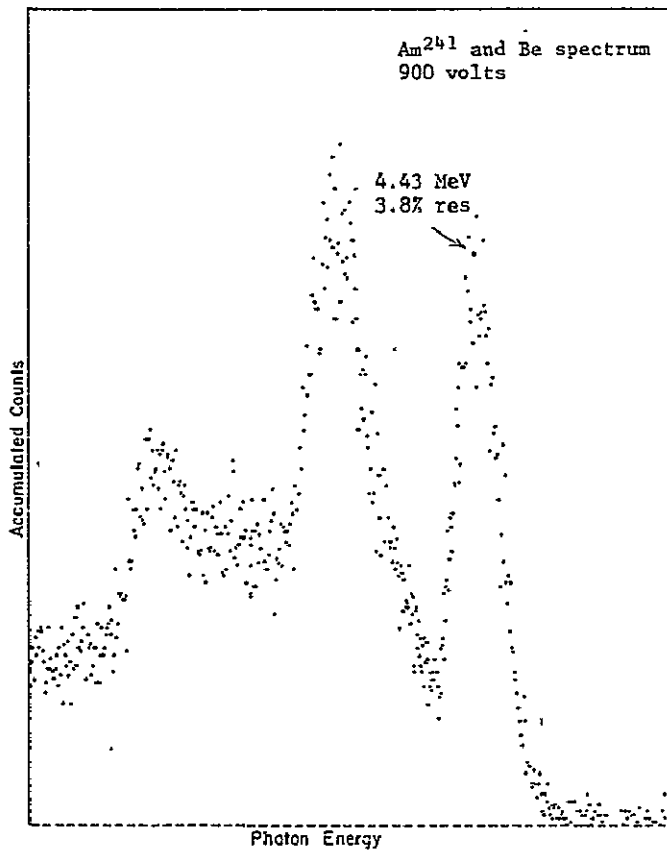
resolution in the singles or sum modes will be less than 7% at 0.662 MeV. The energy resolution expected at the energy of the ^{12}C deexcitation line, 4.43 MeV, is determined from the spectrum shown in Figure 5, which was obtained using an ^{241}Am-Be neutron source. The 4.43 MeV gamma ray results from the reaction ^{9}Be$(\alpha,n)^{12}$C*. The resulting energy resolution is 3.8% FWHM for the same detector used to obtain the data in Figure 4. The 0.51 MeV photon escape peaks will be strongly suppressed in the SMM instrument because of the operation of the various anticoincidence shield elements, most of which have a high efficiency for detecting 0.5 MeV annihilation photons. The expected energy resolution, expressed in energy units, versus incident photon energy is shown in Figure 6 on the right ordinate. These data are preliminary but are representative of what is expected from the completed instrument.

Figure 6. Preliminary estimates of the basic detector properties.

Energy Resolution

Effective Area (cm²)

Energy Resolution (keV)

Effective Area
—— Single Detector
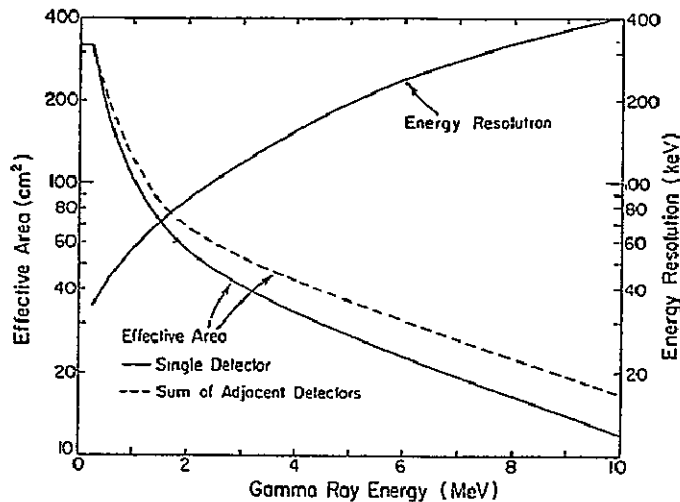--- Sum of Adjacent Detectors

Gamma Ray Energy (MeV)

Figure 6 shows *preliminary* data on the effective area or photopeak sensitivity of the 7 main channel detectors. The lower curve is derived from spectra which are obtained in the singles mode and the upper curve from the summed singles and multiple mode spectra. The data in this figure are a composite taken from several sources:

- Calculations for a 7.6 cm x 7.6 cm NaI geometry by Berger and Selzer. (1964) and Birks (1964),

- A detailed Monte Carlo simulation of the SMM detector geometry carried out by our NRL co-investigators (Kinzer et al., 1977), and

- Actual calibration data from a UNH balloon instrument which used 7 NaI(Tℓ) spectrometers in a geometry very similar to that of the SMM detector.

Dividing the total counting rate in a line by the effective area shown in Figure 6 gives the incident photon flux in that line.

It should be noted that calibration data to be taken with the completed instrument in September 1978 will provide final preflight verification of the energy dependent photopeak sensitivity (or effective area), as well as the energy resolution.

The capabilities of the various detectors in the instrument are listed in Table 2. For the main channel, the energy range for pulse height analysis can be extended up to ∿ 17 MeV by command but ·this will also increase the lower energy for analysis to ∿ 0.7 MeV. This mode will only be activated later in the mission specifically to look for evidence of the 15.11 MeV ^{12}C line in very large flares (cf. Crannell et al., 1977). As mentioned earlier, complete main channel energy spectra are accumulated for ∿ 16 sec for both the singles and multiple mode data; therefore, the minimum time resolution obtainable with these spectra is also 16 sec. However, separate fast time (2 sec) accumulation and readouts are available for three energy intervals. These fast time resolution energy intervals are set at 4.2-4.6 MeV, 4.6-5.6 MeV, and 5.6-6.4 MeV so that the time history of prompt gamma ray lines from ^{12}C and ^{16}O at 4.4 and 6.1 MeV can be studied. This possibility exists, however, only for flares as large or larger than that on 4 August 1972. In addition, a single energy window covering the energy range 350-400 keV for bursts of photons is readout every 0.064 sec for ultrafast time resolution study of bursts of hard X-rays. Again the setting of this window is optimized for very large events so information will be available on the time behavior of fast electrons in a flare.

The full main channel detector only is covered with a separate filter to absorb the intense X-ray flux so pulse pileup effects in the main channel spectra are minimized. This "forward closeout", which is placed outside the experment's thermal shield, consists of a sandwich of 10 mil of Aℓ and 20 mil of Pb.

The basic properties of the high energy detector were described earlier; however, this part of the detector is in principle also sensitive to energetic neutrons (> 20 MeV) as indicated in Table 2. A neutron signature can be identified by a pattern of events in the high energy matrix, distinct from that produced by the high energy gamma rays. Also, in a large flare producing a copious flux of both forms· of radiation, the neutron flux should extend over a larger time period and be delayed by several minutes with respect to the gamma radiation.

The basic purpose of the X-ray detectors is to have correlated X-ray data for identification of the time periods when electron acceleration is occurring at the Sun. It is during these same time periods when it is likely that protons

Table 2   568

Experiment Capabilities*

SEVEN 7.6 cm x 7.6 cm NaI SCINTILLATORS

MAIN DETECTOR

Energy Range:	0.3 TO 17 MeV
Energy Resolution:	$\Delta E/E \leq 7.0\%$ at 0.662 Mev
Intensity Range:	(Fluxes for a typical line)
Minimum Flux	10^{-3} photons $cm^{-2}sec^{-1}$
Maximum Flux	10 photons $cm^{-2}sec^{-1}$
Detection Sensitivity:	20 to 300 cm^2 gamma ray photopeak sensitivity
Temporal Resolution:	16.38 sec (full energy range) 2.05 sec (three energy intervals) 0.064 sec (0.1 to 0.3 MeV)

NaI - CsI SCINTILLATORS

HIGH ENERGY DETECTOR

Gamma Rays:	10 to 100 MeV
Energy Resolution:	$\Delta E/E \sim 1$ (24-Element Matrix)
Intensity Range:	
Minimum Flux	10^{-3} photons $cm^{-2}sec^{-1}$
Sensitivity:	120 cm^2
Neutrons:	>20 MeV
Intensity Range:	
Minimum Flux	3×10^{-2} neutrons $cm^{-2}sec^{-1}$
Sensitivity:	7.5 cm^2
Temporal Resolution: (n and γ)	2 sec

NaI SCINTILLATOR

X-RAY DETECTOR

Energy Range:	10 to 180 keV
Energy Resolution:	$\Delta E/E \sim 1$ (4 channels)
Intensity Range:	
Minimum Flux	~ 10 photons $cm^{-2}sec^{-1}$
Maximum Flux	$\sim 10^6$ photons $cm^{-2}sec^{-1}$
Detection Sensitivity:	2 cm^2 to 20 cm^2
Temporal Resolution:	1 sec

CALIBRATION

Main Detector:	3	Co^{60} gated sources (night)
X-ray Detector:	1	Am^{241} gated source (night)

* The information in this table is based on pre-calibration estimates and therefore is not final.

and other ions producing the nuclear excitation will be accelerated. It should be noted that complete calibration of the main channel and the X-ray detectors occurs during orbital nighttime or approximately every 90 min.

3. EXPECTED RESULTS

Two major improvements have been made in the SMM instrument as compared to the gamma ray spectrometer on OSO-7. First, the earlier instrument utilized a single 3" x 3" NaI(Tℓ) crystal in a rotating spacecraft with an observing duty cycle of 25%, whereas the SMM instrument uses seven 3" x 3" NaI(Tℓ) crystals with a solar observing duty cycle of .100%. Second, full SMM spectra from 300 keV to 9.0 MeV will be accumulated in 16 sec intervals as compared to the 180 sec accumulation time for the OSO-7 experiment. With the larger SMM instrument, it is expected that many more solar gamma ray events will be seen. In Figure 7 we show a plot of the predicted intensity of a solar gamma ray line

Figure 7. Preliminary estimate of gamma ray flare size relative to that of 4 August 1972 necessary to produce an average intensity at 4.4 MeV to be detectable at the 99% confidence level. The detectable intensity is plotted vs. integration time. (The final curve will be determined by the observed inflight background.)
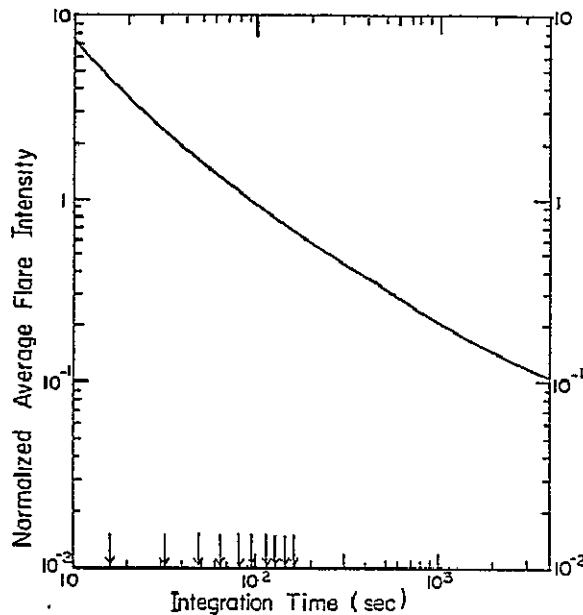
at 4.4 MeV that can be detected for different spectrum integration times. The ordinate.gives the flare intensity normalized to the average flux estimated for the 4.4 MeV line in the 4 August 1972 flare, which was $\sim 3 \times 10^{-2}$ photons $cm^{-2}sec^{-1}$ (Chupp et al., 1975). The curve shown applies to a measurement at the 99% confidence level, which means there is a 99% chance that a given observation of the gamma ray line would be due to an actual solar emission rather than to a fluctuation in the background counting rate [see the earlier paper in these proceedings by Chupp (1978) describing the likelihood method of analysis which we use for calculating this confidence level]. As can be seen, in an integration time of $\sim$ 95 sec ($\sim$ 6 spectral accumulations), it will be possible to identify a spectral line at 4.4 MeV having an intensity level equal to that believed to have been emitted in the 4 August 1972 flare. Correspondingly in $\sim$ 1000 sec it will be possible to detect a 4.4 MeV line intensity of 0.2 of that of the 4 August intensity. This would correspond to a flux of $\sim 6 \cdot x \ 10^{-3}$ photons $cm^{-2}sec^{-1}$. It should be noted that we have assumed that the average gamma ray intensity is constant over the integration time but this may not be the case in practice. Finally, the arrow marks on the abscissa indicate successive basic 16 sec accumulation intervals.

Figure 8 shows a hypothetical solar gamma ray flare counting rate spectrum expected during a 1000 sec exposure to a flare having the gamma ray intensity of the 4.August 1972 flare. This curve is a result of folding the estimated SMM instrument response function generated by Kinzer et al. (1977) into the theoretical flare gamma ray spectrum calculated by Ramaty et al. (1975). It should be recalled that the only experimentally observed lines reported by Chupp et al. (1975) were at 0.51 and 2.22 MeV with suggestions of lines at 4.4 and 6.1 MeV. The other lines shown in Figure 8 are based on the model developed by Ramaty et al. (1975) using standard solar abundances and an assumed spectrum of solar cosmic rays having the same composition. In constructing Figure 8, Kinzer et al. (1977) have superimposed the calculated solar flare spectrum on a predicted background spectrum consisting of contributions from the cosmic diffuse radiation, the Earth's atmosphere, spacecraft background, and a solar gamma ray continuum reported by Suri et al. (1975). A fixed channel width of 20 keV was used in constructing Figure 8 which is reasonable for lines above 1 MeV. In the half MeV region the detector's ability to resolve the 0.511 MeV line is misrepresented. The presence of this line can be seen in Figure 8 but

at the finer channel resolution, of which the SMM detector is capable, this line will be resolved.

Figure 8. Energy spectrum expected during a 1000 sec exposure to a flare having the intensity of the 4 August 1972 flare. Note that the 0.511 MeV line would be resolved with narrower channel width at low energies.
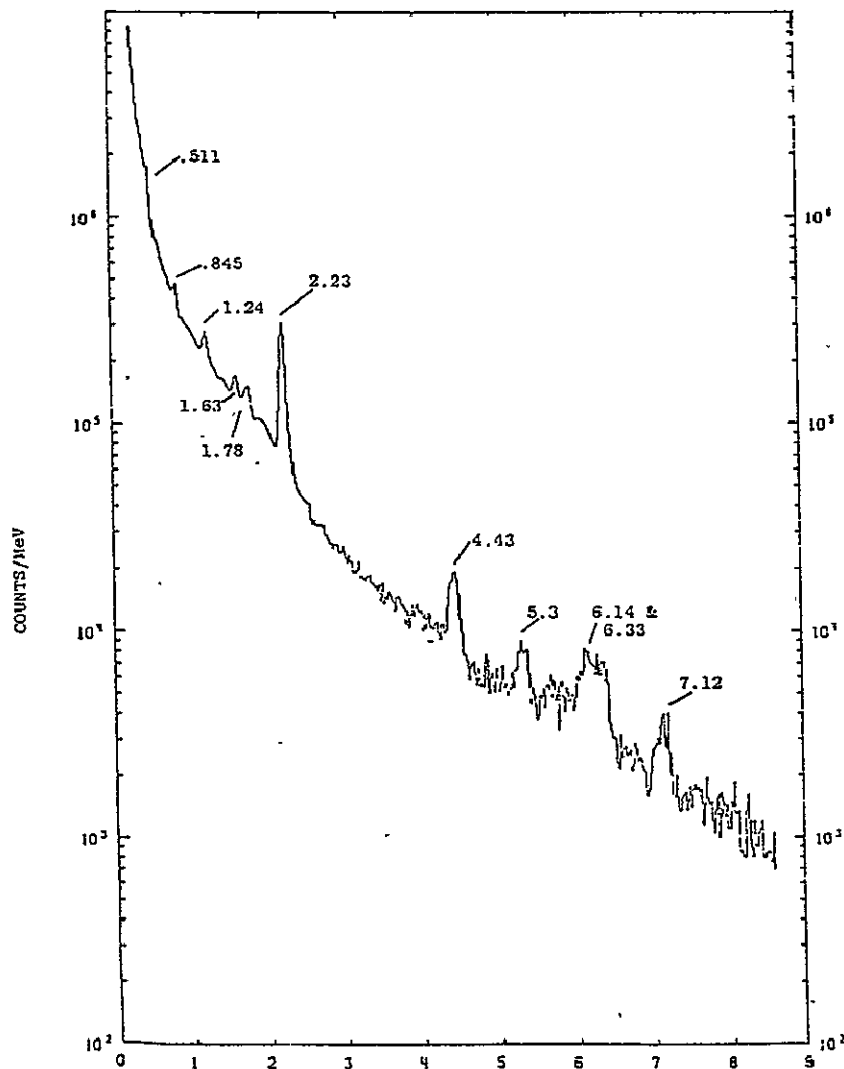

4. GAMMA RAY LINE PARAMETERS

In order to perform gamma ray spectroscopy with the SMM instrument, one must determine accurately its ability to measure the peak energy position and the

width of a gamma ray spectral line. These two quantities depend basically on the energy resolution of the detector (see Figure 6) and the counting statistics available for a given solar gamma ray line event. One of the most interesting applications of such observations would be to measure a Doppler shift in the position of a prompt line such as the 4.4 MeV ^{12}C line, which could indicate the direction of motion of the solar cosmic rays at the Sun as suggested by Ramaty and Crannell (1976).

We have made a preliminary study of this aspect of the SMM instrument's capability by carrying out a Monte Carlo simulation using an assumed incident flux of 4.4 MeV photons and a continuum flux of photons corresponding to strongly broadened lines or a hard X-ray continuum. First, a Monte Carlo run was made with the spectral line at its proper location but broadened by the instrument's

Figure 9. Monte Carlo simulation for 4.44 MeV photons on
SMM project. Dark curves - no Doppler shift;
light curves - 50 keV blue Doppler shift.
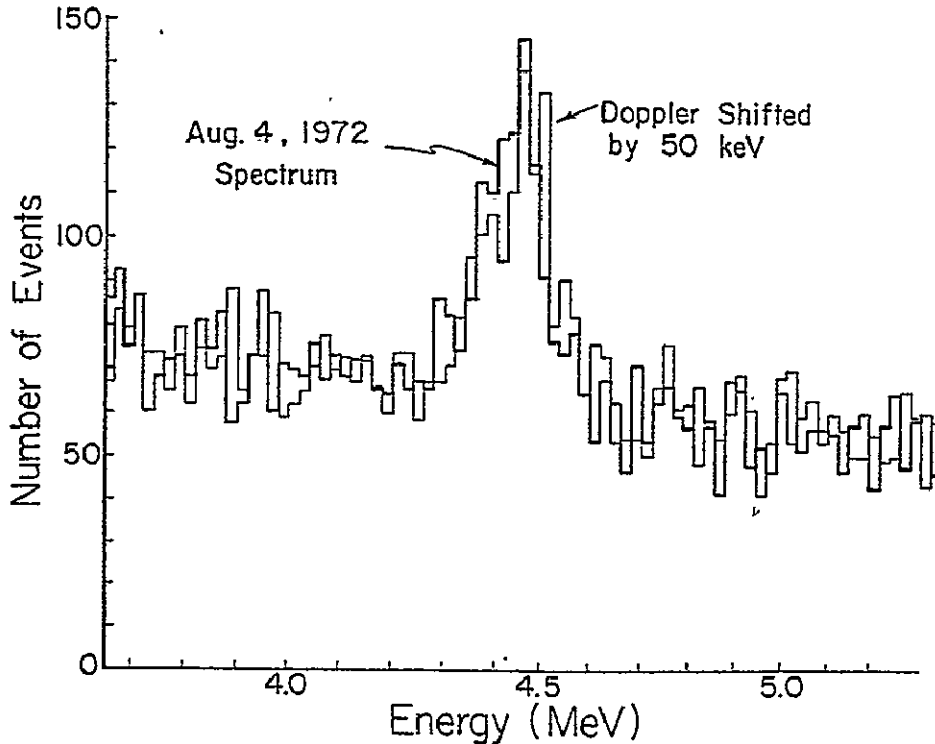
response function followed by introducing an artificial blue Doppler shift of 50 keV in the line's position.

The two resulting spectra are shown in Figure 9. A separation of the two peaks at ∿ 4.4 MeV is just discernable to the eye; however, no detailed statistical analysis of the significance of this shift has as yet been carried out. In Figure 10, we show the corresponding results for the case of a 100 keV blue shift. In this case, the shift is clearly discernable. The integrated counts used in this Monte Carlo simulation correspond to a gamma ray flare comparable to the 4 August 1972 event observed over a total time of 1000 sec. Further studies of the SMM detector's ability to detect Doppler shifts will be carried out after the instrument calibration is completed.

Figure 10. Monte Carlo simulation for 4.44 MeV photons on SMM project. Dark curves – no Doppler shift; light curves – 100 keV Doppler shift.
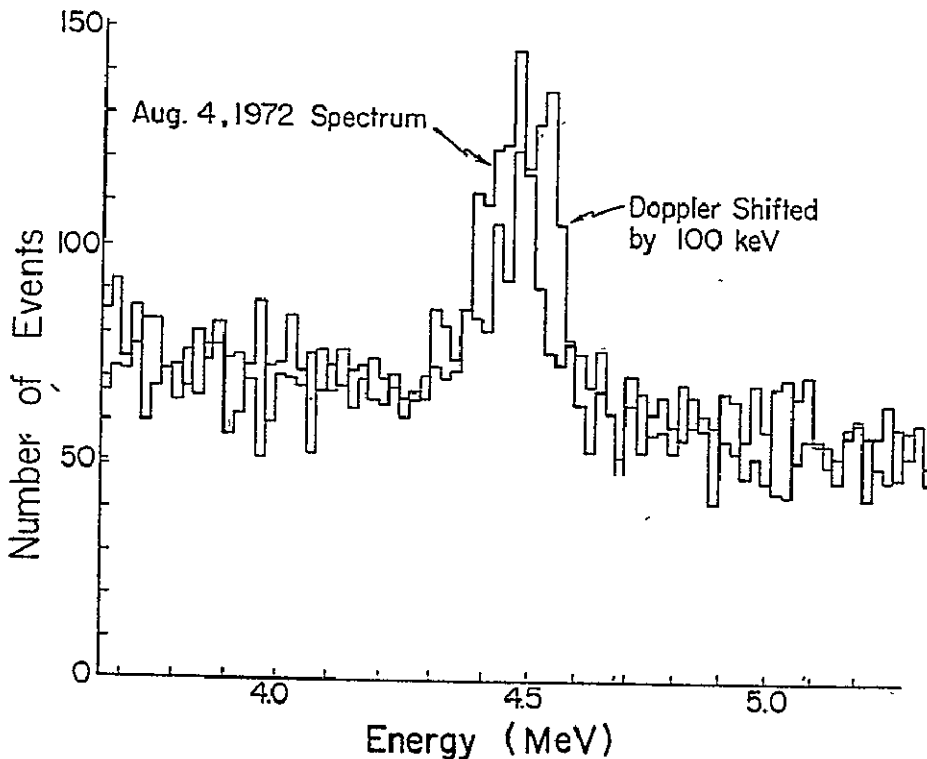
In conclusion, the SMM gamma ray instrument has been designed to detect gamma ray lines with > 99% confidence ·in the range 0.3 MeV to 17 MeV from flares significantly smaller than those of August 1972. Improved energy and time

resolution, increased sensitivity and observational coverage, and extended energy range compared to the OSO-7 instrument give the SMM instrument the capability of substantially refined solar gamma ray spectroscopy.

ACKNOWLEDGEMENTS

REFERENCES

Berger, M. J., and Seltzer, S. M.: 1964, Tables of Energy Losses and Ranges of Electrons and Positrons, NASA SP-3012.

Birks, J. B.: 1964, The Theory and Practice of Scintillation Counting, Pergamon Press, Oxford, England.

Chupp, E. L.: 1978, In these proceedings, see page 42.

Chupp, E. L., Forrest, D. J., and Suri, A. N.: 1975, in S. Kane (ed.) Proceedings of the IAU-COSPAR Symposium, D. Reidel Publishing Company, 68.

Crannell, C. M., Ramaty, R., and Crannell, H.: 1977, Proceedings of 12th ESLAB Symposium, Frascati, Italy, 24-27 May, 213.

Forrest, D. J. and collaborators: 1979, (in preparation).

Forrest, D. J., Higbie, P. R., Orwig, L. E., and Chupp, E. L.: 1972, Nucl. Instrum. Methods 101, 567.

Kinzer, R. L., Kurfess, J. D., Johnson, W. N., and Share, G. H.: 1977 "Monte Carlo Simulation of the SMM γ-Ray Detector", Unpublished Naval Research Report for SMM project collaboration.

Ramaty, R., Crannell, C.: 1976, Astrophys. J. 203, 766.

Ramaty, R., Kozlovsky, B., and Lingenfelter, R.E.: 1975, Space Sci. Rev. 18, 341.

Seiple, A. and collaborators: 1979, (in preparation).

Suri, A. N., Chupp, E. L., Forrest, D. J., and Reppin, C.: 1975, Solar Phys. 43, 415.

$D4B/-12$

N78-32013

THE GAMMA RAY OBSERVATORY

Albert G. Opp

Astrophysics Program
National Aeronautics and Space Administration
Washington, DC   20546

The Gamma Ray Observatory (GRO) will be a large, free-flying space observatory dedicated to the study of the sky in gamma rays. For the purpose of GRO, gamma rays are defined as photons with energies greater than ~100 keV.

The GRO spacecraft will weigh about 10,000 kg, with about 6,500 kg available for scientific instruments, providing about 400 watts of power to the instruments, and about 12,000 bits per second of telemetry. The spacecraft will be launched by the Space Shuttle into a 400 to 500 km circular orbit, inclined at 28.5° to the equator. Launch is planned for 1984. The spacecraft will be three-axis stabilized, with orientation capability of about 20 arc minutes and aspect determination of 2 arc minutes. Absolute timing of 0.1 millisecond will be provided by the spacecraft. The instruments will be co-aligned along one axis of the spacecraft to optimize the spectral coverage of a particular region. We are planning a two-year mission, and are studying possible retrieval by the Shuttle at the end of the mission.

The objectives of GRO are, briefly: to locate and characterize gamma ray sources, in particular peculiar objects such as pulsars, to study diffuse gamma ray emission, both from our galaxy and from extragalactic space, to investigate other galaxies, especially radio galaxies, Seyfert galaxies and QSOs, and to understand the origin of gamma ray bursts.

Gamma ray spectroscopy is one of the important objectives of GRO. Major astrophysical problems such as the origin of the·elements, the nature of compact objects, and particle acceleration could receive answers from observational results obtained by a spectroscopy experiment on this Observatory.

To meet these objectives, a complement of four or five instruments will be selected to fly on GRO. For the purpose of the GRO definition study, the High Energy Astrophysics Management Operations Working Group came up with a 'strawman' payload for GRO, which included one spectroscopy experiment. The actual payload is to be selected following an Announcement of Opportunity (AO), which was released in November 1977. Proposals were due in February 1978. Seventeen proposals were received from 37 different organizations, representing 50 research groups and 150 individual participants. The proposals were reviewed by a peer review subcommittee in May 1978; it is expected that the payload will be chosen before September 1978.

The Gamma Ray Observatory is not yet an approved mission. The Astrophysics Program is recommending it as a new start in fiscal year 1980. It is hoped that this Observatory, carrying a full complement of gamma ray detectors, could firmly establish gamma-ray spectroscopy as a new and vigorous observational science.

OMIT TO END

SYMPOSIUM SUMMARY

L. E. Peterson*
Physics Department
University of California at San Diego
La Jolla, CA   92037

This conference marks the transition from the earlier age of such things as conferences on shielding against background in gamma-ray astronomy to the new age of high-resolution gamma-ray astrophysics. Those struggles have borne fruit in that now we have not only some ideas regarding how to do gamma-ray astronomy, but also excellent preliminary results. With these results, gamma-ray astronomy has moved out of the exploratory era into the time when observations on a serious and intensive basis are needed next. We have seen some older results reviewed here and we have seen new results, with a good deal of discussion in the theoretical context regarding the interaction of these results with the rest of astrophysics.

The first spectroscopic measurements in gamma-ray astronomy were obtained on solar flares, both following theoretical predictions and prompting a considerable amount of theoretical study, in particular such as by Ramaty and Lingenfelter. In solar flares are seen a series of complex lines which are due primarily to the interaction of energetic particles in the solar atmosphere. The intensities of these lines are quite high, observationally, being found to be on the order of a few tenths of a gamma-ray per cm^2 per second. However, the upper limits on cosmic sources that have persisted over the past decade are around 10^{-3} photon per cm^2 per second, at the sensitivity threshold of detectors which have been flown up the present time. At this conference we have been presented with new results which, as I have indicated, confirm some of the older results with observations at that intensity level.

---

*Transcribed by the Editors from the author's tape-recorded talk given at the Symposium.

One of these is the nice work which has been done by Leventhal, MacCallum and Stang at the Bell Telephone and Sandia Labs. In this measurement, the previous observation of Bob Haymes of the 511-keV annihilation gamma ray line from the galactic center region was indeed confirmed. This gives a flavor to the sort of observations we would all hope to make. It indicates the kind of labor that is necessary in order to produce such an accomplishment. This narrow line measurement is a remarkable discovery, and the verification of the 0.5 MeV line is, I think, a keynote to the work that we have seen presented here. The interpretations one can do in an astrophysical sense with this line involve the nature of the interstellar medium near the galactic center, the forms of the annihilation of the positrons, the nature of the positron production mechanisms, and the density and the types of matter in the regions in which these reactions occur.

One source process of narrow-line spectra which was not predicted in early times, but has since proven very important and was much discussed at this meeting, is revealed by the beautiful observations of the Max Planck Institute of the cyclotron line emission from Hercules X-1. The results were presented here by Dr. Trümper, and the comparisons with some of the other measurements have been cleared up, as I see it, at this conference. First of all, the observations of Dr. Trümper were made with an instrument that is considerably more sensitive than the previous instruments that produced the earlier null results. Those were primarily a consequence, I think, of sensitivity limitations which were essentially at the threshold of detection of this particular line. In addition to the verification of the intensity levels close to those reported, the question of time variations of this line is just beginning to unfold; this study will undoubtedly produce much new information useful for the theoretical work which was also discussed at this meeting. I might say

that Dr. Trümper gave a beautiful tutorial on the cylcotron line emission
process, and, in fact, we heard here of a variety of the different kinds of
calculations which involve the details of the mechanisms modelled for the
production of this line. Certainly, much important astrophysical information
can be obtained from the study of this line and its harmonics, regarding the
intensity of the magnetic field, the location of the emission process, the
geometry of the source, and so on; this is what the significance of what these
observations are about.

Another type of observation was reported by the JPL group, of the trans-
ient event observed with germanium detectors. This is a very different class
of activity – a 20 minute transient event in which lines were observed at a
number of different energies. An interpretation which was indicated at this
Conference, due to Lingenfelter, is that these lines may be due to nuclear
processes, such as have been calculated for solar flares, but occurring near
the surface of a neutron star. Several of the talks heard were associated with
theoretical processes which may occur near compact objects; the above interpre-
tation of the JPL event, speculative of course, is that indeed some of these
processes could be observed. This is a good indication, I think, of the viable
kind of interaction between observation and theory that was amply demonstrated
at this Conference.

Another kind of result, not necessarily related to gamma-ray line astronomy,
but which has to do with the general production of gamma rays in distant objects,
was reported by Schönfelder, also of the Max Planck Institute. He reported the
detection of gamma-rays from a discrete source, the Seyfert galaxy NGC4151. The
cosmological implications of this particular discovery concern the origin of the
diffuse gamma-ray component which could be due to the superposition of discrete
source of this type. Being an observationalist, or a 'screwdriver man' more

precisely, I regard many of the mechanisms which were discussed here as being speculative rather than theory, but nevertheless I think these are important for driving the rest of us to produce better observations and for setting a tone to an observational science. Such mechanisms are all involved. In stellar flares, for example, the gamma rays are produced by the process associated with setting up the magnetic fields; the mechanisms associated with the production of light elements and the distribution of these elements in the interstellar medium and the acceleration of cosmic rays are also related to gamma ray line production. There is production associated with supernovae, in which the material is ejected and appears eventually in the interstellar medium while still radioactive. Sources of gamma ray lines are also associated with nova explosions.

Another indication of the viability of this discipline has been demonstrated by the discussions that have taken place in the workshops and experiment sessions where we heard three different but somewhat related topics. First, we heard about detectors and the various processes which are associated with detection phenomena, the observation of cosmic gamma rays at their low intensities and the problems involved in improving the detector sensitivities and their background and instrumental effects. Second, the measurement of nuclear cross sections in laboratory experiments are essential both in order to interpret the astrophysical phenomena and, for us as experimentalists and observationalists, to use these cross sections in order to understand our instrumental and background effects. And third, we have heard about the new experiments to be flown in upcoming spacecraft missions.

To summarize what has taken place at this meeting, then, I think we have seen gamma-ray line astronomy moving from an exploratory phase into a phase where a great amount of theoretical work is occurring, and where the observational work needs to be moved into its intense phase.

The future! First, older data sitting on magnetic tapes must be analyzed. I think one of the elements of this conference had to do with the kinds of effort, the intensity, the methods and the caution which one must use in analyzing these data in order to make sure that the results that we publish are understood and are significant. I think a lot of confusion was clarified in the experimental situation at this particular meeting. Second, there are instruments that will soon be flown, as we heard, both on balloons and on upcoming spacecraft in the next several years; these certainly will produce significant results. We have to think in terms of sensitivity: The sensitivity we have seen so far is on the order of 10^{-3} photons per centimer^2 per second for lines in this energy range. Instruments are designed and are about to be flown, such as one on the HEAO-C, which will have sensitivities in the 10^{-4} range. We have seen already what a small improvement in sensitivity over the past few years has done to this field. So improving it by an order of magnitude, which is possible in the next 5 years, will undoubtedly produce new observational results. Many different conflicting theories have to be tested and proven by the next step in observational sensitivity. By the early 1980's there is a possiblity of having a very much larger observatory, the Gamma Ray Observatory, which will be capable of carrying instruments, not of hundreds of kilograms weight, but measured in masses of 1000 or 2000 kilograms. It is this kind of massive instrument that is required in order to get the sensitivity level into the 10^{-5} photon per centimeter^2 per second range, which is certainly the next observational goal. Finally, more sophisticated, larger area, larger volume instruments must also be flown on balloons. These will become the instruments and the vehicles which we will be using to expand our science for the future.

To summarize this meeting, I think we have all been caught up in the

spirit and the progress that has taken place here. I think we should all contribute to the proceedings of this conference, which are to be published soon. I think it is not unlikely that this conference, amalgamating and collecting a number of diffuse results and setting a tone for the future, will have the same place in the history of gamma-ray astronomy as did the workshop held here on solar flares, way back in 1963.

I think we must thank the organizers of this conference for being very successful in terms of having these people together at an opportune moment in time and at the same time providing a very pleasant and productive meeting.

PROGRAM OF THE SYMPOSIUM

GAMMA RAY SPECTROSCOPY IN ASTROPHYSICS

PROGRAM

APRIL 28, 1978

8:30 AM – Registration

9:00 AM, Morning Session, Chaired by T. L. Cline
(Goddard Space Flight Center)

R. S. Cooper (Director, Goddard Space Flight Center)
Opening Remarks

R. Ramaty (Goddard Space Flight Center)
Theoretical Overview . . . . 20 min.

E. L. Chupp (University of New Hampshire)
Observational Overview . . . . 20 min.

K. C. Hurley (CESR, Toulouse, France)
*Signe 2MP Observations of the 1977,
November 22 Flare* . . . . 10 min.

R. P. Lin (University of California, Berkeley)
Gamma Ray Lines and Solar Flares . . . . . 10 min.

S. A. Colgate (Los Alamos Scientific Laboratories)
*Nuclear Gamma Rays from
Stellar Flares* . . . . 10 min.

J. I. Trombka (Goddard Space Flight Center)
*Discrete Gamma Ray Lines from
the Moon.* . . . . 10 min.

10:45 AM – Coffee

11:00 AM

M. Leventhal (Bell Telephone Laboratories)
*High Resolution Search for Gamma
Ray Lines from the Galactic Center,
Cen A and Cen X-3.* . . . . 20 min.

G. Vedrenne (CESR, Toulouse, France)
*Results of the CESR 1977 Southern
Hemisphere Balloon Flight.* . . . . 10 min.

D. Gilman (Jet Propulsion Laboratory)
*The Galactic Gamma Ray Flux in the
0.6 to 5MeV Range.* . . . . 10 min.

V. Schonfelder (MPI, Garching, Germany)
*Gamma Ray Line Spectroscopy with
a Compton Telescope* . . . . 10 min

R. S. White (University of California, Riverside)
*Search for Broad Gamma Ray Lines
with the UCR Double Compton
Telescope* . . . . 10 min.

C. A. Meegan (Marshall Space Flight Center)
*Results from the 1977 Flight of the
Rice University Gammascope* . . . . 10 min.

12:30 PM – Lunch

2:00 PM, Afternoon Session, Chaired by D. D. Clayton
(Rice University)

A. S. Jacobson (Jet Propulsion Laboratory)
*Observational Evidence for Extrater-
restrial Gamma Ray Line Sources.* . . . . . 20 min.

J. L. Matteson (University of California, San Diego)
*Observations with the A4 Experi-
ment on HEAO-1.* . . . . 10 min.

R. E. Lingenfelter (University of California, Los Angeles)
*Nuclear Gamma Rays from
Compact Objects* . . . . 20 min.

K. Brecher (Massachusetts Institute of Technology)
*Gamma Ray Lines from Neutron
Stars as Probes of Fundamental
Physics* . . . . 10 min.

H. Reeves (CEN, Saclay, France)
*Nuclear Lines and the Nucleo-
Synthesis of the Light Elements.* . . . . . . 10 min.

C. J. Crannell (Goddard Space Flight Center)
*Gamma Ray Line Emission Above
8MeV* . . . . 10 min.

W. D. Arnett (University of Chicago)
Gamma Ray Lines from Supernovae . . . 10 min.

J. W. Truran (University of Illinois)
Gamma Ray Lines from Novae . . . . 10 min.

4:00 PM – Coffee

4:30 PM, Workshop on Gamma Ray Line Detector
Characteristics
Coordinated by G. J. Fishman
(NASA Headquarters)

Topics: *Detection Techniques, Detector Materials,
Background Effects.* . . . . 60 min.

Contributors: J. D. Kurfess (Naval Research Lab-
oratory), K. N. Long (Columbia University)
W. A. Mahoney (Jet Propulsion Laboratory),

A. E. Metzger (Jet Propulsion Laboratory),
R. Novick (Columbia University), R. H. Pehl
(University of California, Berkeley),
J D Willett (Jet Propulsion Laboratory)

**6:00 PM – Cocktails and Dinner at the Goddard
Recreation Center**

APRIL 29, 1978

**9:00 AM, Morning Session, Chaired by M. Shapiro
(Naval Research Laboratory)**

J. Trumper (MPI, Garching, Germany)
Cyclotron Lines from Her X-1 . . . . 20 min.

Ph. Durouchoux (CEN, Saclay, France)
Cyclotron Lines from Her X-1 . . . . 10 min.

B. R. Dennis (Goddard Space Flight Center)
*An Upper Limit on the Cyclotron
Lines from Her X-1 as Observed by
OSO-8* . . . . 10 min.

J. K. Daugherty (Durham, North Carolina)
Theory of Cyclotron Line Emission . . . . 10 min.

R. W. Bussard (Goddard Space Flight Center)
*The Excitation of Energy Levels in
Strong Magnetic Fields by Photons
and Particles* . . . . 10 min.

R. P. Weaver (Goddard Space Flight Center)
*Transfer of Cyclotron Lines through
the Magnetospheric Shell of Her X-1* . . . . 10 min.

P. Meszaros (MPI, Munich, Germany)
Theory of Cyclotron Line Emission . . . . 10 min.

10:30 AM – Coffee

**11:00 AM, Workshop on Laboratory Accelerator
Measurements
Coordinated by N. S. Wall (University of Maryland)**

Topic: *Nuclear Cross Sections of
Astrophysical Significance* . . . . 60 min.

Contributors: D. Bodansky (University of Wash-
ington), C. J. Crannell (Goddard Space Flight
Center), H. L. Crannell (Catholic University),
P. L. Dyer (Michigan State University), J. R.
Lapides (University of Maryland), W. Hornyak
(University of Mayland), D. R. Maxson (Brown
University), R. Ramaty (Goddard Space Flight
Center), J. I. Trombka (Goddard Space Flight
Center)

12:30 PM – Lunch

**2:00 PM, Afternoon Session, Chaired by T. L. Cline
(Goddard Space Flight Center)**

B. J.Teegarden (Goddard Space Flight Center)
*High Resolution Spectroscopy on
ISEE-C.* . . . . 10 min.

G. H. Nakano (Lockheed, Palo Alto)
*High Resolution Spectroscopy on
the Air Force S78-1 Satellite* . . . . 10 min.

J. C. Ling (Jet Propulsion Laboratory)
*High Resolution Spectroscopy on
HEAO-C.* . . . . 10 min.

D. J. Forrest (University of New Hampshire)
*Solar Gamma Ray Astronomy
on SMM* . . . . 10 min.

F. B. McDonald (Goddard Space Flight Center)
The GRO Mission . . . . 10 min.

L. E. Peterson (University of California, San Diego)
Conference Summary. . . . . 20 min.

4:00 PM – Adjournment

NOTES:

LIST OF PARTICIPANTS

ett, W. D.
ico Fermi Inst.
versity of Chicago
3 E. 56th St.
icago, IL 60637

douze, J.
ntre National de La Recherche Scientifique
stitut D'Astrophysique
bis, Blvd. Argo
014 Paris
ANCE

lasubrahmanyan, V. K.
boratory for High Energy Astrophysics
ddard Space Flight Center
eenbelt, MD 20771

dansky, D.
partment of Physics
iversity of Washington
attle, WA 98195

ldt, E. A.
boratory for High Energy Astrophyiscs
ddard Space Flight Center
eenbelt, MD 20771

echer, K.
partment of Physics
ssachusetts Institute of Technology
mbridge, MA 02139

ssard, R. W.
boratory for High Energy Astrophysics
ddard Space Flight Center
eenbelt, MD 20771

nuto, V. M.
ddard Institute for Space Studies
80 Broadway
w York, NY 10025

sarsky, C. J.
ntre d'Etudes Nuclearies de Saclay
P. No. 2
Gif-sur-Yvette
ANCE

erry, M.
ysics Department
iversity of New Hampshire
rham, NH 03824

Chupp, E. L.
Physics Department
University of New Hampshire
Durham, NH 03824

Clayton, D. D.
Department of Space Physics & Astronomy
Rice University
Houston, TX 77001

Cline, T. L.
Laboratory for High Energy Astrophysics
Goddard Space Flight Center
Greenbelt, MD 20771

Coe, M. J.
Laboratory for Astronomy and
   Solar Physics
Goddard Space Flight Center
Greenbelt, MD 20771

Colgate, S. A.
Los Alamos Scientific Laboratory
Los Alamos, NM 87545

Cotin, M.
CEA-CEN Saclay
B. P. #2
Gif-sur-Yvette 91
FRANCE

Cooper, R. S.
Director, Goddard Space Flight Center
Greenbelt, MD 20771

Cramer, J. G.
Nuclear Physics Laboratory
University of Washington
Seattle, WA 98195

Crannell, C. J.
Laboratory for Astronomy and
   Solar Physics
Goddard Space Flight Center
Greenbelt, MD 20771

Crannell, H.
Physics Department
Catholic University of America
Washington, D.C. 20064

Cutler, E. P.
Comtech
5303 Lanham Station Road
Lanham, MD   20801

Daugherty, J. K.
3017 Weymouth St, Apt. 204
Durham, NC   27707

Dean, A. J.
Department of Physics
University of Southampton
United Kingdom

Dennis, B. R.
Laboratory for Astronomy and
   Solar Physics
Goddard Space Flight Center
Greenbelt, MD   20771

Desai, U. D.
Laboratory for High Energy Astrophysics
Goddard Space Flight Center
Greenbelt, MD   20771

Dunphy, P.
Physics Department
University of New Hampshire
Durham, NH   03824

Durouchoux, P.
CEA-CEN Saclay
P. B. #2
Gif-sur-Yvette 91
FRANCE

Dyer, P. L.
Cyclotron Laboratory
Michigan State University
East Lansing, MI   48824

Evans, D. W.
Group P-4
Los Alamos Scientific Laboratory
Los Alamos, NM   87545

Falk, S. W.
Enrico Fermi Institute
University of Chicago
Chicago, IL   60637

Felten, J. E.
Laboratory for High Energy Astrophysics
Goddard Space Flight Center
Greenbelt, MD   20771

Fichtel, C. E.
Laboratory for High Energy Astrophysics
Goddard Space Flight Center
Greenbelt, MD   20771

Fishman, G. J.
Space Science Laboratory
Marshall Space Flight Center
Huntsville, AL   35812

Forrest, D. J.
Physics Department
University of New Hampshire
Durham, NH   03824

Frost, K. J.
Laboratory for Astronomy and
   Solar Physics
Goddard Space Flight Center
Greenbelt, MD   20771

Gilman, D.
Jet Propulsion Laboratory
4800 Oak Grove Drive
Pasadena, CA   91103

Grindlay, J. E.
Center for Astrophysics
60 Garden Street
Cambridge, MA   02138

Hartman, R. C.
Laboratory for High Energy Astrophysics
Goddard Space Flight Center
Greenbelt, MD   20771

Haug, E.
Laboratory for Astronomy and
   Solar Physics
Goddard Space Flight Center
Greenbelt, MD   20771

Kinzer, R. L.
Code 7128.3
Naval Research Laboratory
Washington, D.C.   20375

Haymes, R. C.
Department of Space Physics and
   Astronomy
Rice University
Houston, TX   77001

Higdon, J. C.
Planetary Science Department
University of Arizona
Tucson, AZ   85721

udson, H. S.
hysics Department.
CSD, P. O. Box 109
a Jolla, CA 92037

urley, K.
.E.S.R.
niversity of Toulouse
oulouse, FRANCE

ohnson, W. N., III
. O. Hulburt Center for Space Research
aval Research Laboratory
ashington, D. C. 20375

ones, F. C.
aboratory for High Energy Astrophysics
oddard Space Flight Center
reenbelt, MD 20771

niffen, D. A.
aboratory for High Energy Astrophysics
oddard Space Flight Center
reenbelt, MD 20771

oga, R.
ase Western Reserve University
leveland, OH 44100

urfess, J. D.
aval Research Laboratory
ashington, D.C. 20375

amb, R. C.
hysics Department
owa State University
mes, Iowa 50011

apides, J. R.
aboratory for Astronomy and
   Solar Physics
oddard Space Flight Center
reenbelt, MD 20771

eventhal, M.
oom 1E 349
ell Laboratories
00 Mountain Avenue
urray Hill, NJ 07974

ewin, W. H. G.
pace Research Center
assachusetts Institute of Technology
ambridge, MA 02139

Lin, R. P.
Space Science Laboratory
University of California
Berkeley, CA 94720

Ling, J. C.
Space Science Division
JPL, Bldg. 183-901
Pasadena, CA 91103

Lingenfelter, R. E.
Department of Astronomy
UCLA
Los Angeles, CA 90024

Lockwood, J. A.
University of New Hampshire
Durham, NH 03824

Long, K. S.
Department of Physics
Columbia University
New York, NY 10027

Maccallum, C. J.
Sandia Laboratories MS. 5231
P. O. Box 5800
Albuquerque, NM 87115

Madden, J. J.
Code 403 Project Management Directorate
Goddard Space Flight Center
Greenbelt, MD 20771

Mahoney, W. A.
Space Science Division
JPL, Bldg. 183-901
Pasadena, CA 91103

Matteson, J. L.
Physics Department
University of California, San Diego
La Jolla, CA 92093

Maurer, G. S.
Laboratory for Astronomy and
   Solar Physics
Goddard Space Flight Center
Greenbelt, MD 20771

McDonald, F. B.
Laboratory for High
   Energy Astrophysics
Goddard Space Flight Center
Greenbelt, MD 20771

McGuire, R. F.
Laboratory for High Energy Astrophysics
Goddard Space Flight Center
Greenbelt, MD 20771

Meegan, C. A.
Space Science Laboratory
Marshall Space Flight Center
Huntsville, AL 35812

Meneguzzi, M.
Princeton Observatory
Peyton Hall
Princeton, NJ 08540

Meszaros, P.
Max-Planck Insitut fur
   Physik und Astrophysik
Institut fur Extraterrestrische Physik
8046 Garching
WEST GERMANY

Metzger, A. E.
JPL
4800 Oak Grove Drive
Pasadena, CA 91103

Meyer, P.
Enrico Fermi Institute
University of Chicago
Chicago, IL 60637

Mullan, D. J.
Bartol Research Foundation
University of Delaware
Newark, DE 19711

Muller, D.
University of Chicago
Enrico Fermi Institute
933 E. 56th Street
Chicago, IL 60637

Nakano, G. H.
Department 52-12, Bldg. 205
Lockheed Palo Alto Research Laboratory
3251 Hanover St.
Palo Alto, CA 94304

Northrop, T. G.
Laboratory for High Energy Astrophysics
Goddard Space Flight Center
Greenbelt, MD 20771

Novick, R.
Department of Physics
Columbia University
538 W. 120 St.
New York, NY 10027

Opp, A. G.
NASA Headquarters
Code SC-7
Washington, D.C. 20546

Ormes, J. F.
Laboratory for High Energy Astrophysi
Goddard Space Flight Center
Greenbelt, MD 20771

Pehl, R. H.
Lawrence Laboratory
Berkeley, CA 94720

Peterson, L. E.
Physics Department
University of California, SD
La Jolla, CA 92037

Pieper, G. F.
Director of Sciences
Goddard Space Flight Center
Greenbelt, MD 20771

Pinkau, K.
Max Planck Institut fur
   Extraterrestrische Physik
Garching bei Munchen
WEST GERMANY

Pizzichini, G.
Laboratory for High Energy Astrophysi
Goddard Space Flight Center
Greenbelt, MD 20771

Ramaty, R.
Laboratory for High Energy Astrophysi
Goddard Space Flight Center
Greenbelt, MD 20771

Reeves, H.
Centre d'Etudes Nucleaires de Saclay
B. P. No. 2, Gif-sur-Yvette
Paris, FRANCE

Reppin, C.
Max Planck Institut fur
   Extraterrestrial Physics
Garching bei Munchen
WEST GERMANY

Rose, W. K.
Astronomy Program
University of Maryland
College Park, MD 20742

Riegler, G. R.
Space Science Division
JPL, Bldg. 183-901
Pasadena, CA 91103

Schardt, A. W.
Laboratory for High Energy Astrophysics
Goddard Space Flight Center
Greenbelt, MD 20771

Schmidt, W. K. H.
Max Planck Institut fur Aeronomy
Lindau/Harz, WEST GERMANY

Schonfelder, V.
Max Planck Institute
fur Extraterrestrische Physik
Garching bei Munche
WEST GERMANY

Shapiro, M. M.
Cosmic Ray Physics Lab.
Naval Research Laboratory
Code 7020
Washington, D.C. 20375

Share, G. H.
Naval Research Laboratory
Code 7128.4
Space Science Division
Washington, D.C. 20375

Sommer, M.
Max Planck Institut fur
   Extraterrestrische Physik
Garching bei Munchen
WEST GERMANY

Staubert, R.
Astronomisches Institut der Universitat
   Tubingen
74 Tubingen, WEST GERMANY

Stecker, F. W.
Laboratory for High Energy Astrophysics
Goddard Space Flight Center
Greenbelt, MD 20771

Strickman, M. S.
Code 7128
Naval Research Laboratory
Greenbelt, MD 20771

Strong, I. B.
Physics Division MS 436
Los Alamos Scientific Laboratory
P. O. Box 1663
Los Alamos, NM 87545

Sturrock, P. A.
Institut for Plasma Research
Stanford University
via Crespi
Stanford, CA 94305

Swank, J. H.
Laboratory for High Energy
   Astrophysics
Goddard Space Flight Center
Greenbelt, MD 20771

Teegarden, B. J.
Laboratory for High Energy
   Astrophysics
Goddard Space Flight Center
Greenbelt, MD 20771

Thompson, D. J.
Laboratory for High Energy
   Astrophysics
Goddard Space Flight Center
Greenbelt, MD 20771

Thompson, M. G.
Department of Physics
University of Durham
South Road
Durham, ENGLAND

Trainor, J. H.
Laboratory for High Energy
   Astrophysics
Goddard Space Flight Center
Greenbelt, MD 20771

Trombka, J. I.
Laboratory for Astronomy and
   Solar Physics
Goddard Space Flight Center
Greenbelt, MD 20771

Trumper, J.
Max-Planck Institut fur Physik
   und Astrophysik
Institut fur Extraterrestrische
   Physik
8046 Garching, WEST GERMANY

Truran, J. W.
Department of Astronomy
University of Illinois
Urbana, IL 61801

Tueller, J.
Department of Physics
Washington University
St. Louis, MO   63130

Van Hollebeke, M.
Laboratory for High Energy Astrophysics
Goddard Space Flight Center
Greenbelt, MD   20771

Wall, N. S.
Department of Physics & Astronomy
University of Maryland
College Park, MD   20742

Weaver, R. P.
Laboratory for High Energy Astrophysics
Goddard Space Flight Center
Greenbelt, MD   20771

Webber, W. R.
Space Sciences Center
University of New Hampshire
Durham, NH   03824

White, R. C.
Institute of Geophysics & Planetary Physics
University of California
Riverside, CA   92502

Willet, J. B.
Space Science Division
JPL
4800 Oak Grove Drive
Pasadena, CA   91103

1. Report No. TM 79619	2. Government Accession No.	3. Recipient's Catalog No.
4. Title and Subtitle GAMMA RAY SPECTROSCOPY IN ASTROPHYSICS		5. Report Date
		6. Performing Organization Code 660
7. Author(s) T. L. Cline and R. Ramaty		8. Performing Organization Report No.
9. Performing Organization Name and Address Laboratory for High Energy Astrophysics NASA/GSFC Greenbelt, MD 20771		10. Work Unit No.
		11. Contract or Grant No.
		13. Type of Report and Period Covered
12. Sponsoring Agency Name and Address		
		14. Sponsoring Agency Code

15. Supplementary Notes

16. Abstract.

This volume contains the papers presented at the symposium on "Gamma Ray Spectroscopy in Astrophysics" held at the Goddard Space Flight Center on April 28 and 29, 1978

17. Key Words (Selected by Author(s)) - Gamma Rays Gamma Ray Lines	18. Distribution Statement		
19. Security Classif. (of this report)	20. Security Classif. (of this page)	21. No. of Pages 598	22. Price*